Arthritis & Rheumatology

An Official Journal of the American College of Rheumatology
www.arthritisrheum.org and wileyonlinelibrary.com

Arthritis & Rheumatology

An Official Journal of the American College of Rheumatology
www.arthritisrheum.org and wileyonlinelibrary.com

VOLUME 73 • November 2021 • NO. 11

Systemic Lupus Erythematosus

Clinical Images

Vasculitis

Systemic Sclerosis

Gout

Autoinflammatory Disease

Fibromyalgia

Rheumatology Workforce

Letters

Cover image: The figure on the cover (from Kato et al, pages 2105–2115) shows immunofluorescence staining of bone marrow–derived dendritic cells from a *Copa*^{V242G} heterozygous mutant mouse. Upon stimulation with a stimulator of interferon genes (STING) agonist, STING (red) is prominently localized to the Golgi (green), which is indicated by the intense yellow color.

In this **Issue**

Highlights from this issue of *A&R* | **By Lara C. Pullen, PhD**

IL-34 Reprograms Glycolytic, Osteoclastic RA Macrophages

Rheumatoid arthritis (RA) patients have elevated levels of multiple inflammatory cytokines, some of which act directly on macrophages. Macrophage colony-stimulating factor (M-CSF), for example, promotes M2 macrophages that favor mitochondrial oxygen consumption over glycolysis. In contrast, granulocyte–macrophage colony-stimulating factor (GM-CSF) does the reverse, promoting M1 macrophages that favor glycolysis over mitochondrial oxygen consumption. Macrophages exposed to interleukin-34 (IL-34) diverge from M-CSF–induced M2 or GM-CSF–derived M1 macrophages to become hyperglycolytic M34 macrophages.

p. 2003

Van Raemdonck et al (p. 2003) report that IL-34 remodels hypermetabolic M34 macrophages through interaction with its co-receptor syndecan 1. In individuals with RA, IL-34 also facilitates the cross-regulation between M34 macrophages and effector T cells, resulting in advanced inflammatory bone destruction. Their
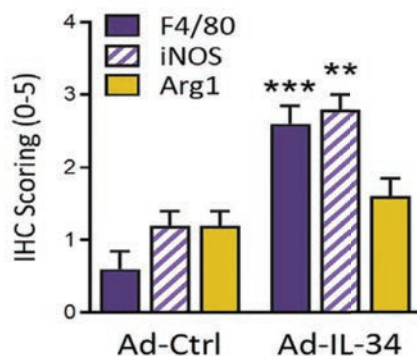
Figure 1. Induction of joint inflammation in mice by local IL-34 expression. Tissue sections were stained for the macrophage markers F4/80, iNOS, and arginase 1.

data demonstrate for the first time that M34 macrophages and effector Th17 cells participate in inflammatory and erosive phenotypes enforced by joint IL-34 expression.

The investigators first documented that syndecan 1 activated IL-34–induced M-CSF receptor phosphorylation and

reprogrammed RA naive cells into distinctive CD14+CD86+GLUT1+ M34 macrophages that expressed elevated levels of IL-1β, CXCL8, and CCL2. When the researchers examined these M34 macrophages in mice, they found that the inflammatory phenotype was accompanied by transcriptional up-regulation of GLUT1, c-Myc, and hypoxia-inducible factor 1α, as well as by amplified pyruvate and l-lactate secretion—all of which were signs of potentiated glycolytic activity.

Since IL-34 is more bioavailable than M-CSF in RA synovial fluid, it can outcompete M-CSF, such that local expression of IL-34 could expand the glycolytic F4/80-positive, inducible nitric oxide synthase (iNOS)-positive macrophage population. This expansion attracted fibroblasts and polarized Th1/Th17 cells, provoking arthritis. The continued crosstalk between murine M34 macrophages and Th1/Th17 cells then further broadened the inflammatory and metabolic phenotypes and resulted in the expansion of IL-34 pathogenicity.

B Cell Depletion Suppresses Profibrotic Macrophage Differentiation in Mouse Model of SSc

In systemic sclerosis (SSc), profibrotic macrophages directly induce fibrosis via interleukin-4 (IL-4), IL-6, IL-13, transforming growth factor β, and CCL18. Since studies in squamous cell carcinoma have suggested that B cell depletion inhibits macrophage differentiation, researchers have hypothesized that B cell depletion may be a reasonable therapy for SSc. Mice with bleomycin-induced SSc (BLM-SSc) are widely used as a model of SSc because they exhibit autoimmune abnormalities and skin and lung fibrosis. Numajiri et al (p. 2086) report that B cell depletion in mice with BLM-SSc suppressed

p. 2086

profibrotic macrophage differentiation and inhibited skin and lung fibrosis.

They found that B cell depletion in mice before BLM induction inhibited fibrosis more strongly than B cell depletion after BLM induction. Because the frequencies of proinflammatory T cells were lower in the post-depletion group than in the pre-depletion group, the authors suggested that the effect of B cell depletion on fibrosis cannot be explained by its effect on T cell differentiation. Instead, they found that profibrotic macrophages were markedly decreased in the pre-depletion group compared to the post-depletion group, suggesting that the B cell depletion was affecting disease through macrophage differentiation.

This hypothesis is supported by the fact that the extent of profibrotic macrophage induction by B cells in SSc patients correlated with the severity of fibrosis. For example, B cells from patients with severely fibrotic diffuse cutaneous SSc with interstitial lung disease had enhanced the expression of CD206 on their monocytes—a noteworthy finding given that CD206 is a marker of profibrotic macrophages. These results suggest that CD11a- and CD22-mediated binding of B cells to macrophages is required for B cell induction of profibrotic macrophages, and the authors conclude by suggesting that their findings point to a new rationale for B cell depletion therapy in SSc.

Details Emerge About Mechanism Behind Estrogen Regulation of Immune Cells

Serine/arginine-rich splicing factor 1 (SRSF1) controls genes involved in T cell function, and patients with systemic lupus erythematosus (SLE) have decreased expression of SRSF1 in their T cells, which correlates with higher SLE Disease Activity Index scores and comorbidity. Ramanujan et al (p. 2052) describe identification of a previously unrecognized molecular link between estrogen and gene regulation of SRSF1 in immune cells.

While SRSF1 could be regulated via translational mechanisms or posttranscriptional regulation of messenger RNA (mRNA), the presence of a long 3′-UTR tail on the *Srsf1* mRNA suggested that the gene's expression is controlled at the posttranscriptional level, presumably by microRNAs (miRNAs) which bind cognate sites within the 3′-UTR and target the mRNA for degradation and/or inhibition of translation. The investigators sought to identify the miRNA that could regulate the *Srsf1* gene at the posttranscriptional level. First, they identified 7 miRNAs that bound the 3′-UTR of the mRNA and appeared from the scientific literature to be implicated in SLE, focusing their efforts on hsa-miR-10b-5p, which showed reliable and consistently robust overexpression under various conditions. Further investigation revealed that overexpression of hsa-miR-10b-5p in transfected cell lines led to decreased levels of SRSF1.

The team then examined the relationship between estrogen, miRNA, and SRSF1, and found that estrogen increased hsa-miR-10b-5p expression in human T cells. Thus, as hypothesized, hsa-miR-10b-5p mediated posttranscriptional regulation of the prototypical splicing regulatory SRSF1 via control of its 3′-UTR activity. When the investigators examined hsa-miR-10b-5p expression levels in human cells, they found that expression was elevated in T cells from healthy women compared to men, and in T cells from SLE patients compared to healthy controls. This study is the first to implicate hsa-miR-10b-5p in SLE, and their findings have potential relevance to systemic autoimmune disease.

Journal Club

A monthly feature designed to facilitate discussion on research methods in rheumatology.

Erosive Hand OA: Incidence and Predictive Characteristics Among Participants in the OA Initiative

McAlindon et al, *Arthritis Rheumatol* 2021;73:2015–2024

Within the spectrum of hand osteoarthritis (OA) exists a subtype differentiated by more pain, presence of inflammation, and presence of joint erosion. Erosive hand OA is present in ~10% of individuals with symptomatic hand OA, giving it a population prevalence comparable to rheumatoid. Treatment is a significant clinical challenge due to the severity of symptoms and the dearth of effective treatments for OA. The distinguishing characteristics of erosive hand OA indicate pathologic processes different from typical OA that could present novel treatment targets. The conjecture that inflammation underlies the development of the erosive subtype of hand OA has led to several clinical trials of anticytokine therapies. However, there are reasons to question the view of erosive hand OA as an inflammatory polyarthritis. The anticytokine trials have been generally negative, and the pathologic appearance of the "erosions" that characterize erosive hand OA suggests damage and subchondral osteolysis more consistent with advanced joint damage than inflammatory pannus. Better understanding the nature of erosive hand OA could help clarify these processes and lead to new and different therapeutic approaches.

McAlindon et al used data from the Osteoarthritis Initiative (OAI), a multicenter cohort study of 4,796 adults with, or at risk for, knee OA, to perform an epidemiologic analysis of erosive hand OA. The rigor and design of the OAI gave researchers the ability to analyze incident erosive hand OA over a 48-month observation period. The availability of hand radiographs at 2 time points enabled the researchers to perform a range of OA severity measures and measure cortical width, a proxy for bone density. The authors used generalized estimating equation models with an underlying Poisson distribution for the dependent variable, robust variance estimator, unstructured correlation matrix, and a log link function, to estimate the relative risk of each SD increase in OA severity for incident erosive hand OA.

Questions

1. What analytic advantages does the longitudinal cohort design offer in relation to previous studies in this field?

2. Does the view of erosive hand OA as an inflammatory arthritis amount to a heuristic error?

3. What is the likely relationship between cortical thinness and erosive hand OA, an association that disappears with adjustment for OA severity?

4. Why might erosive hand OA be associated with reduced body mass index (BMI) when all other OA associations with BMI occur in the opposite direction?

5. Is frailty a useful biologic concept?

Clinical Connections

Protein Mannosylation as a Diagnostic and Prognostic Biomarker of Lupus Nephritis: An Unusual Glycan Neoepitope in SLE

Alves et al, *Arthritis Rheumatol* 2021;73:2069–2077

CORRESPONDENCE
Salomé Pinho, DVM, PhD: salomep@ipatimup.pt
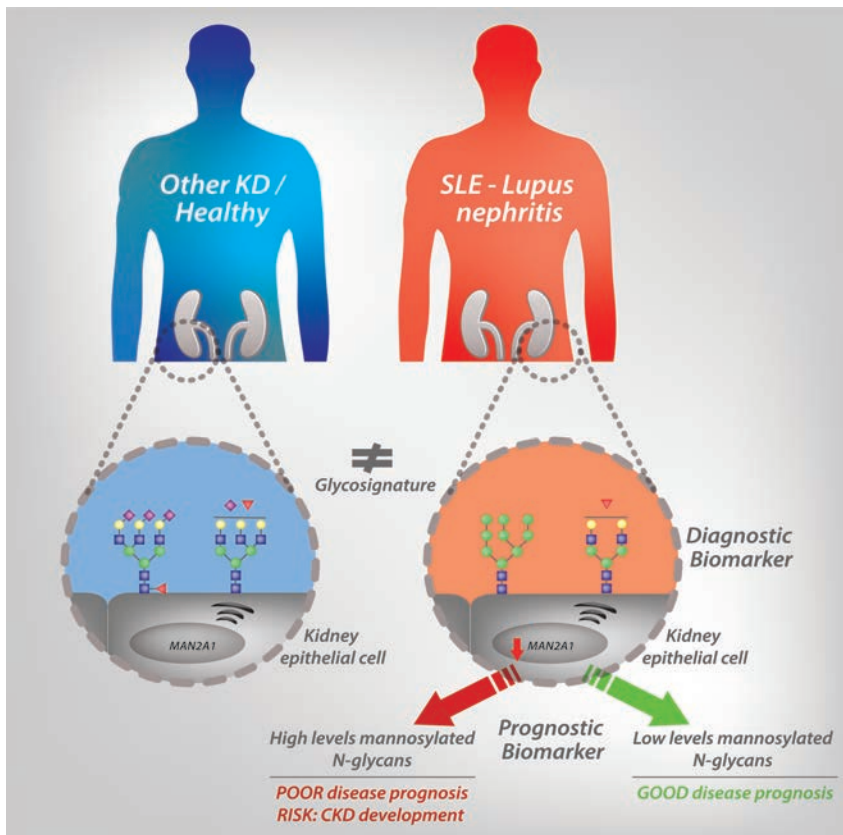
KEY POINTS

• Glycans composition (glycosignature) of kidney tissue distinguishes LN from non-LN patients.

• Kidney epithelial cells from LN patients display an abnormal exposure of microbial-associated mannose-enriched glycans.

• High levels of mannosylated proteins in kidney biopsy from LN patients, at diagnosis, predict the development of chronic kidney disease.

SUMMARY

Changes in protein glycosylation are a hallmark of immune-mediated diseases. Glycans are master regulators of the inflammatory response being important molecules for self–nonself discrimination. In their study, Alves et al reveal the existence of a unique glycan signature in the kidney of systemic lupus erythematosus (SLE) patients with lupus nephritis (LN), characterized by an increased abundance and spatial distribution of unusual mannose-enriched glycans structures. This abnormal exposure of microbial-associated mannosylated glycans at the surface of kidney cells from LN patients was shown to promote an increased recognition by specific glycans-recognizing receptors, expressed by immune cells, potentially contributing to the immunopathogenesis of SLE. Importantly, from a clinical perspective, levels of mannosylation detected in kidney biopsies from LN patients at diagnosis were demonstrated to predict the development of chronic kidney disease (CKD) with 93% specificity.

Value of MRI in Assessing Disease Extent, Relapse Prediction in Early Peripheral SpA

CORRESPONDENCE
Filip Van den Bosch, MD, PhD: filip.vandenbosch@uzgent.be

32 patients with early peripheral SpA

Clinical examination

MRI

Early remission–induction with TNF inhibitor

Resolved enthesitis

Persisting enthesitis

Sustained drug-free remission

Relapse

KEY POINTS

- Lower-extremity MRI detects a much broader pattern of joint and entheseal involvement in patients with early peripheral SpA.

- Enthesitis showed less treatment response compared to synovitis upon MRI assessment.

- Persisting signs of enthesitis on MRI at clinical remission may be a risk factor for subsequent relapse of peripheral SpA after treatment withdrawal.

- Prolonged treatment may be warranted in peripheral SpA patients in clinical remission with residual enthesitis on MRI.

SUMMARY

Peripheral spondyloarthritis (SpA) is a rheumatic inflammatory condition, characterized by inflammation of the joints and entheses predominantly of the lower extremities. Whereas the role of magnetic resonance imaging (MRI) in axial spondyloarthritis is well established, its value in peripheral SpA is still unclear. MRI could play a pivotal role in the assessment of enthesitis, a hallmark of peripheral SpA, which is challenging to diagnose clinically. In this study, Renson et al assessed the inflammatory burden in patients with early peripheral SpA by performing MRI evaluations of lower-extremity joints and entheses at baseline and at clinical remission induced by tumor necrosis factor (TNF) inhibition. This is the first report on the value of MRI in assessing disease extent and prediction of relapse, revealing several clinically relevant findings with implications for the management of early peripheral SpA.

A higher inflammatory burden than clinically anticipated was found in patients with early peripheral SpA, as lower-extremity MRI showed a broader pattern of joint and entheseal involvement. Inflammation on MRI was strongly reduced at the time of clinical remission upon treatment with TNF inhibition. However, a differential response was noted between enthesitis and synovitis, with enthesitis responding less well after TNF inhibition. This may have important implications as our results also indicate that persistent enthesitis on MRI at the time of clinical remission may be a risk factor for subsequent peripheral SpA relapse after treatment withdrawal. Therefore, MRI could play a role in identifying patients who have a more severe disease course in peripheral SpA, which may warrant prolonged treatment.

AMERICAN COLLEGE
of RHEUMATOLOGY
Empowering Rheumatology Professionals

EDITORIAL

Industry Payments to Rheumatologists Ought to Be Going Down, Not Up

Aaron P. Mitchell ![ORCID]

In this issue of *Arthritis & Rheumatology*, Putman et al report their findings regarding the distribution and temporal trends of industry payments to US rheumatologists (1). Their findings are consistent with similar reports from other medical and surgical specialties, and highlight the overarching concern regarding the ability of industry payments to adversely affect care quality within the specific context of rheumatology practice.

The authors analyze Open Payments from 2014 to 2019. This database includes industry-reported records of all transfers of financial value to US physicians and teaching hospitals during this time frame. While there have been anecdotal reports of inaccuracies in Open Payments, it recently underwent audit and review by the Office of the Inspector General and was found to be highly accurate (2). Importantly, Putman and colleagues focused solely on personal payments to physicians—often in the form of in-kind gifts such as meals and travel—and did not include industry funding for research.

Several findings stand out. The first is the temporal trend; industry payments to rheumatologists have been increasing, well above the rate of inflation. This phenomenon has been seen in some, but not all, medical specialties. Medical oncologists, neurologists, and dermatologists have seen payments sharply increase (3–5), while general internists have not. The present study is the first to examine rheumatology specifically, and finds it to be among the specialties with increasing payments. The second remarkable finding is the highly skewed distribution of payments, with a relatively small number of rheumatologists receiving a large majority of the dollar value. This suggests an industry strategy of targeting "key opinion leaders" with higher payments. This group of physicians receives substantial compensation in speaking and consulting fees, whereas the median rheumatologist receives smaller sums that are composed mostly of food and beverage payments, presumably through attendance at "drug talks" or other such events. This is not surprising, as similar patterns have been found for many specialties, and a recent study found that, as measured by its professional society leaders, rheumatology is one of the specialties with the highest degree of key opinion leader–industry ties (6).

Another notable finding is that these payments are concentrated on a relatively small number of drugs; just 10 made up over half of payments. The unifying feature of these drugs is their high cost. The value of payments for these drugs—tens of millions of dollars in some cases—is especially remarkable given that some of them (sarilumab, secukinumab, and apremilast) were not approved until well within the 2014–2019 study period, allowing less time for industry payments to accrue. Similar patterns of rapid payment increases have been observed with other recently approved, high-cost drugs (7).

The picture of industry strategy that emerges from the study by Putman et al and other similar reports is that of intense, sustained key opinion leader–focused marketing soon after the release of a new high-margin drug. This strategy is likely to be successful for two reasons. First, physicians are substantially influenced by their peers' prescribing patterns. Industry payments to a physician increase not only that physician's prescribing but also their peers' prescribing, and key opinion leaders are well positioned to influence a large number of other physicians in this manner (8). Second, physicians also follow their peers in terms of which companies they accept money from (9). Targeting key opinion leaders for industry payments may therefore lead to a larger number of other physicians accepting similar payments, and the potential to be swayed by them, in the future.

Though descriptive in nature, the findings reported by Putman et al have important implications, based on prior findings regarding the consequences of industry payments. In short, work done within medical specialties other than rheumatology suggests that financial relationships between physicians and industry have the potential to adversely affect care quality. Hypothetically, industry spending to promote drugs to physicians could increase dissemination of new, superior drugs, improving patient outcomes. However, the literature suggests this is less often the case. Rather, industry focuses its promotional spending

Aaron P. Mitchell, MD, MPH: Memorial Sloan Kettering Cancer Center, New York, New York.

No potential conflicts of interest relevant to this article were reported.

Address correspondence to Aaron Mitchell, MD, MPH, Department of Epidemiology and Biostatistics, 485 Lexington Avenue, 2nd Floor, New York, NY 10017. Email: mitchea2@mskcc.org.

on treatments that are less innovative and less effective (10,11). Physicians, it seems, naturally gravitate toward the truly game-changing drugs; it is the less innovative drugs that industry has to push harder. The promotion of lower-value drugs is concerning because the literature is also clear on another point: promotional spending works. Receiving industry payments influences physicians' behavior, causing them to increase prescribing of the promoted drug (12). While additional work is needed to investigate whether these same trends hold for rheumatology practice, the implication of these observations is clear: industry money has the potential to shift our prescribing in ways that are unlikely to benefit our patients.

The potential negative consequences of industry payments have become evident in other medical specialties. Oncologists who receive manufacturer payments are more likely to select a more expensive, more toxic drug for the treatment of chronic myeloid leukemia over equally effective alternatives (13). Payments from manufacturers of novel anticoagulants cause physicians to increase prescribing regardless of a patient's bleeding risk (8). Manufacturer payments also increase the prescribing of rebranded generic drugs (14), leading to no therapeutic benefit to the patient but increasing their out-of-pocket costs. The findings of Putman et al suggest that these patterns may apply to rheumatology as well. They note the staggering amount of industry money spent to promote repository corticotropin (Acthar gel), a treatment with nearly nonexistent clinical evidence which has undergone predatory price hikes to rival Martin Shkreli's Daraprim (15,16). Indeed, as the authors note, there are few prescribers of repository corticotropin besides those who receive personal payments from this drug's manufacturer (17). While relatively few rheumatologists prescribe repository corticotropin (approximately half of the 1,743 prescribers in 2015 were rheumatologists), this drug has a substantial financial impact, costing Medicare $0.5 billion per year (17). Similar to what has been observed in other specialties, this likely results in avoidable financial cost to patients without commensurate benefit. Tofacitinib may provide another example, wherein the substantial industry payments may reflect efforts to maintain utilization in the face of increasing safety concerns.

This study has several limitations that warrant mention. By focusing on rheumatologists with Open Payments records, those who never received industry payments are left out of the denominator, causing the reported payment means and medians to be somewhat inflated (this is somewhat accounted for in the geographic analysis, in which the authors impute state-level denominators from the American College of Rheumatology workforce report). This is likely a minor limitation because, based on similar reports of other specialties, the portion of physicians that received no industry payments over the entire 7-year history included in Open Payments is very small. The analysis of physician gender did not account for career stage, which is an important confounder because industry payments are highly correlated with career

stage, and female physicians are younger on average than male physicians. Based on results from other specialties, this gender disparity would likely be reduced in magnitude, but would persist, after adjustment for career stage (18).

From the patient perspective, the practice of industry payments to physicians is increasingly difficult to rationalize. We know that industry promotion focuses on drugs with greater toxicity and/or excessive costs. To the extent that industry payments achieve the desired end of increasing prescriptions, patients may experience avoidable toxicity and out-of-pocket expense. Moreover, industry payments serve no unmet need; through our professional societies and other nonprofit sources, we physicians are fully capable of staying up-to-date on new treatments without relying on industry meals and sponsored events. We should reconsider our participation in a practice which, existing evidence suggests, adversely affects prescribing while contributing to higher health system and patient out-of-pocket costs.

AUTHOR CONTRIBUTIONS

Dr. Mitchell drafted the article, revised it critically for important intellectual content, and approved the final version to be published.

REFERENCES

1. Putman MS, Goldsher JE, Crowson CS, Duarte-García A. Industry payments to practicing US rheumatologists, 2014–2019. Arthritis Rheumatol 2021;73:2138–44.

2. Murrin S. Open Payments Data: review of accuracy, precision, and consistency in reporting. Department of Health and Human Services Office of the Inspector General. August 2018. URL: https://oig.hhs.gov/oei/reports/oei-03-15-00220.pdf.

3. Mitchell AP, Mishra AA, Dey P, Curry MA, Trivedi NA, Haddadin M, et al. The association between drug industry payments and NCCN guideline panel membership. J Clin Oncol 2020;38 Suppl:2068.

4. Robbins NM, Meyer MJ, Bernat JL. Scope and nature of financial conflicts of interest between neurologists and industry: 2013–2016. Neurology 2019;93:438–49.

5. Schlager E, Flaten H, St. Claire C, Maxim E, Dunnick C, Dellavalle RP. Industry payments to dermatologists: updates from the 2016 open payment data. Dermatol Online J 2018;24:13030/qt8r74w3c4.

6. Moynihan R, Albarqouni L, Nangla C, Dunn AG, Lexchin J, Bero L. Financial ties between leaders of influential US professional medical associations and industry: cross sectional study. BMJ 2020;369:m1505.

7. Mitchell AP, Rahman MW, Trivedi NU, Bach PB. Personal payments from pharmaceutical companies to US oncologists increased from 2014-2017 [poster]. Presented at the Academy Health Annual Research Meeting (virtual); 2020 July 28. URL: https://academyhealth.confex.com/academyhealth/2020arm/meetingapp.cgi/Paper/41256.

8. Agha L, Zeltzer D. Drug diffusion through peer networks: the influence of industry payments. National Bureau of Economic Research. October 2019. URL: http://www.nber.org/papers/w26338.

9. Winn AN, Mitchell AP, Fergestrom N, Neuner JM, Trogdon JG. The role of physician professional networks in physicians' receipt of pharmaceutical and medical device industries' payments. J Gen Intern Med 2021 doi: 10.1007/s11606-021-06802-9. E-pub ahead of print.

10. Lexchin J. The relation between promotional spending on drugs and their therapeutic gain: a cohort analysis. CMAJ Open 2017;5:E724–8.

11. Greenway T, Ross JS. US drug marketing: how does promotion correspond with health value? BMJ 2017;357:j1855.

12. Mitchell A, Trivedi N, Gennarelli RL, Chimonas SC, Tabatabai S, Goldberg J, et al. Are financial payments from the pharmaceutical industry associated with physician prescribing? A systematic review. Ann Intern Med 2021;174:353–61.

13. Mitchell AP, Winn AN, Dusetzina SB. Pharmaceutical industry payments and oncologists' selection of targeted cancer therapies in Medicare beneficiaries [letter]. JAMA Intern Med 2018;178:854–6.

14. Sharma M, Vadhariya A, Johnson ML, Marcum ZA, Holmes HM. Association between industry payments and prescribing costly medications: an observational study using open payments and medicare part D data. BMC Health Serv Res 2018;18:236.

15. Duarte-García A, Matteson EL, Shah ND. Older drugs with limited trial evidence: are they worth the expense? The case of repository corticotropin marketed as H.P. Acthar gel. Ann Intern Med 2019;170:791–2.

16. Pollack A. Drug goes from $13.50 a tablet to $750, overnight. New York Times. September 20, 2015. URL: https://www.nytimes.com/2015/09/21/business/a-huge-overnight-increase-in-a-drugs-price-raises-protests.html

17. Hartung DM, Johnston K, Cohen DM, Nguyen T, Deodhar A, Bourdette DN. Industry payments to physician specialists who prescribe repository corticotropin. JAMA Netw Open 2018;1: e180482.

18. Inoue K, Blumenthal DM, Elashoff D, Tsugawa Y. Association between physician characteristics and payments from industry in 2015–2017: observational study. BMJ Open 2019;9:e031010.

AMERICAN COLLEGE
of RHEUMATOLOGY
Empowering Rheumatology Professionals

REVIEW

Is There a Place for Chimeric Antigen Receptor–T Cells in the Treatment of Chronic Autoimmune Rheumatic Diseases?

Cindy Orvain,[1] Morgane Boulch,[2] Philippe Bousso,[3] Yannick Allanore,[4] and Jérôme Avouac[4] (iD)

Chimeric antigen receptor–T (CAR-T) cell therapy is based on specific targeting of tumor antigens, leading to lysis and destruction of tumor cells. The high potency of CAR-T cells in the management of B cell malignancies has been demonstrated. Following the success of this therapeutic strategy, new CAR-T cell–derived constructs that have the ability to eradicate pathogenic B cells or restore tolerance have been developed. The present review discusses how the knowledge and technology generated by the use of CAR-T cells may be translated and integrated into ongoing therapeutic strategies for autoimmune rheumatic diseases. To this end, we describe the details of CAR-T cell technology, as well as the meaningful achievements attained with the use of CAR-T cells in onco-hematology. In addition, we review the preliminary data obtained with CAR-T cells and their derivative constructs in experimental models of autoimmune diseases. Finally, we focus on how CAR-T cell engineering interferes with the pathogenesis of 3 chronic autoimmune rheumatic diseases—rheumatoid arthritis, systemic lupus erythematosus, and systemic sclerosis—and discuss whether these constructs might yield greater efficacy and be associated with fewer adverse events compared to current treatment strategies.

Introduction

Autoimmune rheumatic diseases have a high impact on patients' quality of life and increase the risk of morbidities and mortality, particularly given the chronicity of these diseases and their various organ manifestations and associations with comorbidities. Over the last several decades, earlier diagnosis, new classification criteria, and development of novel therapeutic approaches have improved the management of autoimmune rheumatic diseases (1,2). However, there are still great challenges that need to be addressed. Indeed, standard-of-care treatments are based on immunosuppression aimed at controlling disease activity and dampening immune system overactivation. Conventional synthetic disease-modifying antirheumatic drugs (DMARDs) and biologic/synthetic targeted DMARDs have dramatically improved the prognosis in patients with autoimmune rheumatic diseases (2); nevertheless, despite major therapeutic advances, the response to these therapies may not be adequate in some patients, and long-term drug therapy is required to maintain prolonged clinical remission.

A recent breakthrough in oncology brought new hopes for cancer therapies. Genetic engineering of our immune cells, and especially T cells, has improved the prognosis of B cell cancers that are refractory to conventional therapies (3,4). This technology, called chimeric antigen receptor–T (CAR-T) cell therapy, is based on specific targeting of tumor antigens, leading to the lysis and destruction of tumor cells by modified autologous T cells. CAR-T cells are becoming of great therapeutic interest for autoimmune diseases, given their ability to delete pathologically activated immune cells or reestablish immune tolerance in an organ affected by dysregulated immunity.

The intention of this review was to introduce CAR-T cell technology, describe the achievements attained with the use of CAR-T cells in onco-hematology, and present preliminary data obtained with the use of CAR-T cells and their derivative constructs in experimental models of autoimmune diseases. In addition, this review describes how CAR-T cells may interfere with the pathogenesis of chronic autoimmune rheumatic diseases, and discusses whether greater efficacy may be achieved with these constructs and may

---

[1]Cindy Orvain, PhD: INSERM U1016, CNRS UMR8104, Institut Cochin, Paris, France; [2]Morgane Boulch, PhD: University Paris Diderot, Sorbonne Paris Cité, Paris, France; [3]Philippe Bousso, PhD: Dynamics of Immune Responses Unit, Equipe Labellisée Ligue Contre le Cancer, Institut Pasteur, INSERM U1223, Paris, France; [4]Yannick Allanore, MD, PhD, Jérôme Avouac, MD, PhD: INSERM U1016, CNRS UMR8104, Institut Cochin, Université Paris Descartes, and Service de Rhumatologie, Hôpital Cochin, AP-HP, Paris, France.

be associated with fewer adverse events compared to current treatments. To this end, we searched PubMed for reports published between 1989 and 2021 using any of the following terms: "CAR-T cells," "CAR-T cells AND autoimmunity," "CAAR-T cells," and "CAR-Treg." We found 3,795 published references based on these criteria, and after reading the abstract and/or the full text, we selected 42 articles for the purpose of this review.

CAR-T cell technology

T cells are main effectors of our adaptive immune system. One of their key functions is to kill tumor cells or infected cells after recognition of a specific antigen via their T cell receptor (TCR). This observation led to the emergence of a new therapeutic strategy: redirecting T cells to antigens of interest to overcome natural barriers that they encounter. This concept emerged in the 1990s, and Eshhar and colleagues showed that the combination of TCR constant variant domains and antibody variable domains on T cells induced T cell activation and the lysis of target cells (5). These studies led to the further development of genetically engineered autologous T cells that express a chimeric antigen receptor, or CAR, allowing redirection of these cells to the targeted antigen without the restrictions conferred by the major histocompatibility complex (MHC).

CAR-T cell constructs contain 4 main components: an extracellular antigen-binding domain, a hinge, a transmembrane domain, and an intracellular signaling domain leading to T cell activation (6), as shown in Figure 1A. All of these components are crucial for CAR signaling, and different combinations should be tested to analyze and determine the optimal CAR-T cell response.

Recognition of the CAR target is mediated by an antigen-binding domain composed of variable heavy and light chains of a monoclonal antibody connected by a flexible linker and called single-chain Fv (scFv). The scFv must have high affinity to the target antigen in order to induce CAR signaling and T cell activation. The hinge of CAR-T cells should be flexible to avoid steric hindrance and allow the recognition of the targeted antigen and T cell activity (7). The CAR hinge sequence is similar to amino acid sequences of the CD8, CD28, IgG1, or IgG4 hinge.

The transmembrane domain anchors the scFv in the T cell membrane and is designed using amino acid sequences derived from CD3ζ, CD28, CD4, and CD8α transmembrane domains. The choice of the sequence is critical, since it influences CAR activity (8). Compared to CD28 sequences, CD8α sequences chosen for the hinge and the transmembrane domain were found to be associated with decreased production of interferon-γ (IFNγ) and tumor necrosis factor (TNF) (8). Once the CAR has recognized its target, it induces phosphorylation of immunoreceptor tyrosine–based activation motifs (ITAMs) located on intracellular domains. Once phosphorylated, ITAMs induce the recruitment of effector molecules that lead to T cell activation, cytokine production, and lysis of target cells, as has been observed in unmodified T cells after antigen recognition by the TCR. For several years, this intracellular domain has been engineered to improve its function. The first generation of CAR was composed of only one intracellular activation domain, which was the CD3ζ domain. However, this domain was insufficient to induce activation of resting T cells in vivo (9). This has led to the development of second-generation CARs, characterized by an intracellular domain composed of both activation and costimulation domains. Indeed, human T cells transduced with a CAR containing a fusion of intracellular CD3ζ and CD28 domains display increased proliferation rates, higher production of interleukin-2 (IL-2), and augmented cytotoxic activity (10).
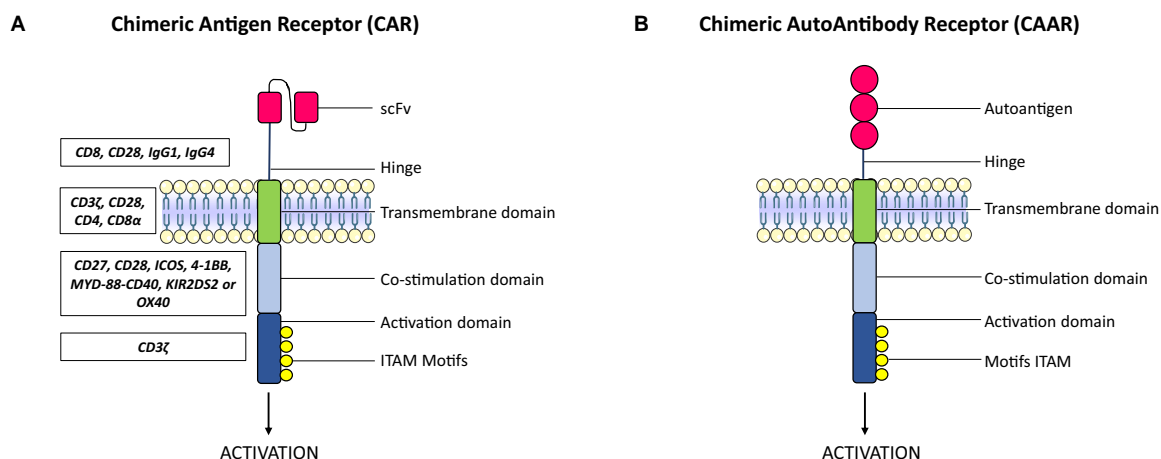
Figure 1. Structure of the chimeric antigen receptor (**A**) and chimeric autoantibody receptor (**B**). Both receptors are composed of activation, costimulation, and transmembrane domains linked to single-chain Fv (scFv) for CAR or an autoantigen for CAAR. The protein sequences that have been used for design of the CAR or the CAAR are shown in the boxes on the left. ITAM = immunoreceptor tyrosine–based activation motif. Color figure can be viewed in the online issue, which is available at http://onlinelibrary.wiley.com/doi/10.1002/art.41812/abstract.

Other studies have investigated the effects of other costimulatory intracellular domains, such as the TNF receptor superfamily protein domain 4-1BB, on the function and fate of CAR-T cells. The 4-1BB domain induces persistence of CAR-T cells and a profile characterized by central memory T cells, whereas the CD28 domain is associated with reduced persistence of CAR-T cells and an effector memory T cell profile (11). It was also shown that a single amino acid residue in CD28 drove T cell exhaustion and hindered the persistence of CD28-based CAR-T cells; indeed, changing asparagine to phenylalanine in the amino acid sequence of CD28-based CAR-T cells (CD28-YMFM) promoted increased persistence of CAR-T cells in vivo and enhanced antitumor activity (12).

To address the lack of persistence of second-generation CAR T cells, some groups have proposed using a combination of the activation CD3ζ domain with 2 intracellular costimulation domains derived from CD27, CD28, inducible T cell costimulator (ICOS), 4-1BB, myeloid differentiation primary response protein 88–CD40, killer cell immunoglobulin-like receptor 2DS2, or OX40, creating third-generation CAR-T cells (13–17). For example, CAR-T cells engineered with a combination of 4-1BB and CD28 displayed increased cytotoxicity and persistence compared to CAR-T cells composed of the 4-1BB intracellular domain only (18). Moreover, mesothelin CAR-T cells designed with ICOS and 4-1BB costimulation domains displayed increased persistence as compared to CAR-T cells composed of the 4-1BB intracellular domain only (19). Further studies are still needed to evaluate the efficacy and safety of third-generation CAR-T cells. In fact, only second-generation CAR-T cells have been approved for therapeutic use by the US Food and Drug Administration (FDA); the list of approved therapies is shown in Table 1.

Recent genetic modifications of CAR-T cells have been performed to enhance their cytokine production, in particular the production of IL-12. Genetic modification of CD19 CAR-T cells to achieve enhanced expression of IL-12 was associated with an increase in antitumor activity in vivo, without being preceded by a preconditioning chemotherapy, in mice infused with an EL4 thymoma cell line expressing human CD19 (20). CAR-T cells that constitutively expressed IL-12 and targeted vascular endothelial growth factor receptor 2 (IL-12/VEGFR2 CAR-T cells) were associated with a regression of established tumors together with long-term CAR-T cell persistence in the tumor tissue (21). Moreover, CAR-T cells that constitutively expressed IL-12 and targeted carcinoembryonic antigen (IL-12/CEA CAR-T cells) led to a more pronounced reduction in tumor volume compared to CAR-T cells that did not express IL-12 and targeted CEA alone (CEA CAR-T cells) (22). Other CAR-T cells have been armed to express IL-7, IL-15, IL-18, or IL-33, and results regarding efficacy of those strategies are reviewed elsewhere (6). These studies showed that the persistence and functions of CAR-T cells are modulated according to study objectives.

CAR-T cells in oncology

CAR-T cells were first utilized in oncology to overcome the failure of natural T cells to eradicate tumor cells. Redirecting T cells against specific antigens expressed by tumor cells has yielded great results in hematologic cancers, specifically in B cell malignancies. CD19 was chosen as the preferential B cell target, since it is expressed during all major stages of B cell maturation (from the pro–B cell state to late plasmablasts), whereas CD20 is mainly expressed during the stage of peripheral B cell maturation (from naive B cells to early plasmablasts) (23). Moreover, CD19 is highly expressed on tumor B cells, and preclinical studies showed a total eradication of systemic lymphoma cells after a single infusion of human CD19 CAR-T cells in mice (24), thus providing the rationale to translate the use of these cells to human patients in the clinic.

Meaningful results were obtained with CD19 CAR-T cell treatment in patients with diffuse large B cell lymphoma or acute lymphoblastic leukemia whose disease was refractory to chemotherapy. Patients with diffuse large B cell or follicular lymphoma had a complete remission rate of 57% (4), while in patients with acute lymphoblastic leukemia, the complete remission rate ranged from 68% to 100% (25). These results

Table 1. CAR-T cell therapies approved by the US Food and Drug Administration

Drug (trade name)	Provider	Target antigen	Costimulation activation domains	Indication	Approval date
Tisagenlecleucel (Kymriah)	Novartis	CD19	4-1BB, CD3ζ	Adults with acute lymphoblastic leukemia	August 30, 2017
Axicabtagene ciloleucel (Yescarta)	Gilead	CD19	CD28, CD3ζ	Adults with relapsed or refractory large B cell lymphoma	October 18, 2017
Brexucabtagene autoleucel (Tecartus)	Gilead	CD19	CD28, CD3ζ	Adults with relapsed or refractory mantle cell lymphoma	June 24, 2020
Lisocabtagene maraleucel (Breyanzi)	Bristol Myers Squibb	CD19	4-1BB, CD3ζ	Adults with relapsed or refractory large B cell lymphoma	February 5, 2021

led to FDA approval of the use of CD19 CAR-T cell therapy in patients with B cell lymphoma and patients with acute lymphoblastic leukemia. However, the success of CAR-T cell therapy in hematologic malignancies was not replicated in patients with solid cancers. The differing outcomes in patients with solid cancers may be related to the lack of specific tumor antigens, which leads to off-tumor toxicities, the loss of the targeted antigen, or the complexity of the immunosuppressive tumor microenvironment, which could prevent CAR-T cell penetration and activity. New engineering strategies to improve CAR-T cell activity in solid tumors are currently under investigation, such as development of CARs with multispecificity, improvement of CAR trafficking, and modification of their sensitivity to inhibitory signals in the tumor microenvironment (6).

Although CAR-T cells can produce durable periods of clinical remission in patients with hematologic malignancies who have an inadequate response to standard therapies, the use of CAR-T cells is limited by potentially severe toxic effects. Cytokine release syndrome (CRS) has been reported to occur in 54–91% of patients treated with CD19 CAR-T cells, and the frequency of severe CRS in that series of patients ranged from 8.3% to 43% (26). Patients usually developed CRS within 1 week after CAR-T cell infusion and experienced fever, hypotension, and respiratory insufficiency, leading, in severe cases, to multiorgan failure. CRS is triggered by CAR-T cell activation after tumor antigen recognition. Indeed, CAR-T cells secrete proinflammatory chemokines and cytokines, leading to the recruitment of immune cells and the production of IL-1 and IL-6 by macrophages (27). Tumor volume and CAR-T cell expansion are important determinants of the severity of CRS, as they regulate the amount of proinflammatory cytokines released (28). Treatment with glucocorticoids, anti–IL-6, anti–IL-1, or anti–granulocyte-macrophage colony-stimulating factor may be used for the treatment of severe or life-threatening CAR-T cell–induced CRS.

CAR-T cells in autoimmunity

Most standard-of-care treatments used in autoimmune diseases are not curative, may cause side effects, and may be associated with a primary or secondary lack of clinical response. Autoimmune diseases are characterized by the activation of the immune system against self antigens, leading to autoantibody production by B cells and tissue destruction by cytotoxic T cells. The success of CAR-T cell therapies in different cancers has led to the development of 3 specific strategies in patients affected by autoimmune diseases (Table 2).

CAR-T cell strategies. Given the successful use of CD19 CAR-T cells in treating B cell malignancies, a first strategy would be to reposition CD19 CAR-T cells as a novel strategy to replace the current B cell depletion therapy in patients with autoimmune diseases (26). Among existing therapies,

rituximab, an anti-CD20 antibody, is the main B cell depletion strategy used in autoimmune diseases. Rituximab has demonstrated efficacy in patients with rheumatoid arthritis (RA), those with multiple sclerosis, and those with antineutrophil cytoplasmic antibody–associated vasculitis (29–31). However, its efficacy was not conclusive in other autoimmune diseases, such as systemic lupus erythematosus (SLE) (32). An incomplete response to rituximab may be related to an insufficient depletion of B cells, which is attributable to sequestration of resistant B cells or long-lived plasma cells in the bone marrow, a site that might be less accessible to rituximab (33). Some patients may develop antibodies directed against the murine parts of the anti-CD20 antibody, which could limit its efficacy (34,35). Based on these results, anti-CD20 humanized antibodies with increased complement-dependent cytotoxicity or antibody-dependent cellular cytotoxicity have been designed, including ocrelizumab or ofatumumab, and are currently approved for the treatment of multiple sclerosis.

Another interesting B cell target is the CD19 antigen, which, when compared to the CD20 antigen, is expressed on more B cell subsets. We could speculate that use of the CD19 antibody may lead to deeper B cell depletion by eradicating pro–B cell, antibody-secreting plasmablasts and some plasma cells (33). Monoclonal anti-CD19 antibodies are currently being investigated in patients with multiple sclerosis and in patients with anti–*N*-methyl-ᴅ-aspartate receptor encephalitis (ClinicalTrials.gov identifiers: NCT04372615 and NCT01585766, respectively).

The expression of CD19 on numerous B cell subsets and successful B cell eradication by CD19 CAR-T cells in patients with acute B cell lymphoblastic leukemia drove physicians to investigate CD19 CAR-T cells in murine models of autoimmune diseases. In an experimental mouse model of SLE, the infusion of CD19 CAR-T cells in (NZB × NZW)F1 and MRL*fas/fas* mice led to complete depletion of CD19+ B cells and autoantibody production, a reversion of disease manifestations in target organs, and an extended mouse lifespan (36) (Table 2). Moreover, clinical trials using CD19 CAR-T cells showed a persistence of B cell aplasia following administration of a single dose of CD19 CAR-T cells, in contrast to the effects of B cell–depleting antibodies, which need to be infused regularly to maintain B cell aplasia (37).

In addition to the treatment strategy of B cell depletion, other types of CAR-T cells have been designed to target autoreactive immune cells in preclinical autoimmune diabetes mellitus. NOD mice develop autoimmune diabetes through a process in which the B:9-23 peptide from the insulin B-chain is presented by the MHC class II gene I-A^{g7} to pathogenic B:9-23–specific CD4+ cells. A single infusion of CAR-T cells directed against this MHC class II complex in NOD mice delayed the onset of diabetes when compared to that observed in control CAR-T cell–treated mice (38). However, this infusion did not provide long-term protection against autoimmune diabetes development, likely due to a lack of CAR-T cell persistence.

Table 2. CAR-T cell strategies developed in experimental models of autoimmunity*

Strategy, disease	Targeted antigen	Mouse model	Costimulation/ activation domains	Outcomes	Reference
CAR-T cells					
Type 1 diabetes	MHC I-A^{g7}-B:9-23(R3)	NOD mice	CD28/CD3ζ or CD28/CD137/CD3ζ	Delayed occurrence of type 1 diabetes	Zhang et al (38)
Lupus	CD19	(NZB × NZW)F1 or MRL$^{fas/fas}$ mice	CD28/CD3ζ	Sustained B cell depletion; decreased autoantibody production; increased survival	Kansal et al (36)
CAAR-T cells					
Pemphigus vulgaris	Dsg-3	Pemphigus vulgaris hybridoma (NOD *scid* gamma mice)	CD137/CD3ζ	Specific deletion of Dsg-3 B cells; decrease in Dsg-3 antibodies	Ellebrecht et al (40)
CAR-Treg cells					
Multiple sclerosis	MOG	EAE	CD28/CD3ζ	Migration of CAR-Treg cells in brain; reduced disease symptoms; decrease in proinflammatory cytokines in brain	Fransson et al (52)
Colitis	CEA	TNBS-induced colitis	CD28/FcRy	Migration of CEA CAR-Treg cells in colon mucosa	Elinav et al (47)
Colitis	CEA	CEABAC or transfer of CEA-specific CD4+ cells	CD28/CD3ζ	Amelioration of colitis; improved survival	Blat et al (53)
Colorectal cancer	CEA	DSS-induced colitis	CD28/CD3ζ	Accumulation of CAR-Treg cells in colon; suppression of colitis	Blat et al (53)
Type 1 diabetes	Insulin	NOD mice	CD28/CD3ζ	Decreased colorectal tumor burden; no prevention of diabetes occurrence	Tenspolde et al (55)

* CAR = chimeric antigen receptor; MHC = major histocompatibility complex; Dsg-3 = desmoglein-3; MOG = myelin oligodendrocyte glycoprotein; EAE = experimental autoimmune encephalitis; CEA = carcinoembryonic antigen; TNBS = 2,4,6-trinitrobenzenesulfonic acid; CEABAC = carcinoembryonic antigen with a human bacterial artificial chromosome; DSS = dextran sulfate sodium.

An important point to consider before initiation of CAR-T cell therapy in patients affected by autoimmune diseases is the patient's basal state of inflammation, defined according to the presence and levels of inflammatory cytokines produced by M1 macrophages infiltrating the lesional tissue (39). For this reason, it is tempting to speculate that development of CRS in patients with autoimmune diseases treated with CAR-T cells might be more severe. Thus, the use of CAR-T cells in these patients would only be conceivable after treatment with immunosuppressive drugs or other targeted therapies has been initiated.

Chimeric autoantibody receptor–T (CAAR-T) cell strategies. In the development of CAR-T cell therapies, it was observed that pathologic cells, including tumor cells, could be targeted and then eradicated. B cells in autoimmune diseases produce autoantibodies that promulgate organ dysfunction. To target these autoimmune B cells, CAAR-T cells have been engineered. In contrast to the specific expression by CAR-T cells of receptors for molecules expressed on pathologic cells, CAAR-T cells express an extracellular autoantigen recognized by the B cell receptor (BCR), as shown in Figure 1B. This extracellular domain is linked to a transmembrane domain, a costimulation domain, and an activation domain, similar to the intracellular part of CARs. Thus, autoantigen recognition by autoreactive B cells leads to CAAR activation and specific lysis of pathogenic B cells (40). The proof of concept of this approach was presented in a study conducted in a preclinical mouse model of pemphigus vulgaris (PV). The aim of that study was to test the efficacy of CAAR-T cells expressing the PV autoantigen desmoglein-3 (Dsg-3) fused to the CD137–CD3ζ signaling domains as a strategy to deplete

pathogenic B cells. After infusion of Dsg-3 CAAR-T cells, specific elimination of B cells carrying a BCR directed against the Dsg-3 antigen was observed, both in the presence and in the absence of soluble Dsg-3–IgG. Moreover, Dsg-3 CAAR-T cells engrafted and persisted in mice even in the absence of their antigen (40) (Table 2).

Recently, Dsg-3 CAAR-T cells have been shown to lyse primary human anti–Dsg-3–IgG B cells isolated from patients with PV. Moreover, injection of Dsg-3 CAAR-T cells in a murine model of active PV improved mucocutaneous erosions and induced a decrease in serum anti–Dsg-3 antibodies (41). This new CAR strategy may be a promising approach in the treatment of autoimmune diseases that are characterized by pathologic B cells and autoantibodies. However, some disease aspects should be studied before initiating a CAAR-T cell therapeutic approach. Indeed, the pathologic role of autoantibodies should be demonstrated in the disease pathogenesis and then the sequence and molecular structure of the autoantigen targeted by pathogenic autoantibodies must be characterized, in order to design suitable CAAR-T cells (42). Future studies will need to focus on the pathogenic role of autoantibodies and characterize the target autoantigens in autoimmune diseases in which B cells contribute to disease development.

CAR-Treg cell strategies. The numbers and functions of Treg cells are altered in autoimmune diseases, leading to a defect in tolerance, dysregulation of immunity, inflammation, and emergence of autoimmune cells (43). Several therapeutic strategies based on Treg cell function have been proposed to restore tolerance in affected tissues. Infusion of low-dose IL-2 as a strategy to stimulate the expansion of Treg cells has been shown to increase the Treg cell:Teff cell ratio and to improve the Clinical Global Impression score in a phase I/IIa study that included patients affected by different autoimmune diseases (44). Other phase I/II studies showed increased Treg cell expansion after infusion of low-dose IL-2 in patients with SLE or patients with type 1 diabetes (45). Nevertheless, IL-2 therapy is limited in that it has a short half-life, it requires repeated injections, and an anti-drug immune response may occur.

Polyclonal Treg cell infusion has a good safety profile, and the benefits of this strategy have been demonstrated in patients with type 1 diabetes and those with graft-versus-host disease; other clinical trials in patients with Crohn's disease and those with pemphigus are ongoing (46). However, the use of polyclonal Treg cells is limited by their lack of specificity, leading to reduced anti-infection and anti-tumor immune responses. Thus, Treg cells including a transgenic TCR or a CAR were further designed to target specific antigens, and these have displayed a better ability to suppress effector responses compared to polyclonal Treg cell infusion (46). However, a transgenic TCR can only recognize the antigen presented by MHC molecules, which requires a specific TCR design for each patient, and therefore the large-scale development of this approach may be limited.

The limitations of this approach have led to development of a CAR directed against a specific antigen within an affected tissue that could be recognized without MHC restriction. Elinav et al demonstrated that mouse CAR-Treg cells accumulated at the site of the target antigen and induced bystander suppression (47). This phenomenon demonstrates that CAR-Treg cells target antigens that are not necessarily expressed on the cell surface, leading to immune suppression in the affected organ. Moreover, Treg cells have been shown to inhibit dendritic cell (DC) differentiation and maturation (48,49) and could limit migration of inflammatory DCs in draining lymph nodes (50). We hypothesize that CAR-Treg cells will also modulate DC function in affected tissues and secondary lymphoid organs. Restoring immune tolerance with CAR-Treg cells may be a relevant strategy (Table 2), but CAR-Treg cell plasticity and stability should be maintained to avoid their conversion into inflammatory cells (51). Additional studies should be conducted regarding their persistence in targeted tissues.

CAR-Treg cells in experimental autoimmune encephalitis (EAE). CAR-expressing Treg cells directed against the antigen myelin oligodendrocyte glycoprotein (MOG) showed suppressive capacity in vitro and could efficiently access various regions in the brain via intranasal cell delivery in a mouse model of EAE. Mice displayed decreased severity of disease symptoms and brain inflammation, and remained healthy after a second challenge with the MOG peptide. These findings highlight the sustained effects of engineered CAR-Treg cells (52).

CAR-Treg cells in colitis. A CAR-Treg cell directed against the 2,4,6-trinitrophenyl (TNP) antigen was assessed in a mouse model of 2,4,6-trinitrobenzenesulfonic acid–induced colitis. Mice infused with TNP-expressing CAR-Treg cells had a better survival compared to mice infused with wild-type Treg cells (75% versus 40%), and the colitis score in TNP-expressing CAR-Treg cell–treated mice was lower (47). The same investigators induced experimental colitis in CEA-transgenic mice by irradiating the mice and injecting them with CEA-expressing CD4+ Teff cells. The mice were then treated with CEA-specific CAR-Treg cells or CAR-Treg cells that were not specific for the target antigen (irrelevant CAR-Treg cells). On day 6 postinjection, the investigators observed accumulation of CEA CAR-Treg cells in the colon of diseased mice, which was associated with inhibition of abdominal accumulation of CEA CAR CD4+ Teff cells. They also noted that after the induction of lethal colitis, the lifespan of the CEA CAR-Treg cell–treated mice was longer than that of mice that had received irrelevant CAR Treg cells.

In another experimental colitis mouse model, in which colorectal cancer was induced in mice by injection of dextran sulfate sodium, the effect of CEA CAR Treg cell treatment was compared to that of irrelevant CAR-Treg cells. The tumor score, defined by the percentage of the tumor-occupied colon circumference, was significantly decreased in mice receiving CEA CAR Treg cells compared to those receiving irrelevant CAR-Treg cells, suggesting a protective effect of these cells against colorectal cancer

development. This result is of importance, given the increased risk of colorectal cancers in patients affected by ulcerative colitis (53).

CAR-Treg cells in type I diabetes. The first observations following polyclonal Treg cell infusion in patients with type 1 diabetes provided evidence showing a persistence of transferred Treg cells up to 1 year after infusion, and demonstrated a good safety profile of the procedure (54). The infusion of CAR-Treg cells directed against insulin in NOD mice was also associated with CAR-Treg cell persistence in mice, but showed no benefit in terms of preventing the occurrence of type 1 diabetes. These findings support the need for further studies (55).

CAR-Treg cells in graft-versus-host disease. Interestingly, a recent study performed by Imura et al demonstrated the in vitro suppression of IgG antibody production and differentiation of B cells by CD19 CAR-Treg cells. In the same study, a strategy of infusion of CD19 CAR-Treg cells in immunodeficient mice reconstituted with human peripheral blood mononuclear cells led to suppression of antibody production and reduction in the risk of graft-versus-host disease (56).

Application of CAR-T cells in human autoimmune rheumatic diseases

Several issues may be encountered in the use of current treatments for autoimmune rheumatic diseases, including increased rates of infection due to a strong immunosuppressive effect, and the need for regular injections to maintain disease remission. Moreover, the development of anti-drug antibodies, which can lead to treatment failure or injection-site reactions, has also been observed with the use of monoclonal antibody treatments. The development of CAR T cells may represent an innovative way to counteract several of the limitations of biologic therapies, e.g., issues encountered with short- or long-term use of rituximab, including adverse effects from repeated injections of rituximab, incomplete B cell depletion (57), or immunogenicity (34,35). CD19 CAR-T cell therapy requires only one infusion and induces total B cell aplasia over several years (37). Moreover, the preexisting humoral immunity that was present before CD19 CAR-T cell therapy is conserved after treatment (58). CAAR-T cells could be used to deplete, specifically, pathogenic B cells, and CAR-Treg cells may be a promising therapy to promote localized tolerance in organs affected by autoimmune rheumatic diseases.

Several CAR-T cell preclinical approaches have been studied or are ongoing in patients with autoimmune rheumatic diseases. These include RA, SLE, and systemic sclerosis (SSc).

CAR-T cells in RA. Anti–citrullinated protein antibodies (ACPAs) are well described in patients with RA and could have a pathogenic role. ACPAs against citrullinated vimentin (CV) have been shown to enhance osteoclastogenesis and high bone resorption in mice (59), suggesting that B cells have a pathologic role. The efficacy of rituximab has been demonstrated in patients with active RA, especially in patients with high ACPA titers (60). Thus, we may hypothesize that the development of CAAR-T cells expressing citrullinated antigens would allow a specific deletion of anticitrulline B cells, while saving protective B cells (Figure 2).
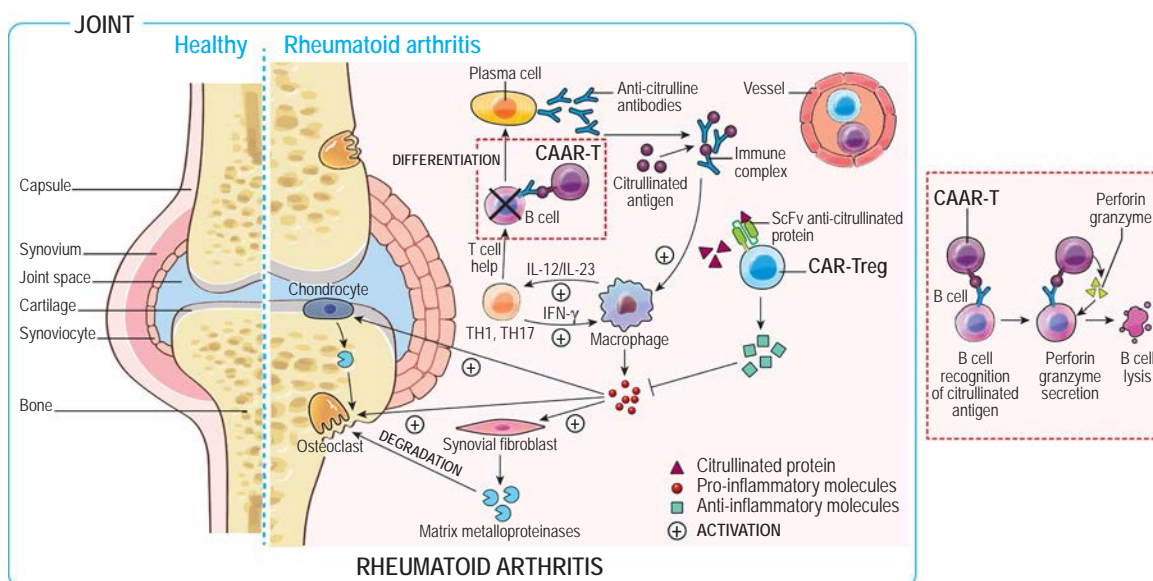
Figure 2. Direction of potential future research strategies for targeting pathologic cells in patients with rheumatoid arthritis (RA). Presentation of citrullinated neoepitopes to autoimmune B cells leads to autoantibody production, which could be broken with a CAAR-T cell bearing a citrullinated antigen. Use of CAR-Treg cells directed against citrullinated vimentin could reestablish tolerance in the joints of RA patients. The smaller diagram on the right depicts how CAAR-T cells deplete pathogenic B cells. IL-12 = interleukin-12; IFNγ = interferon-γ (see Figure 1 for other definitions).

Another original strategy to target pathogenic B cells has been proposed by Zhang and colleagues. Immunodominant antigens targeted by autoantibodies were identified and coupled to fluorescein isothiocyanate (FITC). Zhang's group then engineered FITC-labeled CAR-T cells that had the ability to recognize FITC-labeled immunodominant antigens fixed on autoreactive B cells in the blood of RA patients, leading to lysis of pathogenic B cells. In analyzing how FITC-labeled CAR-T cells produced lysis of autoreactive B cells, Zhang and colleagues observed that FITC-labeled CAR-T cells specifically killed B cells that recognized FITC-labeled citrullinated autoantigens in vitro, supporting the efficacy of this approach (61).

Induction of tolerance by specific CAR-Treg cells in the synovium of affected joints in patients with RA also seems to be a promising strategy (Figure 2). CV has been identified as a specific antigen that is found exclusively in the extracellular matrix of the inflamed synovial tissue of RA patients (62). Preliminary unpublished data have suggested that engineered CAR-Treg cells directed against CV may react with CV expressed in RA synovial fluid. Future studies are needed to investigate the effects of CV-expressing CAR-Treg cells in preclinical RA.

CAR-T cells in SLE. SLE is characterized by pathologic autoantibody production, leading to immune complex formation on the tissues, followed by complement activation and then tissue destruction (63). Treatments include low-dose glucocorticoids, antimalarial drugs, immunosuppressive drugs, and specific biologic agents targeting B cells (1). Belimumab, which targets the cytokine BAFF, is the single licensed biologic drug for SLE management (64,65). To avoid the side effects of current autoimmune rheumatic disease treatments, a strategy of repositioning CD19

CAR-T cells has been proposed by Kansal et al. They reported observations of a complete and sustained depletion of CD19+ B cells using CD19 CAR-T cells in 2 murine models of lupus, which resulted in increased mouse survival. This is likely related to the significant decrease in levels of anti-DNA IgG and IgM in the serum of treated mice. Moreover, Kansal and colleagues observed that in mice with lupus, at 7 months after they had received a single injection of CD19 CAR-T cells and then been re-injected, CD8+ T cells isolated from the mice still had the capacity to deplete CD19+ B cells, indicating the persistence and action of CD19 CAR-T cells (36). Another recent study showed that infusion of CD19 CAR-T cells in MRL-*lpr* mice before the onset of disease or after disease initiation improved lupus symptoms, prolonged the lifespan of the mice, and delayed the progression of lupus (66). These results are promising, and the translation to human clinical trials now needs to be addressed.

In patients with SLE, CD19 CAR-T cells are expected to deplete total B cells, leading to decreased production of antibodies. Based on recent studies performed in patients with PV, the refinement of B cell targeting by engineering CAAR-T cells may also be proposed. However, SLE displays a huge diversity of autoantibodies (~180), suggesting that there are numerous autoantigens that could be targeted (67). Double-stranded DNA and nuclear antigens have been well described as having a role in tissue injury. The design of CAAR-T cells directed against these antigens could be interesting and should be evaluated in lupus mouse models, as they may be potentially effective in depleting specific pathogenic B cells (Figure 3). Inducing tolerance in affected tissue by using Treg cells or CAR-Treg cells may also be a relevant strategy. Indeed, in a study by Dall'Era et al, autologous Treg cell infusion in an SLE patient with skin involvement increased the activation of Treg cells
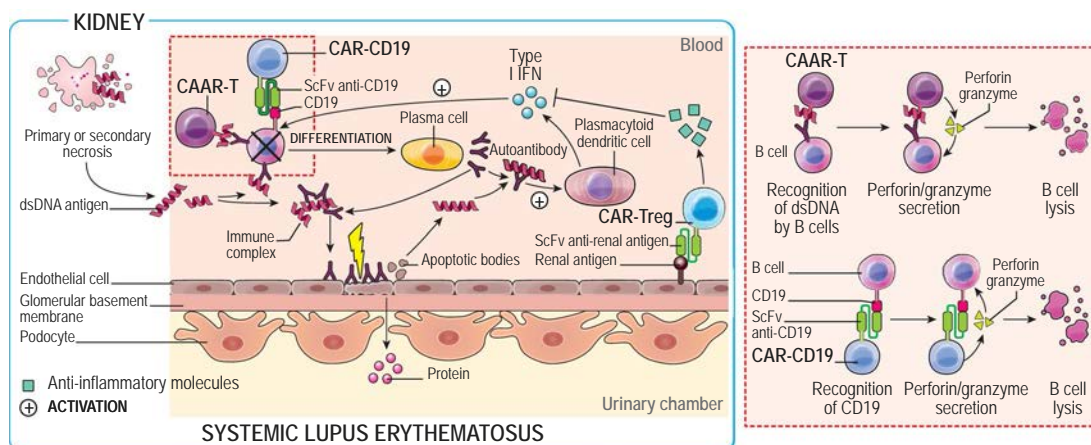
Figure 3. Direction of potential future research strategies for targeting pathologic cells in patients with systemic lupus erythematosus. A defect in clearance of apoptotic cells leads to liberation of double-stranded DNA (dsDNA), production of autoantibodies by B cells, and immune complex formation. CD19-expressing CAR-T cells may drive B cell depletion and stop immune complex formation. CAR-Treg cells specific for a renal antigen could secrete antiinflammatory molecules that limit B cell activation and differentiation. The smaller diagram on the right depicts how dsDNA-expressing CAAR-T cells and CD19-expressing CAR-T cells deplete pathogenic B cells and CD19-expressing B cells, respectively. IFN = interferon (see Figure 1 for other definitions). Color figure can be viewed in the online issue, which is available at http://onlinelibrary.wiley.com/doi/10.1002/art.41812/abstract.

in the inflamed skin and reduced the infiltration of IFNγ-expressing CD4+ Teff cells (68). A study by He et al showed that treatment with a low dose of IL-2 led to marked reductions in disease activity and increased numbers of Treg cells in the blood of patients with SLE (69). This result was confirmed by another group (44). Based on these studies, we hypothesize that targeting CAR-Treg cells to the skin or kidneys will induce tolerance and reduce inflammation in the affected tissues (Figure 3).

CAR-T cells in SSc. Significant progress in better controlling the vascular component of the disease has been achieved in patients with SSc. In addition, nintedanib (tyrosine kinase inhibitor) (approved by both the FDA and the European Medicines Agency) and tocilizumab (approved by the FDA) have recently been approved for the treatment of interstitial lung disease (ILD) associated with SSc (70). However, therapies with larger effects on SSc-ILD and other therapies with broader disease-modifying properties are eagerly awaited. CD19 CAR-T cells could be an interesting strategy, given the dysregulation of B cell homeostasis in SSc (71–74) and the positive signal observed with rituximab in skin fibrosis (75–77). However, the depletion of total B cells, including cells that produce protective antibodies, could lead to an increased risk of infections. To overcome this, we might consider a strategy targeting B cells that are responsible for the generation of

autoantibodies involved in the pathogenesis of SSc, such as anti-endothelial or anti-fibroblast antibodies, which contribute to the increased activation of these cells (78). Identification of antigens targeted by these pathogenic B cells could lead to the design of specific CAAR-T cells that would facilitate the deletion of these B cells (Figure 4).

Moreover, changes in the numbers of Treg cells and functional changes in the Treg cell population have been described in patients with SSc. Decreased Treg cell numbers have been observed in patients with SSc, except for those with early-phase or active disease (79). It would be interesting to design CAR-Treg cells that would be directed to specific skin and lung antigens, to investigate the induction of tolerance in the early and late phases of SSc. We hypothesize that early treatment with CAR-Treg cells may alleviate inflammation and promote physiologic tissue repair in affected tissue (as depicted in Figure 4). However, we could not speculate on the implication of late infusion of CAR-Treg cells as a strategy for resolution of fibrosis. Further investigations assessing the effect of tolerance induction at different stages of fibrosis will be needed. Interestingly, a recent study has shown that targeting fibroblast activation protein (FAP) with the use of CAR T cells induces a significant reduction in cardiac fibrosis and restoration of function after injury in mice, as a result of the deletion of FAP+ fibroblasts (80). It would be interesting to
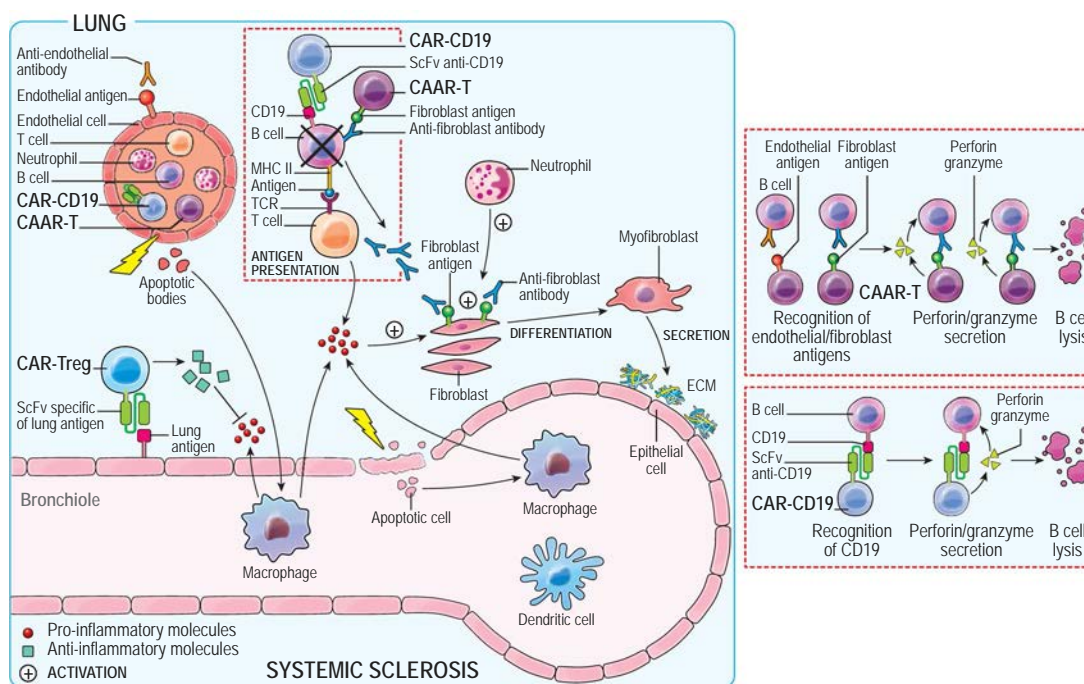
Figure 4. Direction of potential future research strategies for targeting pathologic cells in patients with systemic sclerosis. Phagocytosis of endothelial cell apoptotic bodies by macrophages leads to production of proinflammatory molecules, recruitment of immune cells, presentation of autoantigens, and, ultimately, production of anti-fibroblast or anti-endothelial antibodies. Depletion of pathogenic cells by CD19-expressing CAR-T cells and CAAR-T cells, specifically those targeting fibroblasts or endothelial antigens, could limit fibroblast activation and extracellular matrix (ECM) protein production. A CAR-Treg cell construct against a lung antigen could reestablish tolerance in the lung. Smaller diagrams on the right depict how endothelial/fibroblast-targeting CAAR-T cells and CD19-targeting CAR-T cells deplete pathogenic B cells and CD19-expressing B cells, respectively. MHC II = major histocompatibility complex class II; TCR = T cell receptor (see Figure 1 for other definitions). Color figure can be viewed in the online issue, which is available at http://onlinelibrary.wiley.com/doi/10.1002/art.41812/abstract.

find a specific myofibroblast protein that could be targeted by CAR-T cells.

Conclusions

The high potency of CAR-T cell therapies as a management strategy for B cell malignancies has been demonstrated in recent years. This has caught the attention of researchers in other fields, especially in the field of autoimmunity. Dsg-3–expressing CAAR-T cells in PV, CD19-expressing CAR-T cells in SLE, and MOG-expressing CAR-Treg cells in EAE have shown promising results, providing novel prospects for the treatment of autoimmune rheumatic diseases. Indeed, CD19 CAR-T cells have been evaluated in patients with myasthenia gravis (ClinicalTrials.gov identifier: NCT04146051), and BCMA CAR-T cells have been used in patients with relapsed/refractory antibody-associated idiopathic inflammatory diseases of the nervous system (ClinicalTrials.gov identifier: NCT04561557). Evaluation of the maximal tolerated dose of Dsg-3 CAAR-T cells in patients with PV is ongoing (ClinicalTrials.gov identifier: NCT04422912). A CAAR-T cell construct directed against antigens that are targeted by autoantibodies is a promising approach for achieving deletion of pathogenic B cells in RA, SLE, and SSc. Infusion of polyclonal Treg cells or low-dose IL-2 in patients with autoimmune diseases has shown that re-induction of tolerance is possible. Novel CAR-Treg cell designs will allow their targeting in appropriate tissues affected by autoimmune rheumatic diseases. For this reason, it is necessary to identify the specific antigens expressed by affected tissues in autoimmunity. The stability of CAR-Treg cells is also an important consideration, to avoid any reversal plasticity, which could exacerbate autoimmune responses.

There are some potential limitations to CAR-T cell therapy. The use of CAR-T cells can result in some severe side effects, including development of CRS. In addition, the cost associated with this type of therapy is a concern. For example, in the treatment of patients with diffuse large B cell lymphoma, use of CD19 CAR-T cells has a cost-effectiveness of $150,000/quality-adjusted life years, while use of rituximab has a cost-effectiveness of $61,984/life-year gained (81,82). Even though a large amount of research remains to be done, derived CAR T cell constructs could provide an effective therapeutic arsenal for the management of autoimmune rheumatic diseases for which "curative" treatments are currently lacking.

AUTHOR CONTRIBUTIONS

All authors were involved in drafting the article or revising it critically for important intellectual content, and all authors approved the final version to be published. Dr. Avouac had full access to all of the data in the study and takes responsibility for the integrity of the data and the accuracy of the data analysis.
Study conception and design. Bousso, Allanore, Avouac.
Acquisition of data. Orvain, Boulch, Avouac.
Analysis and interpretation of data. Orvain, Boulch, Bousso, Allanore, Avouac.

REFERENCES

1. Gatto M, Zen M, Iaccarino L, Doria A. New therapeutic strategies in systemic lupus erythematosus management [review]. Nat Rev Rheumatol 2019;15:30–48.

2. Smolen JS, Aletaha D, McInnes IB. Rheumatoid arthritis. Lancet 2016;388:2023–38.

3. Park JH, Rivière I, Gonen M, Wang X, Sénéchal B, Curran KJ, et al. Long-term follow-up of CD19 CAR therapy in acute lymphoblastic leukemia. N Engl J Med 2018;378:449–59.

4. Schuster SJ, Svoboda J, Chong EA, Nasta SD, Mato AR, Anak Ö, et al. Chimeric antigen receptor T cells in refractory B-cell lymphomas. N Engl J Med 2017;377:2545–54.

5. Gross G, Waks T, Eshhar Z. Expression of immunoglobulin-T-cell receptor chimeric molecules as functional receptors with antibody-type specificity. Proc Natl Acad Sci U S A 1989;86:10024–8.

6. Rafiq S, Hackett CS, Brentjens RJ. Engineering strategies to overcome the current roadblocks in CAR T cell therapy [review]. Nat Rev Clin Oncol 2020;17:147–67.

7. Hudecek M, Sommermeyer D, Kosasih PL, Silva-Benedict A, Liu L, Rader C, et al. The nonsignaling extracellular spacer domain of chimeric antigen receptors is decisive for *in vivo* antitumor activity. Cancer Immunol Res 2015;3:125–35.

8. Alabanza L, Pegues M, Geldres C, Shi V, Wiltzius JJ, Sievers SA, et al. Function of novel anti-CD19 chimeric antigen receptors with human variable regions is affected by hinge and transmembrane domains. Mol Ther 2017;25:2452–65.

9. Brocker T, Karjalainen K. Signals through T cell receptor-ζ chain alone are insufficient to prime resting T lymphocytes. J Exp Med 1995;181:1653–9.

10. Maher J, Brentjens RJ, Gunset G, Rivière I, Sadelain M. Human T-lymphocyte cytotoxicity and proliferation directed by a single chimeric TCRζ /CD28 receptor. Nat Biotechnol 2002;20:70–5.

11. Kawalekar OU, O'Connor RS, Fraietta JA, Guo L, McGettigan SE, Posey AD, et al. Distinct signaling of coreceptors regulates specific metabolism pathways and impacts memory development in CAR T cells. Immunity 2016;44:380–90.

12. Guedan S, Madar A, Casado-Medrano V, Shaw C, Wing A, Liu F, et al. Single residue in CD28-costimulated CAR-T cells limits long-term persistence and antitumor durability. J Clin Invest 2020;130:3087–97.

13. Song DG, Powell DJ. Pro-survival signaling via CD27 costimulation drives effective CAR T-cell therapy. OncoImmunology 2012;1:547–9.

14. Guedan S, Chen X, Madar A, Carpenito C, McGettigan SE, Frigault MJ, et al. ICOS-based chimeric antigen receptors program bipolar TH17/TH1 cells. Blood 2014;124:1070–80.

15. Hombach AA, Heiders J, Foppe M, Chmielewski M, Abken H. OX40 costimulation by a chimeric antigen receptor abrogates CD28 and IL-2 induced IL-10 secretion by redirected CD4+ T cells. OncoImmunology 2012;1:458–66.

16. Wang E, Wang LC, Tsai CY, Bhoj V, Gershenson Z, Moon E, et al. Generation of potent T-cell immunotherapy for cancer using DAP12-based, multichain, chimeric immunoreceptors. Cancer Immunol Res 2015;3:815–26.

17. Mata M, Gerken C, Nguyen P, Krenciute G, Spencer DM, Gottschalk S. Inducible activation of MyD88 and CD40 in CAR T cells results in controllable and potent antitumor activity in preclinical solid tumor models. Cancer Discov 2017;7:1306–19.

18. Tammana S, Huang X, Wong M, Milone MC, Ma L, Levine BL, et al. 4–1BB and CD28 signaling plays a synergistic role in redirecting

umbilical cord blood T cells against B-cell malignancies. Hum Gene Ther 2010;21:75–86.

19. Guedan S, Posey AD, Shaw C, Wing A, Da T, Patel PR, et al. Enhancing CAR T cell persistence through ICOS and 4–1BB costimulation. JCI Insight 2018;3:e96976.

20. Pegram HJ, Lee JC, Hayman EG, Imperato GH, Tedder TF, Sadelain M, et al. Tumor-targeted T cells modified to secrete IL-12 eradicate systemic tumors without need for prior conditioning. Blood 2012;119:4133–41.

21. Chinnasamy D, Yu Z, Kerkar SP, Zhang L, Morgan RA, Restifo NP, et al. Local delivery of interleukin-12 using T cells targeting VEGF receptor-2 eradicates multiple vascularized tumors in mice. Clin Cancer Res 2012;18:1672–83.

22. Chmielewski M, Kopecky C, Hombach AA, Abken H. IL-12 release by engineered T cells expressing chimeric antigen receptors can effectively muster an antigen-independent macrophage response on tumor cells that have shut down tumor antigen expression. Cancer Res 2011;71:5697–706.

23. Blanc V, Bousseau A, Caron A, Carrez C, Lutz RJ, Lambert JM. SAR3419: an anti-CD19-maytansinoid immunoconjugate for the treatment of B-cell malignancies. Clin Cancer Res 2011;17:6448–58.

24. Brentjens RJ, Latouche JB, Santos E, Marti F, Gong MC, Lyddane C, et al. Eradication of systemic B-cell tumors by genetically targeted human T lymphocytes co-stimulated by CD80 and interleukin-15. Nat Med 2003;9:279–86.

25. Sadelain M, Rivière I, Riddell S. Therapeutic T cell engineering. Nature 2017;545:423–31.

26. Hay KA, Hanafi LA, Li D, Gust J, Liles WC, Wurfel MM, et al. Kinetics and biomarkers of severe cytokine release syndrome after CD19 chimeric antigen receptor–modified T-cell therapy. Blood 2017;130:2295–306.

27. Larson RC, Maus MV. Recent advances and discoveries in the mechanisms and functions of CAR T cells [review]. Nat Rev Cancer 2021;21:145–61.

28. Mueller KT, Waldron E, Grupp SA, Levine JE, Laetsch TW, Pulsipher MA, et al. Clinical pharmacology of tisagenlecleucel in B-cell acute lymphoblastic leukemia. Clin Cancer Res 2018;24:6175–84.

29. Edwards JC, Szczepański L, Szechiński J, Filipowicz-Sosnowska A, Emery P, Close DR, et al. Efficacy of B-cell–targeted therapy with rituximab in patients with rheumatoid arthritis. N Engl J Med 2004;350:2572–81.

30. Guillevin L, Pagnoux C, Karras A, Khouatra C, Aumaître O, Cohen P, et al. Rituximab versus azathioprine for maintenance in ANCA-associated vasculitis. N Engl J Med 2014;371:1771–80.

31. Hauser SL, Waubant E, Arnold DL, Vollmer T, Antel J, Fox RJ, et al. B-cell depletion with rituximab in relapsing–remitting multiple sclerosis. N Engl J Med 2008;358:676–88.

32. Merrill JT, Neuwelt CM, Wallace DJ, Shanahan JC, Latinis KM, Oates JC, et al. Efficacy and safety of rituximab in moderately-to-severely active systemic lupus erythematosus: the randomized, double-blind, phase II/III systemic lupus erythematosus evaluation of rituximab trial. Arthritis Rheum 2010;62:222–33.

33. Crickx E, Weill JC, Reynaud CA, Mahévas M. Anti-CD20–mediated B-cell depletion in autoimmune diseases: successes, failures and future perspectives [review]. Kidney Int 2020;97:885–93.

34. Combier A, Nocturne G, Henry J, Belkhir R, Pavy S, Le Tiec C, et al. Immunization to rituximab is more frequent in systemic autoimmune diseases than in rheumatoid arthritis: ofatumumab as alternative therapy. Rheumatology (Oxford) 2020;59:1347–54.

35. Emery P, Fleischmann R, Filipowicz-Sosnowska A, Schechtman J, Szczepanski L, Kavanaugh A, et al. The efficacy and safety of rituximab in patients with active rheumatoid arthritis despite methotrexate treatment: results of a phase IIB randomized, double-blind, placebo-controlled, dose-ranging trial. Arthritis Rheum 2006;54:1390–400.

36. Kansal R, Richardson N, Neeli I, Khawaja S, Chamberlain D, Ghani M, et al. Sustained B cell depletion by CD19-targeted CAR T cells is a highly effective treatment for murine lupus. Sci Transl Med 2019;11:eaav1648.

37. Mueller KT, Maude SL, Porter DL, Frey N, Wood P, Han X, et al. Cellular kinetics of CTL019 in relapsed/refractory B-cell acute lymphoblastic leukemia and chronic lymphocytic leukemia. Blood 2017;130:2317–25.

38. Zhang L, Sosinowski T, Cox AR, Cepeda JR, Sekhar NS, Hartig SM, et al. Chimeric antigen receptor (CAR) T cells targeting a pathogenic MHC class II:peptide complex modulate the progression of autoimmune diabetes. J Autoimmun 2019;96:50–8.

39. Ma WT, Gao F, Gu K, Chen DK. The role of monocytes and macrophages in autoimmune diseases: a comprehensive review. Front Immunol 2019;10:1140.

40. Ellebrecht CT, Bhoj VG, Nace A, Choi EJ, Mao X, Cho MJ, et al. Reengineering chimeric antigen receptor T cells for targeted therapy of autoimmune disease. Science 2016;353:179–84.

41. Lee J, Lundgren DK, Mao X, Manfredo-Vieira S, Nunez-Cruz S, Williams EF, et al. Antigen-specific B cell depletion for precision therapy of mucosal pemphigus vulgaris. J Clin Invest 2020;130:6317–24.

42. Chatenoud L. Precision medicine for autoimmune disease. Nat Biotechnol 2016;34:930–2.

43. Klatzmann D, Abbas AK. The promise of low-dose interleukin-2 therapy for autoimmune and inflammatory diseuses [review]. Nat Rev Immunol 2015;15:283–94.

44. Rosenzwajg M, Lorenzon R, Cacoub P, Pham HP, Pitoiset F, El Soufi K, et al. Immunological and clinical effects of low-dose interleukin-2 across 11 autoimmune diseases in a single, open clinical trial. Ann Rheum Dis 2019;78:209–17.

45. Tahvildari M, Dana R. Low-dose IL-2 therapy in transplantation, autoimmunity, and inflammatory diseases. J Immunol 2019;203:2749–55.

46. Rana J, Biswas M. Regulatory T cell therapy: current and future design perspectives. Cell Immunol 2020;356:104193.

47. Elinav E, Waks T, Eshhar Z. Redirection of regulatory T cells with predetermined specificity for the treatment of experimental colitis in mice. Gastroenterology 2008;134:2014–24.

48. Onishi Y, Fehervari Z, Yamaguchi T, Sakaguchi S. Foxp3+ natural regulatory T cells preferentially form aggregates on dendritic cells in vitro and actively inhibit their maturation. Proc Natl Acad Sci U S A 2008;105:10113–8.

49. Mavin E, Nicholson L, Rafez Ahmed S, Gao F, Dickinson A, Wang X. Human regulatory T cells mediate transcriptional modulation of dendritic cell function. J Immunol 2017;198:138–46.

50. Alissafi T, Hatzioannou A, Ioannou M, Sparwasser T, Grün JR, Grützkau A, et al. De novo–induced self-antigen–specific Foxp3+ regulatory T cells impair the accumulation of inflammatory dendritic cells in draining lymph nodes. J Immunol 2015;194:5812–24.

51. Zhou X, Bailey-Bucktrout SL, Jeker LT, Penaranda C, Martínez-Llordella M, Ashby M, et al. Instability of the transcription factor Foxp3 leads to the generation of pathogenic memory T cells in vivo. Nat Immunol 2009;10:1000–7.

52. Fransson M, Piras E, Burman J, Nilsson B, Essand M, Lu B, et al. CAR/FoxP3-engineered T regulatory cells target the CNS and suppress EAE upon intranasal delivery. J Neuroinflammation 2012;9:576.

53. Blat D, Zigmond E, Alteber Z, Waks T, Eshhar Z. Suppression of murine colitis and its associated cancer by carcinoembryonic antigen-specific regulatory T cells. Mol Ther 2014;22:1018–28.

54. Bluestone JA, Buckner JH, Fitch M, Gitelman SE, Gupta S, Hellerstein MK, et al. Type 1 diabetes immunotherapy using polyclonal regulatory T cells. Sci Transl Med 2015;7:315ra189.

55. Tenspolde M, Zimmermann K, Weber LC, Hapke M, Lieber M, Dywicki J, et al. Regulatory T cells engineered with a novel insulin-specific chimeric antigen receptor as a candidate immunotherapy for type 1 diabetes. J Autoimmun 2019;103:102289.

56. Imura Y, Ando M, Kondo T, Ito M, Yoshimura A. CD19-targeted CAR regulatory T cells suppress B cell pathology without GvHD. JCI Insight 2020;5:e136185.

57. Vital EM, Rawstron AC, Dass S, Henshaw K, Madden J, Emery P, et al. Reduced-dose rituximab in rheumatoid arthritis: efficacy depends on degree of B cell depletion. Arthritis Rheum 2011;63:603–8.

58. Bhoj VG, Arhontoulis D, Wertheim G, Capobianchi J, Callahan CA, Ellebrecht CT, et al. Persistence of long-lived plasma cells and humoral immunity in individuals responding to CD19-directed CAR T-cell therapy. Blood 2016;128:360–70.

59. Harre U, Georgess D, Bang H, Bozec A, Axmann R, Ossipova E, et al. Induction of osteoclastogenesis and bone loss by human autoantibodies against citrullinated vimentin. J Clin Invest 2012;122:1791–802.

60. Tak PP, Rigby WF, Rubbert-Roth A, Peterfy CG, van Vollenhoven RF, Stohl W, et al. Inhibition of joint damage and improved clinical outcomes with rituximab plus methotrexate in early active rheumatoid arthritis: the IMAGE trial. Ann Rheum Dis 2011;70:39–46.

61. Zhang B, Wang Y, Yuan Y, Sun J, Liu L, Huang D, et al. In vitro elimination of autoreactive B cells from rheumatoid arthritis patients by universal chimeric antigen receptor T cells. Ann Rheum Dis 2021;80:176–84.

62. Van Steendam K, Tilleman K, De Ceuleneer M, De Keyser F, Elewaut D, Deforce D. Citrullinated vimentin as an important antigen in immune complexes from synovial fluid of rheumatoid arthritis patients with antibodies against citrullinated proteins. Arthritis Res Ther 2010;12:R132.

63. Tsokos GC. Systemic lupus erythematosus. N Engl J Med 2011;365:2110–21.

64. Furie R, Petri M, Zamani O, Cervera R, Wallace DJ, Tegzová D, et al. A phase III, randomized, placebo-controlled study of belimumab, a monoclonal antibody that inhibits B lymphocyte stimulator, in patients with systemic lupus erythematosus. Arthritis Rheum 2011;63:3918–30.

65. Navarra SV, Guzmán RM, Gallacher AE, Hall S, Levy RA, Jimenez RE, et al. Efficacy and safety of belimumab in patients with active systemic lupus erythematosus: a randomised, placebo-controlled, phase 3 trial. Lancet 2011;377:721–31.

66. Jin X, Xu Q, Pu C, Zhu K, Lu C, Jiang Y, et al. Therapeutic efficacy of anti-CD19 CAR-T cells in a mouse model of systemic lupus erythematosus. Cell Mol Immunol 2021;18:1869–903.

67. Yaniv G, Twig G, Shor DB, Furer A, Sherer Y, Mozes O, et al. A volcanic explosion of autoantibodies in systemic lupus erythematosus: a diversity of 180 different antibodies found in SLE patients [review]. Autoimmun Rev 2015;14:75–9.

68. Dall'Era M, Pauli ML, Remedios K, Taravati K, Sandova PM, Putnam AL, et al. Adoptive Treg cell therapy in a patient with systemic lupus erythematosus. Arthritis Rheumatol 2019;71:431–40.

69. He J, Zhang R, Shao M, Zhao X, Miao M, Chen J, et al. Efficacy and safety of low-dose IL-2 in the treatment of systemic lupus erythematosus: a randomised, double-blind, placebo-controlled trial. Ann Rheum Dis 2020;79:141–9.

70. Distler O, Highland KB, Gahlemann M, Azuma A, Fischer A, Mayes MD, et al. Nintedanib for systemic sclerosis–associated interstitial lung disease. N Engl J Med 2019;380:2518–28.

71. Soto L, Ferrier A, Aravena O, Fonseca E, Berendsen J, Biere A, et al. Systemic sclerosis patients present alterations in the expression of molecules involved in B-cell regulation. Front Immunol 2015;6:496.

72. Asano N, Fujimoto M, Yazawa N, Shirasawa S, Hasegawa M, Okochi H, et al. B lymphocyte signaling established by the CD19/CD22 loop regulates autoimmunity in the tight-skin mouse. Am J Pathol 2004;165:641–50.

73. Bosello S, Angelucci C, Lama G, Alivernini S, Proietti G, Tolusso B, et al. Characterization of inflammatory cell infiltrate of scleroderma skin: B cells and skin score progression. Arthritis Res Ther 2018;20:75.

74. Lafyatis R, O'Hara C, Feghali-Bostwick CA, Matteson E. B cell infiltration in systemic sclerosis–associated interstitial lung disease. Arthritis Rheum 2007;56:3167–8.

75. Elhai M, Boubaya M, Distler O, Smith V, Matucci-Cerinic M, Alegre Sancho JJ, et al. Outcomes of patients with systemic sclerosis treated with rituximab in contemporary practice: a prospective cohort study. Ann Rheum Dis 2019;78:979–87.

76. Thiebaut M, Launay D, Rivière S, Mahévas T, Bellakhal S, Hachulla E, et al. Efficacy and safety of rituximab in systemic sclerosis: French retrospective study and literature review. Autoimmun Rev 2018;17:582–7.

77. Daoussis D, Melissaropoulos K, Sakellaropoulos G, Antonopoulos I, Markatseli TE, Simopoulou T, et al. A multicenter, open-label, comparative study of B-cell depletion therapy with rituximab for systemic sclerosis-associated interstitial lung disease. Semin Arthritis Rheum 2017;46:625–31.

78. Choi MY, Fritzler MJ. Progress in understanding the diagnostic and pathogenic role of autoantibodies associated with systemic sclerosis. Curr Opin Rheumatol 2016;28:586–94.

79. Frantz C, Auffray C, Avouac J, Allanore Y. Regulatory T cells in systemic sclerosis [review]. Front Immunol 2018;9:2356.

80. Aghajanian H, Kimura T, Rurik JG, Hancock AS, Leibowitz MS, Li L, et al. Targeting cardiac fibrosis with engineered T cells [letter]. Nature 2019;573:430–3.

81. Lin JK, Muffly LS, Spinner MA, Barnes JI, Owens DK, Goldhaber-Fiebert JD. Cost effectiveness of chimeric antigen receptor T-cell therapy in multiply relapsed or refractory adult large B-cell lymphoma. J Clin Oncol 2019;37:2105–19.

82. Khor S, Beca J, Krahn M, Hodgson D, Lee L, Crump M, et al. Real world costs and cost-effectiveness of rituximab for diffuse large B-cell lymphoma patients: a population-based analysis. BMC Cancer 2014;14:586.

AMERICAN COLLEGE
of RHEUMATOLOGY
Empowering Rheumatology Professionals

Definition and Validation of the American College of Rheumatology 2021 Juvenile Arthritis Disease Activity Score Cutoffs for Disease Activity States in Juvenile Idiopathic Arthritis

Chiara Trincianti,[1] Evert Hendrik Pieter Van Dijkhuizen,[2] Alessandra Alongi,[3] Marta Mazzoni,[3] Joost F. Swart,[4] Irina Nikishina,[5] Pekka Lahdenne,[6] Lidia Rutkowska-Sak,[7] Tadej Avcin,[8] Pierre Quartier,[9] Violeta Panaviene,[10] Yosef Uziel,[11] Chris Pruunsild,[12] Veronika Vargova,[13] Soamarat Vilaiyuk,[14] Pavla Dolezalova,[15] Sarah Ringold,[16] Marco Garrone,[3] Nicolino Ruperto,[3] Angelo Ravelli,[17] and Alessandro Consolaro,[18] for the Paediatric Rheumatology International Trials Organisation

> *This work has been approved by the American College of Rheumatology (ACR) Board of Directors. This signifies that it has been quantitatively validated using patient data, and it has undergone validation based on an independent data set. All ACR-approved criteria sets are expected to undergo intermittent updates. The ACR is an independent, professional, medical and scientific society that does not guarantee, warrant, or endorse any commercial product or service.*

Objective. To develop and validate new Juvenile Arthritis Disease Activity Score 10 (JADAS10) and clinical JADAS10 (cJADAS10) cutoffs to separate the states of inactive disease (ID), minimal disease activity (MiDA), moderate disease activity (MoDA), and high disease activity (HDA) in children with oligoarthritis and with rheumatoid factor–negative polyarthritis, based on subjective disease assessment by the treating pediatric rheumatologist.

[1]Chiara Trincianti, MD: Università degli Studi di Genova, Genoa, Italy; [2]Evert Hendrik Pieter Van Dijkhuizen, MD, PhD: Wilhelmina Children's Hospital, Utrecht, The Netherlands, and Istituto Giannina Gaslini, IRCCS and Clinica Pediatrica e Reumatologia, Genoa, Italy; [3]Alessandra Alongi, MD, PhD, Marta Mazzoni, MD, Marco Garrone, MA, Nicolino Ruperto, MD, MPH: Istituto Giannina Gaslini, IRCCS and Clinica Pediatrica e Reumatologia, Genoa, Italy; [4]Joost F. Swart, MD, PhD: Wilhelmina Children's Hospital, Utrecht, The Netherlands; [5]Irina Nikishina, MD, PhD: V. A. Nasonova Research Institute of Rheumatology, Moscow, Russia; [6]Pekka Lahdenne, MD, PhD: New Children's Hospital and Helsinki University Hospital, Helsinki, Finland; [7]Lidia Rutkowska-Sak, MD, PhD: National Institute of Geriatrics, Rheumatology, and Rehabilitation, Warsaw, Poland; [8]Tadej Avcin, MD, PhD: University Children's Hospital and University Medical Centre Ljubljana, Ljubljana, Slovenia; [9]Pierre Quartier, MD: Université Paris-Descartes, Institut IMAGINE, Centre de Référence National pour les Rhumatismes Inflammatoires et les Maladies Auto-Immunes Systémiques Rares de l'Enfant (RAISE), Hôpital Necker-Enfants Malades, AP-HP, Paris, France; [10]Violeta Panaviene, MD, PhD: Children's Hospital, Affiliate of Vilnius University Hospital Santaros Clinic and Clinic of Children's Diseases, Vilnius University, Vilnius, Lithuania; [11]Yosef Uziel, MD: Meir Medical Centre and Kfar Saba and Sackler School of Medicine, Tel Aviv University, Tel Aviv, Israel; [12]Chris Pruunsild, MD, PhD: Tartu University Hospital Children's Clinic, and University of Tartu Institute of Clinical Medicine, Tartu, Estonia; [13]Veronika Vargova, MD, PhD: Pavol Jozef Šafárik University in Košice, Kosice, Slovakia; [14]Soamarat Vilaiyuk, MD: Ramathibodi Hospital and Mahidol University, Bangkok, Thailand; [15]Pavla Dolezalova, MD, PhD: Charles University in Prague and General University Hospital, Prague, Czech Republic; [16]Sarah Ringold, MD, MS: Seattle Children's Hospital, Seattle, Washington; [17]Angelo Ravelli, MD: Università degli Studi di Genova, Istituto Giannina Gaslini, IRCCS and Clinica Pediatrica e Reumatologia, Genoa, Italy, and Sechenov First Moscow State Medical University, Moscow, Russia; [18]Alessandro Consolaro, MD, PhD: Università degli Studi di Genova, Istituto Giannina Gaslini, IRCCS, and Clinica Pedietrica e Reumatologia, Genoa, Italy.

Methods. The cutoffs definition cohort was composed of 1,936 patients included in the multinational Epidemiology, Treatment and Outcome of Childhood Arthritis (EPOCA) study. Using the subjective physician rating as an external criterion, 4 methods were applied to identify the cutoffs: mapping, Youden index, 90% specificity, and maximum agreement. The validation cohort included 4,014 EPOCA patients, patients from 2 randomized trials, and 88 patients from the PharmaChild registry. Cutoff validation was conducted by assessing discriminative and predictive ability.

Results. The JADAS10 cutoffs were 1.4, 4, and 13, respectively, for oligoarthritis and 2.7, 6, and 17, respectively, for polyarthritis. The cJADAS10 cutoffs were 1.1, 4, and 12, respectively, for oligoarthritis and 2.5, 5, and 16, respectively, for polyarthritis. The cutoffs discriminated strongly among different levels of pain and morning stiffness, between patients who were and those who were not prescribed a new medication, and between different levels of improvement in clinical trials. Achievement of ID and MiDA according to the new JADAS cutoffs at least twice in the first year of disease predicted better outcome at 2 years.

Conclusion. The 2021 JADAS and cJADAS cutoffs revealed good metrologic properties in both definition and validation samples, and are therefore suitable for use in clinical trials and routine practice.

INTRODUCTION

Juvenile idiopathic arthritis (JIA) is a chronic inflammatory disease with a widely variable clinical course and outcome (1). Persistently active disease and uncontrolled synovial inflammation may cause structural joint damage (2), which may in turn lead to serious impairment of physical function and have marked impact on the quality of life of children and their families (3,4). Thus, regular assessment of the level of disease activity in children with JIA is fundamental to monitor the course of the disease over time and the effectiveness of therapeutic interventions. A precise measurement of disease activity may also have prognostic implications. For instance, achievement of the state of inactive disease (ID) at least once in the first 5 years was found to be associated with lower levels of long-term damage and functional impairment (5). Furthermore, the time spent in the state of active disease in the first 2 years was the most significant factor associated with the duration of active disease over the following years (6).

In the last decade, the use of composite disease activity scores in JIA has gained increasing popularity. These tools enable an easy and pragmatic approach to the quantification of disease activity by providing a summary number on a continuous scale, which is calculated by calculating the simple arithmetic sum of the scores of their individual components. The first composite disease activity score for JIA was developed in 2009 and was named the Juvenile Arthritis Disease Activity Score (JADAS) (7). The JADAS includes the following 4 measures: physician global assessment of disease activity measured on a 0–10 visual analog scale (VAS), parent/patient global assessment of child well-being measured on a 0–10 VAS, count of joints with active disease among the total assessed (10, 27, or 71 joints depending on the version), and the erythrocyte sedimentation rate (ESR) or C-reactive protein (CRP) level (8), both normalized to a 0–10 scale. A simplified, 3-item version of the score called the clinical JADAS (cJADAS), which excludes the acute-phase reactants, was subsequently published (9). Among the different versions of the score, the JADAS10 and the cJADAS10 have been more widely adopted as they are simpler than and equally effective as the other versions.

Proper interpretation of the scores obtained with JADAS calculation requires the definition of criteria for identifying high and low levels of disease activity (10). Cutoff values to separate the states of ID, minimal disease activity (MiDA), moderate disease activity (MoDA), and high disease activity (HDA) were established for both the JADAS (11,12) and the cJADAS (13). These cutoffs were defined with reference to published criteria for clinically inactive disease (CID) (14) and MiDA (15). At the time of previous cutoff definition, these criteria were considered as the only available external reference. However, use of these criteria has some limitations. The published criteria for CID include 3 of the 4 items in the JADAS, all of which must be scored zero. Thus, the variability of the JADAS in a patient who meets the criteria for CID can only be due to the fourth component, i.e., the parent/patient global assessment of the child's well-being. Similar concerns could be raised with regard to the definition of MiDA and the related JADAS cutoffs. Previous cutoffs for HDA were based on the treatment choices made by the treating physician. Potential limitations of the latter approach are that therapeutic choices may be driven by factors other than disease activity and that therapeutic decisions may vary across pediatric rheumatologists practicing in diverse geographic settings or with different clinical experience.

In a recently completed project (16), a large multinational cohort of JIA patients was enrolled and data collected on the treating physician's subjective rating of disease activity. In the present study, we took advantage of this large data set to develop and test new JADAS10 and cJADAS10 cutoffs for oligoarthritis and rheumatoid factor (RF)–negative polyarthritis disease activity states based on the subjective perception of international pediatric rheumatologists.

PATIENTS AND METHODS

Patient population used for the development of JADAS cutoffs. The cutoff definition cohort was selected from among the consecutive JIA patients included in the multinational Epidemiology, Treatment and Outcome of Childhood Arthritis (EPOCA) study (16), whose aims were to investigate the prevalence of JIA categories in different geographic areas, to gain

information on the treatments prescribed by international pediatric rheumatologists, and to assess the disease and health status of children with JIA living in diverse parts of the world. The EPOCA study included 9,081 patients enrolled in 49 countries between April 4, 2011 and November 21, 2016. For the purpose of the study, each JIA patient underwent a cross-sectional visit, during which the treating physician was asked to subjectively rate the disease status as ID, MiDA, MoDA, or HDA.

The oligoarthritis cutoff definition cohort consisted of the patients enrolled at the 20 centers that provided the largest sample of patients with persistent oligoarthritis. The number of oligoarthritis patients in each center ranged from 35 to 65. The polyarthritis cutoff definition cohort consisted of the patients enrolled at the 20 centers that provided the largest sample of patients with extended oligoarthritis and RF-negative polyarthritis. The number of polyarthritis patients in each center ranged from 35 to 65.

Patient populations used for the validation of JADAS cutoffs. Patients in the EPOCA study who had oligoarthritis or polyarthritis according to the International League of Associations for Rheumatology categorization (17) (subclassified as above) and who were not part of the cutoff definition cohort were included in the cutoff validation cohort. In addition, we obtained longitudinal data from 2 randomized clinical trials. The first (the TRIMECA trial [Comparison of the Efficacy of Intraarticular Corticosteroid Therapy Administered Alone or in Combination with Methotrexate in Children with JIA]) was a multicenter randomized clinical trial conducted in Italy between July 7, 2009 and March 31, 2013, which compared intraarticular glucocorticoid injections alone versus intraarticular glucocorticoid injections plus methotrexate in the treatment of oligoarticular JIA in a study population of 207 patients (18). The second was a randomized controlled trial conducted between February 2004 and June 2006, which assessed the efficacy and safety of abatacept withdrawal versus continuation in 190 patients with JIA (19). In the latter data set, only patients with extended oligoarticular arthritis and RF-negative polyarthritis were considered for cutoff validation.

To assess predictive ability, a fourth sample of patients was obtained from PharmaChild (20), a multinational registry to assess the long-term safety and efficacy of medications in children with JIA. We included all patients who had undergone at least 4 prospective visits in the first year of observation and a complete clinical assessment at 2 years after enrollment.

Methods used to calculate the cutoffs. The methodology for the definition of rheumatoid arthritis disease activity states based on the Clinical Disease Activity Index (CDAI) and the Simplified Disease Activity Index (SDAI) (10) was adapted for the present study. The following 4 methods were used to identify cutoffs in the JADAS10 and cJADAS10 to distinguish the states of ID, MiDA, MoDA, and HDA in oligoarthritis and RF-negative polyarthritis: mapping, Youden index, 90% specificity, and agreement.

The median of the values obtained with the 4 methods was retained as the cutoff for each disease activity state. For these analyses, we used the OptimalCutpoints package for R statistics, version 3.3.3 (21). This application computes optimal cut points for diagnostic tests or continuous markers and allows for selection of different approaches.

Mapping. For definition of the cutoff separating the states of ID and MiDA, the 75th percentile values of the JADAS10 and cJADAS10 in patients judged by their treating physician as having ID were retained. For definition of the cutoff separating the states of MiDA and MoDA, the 75th percentile values of the JADAS10 and cJADAS10 in patients judged as having ID or MiDA were retained. For definition of the cutoff separating the states of MoDA and HDA, the 25th percentile values of the JADAS10 and cJADAS10 in patients judged by their treating physician as having HDA were retained. Since for this analysis we considered it important to assign the same weight to each center regardless of the number of patients studied at the center, the cutoff values were retained separately for each center. The 20 values obtained for each cutoff were then averaged.

Youden index. The Youden index (J) identifies the maximum potential effectiveness of a biomarker through receiver operating characteristic (ROC) curve analysis. It is calculated with the formula $J = max_c = (Se_c + Sp_c - 1)$, where max_c is the maximally effective cutoff, Se_c is the cutoff with the maximum sensitivity, and Sp_c is the cutoff with the maximum specificity. The cutoff that achieves this threshold is considered the best cutoff because it is the one that optimizes the discriminative ability of the evaluated parameter when sensitivity and specificity are weighted equally (22,23). For each of the 3 cutoffs, patients were divided into 2 mutually exclusive groups, coded as 0 or 1. For the cutoff separating ID from MiDA, the first group comprised patients judged as having ID by the attending physician and the second comprised patients judged as having MiDA, MoDA, or HDA; for the cutoff separating MiDA from MoDA, the first group comprised patients judged as having ID or MiDA and the second comprised patients judged as having MoDA or HDA; for the cutoff separating MoDA from HDA, the first group comprised patients judged as having ID, MiDA, or MoDA and the second comprised patients judged as having HDA.

Ninety percent fixed specificity. With the 90% fixed specificity method, the 3 values identifying the states of ID, MiDA, MoDA, and HDA were obtained by fixing the specificity at 90% in the ROC curve analysis and considering the attending physician rating as the gold standard. This approach was chosen to minimize the rate of misclassification of patients with moderate/high disease activity as having inactive disease (24,25).

Evaluation of agreement. The analysis of agreement was based on the kappa statistic, which assesses the agreement beyond chance between 2 dichotomous ratings, using OptimalCutpoints for R statistics. The first rating was obtained using all

Table 1. JADAS10 and cJADAS10 cutoff values for classification of disease activity in children with juvenile idiopathic arthritis (oligoarthritis or polyarthritis) according to 4 different methods for determining optimal cutoffs*

Diagnosis, disease state distinction, JADAS version	Method for optimal cutoff determination					Sensitivity of chosen cutoff value	Specificity of chosen cutoff value	AUC
	75th percentile†	Youden index‡	90% specificity§	Kappa¶	Median#			
Oligoarthritis								
ID to MiDA								
JADAS10	1.5	1.2	1.9	1.2	1.4	76.1	93.6	0.919
cJADAS10	1.2	1.0	1.5	1.0	1.1	79.5	92.9	0.922
MiDA to MoDA								
JADAS10	3.9	4.0	4.2	9.2	4.0	77.4	90.7	0.923
cJADAS10	3.4	4.0	3.5	6.5	4.0	80.5	87.0	0.924
MoDA to HDA								
JADAS10	14.4	12.5	10.5	18.0	13.0	83.3	95.9	0.974
cJADAS10	14.3	10.0	9.5	15.0	12.0	76.2	95.0	0.971
Polyarthritis								
ID to MiDA								
JADAS10	2.6	2.7	2.3	3.0	2.7	79.1	90.2	0.925
cJADAS10	2.5	2.5	2.0	3.0	2.5	81.0	89.0	0.924
MiDA to MoDA								
JADAS10	5.1	5.9	5.9	9.9	6.0	79.8	88.6	0.927
cJADAS10	5.0	5.0	5.0	7.5	5.0	76.0	92.2	0.924
MoDA to HDA								
JADAS10	18.9	11.0	12.5	21.0	17.0	82.6	93.3	0.961
cJADAS10	19.0	10.5	12.5	19.0	16.0	81.5	93.9	0.960

* JADAS10 = Juvenile Arthritis Disease Activity Score 10; cJADAS10 = clinical JADAS10; AUC = area under the receiver operating characteristic curve; ID = inactive disease; MiDA = minimal disease activity; MoDA = moderate disease activity; HDA = high disease activity.
† Cutoff according to the 75th percentile of the cumulative score distribution.
‡ Cutoff, according to the Youden index (22,23), that best distinguishes between patients divided into 2 mutually exclusive groups coded as 0 or 1.
§ Cutoff according to fixed 90% specificity.
¶ Cutoff with best agreement according to kappa analysis.
# Median value among tentative cutoffs and chosen cutoff value.

possible JADAS10 and cJADAS10 values as hypothetical test criteria. To obtain the second rating, the categorical ratings from each attending physician (ID, MiDA, MoDA, or HDA) were dichotomized and were coded as 0 or 1, using the same approach as in the Youden index analysis. The software calculates the cutoff value with the highest kappa statistic.

Analyses performed to validate the cutoffs. Cutoff validation was based on assessment of discriminative and predictive ability. We tested whether the disease activity states according to the new cutoffs could discriminate 1) between patients in a cross-sectional sample with differing levels of various health outcomes, and 2) among different levels of response to a new treatment in 2 randomized clinical trials. Then, we tested the ability of JADAS10 and cJADAS10 states in the first year to predict clinically inactive disease at 2 years.

Ability to discriminate between different health states. In the EPOCA study, the median and interquartile range (IQR) level of pain on a 0–10-cm VAS (0 = no pain; 10 = maximum possible pain), the median and IQR count of joints with restricted function, the median level of physical function measured with the Juvenile Arthritis Functional Ability Scale (26) (range 0–45, where 0 is normal physical function), the percentage of parents who reported being not satisfied with current disease outcome, the percentage of patients with morning stiffness lasting >15 minutes, and the percentage of patients who were prescribed a new therapy for JIA at the study visit were compared across disease activity states defined by JADAS10 and cJADAS10 cutoffs. It was predicted that the values of all the above parameters would increase progressively from ID to HDA, although the changes in physical function and count of joints with restricted function were expected to be less pronounced as these indicators are affected by both disease activity and damage. Quantitative measures were compared by Kruskal-Wallis test with Dunn's post hoc test. Percentages were compared by chi-square test, with Bonferroni correction used for post hoc analysis.

Ability to discriminate among different levels of improvement. Patients at the 4-month visit in the open-label portion of the abatacept trial and at the 3-month visit in the TRIMECA trial were divided, according to the level of the American College of Rheumatology (ACR) Pediatric (Pedi) response (27), into 6 mutually exclusive groups: nonresponders, and ACR Pedi 30, 50, 70, 90, and 100 responders. For each level of response, we calculated the proportion of patients with ID, MiDA, MoDA, and HDA according to the new JADAS cutoffs. We expected that the proportion of patients with ID, MiDA, and MoDA would increase and that the proportion of patients with HDA would decrease when a higher level of improvement was met (moving from nonresponders to ACR Pedi 100 responders). We also expected that in both trials a higher proportion of patients would have had JADAS10 and cJADAS10 scores above the cutoffs for HDA cutoffs at the baseline visit.

Ability to predict future disease outcome. Among subjects in the PharmaChild registry, we compared the median and IQR number of visits with JADAS10 and cJADAS10 scores below the cutoffs for ID and MiDA and above the cutoffs for HDA in the first year of observation between patients who were and those who were not categorized as having CID according to the 2011 ACR JIA criteria (14) at 2 years. We also compared, using the same end point, the percentage of patients who had and those who did not have 2 or more visits with ID, MiDA, or HDA in the first year of observation. We expected that patients whose disease was clinically inactive at 2 years according to the ACR JIA criteria would have a higher number of visits with ID or MiDA and a lower number of visits with HDA in the first year. The inclusion of the state of MoDA was not considered meaningful for this analysis, because it was not expected that the number of visits in this intermediate state could predict the disease outcome.

Comparison with 2012–2014 cutoffs. The analyses described above were repeated using cutoffs published in 2012–2014 (11–13), and the statistical performance of the older versus the newer set of criteria was compared for each analysis (see below). The complete results of comparative validation of 2012–2014 cutoffs are presented in the Supplementary Appendix,

Table 2. Disease activity states based on the JADAS10 and cJADAS10, according to 2021 cutoffs and 2012–2014 cutoffs*

Disease activity state	2021 cutoffs		2012–2014 cutoffs	
	JADAS10	cJADAS10	JADAS10	cJADAS10
Oligoarthritis				
Inactive disease	≤1.4	≤1.1	≤1	≤1
Minimal disease activity	1.5–4	1.2–4	1.1–2	1.1–1.5
Moderate disease activity	4.1–13	4.1–12	2.1–4.2	1.51–4
High disease activity	>13	>12	>4.2	>4
Polyarthritis				
Inactive disease	≤2.7	≤2.5	≤1	≤1
Minimal disease activity	2.8–6	2.6–5	1.1–3.8	1.1–2.5
Moderate disease activity	6.1–17	5.1–16	3.9–10.5	2.51–8.5
High disease activity	>17	>16	>10.5	>8.5

* JADAS10 = Juvenile Arthritis Disease Activity Score 10; cJADAS10 = clinical JADAS10.

available on the *Arthritis & Rheumatology* website at http://onlin elibrary.wiley.com/doi/10.1002/art.41879/abstract.

RESULTS

Definition of cutoffs. The cutoff selection cohort comprised 979 patients with oligoarthritis and 957 patients with polyarthritis. Demographic and clinical features of the patients are shown in Supplementary Table 1, on the *Arthritis & Rheumatology* website at http://onlinelibrary.wiley.com/doi/10.1002/art.41879/abstract.

The JADAS10 and cJADAS10 cutoffs obtained with the 4 different statistical approaches and the final 3 cutoffs, calculated as the median of the 4 values to define the 4 disease states (ID, MiDA, MoDA, and HDA) in oligoarthritis and polyarthritis, are shown in Table 1. Table 2 presents the comparison of the current proposed cutoffs (2021 cutoffs) with cutoffs published in 2012–2014 (11–13). All of the 2021 cutoffs were higher than the 2012–2014 cutoffs.

Validation of cutoffs. *Ability to discriminate between different health states.* A total of 1,859 and 2,155 patients with oligoarthritis and polyarthritis, respectively, from the EPOCA study were included in this analysis; demographic and clinical features are shown in Supplementary Table 1. The level of pain increased progressively from ID through HDA in both patient groups, based on either JADAS10 or cJADAS10 cutoffs (Figure 1). Likewise, the count of joints with restricted function and the physical function score worsened progressively throughout the same states ($P < 0.001$). However, Dunn's post hoc test revealed that among patients with oligoarthritis, only pain and physical function were different between all 4 disease activity states ($P < 0.001$ for all comparisons), whereas the count of joints with restricted function did not differ between patients with ID and patients with MiDA ($P = 0.18$ for JADAS10, $P = 0.14$ for cJADAS10). The proportion of parents not satisfied with illness outcome and the proportions of patients with morning stiffness and with newly prescribed medications at the time of the visit increased progressively from ID through HDA (Figure 2).

In the same data sets, using 2012–2014 cutoffs for oligoarthritis, the level of pain and functional ability and the count of joints with restricted function were not significantly different between patients with MiDA and patients with MoDA, for both the JADAS10 and the cJADAS10 (Figure 1 in the Supplementary Appendix, on the *Arthritis & Rheumatology* website at http://onlinelibrary.wiley.com/doi/10.1002/art.41879/abstract). Using the 2021 cutoffs, all comparisons in post hoc analyses of polyarthritis were significant.
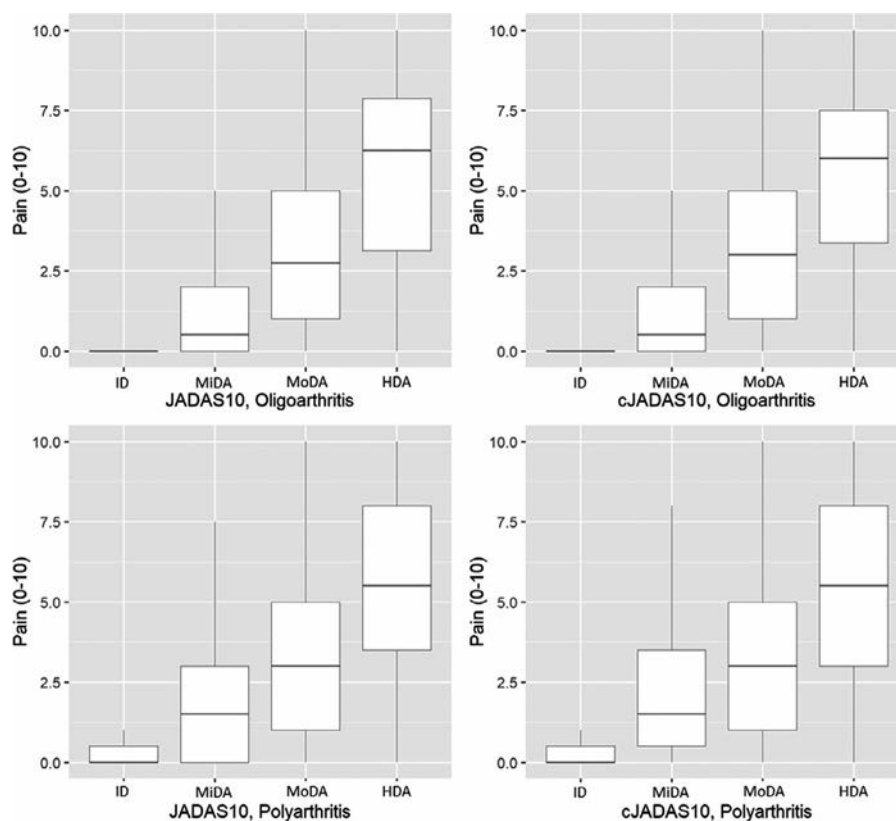
Figure 1. Comparison of the level of pain, measured on a 21-point 0–10 Likert scale, at visits (n = 1,908 for oligoarthritis and 2,489 for polyarthritis) in the Epidemiology, Treatment and Outcome of Childhood Arthritis study among patients with Juvenile Arthritis Disease Activity Score 10 (JADAS10)– and clinical JADAS10 (cJADAS10)–based inactive disease (ID), those with minimal disease activity (MiDA), those with moderate disease activity (MoDA), and those with high disease activity (HDA). Data are presented as box plots, where the boxes represent the 25th to 75th percentiles, the lines within the boxes represent the median, and the lines outside the boxes represent the range. $P < 0.001$ for comparison of disease states.

JADAS10 - Oligoarthritis

JADAS10 - Polyarthritis

cJADAS10 - Oligoarthritis

cJADAS10 - Polyarthritis
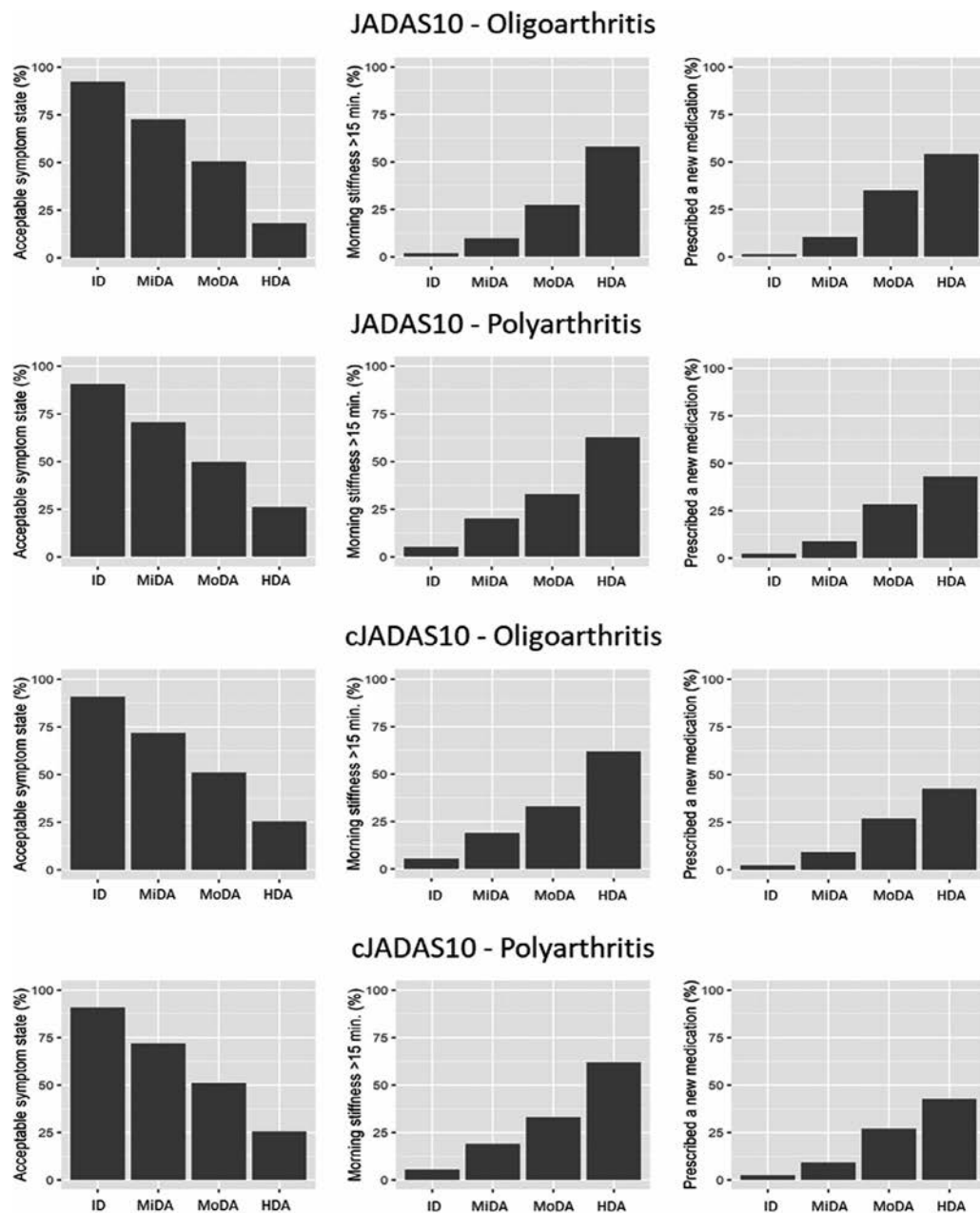
Figure 2. Percentage of patients whose parents described the patient's symptom status as acceptable, who had morning stiffness of >15 minutes, and who were prescribed a new medication for juvenile idiopathic arthritis at visits (n = 1,908 for oligoarthritis and 2,489 for polyarthritis) in the Epidemiology, Treatment and Outcome of Childhood Arthritis study among patients with Juvenile Arthritis Disease Activity Score 10 (JADAS10)– and clinical JADAS10 (cJADAS10)–based inactive disease (ID), those with minimal disease activity (MiDA), those with moderate disease activity (MoDA), and those with high disease activity (HDA). In post hoc analyses with Bonferroni correction, all comparisons were significant at $P < 0.001$ with the following exceptions: $P = 0.04$ for the comparison of morning stiffness frequency in oligoarthritis patients between the cJADAS10 states of MiDA and MoDA, and $P = 0.37$ for the comparison of the frequency of new therapy prescription in oligoarthritis patients between the cJADAS10 states of MiDA and MoDA.

In oligoarthritis and polyarthritis, the frequency of new medication prescription was not different between patients with ID and patients with MiDA according to 2012–2014 cutoffs for JADAS10 and cJADAS10. Additionally, in oligoarthritis, the frequency of morning stiffness was not different between patients with MiDA and patients with MoDA according to 2012–2014 cutoffs for JADAS10 and cJADAS10 (Figure 2 in the Supplementary Appendix).

Ability to discriminate among different levels of improvement. The analysis included 148 oligoarthritis patients enrolled in the TRIMECA trial and 99 polyarthritis patients included in the abatacept trial. In the TRIMECA trial, all patients who exhibited an ACR Pedi 30 response at 3 months met the JADAS10 cutoffs for MoDA, whereas none met the cutoffs for ID and MiDA; of the 51 patients who exhibited an ACR Pedi 100 response,

Table 3. JIA patients with JADAS10 and cJADAS10 below the cutoff for inactive disease, with JADAS10 and cJADAS10 below the cutoff for minimal disease activity, and with JADAS10 and cJADAS10 above the cutoff for high disease activity in at least 2 visits in the first year of PharmaChild registry participation, among those with and those without clinically inactive disease according to ACR criteria at 2 years*

Visits in the first year†	Active disease at 2 years (n = 44)	Clinically inactive disease at 2 years (n = 44)	P
≥2 with ID by JADAS10	12 (27.3)	37 (84.1)	<0.001
≥2 with ID by cJADAS10	13 (29.5)	38 (86.4)	<0.001
≥2 with MiDA by JADAS10‡	27 (61.4)	42 (95.5)	<0.001
≥2 with MiDA by cJADAS10‡	26 (59.1)	42 (95.5)	<0.001
≥2 with HDA by JADAS10	7 (15.9)	1 (2.3)	0.064
≥2 with HDA by cJADAS10	8 (18.2)	0 (0.0)	0.009

* Values are the number (%). JIA = juvenile idiopathic arthritis; JADAS10 = Juvenile Arthritis Disease Activity Score 10; cJADAS10 = clinical JADAS10; ACR = American College of Rheumatology; ID = inactive disease; MiDA = minimal disease activity; HDA = high disease activity.
† Only patients with at least 4 visits in the first year of PharmaChild registry participation were included.
‡ Including patients with ID.

65%, 98%, and 100% met the JADAS10 cutoffs for ID, MiDA, and MoDA, respectively (Supplementary Figure 1A, http://online library.wiley.com/doi/10.1002/art.41879/abstract). Similar data were obtained with the cJADAS10 (Supplementary Figure 1B). Of note, 1 patient in whom ID was achieved according to the JADAS10 and cJADAS10 was considered a nonresponder according to the ACR Pedi definition, due to an increase in the number of joints with limitation and a worsening in the level of physical function. The percentages of patients with JADAS10 and cJADAS10 above the cutoffs for HDA at trial baseline were 49% and 51%, respectively.

In the abatacept trial, 0%, 6%, and 56% of the patients with an ACR Pedi 30 response at 4 months met the JADAS10 cutoffs for ID, MiDA, and MoDA, respectively (Supplementary Figure 1C, http://onlinelibrary.wiley.com/doi/10.1002/art.41879/abstract); of those who exhibited an ACR Pedi 70 response, 31%, 75%, and 100% met the JADAS10 cutoffs for ID, MiDA, and MoDA, respectively. Findings with the cJADAS10 were similar (Supplementary Figure 1D). The percentages of patients with JADAS10 and cJADAS10 scores above the cutoffs for HDA at trial baseline were 63% and 68%, respectively.

According to 2012–2014 cutoffs, at least 50% of the patients with an ACR Pedi 30 to ACR Pedi 90 response in the TRIMECA trial would be classified as having HDA. In the abatacept trial, the percentage of patients with MiDA among patients who were ACR Pedi 70 responders according to 2012–2014 cutoffs did not exceed 40% (Figure 3 in the Supplementary Appendix, http://online library.wiley.com/doi/10.1002/art.41879/abstract).

Ability to predict future disease outcome. The PharmaChild longitudinal sample included 88 patients, 33 of whom had persistent oligoarthritis. Among the patients with CID (n = 44) and those without CID (n = 44) by ACR JIA criteria at 2 years, the median number of visits with a JADAS10 score below the cutoff for ID, a JADAS10 score below the cutoff for MiDA, and a JADAS10 score above the cutoff for HDA, respectively, in

the first year was 4 (IQR 2–5), 5 (IQR 4–5), and 0 (IQR 0–0) in those whose disease was clinically inactive at 2 years, and 1 (IQR 0–2), 3 (IQR 1–4), and 0 (IQR 0–1) in those whose disease was not clinically inactive at 2 years (P < 0.001, P < 0.001, and P = 0.031, respectively). Similar results were obtained with the cJADAS10 (data not shown). Among the patients with CID according to the ACR criteria at 2 years, the percentage of visits in the first year in which the patient had ID or MiDA was higher, and the percentage in which the patient had HDA was lower, compared to the percentages among patients whose disease was active at 2 years (Table 3). Results from the same analysis performed using 2012–2014 cutoffs are shown in Table 1 in the Supplementary Appendix.

DISCUSSION

In this study, we defined cutoffs in the JADAS10 and cJADAS10 that correspond to the states of ID, MiDA, MoDA, and HDA in juvenile oligoarthritis and RF-negative polyarthritis, based on the subjective perception of disease activity level by pediatric rheumatologists from different regions of the world. We propose that the new cutoffs be called the 2021 JADAS10 and cJADAS10 cutoffs, to distinguish them from the previous cutoffs developed in 2012 and 2014 (11–13). Cutoff development was conducted using a large multinational data set comprising nearly 2,000 patients enrolled in 35 pediatric rheumatology centers located in 49 countries on 5 continents. The large sample size and the wide geographic distribution of the centers make the study findings likely generalizable to patients with various JIA phenotypes and treated with different approaches. Notably, the new cutoffs are closer to the JADAS thresholds identified by Swart et al for treatment escalation from a cohort of JIA patients seen at an academic center (28).

We considered it necessary to develop new cutoff values because previous JADAS and cJADAS cutoffs were developed

using formal criteria for CID (14) and MiDA (15) as reference standards, but both of these definitions comprise some JADAS components, making it difficult to avoid circular reasoning. Indeed, the definition of CID includes the count of joints with active arthritis, the physician global assessment of disease activity, and measurement of an acute-phase reactant. The definition of MiDA is centered on the count of joints with active arthritis, the physician global assessment of disease activity, and the parent/patient assessment of well-being. Another limitation of 2012–2014 cutoffs was the use of the physician's treatment decisions, collected retrospectively, as an external criterion. This approach did not take into account the fact that treatment changes could be driven by factors other than disease activity, such as drug intolerance or increased body weight. Furthermore, therapeutic choices may vary between physicians from different regions and according to their particular expertise and local availabilities of treatments.

For definition of the cutoffs, we adapted the methodology used by Aletaha et al (10) for the establishment of the CDAI and SDAI cutoffs. However, unlike that study, in which physicians rated multiple hypothetical patient profiles, we performed a more direct assessment by capturing disease activity ratings using actual patients. Because the proposed 2021 cutoffs are derived from real-life perception of patient disease activity by treating physicians, they may have greater face validity and practical relevance than the 2012–2014 cutoffs. The cutoff values were obtained by applying 4 different methods; of note, the tentative cutoffs yielded by agreement analysis were consistently higher than those yielded by different approaches, with the exception of the cutoff separating ID from MiDA. While the new cutoffs for distinguishing between ID and MiDA are very close to previous ones for oligoarthritis, they appear to be less stringent for polyarthritis. All cutoffs for the other disease activity states are notably higher in the new set.

The new cutoffs were validated using 4 different samples, including nearly 5,000 JIA patients. In cross-validation analyses, cutoff values differentiated well between levels of disease severity, as measured in terms of pain and count of joints with restricted function, and between patients who had or did not have morning stiffness or whose parents were satisfied or not satisfied with the outcome of the illness. In addition, the cutoffs revealed a strong ability to discriminate between different levels of ACR Pedi response in 2 randomized clinical trials. Notably, the cutoff values separating ID from MiDA in polyarthritis were met in a sizable proportion of cases only among patients with at least an ACR Pedi 70 response, which is in accordance with our previous findings that only an improvement in symptoms of at least 70% makes a substantial difference in disease status in patients with JIA (5). Nearly all ACR Pedi 100 responders with polyarthritis and the large majority with oligoarthritis met the cutoffs for ID. Finally, in the PharmaChild registry, achievement of the new cutoffs in the first year of observation was found to predict the attainment of disease remission at 2 years.

Our results should be interpreted in light of some potential caveats. The assessors were not provided any background information on the definition of the various disease states that could help to enhance standardization of assessments. Furthermore, although the wide geographic representation of the pediatric rheumatologists who provided their ratings is a strength of our study, it could be argued that perception of disease activity may vary between physicians practicing in different regions or with diverse expertise and treatment availability. However, the fact that the reported cutoffs were based on the judgment of physicians from a large number of countries may lead to their widespread acceptance and use and foster the harmonization of clinical assessment in JIA. In addition, we decided to limit our study only to oligoarthritis and RF-negative polyarthritis owing to the wide clinical homogeneity between these 2 JIA categories. The application of the new cutoffs in different JIA categories, and in particular to RF-positive patients, who are included in most clinical trials on polyarthritis, requires validation. Recently, a systemic JIA–specific version of the JADAS was developed and validated (29), and cutoffs specific to this tool are needed. Finally, it must be acknowledged that part of the validation analysis (predictive ability assessment and ability to discriminate among different levels of improvement) was performed in a smaller subset of patients.

The comparison of the newer versus the older sets of criteria showed a better discriminative ability with the 2021 cutoffs, particularly for oligoarthritis. Moreover, the disease activity states based on the new cutoffs appear more consistent with the response to treatment defined with the ACR Pedi criteria in 2 clinical trials. In the comparison of predictive ability, the performances of cutoffs for inactive disease were similar. Compared to use of the 2012–2014 cutoffs, the percentage of patients with active disease at 2 years was relevantly higher among those who had at least 2 visits with a JADAS score below the cutoff for MiDA in the first year according to the 2021 cutoffs. Among patients with HDA at ≥2 visits in the first year according to 2021 cutoffs, a lower proportion had clinically inactive disease at 2 years.

In conclusion, we have developed a new set of JADAS10 and cJADAS10 cutoffs for the different disease activity states in JIA, which were based on the subjective perception of the level of disease activity by a multinational sample of pediatric rheumatologists. In validation analyses, the cutoffs demonstrated a strong ability to discriminate between different levels of disease severity and treatment response and to predict the achievement of long-term disease remission. Future studies should assess the 2021 cutoffs in other prospective patient cohorts and compare their metrologic performances to those of the 2012–2014 cutoffs.

ACKNOWLEDGMENTS

AUTHOR CONTRIBUTIONS

All authors were involved in drafting the article or revising it critically for important intellectual content, and all authors approved the final version to be published. Dr. Consolaro had full access to all of the data in the study and takes responsibility for the integrity of the data and the accuracy of the data analysis.

Study conception and design. Ruperto, Ravelli, Consolaro.

Acquisition of data. Nikishina, Lahdenne, Rutkowska-Sak, Avcin, Quartier, Panaviene, Uziel, Pruunsild, Vargova, Vilaiyuk, Dolezalova, Ringold, Garrone.

Analysis and interpretation of data. Trincianti, Van Dijkhuizen, Alongi, Mazzoni, Swart.

REFERENCES

1. Ravelli A, Martini A. Juvenile idiopathic arthritis [review]. Lancet 2007;369:767–78.

2. Viola S, Felici E, Magni-Manzoni S, Pistorio A, Buoncompagni A, Ruperto N, et al. Development and validation of a clinical index for assessment of long-term damage in juvenile idiopathic arthritis. Arthritis Rheum 2005;52:2092–102.

3. Brunner HI, Higgins GC, Wiers K, Lapidus SK, Olson JC, Onel K, et al. Health-related quality of life and its relationship to patient disease course in childhood-onset systemic lupus erythematosus. J Rheumatol 2009;36:1536–45.

4. Duffy CM. Measurement of health status, functional status, and quality of life in children with juvenile idiopathic arthritis: clinical science for the pediatrician. Pediatr Clin North Am 2005;52:359–72.

5. Bartoli M, Taro M, Magni-Manzoni S, Pistorio A, Traverso F, Viola S, et al. The magnitude of early response to methotrexate therapy predicts long-term outcome of patients with juvenile idiopathic arthritis. Ann Rheum Dis 2008;67:370–4.

6. Albers HM, Brinkman DM, Kamphuis SS, Van Suijlekom-Smit LW, Van Rossum MA, Hoppenreijs EP, et al. Clinical course and prognostic value of disease activity in the first two years in different subtypes of juvenile idiopathic arthritis. Arthritis Care Res (Hoboken) 2010;62:204–12.

7. Consolaro A, Ruperto N, Bazso A, Pistorio A, Magni-Manzoni S, Filocamo G, et al. Development and validation of a composite disease activity score for juvenile idiopathic arthritis. Arthritis Rheum 2009;61:658–66.

8. Nordal EB, Zak M, Aalto K, Berntson L, Fasth A, Herlin T, et al. Validity and predictive ability of the juvenile arthritis disease activity score based on CRP versus ESR in a Nordic population-based setting. Ann Rheum Dis 2012;71:1122–7.

9. McErlane F, Beresford MW, Baildam EM, Chieng SE, Davidson JE, Foster HE, et al. Validity of a three-variable Juvenile Arthritis Disease Activity Score in children with new-onset juvenile idiopathic arthritis. Ann Rheum Dis 2013;72:1983–8.

10. Aletaha D, Ward MM, Machold KP, Nell VP, Stamm T, Smolen JS. Remission and active disease in rheumatoid arthritis: defining criteria for disease activity states. Arthritis Rheum 2005;52:2625–36.

11. Consolaro A, Bracciolini G, Ruperto N, Pistorio A, Magni-Manzoni S, Malattia C, et al. Remission, minimal disease activity, and acceptable symptom state in juvenile idiopathic arthritis: defining criteria based on the juvenile arthritis disease activity score. Arthritis Rheum 2012;64:2366–74.

12. Consolaro A, Ruperto N, Bracciolini G, Frisina A, Gallo MC, Pistorio A, et al. Defining criteria for high disease activity in juvenile idiopathic arthritis based on the juvenile arthritis disease activity score. Ann Rheum Dis 2014;73:1380–3.

13. Consolaro A, Negro G, Gallo MC, Bracciolini G, Ferrari C, Schiappapietra B, et al. Defining criteria for disease activity states in nonsystemic juvenile idiopathic arthritis based on a three-variable juvenile arthritis disease activity score. Arthritis Care Res (Hoboken) 2014;66:1703–9.

14. Wallace CA, Giannini EH, Huang B, Itert L, Ruperto N, for the Childhood Arthritis Rheumatology Research Alliance (CARRA), the Pediatric Rheumatology Collaborative Study Group (PRCSG), and the Paediatric Rheumatology International Trials Organisation (PRINTO). American College of Rheumatology provisional criteria for defining clinical inactive disease in select categories of juvenile idiopathic arthritis. Arthritis Care Res (Hoboken) 2011;63:929–36.

15. Magni-Manzoni S, Ruperto N, Pistorio A, Sala E, Solari N, Palmisani E, et al. Development and validation of a preliminary definition of minimal disease activity in patients with juvenile idiopathic arthritis. Arthritis Rheum 2008;59:1120–7.

16. Consolaro A, Giancane G, Alongi A, van Dijkhuizen EH, Aggarwal A, Al-Mayouf SM, et al. Phenotypic variability and disparities in treatment and outcomes of childhood arthritis throughout the world: an observational cohort study. Lancet Child Adolesc Health 2019;3: 255–63.

17. Petty RE, Southwood TR, Manners P, Baum J, Glass DN, Goldenberg J, et al. International League of Associations for Rheumatology classification of juvenile idiopathic arthritis: second revision, Edmonton, 2001. J Rheumatol 2004;31:390–2.

18. Ravelli A, Davi S, Bracciolini G, Pistorio A, Consolaro A, van Dijkhuizen EH, et al. Intra-articular corticosteroids versus intra-articular corticosteroids plus methotrexate in oligoarticular juvenile idiopathic arthritis: a multicentre, prospective, randomised, open-label trial. Lancet 2017;389:909–16.

19. Ruperto N, Lovell DJ, Quartier P, Paz E, Rubio-Perez N, Silva CA, et al. Abatacept in children with juvenile idiopathic arthritis: a randomised, double-blind, placebo-controlled withdrawal trial. Lancet 2008;372:383–91.

20. Swart J, Giancane G, Horneff G, Magnusson B, Hofer M, Alexeeva E, et al. Pharmacovigilance in juvenile idiopathic arthritis patients treated with biologic or synthetic drugs: combined data of more than 15,000 patients from Pharmachild and national registries. Arthritis Res Ther 2018;20:285.

21. López-Ratón M, Rodríguez-Álvarez M, Cadarso-Suárez C, Gude-Sampedro F. OptimalCutpoints: an R package for selecting optimal cutpoints in diagnostic tests. J Stat Softw 2014;61:v06i08.

22. Youden WJ. Index for rating diagnostic tests. Cancer 1950;3:32–5.

23. Ruopp MD, Perkins NJ, Whitcomb BW, Schisterman EF. Youden Index and optimal cut-point estimated from observations affected by a lower limit of detection. Biom J 2008;50:419–30.

24. Perkins NJ, Schisterman EF. The inconsistency of "optimal" cut-points obtained using two criteria based on the receiver operating characteristic curve. Am J Epidemiol 2006;163:670–5.

25. Machado P, Landewe R, Lie E, Kvien TK, Braun J, Baker D, et al. Ankylosing Spondylitis Disease Activity Score (ASDAS): defining cut-off values for disease activity states and improvement scores. Ann Rheum Dis 2011;70:47–53.

26. Filocamo G, Sztajnbok F, Cespedes-Cruz A, Magni-Manzoni S, Pistorio A, Viola S, et al. Development and validation of a new short and simple measure of physical function for juvenile idiopathic arthritis. Arthritis Rheum 2007;57:913–20.

27. Giannini EH, Ruperto N, Ravelli A, Lovell DJ, Felson DT, Martini A. Preliminary definition of improvement in juvenile arthritis. Arthritis Rheum 1997;40:1202–9.

28. Swart JF, van Dijkhuizen EH, Wulffraat NM, de Roock S. Clinical Juvenile Arthritis Disease Activity Score proves to be a useful tool in treat-to-target therapy in juvenile idiopathic arthritis. Ann Rheum Dis 2018;77:336–42.

29. Tibaldi J, Pistorio A, Aldera E, Puzone L, El Miedany Y, Pal P, et al. Development and initial validation of a composite disease activity score for systemic juvenile idiopathic arthritis. Rheumatology (Oxford) 2020;59:3505–14.

AMERICAN COLLEGE
of RHEUMATOLOGY
Empowering Rheumatology Professionals

Lupus Anticoagulant Single Positivity During the Acute Phase of COVID-19 Is Not Associated With Venous Thromboembolism or In-Hospital Mortality

Nicolas Gendron,[1] 🆔 Marie-Agnès Dragon-Durey,[2] Richard Chocron,[3] Luc Darnige,[1] Georges Jourdi,[4] Aurélien Philippe,[1] Camille Chenevier-Gobeaux,[5] Jérôme Hadjadj,[6] Jérôme Duchemin,[4] Lina Khider,[7] Nader Yatim,[8] Guillaume Goudot,[7] Daphné Krzisch,[9] Benjamin Debuc,[10] Laetitia Mauge,[11] Françoise Levavasseur,[12] Frédéric Pene,[13] Jeremy Boussier,[8] Elise Sourdeau,[4] Julie Brichet,[9] Nadège Ochat,[9] Claire Goulvestre,[14] Christophe Peronino,[1] Tali-Anne Szwebel,[8] Franck Pages,[2] Pascale Gaussem,[15] Charles-Marc Samama,[16] Cherifa Cheurfa,[17] Benjamin Planquette,[18] Olivier Sanchez,[18] Jean-Luc Diehl,[19] Tristan Mirault,[7] Michaela Fontenay,[20] Benjamin Terrier,[21] 🆔 and David M. Smadja[22]

Objective. The clinical relevance of antiphospholipid antibodies (aPLs) in COVID-19 is controversial. This study was undertaken to investigate the prevalence and prognostic value of conventional and nonconventional aPLs in patients with COVID-19.

Methods. This was a multicenter, prospective observational study in a French cohort of patients hospitalized with suspected COVID-19.

Results. Two hundred forty-nine patients were hospitalized with suspected COVID-19, in whom COVID-19 was confirmed in 154 and not confirmed in 95. We found a significant increase in lupus anticoagulant (LAC) positivity among patients with COVID-19 compared to patients without COVID-19 (60.9% versus 23.7%; $P < 0.001$), while prevalence of conventional aPLs (IgG and IgM anti–β_2-glycoprotein I and IgG and IgM anticardiolipin isotypes) and nonconventional aPLs (IgA isotype of anticardiolipin, IgA isotype of anti-β_2-glycoprotein I, IgG and IgM isotypes of anti–phosphatidylserine/prothrombin, and IgG and IgM isotypes of antiprothrombin) was low in both groups. Patients with COVID-19 who were positive for LAC, as compared to patients with COVID-19 who were negative for LAC, had higher levels of fibrinogen (median 6.0 gm/liter [interquartile range 5.0–7.0] versus 5.3 gm/liter [interquartile range 4.3–6.4]; $P = 0.028$) and C-reactive protein (CRP) (median 115.5 mg/liter [interquartile range 66.0–204.8] versus 91.8 mg/liter [interquartile range 27.0–155.1]; $P = 0.019$). Univariate analysis did not show any association between LAC positivity and higher risks of venous thromboembolism (VTE) (odds ratio 1.02 [95% confidence interval 0.44–2.43], $P = 0.95$) or in-hospital mortality (odds ratio 1.80 [95% confidence interval 0.70–5.05], $P = 0.24$). With and without adjustment for CRP level, age, and sex, Kaplan-Meier survival curves according to LAC positivity confirmed the absence of an association with VTE or in-hospital mortality (unadjusted $P = 0.64$ and $P = 0.26$, respectively; adjusted hazard ratio 1.13 [95% confidence interval 0.48–2.60] and 1.80 [95% confidence interval 0.67–5.01], respectively).

Conclusion. Patients with COVID-19 have an increased prevalence of LAC positivity associated with biologic markers of inflammation. However, LAC positivity at the time of hospital admission is not associated with VTE risk and/or in-hospital mortality.

INTRODUCTION

COVID-19 is caused by SARS–CoV-2 and is associated with nonspecific respiratory syndromes, ranging from mild upper airway symptoms to hypoxemia requiring mechanical ventilation support (1–3). An important feature of COVID-19 is the associated coagulopathy that correlates with disease severity and in-hospital mortality (4,5), without any sign of disseminated intravascular coagulopathy (6), in contrast to previous reports (5). There are increasing reports of venous thromboembolism (VTE) and arterial thrombosis irrespective of the use of pharmacologic thromboprophylaxis (7–14). Both macrothrombosis, in particular pulmonary embolism (PE) (15), and microthrombosis in the lungs have been largely described (16). Microthrombosis could be a consequence of vascular injury and the link between coagulopathy and COVID-19 severity and/or mortality (17).

Antiphospholipid syndrome (APS) is an acquired thrombophilia leading to the use of long-term anticoagulation therapy (18). Classification of APS requires the presence of 1 clinical event (thrombosis or pregnancy morbidity) and persistently positive laboratory test results for at least 1 antiphospholipid antibody (aPL), the latter including lupus anticoagulant (LAC), anticardiolipin antibody (aCL), and IgG and/or IgM anti–β_2-glycoprotein I (anti-β_2GPI) antibodies (19,20). Autoantibodies to phospholipids and phospholipid-binding proteins such as antiprothrombin (anti-PT), aCL, or anti-β_2GPI are involved in leukocyte and endothelial activation and induce both VTE and arterial thrombosis. A combination of positive results of aPL testing, and particularly triple positivity (LAC and aCL, anti-β_2GPI, same isotype, IgG and/or IgM) identifies patients at high risk for thrombosis and allows a more confident diagnosis of APS. Furthermore, very often, triple-positive patients are also positive for anti–phosphatidylserine/prothrombin antibodies (anti-PS/PT) (tetra-positive patients), adding further risk for thromboembolic events to the usual aPL profile (21). Moreover, aPLs are not specific to APS but can be detected in healthy individuals and in different clinical settings, including autoimmune conditions, some drug treatments, or infectious disease (18). The occurrence of aPLs has been largely described during viral infections (22), and their pathogenicity in these contexts remains controversial.

During the COVID-19 outbreak, several reports described a potential association between aPLs and thrombotic events (23). Previous studies exploring LAC demonstrated between 45% and 88% positivity among different cohorts in the medical ward and/or intensive care unit (ICU) settings (10,23–25). Only 1 study suggested in vitro that aPL positivity in sera of patients with COVID-19 could be prothrombotic, but LAC was not assessed (26). To the best of our knowledge, there is no large cohort study that includes complete screening for LAC and associated aPLs. Moreover, the association of aPLs with VTE or in-hospital mortality in patients with COVID-19 is still a matter of debate. In the present study, we aimed to investigate the prevalence of conventional and nonconventional aPLs and explore their relevance to VTE and mortality outcomes in a large cohort of 249 patients with suspected COVID-19.

PATIENTS AND METHODS

Study design and population. This multicenter, prospective, observational cohort study was conducted at 2 university hospitals in Paris: Hôpital Européen Georges Pompidou and Hôpital Cochin. Patients with suspected SARS–CoV-2 infection were prospectively included from March 14, 2020 to April 20, 2020. Inclusion criteria were age >18 years, and presentation to the emergency department of either hospital with an infectious syndrome and suspected COVID-19 meeting criteria for hospital admission, or direct admission to the hospital. Patients with suspected COVID-19 had ≥1 of the following: fever, headache, myalgia, cough, dyspnea, rhinorrhea, or digestive symptoms. All patients with suspected COVID-19 were tested for SARS–CoV-2 infection by nasopharyngeal swab and screened for

Paris, France; [8]Nader Yatim, MD, Jeremy Boussier, MD, Tali-Anne Szwebel, MD: Translational Immunology Lab, Department of Immunology, Institut Pasteur, and Department of Internal Medicine, National Referral Center for Rare Systemic Autoimmune Diseases, APHP-CUP, F-75015 Paris, France; [9]Daphné Krzisch, MD, Julie Brichet, BSc, Nadège Ochat, BSc: Université de Paris, Hematology Department, APHP-CUP, F-75015 Paris, France; [10]Benjamin Debuc, MD: Université de Paris, Innovative Therapies in Haemostasis, INSERM, F-75006, and Plastic Surgery Department, APHP-CUP, F-75015 Paris, France; [11]Laetitia Mauge, PharmD, PhD: Université de Paris, PARCC, INSERM, F-75015, and Hematology Department, APHP-CUP, F-75015 Paris, France; [12]Françoise Levavasseur, BSc: Université de Paris, Institut Cochin, INSERM, F-75014 Paris, France; [13]Frédéric Pene, MD: Intensive Care Medicine, APHP-CUP, F-75014 Paris, France; [14]Claire Goulvestre, MD: Immunology Department, APHP-CUP, F-75014 Paris, France; [15]Pascale Gaussem, PharmD, PhD: Université de Paris, Innovative Therapies in Haemostasis, INSERM, F-75006, and Hematology Department, APHP-CUP, F-75015 Paris, France; [16]Charles-Marc Samama, MD, PhD: Université de Paris, Innovative Therapies in Haemostasis, INSERM, F-75006, and Anaesthesia, Intensive Care and Perioperative Medicine Department, APHP-CUP, F-75014 Paris, France; [17]Cherifa Cheurfa, MD: Anaesthesia, Intensive Care and Perioperative Medicine Department, APHP-CUP, F-75014 Paris, France; [18]Benjamin Planquette, MD, PhD, Olivier Sanchez, MD, PhD: Université de Paris, Innovative Therapies in Haemostasis, INSERM, F-75006, and Respiratory Medicine Department and Biosurgical Research Lab (Carpentier Foundation), APHP-CUP, F-75015 Paris, France and F-CRIN INNOVTE, Saint-Étienne, France; [19]Jean-Luc Diehl, MD, PhD: Université de Paris, Innovative Therapies in Haemostasis, INSERM, F-75006, and Intensive Care Unit and Biosurgical Research Lab (Carpentier Foundation), APHP-CUP, F-75015 Paris, France; [20]Michaela Fontenay, MD, PhD: Université de Paris, Institut Cochin, INSERM, and Hematology Department APHP-CUP, F-75014 Paris, France; [21]Benjamin Terrier, MD, PhD: Université de Paris, PARCC, INSERM U970, F-75015, and Department of Internal Medicine, National Referral Center for Rare Systemic Autoimmune Diseases, APHP-CUP, F-75014 Paris, France; [22]David M. Smadja, PharmD, PhD: Université de Paris, Innovative Therapies in Haemostasis, INSERM, F-75006, and Hematology Department and Biosurgical Research Lab (Carpentier Foundation), APHP-CUP, F-75015 Paris, France and F-CRIN INNOVTE, Saint-Étienne, France.

hospitalization criteria based on local guidelines (27) and defined as described in Supplementary Table 1 (available on the *Arthritis & Rheumatology* website at http://onlinelibrary.wiley.com/doi/10.1002/art.41777/abstract). Patients with suspected COVID-19 who met the hospitalization criteria were admitted to dedicated departments (medical ward or ICU) while awaiting laboratory confirmation of SARS–CoV-2 infection. A SARS–CoV-2 infection diagnosis was confirmed by a positive result of a reverse transcriptase–polymerase chain reaction (RT-PCR) assay and/or typical computed tomography (CT) scan findings of pneumonia related to COVID-19.

The study was performed in accordance with the Declaration of Helsinki. All patients provided written informed consent before they were enrolled (secondary ID: SARCODO 2020-A01048-31; ClinicalTrials.gov identifier: NCT04624997). Baseline characteristics (i.e., demographics, treatment, cardiovascular risk factors, and body mass index [BMI]), clinical data, biologic data, and CT scan evaluations were obtained from the medical records of all included patients, using standardized data collection methods.

Laboratory confirmation of SARS–CoV-2 infection. Nasopharyngeal swabs were collected at hospital admission in a universal transport medium using an Xpert nasopharyngeal sample collection kit as previously described (28). SARS–CoV-2 was detected using an Allplex 2019-nCoV assay (Seegene), a multiplex

Table 1. Demographic, clinical, and laboratory features of patients at the time of admission, according to COVID-19 viral status*

	Non–COVID-19 patients (n = 95)	Patients with COVID-19 (n = 154)	*P*
Male, no. (%)	43 (45.3)	111 (72.1)	<0.001
Age, years	76.0 (56.0–87.0)	59.0 (51.0–72.0)	<0.001
BMI, kg/m²	24.2 (21.4–26.6)	27.1 (24.5–31.5)	<0.001
Days from disease onset to hospital admission	4.0 (1.0–7.0)	7.0 (4.0–8.0)	0.001
CV risk factors, no. (%)			
Hypertension	51 (53.7)	66 (42.9)	0.037
Dyslipidemia	21 (22.1)	29 (18.8)	0.24
Diabetes mellitus	2 (2.1)	36 (23.4)	<0.001
Chronic kidney disease	13 (13.7)	15 (9.7)	0.27
Medical history, no. (%)			
Cancer	26 (27.4)	18 (11.7)	0.03
Coronary heart disease	10 (10.5)	7 (4.5)	0.002
Stroke	10 (10.5)	7 (4.5)	–
Clinical features			
Fever, no. (%)	31 (32.6)	132 (85.7)	<0.001
Headache, no. (%)	9 (9.5)	42 (27.3)	<0.001
Cough, no. (%)	40 (42.1)	122 (79.2)	<0.001
Productive cough, no. (%)	5 (5.3)	15 (9.7)	0.43
Dyspnea, no. (%)	59 (62.1)	106 (68.8)	0.42
Myalgia, no. (%)	12 (12.6)	62 (40.3)	<0.001
Diarrhea, no. (%)	12 (12.6)	38 (24.7)	0.064
Pneumonia on CT scan, no. (%)	26 (27.4)	116 (75.3)	<0.001
ARDS, no. (%)	2 (2.1)	45 (29.2)	<0.001
ICU admission, no. (%)	6 (6.3)	88 (57.1)	<0.001
Temperature, °C	37.1 (36.6–37.5)	38.3 (37.7–39.0)	<0.001
SpO₂, %	96.0 (92.0–98.0)	93.0 (89.1–96.0)	<0.001
Respiratory rate, breaths per minute	18.0 (16.0–22.0)	20.5 (18.0–27.8)	0.001
Pulse rate, beats per minute	87.0 (78.0–100.0)	92.0 (80.8–105.3)	0.17
Laboratory features			
White blood cell count, ×10⁹/liter	8.20 (6.45–11.1)	6.40 (4.60–9.00)	<0.001
Hemoglobin, gm/liter	134.0 (115.0–145.0)	128.5 (113.0–143.3)	0.23
Platelet count, ×10⁹/liter	223.5 (181.8–265.3)	196.5 (148.3–281.3)	0.074
Polynuclear neutrophils, ×10⁹/liter	6.44 (4.32–9.41)	4.83 (3.17–7.51)	0.005
Lymphocytes, ×10⁹/liter	1.17 (0.83–1.72)	0.95 (0.66–1.25)	0.001
Monocytes, ×10⁹/liter	0.60 (0.42–0.83)	0.37 (0.25–0.56)	<0.001
CRP, mg/liter	13.6 (2.5–97.6)	104.2 (47.3–173.9)	<0.001
Plasma creatinine, µmoles/liter	78.0 (62.0–110.0)	75.0 (62.0–102.0)	0.78
K-APTT, seconds	29.1 (27.8–32.0)	32.0 (30.0–35.4)	<0.001
PT ratio, %	97.0 (85.8–107.0)	92.0 (81.0–99.0)	0.003
Fibrinogen, gm/liter	4.30 (3.35–5.15)	5.70 (4.85–7.00)	<0.001
ᴅ-dimer, ng/ml	894.0 (430.0–2,266.3)	1,170.0 (702.5–2325.5)	0.039
Fibrin monomers, µg/ml	<7.0 (<7.0–<7.0)	<7.0 (<7.0–<7.0)	0.15

* Except where indicated otherwise, values are the median (interquartile range). BMI = body mass index; CV = cardiovascular; CT = computed tomography; ARDS = acute respiratory distress syndrome; ICU = intensive care unit; CRP = C-reactive protein; K-APTT = kaolin activated partial thromboplastin time; PT = thromboplastin time.

RT-PCR assay that detects 3 target genes (E gene, RdRP gene, and N gene) in real time in a single tube. Data were automatically analyzed using Seegene viewer software. Only qualitative data were considered.

Routine blood evaluations. All samples were collected in EDTA, sodium heparin, or 0.129*M* 9NC trisodium citrate tubes (BD Vacutainer) at the time of admission. Routine laboratory tests were complete blood cell count and creatinine, C-reactive protein (CRP), interleukin-6 (IL-6), and ferritin levels. Global coagulation tests were activated partial thromboplastin time (APTT) (kaolin activated partial thromboplastin [K-APTT] and CK Prest APTT; Diagnostica Stago), prothrombin time (PT) ratio (%), fibrinogen, and soluble fibrin monomer using STA-Liatest FM explored on a STA-R Max coagulometer (both from Diagnostica Stago) as previously described (26). D-dimer levels were determined using a Vidas D-dimer assay (BioMérieux) according to the manufacturer's instructions.

LAC testing. LAC assays were performed at the local center in accordance with the International Society on Thrombosis and Haemostasis Scientific Standardization Committee guidelines (29). Briefly, citrated blood was double centrifuged for 15 minutes at 2,000*g* at room temperature. The obtained platelet-poor plasma was analyzed for prolonged clotting time using 2 tests (i.e., APTT and dilute Russell's viper venom time [dRVVT]) based on different principles. LAC testing was performed using a 3-step procedure, i.e., for screening, mixing, and confirmation. For the dRVVT test, reagents LA1 and LA2 (Siemens) were used, and for the APTT test, automated APTT (Trinity Biotech) and a reagent with weak sensitivity to LAC (CK Prest) were used. The dRVVT assay contains a heparin-neutralizer that is able to quench unfractionated or low molecular weight heparin (up to 1.0 IU/ml)

that might lead to false-positive detection of LAC. In case of LAC testing in the setting of unfractionated heparin/low molecular weight heparin, anti–factor Xa activity was quantified and verified to be below the heparin-neutralizer cutoff of 1.0 IU/ml (Supplementary Table 2, available on the *Arthritis & Rheumatology* website at http://onlinelibrary.wiley.com/doi/10.1002/art.41777/abstract).

Solid-phase aPL testing. Using Bio-Flash chemiluminescent immunoassay technology (Quanta Flash β_2 GP1; Inova Diagnostics), IgG, IgM, and IgA aCL and anti-β_2GPI antibodies were measured in the plasma, with a cutoff value (99th percentile) of 20 arbitrary units (AU), as previously described (30). IgM and IgG anti-PS/PT antibodies were measured in the serum by Quanta Lite enzyme-linked immunosorbent assay (ELISA) (Inova Diagnostics), with a cutoff value (99th percentile) of 30 AU, as previously described (30). IgG and IgM anti-PT antibodies were measured by ELISA (Orgentec Diagnostika), with a cutoff value (99th percentile) of 10 AU.

Statistical analysis. Continuous data are shown as the median (interquartile range [IQR]), and categorical data are shown as percentages. Patients were compared according to COVID-19 viral status and LAC positivity. The Mann-Whitney test was used for assessment of continuous variables, and Fisher's exact test for categorical variables. In the multivariate analysis, we used a logistic regression model to identify risk factors for VTE and in-hospital mortality. The model was adjusted for age, sex, and CRP level (as a binary variable dichotomized according to the median value). In the survival analysis, the start of the study was triggered at the time of diagnosis of SARS–CoV-2 infection and hospitalization. The end of the study was defined either by the death of the patient during hospitalization or by discharge
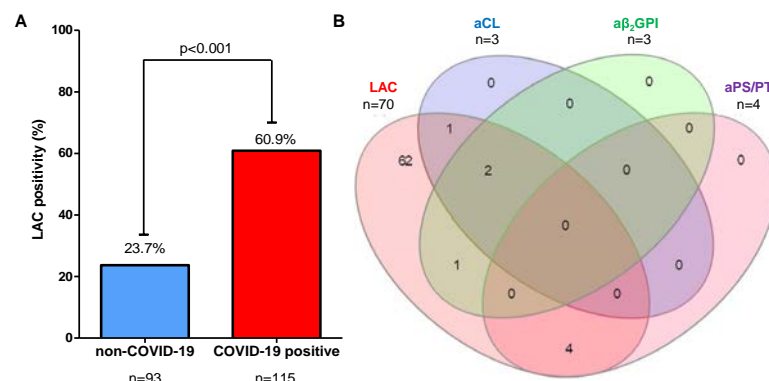
Figure 1. Prevalence of lupus anticoagulant (LAC) positivity in COVID-19 patients admitted to the hospital and its association with other antiphospholipid antibodies (aPLs). **A**, LAC positivity at the time of admission in 115 patients with COVID-19 compared to 93 patients without COVID-19, showing a significant difference between the groups (70 of 115 COVID-19 patients versus 22 of 93 non–COVID-19 patients positive for LAC). **B**, Venn diagram, created using a web-based tool (40), of aPL profiles among patients with COVID-19, showing positivity for each antibody subset either overlapping or not overlapping with positivity for LAC. The findings show that positivity for IgG or IgM anticardiolipin antibody (aCL), IgG or IgM anti–β_2-glycoprotein I (aβ_2GPI), and IgM anti–phosphatidylserine/prothrombin complex (aPS/PT) (no patients with COVID-19 were positive for IgG anti-PS/PT) was infrequent.

from the hospital. Survival time was calculated as the difference between the date of the diagnosis of SARS–CoV-2 infection and the date of event occurrence (VTE and in-hospital mortality) or the date of hospital discharge. We used the Cox proportional hazards model adjusted for age, sex, and CRP level to investigate the relationship between LAC positivity and patient outcomes (VTE or in-hospital mortality). The Kaplan-Meier method was used to represent the Cox proportional hazards model results according to LAC positivity. In the unadjusted survival analysis, survival curves were compared by log rank test. All analyses were performed using R studio software, including R version 3.6.3. P values (2-sided) less than 0.05 were considered significant.

RESULTS

Study population. A total of 249 patients admitted with suspected COVID-19 were included. Among them, 154 (61.8%) had confirmed COVID-19, whereas 95 (38.2%) did not have COVID-19 and were ultimately found to have other diagnoses (Supplementary Table 3, available on the *Arthritis & Rheumatology* website at http://onlinelibrary.wiley.com/doi/10.1002/art.41777/abstract). These 2 groups were not strictly comparable in terms of sex, age, BMI, cardiovascular risk factors, medical history, clinical features, and symptoms (Table 1). The group with COVID-19 had a higher proportion of male patients, higher BMI, and a higher frequency of fever and respiratory symptoms described in COVID-19 (1–3). At the time of admission, when compared to non–COVID-19 patients, patients with COVID-19 were more likely to have dyspnea, decreased SpO_2, pneumonia on CT scan, and increased respiratory rate and were more likely to be referred to the ICU, in particular, for acute respiratory distress syndrome. In terms of laboratory features related to coagulation disorders, patients with COVID-19 had higher median D-dimer levels, longer K-APTT, and lower PT ratio. In patients with COVID-19, fibrin monomers were negative and associated with hyperfibrinogenemia without thrombocytopenia.

Higher prevalence of positivity for LAC, but not other aPLs, in patients with COVID-19. LAC was assessed at the time of admission in the majority of patients with confirmed COVID-19 and patients without COVID-19. When compared to non–COVID-19 patients, we observed a higher prevalence of LAC positivity among patients with confirmed COVID-19 (60.9% versus 23.7%; $P < 0.001$) (Figure 1A). Interestingly, among all patients with COVID-19 who were tested for LAC, 9 (7.8%) received hydroxychloroquine at the time of admission, and among them, 6 (67%) were positive for LAC and 3 (33%) were negative for LAC.

The prevalence of positive findings on solid-phase immunoassays for conventional and nonconventional markers of APS in patients with and those without COVID-19 is described in Table 2. IgG, IgM, and IgA aCL positivity was infrequent in both groups (3.2%,

Table 2. Results of solid-phase immunoassays for conventional and nonconventional aPLs*

	Non–COVID-19 patients	Patients with COVID-19	P
IgG aCL			
Titer, median (IQR)	3.0 (2.6–5.5)	3.0 (3.0–9.0)	<0.001
Positive result	3 (3.2)	9 (5.8)	0.088
Missing data	0 (0.0)	6 (3.9)	
IgM aCL			
Titer, median (IQR)	2.8 (1.4–5.5)	2.0 (1.0–3.0)	0.019
Positive result	7 (7.4)	2 (1.3)	0.008
Missing data	0 (0.0)	6 (3.9)	
IgA aCL			
Titer, median (IQR)	2.3 (1.8–4.6)	2.0 (2.0–4.0)	0.22
Positive result	2 (2.1)	3 (1.9)	<0.001
Missing data	2 (2.1)	57 (37.0)	
IgG anti-β_2GPI			
Titer, median (IQR)	6.4 (6.4–6.4)	6.0 (6.0–6.0)	<0.001
Positive result	1 (1.1)	5 (3.2)	0.078
Missing data	0 (0.0)	6 (3.9)	
IgM anti-β_2GPI			
Titer, median (IQR)	1.1 (1.1–2.1)	1.0 (1.0–2.0)	<0.001
Positive result	4 (4.2)	3 (1.9)	0.091
Missing data	0 (0.0)	6 (3.9)	
IgA anti-β_2GPI			
Titer, median (IQR)	4.0 (4.0–4.0)	4.0 (4.0–4.0)	0.55
Positive result	2 (2.1)	2 (1.3)	<0.001
Missing data	2 (2.1)	56 (36.4)	
IgG anti-PS/PT			
Titer, median (IQR)	6.0 (4.0–9.0)	5.0 (4.0–6.0)	0.007
Positive result	0 (0.0)	0 (0.0)	NA
Missing data	0 (0.0)	0 (0.0)	
IgM anti-PS/PT			
Titer, median (IQR)	12.0 (6.0–17.0)	8.0 (5.0–13.0)	0.013
Positive result	10 (10.5)	7 (4.5)	0.12
Missing data	0 (0.0)	0 (0.0)	
IgG anti-PT			
Titer, median (IQR)	4.0 (3.0–6.0)	5.0 (3.0–6.7)	0.12
Positive result	7 (7.4)	11 (7.1)	0.22
Missing data	0 (0.0)	39 (25.3)	
IgM anti-PT			
Titer, median (IQR)	2.0 (1.0–3.0)	3.0 (1.9–4.0)	<0.001
Positive result	5 (5.3)	10 (6.5)	0.003
Missing data	0 (0.0)	39 (25.3)	
LAC assay			
Positive result among tested patients	22/93 (23.7)	70/115 (60.9)	<0.001
Missing data	2 (2.1)	39 (23.2)	

* Except where indicated otherwise, values are the number (%). aPLs = antiphospholipid antibodies; aCL = anticardiolipin antibody; IQR = interquartile range; anti-β_2GPI = anti–β_2-glycoprotein I; anti-PS/PT = anti–phosphatidylserine/prothrombin antibodies; NA = not applicable; anti-PT = antiprothrombin antibody; LAC = lupus anticoagulant.

7.4%, and 2.1%, respectively, in non–COVID-19 patients and 5.8%, 1.3%, and 1.9% in patients with COVID-19. IgM aCLs were significantly more frequent in non–COVID-19 patients ($P = 0.008$). IgG, IgM, and IgA anti-β_2GPI positivity was infrequent in both groups (1.1%, 4.2%, and 2.1%, respectively, in non–COVID-19 patients versus 3.2%, 1.9%, and 1.3% in patients with COVID-19). IgA anti-β_2GPI antibodies were significantly more frequent in non–COVID-19 patients ($P < 0.001$). IgG and IgM anti-PS/PT antibody

Table 3. Demographic, clinical, and laboratory features of patients with COVID-19 at the time of admission according to LAC status*

	LAC negative (n = 45)	LAC positive (n = 70)
Demographic features		
Male	37 (82.2)	48 (68.6)
Age, median (IQR) years	59.0 (45.0–74.0)	59.5 (52.0–72.0)
BMI, median (IQR) kg/m²	27.3 (24.7–32.1)	27.2 (25.3–30.7)
Time from disease onset to hospital admission, median (IQR) days	5.0 (3.0–9.0)	7.0 (4.0–8.0)
CV risk factors		
Hypertension	18 (40.0)	33 (47.1)
Dyslipidemia	9 (20.0)	16 (22.9)
Diabetes	10 (22.2)	20 (28.6)
Chronic kidney disease	5 (11.1)	9 (12.9)
Medical history		
Cancer	6 (13.3)	7 (10.0)
Coronary heart disease	22 (48.9)	42 (60)
Atrial fibrillation	4 (8.9)	4 (5.7)
Stroke	3 (6.7)	4 (5.7)
Previous DVT	1 (2.2)	1 (1.4)
Previous PE	2 (4.4)	1 (1.4)
Clinical features		
Fever	34 (75.6)	62 (88.6)
Headache	16 (35.6)	24 (34.3)
Cough	33 (73.3)	55 (78.6)
Productive cough	10 (22.2)	5 (7.1)†
Dyspnea	25 (55.6)	48 (68.6)
Myalgia	17 (37.8)	27 (38.6)
Diarrhea	11 (24.4)	13 (18.6)
Pneumonia on CT scan	30 (66.7)	50 (71.4)
ARDS	15 (33.3)	21 (30.0)
Temperature, median (IQR) °C	38.0 (37.4–38.5)	38.4 (37.7–38.8)
SpO₂, median (IQR) %	94.0 (89.3–96.0)	92.8 (89.1–95.0)
Laboratory features		
K-APTT, median (IQR) seconds	31.0 (29.2–33.0)	31.9 (30.0–34.0)
PT ratio, median (IQR)	87.0 (80.8–99.0)	93.0 (84.8–102.3)
Fibrinogen, median (IQR) gm/liter	5.3 (4.3–6.4)	6.0 (5.0–7.0)‡
D-dimer, median (IQR) ng/ml	1,503.0 (807.0–2,658.0)	981.0 (634.8–1891.8)
Fibrin monomers, median (IQR) µg/ml	<7.0 (<7.0–<7.0)	<7.0 (<7.0–<7.0)
Plasma creatinine, median (IQR) µmoles/liter	80.5 (58.5–101.8)	79.5 (68.0–117.8)
CRP, median (IQR) mg/liter	91.8 (27.0–155.1)	115.5 (66.0–204.8)§
IL-6, median (IQR) pg/ml	36.0 (16.3–82.5)	28.70 (12.7–97.8)
Ferritin, median (IQR) µg/liter	909.0 (336.0–1,718.0)	731.0 (270.5–1,040.5)
Peak blood test levels during hospitalization		
Plasma creatinine, median (IQR) µmoles/liter	94.5 (74.8–140.5)	101.0 (79.5–278.5)
CRP, median (IQR) mg/liter	148.2 (98.5–237.3)	170.95 (106.8–282.5)
Ferritin, median (IQR) µg/liter	1,005.0 (336.0–2,797.0)	931.50 (377.5–1578.2)
Fibrinogen, median (IQR) gm/liter	7.12 (4.92–8.60)	7.00 (5.60–9.11)
D-dimer, median (IQR) ng/ml	3,767.0 (1,430.0–6,528.5)	3,399.0 (832.8–9,490.5)
Outcomes		
ICU admission	25 (55.6)	43 (61.4)
Length of ICU stay, median (IQR) days	17.0 (5.0–25.0)	18.0 (5.0–30.0)
VTE¶	12 (26.8)	19 (27.1)
Symptomatic PE	10 (22.2)	15 (21.4)
Symptomatic DVT	5 (11.1)	6 (8.6)
Renal replacement therapy	7 (15.6)	16 (22.9)
Discharged	31 (68.9)	39 (55.7)
Deceased	7 (15.6)	17 (24.3)

* Except where indicated otherwise, values are the number (%). LAC = lupus anticoagulant; IQR = interquartile range; BMI = body mass index; CV = cardiovascular; CT = computed tomography; ARDS = acute respiratory distress syndrome; K-APTT = kaolin activated partial thromboplastin time; PT = thromboplastin time; CRP = C-reactive protein; IL-6 = interleukin-6; ICU = intensive care unit; VTE = venous thromboembolism.
† P = 0.029 versus LAC-negative patients.
‡ P = 0.028 versus LAC-negative patients.
§ P = 0.019 versus LAC-negative patients.
¶ Deep vein thrombosis (DVT) alone, pulmonary embolism (PE) alone, or DVT and PE combined.

Table 4. Association between LAC positivity, VTE, and in-hospital mortality outcomes, determined using logistic regression analysis*

	Univariate analysis		Multivariate analysis	
	OR (95% CI)	P	OR (95% CI)	P
Risk of VTE				
LAC status				
Negative	–	–	–	–
Positive	1.02 (0.44–2.43)	0.95	1.01 (0.42–2.48)	0.98
CRP level†				
<104.2 mg/liter	–	–	–	–
≥104.2 mg/liter	1.70 (0.79–3.75)	0.18	1.67 (0.70–4.15)	0.26
Sex				
Female	–	–	–	–
Male	1.16 (0.50–2.84)	0.74	0.96 (0.35–2.84)	0.93
Age	1.01 (0.98–1.03)	0.67	1.00 (0.97–1.03)	0.94
Risk of in-hospital mortality				
LAC status				
Negative	–	–	–	–
Positive	1.80 (0.70–5.05)	0.24	1.69 (0.58–5.35)	0.35
CRP level†				
<104.2 mg/liter	–	–	–	–
≥104.2 mg/liter	5.72 (2.17–18.03)	0.001	3.30 (1.12–11.32)	0.039
Sex				
Female	–	–	–	–
Male	1.56 (0.62–4.51)	0.37	2.35 (0.61–11.95)	0.25
Age	1.04 (1.01–1.08)	0.004	1.04 (1.01–1.09)	0.030

* LAC = lupus anticoagulant; VTE = venous thromboembolism; OR = odds ratio; 95% CI = 95% confidence interval; CRP = C-reactive protein.
† Dichotomized according to the median value.

positivity was 0.0% and 10.5%, respectively, in non–COVID-19 patients, compared to 0.0% and 4.5% in patients with COVID-19, with no significant difference between the groups. Finally, IgG and IgM anti-PT positivity was 7.4% and 5.3% in non–COVID-19 patients, compared to 7.1% and 6.5% in patients with COVID-19. IgM anti-PT antibodies were significantly more frequent in patients with COVID-19 ($P = 0.003$). Among the 70 patients with COVID-19 with LAC positivity, 62 (88.6%) were negative for other aPLs and 8 (11.4%) were positive for ≥1 other aPL (IgG or IgM aCL and/or anti-β_2GPI, and/or anti-PS/PT) (Figure 1B).

Association of LAC positivity in COVID-19 with markers of inflammation, but not with VTE or in-hospital mortality. Among patients with COVID-19, those with and those without LAC positivity were comparable in terms of sex, age, BMI, cardiovascular risk factors, medical history, and time from disease onset to hospitalization (Table 3). Furthermore, risk factors for VTE (i.e., age, BMI, cancer, previous deep vein thrombosis/PE) did not differ between groups ($P > 0.05$ for each). However, when compared to patients who were negative for LAC, patients with COVID-19 who were positive for LAC had higher levels of fibrinogen (median 6.0 gm/liter [IQR 5.0–7.0] versus 5.3 gm/liter [IQR 4.3–6.4]; $P = 0.028$) and CRP (median 115.5 mg/liter [IQR 66.0–204.8] versus 91.8 mg/liter [IQR 27.0–155.1]; $P = 0.019$). Strikingly, levels of IL-6 and ferritin were not significantly different between COVID-19 patients who were positive for LAC and those who were negative for LAC.

The percentages of patients who were referred to the ICU who developed VTE and who died in the hospital were not significantly different between LAC-negative and LAC-positive patients with COVID-19 (55.6% versus 61.4%, 26.8% versus 27.1%, and 15.6% versus 24.3%, respectively; $P > 0.05$ for each).

In both univariate and multivariate analyses adjusted for CRP level, age, and sex, LAC positivity was not associated with higher risk of VTE (odds ratio 1.02 [95% confidence interval 0.44–2.43], $P = 0.95$ and odds ratio 1.01 [95% confidence interval 0.42–2.48], $P = 0.98$, respectively) (Table 4). Furthermore, LAC positivity was not associated with higher in-hospital mortality in either the univariate analysis (odds ratio 1.80 [95% confidence interval 0.70–5.05], $P = 0.24$) or the multivariate analysis (odds ratio 1.69 [95% confidence interval 0.58–5.35], $P = 0.35$), in contrast to age (odds ratio 1.04 [95% confidence interval 1.01–1.09], $P = 0.030$) and CRP level (odds ratio 3.30 [95% confidence interval 1.12–11.32], $P = 0.039$ in the multivariate analysis). Finally, Kaplan-Meier survival curves showed that in patients with COVID-19, LAC positivity at the time of admission did not predict the risk of VTE ($P = 0.64$) or in-hospital mortality ($P = 0.26$), even after adjustment for CRP level, age, and sex (Figure 2).

DISCUSSION

COVID-19–associated coagulopathy is associated with microthrombosis, VTE, and arterial thrombotic complications (14,15,31). To the best of our knowledge, the present study is
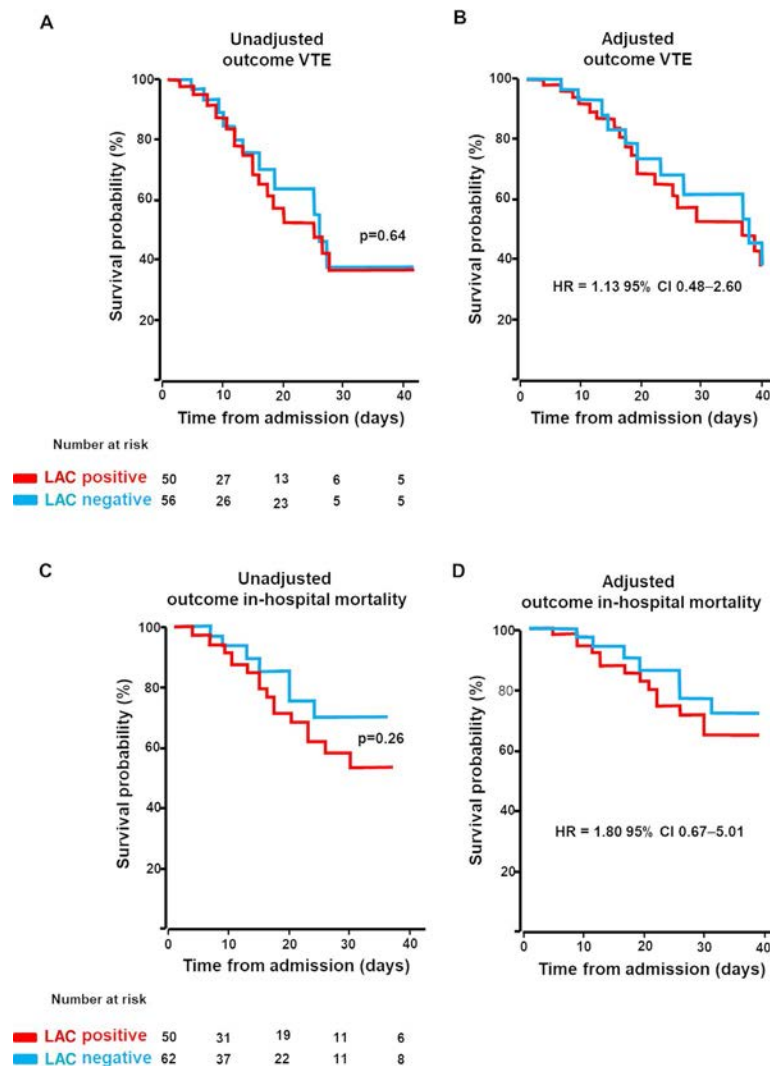
Figure 2. Kaplan-Meier survival curves showing the prognostic value of lupus anticoagulant (LAC) positivity at the time of admission with COVID-19. **A** and **B**, Development of venous thromboembolism (VTE) in patients with COVID-19 according to positivity or negativity for LAC, in an unadjusted analysis (**A**) and after adjustment for C-reactive protein level, age, and sex (**B**). **C** and **D**, In-hospital mortality in patients with COVID-19 according to positivity or negativity for LAC, in an unadjusted analysis (**C**) and after adjustment for C-reactive protein level, age, and sex (**D**). HR = hazard ratio; 95% CI = 95% confidence interval.

the first to test all aPLs in a large cohort of patients with suspected COVID-19, including both confirmed and nonconfirmed COVID-19 cases. We explored the relevance of conventional and nonconventional markers of APS at the time of admission with COVID-19 to assess whether they might play a role in disease prognosis. As described previously (10,23–25), we found a high prevalence of LAC in patients with COVID-19 in contrast with the low prevalence of IgG and IgM aCLs and IgG and IgM anti-β_2GPI antibodies detected by solid-phase immunoassay. LAC positivity in patients with COVID-19 was significantly associated with markers of inflammation such as fibrinogen and CRP levels, but not IL-6 or ferritin levels. Discrepancies between various markers of inflammation and LAC in terms of their association with COVID-19 suggested that those markers of inflammation do not have the same relevance in COVID-19. Further studies are needed to

decipher the exact involvement of inflammatory proteins in COVID-19 severity and/or COVID-19–associated coagulopathy. LAC testing during the acute phase of inflammatory conditions is not recommended because high CRP and fibrinogen levels may induce false-positive results (29,32,33).

Early during the COVID-19 outbreak, Zhang et al described 3 critical cases of COVID-19, characterized by the absence of LAC and the presence of IgA aCLs, and IgA and IgG anti-β_2GPI antibodies; more details on titers were not reported (34). The 3 patients experienced ischemic events associated with multifocal thrombosis. In patients with infectious conditions, aPLs can be transitorily positive (22), and these antibodies are rarely associated with thrombotic events; therefore, this association is not reliably prognostic in critically ill patients. Whether aPLs in patients with COVID-19 are similar to those in patients with other infectious diseases such

as hepatitis C virus (HCV), HBV, and HIV remain to be determined (18,22). A previous report on 56 patients with COVID-19 described the association of IgG aCL levels with COVID-19 severity (35), but LAC positivity was not tested. Results of one study suggested that aPL positivity could be prothrombotic in vitro and in vivo after accelerated venous thrombosis was observed in mice injected with IgG purified from the serum of aPL-positive patients with COVID-19 (26). However, a major flaw of that study is the absence of aPL specificity in the purified IgG of the patients with COVID-19. LAC was not assessed in the study.

A limitation of our study is the small sample size in both groups and the heterogeneity of the non–COVID-19 control group. In our study, we demonstrated that LAC positivity in patients with COVID-19 was not associated with VTE, in particular PE, or with a poorer prognosis. Our results are in accordance with previous studies of smaller cohorts that suggest the lack of association between aPLs and COVID-19 severity and/or VTE (24,25,36). The high prevalence of stroke (13) or VTE in patients with severe COVID-19 (15,30), in particular PE, is unusual and has rarely been observed in other viral infections such as influenza (8). In the study by Devreese et al, 10 patients with COVID-19 were retested 1 month after the first test, and all but 1 patient who initially tested positive for LAC were negative (37). This reinforces the hypothesis that LAC may be transient and/or artefactual due to the acute phase of infection and increased CRP and fibrinogen levels. Furthermore, Pengo et al showed that among patients with suspected APS, the initial single aPL–positive phenotype was confirmed in only 40% (38).

LACs are heterogeneous antibodies detected under various clinical circumstances in which cellular damage due to infectious, autoimmune, or inflammatory stimuli leads to plasma membrane remodeling, including the release of membrane microparticles and exposure of anionic phospholipids. LAC activity may be induced by anti-β_2GPI and/or anti-PT antibodies that provoke a dimerization of β_2GPI and/or prothrombin enhancing their affinity to negatively charge phospholipid (39). Strikingly, this high prevalence of LAC/aPLs in patients with COVID-19 has rarely been observed with other pathologies, which probably reveals significant or massive cellular destruction that is specific to COVID-19.

Medium/low aPL titers were consistently found in patients with COVID-19. We acknowledge that in the present study, aPL testing was performed during the acute phase, which is discouraged according to the guidelines because of potential interference. The guidelines recommend retesting after 3 months to avoid overdiagnosis by classification of transient positivity of aPLs (19,20,33). Of note, heparin therapy was not an issue for LAC testing in our study because our reagents contain heparin neutralizers, and anti–factor Xa activity in patients receiving anticoagulation treatment with heparin was below the cutoff of the neutralizer.

In summary, our study demonstrates that in COVID-19, similar to other acute infectious inflammatory diseases, there is a high prevalence of LAC positivity, but the latter is not associated with VTE and/or in-hospital mortality. LAC and aPL testing is not recommended and must be discouraged during the acute phase of COVID-19, as is the case in other viral infections. In any case, biologic confirmation after recovery is necessary.

AUTHOR CONTRIBUTIONS

All authors were involved in drafting the article or revising it critically for important intellectual content, and all authors approved the final version to be published. Dr. Gendron had full access to all of the data in the study and takes responsibility for the integrity of the data and the accuracy of the data analysis.

Study conception and design. Gendron, Dragon-Durey, Chocron, Darnige, Fontenay, Terrier, Smadja.
Acquisition of data. Gendron, Dragon-Durey, Chocron, Darnige, Jourdi, Philippe, Chenevier-Gobeaux, Hadjadj, Duchemin, Khider, Yatim, Goudot, Krzisch, Debuc, Mauge, Levavasseur, Pene, Boussier, Sourdeau, Brichet, Ochat, Goulvestre, Peronino, Szwebel, Pages, Gaussem, Samama, Cheurfa, Planquette, Sanchez, Diehl, Mirault, Fontenay, Terrier, Smadja.
Analysis and interpretation of data. Gendron, Dragon-Durey, Chocron, Darnige, Fontenay, Terrier, Smadja.

REFERENCES

1. Guan WJ, Ni ZY, Hu Y, Liang WH, Ou CQ, He JX, et al. Clinical characteristics of coronavirus disease 2019 in China. N Engl J Med 2020;382:1708–20.

2. Huang C, Wang Y, Li X, Ren L, Zhao J, Hu Y, et al. Clinical features of patients infected with 2019 novel coronavirus in Wuhan, China. Lancet 2020;395:497–506.

3. Chen N, Zhou M, Dong X, Qu J, Gong F, Han Y, et al. Epidemiological and clinical characteristics of 99 cases of 2019 novel coronavirus pneumonia in Wuhan, China: a descriptive study. Lancet 2020;395:507–13.

4. Zhou F, Yu T, Du R, Fan G, Liu Y, Liu Z, et al. Clinical course and risk factors for mortality of adult inpatients with COVID-19 in Wuhan, China: a retrospective cohort study. Lancet 2020;395:1054–62.

5. Tang N, Li D, Wang X, Sun Z. Abnormal coagulation parameters are associated with poor prognosis in patients with novel coronavirus pneumonia. J Thromb Haemost 2020;18:844–7.

6. Khider L, Gendron N, Goudot G, Chocron R, Hauw-Berlemont C, Cheng C, et al. Curative anticoagulation prevents endothelial lesion in COVID-19 patients. J Thromb Haemost 2020;18:2391–9.

7. Leonard-Lorant I, Delabranche X, Severac F, Helms J, Pauzet C, Collange O, et al. Acute pulmonary embolism in COVID-19 patients on CT angiography and relationship to D-dimer levels [letter]. Radiology 2020;296:E189–91.

8. Poissy J, Goutay J, Caplan M, Parmentier E, Duburcq T, Lassalle F, et al. Pulmonary embolism in patients with COVID-19: awareness of an increased prevalence [letter]. Circulation 2020;142:184–6.

9. Klok FA, Kruip MJ, van der Meer NJ, Arbous MS, Gommers D, Kant KM, et al. Confirmation of the high cumulative incidence of thrombotic complications in critically ill ICU patients with COVID-19: an updated analysis. Thromb Res 2020;191:148–50.

10. Helms J, Tacquard C, Severac F, Leonard-Lorant I, Ohana M, Delabranche X, et al. High risk of thrombosis in patients with severe SARS-CoV-2 infection: a multicenter prospective cohort study. Intensive Care Med 2020;46:1089–98.

11. Middeldorp S, Coppens M, van Haaps TF, Foppen M, Vlaar AP, Müller MC, et al. Incidence of venous thromboembolism in hospitalized patients with COVID-19. J Thromb Haemost 2020;18:1995–2002.

12. Llitjos JF, Leclerc M, Chochois C, Monsallier JM, Ramakers M, Auvray M, et al. High incidence of venous thromboembolic events in anticoagulated severe COVID-19 patients. J Thromb Haemost 2020;18:1743–6.

13. Merkler AE, Parikh NS, Mir S, Gupta A, Kamel H, Lin E, et al. Risk of ischemic stroke in patients with coronavirus disease 2019 (COVID-19) vs patients with influenza. JAMA Neurol 2020;77:1–7.

14. Lodigiani C, Iapichino G, Carenzo L, Cecconi M, Ferrazzi P, Sebastian T, et al. Venous and arterial thromboembolic complications in COVID-19 patients admitted to an academic hospital in Milan, Italy. Thromb Res 2020;191:9–14.

15. Planquette B, Le Berre A, Khider L, Yannoutsos A, Gendron N, de Torcy M, et al. Prevalence and characteristics of pulmonary embolism in 1042 COVID-19 patients with respiratory symptoms: a nested case-control study. Thromb Res 2020;197:94–9.

16. Ackermann M, Verleden SE, Kuehnel M, Haverich A, Welte T, Laenger F, et al. Pulmonary vascular endothelialitis, thrombosis, and angiogenesis in Covid-19. N Engl J Med 2020;383:120–8.

17. Diehl JL, Peron N, Chocron R, Debuc B, Guerot E, Hauw-Berlemont C, et al. Respiratory mechanics and gas exchanges in the early course of COVID-19 ARDS: a hypothesis-generating study. Ann Intensive Care 2020;10:95.

18. Schreiber K, Sciascia S, de Groot PG, Devreese K, Jacobsen S, Ruiz-Irastorza G, et al. Antiphospholipid syndrome [review]. Nat Rev Dis Primer 2018;4:17103.

19. Miyakis S, Lockshin MD, Atsumi T, Branch DW, Brey RL, Cervera R, et al. International consensus statement on an update of the classification criteria for definite antiphospholipid syndrome (APS). J Thromb Haemost 2006;4:295–306.

20. Devreese KM, Ortel TL, Pengo V, de Laat B. Laboratory criteria for antiphospholipid syndrome: communication from the SSC of the ISTH. J Thromb Haemost 2018;16:809–13.

21. Pengo V. Additional laboratory tests to improve on the diagnosis of antiphospholipid syndrome. J Thromb Haemost 2020;18:1846–8.

22. Abdel-Wahab N, Talathi S, Lopez-Olivo MA, Suarez-Almazor ME. Risk of developing antiphospholipid antibodies following viral infection: a systematic review and meta-analysis. Lupus 2018;27:572–83.

23. Harzallah I, Debliquis A, Drénou B. Lupus anticoagulant is frequent in patients with Covid-19 [letter]. J Thromb Haemost 2020;18:2064–5.

24. Siguret V, Voicu S, Neuwirth M, Delrue M, Gayat E, Stépanian A, et al. Are antiphospholipid antibodies associated with thrombotic complications in critically ill COVID-19 patients? [letter]. Thromb Res 2020;195:74–6.

25. Ferrari E, Sartre B, Squara F, Contenti J, Occelli C, Lemoel F, et al. High prevalence of acquired thrombophilia without prognosis value in patients with coronavirus disease 2019. J Am Heart Assoc 2020;9:e017773.

26. Zuo Y, Estes SK, Ali RA, Gandhi AA, Yalavarthi S, Shi H, et al. Prothrombotic autoantibodies in serum from patients hospitalized with COVID-19. Sci Transl Med 2020;12:eabd3876.

27. Smadja DM, Guerin CL, Chocron R, Yatim N, Boussier J, Gendron N, et al. Angiopoietin-2 as a marker of endothelial activation is a good predictor factor for intensive care unit admission of COVID-19 patients. Angiogenesis 2020;23:611–20.

28. Péré H, Podglajen I, Wack M, Flamarion E, Mirault T, Goudot G, et al. Nasal swab sampling for SARS-CoV-2: a convenient alternative in time of nasopharyngeal swab shortage [letter]. J Clin Microbiol 2020;58:e00721–20.

29. Pengo V, Tripodi A, Reber G, Rand JH, Ortel TL, Galli M, et al. Update of the guidelines for lupus anticoagulant detection. J Thromb Haemost 2009;7:1737–40.

30. Litvinova E, Darnige L, Kirilovsky A, Burnel Y, de Luna G, Dragon-Durey MA. Prevalence and significance of non-conventional antiphospholipid antibodies in patients with clinical APS criteria. Front Immunol 2018;9:2971.

31. Nopp S, Moik F, Jilma B, Pabinger I, Ay C. Risk of venous thromboembolism in patients with COVID-19: a systematic review and meta-analysis. Res Pract Thromb Haemost 2020;4:1178–91.

32. Eschwège V, Seddiki S, Robert A. The tissue thromboplastin inhibition test in the detection of lupus anticoagulants: importance of a correction factor eliminating the influence of fibrinogen level. Thromb Haemost 1996;76:65–8.

33. Devreese KM, de Groot PG, de Laat B, Erkan D, Favaloro EJ, Mackie I, et al. Guidance from the Scientific and Standardization Committee for lupus anticoagulant/antiphospholipid antibodies of the International Society on Thrombosis and Haemostasis. J Thromb Haemost 2020;18:2828–39.

34. Zhang Y, Xiao M, Zhang S, Xia P, Cao W, Jiang W, et al. Coagulopathy and antiphospholipid antibodies in patients with Covid-19. N Engl J Med 2020;382:e38.

35. Bertin D, Brodovitch A, Beziane A, Hug S, Bouamri A, Mege JL, et al. Anticardiolipin IgG autoantibody level is an independent risk factor for COVID-19 severity [letter]. Arthritis Rheumatol 2020;72:1953–5.

36. Borghi MO, Beltagy A, Garrafa E, Curreli D, Cecchini G, Bodio C, et al. Anti-phospholipid antibodies in COVID-19 are different from those detectable in the anti-phospholipid syndrome. Front Immunol 2020;11:584241.

37. Devreese KM, Linskens EA, Benoit D, Peperstraete H. Antiphospholipid antibodies in patients with COVID-19: a relevant observation? J Thromb Haemost 2020;18:2191–201.

38. Pengo V, Ruffatti A, Del Ross T, Tonello M, Cuffaro S, Hoxha A, et al. Confirmation of initial antiphospholipid antibody positivity depends on the antiphospholipid antibody profile. J Thromb Haemost 2013;11:1527–31.

39. Simmelink MJ, Horbach DA, Derksen RH, Meijers JC, Bevers EM, Willems GM, et al. Complexes of anti-prothrombin antibodies and prothrombin cause lupus anticoagulant activity by competing with the binding of clotting factors for catalytic phospholipid surfaces. Br J Haematol 2001;113:621–9.

40. Heberle H, Meirelles GV, da Silva FR, Telles GP, Minghim R. InteractiVenn: a web-based tool for the analysis of sets through Venn diagrams. BMC Bioinformatics 2015;16:169.

AMERICAN COLLEGE
of RHEUMATOLOGY
Empowering Rheumatology Professionals

Differences in the Oral Microbiome in Patients With Early Rheumatoid Arthritis and Individuals at Risk of Rheumatoid Arthritis Compared to Healthy Individuals

Johanna M. Kroese,[1] [ID] Bernd W. Brandt,[1] [ID] Mark J. Buijs,[1] Wim Crielaard,[1] Frank Lobbezoo,[1] [ID]
Bruno G. Loos,[1] [ID] Laurette van Boheemen,[2] [ID] Dirkjan van Schaardenburg,[2] [ID] Egija Zaura,[1] [ID] and
Catherine M. C. Volgenant[1] [ID]

Objective. It has been suggested that rheumatoid arthritis (RA) may originate at the oral mucosa. The aim of the present study was to assess the oral microbiome and periodontal condition in patients with early RA and individuals at risk of developing RA compared to healthy controls.

Methods. Three groups were recruited (n = 50 participants per group): 1) patients with early RA (meeting the American College of Rheumatology/European Alliance of Associations for Rheumatology 2010 classification criteria), 2) individuals at risk of developing RA (those with arthralgia who were positive for RA-associated autoantibodies), and 3) healthy controls. A periodontal examination was conducted to assess the presence of bleeding on probing (BOP), pocket probing depth (PPD), and periodontal inflamed surface area (PISA). The microbial composition of subgingival dental plaque, saliva, and tongue coating was assessed using 16S ribosomal DNA amplicon sequencing, and findings were compared between groups with permutational multivariate analysis of variance (PERMANOVA).

Results. There were no significant differences in any of the 3 periodontal variables between patients with early RA, at-risk individuals, and healthy controls ($P = 0.70$ for BOP, $P = 0.30$ for PPD, and $P = 0.57$ for PISA, by Kruskal-Wallis test). PERMANOVA analyses comparing microbial composition between the groups showed significant differences in the microbial composition of saliva (F = 2.08, $P = 0.0002$) and tongue coating (F = 2.04, $P = 0.008$), but not subgingival dental plaque (F = 0.948, $P = 0.51$). However, in post hoc tests, no significant differences in microbial composition of the saliva or tongue coating were observed between the early RA group and the at-risk group (F = 1.12, $P = 0.28$ for saliva; F = 0.834, $P = 0.59$ for tongue coating). In assessing microbial diversity based on the number of zero-radius operational taxonomic units per sample, *Prevotella* in the saliva and *Veillonella* in the saliva and tongue coating were each found at a higher relative abundance in samples from patients with early RA and at-risk individuals compared to healthy controls.

Conclusion. The results show similarities in the oral microbiome between patients with early RA and at-risk individuals, since in both groups, the oral microbiome was characterized by an increased relative abundance of potentially proinflammatory species when compared to that in healthy controls. These findings suggest a possible association between the oral microbiome and the onset of RA.

INTRODUCTION

Rheumatoid arthritis (RA) is a chronic inflammatory joint disease that is frequently accompanied by autoantibodies such as rheumatoid factor (RF) and antibodies against citrullinated

proteins (ACPAs) (1). These antibodies are often present several years before the onset of clinically apparent RA (2).

It has been suggested that RA originates at mucosal sites, such as the gut and oral mucosa (3,4). Periodontitis—a chronic inflammation of the gingiva, the tooth-supporting connective

---

[1]Johanna M. Kroese, DDS, Bernd W. Brandt, PhD, Mark J. Buijs, Wim Crielaard, PhD, Frank Lobbezoo, DDS, PhD, Bruno G. Loos, DDS, MSc, PhD, Egija Zaura, DDS, PhD, Catherine M. C. Volgenant, DDS, PhD: University of Amsterdam and Vrije Universiteit Amsterdam, Amsterdam, The Netherlands; [2]Laurette van Boheemen, MD, Dirkjan van Schaardenburg, MD, PhD: Amsterdam Rheumatology and Immunology Center, Reade, and Amsterdam University Medical Center, Amsterdam, The Netherlands.

tissues, and the alveolar bone—displays pathogenic similarities to RA, and several studies have shown an association between periodontal disease and RA (5). In previous studies on the oral microbiome in relation to RA, there was a particular interest in *Porphyromonas gingivalis*, a bacterium associated with periodontal disease (6). Because of its capacity to generate citrullinated proteins, *P gingivalis* could potentially trigger production of ACPAs and thereby initiate an RA-associated immune response (1).

However, findings from previous studies, both in RA patients and in individuals at risk of developing RA, have suggested that further investigations are needed and should focus on the microbiome as a whole, rather than on specific species (7–9). Since the oral microbiome may play a role in the onset of RA, and could thus be a potential target in the prediction or even prevention of RA, information on the oral microbiome in patients with early RA and individuals at risk of developing RA would be relevant. However, data on these specific groups are currently very limited. Our aim was therefore to assess the oral microbiome and the periodontal condition in patients with early RA and individuals at risk of developing RA in comparison to healthy controls.

PATIENTS AND METHODS

Study design and ethics approval. This study is based on baseline data obtained from a larger parent cohort study; a full description of the protocol has been published elsewhere (10) and is outlined in more detail below. Information on the methods used for sample processing is provided in the Supplementary Methods (available on the *Arthritis & Rheumatology* website at http://online library.wiley.com/doi/10.1002/art.41780/abstract). The protocol was approved by the accredited Medical Ethical Committees of Slotervaart Hospital and Reade (METc Slotervaartziekenhuis and Reade; approval no. U/17.056/P1719), and details on the protocol are included in the Dutch National Trial Register (trial no. NTR6362; https://www.trialregister.nl/trial/6198).

Participants and recruitment. For this study, 3 groups of participants were recruited: 1) patients with early RA, 2) individuals at risk of developing RA, and 3) a healthy control group of subjects without autoimmune conditions. Groups 1 and 2 were recruited at Reade, a rheumatology clinic in Amsterdam, The Netherlands. Group 1 consisted of patients diagnosed as having RA within the previous year and fulfilling the American College of Rheumatology/ European Alliance of Associations for Rheumatology 2010 classification criteria for RA (11). For group 2, participants were recruited from among individuals at risk of developing RA in the Reade cohort (12–14). Participants in this at-risk cohort have inflammatory-type arthralgia combined with increased serum levels of RF and/or ACPAs. Participants in group 3 were healthy subjects recruited at the Academic Centre for Dentistry Amsterdam, without selection for oral status, and were matched to the participants in groups 1 and 2 by sex and age (±5 years). All participants were age ≥18 years,

had a minimum of 12 natural teeth, and gave written informed consent. All clinical examinations and sampling took place at Reade and were performed by a single trained dentist (JMK).

Outcome variables. *General health.* All participants completed a medical questionnaire prior to the research visit, to identify possible confounders such as comorbid conditions. During the research visit, additional questions were asked about the subject's use of antibiotics during the preceding 3 months. Venous blood samples were collected to determine the serum levels of RF and ACPAs. Blood samples were processed in the hematology laboratory at OLVG Hospital in Amsterdam, using Phadia antibody detection assays (250 EliA IgM and Phadia 250 EliA cyclic citrullinated peptide antibody tests). In accordance with the manufacturer's recommendations, individuals with RF levels >5.0 kU/ liter and/or ACPA levels >10.0 kU/liter were considered seropositive; otherwise, participants were considered seronegative.

Oral health. Participants were asked about the amount of time lapsed since brushing their teeth, and about their regular practice of additional oral hygiene measures, e.g., mouth rinse and tongue cleaning. An intraoral examination was performed to determine the total number of teeth present, the number of decayed, missing, and filled teeth, and the presence or absence of a removable (partial) denture.

Collection of samples for microbiome analyses. Participants were instructed not to perform any oral hygiene measures for 24 hours, and not to eat or drink anything except water for 2 hours prior to their research visit. During the visit, a subgingival dental plaque sample, saliva sample, and tongue coating sample were collected. The microbial composition of the samples was assessed using 16S ribosomal DNA amplicon sequencing. A thorough description of the sample collection and processing is available in the Supplementary Methods (http://onlinelibrary.wiley. com/doi/10.1002/art.41780/abstract).

Periodontal examination. The periodontal examination included identification of bleeding on probing (BOP) (absent versus present) and measurement of pocket probing depth (PPD) (measured in millimeters) on 6 sites for each tooth (mesiobuccal, midbuccal, distobuccal, mesiolingual, midlingual, and distolingual). BOP values are expressed as a percentage of the full-mouth BOP. When calculating this percentage, data from the tooth from which a subgingival plaque sample was collected were not used. The dentist performing the examination of BOP and PPD (JMK) was trained by a periodontist.

Based on the PPD data obtained, a Community Periodontal Index of Treatment Need (CPITN) score (15) was calculated, and this score was used to categorize participants according to periodontitis status. Participants were categorized as either having suspected severe periodontitis (a CPITN score of 4) or not having suspected severe periodontitis (a CPITN score of 0–3). This means

that a PPD of ≥6 mm in at least one tooth would be needed for a patient to be classified as having suspected severe periodontitis.

To quantify the total burden of periodontal inflammation, the total periodontal inflamed surface area (PISA) was calculated. This measurement of inflammatory burden was carried out using the method described by Nesse et al (16).

Statistical analysis. Descriptive statistics were used to describe the characteristics of the study population. For continuous variables, one-way analysis of variance was performed to compare the mean values for normally distributed variables between the 3 groups; for non–normally distributed variables, a Kruskal-Wallis test was used. Possible differences in categorical variables between groups were tested with a chi-square test. A 2-sided alpha level of 0.05 was used as the threshold for statistical significance.

Microbiome data among the 3 groups were analyzed for both microbial composition and microbial diversity in all 3 periodontal niches: the plaque, saliva, and tongue coating. Details on these analyses are available in the Supplementary Methods (http://onlinelibrary.wiley.com/doi/10.1002/art.41780/abstract).

In addition, since the presence of ACPAs is a more relevant predictor of RA than is the presence of RF (17), we compared 2 subgroups of individuals within the at-risk group according to ACPA status ACPA-positive versus ACPA-negative at-risk individuals. Possible confounding factors and periodontal variables, as well as the microbiome composition in all 3 niches, were compared between these 2 subgroups.

RESULTS

Characteristics of the study population. From November 2017 until July 2019, 150 participants were included, comprising 50 participants per group (Table 1). Patients in the early RA

group were included in the study at a mean ± SD 3.1 ± 1.7 months after having received the diagnosis of RA. The majority of patients with early RA had been receiving treatment with methotrexate, mostly in combination with prednisone (Table 1), in accordance with the Dutch Society for Rheumatology national guidelines on drug treatment for RA (18).

The 3 groups were compared with regard to factors that could influence the oral microbiome: smoking status, alcohol consumption, use of drugs, use of painkillers during the preceding 24 hours, use of antibiotics during the preceding 3 months, wearing removable dentures, regular tongue cleaning, regular use of mouth rinse, number of decayed, missing, and filled teeth, time since eating/drinking before the research visit, and time since practice of oral hygiene before the research visit (see Supplementary Table 1, available on the *Arthritis & Rheumatology* website at http://onlinelibrary.wiley.com/doi/10.1002/art.41780/abstract). No differences in any of these characteristics were observed between the groups, except for the amount of time since practice of oral hygiene, which was carried out significantly more recently by patients in the early RA group compared to subjects in the other 2 groups.

Periodontal health. There was no difference in the percentage of BOP, median PPD, or median PISA between the 3 groups (Table 2). A trend toward a higher prevalence of severe periodontitis was seen in the early RA group and at-risk group compared to the healthy control group, with the prevalence of severe periodontitis incrementally increasing from the healthy control group to the at-risk group, and from the at-risk group to the early RA group. However, no significant between-group differences in the prevalence of severe periodontitis were found (Table 2).

Table 1. Characteristics of the study population by group*

	Early RA (n = 50)	At risk of RA (n = 50)	Healthy controls (n = 50)
Age, mean ± SD years	52.1 ± 13.2	51.4 ± 10.3	51.2 ± 11.0
Sex, female	39 (78)	38 (76)	38 (76)
RF positive	37 (74)	46 (92)	0 (0)
ACPA positive	31 (62)	24 (48)	0 (0)
Both RF and ACPA positive	38 (76)	50 (100)	0 (0)
Pharmacologic treatment for RA			
Methotrexate	44 (88)	–	–
Prednisone	39 (78)	–	–
Other	4 (8)	–	–
No pharmacologic treatment	2 (4)	–	–

* There were no significant differences between the groups in any of the listed characteristics, as determined by one-way analysis of variance or chi-square test. A between-group difference in frequency of rheumatoid factor (RF) and/or anti–citrullinated protein antibody (ACPA) positivity was not tested, because seropositivity was an inclusion criterion for the group of individuals at risk of developing rheumatoid arthritis (RA) and an exclusion criterion for the healthy control group, and therefore the difference was obvious. Additional characteristics are listed in Supplementary Table 1 (available on the *Arthritis & Rheumatology* website at http://onlinelibrary.wiley.com/doi/10.1002/art.41780/abstract). Except where indicated otherwise, values are the number (%) of participants.

Table 2. Periodontal assessments in the study groups*

	Early RA (n = 50)	At risk of RA (n = 50)	Healthy controls (n = 50)
BOP, median (IQR) %	19.3 (9.9–35.4)	15.4 (7.4–32.5)	17.5 (8.5–27.5)
PPD (total 6 sites per tooth)			
Plaque sample tooth, median (IQR) mm	2.5 (2.3–3.0)	2.6 (2.3–3.0)	2.5 (2.2–2.8)
All samples, median (IQR) mm	2.2 (2.0–2.6)	2.2 (2.0–2.5)	2.1 (1.9–2.5)
No. of pockets ≥6 mm, median (IQR)	0 (0–0.25)	0 (0–0)	0 (0–0)
PISA, median (IQR) mm^2	258.3 (108.4–398.3)	191.3 (72.5–431.8)	181.4 (91.2–369.4)
CPITN score 4, no. (%)	12 (24)	10 (20)	7 (14)

* There were no significant differences between the groups in any of the 3 periodontal variables assessed ($P =$ 0.70 for bleeding on probing [BOP], $P = 0.30$ for pocket probing depth [PPD], and $P = 0.57$ for periodontal inflamed surface area [PISA], by Kruskal-Wallis test) or in the Community Periodontal Index of Treatment Needs (CPITN) PPD score ($P = 0.21$, by chi-square test with linear association). RA = rheumatoid arthritis; IQR = interquartile range.

ACPA-positive versus ACPA-negative at-risk individuals. A separate analysis was performed to compare at-risk individuals who were ACPA positive (n = 24) to those who were ACPA negative (n = 26) with regard to all of the above-mentioned possible confounding factors and periodontal variables. No significant differences were found between these 2 subgroups of at-risk individuals stratified by ACPA status (data not shown).

Microbiologic signatures. After processing, the periodontal samples obtained from all subjects were found to have a total of 948 zero-radius operational taxonomic units (zOTUs). After subsampling at 3,500 reads per sample, 942 zOTUs remained, with a mean of 130 zOTUs per sample. Eight samples (2 plaque, 4 saliva, and 2 tongue coating samples) were excluded from further analyses because the number of reads was too low. Because patients in the early RA group had performed oral hygiene practices significantly more recently before the research visit as compared to participants in the other 2 groups, and brushing could influence the oral microbiome, this variable was taken into account when analyzing group differences by permutational multivariate analysis of variance (PERMANOVA).

Microbial diversity of the 3 periodontal niches (the plaque, saliva, and tongue coating) in all samples was measured using the Shannon Diversity Index, as well as by determining the number of zOTUs per sample and the Bray-Curtis distance as an index of microbial diversity. The results in each niche are reported below and in Supplementary Table 2 (available on the *Arthritis & Rheumatology* website at http://onlinelibrary.wiley.com/doi/10.1002/art.41780/abstract).

Plaque samples. There was no difference among the groups in the microbial composition of the plaque samples, as determined in analyses based on the number of hours since practice of oral hygiene (F = 1.58, $P = 0.07$ by two-way PERMANOVA) and in analyses based on the groups being compared (F = 0.948, $P = 0.51$ by two-way PERMANOVA). Results of principal components analysis (PCA) did not reveal any clustering of plaque microbial composition by group (Figure 1A).

Saliva samples. The microbial composition of saliva differed significantly among the groups, irrespective of the number of hours since practice of oral hygiene (F = 2.27, $P = 0.004$ by two-way PERMANOVA) and irrespective of the groups being compared (F = 2.08, $P = 0.0002$ by two-way PERMANOVA). PCA showed that the microbial composition of saliva samples from the healthy control group clustered together (Figure 1B). This was confirmed by results of the post hoc, pairwise two-way PERMANOVA analyses based on the number of hours since practice of oral hygiene and those based on the groups being compared, with evidence of a significant difference in the saliva microbial composition between the healthy control group and the early RA group (F = 2.66, $P < 0.001$) and between the healthy control group and the at-risk group (F = 2.56, $P = 0.001$), but not between the early RA group and the at-risk group (F = 1.12, $P = 0.28$).

Tongue coating samples. The microbial composition of the tongue coating samples was also significantly different among the groups, irrespective of the number of hours since practice of oral hygiene (F = 1.97, $P = 0.033$ by two-way PERMANOVA) and irrespective of the groups being compared (F = 2.04, $P = 0.008$ by two-way PERMANOVA). Similar to the findings in the saliva, the microbial composition of the tongue coating samples from the healthy control group clustered together (Figure 1C). This was confirmed by post hoc, pairwise two-way PERMANOVA analyses based on the number of hours since practice of oral hygiene and those based on the groups being compared with a significant difference in tongue coating microbial composition observed between the healthy control group and the early RA group (F = 2.75, $P = 0.005$) and between the healthy control group and the at-risk group (F = 2.59, $P = 0.01$), but not between the early RA group and the at-risk group (F = 0.834, $P = 0.59$).

ACPA-positive versus ACPA-negative at-risk individuals. For all 3 niches, a separate one-way PERMANOVA analysis was performed to compare ACPA-positive and ACPA-negative individuals at risk of developing RA. No significant differences in microbial composition in any of the 3 niches were found between these 2 subgroups (data not shown).
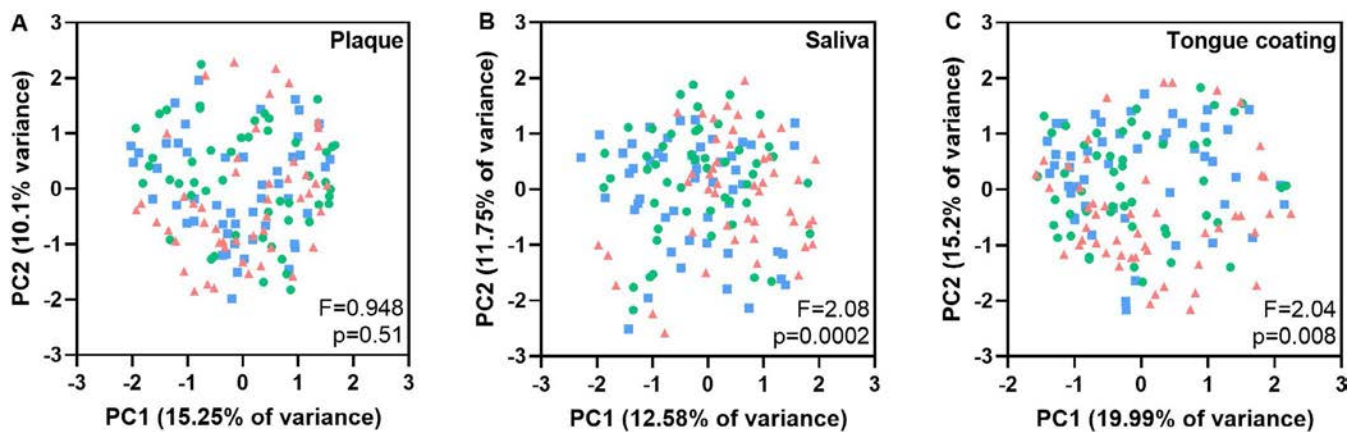
Figure 1. Principal components analysis plots, including the first and second principal components (PC1 and PC2, respectively), displaying microbiologic composition signatures of the subgingival dental plaque (**A**), saliva (**B**), and tongue coating (**C**) in patients with early rheumatoid arthritis (RA) (blue), individuals at risk of developing RA (green), and healthy controls (orange). The F value was calculated using two-way permutational multivariate analysis of variance, based on the number of hours since practice of oral hygiene and based on the groups being compared.

Discriminative zOTUs. *Saliva samples.* Twenty-five zOTUs in the saliva significantly discriminated among the groups, of which 7 had a relative abundance of ≥0.01 in at least 1 group (see Supplementary Table 3, available on the *Arthritis & Rheumatology* website at http://onlinelibrary.wiley.com/doi/10.1002/art.41780/abstract). Post hoc Mann-Whitney U tests showed that the significant results were predominantly attributable to the difference between the early RA and at-risk groups and the healthy control group, rather than to the difference between the early RA group and the at-risk group (Supplementary Table 3 [http://onlinelibrary.wiley.com/doi/10.1002/art.41780/abstract]). *Prevotella salivae* (zOTU 25), *Veillonella* (zOTU 4), and *Prevotella* (zOTU 10) were more abundant in the early RA group and at-risk group compared to the healthy control group (Figures 2A–C), while *Neisseria flavescens/subflava* (zOTU 7), *Porphyromonas pasteri/sp._oral_taxon_278* (zOTU 15), and *Veillonella parvula* (zOTU 12) were more abundant in the healthy control group compared to the other 2 groups. Only *Fusobacterium periodonticum* (zOTU 13) was more abundant in the at-risk group and the healthy control group compared to the early RA group, while no difference was found between the at-risk group and the healthy control group.

Tongue coating samples. Nineteen zOTUs in the tongue coating samples significantly discriminated among the groups, of which 4 had a relative abundance of ≥0.01 in at least 1 group (see Supplementary Table 4, available on the
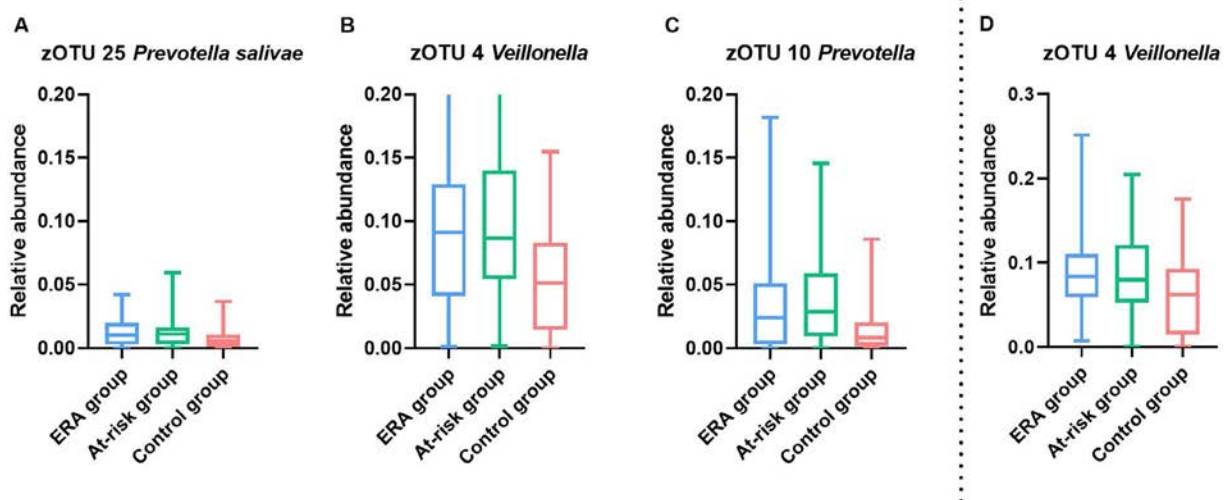
Figure 2. Relative abundance of zero-radius operational taxonomic units (zOTUs) in the saliva (*Prevotella salivae*, *Veillonella*, and *Prevotella* species) (**A–C**) and tongue coating (*Veillonella* species) (**D**) in patients with early rheumatoid arthritis (ERA), individuals at risk of developing RA, and healthy controls. The relative abundance of microbial species was assessed as the number of zOTUs, which helped discriminate among the groups according to linear discriminant analysis incorporating effect size. Results are shown as box plots. Each box represents the 25th to 75th percentiles. Lines inside the boxes represent the median. Lines outside the boxes represent the minimum and maximum.

Arthritis & Rheumatology website at http://onlinelibrary.wiley.com/doi/10.1002/art.41780/abstract). Again, the significant results were predominantly attributable to the difference between the early RA and at-risk groups and the healthy control group, rather than to the difference between the early RA group and the at-risk group (Supplementary Table 4). While *Veillonella* (zOTU 4) was more abundant in the early RA group and the at-risk group (Figure 2D), *Neisseria flavescens/subflava* (zOTU 7) and *Streptococcus dentisani/infantis/mitis/oralis/sp._oral_taxon_058* (zOTU 1) were more abundant in the healthy control group compared to the other 2 groups. *Fusobacterium periodonticum* (zOTU 13) was more abundant in the healthy control group compared to the early RA group, while no differences were found in the at-risk group compared to both other groups.

P gingivalis. The genus *P gingivalis* was not identified as a discriminative zOTU. One of the zOTUs–*P gingivalis* zOTU 116–did classify as *P gingivalis*, but had an overall low abundance in all 3 niches and did not differ among the groups; in all 3 groups, the median relative abundance of *P gingivalis* zOTU 116 in all 3 niches was 0 (in the plaque, $P = 0.37$; in the saliva, $P = 0.47$; in the tongue coating, $P = 0.12$, by Kruskal-Wallis test).

DISCUSSION

The microbial composition of the stimulated saliva and tongue coating, but not that of the subgingival dental plaque, in patients with early RA and individuals at risk of RA significantly differed when compared to an age- and sex-matched healthy control group. *Prevotella* and *Veillonella*—both being gram-negative anaerobes—were found at a higher relative abundance in the saliva, and *Veillonella* was also found at a higher relative abundance in the tongue coating, both in the patients with early RA and in the at-risk individuals compared to healthy controls. However, in saliva, there was also another zOTU that classified as a different species, belonging to the genus *Veillonella*, which was present at a higher relative abundance in the healthy control group compared to the other 2 groups.

The increased relative abundance of the genus *Prevotella* in patients with early RA is consistent with the findings from a study by Scher et al in patients with new-onset RA (7), and with the findings from a study by Correa et al in patients with established RA (19). Furthermore, studies on the gut microbiome have also shown an increased relative abundance of *Prevotella* species in patients with early RA (3) and at-risk individuals (20). Some *Prevotella* strains are capable of promoting chronic inflammation, by stimulating local cytokine production and induction of mucosal inflammation, which in turn can lead to systemic dissemination of inflammatory mediators (21). Furthermore, results of one study suggested that a possible translocation of oral *Prevotella* species or their DNA to joint tissues occurs in patients with RA (22). The increased relative abundance of this potentially proinflammatory genus in patients with early RA and at-risk individuals suggests a link between the

oral microbiome and RA (8), and microbiome dysbiosis may contribute to the induction of arthritis. Additionally, dysbiosis in both the oral and gut microbiome is partially resolved after the start of pharmacologic treatment for RA (23), further supporting an association between the microbiome and RA development. However, the currently available literature is insufficient to establish a causal link and to fully elucidate the biologic mechanisms involved (22).

Furthermore, the potential presence of a reversed pathway needs to be considered, whereby active inflammation or the characteristics of inflammation in susceptible subjects may provide an environment in which *Prevotella* species would attain ecologic advantages and emerge at larger numbers. When RA has been treated with specific medications (23), the ecology tends to revert to a situation less favorable for *Prevotella*. Thus, the possible influence of treatments for systemic RA on the oral microbiome is overall a factor to consider when interpreting the findings in patients with early RA (24).

Due to the early stage of the disease, most patients with early RA in the present study had been receiving the same treatment, and thus heterogeneity within this group was not an issue. However, it does mean that there was a notable difference in comparison to the at-risk group and the control group, potentially leading to a bias in the results. By including the patients with early RA during the first few months after the start of the treatment, we attempted to limit this bias. Interestingly, the results showed an increased relative abundance of *Prevotella* in the early RA group, with similar findings in the at-risk group, possibly indicating that the influence of pharmacologic treatment was limited. However, it should be mentioned that future research should preferably include patients with early RA who are not receiving any immunomodulatory therapy.

This study is the first to report on the microbial composition of several oral niches in individuals at risk of RA. In a study by Mankia et al, ACPA-positive at-risk individuals were assessed for the presence of *P gingivalis* and *Aggregatibacter actinomycetemcomintans* (in subgingival plaque only), with the results showing an increased relative abundance of *P gingivalis* in at-risk individuals compared to healthy controls (25). However, the current study showed an overall low abundance of *P gingivalis*, and did not identify *P gingivalis* as a relevant bacterium for discrimination between the groups. Also, we did not observe any differences between the ACPA-positive and ACPA-negative at-risk groups. Interestingly, our results do show an increased relative abundance of the *Veillonella* and *Prevotella* species in the at-risk group, similar to the findings in the early RA group. This is consistent with the findings from a study by Tong et al, in which both patients with RA and at-risk individuals showed an increased abundance of *Prevotella* in saliva (26).

Furthermore, for most of the discriminative zOTUs, the relative abundance did not significantly differ between the early RA group and the at-risk group. This corresponds to our observations of overall similarities in the oral microbiome between patients with early RA and at-risk individuals, despite the microbial variety within

these groups, which should always be considered when interpreting Bray-Curtis distances between groups. Taken together, these findings indicate a possible role for oral microbial dysbiosis in the induction of arthritis, similar to previous findings on the gut microbiome (3). It also corresponds to the findings from a study by Cheng et al, in which at-risk individuals, patients with early RA, and controls showed differences in bacterial diversity and composition, and a role for oral microbiome dysbiosis in RA onset was suggested (9). Collectively, the current findings and previously published data suggest that bacterial colonization on any mucosal tissue might trigger aberrant inflammatory reactions; this is not, per se, restricted to bacteria from periodontal pockets. However, the possibility of a reversed pathway, as mentioned earlier, cannot be excluded, due to the cross-sectional nature of the data.

Regarding measures of periodontal health and possible confounding factors, this study did not show any between-group differences. This is a major strength of the current study, since clinical differences between groups are often an issue that complicates the interpretation of the results in microbiome studies (27). In contrast to our study findings, the study by Mankia and colleagues showed that ACPA-positive at-risk individuals had a higher prevalence of periodontal disease compared to the control group (25). These contradictory findings might be explained by differences in the case definition of periodontitis. Furthermore, the percentage of subjects with severe periodontitis in the healthy control group in the current study is representative of the overall prevalence of severe periodontitis observed in Western populations (28), while in the study by Mankia and colleagues, the prevalence of periodontitis was relatively high, but severe cases were not specified (25). Nonetheless, although not significant, the current results do show a trend toward a higher prevalence of severe periodontitis in patients with early RA and at-risk individuals compared to healthy controls.

A somewhat surprising result of this study is the absence of a difference among the groups in the microbial composition of the subgingival dental plaque. Whereas a role for periodontal disease and associated bacteria in the onset of RA was previously hypothesized (25), which would thus lead to a profound difference in the plaque microbiome between the groups, the results of the present study do not support this hypothesis. A possible explanation for this is that a significant difference in periodontal disease was not observed among the 3 groups, and thus there was no difference in the relative abundance of associated bacteria. Furthermore, the composition of dental plaque can be influenced by several factors, e.g., local immunologic reactions, diet, and oral hygiene, whereas the tongue coating was shown to be the most stable oral niche in terms of microbiome composition (29). Although we attempted to limit the influence of systemic treatment for RA, as described earlier, it may also partly explain the similarities in the plaque microbiome between the early RA group and the healthy control group, because the use of prednisone was shown to be associated with a healthier

subgingival microbiome in patients with RA (24). This effect may be more pronounced in the subgingival plaque compared to the saliva and tongue coating, due to the direct contact of the subgingival niche to the circulatory system. However, further research is necessary to support this hypothesis.

To complement the currently available cross-sectional data, future studies should also include a longitudinal aspect, preferably with large cohorts and consistent data collection, to aid in the application of advanced methods, including the use of artificial intelligence, for prediction of an oral–systemic RA link (27). The results of the present study indicate that there are similarities in the oral microbiome between patients with early RA and at-risk individuals, as both groups had an increased relative abundance of potentially proinflammatory species when compared to healthy controls. These findings thus point toward a possible role of the oral microbiome in the onset of RA.

ACKNOWLEDGMENT

AUTHOR CONTRIBUTIONS

All authors were involved in drafting the article or revising it critically for important intellectual content, and all authors approved the final version to be published. Ms Kroese had full access to all of the data in the study and takes responsibility for the integrity of the data and the accuracy of the data analysis.
Study conception and design. Kroese, Crielaard, Lobbezoo, Loos, van Schaardenburg, Volgenant.
Acquisition of data. Kroese, van Boheemen.
Analysis and interpretation of data. Kroese, Brandt, Buijs, Loos, Zaura, Volgenant.

REFERENCES

1. Malmstrom V, Catrina AI, Klareskog L. The immunopathogenesis of seropositive rheumatoid arthritis: from triggering to targeting [review]. Nat Rev Immunol 2017;17:60–75.

2. Nielen MM, van Schaardenburg D, Reesink HW, van de Stadt RJ, van der Horst-Bruinsma IE, de Koning MH, et al. Specific autoantibodies precede the symptoms of rheumatoid arthritis: a study of serial measurements in blood donors. Arthritis Rheum 2004;50:380–6.

3. Maeda Y, Takeda K. Host-microbiota interactions in rheumatoid arthritis. Exp Mol Med 2019;51:1–6.

4. Konig MF. The microbiome in autoimmune rheumatic disease [review]. Best Pract Res Clin Rheumatol 2020;34:101473.

5. Cheng Z, Meade J, Mankia K, Emery P, Devine DA. Periodontal disease and periodontal bacteria as triggers for rheumatoid arthritis. Best Pract Res Clin Rheumatol 2017;31:19–30.

6. Mysak J, Podzimek S, Sommerova P, Lyuya-Mi Y, Bartova J, Janatova T, et al. *Porphyromonas gingivalis*: major periodontopathic pathogen overview. J Immunol Res 2014;2014:476068.

7. Scher JU, Ubeda C, Equinda M, Khanin R, Buischi Y, Viale A, et al. Periodontal disease and the oral microbiota in new-onset rheumatoid arthritis. Arthritis Rheum 2012;64:3083–94.

8. Lopez-Oliva I, Paropkari AD, Saraswat S, Serban S, Yonel Z, Sharma P, et al. Dysbiotic subgingival microbial communities in periodontally healthy patients with rheumatoid arthritis. Arthritis Rheumatol 2018;70:1008–13.

9. Cheng Z, Do T, Mankia K, Meade J, Hunt L, Clerehugh V, et al. Dysbiosis in the oral microbiomes of anti-CCP positive individuals at risk of developing rheumatoid arthritis. Ann Rheum Dis 2020;80:162–8.

10. Kroese JM, Volgenant CM, van Schaardenburg D, Loos BG, Crielaard W, Lobbezoo F. Temporomandibular joint function, periodontal health, and oral microbiome in early rheumatoid arthritis and at-risk individuals: a prospective cohort study protocol. BDJ Open 2020;6:7.

11. Aletaha D, Neogi T, Silman AJ, Funovits J, Felson DT, Bingham CO III, et al. 2010 rheumatoid arthritis classification criteria: an American College of Rheumatology/European League Against Rheumatism collaborative initiative. Arthritis Rheum 2010;62:2569–81.

12. Van Beers-Tas MH, Marotta A, Boers M, Maksymowych WP, van Schaardenburg D. A prospective cohort study of 14-3-3η in ACPA and/or RF-positive patients with arthralgia. Arthritis Res Ther 2016;18:76.

13. Van Beers-Tas MH, Blanken AB, Nielen MM, Turkstra F, van der Laken CJ, Reynders MM, et al. The value of joint ultrasonography in predicting arthritis in seropositive patients with arthralgia: a prospective cohort study. Arthritis Res Ther 2018;20:279.

14. Holla JF, van Beers-Tas MH, van de Stadt LA, Landewé R, Twisk JW, Dekker J, et al. Depressive mood and low social support are not associated with arthritis development in patients with seropositive arthralgia, although they predict increased musculoskeletal symptoms. RMD Open 2018;4:e000653.

15. Ainamo J, Barmes D, Beagrie G, Cutress T, Martin J, Sardo-Infirri J. Development of the World Health Organization (WHO) Community Periodontal Index of Treatment Needs (CPITN). Int Dent J 1982;32:281–91.

16. Nesse W, Abbas F, van der Ploeg I, Spijkervet FK, Dijkstra PU, Vissink A. Periodontal inflamed surface area: quantifying inflammatory burden. J Clin Periodontol 2008;35:668–73.

17. Bos WH, Wolbink GJ, Boers M, Tijhuis GJ, de Vries N, van der Horst-Bruinsma IE, et al. Arthritis development in patients with arthralgia is strongly associated with anti-citrullinated protein antibody status: a prospective cohort study. Ann Rheum Dis 2010;69:490–4.

18. Dutch Society for Rheumatology. NVR richtlijn medicamenteuze behandeling van reumatoïde artritis; 2020. URL: https://richtlijnendatabase.nl/richtlijn/reumato_de_artritis_ra/startpagina_-_reumatoide_artritis.html#tab-content-general.

19. Correa JD, Fernandes GR, Calderaro DC, Mendonca SM, Silva JM, Albiero ML, et al. Oral microbial dysbiosis linked to worsened periodontal condition in rheumatoid arthritis patients. Sci Rep 2019;9:8379.

20. Alpizar-Rodriguez D, Lesker TR, Gronow A, Gilbert B, Raemy E, Lamacchia C, et al. Prevotella copri in individuals at risk for rheumatoid arthritis. Ann Rheum Dis 2019;78:590–3.

21. Larsen JM. The immune response to Prevotella bacteria in chronic inflammatory disease [review]. Immunology 2017;151:363–74.

22. Iljazovic A, Amend L, Galvez EJ, de Oliveira R, Strowig T. Modulation of inflammatory responses by gastrointestinal Prevotella spp.: from associations to functional studies [review]. Int J Med Microbiol 2021;311:151472.

23. Zhang X, Zhang D, Jia H, Feng Q, Wang D, Liang D, et al. The oral and gut microbiomes are perturbed in rheumatoid arthritis and partly normalized after treatment. Nat Med 2015;21:895–905.

24. Beyer K, Zaura E, Brandt BW, Buijs MJ, Brun JG, Crielaard W, et al. Subgingival microbiome of rheumatoid arthritis patients in relation to their disease status and periodontal health. PLoS One 2018;13:e0202278.

25. Mankia K, Cheng Z, Do T, Hunt L, Meade J, Kang J, et al. Prevalence of periodontal disease and periodontopathic bacteria in anti-cyclic citrullinated protein antibody-positive at-risk adults without arthritis. JAMA Netw Open 2019;2:e195394.

26. Tong Y, Zheng L, Qing P, Zhao H, Li Y, Su L, et al. Oral microbiota perturbations are linked to high risk for rheumatoid arthritis. Front Cell Infect Microbiol 2019;9:475.

27. Seneviratne CJ, Balan P, Suriyanarayanan T, Lakshmanan M, Lee DY, Rho M, et al. Oral microbiome-systemic link studies: perspectives on current limitations and future artificial intelligence-based approaches. Crit Rev Microbiol 2020;46:288–99.

28. Albandar JM. Underestimation of periodontitis in NHANES surveys. J Periodontol 2011;82:337–41.

29. Zaura E, Pappalardo VY, Buijs MJ, Volgenant CM, Brandt BW. Optimizing the quality of clinical studies on oral microbiome: a practical guide for planning, performing, and reporting [review]. Periodontol 2000 2021;85:210–36.

Relationship Between Rheumatoid Arthritis and Pulmonary Function Measures on Spirometry in the UK Biobank

Lauren Prisco,[1] Matthew Moll,[2] Jiaqi Wang,[1] Brian D. Hobbs,[2] Weixing Huang,[1] Lily W. Martin,[1] Vanessa L. Kronzer,[3] ID Sicong Huang,[2] ID Edwin K. Silverman,[2] Tracy J. Doyle,[2] Michael H. Cho,[2] and Jeffrey A. Sparks[2] ID

Objective. To investigate the independent relationship of rheumatoid arthritis (RA) to the type and severity of pulmonary patterns on spirometry compared to the pulmonary patterns in general population controls.

Methods. In this cross-sectional study, we investigated the association of RA with pulmonary function measures on spirometry among subjects in the UK Biobank who underwent spirometry for research purposes. RA cases were identified based on self-report and current disease-modifying antirheumatic drug/glucocorticoid use. Controls were subjects without RA from the general population. Outcome measures included continuous forced expiratory volume in 1 second percent predicted (FEV_1%) and forced vital capacity percent predicted (FVC%), type of spirometric pattern (restrictive or obstructive), and severity of the restrictive or obstructive pattern. We used multivariable regression to estimate the effects in RA cases compared to the effects in controls, adjusting for age, sex, body mass index, and smoking status/pack-years.

Results. Among 350,776 analyzed subjects who underwent spirometry (mean age 56.3 years; 55.8% female; 45.5% ever smokers), we identified 2,008 cases of treated RA. In multivariable analyses, RA was associated with lower FEV_1% (β = –2.93 [95% confidence interval (95% CI) –3.63, –2.24]), FVC% (β = –2.08 [95% CI –2.72, –1.45]), and FEV_1/FVC (β = –0.008 [95% CI –0.010, –0.005]) compared to controls. RA was additionally associated with restrictive patterns (odds ratio [OR] 1.36 [95% CI 1.21, 1.52]) and obstructive patterns (OR 1.21 [95% CI 1.07, 1.37]) independent of confounders, and was most strongly associated with severe restrictive and obstructive patterns.

Conclusion. RA is associated with increased odds of restrictive and obstructive patterns, and this relationship is not explained by confounders, including smoking status. In addition to restrictive lung disease, clinicians should also be aware that airway obstruction may be a pulmonary manifestation of RA.

INTRODUCTION

Pulmonary manifestations of rheumatoid arthritis (RA) are associated with high morbidity and mortality (1–7). Established pulmonary manifestations of RA include restrictive processes (2,4,8,9) (such as interstitial lung disease [ILD]) and obstructive processes (3,10–13) (such as bronchiectasis). Emerging research suggests that airway diseases may be common in RA and may not be explained by smoking status (12,14).

Pulmonary function testing (PFT), often obtained using spirometry, is an important tool for broadly classifying lung diseases into restrictive or obstructive lung processes, and PFT can

also be used when screening for and monitoring pulmonary diseases (15). Previous studies have investigated the relationship between RA and restrictive or obstructive pulmonary abnormalities in RA patients compared to general population controls (9,16–18). Only one study showed an association between RA and restrictive patterns on PFT (17), and no studies demonstrated a significant association of RA with obstructive patterns (9,16,17). However, since these studies were limited by small sample sizes and a lack of detailed data on smoking (9,16,17), the relationship between RA and restrictive and obstructive pulmonary deficits independent of confounders, such as smoking status, is unclear.

We aimed to investigate the type and severity of pulmonary patterns using spirometry in a large sample of the UK Biobank by comparing RA patients to general population controls. In the UK Biobank, spirometry was performed for research purposes (not only in those with suspected or known lung disease), with detailed data available regarding potential confounders, including smoking status. We hypothesized that RA would be associated with increased risk of restrictive and obstructive patterns on spirometry.

PATIENTS AND METHODS

Study population and design. The UK Biobank is a prospective study of over 500,000 participants, ages 40–69 years. Details regarding the design of the UK Biobank study were previously reported in detail (19). Briefly, a random sample of adults was recruited between 2006 and 2010 from the NHS registry (20). Baseline visits were conducted at 22 sites across the UK. Questionnaires assessed smoking status/pack-years, as well as medical history. Study staff determined each subject's height and weight, and findings from spirometric assessment of the lung, among other measures, were noted (19). Data were also linked with electronic health records to obtain administrative information such as Read codes and medication usage. The overall UK Biobank received ethics approval from the North West Multi-centre Research Ethics Committee. All subjects provided informed consent before participation. This secondary data analysis study was approved by the Mass General Brigham Institutional Review Board.

We performed a cross-sectional analysis of the UK Biobank investigating the association of RA with pulmonary function measures on spirometry compared to that in general population controls. For this analysis, among the subjects who underwent spirometry, we only included those whose measurements, including both the continuous forced expiratory volume in 1 second (FEV_1) and the forced vital capacity (FVC), passed quality control (more details on these measures are discussed below). We also required smoking data, since this was a key covariate. A flow diagram illustrating the analyzed study sample is included in Supplementary Figure 1 (available on the *Arthritis & Rheumatology* website at http://online library.wiley.com/doi/10.1002/art.41791/abstract).

Defining RA cases and controls without RA as the primary exposure variable. The primary exposure variable was the diagnosis of RA relative to general population controls without RA. As in previous UK Biobank studies, RA cases were identified by self-report and current use of disease-modifying antirheumatic drugs (DMARDs) or systemic glucocorticoids (21,22). A previous study using a similar case definition for RA reported a positive predictive value (PPV) of 88% (22). Current DMARD use and/or glucocorticoid use was identified through electronic health records. A subset of patients with RA had rheumatoid factor (RF) tested for research purposes from donated blood in the UK Biobank. We excluded participants who self-reported RA but who did not fulfill the current definition of an RA case from the analysis. General population controls were subjects who had no self-reported history of RA.

Pulmonary function measures. Spirometry was performed for research purposes by trained respiratory therapists using the research protocol, as previously described (19). Spirometric measurements were made using a Pneumotrac 6800 Spirometer (Vitalograph). Spirometry was not performed on a small subset of participants with self-reported contraindications to spirometry (e.g., recent chest infection or myocardial infarction; recent chest, abdominal, or eye surgery; or history of a detached retina or pneumothorax). Bronchodilator medication was not administered.

FEV_1 and FVC were derived from volume–time series spirometry data, with validation by comparing the values against the acceptable range of automated spirometry values. The back-extrapolated volume was determined, allowing a volume difference of 250 ml between each of 3 consecutive spirometer blows, to determine the "best" measurement for the FEV_1 and FVC, as previously described (23). The FEV_1/FVC ratio was then calculated from the best values. The FEV_1 and FVC percent predicted values ($FEV_{1\%}$ and FVC%, respectively) were calculated with adjustments for age, sex, race, and height of the individual, as previously described (24). Among a subset of participants with acceptable forced expiratory flow, midexpiratory phase ($FEF_{25-75\%}$) measurements, we calculated the percent predicted values for $FEF_{25-75\%}$ as an additional indicator of expiratory airflow limitation and early airway obstruction (24).

Assessment of abnormal spirometric patterns as the primary outcome. The coprimary outcomes were presence of a restrictive abnormal spirometric pattern and presence of an obstructive abnormal spirometric pattern; these outcomes were considered mutually exclusive. Restrictive pattern was defined as no obstructive pattern (FEV_1/FVC ≥ 0.7) and an FVC% value less than the calculated lower limit of normal (LLN) of FVC, consistent with prior clinical and research definitions used for identifying restrictive patterns using only spirometry (25). Obstructive pattern was defined as an FEV_1/FVC ratio of <0.7, the standard cutoff point in both clinical practice and research studies (14,25,26).

Determination of continuous spirometry data and defining the level of severity of restrictive and obstructive patterns as secondary outcomes. The secondary outcomes of this study were $FEV_1\%$, FVC%, FEV_1/FVC, and $FEF_{25-75\%}$ (among the subset in which this measurement was taken), as well as the level of severity (mild, moderate, severe) of the restrictive or obstructive pattern. Severity levels for both the restrictive and obstructive patterns were defined based on the degree of FEV_1 impairment, according to standard clinical and research cutoff points (25,27,28), with mild defined as an $FEV_1\%$ of ≥70%, moderate as an $FEV_1\%$ of ≥50% to <70%, and severe as an $FEV_1\%$ of <50%. In addition, the restrictive pattern had to be associated with an FVC% less than the LLN and an FEV_1/FVC ratio of ≥0.7, while the obstructive pattern had to be associated with an FEV_1/FVC ratio of <0.7.

Identification of covariates. We considered covariates that have been associated with RA and/or pulmonary function abnormalities (29–34). Covariates were obtained at the same time that each subject in the UK Biobank underwent spirometry. Age (in years; continuous variable) and sex were sociodemographic variables. Lifestyle factors included height and weight, which were used to calculate body mass index (BMI) (in kg/m^2; continuous variable), as well as smoking status (never/past/current) and pack-years (continuous variable) by self-report. The presence of chronic respiratory illnesses (asthma, bronchiectasis, chronic obstructive pulmonary disease [COPD], ILD, and idiopathic pulmonary fibrosis [IPF]) was identified by self-report.

Statistical analysis. Descriptive statistics for baseline covariates and spirometric outcomes were reported for the subjects overall and according to RA status. We compared spirometric results in RA subjects to those in controls using t-tests for continuous variables and chi-square tests for categorical variables.

We performed a linear regression analysis to estimate β coefficients and 95% confidence intervals (95% CIs) for the continuous spirometric values stratified by RA status. General population controls were the reference group in the models. We adjusted the main multivariable models for potential confounders consisting of age, sex, smoking status and pack-years, and BMI. Additionally, we adjusted the multivariable model for history of chronic respiratory disease, since RA is known to have pulmonary manifestations (1,5). This model was considered exploratory, since development of respiratory diseases may be a causal effect that occurs between the onset of RA and development of spirometric abnormalities. We also performed separate analyses stratified by sex, history of chronic respiratory disease, and smoking status.

We performed a logistic regression analysis to estimate odds ratios (ORs) and 95% CIs for obstructive and restrictive spirometric patterns, stratified by RA status. We further adjusted the multivariable model for history of chronic respiratory disease and performed separate analyses additionally stratified by sex and history of chronic respiratory disease.

To further investigate the role of smoking and known chronic respiratory disease as they pertain to the development of RA and risk of abnormal spirometric patterns, we constructed logistic regression models stratified by smoking status (never compared to ever smokers) and known chronic respiratory disease (absence compared to presence) and tested for their interactions in relation to the development of RA and risk of spirometric abnormalities. Among the subset of patients reporting a status of ever smoker, we created an additional model adjusting for smoking status (current/past) and continuous pack-years. We also stratified the model by sex (men versus women) and tested for interactions.

For the ordinal severity analyses, we performed a multinomial ordinal regression analysis to obtain ORs and 95% CIs for the severity of restrictive or obstructive pattern spirometric abnormalities, stratified by RA status and adjusted for the same covariates as those in the model. In a separate analysis restricted to RA cases only, we compared the coprimary outcomes of restrictive patterns and obstructive patterns on spirometry between patients with RF-positive RA and patients with RF-negative RA.

Statistical significance was defined as a 2-sided P value less than 0.05. Analyses were performed using SAS 9.4 (SAS Institute).

RESULTS

Study sample characteristics. The study sample was composed of 350,776 subjects who underwent spirometry for research purposes. The demographic and clinical characteristics of the subjects at the time that spirometry was conducted are listed in Table 1. The mean ± SD age was 56.3 ± 8.1 years,

Table 1. Characteristics of the RA cases at the time of spirometry and general population controls in the UK Biobank (total n = 350,776)*

	RA cases (n = 2,008)	Controls (n = 348,768)
Age, mean ± SD years	59.1 ± 7.0	56.2 ± 8.1
Sex, female	1,453 (72.4)	194,292 (55.7)
European ancestry	1,865 (92.9)	321,285 (92.1)
Smoking		
Pack-years, mean ± SD	13.3 ± 17.0	9.7 ± 14.6
Status		
Never	911 (45.4)	190,369 (54.6)
Past	877 (43.7)	123,225 (35.3)
Current	220 (11.0)	35,174 (10.1)
BMI, mean ± SD kg/m^2	27.7 ± 5.2	27.3 ± 4.7
Any self-reported chronic respiratory disease	362 (18.0)	46,038 (13.2)
Asthma	295 (14.7)	42,398 (12.2)
COPD	81 (4.0)	4,844 (1.4)
Bronchiectasis	18 (0.9)	650 (0.2)
ILD	6 (0.3)	151 (0.04)
IPF	4 (0.2)	58 (0.02)

* Except where indicated otherwise, values are the number (%) of subjects. RA = rheumatoid arthritis; BMI = body mass index; COPD = chronic obstructive pulmonary disease; ILD = interstitial lung disease; IPF = idiopathic pulmonary fibrosis.

and 55.8% were women. We identified a total of 2,008 subjects who met the case definition of RA. Compared to general population controls, RA cases were more likely to be older, women, and ever smokers, and more likely to have a higher number of pack-years of smoking and a history of chronic respiratory disease (asthma, COPD, bronchiectasis, ILD, and IPF). Among RA cases (n = 9) whose blood was tested for RF for research purposes, 86.1% were seropositive.

Results of spirometry in RA cases compared to controls. Spirometric results (continuous variable) stratified by RA case status are shown in Table 2. A restrictive pattern was observed by spirometry in 18.1% of RA cases and 14.1% of general population controls. Obstructive patterns were found in 19.1% of RA cases and 13.8% of general population controls. Additional subgroup analyses of the spirometric results (continuous variable) are shown in Supplementary Tables 1–4 (available on the *Arthritis & Rheumatology* website at http://onlinelibrary. wiley.com/doi/10.1002/art.41791/abstract). Table 3 shows the association of the presence of RA with spirometric results (continuous variable). RA was associated with a statistically significantly lower $FEV_1\%$ (β = –2.93 [95% CI –3.63, –2.24]), FVC% (β = –2.08 [95% CI –2.72, –1.45]), FEV_1/FVC (β = –0.008 [95% CI –0.010, –0.005]), and $FEF_{25–75\%}$ (β = –4.79 [95% CI –6.08, –3.49]) as compared to that in general population controls, after adjusting for age, sex, smoking status, pack-years, and BMI.

Table 2. Spirometry results in the patients with RA compared to general population controls from the UK Biobank (total n = 350,776)*

	RA cases (n = 2,008)	Controls (n = 348,768)	P
$FEV_1\%$	87.5 ± 17.5	91.5 ± 16.3	<0.0001
FVC%	90.0 ± 15.9	93.0 ± 15.0	<0.0001
FEV_1/FVC	0.748 ± 0.072	0.761 ± 0.064	<0.0001
$FEF_{25–75\%}$†	82.3 ± 29.4	89.3 ± 29.2	<0.0001
Restrictive pattern, no. (%)‡	363 (18.1)	49,072 (14.1)	<0.0001
Mild	228 (11.4)	33,657 (9.7)	<0.0001
Moderate	122 (6.1)	14,206 (4.1)	–
Severe	13 (0.7)	1,209 (0.4)	–
Obstructive pattern, no. (%)§	383 (19.1)	48,258 (13.8)	<0.0001
Mild	127 (6.3)	21,323 (6.1)	<0.0001
Moderate	220 (11.0)	23,558 (6.8)	–
Severe	36 (1.8)	3,377 (1.0)	–

* Except where indicated otherwise, values are the mean ± SD.
† There were missing data on forced expiratory flow, midexpiratory phase ($FEF_{25–75\%}$) for 162 rheumatoid arthritis (RA) cases and 24,611 controls.
‡ A restrictive pulmonary pattern on spirometry was defined as a ratio of forced expiratory volume in 1 second percent predicted ($FEV_1\%$) to forced vital capacity percent predicted (FVC%) of ≥0.7 and an FVC% of less than the lower limit of normal. Severity categories were defined as follows: mild = FEV_1/FVC ≥0.7 and $FEV_1\%$ ≥70%; moderate = FEV_1/FVC ≥0.7 and $FEV_1\%$ ≥50% to <70%; severe = FEV_1/FVC ≥0.7 and $FEV_1\%$ <50%.
§ An obstructive pulmonary pattern on spirometry was defined as an FEV_1/FVC ratio of <0.7. Severity categories were defined as follows: mild = FEV_1/FVC <0.7 and $FEV_1\%$ ≥80%; moderate = FEV_1/FVC <0.7 and $FEV_1\%$ of ≥50% to <80%; severe = FEV_1/FVC <0.7 and $FEV_1\%$ <50%.

Table 3. Association of RA cases with specific spirometry measures compared to general population controls, based on linear regression analyses*

Spirometry result	Unadjusted model	Multivariable model†
↓ $FEV_1\%$	–4.00 (–4.72, –3.29)	–2.93 (–3.63, –2.24)
↓ FVC%	–2.91 (–3.57, –2.26)	–2.08 (–2.72, –1.45)
↓ FEV_1/FVC	–0.013 (–0.016, –0.010)	–0.008 (–0.010, –0.005)
↓ $FEF_{25–75\%}$‡	–7.02 (–8.35, –5.68)	–4.79 (–6.08, –3.49)

* Values are β coefficients (95% confidence interval) for the association between decreased values on spirometry and presence of rheumatoid arthritis (RA), among subjects in the UK Biobank (total n = 350,776). $FEV_1\%$ = forced expiratory volume in 1 second percent predicted; FVC% = forced vital capacity percent predicted.
† Adjusted for age, sex, smoking status (never/past/current), number of pack-years of smoking (continuous variable), and body mass index (continuous variable).
‡ The study sample size for the forced expiratory flow, midexpiratory phase ($FEF_{25–75\%}$) was 326,003 cases.

Type of abnormal spirometric pattern in RA cases compared to controls. The association of RA with restrictive and obstructive pulmonary patterns on spirometry is shown in Table 4. RA cases had a multivariable OR of 1.36 (95% CI 1.21, 1.53) for restrictive patterns and 1.31 (95% CI 1.16, 1.47) for obstructive patterns compared to general population controls. These associations remained after further adjusting for known chronic respiratory illness.

We assessed the impact of smoking status on the association of RA with the type of pulmonary pattern, using separate models stratified by smoking status (never or ever smokers) and known chronic respiratory disease (absence or presence) (Table 5). In each smoking status stratum, associations between RA and restrictive and obstructive patterns were still significant. Among individuals without known chronic respiratory disease, there were significant associations between RA and restrictive and obstructive patterns. There were no significant interactions between RA case status and smoking status or known chronic respiratory disease for restrictive patterns or obstructive patterns (for the interaction of case status and smoking, P = 0.88 for restrictive spirometric patterns and P = 0.76 for obstructive spirometric patterns; for the interaction of case status and known chronic respiratory disease, P = 0.40 for restrictive spirometric patterns and P = 0.84 for obstructive spirometric patterns). Among individuals with no known respiratory disease, RA cases had significantly higher odds of both restrictive patterns (OR 1.43 [95% CI 1.26, 1.62]) and obstructive patterns (OR 1.24 [95% CI 1.07, 1.43]).

We also assessed the impact of sex (male versus female) on the association of RA with the type of abnormal spirometric pattern using a stratified model. There was no interaction with sex in the association of RA with restrictive or obstructive pulmonary patterns (Supplementary Table 5, available on the *Arthritis & Rheumatology* website at http://onlinelibrary.wiley.com/doi/10.1002/

Table 4. Odds ratios (ORs) for the type of pulmonary pattern observed on spirometry in RA cases relative to general population controls*

	Restrictive pattern		Obstructive pattern	
	OR	95% CI	OR	95% CI
Unadjusted model				
RA cases	1.35	1.20, 1.51	1.47	1.31, 1.64
Controls	1.00	Referent	1.00	Referent
Multivariable model 1†				
RA cases	1.36	1.21, 1.53	1.31	1.16, 1.47
Controls	1.00	Referent	1.00	Referent
Multivariable model 2‡				
RA cases	1.36	1.21, 1.52	1.21	1.07, 1.37
Controls	1.00	Referent	1.00	Referent

* Values are ORs with 95% confidence intervals (95% CIs) for the likelihood of rheumatoid arthritis (RA) cases having a restrictive or obstructive pulmonary pattern relative to general population controls in the UK Biobank (total n = 350,776). Restrictive pattern is defined as a ratio of forced expiratory volume in 1 second (FEV_1) to forced vital capacity (FVC) of ≥0.7 and an FVC less than the lower limit of normal. Obstructive pattern is defined as an FEV_1/FVC <0.7.
† Adjusted for age, sex, smoking status (never/past/current), number of pack-years of smoking (continuous variable), and body mass index (continuous variable).
‡ Adjusted for the same variable as in model 1 and additionally adjusted for known respiratory illness.

art.41791/abstract). Additional subgroup analyses of the types of patterns are shown in Supplementary Tables 6–8.

A separate analysis was conducted among RA cases only, to analyze and compare the risk of the 2 spirometric patterns according to RF status (n = 900). Compared to RF-negative patients, those who were positive for RF had a hazard ratio (HR) of 2.30 (95% CI 1.20, 4.42) for a restrictive spirometric pattern, after multivariable adjustment. There was no association of RF-positive RA with obstructive spirometric patterns (OR 1.00 [95% CI 0.60, 1.66]) when compared to that in RF-negative RA

(Supplementary Table 9, available on the *Arthritis & Rheumatology* website at http://onlinelibrary.wiley.com/doi/10.1002/art.41791/abstract).

Severity of pulmonary patterns in RA cases compared to controls. RA was associated with significantly increased odds of having mild, moderate, or severe restrictive pulmonary patterns compared to those observed in general population controls, with ORs of 1.29 (95% CI 1.12, 1.49), 1.45 (95% CI 1.20, 1.75), and 1.86 (95% CI 1.08, 3.23),

Table 5. Odds ratios for the type of pulmonary pattern observed on spirometry in RA cases relative to general population controls according to smoking status and chronic respiratory disease status*

	Restrictive pattern		Obstructive pattern	
	RA cases	Controls	RA cases	Controls
Never smokers (n = 191,280)				
Unadjusted	1.44 (1.22, 1.70)	1.00 (referent)	1.26 (1.03, 1.53)	1.00 (referent)
Multivariable model 1†	1.43 (1.21, 1.70)	1.00 (referent)	1.28 (1.05, 1.56)	1.00 (referent)
Ever smokers (n = 159,496)				
Unadjusted	1.29 (1.10, 1.51)	1.00 (referent)	1.46 (1.27, 1.68)	1.00 (referent)
Multivariable model 1†	1.32 (1.12, 1.55)	1.00 (referent)	1.40 (1.21, 1.61)	1.00 (referent)
Multivariable model 2‡	1.29 (1.10, 1.52)	1.00 (referent)	1.31 (1.14, 1.52)	1.00 (referent)
No known chronic respiratory disease (n = 304,376)				
Unadjusted	1.40 (1.23, 1.58)	1.00 (referent)	1.38 (1.21, 1.59)	1.00 (referent)
Multivariable‡	1.43 (1.26, 1.62)	1.00 (referent)	1.24 (1.07, 1.43)	1.00 (referent)
Known chronic respiratory disease (n = 46,400)				
Unadjusted	1.11 (0.84, 1.47)	1.00 (referent)	1.36 (1.10, 1.69)	1.00 (referent)
Multivariable‡	1.08 (0.81, 1.43)	1.00 (referent)	1.16 (0.93, 1.46)	1.00 (referent)

* Values are the odds ratio (95% confidence interval) for the likelihood of rheumatoid arthritis (RA) cases having a restrictive or obstructive pulmonary pattern relative to general population controls in the UK Biobank (total n = 350,776). Restrictive pattern is defined as a ratio of forced expiratory volume in 1 second (FEV_1) to forced vital capacity (FVC) of ≥0.7 and an FVC less than the lower limit of normal. Obstructive pattern is defined as an FEV_1/FVC <0.7. There was no statistically significant interaction for any of the subgroups examined for both outcomes (*P* > 0.05).
† Adjusted for age, sex, and body mass index (continuous variable).
‡ Adjusted for age, sex, smoking status (current or past), number of pack-years of smoking (continuous variable), and body mass index (continuous variable).
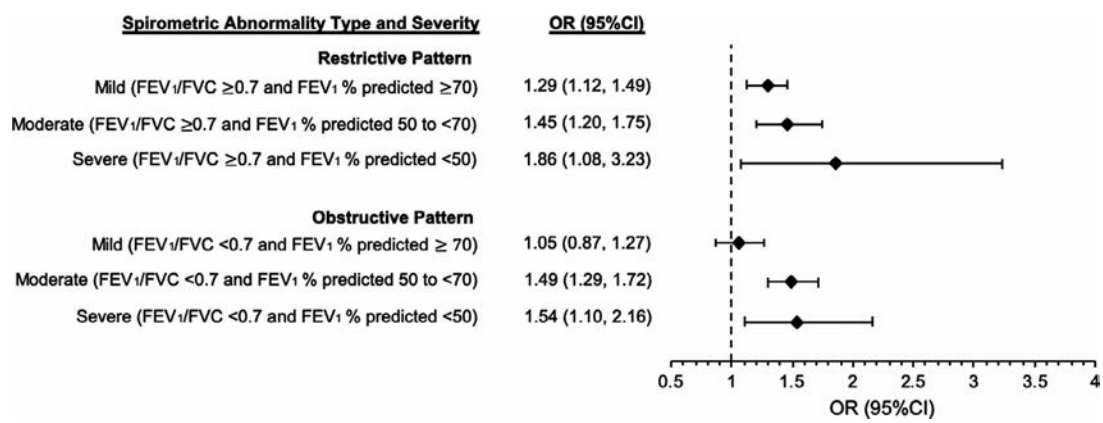
Figure 1. Multivariable odds ratios (ORs) for type and severity of pulmonary patterns on spirometry. The odds of having a mild, moderate, or severe restrictive or obstructive pulmonary pattern were assessed in cases with rheumatoid arthritis relative to general population controls in the UK Biobank (n = 350,776), adjusting for age, sex, smoking status (never/past/current), number of pack-years of smoking (continuous variable), and body mass index (continuous variable). 95% CI = 95% confidence interval; FEV_1% = forced expiratory volume in 1 second percent predicted; FVC% = forced vital capacity percent predicted.

respectively (Figure 1). Furthermore, among patients with RA, the odds of having a moderate obstructive pulmonary pattern and severe obstructive pulmonary pattern were increased (ORs of 1.49 [95% CI 1.29, 1.72] and 1.54 [95% CI 1.10, 2.16], respectively, relative to general population controls).

DISCUSSION

In this large study of over 350,000 subjects who underwent spirometry for research purposes, we found that RA was strongly associated with increased odds of both restrictive and obstructive pulmonary patterns on spirometry. We showed that RA was associated with 36% increased odds of a restrictive pulmonary pattern and 21% increased odds of an obstructive pulmonary pattern, with the most marked risk of severe patterns. These results were not explained by possible confounding due to smoking status, age, sex, or BMI. Our findings suggest that, in addition to restrictive lung diseases such as RA-associated ILD (RA-ILD), obstructive lung diseases may be an important pulmonary manifestation of RA, even in never smokers. Moreover, we found that RA cases without a history of known chronic respiratory disease had a higher risk of restrictive and obstructive spirometric patterns, suggesting that our findings are not explained by higher rates of known underlying lung disease among RA patients. These findings, rather, suggest that the abnormalities observed on spirometry may be related to the pathogenesis of RA, since obstructive lung diseases, including COPD and asthma, are highly associated with an increased risk of developing RA (35). Moreover, either the RA disease process or its treatment may affect the thorax, lung parenchyma, and airways. However, it is important to note that smoking still contributes to pulmonary diseases and dysfunction in RA, since mucosal inflammation may produce RA-related autoantibodies prior to clinical RA onset (36,37).

Prior studies investigated the relationship between the prevalence of RA and the physiologic and functional features of the lungs (16–18). One prospective study of 25 RA patients and 21 healthy controls found that RA patients had relatively normal spirometric results but had reduced aerobic capacity and respiratory muscle strength and endurance compared to that of controls (16). However, researchers were not able to adjust these results for important confounders, such as age, sex, and smoking status and were limited by sample size (16). In contrast, our study was able to demonstrate a statistically significant association between RA and reduced lung function compared to general population controls, even after adjusting for confounders. While our study evaluated the relationship between prevalent RA and pulmonary function, a large Swedish nested case–control study found no association between a restrictive or obstructive spirometric pattern and subsequent incident RA (9).

RA is known to be associated with restrictive lung diseases, such as RA-ILD (2,4,8,9). A prospective cross-sectional study of 155 RA patients and 95 controls found that RA patients were more likely to have PFT abnormalities suggestive of restriction (e.g., reduced FVC and total lung capacity) (17). However, after stratifying patients by smoking status, this association remained only among current smokers. Unlike previous studies, we had detailed covariate data, including smoking status and pack-years, and were able to perform adjusted and stratified multivariable analyses to investigate the independent relationship between prevalent RA and pulmonary function abnormalities and were able to estimate the strength of the association between RA and restrictive pulmonary patterns on spirometry.

Emerging research suggests an association between RA and obstructive lung disease not explained by smoking (36,38–40). However, results of previous studies were inconsistent with regard to the presence and severity of lung obstruction in patients with RA (3,6,10–12,16). A longitudinal study of 594 RA patients and 596 controls demonstrated that RA was associated with

an increased risk of developing incident clinical obstructive lung disease (HR 1.54 [95% CI 1.01, 2.34]) (3) during lengthy clinical follow-up, but not all patients had PFT measures, since clinical data were used. Another prospective study of 100 RA patients and 88 patients with other types of systemic rheumatic diseases found that obstructive lung disease was more frequent among RA patients compared to controls with other types of systemic rheumatic diseases (12). These studies provide support for our finding that prevalent RA is associated with increased odds of an obstructive spirometric pattern, with the most marked risk of a severe obstructive pattern.

Clinically detected forms of RA-ILD and other RA-related lung diseases are generally thought to be relatively uncommon, though emerging research shows that subclinical forms may be common (7,18,41). Inflammation at mucosal surfaces, including the lungs, may produce anti–citrullinated protein antibodies (ACPAs) prior to onset of clinical RA (36,37). A prospective study of 48 ACPA-positive subjects (21 without arthritis, 10 with early RA, and 17 with longstanding RA) who underwent PFTs, cardiopulmonary exercise testing, and high-resolution computed tomography showed that subclinical lung abnormalities occur early in RA pathogenesis (18). $FEF_{25-75\%}$ is an early marker of obstruction (42–45). Previous studies have shown a statistically significant association between RA and reduced $FEF_{25-75\%}$, suggesting that obstruction may be common in RA (10,46). Similarly, we found that RA was associated with a 4.79% lower $FEF_{25-75\%}$ value compared to that of controls after multivariable adjustment, suggesting that small airway narrowing and early airway obstruction may be clinically detectable in RA patients. Prior studies have also demonstrated an association between seropositivity for both RF and ACPA in RA-related pulmonary diseases independent of smoking status (14,47). A cross-sectional study of 1,272 RA patients who had PFTs performed for clinical purposes demonstrated that patients with seropositive RA had a 2-fold increased risk of PFT abnormalities compared to those with seronegative RA (14). Further research is needed to elucidate how the RA disease process and/or treatments may affect lung parenchyma and airways.

Strengths of our study include the large sample size and generalizability to the UK population, along with access to both research data and electronic health record data. While our study sample was large, many participants of the UK Biobank were excluded, mostly due to not undergoing spirometry. Among the entire UK Biobank data set, 0.57% of patents fulfilled the definition of an RA case compared to 0.61% of patients in our analyzed sample. The distribution of women in the UK Biobank at the time of our study was 54.2% (26), which is similar to the distribution of women in the control group in our study (55.7%). The mean age of the subjects in the entire UK Biobank at the time of our study was 56.5 years (26), which is similar to the mean age of 56.2 years in the control group in our study. Therefore, we find it unlikely that a selection bias related to obtaining spirometry and RA case status could explain our results. All analyzed subjects underwent spirometry performed by trained respiratory therapists using a standard research protocol. Using spirometry allowed us to assess for pulmonary abnormalities, and the association of RA with abnormal spirometric patterns remained among the subset without known chronic respiratory diseases. We also had access to detailed covariate data, including smoking status and pack-years, as well as BMI and self-reported history of chronic respiratory disease.

Our study also has some limitations. Our definition of RA was based on self-report of RA and current treatment with RA-specific medications. Self-report may be prone to misclassification, so we additionally required disclosure of current treatment, which has acceptable validity (PPV 88%) (22). To further limit this possibility, one of our inclusion criteria for controls was requiring that subjects have no reported history of RA, which allowed us to lower the possibility that some of the controls potentially had ambiguous RA or untreated RA, but it is possible that some of the control subjects had unrecognized RA. However, misclassification of the exposure status would be expected to bias results toward the null, so it would not explain our findings. In our study, the prevalence of RA was 0.61%, consistent with the results of two recent meta-analyses (48,49). Moreover, 84% of the RA cases in the UK Biobank that we analyzed were patients who were seropositive for RF and whose demographic characteristics were consistent with those typically observed in studies of RA patients. Among RA patients, 86% were RF-positive, which is higher than what was typically observed in previous RA studies (14).

While this further demonstrates the validity of our definition of an RA case, there were relatively few cases of RF-negative RA. We were limited in our ability to compare RF-positive RA cases to RF-negative RA cases, and our results may be most applicable to patients with seropositive RA. While we recorded spirometric measures in a large sample size using a research protocol with detailed quality control, we did not have complete PFT measures (such as lung volume or diffusing capacity for carbon monoxide) which would be necessary to definitively diagnose the presence of a restrictive lung disease or to identify those with a mixed pattern. Therefore, it is possible that some patients classified as having an obstructive pattern may also have a restrictive pattern. Moreover, restrictive lung diseases, such as ILD, are a well-described RA complication, and spirometry is the clinical standard to identify patients with obstructive lung disease. We were not able to analyze spirometry results in patients after they had received bronchodilator treatment, which would have been helpful to assess for reversible airway obstruction in individuals with obstructive pulmonary deficits. We did not have data concerning pulmonary symptoms or previous infections or RA characteristics, such as disease activity, serostatus, medication history, or severity or duration of articular symptoms. In a subset of patients, blood samples were tested for RF for research purposes, but ACPAs were not measured. Additionally, other inhalants, such as passive smoking, air pollution, or electronic cigarette use, were not included as study variables and may have impacted results. After

excluding spirometric measures that did not pass quality control, our sample consisted mostly of individuals with European ancestry, so results may not be generalizable to more diverse populations.

Our study was cross-sectional, and data were collected between 2006 and 2010. We did not have access to records of the entire history of RA treatment that patients may have received, and these could have affected lung health. Therefore, we were unable to investigate the impact of specific RA medications on spirometric abnormalities. Since the landscape of RA treatments has changed over time, there may be temporal influences that we could not address within the timeframe of our current study, but which could potentially be addressed in future longitudinal studies assessing the impact of specific RA medications on lung health.

In conclusion, we found that RA was associated with increased odds of having a restrictive and/or obstructive pulmonary pattern evident on spirometry. These associations were most marked for severe patterns and were not explained by smoking. These results suggest that RA may be associated with obstructive lung disease in addition to the previously known association of RA with restrictive lung disease. Clinicians should be aware that both restrictive and obstructive spirometric abnormalities are more common in RA patients and do not appear to be attributable to a history of smoking.

ACKNOWLEDGMENTS

AUTHOR CONTRIBUTIONS

All authors were involved in drafting the article or revising it critically for important intellectual contact, and all authors approved the final version to be published. Dr. Sparks had full access to all of the data in the study and takes responsibility for the integrity of the data and the accuracy of the data analysis.
Study conception and design. Sparks.
Acquisition of data. Moll, Hobbs, Cho, Sparks.
Analysis and interpretation of data. Prisco, Moll, Wang, Hobbs, W. Huang, Martin, Kronzer, S. Huang, Silverman, Doyle, Cho, Sparks.

REFERENCES

1. England BR, Sayles H, Michaud K, Caplan L, Davis LA, Cannon GW, et al. Cause-specific mortality in male US veterans with rheumatoid arthritis. Arthritis Care Res (Hoboken) 2016;68:36–45.

2. Hyldgaard C, Hilberg O, Pedersen AB, Ulrichsen SP, Lokke A, Bendstrup E, et al. A population-based cohort study of rheumatoid arthritis-associated interstitial lung disease: comorbidity and mortality. Ann Rheum Dis 2017;76:1700–6.

3. Nannini C, Medina-Velasquez YF, Achenbach SJ, Crowson CS, Ryu JH, Vassallo R, et al. Incidence and mortality of obstructive lung disease in rheumatoid arthritis: a population-based study. Arthritis Care Res (Hoboken) 2013;65:1243–50.

4. Doyle TJ, Dellaripa PF, Batra K, Frits ML, Iannaccone CK, Hatabu H, et al. Functional impact of a spectrum of interstitial lung abnormalities in rheumatoid arthritis. Chest 2014;146:41–50.

5. Sparks JA, Chang SC, Liao KP, Lu B, Fine AR, Solomon DH, et al. Rheumatoid arthritis and mortality among women during 36 years

6. Pappas DA, Giles JT, Connors G, Lechtzin N, Bathon JM, Danoff SK. Respiratory symptoms and disease characteristics as predictors of pulmonary function abnormalities in patients with rheumatoid arthritis: an observational cohort study. Arthritis Res Ther 2010;12:R104.

7. Sparks JA, Jin Y, Cho SK, Vine S, Desai R, Doyle TJ, et al. Prevalence, incidence, and cause-specific mortality of rheumatoid arthritis-associated interstitial lung disease among older rheumatoid arthritis patients. Rheumatology (Oxford) 2021;60:3689–98.

8. Raimundo K, Solomon JJ, Olson AL, Kong AM, Cole AL, Fischer A, et al. Rheumatoid arthritis-interstitial lung disease in the United States: prevalence, incidence, and healthcare costs and mortality. J Rheumatol 2019;46:360–9.

9. Bergstrom U, Jacobsson LT, Nilsson JA, Berglund G, Turesson C. Pulmonary dysfunction, smoking, socioeconomic status and the risk of developing rheumatoid arthritis. Rheumatology (Oxford) 2011;50:2005–13.

10. Geddes DM, Webley M, Emerson PA. Airways obstruction in rheumatoid arthritis. Ann Rheum Dis 1979;38:222–5.

11. Collins RL, Turner RA, Johnson AM, Whitley NO, McLean RL. Obstructive pulmonary disease in rheumatoid arthritis. Arthritis Rheum 1976;19:623–8.

12. Vergnenegre A, Pugnere N, Antonini MT, Arnaud M, Melloni B, Treves R, et al. Airway obstruction and rheumatoid arthritis. Eur Respir J 1997;10:1072–8.

13. Halbert RJ, Isonaka S, George D, Iqbal A. Interpreting COPD prevalence estimates: what is the true burden of disease? Chest 2003;123:1684–92.

14. Huang S, He X, Doyle TJ, Zaccardelli A, Marshall AA, Friedlander HM, et al. Association of rheumatoid arthritis-related autoantibodies with pulmonary function test abnormalities in a rheumatoid arthritis registry. Clin Rheumatol 2019;38:3401–12.

15. Ciancio N, Pavone M, Torrisi SE, Vancheri A, Sambataro D, Palmucci S, et al. Contribution of pulmonary function tests (PFTs) to the diagnosis and follow up of connective tissue diseases [review]. Multidiscip Respir Med 2019;14:17.

16. Cimen B, Deviren SD, Yorgancloğlu ZR. Pulmonary function tests, aerobic capacity, respiratory muscle strength and endurance of patients with rheumatoid arthritis. Clin Rheumatol 2001;20:168–73.

17. Hyland RH, Gordon DA, Broder I, Davies GM, Russell ML, Hutcheon MA, et al. A systematic controlled study of pulmonary abnormalities in rheumatoid arthritis. J Rheumatol 1983;10:395–405.

18. Lucchino B, Di Paolo M, Gioia C, Vomero M, Diacinti D, Mollica C, et al. Identification of subclinical lung involvement in ACPA-positive subjects through functional assessment and serum biomarkers. Int J Mol Sci 2020;21:5162.

19. UK Biobank. UK Biobank: protocol for a large-scale prospective epidemiological resource. March 2007. URL: https://www.ukbiobank.ac.uk/media/gnkeyh2q/study-rationale.pdf.

20. Allen N, Downey P, Peakman T, Danesh J, Elliott P, Gallacher J, et al. UK Biobank: current status and what it means for epidemiology. Health Policy Technol 2012;1:123–6.

21. Siebert S, Lyall DM, Mackay DF, Porter D, McInnes IB, Sattar N, et al. Characteristics of rheumatoid arthritis and its association with major comorbid conditions: cross-sectional study of 502 649 UK Biobank participants. RMD Open 2016;2:e000267.

22. McQueenie R, Nicholl BI, Jani BD, Canning J, Macdonald S, McCowan C, et al. Patterns of multimorbidity and their effects on adverse outcomes in rheumatoid arthritis: a study of 5658 UK Biobank participants. BMJ Open 2020;10:e038829.

23. Shrine N, Guyatt AL, Erzurumluoglu AM, Jackson VE, Hobbs BD, Melbourne CA, et al. New genetic signals for lung function highlight pathways and chronic obstructive pulmonary disease associations across multiple ancestries. Nat Genet 2019;51:481–93.

24. Hankinson JL, Odencrantz JR, Fedan KB. Spirometric reference values from a sample of the general US population. Am J Respir Crit Care Med 1999;159:179–87.

25. Pellegrino R, Viegi G, Brusasco V, Crapo RO, Burgos F, Casaburi R, et al. Interpretative strategies for lung function tests. Eur Respir J 2005;26:948–68.

26. Johnson JD, Theurer WM. A stepwise approach to the interpretation of pulmonary function tests. Am Fam Physician 2014;89:359–66.

27. Dempsey TM, Scanlon PD. Pulmonary function tests for the generalist: a brief review. Mayo Clin Proc 2018;93:763–71.

28. Vogelmeier CF, Criner GJ, Martinez FJ, Anzueto A, Barnes PJ, Bourbeau J, et al. Global strategy for the diagnosis, management, and prevention of chronic obstructive lung disease 2017 report: GOLD executive summary. Arch Bronconeumol 2017;53:128–49.

29. Sparks JA, Karlson EW. The roles of cigarette smoking and the lung in the transitions between phases of preclinical rheumatoid arthritis [review]. Curr Rheumatol Rep 2016;18:15.

30. Marchand NE, Sparks JA, Tedeschi SK, Malspeis S, Costenbader KH, Karlson EW, et al. Abdominal obesity in comparison with general obesity and risk of developing rheumatoid arthritis in women. J Rheumatol 2021;48:165–73.

31. Xiao D, Chen Z, Wu S, Huang K, Xu J, Yang L, et al. Prevalence and risk factors of small airway dysfunction, and association with smoking, in China: findings from a national cross-sectional study. Lancet Respir Med 2020;8:1081–93.

32. Fletcher C, Peto R. The natural history of chronic airflow obstruction. Br Med J 1977;1:1645–8.

33. Costa D, Barbalho MC, Miguel GP, Forti EM, Azevedo JL. The impact of obesity on pulmonary function in adult women. Clinics (Sao Paulo) 2008;63:719–24.

34. Melo LC, Silva MA, Calles AC. Obesity and lung function: a systematic review. Einstein (Sao Paulo) 2014;12:120–5.

35. Kronzer VL, Westerlind H, Alfredsson L, Crowson CS, Nyberg F, Tornling G, et al. Respiratory diseases as risk factors for seropositive and seronegative rheumatoid arthritis and in relation to smoking. Arthritis Rheumatol 2021;73:61–8.

36. Zaccardelli A, Liu X, Ford JA, Cui J, Lu B, Chu SH, et al. Elevated anti–citrullinated protein antibodies prior to rheumatoid arthritis diagnosis and risks for chronic obstructive pulmonary disease or asthma. Arthritis Care Res (Hoboken) 2021;73:498–509.

37. Perry E, Kelly C, Eggleton P, De Soyza A, Hutchinson D. The lung in ACPA-positive rheumatoid arthritis: an initiating site of injury? [review]. Rheumatology (Oxford) 2014;53:1940–50.

38. Ford JA, Liu X, Chu SH, Lu B, Cho MH, Silverman EK, et al. Asthma, chronic obstructive pulmonary disease, and subsequent risk for incident rheumatoid arthritis among women: a prospective cohort study. Arthritis Rheumatol 2020;72:704–13.

39. Friedlander HM, Ford JA, Zaccardelli A, Terrio AV, Cho MH, Sparks JA. Obstructive lung diseases and risk of rheumatoid arthritis [review]. Expert Rev Clin Immunol 2020;16:37–50.

40. Sparks JA, Lin TC, Camargo CA Jr, Barbhaiya M, Tedeschi SK, Costenbader KH, et al. Rheumatoid arthritis and risk of chronic obstructive pulmonary disease or asthma among women: a marginal structural model analysis in the Nurses' Health Study. Semin Arthritis Rheum 2018;47:639–48.

41. Robles-Perez A, Luburich P, Bolivar S, Dorca J, Nolla JM, Molina-Molina M, et al. A prospective study of lung disease in a cohort of early rheumatoid arthritis patients. Sci Rep 2020;10:15640.

42. Ciprandi G, Cirillo I, Klersy C, Marseglia GL, Vizzaccaro A, Pallestrini E, et al. Role of FEF25-75 as an early marker of bronchial impairment in patients with seasonal allergic rhinitis. Am J Rhinol 2006;20:641–7.

43. Kwon DS, Choi YJ, Kim TH, Byun MK, Cho JH, Kim HJ, et al. FEF25-75% values in patients with normal lung function can predict the development of chronic obstructive pulmonary disease. Int J Chron Obstruct Pulmon Dis 2020;15:2913–21.

44. Patterson GM, Wilson S, Whang JL, Harvey J, Agacki K, Patel H, et al. Physiologic definitions of obliterative bronchiolitis in heart-lung and double lung transplantation: a comparison of the forced expiratory flow between 25% and 75% of the forced vital capacity and forced expiratory volume in one second. J Heart Lung Transplant 1996;15:175–81.

45. Malerba M, Radaeli A, Olivini A, Damiani G, Ragnoli B, Sorbello V, et al. Association of FEF25-75% impairment with bronchial hyperresponsiveness and airway inflammation in subjects with asthma-like symptoms. Respiration 2016;91:206–14.

46. Chung MH, Lee HG, Kwon SS, Park SH, Kim KJ, Jung JI, et al. Airway obstruction in rheumatoid arthritis: CT manifestations, correlated with pulmonary function testing. Yonsei Med J 2004;45:443–52.

47. Zhu J, Zhou Y, Chen X, Li J. A metaanalysis of the increased risk of rheumatoid arthritis-related pulmonary disease as a result of serum anticitrullinated protein antibody positivity. J Rheumatol 2014;41:1282–9.

48. Almutairi K, Nossent J, Preen D, Keen H, Inderjeeth C. The global prevalence of rheumatoid arthritis: a meta-analysis based on a systematic review. Rheumatol Int 2021;41:863–77.

49. Almutairi KB, Nossent JC, Preen DB, Keen HI, Inderjeeth CA. The prevalence of rheumatoid arthritis: a systematic review of population-based studies. J Rheumatol 2021;48:669–76.

AMERICAN COLLEGE
of RHEUMATOLOGY
Empowering Rheumatology Professionals

Interleukin-34 Reprograms Glycolytic and Osteoclastic Rheumatoid Arthritis Macrophages via Syndecan 1 and Macrophage Colony-Stimulating Factor Receptor

Katrien Van Raemdonck,[1] Sadiq Umar,[1] Karol Palasiewicz,[1] Michael V. Volin,[2] Hatem A. Elshabrawy,[3] Bianca Romay,[4] Chandana Tetali,[4] Azam Ahmed,[4] (iD) M. Asif Amin,[5] Ryan K. Zomorrodi,[4] Nadera Sweiss,[4] and Shiva Shahrara[1] (iD)

Objective. In rheumatoid arthritis (RA), elevated serum interleukin-34 (IL-34) levels are linked with increased disease severity. IL-34 binds to 2 receptors, macrophage colony-stimulating factor receptor (M-CSFR) and syndecan 1, which are coexpressed in RA macrophages. Expression of both IL-34 and syndecan 1 is strikingly elevated in the RA synovium, yet their mechanisms of action remain undefined. This study was undertaken to investigate the mechanism of action of IL-34 in RA.

Methods. To characterize the significance of IL-34 in immunometabolism, its mechanism of action was elucidated in joint macrophages, fibroblasts, and T effector cells using RA and preclinical models.

Results. Intriguingly, syndecan 1 activated IL-34–induced M-CSFR phosphorylation and reprogrammed RA naive cells into distinctive CD14+CD86+GLUT1+ M34 macrophages that expressed elevated levels of IL-1β, CXCL8, and CCL2. In murine M34 macrophages, the inflammatory phenotype was accompanied by potentiated glycolytic activity, exhibited by transcriptional up-regulation of GLUT1, c-Myc, and hypoxia-inducible factor 1α (HIF-1α) and amplified pyruvate and L-lactate secretion. Local expression of IL-34 provoked arthritis by expanding the glycolytic F4/80-positive, inducible nitric oxide synthase (iNOS)–positive macrophage population, which in turn attracted fibroblasts and polarized Th1/Th17 cells. The cross-talk between murine M34 macrophages and Th1/Th17 cells broadened the inflammatory and metabolic phenotypes, resulting in the expansion of IL-34 pathogenicity. Consequently, IL-34–instigated joint inflammation was alleviated in RAG$^{-/-}$ mice compared to wild-type mice. Syndecan 1 deficiency attenuated IL-34–induced arthritis by interfering with joint glycolytic M34 macrophage and osteoclast remodeling. Similarly, inhibition of glycolysis by 2-deoxy-D-glucose reversed the joint swelling and metabolic rewiring triggered by IL-34 via HIF-1α and c-Myc induction.

Conclusion. IL-34 is a novel endogenous factor that remodels hypermetabolic M34 macrophages and facilitates their cross-regulation with T effector cells to advance inflammatory bone destruction in RA.

INTRODUCTION

Rheumatoid arthritis (RA) is an autoimmune disorder characterized by an abundance of inflammatory cytokines, propagating immune cell infiltration, painful joint swelling, and late-stage cartilage and bone erosion (1). Macrophages contribute substantially to this cytokine-rich inflammatory milieu

(2). Independent of the underlying cause of RA, activated macrophages are highly involved in pannus remodeling and radiologic progression (3,4). RA standard of care therapies primarily target tumor necrosis factor (TNF) and interleukin-6 (IL-6) function; however, up to 50% of patients either do not respond or lose their responsiveness to these therapies over time.

Earlier studies have shown that RA naive CD4+ T cells undergo a distinct metabolic reconfiguration, shifting from glucose metabolism to the pentose phosphate pathway, which supports a biased Th1/Th17 polarization (5,6). RA fibroblasts activated with platelet-derived growth factor (PDGF) or TNF can increase glucose metabolism via glycolysis and oxidative phosphorylation (7–9). Studies in cancer, atherosclerosis, and obesity have revealed that polarization of classically activated (M1) macrophages promotes metabolic reprogramming toward glycolysis and away from oxidative phosphorylation (10,11). Recent reports elucidated that hypermetabolic ATP[high]ROS[high] macrophages are characterized by hyperglycolysis, which is linked to the expansion of glucose transporters and glycolytic enzymes (12,13). Yet, the endogenous factors and the mechanism by which RA macrophages are reprogrammed remain unclear.

Recently, IL-34 has gained interest as a novel biomarker for RA (14). Serum levels of IL-34 correlate with several RA markers, including C-reactive protein level, erythrocyte sedimentation rate, rheumatoid factor, and anti–cyclic citrullinated peptide antibody level (15). A correlation was also found between synovial IL-34 expression and the accumulation of leukocytes in RA synovial fluid (SF) (14). Additionally, IL-34 expression and function have been implicated in other diseases, such as breast and lung cancer, liver fibrosis, type 2 diabetes mellitus, and cardiovascular dysfunction (16,17). The mechanism of action of IL-34 has predominantly been attributed to macrophage colony-stimulating factor receptor (M-CSFR), a receptor shared with M-CSF. M-CSF binding to M-CSFR cultivates immunosuppressive alternatively activated (M2) macrophages (18,19). In contrast, the impact of IL-34 on the macrophage profile remains unresolved. Conflicting reports support either an inflammatory (20) or an immunosuppressive (21,22) phenotype for IL-34–differentiated (M34) macrophages. This controversy carries over to the indirect effect of IL-34 on T effector cell polarization. IL-34 has been reported to stimulate Th17 cell polarization, via IL-1α and IL-6, thereby aggravating autoimmune RA pathogenesis (15,20,23). In contrast, others have demonstrated that the immunoregulatory macrophages polarized by IL-34 promote transplant tolerance by expanding the FoxP3+ Treg cell population (24).

Interestingly, syndecan 1, a heparan sulfate proteoglycan that functions as a co-receptor of M-CSFR, modulates the biologic activity of IL-34 (25). Since M-CSF does not bind to syndecan 1, its involvement could account for a distinct pathway that is unique to IL-34–mediated pathology. Although an extensive number of studies have shown that syndecan 1 potentiates tumorigenesis by regulating cancer cell invasion, survival, and metastasis (26,27), its pathogenic role in RA is undetermined.

We investigated the arthritogenic potential of IL-34 and syndecan 1 and their impact on RA immunometabolism. It was observed that in RA macrophages, syndecan 1 triggers M-CSFR phosphorylation upon IL-34 binding. IL-34 rewired naive cells into glycolytic CD14+CD86+GLUT1+ M34 macrophages,

which were disrupted by M-CSFR or syndecan 1 blockade. In SDC-1^{−/−} and RAG^{−/−} mice, dysregulation of the reprogramming of M34 macrophages and their deficient cross-talk with Th1/Th17 cells reversed IL-34–elicited joint inflammation and osteoclast formation. Furthermore, 2-deoxy-D-glucose (2-DG) therapy confirmed that M34 macrophage metabolic remodeling via hypoxia-inducible factor 1α (HIF-1α) and c-Myc may be indispensable for IL-34–induced arthritis. In short, restricting the function of IL-34 or its co-receptors may provide a promising therapeutic strategy for RA patients.

MATERIALS AND METHODS

Patient samples. Peripheral blood and SF samples were collected according to our protocol approved by The University of Illinois at Chicago Institutional Ethics Review Board. Normal subjects, patients with osteoarthritis (OA), and patients with RA participated in this study after providing informed consent. RA patients were diagnosed according to the American College of Rheumatology 1987 revised criteria (28). Human peripheral blood mononuclear cells were isolated by density-gradient centrifugation using Ficoll-Paque Premium. Monocytes were negatively selected using an EasySep human monocyte enrichment kit (StemCell Technologies) according to the manufacturer's instructions. Monocytes were cultured in 20% fetal bovine serum (FBS)/RPMI for 2–3 days to obtain in vitro differentiated naive macrophages. RA fibroblast-like synoviocytes (FLS) were isolated from fresh RA synovial tissue (ST) digested with Dispase/Collagenase/DNase, as previously described (29,30). More detail about the study design, methods, and the antibodies used for flow cytometry, immunohistochemistry, and Western blotting are provided in the Supplementary Methods, available on the *Arthritis & Rheumatology* website at http://onlinelibrary.wiley.com/doi/10.1002/art.41792/abstract.

Western blot analysis. Cell lysates from in vitro differentiated macrophages, peripheral blood T cells, or RA FLS were probed for syndecan 1 and M-CSFR to validate receptor expression. Actin was detected to confirm equal loading. Blots were probed for phosphorylated signaling molecules or activated phosphorylated M-CSFR (Y723) compared to either actin or GAPDH.

Flow cytometric analysis. Negatively selected monocytes were differentiated in vitro and stimulated with IL-34 (300 ng/ml) or left untreated (control) for 24 hours before staining with fluorescein isothiocyanate–conjugated CD14, allophycocyanin-conjugated CD86, and phycoerythrin (PE)–Cy7–conjugated CD206 antibodies or DAPI. Viable (DAPI-negative) cells were analyzed for double-positive CD14+CD86+, CD14+CD206+, and CD14+GLUT1+ populations. Untreated, viable (DAPI-negative) RA FLS were stained with PE-conjugated protein tyrosine phosphatase receptor type Z1 (PTPRZ1) antibody to determine baseline PTPRZ1 surface expression. Antibody concentrations

are indicated in Supplementary Table 1, available on the *Arthritis & Rheumatology* website at http://onlinelibrary.wiley.com/doi/10.1002/art.41792/abstract. Supplementary Figure 1, available on the *Arthritis & Rheumatology* website at http://onlinelibrary. wiley.com/doi/10.1002/art.41792/abstract, shows the gating strategy used.

Seahorse cell energy phenotype test. Glycolytic capacity (extracellular acidification rate [ECAR]) and oxygen consumption (oxygen consumption rate [OCR]) were measured using a Seahorse XF Cell Energy Phenotype Test kit (Agilent Technologies), according to the manufacturer's instructions, in RAW 264.7 cells (5×10^3 cells/well) treated with control (phosphate buffered saline [PBS]) or IL-34. Cells were preconditioned with the stimuli in 0% FBS/Dulbecco's modified Eagle's medium for 24 hours before ECAR and OCR assessment.

Osteoclastogenesis assay. Osteoclastogenesis was evaluated following the previously described protocol (31). Bone marrow (BM)–derived myeloid precursors (4 days of culture with M-CSF) cultured in 10% FBS/α-minimum essential medium were either left untreated (control) or conditioned with suboptimal levels of RANKL/M-CSF (both 15 ng/ml), with or without IL-34 (300 ng/ml). Stimulation media was refreshed 2 times per week for 2 weeks and tartrate-resistant acid phosphatase (TRAP)–positive osteoclasts were stained (387A-1KT; Sigma-Aldrich).

Animals. All animal studies were approved by The University of Illinois at Chicago Animal Care and Use Committee. Wild-type (WT) and RAG1$^{-/-}$ (RAG$^{-/-}$) C57BL/6 mice were purchased from The Jackson Laboratory. SDC-1$^{-/-}$ mice were generated as previously described (26) and kindly provided by Dr. Caroline Alexander (University of Wisconsin–Madison). Mice (ages 8 weeks or older) were given intraarticular (IA) injections of control adenovirus (Ad-Control) or Ad-IL-34 (3×10^{10} viral particles/ankle), on days 0, 7, and 14. Mice treated with 2-DG were injected intraperitoneally with 7.5 mg/kg body weight 2-DG on days 0, 3, 7, 9, 11, 14, and 15. Mice were euthanized on different days as specified in the figure legends.

Immunohistochemistry. Formalin-fixed, paraffin-embedded human tissue samples were sectioned. Normal, OA, and RA ST samples were stained to quantify IL-34, M-CSFR, syndecan 1, and PTPRZ1 presentation. Staining was scored on a scale of 0–5 in a blinded manner, and distinguished within the synovial lining, sublining, and vasculature (29,32). Formalin-fixed mouse ankles were decalcified and paraffin-embedded. Slides were deparaffinized in xylene, and antigen retrieval was achieved as previously described (33). Mouse ankle sections were stained for macrophage markers (F4/80, inducible nitric oxide synthase [iNOS], and arginase 1), T cell marker (CD3), and fibroblast marker (vimentin), or for the transcription factors c-Myc and HIF-1α. Supplementary

Table 1 specifies the antibodies used and their dilutions. The stained joint tissues were scored on a scale of 0–5 for inflammation, synovial lining thickness, and bone erosion (29,32).

Statistical analysis. GraphPad Prism software version 8 was used to generate figures and to perform statistical analysis. Bar graphs show the mean ± SEM. Box plots were used to visualize data distribution, from minimum to maximum with a center line showing the median. Where appropriate, individual data points are shown. Analysis of variance was first used to verify statistical significance when comparing multiple groups. Differences between the 2 groups were evaluated by an unpaired 2-tailed *t*-test unless otherwise specified.

RESULTS

Elevated expression of IL-34 and syndecan 1 in RA synovium. Experiments were conducted to characterize the expression and functional significance of IL-34 and its receptors in RA. Levels of IL-34, M-CSF, and granulocyte–macrophage colony-stimulating factor (GM-CSF) were quantified in plasma from normal controls, OA patients, and RA patients, as well as in OA SF and RA SF. Although IL-34 levels were comparable among all plasma samples, the IL-34 concentration was significantly higher (12 fold) in RA SF compared to OA SF, whereas M-CSF and GM-CSF levels did not differ significantly between RA SF and OA SF (Figure 1A). Histologic analysis substantiated the elevated expression of IL-34 in RA compared to OA and normal ST lining and sublining (Figure 1B and Supplementary Figure 2A, *Arthritis & Rheumatology* website at http://onlinelibrary.wiley.com/doi/10.1002/art.41792/abstract). However, M-CSFR expression was similar in the lining and sublining of all ST samples, with a modest increase observed in RA and OA vasculature (Figure 1C and Supplementary Figure 2B).

While M-CSFR is the primary receptor for IL-34, a co-receptor that modulates IL-34/M-CSFR signaling has been identified. We confirmed that IL-34 binds to the proteoglycan syndecan 1 (2.5 μg) with a 50% maximum response concentration of 3 ng/ml (Figure 1D). Histologic analysis revealed that syndecan 1 presentation was expanded in RA compared to OA and normal ST lining and sublining (Figure 1E and Supplementary Figure 2C). The endothelial distribution of syndecan 1 was similarly amplified in RA and OA ST compared to normal ST. Next, the expression of receptors for IL-34 was evaluated in RA macrophages, T cells, and FLS (Figure 1F). Unlike syndecan 1, which was expressed on RA macrophages, T cells, and RA FLS, M-CSFR expression was restricted to RA macrophages, as its extra- and intracellular domains were present only on these cells (140 and 52 kd). Fluorescence microscopy confirmed that IL-34 and its receptors, M-CSFR and syndecan 1, colocalize in RA ST, particularly in the lining layer (Supplementary Figure 2D). These results indicate that IL-34 levels are highly potentiated in RA SF and ST,
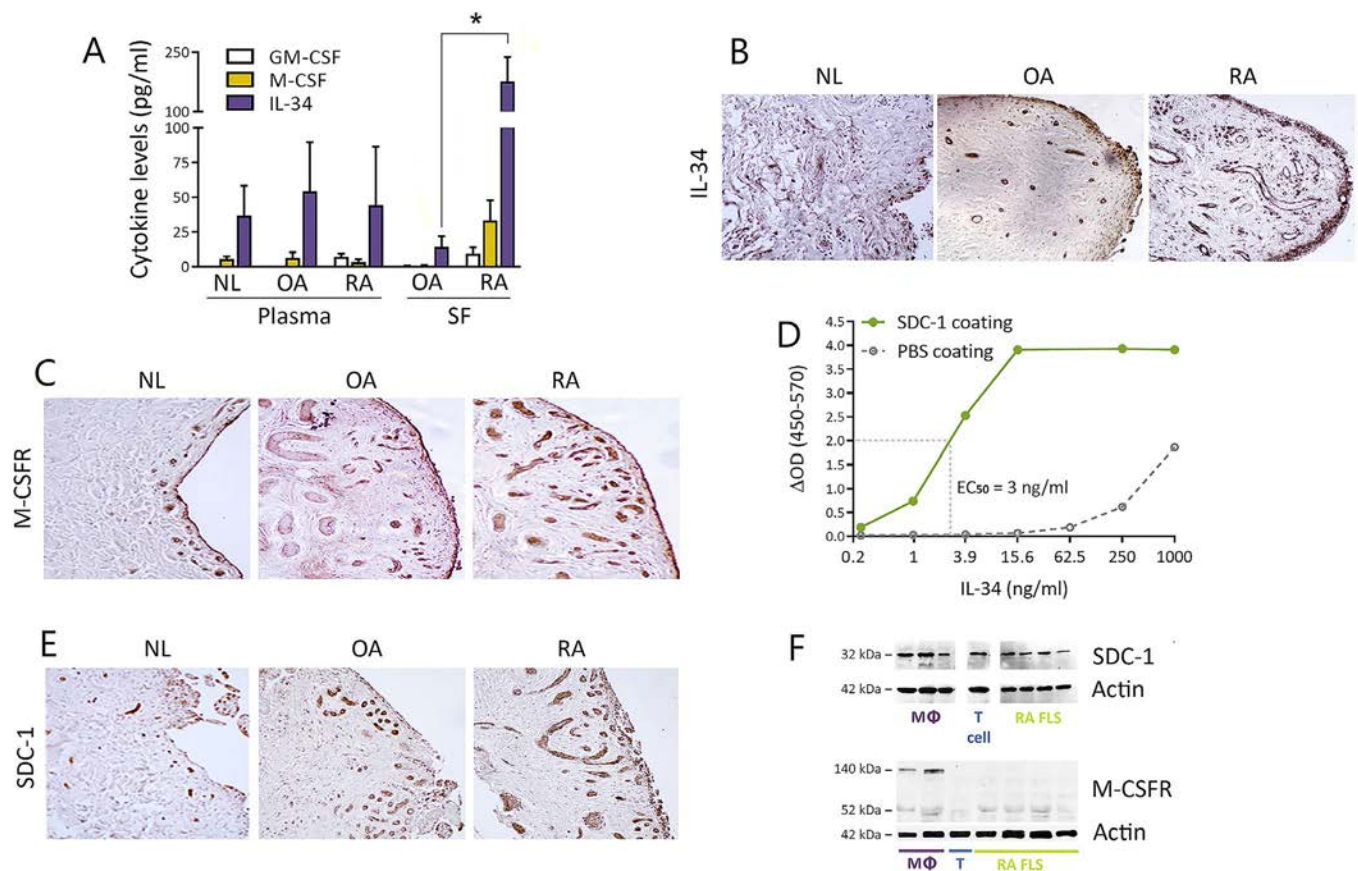
Figure 1. Expression of interleukin-34 (IL-34) and its receptors, macrophage colony-stimulating factor receptor (M-CSFR) and syndecan 1 (SDC-1), in specimens from normal (NL) controls, patients with osteoarthritis (OA), and patients with rheumatiod arthritis (RA). **A**, Granulocyte–macrophage colony-stimulating factor (GM-CSF), M-CSF, and IL-34 protein concentrations were determined in normal, OA, and RA plasma and synovial fluid (SF) samples. Bars show the mean ± SEM (n = 39 normal plasma samples, 10 OA plasma and 32 OA SF samples, and 39 RA plasma and 45 RA SF samples). * = $P < 0.05$. **B**, **C**, and **E**, Normal, OA, and RA synovial tissue samples were stained for IL-34 (n = 9 normal, 11 OA, and 9 RA samples) (**B**), M-CSFR (n = 9 normal, 11 OA, and 8 RA samples) (**C**), and syndecan 1 (n = 8 normal, 10 OA, and 10 RA samples) (**E**) and scored on a scale of 0–5 (Supplementary Figures 2A–C, available on the *Arthritis & Rheumatology* website at http://online library.wiley.com/doi/10.1002/art.41792/abstract). Representative results are shown. Original magnification × 200. **D**, A biotinylated anti–IL-34 antibody was used to compare the amount of IL-34 retained on a recombinant syndecan 1–coated plate versus a phosphate buffered saline (PBS)–coated plate, both incubated with various doses of IL-34 (0.24–1,000 ng/ml). EC_{50} = 50% maximum response concentration. **F**, Western blot analysis was used to evaluate the expression of syndecan 1 (32 kd) and M-CSFR (full-length: 140 kd; intracellular domain: 52 kd) in RA peripheral blood macrophages (Mφ), T cells, and fibroblast-like synoviocytes (FLS). Equal loading was confirmed by quantifying actin (42 kd).

and that macrophages, by expressing the syndecan 1/M-CSFR receptor complex, are the main effector cells that control IL-34 activity.

Immune cell extravasation and joint inflammation triggered by local IL-34 expression. Next, experiments were performed to evaluate the arthritogenic potential of IL-34. IA administration of IL-34 triggered progressive joint inflammation in mice (Figure 2A), along with exacerbated lining thickness and immune cell infiltration (Figure 2B and Supplementary Figure 3A, available on the *Arthritis & Rheumatology* website at http://onlinelibrary.wiley.com/doi/10.1002/art.41792/ abstract). Histologic analysis revealed that IL-34–induced joint inflammation was accompanied by the accumulation of F4/80-positive macrophages, predominantly characterized as

inflammatory iNOS-positive cells (Figure 2C and Supplementary Figure 3B). In contrast, the number of macrophages positive for F4/80 and arginase 1 was unchanged in mice with IL-34–induced arthritis relative to control mice. Consistent with these findings, mice with IL-34–induced arthritis had higher expression of monokines such as CCL5 (302 fold), IL-1β (36 fold), TNF (27 fold), CCL2 (24 fold), CXCL2 (20 fold), and IL-12 (4 fold) compared to control mice (Figures 2D and E).

In mice with IL-34–induced arthritis, the transcriptome data were validated by the increased joint protein levels of CCL5, IL-1β, CCL2, and IL-6 (12-fold to 1,407-fold higher than in control mice) (Supplementary Figures 3C–F). Except for RANKL, transcription of the osteoclastogenic markers, RANK, NFATc, cathepsin K, and TRAP, was up-regulated, by 15, 3, 7, and 12 fold, respectively, in joints from mice with IL-34–induced arthritis compared to their
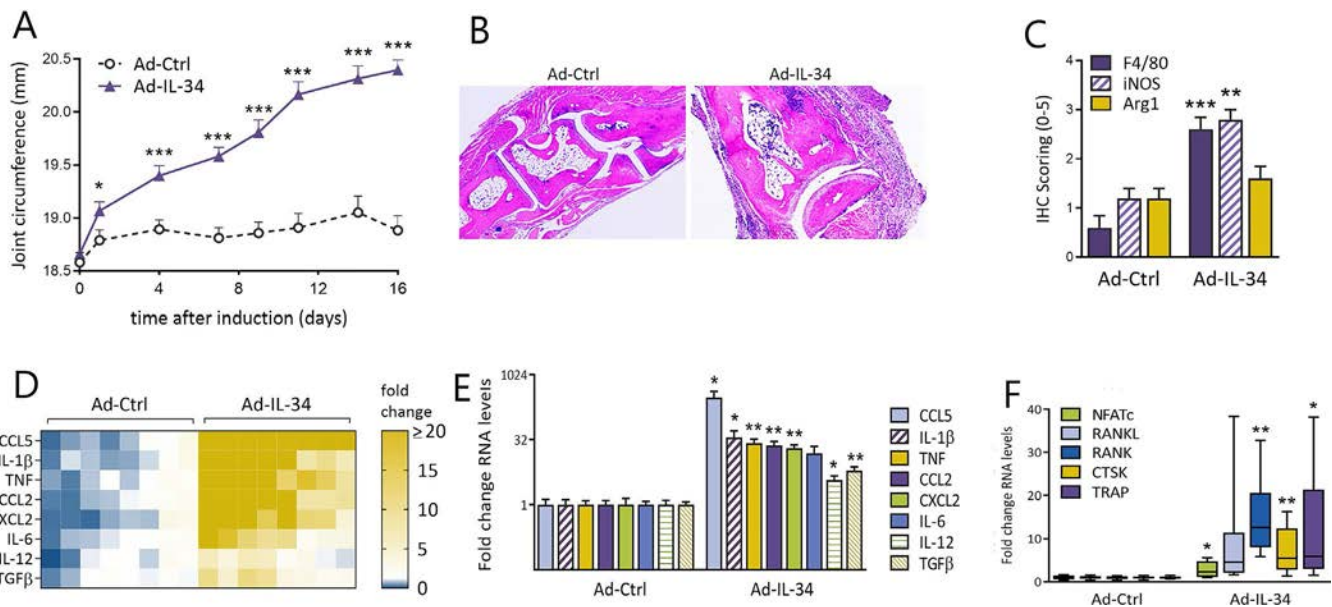
Figure 2. Induction of joint inflammation in mice by local interleukin-34 (IL-34) expression. Wild-type mice were injected intraarticularly with Ad-Ctrl or Ad-IL-34 once a week. **A,** Joint circumference was monitored over 16 days (n = 16 ankles per group). Sixteen days after arthritis onset, mice were euthanized and joints were processed for immunohistochemical (IHC) analysis, quantitative reverse transcriptase–polymerase chain reaction (qRT-PCR), and protein estimation. **B,** Tissue sections from mice treated as indicated were stained with hematoxylin and eosin and scored on a scale of 0–5 for synovial lining thickness, inflammation, and bone erosion (Supplementary Figure 3A, available on the *Arthritis & Rheumatology* website at http://onlinelibrary.wiley.com/doi/10.1002/art.41792/abstract). Representative results are shown (n = 5 ankles per group). Original magnification × 100. **C,** Tissue sections were stained for the macrophage markers F4/80, inducible nitric oxide synthase (iNOS), and arginase 1 (Arg1) (Supplementary Figure 3B), and staining was scored on a scale of 0–5 (n = 5 ankles per group). **D–F,** Levels of RNA for various monokines (**D** and **E**) and osteoclastic factors (**F**) in the joints of mice treated with control or Ad-IL-34 were determined by qRT-PCR (n = 8 ankles per group). Values in **A, C,** and **E** are the mean ± SEM. In **F,** data are shown as box plots. Each box represents the 25th to 75th percentiles. Lines inside the boxes represent the median. Lines outsie the boxes represent the minimum and maximum values. * = $P < 0.05$; ** = $P < 0.01$; *** = $P < 0.001$, versus control. TNF = tumor necrosis factor; TGFβ = transforming growth factor β; CTSK = cathepsin K; TRAP = tartrate-resistant acid phosphatase. Color figure can be viewed in the online issue, which is available at http://onlinelibrary.wiley.com/doi/10.1002/art.41792/abstract.

control counterparts (Figure 2F). Taken together, these findings demonstrate that local IL-34 provokes arthritis, characterized by inflammatory macrophages positive for F4/80 and iNOS, and RANK^high osteoclasts.

Remodeling of monocytes into inflammatory M34 macrophages by IL-34 in a syndecan 1–dependent manner. Expression of IL-34 and its co-receptors in RA macrophages, as well as the amplified transcription of monokines in mice with IL-34–induced arthritis, implied that macrophages are both producers of and responders to IL-34. To delineate the mechanism of action of IL-34 in connection with syndecan 1, we examined the activation of M-CSFR and its downstream pathways. IL-34 binding triggered M-CSFR phosphorylation (tyrosine Y723), which was accompanied by the activation of the ERK and p38 MAPK pathways (Supplementary Figures 3I and J). In RA macrophages, pretreatment with syndecan 1 antibody markedly reduced M-CSFR (tyrosine Y723) and ERK phosphorylation triggered by IL-34 stimulation (Figure 3A and Supplementary Figures 3G and H). This suggests that syndecan 1 controls the initial M-CSFR activation and its downstream signaling pathways.

Naive progenitor cells stimulated with IL-34 exhibited a significant increase in CD14+CD86+ macrophage frequency (Figure 3B and Supplementary Figure 4A, available on the *Arthritis & Rheumatology* website at http://onlinelibrary.wiley.com/doi/10.1002/art.41792abstract). Consistent with these findings, while the mean fluorescence intensity (MFI) for CD14+CD206+ macrophages remained unchanged, IL-34 activation expanded the MFI for CD14+CD86+ macrophages (Supplementary Figure 4A). Reprogramming of nonactivated (M0) cells into M34 macrophages by IL-34 transformed their cytokine profile. In M34 macrophages, transcription of IL-1β, CXCL8, and CCL2 was up-regulated (3–4 fold), whereas IL-10 expression was diminished and transforming growth factor β (TGFβ) levels were unaffected (Figure 3C and Supplementary Figure 4B). Moreover, we substantiated that RA M34 macrophages secrete higher levels of CXCL8, CCL2, TNF, and IL-6 (Supplementary Figure 4C). Nevertheless, this distinct profile of M34 macrophages was disrupted by M-CSFR or syndecan 1 antibodies, as indicated by the down-regulated TNF, IL-6, and CCL2 production (up-regulation reduced by 50–70%). In conclusion, blockade of M-CSFR and syndecan 1 function reversed the M34 macrophage inflammatory profile in RA.
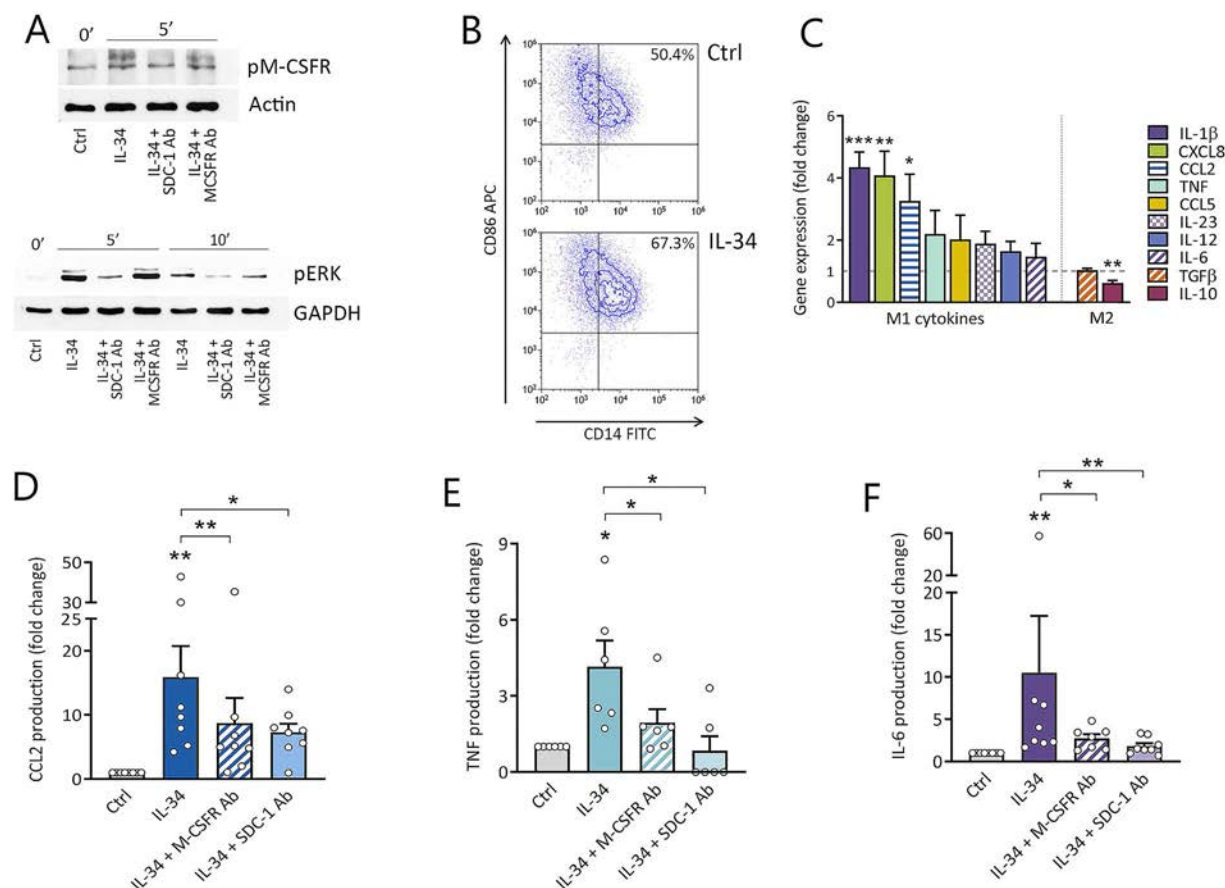
Figure 3. Dependence of IL-34–differentiated (M34) macrophage signaling and signature on syndecan 1 ligation. **A**, Cells were preincubated with buffer, anti–syndecan 1 antibody (Ab; 1:100), or anti–M-CSFR antibody (10 μg/ml) for 2 hours before stimulation with IL-34 (100 ng/ml) for 5 or 10 minutes, and lysates were used for Western blot quantification of pM-CSFR and pERK. Results are representative of 4 independent experiments. **B**, In vitro differentiated macrophages derived from negatively selected RA monocytes were treated with control or stimulated with IL-34 (300 ng/ml) for 24 hours and then stained with antibodies against CD14, CD86, and CD206 for flow cytometry. Results are representative of 5 experiments. Among CD14+ gated cells, the mean fluorescence intensity of CD86 and CD206 staining was determined (n = 5 samples per group) (Supplementary Figure 4A, available on the *Arthritis & Rheumatology* website at http://onlinelibrary.wiley.com/doi/10.1002/art.41792/ abstract). **C**, Quantitative reverse transcriptase–polymerase chain reaction analysis was performed to determine the expression of M1 and M2 cytokines by in vitro differentiated RA macrophages stimulated with IL-34 (300 ng/ml) for 8 hours. Bars show the mean ± SEM fold change compared to control (n = 4 samples per group). * = $P < 0.05$; ** = $P < 0.01$; *** = $P < 0.001$ versus control. **D–F**, Prior to IL-34 stimulation, RA cells were treated with control or preincubated with anti–syndecan 1 antibody (1:100) or anti–M-CSFR antibody (10 μg/ml). Induction of CCL2 (n = 8 samples per group) (**D**), tumor necrosis factor (TNF; n = 6 samples per group) (**E**), and IL-6 (n = 8 samples per group) (**F**) protein was measured. Symbols represent individual samples; bars show the mean ± SEM. * = $P < 0.05$; ** = $P < 0.01$, IL-34 versus control, by Wilcoxon's signed rank test; neutralizing antibody versus IL-34 alone, by Wilcoxon's 1-tailed matched pairs signed rank test. APC = allophycocyanin; FITC = fluorescein isothiocyanate; TGFβ = transforming growth factor β (see Figure 1 for other definitions). Color figure can be viewed in the online issue, which is available at http://onlinelibrary.wiley.com/doi/10.1002/art.41792/abstract.

Subsequently, we asked if IL-34 could influence other myeloid cell functions, such as phagocytosis. We found that in RA macrophages, IL-34 interfered with zymosan-triggered phagocytosis similar to the established inhibitor cytochalasin D (Supplementary Figure 4D). These results indicate that IL-34 advances the inflammatory phenotype in RA macrophages by disrupting phagocytosis.

Reprogramming of naive myeloid cells into glycolytic M34 macrophages by IL-34. RA macrophage reprogramming, instigated by IL-34, expands the population of CD14+GLUT1+ cells (Figure 4A and Supplementary Figure 4E).

In addition, in murine macrophages the ECAR (which reflects glycolysis) was increased by IL-34 in a dose-dependent manner for the entire duration of the experiment (0–55 minutes) (Figure 4B). In contrast, only a brief, transient escalation of the OCR (which reflects oxidative phosphorylation) was noted in IL-34–activated murine macrophages following carbonyl cyanide-4 (trifluoromethoxy) phenylhydrazone treatment, which maximizes oxidative potential (Supplementary Figure 4F). Consistent with their increased glycolytic metabolism, IL-34–differentiated BM-derived macrophages produced higher levels of L-lactate and pyruvate (Figure 4C).
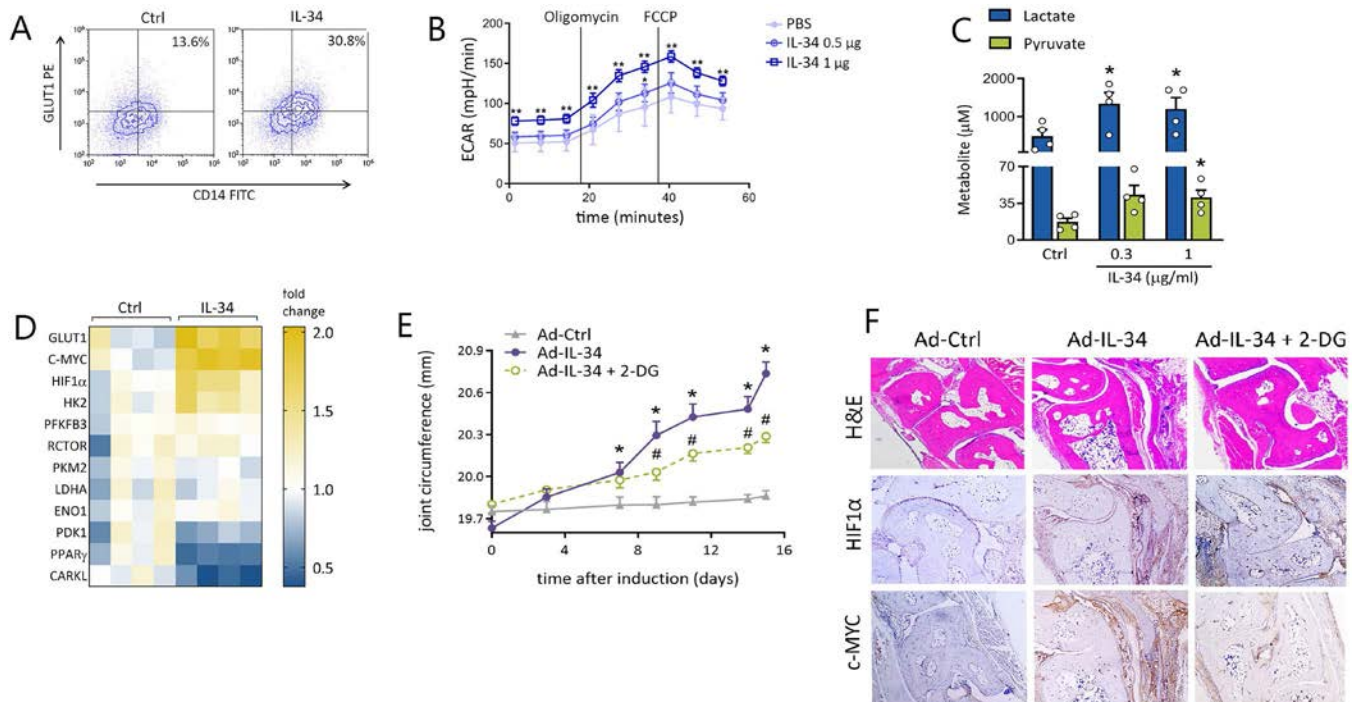
Figure 4. Promotion of progressive inflammation by interleukin-34 (IL-34)–induced metabolic changes. **A**, In vitro differentiated macrophages, derived from negatively selected monocytes, were treated with control or stimulated with IL-34 (300 ng/ml) for 24 hours. A representative contour plot is shown. Values are the mean percentage of CD14+GLUT1+ cells (n = 5 samples per group). Significance was evaluated using a paired *t*-test. **B**, A Seahorse cell energy phenotype assay was used to determine the glycolytic capacity (extracellular acidification rate [ECAR]) of phosphate buffered saline (PBS)–treated versus IL-34–pretreated RAW 264.7 cells (n = 5 samples per group). **C**, The concentration of L-lactate and pyruvate in the conditioned media of murine macrophages (treated with PBS or IL-34 for 24 hours) was determined colorimetrically. Symbols represent individual mice (n = 4 per group); bars show the mean ± SEM. **D**, Under hypoglycemic conditions, murine bone marrow–derived macrophages were left untreated or stimulated with IL-34 (1 µg/ml) for 6 hours, and the expression of metabolic genes was examined by quantitative reverse transcriptase–polymerase chain reaction (n = 4 samples per group). **E**, Wild-type mice were injected intraarticularly with Ad-Ctrl or Ad-IL-34 once per week. The mice that received Ad-IL-34 were treated intraperitoneally with either 2-deoxy-D-glucose (2-DG) or placebo, and joint circumference was monitored over 16 days (n = 10 ankles per group). **F**, Tissue sections from mice treated as indicated were stained with hematoxylin and eosin (H&E) or stained for hypoxia-inducible factor 1α (HIF-1α) or c-Myc and scored on a scale of 0–5 (n = 4 ankles per group) (Supplementary Figures 4I and J, available on the *Arthritis & Rheumatology* website at http://onlinelibrary.wiley.com/doi/10.1002/art.41792/abstract). Original magnification × 100. In **B** and **E**, values are the mean ± SEM. * = $P < 0.05$; ** = $P < 0.01$, versus control; # = $P <$ Ad-IL-34 versus Ad-IL-34 plus 2-DG. PE = phycoerythrin; FITC = fluorescein isothiocyanate; FCCP = carbonyl cyanide-4 (trifluoromethoxy) phenylhydrazone. Color figure can be viewed in the online issue, which is available at http://onlinelibrary.wiley.com/doi/10.1002/art.41792/abstract.

These murine M34 macrophages exhibited a skewed profile, which favored glycolytic factors over the pentose phosphate pathway or oxidative regulators, which resulted in a reduction in CARKL and peroxisome proliferator–activated receptor γ levels (Figure 4D). Accordingly, compared to nonarthritic mice, joints from mice with IL-34–induced arthritis displayed a significant up-regulation of the master modulators of glycolysis, GLUT1 (2 fold) and PFKFB3 (2 fold), as well as the glycolytic transcription factors c-Myc (3 fold) and HIF-1α (4 fold) (Supplementary Figure 4G). Since M34 macrophage polarization was linked to increased GLUT1 and glucose uptake, blood glucose concentration was down-regulated following 15 minutes and 30 minutes of glucose injection in arthritic compared to control mice (Supplementary Figure 4H).

Intriguingly, we showed that IP injection of 2-DG, an inhibitor of glycolysis, alleviates IL-34–induced joint swelling (Figure 4E).

Morphologic analysis confirmed that expression of c-Myc and HIF-1α, as well as macrophages positive for F4/80 and iNOS, and CD3+ T cell infiltration, were curtailed in mice with IL-34–induced arthritis that received 2-DG therapy compared to those that received placebo (Figure 4F and Supplementary Figures 4J–L). Joint lining thickness and inflammation were similarly reversed by 2-DG treatment (Figure 4F and Supplementary Figure 4I). Taken together, our findings demonstrate for the first time that IL-34 is an endogenous factor that can reprogram RA macrophage metabolic activity.

Induction of RA FLS migration by IL-34, independently of syndecan 1 and M-CSFR. In vivo, ectopic IL-34 expression expanded joint vimentin-positive fibroblast infiltration (Supplementary Figure 5A, available on the *Arthritis & Rheumatology* website

at http://onlinelibrary.wiley.com/doi/10.1002/art.41792/abstract). In vitro, IL-34 did not significantly activate any of the signaling pathways evaluated in RA FLS, although a trend was observed for p38 phosphorylation (Supplementary Figure 5B). As previously established, RA FLS abundantly express syndecan 1 (Figure 1F). Despite the lack of full-length M-CSFR in RA FLS, IL-34 markedly activated FLS migration compared to control treatment (Supplementary Figure 5C). Surprisingly, blockade of syndecan 1 or M-CSFR function was incapable of preventing IL-34–induced RA FLS migration.

Since IL-34 has also been reported to induce M-CSFR–independent signaling through PTPRZ1, we examined the role of this proteoglycan. IL-34–mediated RA FLS migration was reduced by anti-PTPRZ1 antibody treatment (Supplementary Figure 5D), despite the rather modest expression of PTPRZ1 on RA FLS (6% PTPRZ1-positive RA FLS) (Supplementary Figure 5E). Unlike syndecan 1, PTPRZ1 expression was not elevated in RA or OA ST compared to normal ST (Supplementary Figure 5F). Due to the missing connection between PTPRZ1 and RA pathogenesis, this IL-34 study was focused on syndecan 1 and its modulation of IL-34/M-CSFR activity. In short, we found that IL-34 triggers

joint as well as RA FLS recruitment independent of its primary co-receptors.

RA FLS inflammatory response and immunometabolism were not modulated by IL-34. IL-34 reprogrammed macrophages positive for syndecan 1 and M-CSFR into glycolytic and inflammatory M34 macrophages, while the transcription and/or translation of IL-6, CXCL8, CCL2, and CCL5 were unaffected by IL-34 in RA FLS (Supplementary Figures 5G and H). Corroborating these data, transcriptional regulation of GLUT1, HK2, PFKFB3, PKM2, LDHA, c-Myc, and HIF-1α was unchanged by IL-34 stimulation (Supplementary Figure 5I). Taken together, these results support the notion that the syndecan 1/M-CSFR complex is indispensable for the inflammatory and hyperglycolytic effects of IL-34, as seen in RA macrophages.

Contribution of T effector cells to IL-34-induced arthritis. IL-34 promotes Th17 cell polarization of syndecan 1–positive, M-CSFR–negative CD4+ T cells in an indirect manner (15,20,23). We found that IL-34–induced Th17 cell differentiation of murine
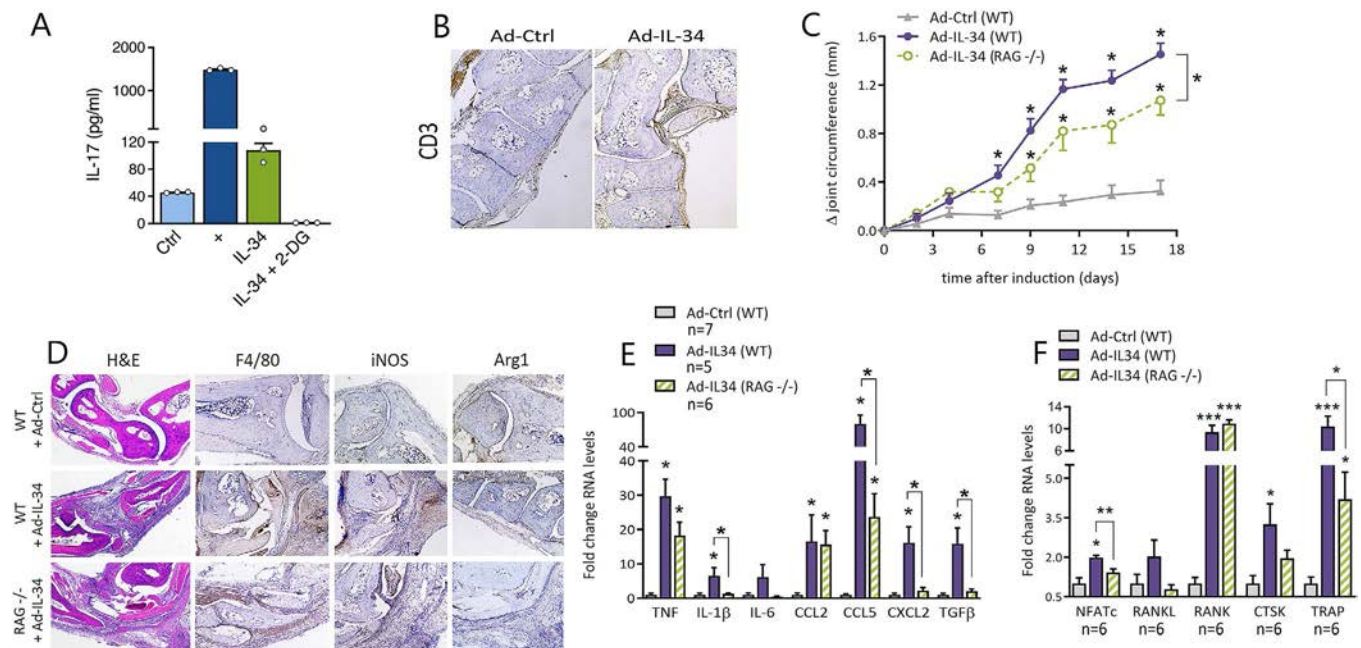
Figure 5. Contribution of T cells to IL-34–induced joint inflammation. **A,** Supernatant levels of IL-17 were measured in bone marrow–derived macrophage/splenocyte cocultures (cultured for 5 days) treated with control or IL-34 (1 μg/ml) in the presence or absence of 2-deoxy-D-glucose (2-DG; 5 m*M*). As a positive control (+) cocultures were stimulated with TGFβ (1 ng/ml) plus IL-6 (20 ng/ml). Symbols represent individual samples (n = 3 per group); bars show the mean ± SEM. **B,** Wild-type (WT) mice were treated with Ad-Ctrl or Ad-IL-34 on days 0, 7, and 14, and were euthanized on day 16. Joint CD3+ T cells were stained, and immunostaining was scored on a scale of 0–5 (n = 5 ankles per group) (Supplementary Figure 6A, available on the *Arthritis & Rheumatology* website at http://onlinelibrary.wiley.com/doi/10.1002/art.41792/abstract). Original magnification × 100. **C,** WT and RAG$^{-/-}$ mice were injected intraarticularly with Ad-Ctrl or Ad-IL-34 once per week, and joint circumference was monitored until day 17. Values are the mean ± SEM (n = 10 ankles per group). **D,** Mouse ankle joints were stained with hematoxylin and eosin (H&E) or for F4/80, iNOS, and arginase 1. H&E and positive macrophage immunostaining were scored on a scale of 0–5 (n = 4 ankles per group) (Supplementary Figures 6D and E). Original magnification × 100. **E** and **F,** Joint expression levels of monokines (**E**) and osteoclastic factors (**F**) in mice were determined by quantitative reverse transcriptase–polymerase chain reaction. Bars show the mean ± SEM. * = P < 0.05; ** = P < 0.01; *** = P < 0.001 versus control or as indicated. See Figure 2 for other definitions. Color figure can be viewed in the online issue, which is available at http://onlinelibrary.wiley.com/doi/10.1002/art.41792/abstract.

splenocytes co-cultured with BM-derived macrophages requires glycolytic cell metabolism, as 2-DG treatment diminished this process (Figure 5A). In addition to macrophages, CD3+ T cell infiltration was potentiated in the ankle joints of mice with IL-34–induced arthritis (Figure 5B and Supplementary Figure 6A, available on the *Arthritis & Rheumatology* website at http://onlinelibrary.wiley.com/doi/10.1002/art.41792/abstract). Furthermore, IL-34 amplified joint Th1/Th17 cell polarization, as reflected by exacerbated interferon-γ and IL-17 production (Supplementary Figures 6B and C).

To confirm the involvement of T cells in IL-34–induced arthritis, RAG$^{-/-}$ mice were injected IA with IL-34. IL-34–induced joint swelling was mitigated in RAG$^{-/-}$ compared to wild-type (WT) mice starting on day 9 and throughout the study (Figure 5C). Morphologic analysis demonstrated that the synovial lining was similarly aggravated by local IL-34 expression in RAG$^{-/-}$ and WT mice (Figure 5D

and Supplementary Figure 6D). The number of joint macrophages positive for F4/80 and iNOS was not disrupted in RAG$^{-/-}$ mice compared to WT mice that received local IL-34 administration (Figure 5D and Supplementary Figure 6E). Despite this finding, expansion of joint IL-1β, CCL5, CXCL2, and TGFβ levels (but not TNF or CCL2 levels) was reduced in RAG$^{-/-}$ mice with IL-34–induced arthritis compared to WT mice with IL-34–induced arthritis (Figure 5E).

Nonetheless, IL-34–induced bone erosion was downregulated in RAG$^{-/-}$ mice relative to WT mice, in part due to the absence of T cell–produced RANKL (Figure 5F). Loss of RANKL function in RAG$^{-/-}$ mice interfered with IL-34–induced upregulation of NFATc and TRAP but not cathepsin K (Figure 5F). Overall, IL-34–induced arthritis is exacerbated by T cell involvement, yet macrophages initiate and shape the signature IL-34–driven arthritic phenotype.
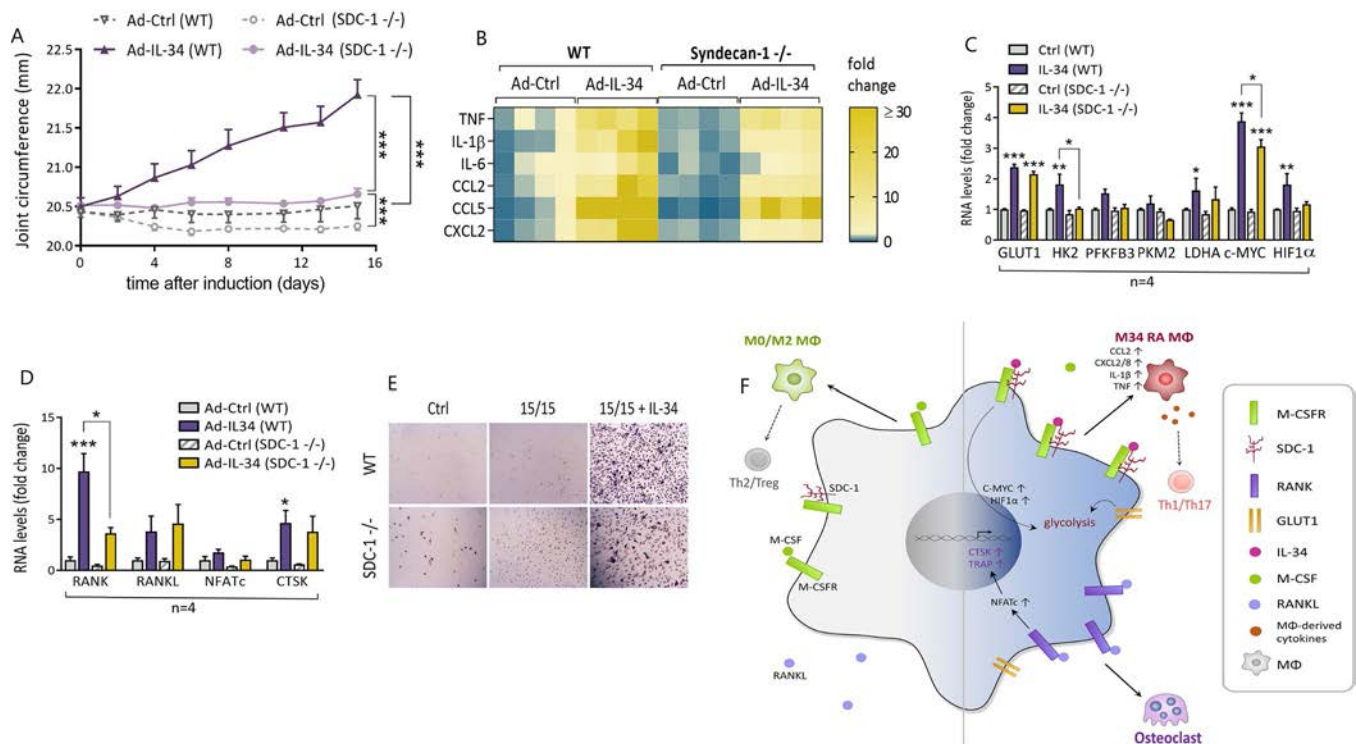
Figure 6. Modulation of interleukin-34 (IL-34)–driven joint inflammation, glycolysis, and osteoclastogenesis by syndecan 1 (SDC-1). Wild-type (WT) and SDC-1$^{-/-}$ mice were injected intraarticularly with Ad-Ctrl or Ad-IL-34 once per week. **A**, Mouse joint circumference was monitored over 15 days. Values are the mean ± SEM (n = 7 for WT mice treated with Ad-Ctrl; n = 8 for all other groups). *** = $P < 0.001$, by Mann-Whitney nonparametric test. **B**, Transcriptional regulation of joint inflammatory mediators was evaluated by quantitative reverse transcriptase–polymerase chain reaction (qRT-PCR) (n = 4 ankles per group). **C**, Under hypoglycemic conditions, bone marrow–derived macrophages from WT and SDC-1$^{-/-}$ mice were left untreated or stimulated with IL-34 (1 μg/ml) for 6 hours, and the expression of glycolytic genes was examined by qRT-PCR. **D**, Transcription levels of joint osteoclastic factors were determined by qRT-PCR in WT and SDC-1$^{-/-}$ mice that received local injection of Ad-Ctrl or Ad-IL-34. In **C** and **D**, bars show the mean ± SEM (n = 4 ankles per group). * = $P < 0.05$; ** = $P < 0.01$; *** = $P < 0.001$ versus control or as indicated. **E**, To assess osteoclastogenesis in vitro, bone marrow–derived preosteoclasts from WT and SDC-1$^{-/-}$ mice were left untreated (Ctrl), cultured under suboptimal conditions (15 ng/ml macrophage colony-stimulating factor [M-CSF] and 15 ng/ml RANKL [15/15]), or exposed to 15/15 and IL-34 (300 ng/ml). Following 14 days of differentiation (fresh stimuli twice per week), tartrate-resistant acid phosphatase (TRAP) staining was performed and TRAP-positive multinuclear osteoclasts were counted (n = 4 ankles per group) (Supplementary Figure 6G). Original magnification × 300. **F**, IL-34 binding to M-CSF receptor (M-CSFR)/syndecan 1 cultivates rheumatoid arthritis (RA) inflammatory and glycolytic M34 macrophages (Mφ) that are predisposed to osteoclastogenesis. HIF-1α = hypoxia-inducible factor 1α. Color figure can be viewed in the online issue, which is available at http://onlinelibrary.wiley.com/doi/10.1002/art.41792/abstract.

Syndecan 1 defines the IL-34–induced immunostimulatory phenotype. To solidify the importance of syndecan 1 as a central modulator of IL-34–mediated disease, genetically modified mice lacking syndecan 1 were utilized (26). Progression of IL-34–induced arthritis was severely reduced in SDC-1$^{-/-}$ mice throughout the study (Figure 6A). Notably, in the absence of syndecan 1, local expression of IL-34 did provoke minor joint swelling, perhaps due to marginal M-CSFR activation. In mice with IL-34–induced arthritis, up-regulation of joint IL-1β, CCL2, CXCL2, and CCL5 levels, but not TNF levels, was impaired in SDC-1$^{-/-}$ mice compared to WT mice (reduced by 81%, 66%, 84%, and 57%, respectively) (Figure 6B and Supplementary Figure 6F).

In murine BM-derived macrophages, transcription of several components of the glycolytic pathway, including GLUT1, HK2, LDHA, c-Myc, and HIF-1α, was amplified by IL-34 stimulation (Figure 6C). Although expression of HK2 and c-Myc was suppressed, levels of GLUT1, LDHA, and HIF-1α remained unchanged in IL-34–activated SDC-1$^{-/-}$ mouse progenitor cells relative to controls (Figure 6C). Taken together, these findings indicate that the interaction between IL-34 and syndecan 1 shifts naive cells to glycolytic M34 macrophages that have a unique inflammatory and metabolic phenotype.

Requirement of syndecan 1 for osteoclasts differentiated by IL-34. In IL-34–induced arthritis, we demonstrated that the formation of TRAP-positive osteoclasts was in part due to increased RANK expression, which was disrupted in SDC-1$^{-/-}$ mice (Figure 6D). TRAP staining corroborated that IL-34–induced osteoclast formation was compromised in SDC-1$^{-/-}$ mouse progenitor cells compared to WT mice (Figure 6E and Supplementary Figure 6G). Taken together, our data indicate that syndecan 1–positive macrophages in conjunction with T cells advance IL-34–modulated osteoclastogenesis in part through RANK/RANKL function.

DISCUSSION

The present study describes a novel role for IL-34 and its co-receptor syndecan 1 in RA pathogenesis. We showed that syndecan 1 regulates myeloid IL-34/M-CSFR signaling and downstream functions. Activation of the receptor complex syndecan 1/M-CSFR is essential for the reconfiguration of naive cells to glycolytic and inflammatory CD14+CD86+GLUT1^{high} M34 macrophages. Arthritic IL-34–differentiated macrophages positive for F4/80 and iNOS are characterized by the transcriptional up-regulation of glycolytic mediators, HIF-1α and c-Myc, which are dysregulated by systemic 2-DG therapy. Intriguingly, syndecan 1 or T cell deficiency counteracts IL-34–induced joint inflammation and osteoclastic erosion in part by interfering with hyperglycolytic activity (Figure 6F).

The higher bioavailability of IL-34 compared to M-CSF in the RA SF emphasizes its ability to outcompete M-CSF for M-CSFR binding. In contrast to the shared receptor M-CSFR, the co-receptor syndecan 1, which does not bind M-CSF, is highly up-regulated in RA ST lining and sublining. Joint GM-CSF levels are also less abundant than IL-34 levels, and GM-CSF does not compete for M-CSFR or syndecan 1 binding. A growing body of evidence has demonstrated that IL-34 is involved in various pathologies, particularly in arthritis (14,34). We showed that in RA macrophages, phosphorylation of M-CSFR by IL-34 is dependent on syndecan 1. Others have shown that syndecan 1 antibody impairs IL-34–mediated monocyte migration (35). Syndecan 1 manipulates the binding affinity of IL-34 to M-CSFR (27), hence remodeling joint macrophages to glycolytic and osteoclastic phenotypes.

Syndecan 1 expression is potentiated in a range of inflammatory as well as malignant disorders (36). In cancer, elevated syndecan 1 levels are linked to exacerbated tumor size and poor prognosis. Syndecan 1 is involved in tumor invasion, proliferation, apoptosis, and angiogenesis (37). Thus, inhibitory syndecan 1 peptides and anti–syndecan 1 antibody have been generated for immunotherapy of different cancers (38). Consistent with its pathogenic implications, we show that syndecan 1 expression was highly up-regulated in RA compared to normal ST lining and sublining, attributed to macrophages, T cells, and RA FLS. Similar to RA joints, syndecan 1 is highly expressed on psoriatic arthritis ST mononuclear infiltrates, while it is barely detectable in OA ST (39). In contrast, others have suggested that syndecan 1 is involved in early-stage cartilage degeneration in experimental OA (40). It has also been shown that cannabinoid therapy attenuates OA disease activity by suppressing syndecan 1 expression (41). Nevertheless, we demonstrated that syndecan 1 up-regulation in OA relative to normal ST samples was restricted to the vasculature. A limitation of this study was that RA ST samples were obtained from de-identified patients, and therefore the expression levels of IL-34, M-CSFR, and syndecan 1 could not be linked to clinical parameters.

Our data underline that IL-34–differentiated macrophages diverge from M-CSF–induced M2 or GM-CSF–derived M1 macrophages (42). The pathogenic M34 macrophages do not rely as heavily on IL-6 or TNF, both of which are successfully targeted by current RA biologic therapies. Additionally, M34 macrophages displayed a glycolytic profile akin to that of hypermetabolic RA macrophages, yet deviating from the metabolic signature reported in lipopolysaccharide (LPS)–induced M1 macrophages. IL-34 potentiates the expression of 2 central glycolytic transcription factors, c-Myc and HIF-1α, resembling RA macrophages (43–45). However, LPS has been shown to up-regulate HIF-1α exclusively, while suppressing c-Myc transcription (46). In mice with IL-34–induced arthritis, 2-DG therapy interfered with c-Myc and HIF-1α amplification and joint swelling, highlighting that the glycolytic rewiring is linked to the IL-34–modulated inflammatory phenotype. Intriguingly, both c-Myc and HIF-1α have also been shown to instigate osteoclast formation (47). In addition to metabolic activity, RANK^{high} M34 osteoclast progenitor cells are exceptionally sensitive to T cell–derived RANKL and are prone to undergo osteoclastogenesis.

In macrophages, M-CSF, unlike GM-CSF, favors mitochondrial oxygen consumption over glycolysis, as determined by

the OCR:ECAR ratio (48). IL-34 has been suggested to induce M2 macrophage differentiation and enhance mitochondrial oxidative phosphorylation via the AMP-activated protein kinase pathway (21). In contrast, our findings identify IL-34 as a glycolytic stimulus, as evidenced by prolonged ECAR/OCR activity, accentuated pyruvate and L-lactate secretion, and transcriptional upregulation of metabolic intermediates in macrophages. Intriguingly, IL-34–driven metabolic reprogramming is expanded beyond macrophages, since 2-DG treatment negates IL-34–instigated Th17 cell polarization, suggesting that hypermetabolic activity is responsible for M34 macrophage cross-regulation with Th17 cells.

We noted that a wider range of cytokines was expressed in mice with IL-34–induced arthritis than in RA macrophages differentiated by IL-34. Perhaps Th1/Th17 cell differentiation in mice with IL-34–induced arthritis exacerbates M34 macrophage immunometabolism. Extending these findings, joint inflammation and bone erosion advanced by local IL-34 were ameliorated in T cell–deficient RAG$^{-/-}$ mice compared to WT mice due to impaired joint IL-1β, CCL5, CXCL2, and NFATc expression. In SDC-1$^{-/-}$ mice, IL-34–induced joint inflammation was alleviated through a similar mechanism as in RAG$^{-/-}$ mice (IL-1β, CCL5, CXCL2); nevertheless, osteoclastogenesis was restrained via RANK reduction. Hence, the cross-talk between the metabolic T effector cells and M34 preosteoclasts plays a critical role in IL-34–elicited inflammatory erosion. Consistent with these observations, earlier studies have illustrated that IL-34 is responsible for Th17 cell differentiation (15,20,23). Controversially, others have reported that IL-34–stimulated macrophages promote CD4+FoxP3+ Treg differentiation and thereby facilitate allograft tolerance (24).

Although TNF and PDGF promote hypermetabolic activity in RA FLS (9), neither their immunometabolic nor inflammatory profile is altered by IL-34 stimulation. In contrast to our findings, IL-6 and CXCL8 were secreted from lung fibroblasts in response to IL-34 stimulation (49). Interestingly, while IL-34 advances RA FLS migration, this function is disconnected from the inflammatory or glycolytic activity in these cells. Hence, the inability of syndecan 1 or M-CSFR blockade to negate IL-34–triggered motility suggested that RA FLS trafficking was fostered by an alternative pathway. Remarkably, IL-34 can function independently of M-CSFR or syndecan 1, through a different heparan sulfate proteoglycan, namely, PTPRZ1 (50). Modest levels of PTPRZ1 in RA FLS were shown to be responsible, at least in part, for the IL-34–mediated infiltration. However, unlike syndecan 1, PTPRZ1 is similarly expressed in RA compared to OA and normal ST samples. This is a departure from the magnified expression of PTPRZ1 on glioblastoma and colorectal cancer cells and its implication in advancing other IL-34–mediated pathologies (50,51).

Taken together, our data show for the first time that hyperglycolytic M34 macrophages and effector Th17 cells participate in inflammatory and erosive phenotypes enforced by joint IL-34 expression. While our preclinical data are promising, the therapeutic potential of IL-34 and its downstream metabolic intermediates remains to be elucidated.

ACKNOWLEDGMENTS

AUTHOR CONTRIBUTIONS

All authors were involved in drafting the article or revising it critically for important intellectual content, and all authors approved the final version to be published. Dr. Shahrara had full access to all of the data in the study and takes responsibility for the integrity of the data and the accuracy of the data analysis.

Study conception and design. Van Raemdonck, Shahrara.
Acquisition of data. Van Raemdonck, Umar, Palasiewicz, Volin, Romay, Tetali, Ahmed, Zomorrodi, Shahrara.
Analysis and interpretation of data. Van Raemdonck, Umar, Palasiewicz, Elshabrawy, Amin, Sweiss, Shahrara.

REFERENCES

1. Brennan FM, McInnes IB. Evidence that cytokines play a role in rheumatoid arthritis [review]. J Clin Invest 2008;118:3537–45.

2. McInnes IB, Buckley CD, Isaacs JD. Cytokines in rheumatoid arthritis: shaping the immunological landscape [review]. Nat Rev Rheumatol 2016;12:63–8.

3. McInnes IB, Schett G. The pathogenesis of rheumatoid arthritis [review]. N Engl J Med 2011;365:2205–19.

4. Mulherin D, Fitzgerald O, Bresnihan B. Synovial tissue macrophage populations and articular damage in rheumatoid arthritis. Arthritis Rheum 1996;39:115–24.

5. Weyand CM, Goronzy JJ. Immunometabolism in early and late stages of rheumatoid arthritis [review]. Nat Rev Rheumatol 2017;13:291–301.

6. Yang Z, Shen Y, Oishi H, Matteson EL, Tian L, Goronzy JJ, et al. Restoring oxidant signaling suppresses proarthritogenic T cell effector functions in rheumatoid arthritis. Sci Transl Med 2016;8:331ra38.

7. Biniecka M, Canavan M, McGarry T, Gao W, McCormick J, Cregan S, et al. Dysregulated bioenergetics: a key regulator of joint inflammation. Ann Rheum Dis 2016;75:2192–200.

8. Garcia-Carbonell R, Divakaruni AS, Lodi A, Vicente-Suarez I, Saha A, Cheroutre H, et al. Critical role of glucose metabolism in rheumatoid arthritis fibroblast-like synoviocytes. Arthritis Rheumatol 2016;68:1614–26.

9. Falconer J, Murphy AN, Young SP, Clark AR, Tiziani S, Guma M, et al. Synovial cell metabolism and chronic inflammation in rheumatoid arthritis [review]. Arthritis Rheumatol 2018;70:984–99.

10. Geeraerts X, Bolli E, Fendt SM, van Ginderachter JA. Macrophage metabolism as therapeutic target for cancer, atherosclerosis, and obesity [review]. Front Immunol 2017;8:289.

11. Viola A, Munari F, Sanchez-Rodriguez R, Scolaro T, Castegna A. The metabolic signature of macrophage responses [review]. Front Immunol 2019;10:1462.

12. Zeisbrich M, Yanes RE, Zhang H, Watanabe R, Li Y, Brosig L, et al. Hypermetabolic macrophages in rheumatoid arthritis and coronary artery disease due to glycogen synthase kinase 3b inactivation. Ann Rheum Dis 2018;77:1053–62.

13. Yoon BR, Oh YJ, Kang SW, Lee EB, Lee WW. Role of SLC7A5 in metabolic reprogramming of human monocyte/macrophage immune responses. Front Immunol 2018;9:53.

14. Chemel M, Le Goff B, Brion R, Cozic C, Berreur M, Amiaud J, et al. Interleukin 34 expression is associated with synovitis severity in rheumatoid arthritis patients. Ann Rheum Dis 2012;71:150–4.

15. Wang B, Ma Z, Wang M, Sun X, Tang Y, Li M, et al. IL-34 upregulated Th17 production through increased IL-6 expression by rheumatoid fibroblast-like synoviocytes. Mediators Inflamm 2017;2017:1567120.

16. Rietkotter E, Bleckmann A, Bayerlova M, Menck K, Chuang HN, Wenske B, et al. Anti-CSF-1 treatment is effective to prevent carcinoma invasion induced by monocyte-derived cells but scarcely by microglia. Oncotarget 2015;6:15482–93.

17. Ge Y, Huang M, Yao YM. Immunomodulation of interleukin-34 and its potential significance as a disease biomarker and therapeutic target [review]. Int J Biol Sci 2019;15:1835–45.

18. Hamilton TA, Zhao C, Pavicic PG Jr, Datta S. Myeloid colony-stimulating factors as regulators of macrophage polarization [review]. Front Immunol 2014;5:554.

19. Huang SC, Smith AM, Everts B, Colonna M, Pearce EL, Schilling JD, et al. Metabolic reprogramming mediated by the mTORC2-IRF4 signaling axis is essential for macrophage alternative activation. Immunity 2016;45:817–30.

20. Foucher ED, Blanchard S, Preisser L, Descamps P, Ifrah N, Delneste Y, et al. IL-34- and M-CSF-induced macrophages switch memory T cells into Th17 cells via membrane IL-1α. Eur J Immunol 2015;45:1092–102.

21. Boulakirba S, Pfeifer A, Mhaidly R, Obba S, Goulard M, Schmitt T, et al. IL-34 and CSF-1 display an equivalent macrophage differentiation ability but a different polarization potential. Sci Rep 2018;8:256.

22. Liu Y, Liu H, Zhu J, Bian Z. Interleukin-34 drives macrophage polarization to the M2 phenotype in autoimmune hepatitis. Pathol Res Pract 2019;215:152493.

23. Wang B, Tang Y, Sun X, Ouyang X, Li H, Wei J, et al. Increased IL-6 expression on THP-1 by IL-34 stimulation up-regulated rheumatoid arthritis Th17 cells. Clin Rheumatol 2018;37:127–37.

24. Bezie S, Picarda E, Ossart J, Tesson L, Usal C, Renaudin K, et al. IL-34 is a Treg-specific cytokine and mediates transplant tolerance. J Clin Invest 2015;125:3952–64.

25. Baghdadi M, Umeyama Y, Hama N, Kobayashi T, Han N, Wada H, et al. Interleukin-34, a comprehensive review. J Leukoc Biol 2018;104:931–51.

26. Alexander CM, Reichsman F, Hinkes MT, Lincecum J, Becker KA, Cumberledge S, et al. Syndecan-1 is required for Wnt-1-induced mammary tumorigenesis in mice. Nat Genet 2000;25:329–32.

27. Teng YH, Aquino RS, Park PW. Molecular functions of syndecan-1 in disease [review]. Matrix Biol 2012;31:3–16.

28. Arnett FC, Edworthy SM, Bloch DA, McShane DJ, Fries JF, Cooper NS, et al. The American Rheumatism Association 1987 revised criteria for the classification of rheumatoid arthritis. Arthritis Rheum 1988;31:315–24.

29. Pickens SR, Chamberlain ND, Volin MV, Pope RM, Mandelin AM II, Shahrara S. Characterization of CCL19 and CCL21 in rheumatoid arthritis. Arthritis Rheum 2011;63:914–22.

30. Pickens SR, Chamberlain ND, Volin MV, Pope RM, Talarico NE, Mandelin AM II, et al. Characterization of interleukin-7 and interleukin-7 receptor in the pathogenesis of rheumatoid arthritis. Arthritis Rheum 2011;63:2884–93.

31. Kim SJ, Chang HJ, Volin MV, Umar S, Van Raemdonck K, Chevalier A, et al. Macrophages are the primary effector cells in IL-7-induced arthritis. Cell Mol Immunol 2020;17:728–40.

32. Umar S, Palasiewicz K, Van Raemdonck K, Volin MV, Romay B, Amin MA, et al. IRAK4 inhibition: a promising strategy for treating RA joint inflammation and bone erosion. Cell Mol Immunol 2020. doi: 10.1038/s41423-020-0433-8. E-pub ahead of print.

33. Van Raemdonck K, Umar S, Palasiewicz K, Volkov S, Volin MV, Arami S, et al. CCL21/CCR7 signaling in macrophages promotes joint inflammation and Th17-mediated osteoclast formation in rheumatoid arthritis. Cell Mol Life Sci 2020;77:1387–99.

34. Chang SH, Choi BY, Choi J, Yoo JJ, Ha YJ, Cho HJ, et al. Baseline serum interleukin-34 levels independently predict radiographic progression in patients with rheumatoid arthritis. Rheumatol Int 2015;35:71–9.

35. Segaliny AI, Brion R, Mortier E, Maillasson M, Cherel M, Jacques Y, et al. Syndecan-1 regulates the biological activities of interleukin-34. Biochim Biophys Acta 2015;1853:1010–21.

36. Fears CY, Woods A. The role of syndecans in disease and wound healing [review]. Matrix Biol 2006;25:443–56.

37. Palaiologou M, Delladetsima I, Tiniakos D. CD138 (syndecan-1) expression in health and disease [review]. Histol Histopathol 2014;29:177–89.

38. Rousseau C, Ferrer L, Supiot S, Bardies M, Davodeau F, Faivre-Chauvet A, et al. Dosimetry results suggest feasibility of radioimmunotherapy using anti-CD138 (B-B4) antibody in multiple myeloma patients. Tumour Biol 2012;33:679–88.

39. Patterson AM, Cartwright A, David G, Fitzgerald O, Bresnihan B, Ashton BA, et al. Differential expression of syndecans and glypicans in chronically inflamed synovium. Ann Rheum Dis 2008;67:592–601.

40. Salminen-Mankonen H, Saamanen AM, Jalkanen M, Vuorio E, Pirila L. Syndecan-1 expression is upregulated in degenerating articular cartilage in a transgenic mouse model for osteoarthritis. Scand J Rheumatol 2005;34:469–74.

41. Kong Y, Wang W, Zhang C, Wu Y, Liu Y, Zhou X. Cannabinoid WIN55,2122 mesylate inhibits ADAMTS4 activity in human osteoarthritic articular chondrocytes by inhibiting expression of syndecan1. Mol Med Rep 2016;13:4569–76.

42. Ushach I, Zlotnik A. Biological role of granulocyte macrophage colony-stimulating factor (GM-CSF) and macrophage colony-stimulating factor (M-CSF) on cells of the myeloid lineage [review]. J Leukoc Biol 2016;100:481–9.

43. Asahara H, Hasunuma T, Kobata T, Inoue H, Muller-Ladner U, Gay S, et al. In situ expression of protooncogenes and Fas/Fas ligand in rheumatoid arthritis synovium. J Rheumatol 1997;24:430–5.

44. Pap T, Nawrath M, Heinrich J, Bosse M, Baier A, Hummel KM, et al. Cooperation of Ras- and c-Myc–dependent pathways in regulating the growth and invasiveness of synovial fibroblasts in rheumatoid arthritis. Arthritis Rheum 2004;50:2794–802.

45. Roivainen A, Soderstrom KO, Pirila L, Aro H, Kortekangas P, Merilahti-Palo R, et al. Oncoprotein expression in human synovial tissue: an immunohistochemical study of different types of arthritis. Br J Rheumatol 1996;35:933–42.

46. Liu L, Lu Y, Martinez J, Bi Y, Lian G, Wang T, et al. Proinflammatory signal suppresses proliferation and shifts macrophage metabolism from Myc-dependent to HIF1α-dependent. Proc Natl Acad Sci U S A 2016;113:1564–9.

47. Park-Min KH. Metabolic reprogramming in osteoclasts [review]. Semin Immunopathol 2019;41:565–72.

48. Izquierdo E, Cuevas VD, Fernandez-Arroyo S, Riera-Borrull M, Orta-Zavalza E, Joven J, et al. Reshaping of human macrophage polarization through modulation of glucose catabolic pathways. J Immunol 2015;195:2442–51.

49. Zhou J, Sun X, Zhang J, Yang Y, Chen D, Cao J. IL-34 regulates IL-6 and IL-8 production in human lung fibroblasts via MAPK, PI3K-Akt, JAK and NF-κB signaling pathways. Int Immunopharmacol 2018;61:119–25.

50. Nandi S, Cioce M, Yeung YG, Nieves E, Tesfa L, Lin H, et al. Receptor-type protein-tyrosine phosphatase ζ is a functional receptor for interleukin-34. J Biol Chem 2013;288:21972–86.

51. Franze E, Dinallo V, Rizzo A, Di Giovangiulio M, Bevivino G, Stolfi C, et al. Interleukin-34 sustains pro-tumorigenic signals in colon cancer tissue. Oncotarget 2018;9:3432–45.

Erosive Hand Osteoarthritis: Incidence and Predictive Characteristics Among Participants in the Osteoarthritis Initiative

Timothy E. McAlindon,[1] Jeffrey B. Driban,[1] ID Mary B. Roberts,[2] Jeffrey Duryea,[3] ID Ida K. Haugen,[4] ID
Lena F. Schaefer,[3] Stacy E. Smith,[3] Alexander Mathiessen,[5] ID and Charles Eaton[2] ID

Objective. To evaluate age, sex, race, osteoarthritis (OA) severity, metabolic factors, and bone health as risk factors for erosive hand OA at baseline and its incidence over a 48-month period.

Methods. This was a longitudinal cohort study that included participants from the Osteoarthritis Initiative (OAI) with complete hand radiographs from baseline and 48-month visits who were eligible at baseline for incident erosive hand OA (i.e., had or were at risk for knee OA [criterion for OAI inclusion] and did not currently have erosive hand OA). Individuals were classified as having erosive hand OA if the Kellgren/Lawrence (K/L) grade was ≥2 in at least 1 interphalangeal joint on 2 different fingers and central erosion was present in at least 1 joint.

Results. Of the 3,365 individuals without prevalent erosive hand OA at baseline, 86 (2.6%) developed erosive hand OA during the 48-month period. Risk factors included older age (relative risk [RR] per SD 1.63 [95% confidence interval 1.35–1.97]), female sex (RR 2.47 [95% confidence interval 1.52–4.02]), greater OA severity (sum K/L grade 13.9 versus 5.3; $P < 0.001$), and less cortical width (1.38 mm versus 1.52 mm; $P < 0.001$). After 48 months, subjects who had developed erosive hand OA were characterized by greater progression of radiographic OA (i.e., joint space narrowing, K/L grade progression [RR 1.35], and loss of cortical thickness [RR 1.23]), adjusted for age, sex, race, body mass index, and baseline OA severity (sum K/L grade).

Conclusion. These findings demonstrate that erosive hand OA is more common in older women and is strongly associated with severity of articular structural damage and its progression. Individuals who develop erosive hand OA have thinner bones prior to erosive hand OA development and as it progresses, suggesting that erosive hand OA is a disorder of skeletal frailty.

INTRODUCTION

Osteoarthritis (OA) of the hands is common, with a prevalence reaching 80% in older populations and generally causing mild

symptoms (1–3). However, among hands with OA there is a recognizable subset that is differentiated by the degree of OA severity, the presence of radiographic central joint erosions (4,5), and sometimes clinically evident inflammation (6,7). The population

Eaton, MD, MS: Care New England Medical Group Family Care Center and Internal Medicine, Pawtucket, Rhode Island, and Brown University, Providence, Rhode Island; [3]Jeffrey Duryea, PhD, Lena F. Schaefer, MD, Stacy E. Smith, MD: Brigham and Women's Hospital and Harvard Medical School, Boston, Massachusetts; [4]Ida K. Haugen, MD, PhD: Diakonhjemmet Hospital, Oslo, Norway; [5]Alexander Mathiessen, MD: Brigham and Women's Hospital and Harvard Medical School, Boston, Massachusetts, and Diakonhjemmet Hospital, Oslo, Norway.

prevalence of this erosive hand OA phenotype is estimated to be 2.8% among those over 55 years of age (which exceeds the typical prevalence of rheumatoid arthritis [8]) but 10.2% among individuals with symptomatic hand OA (9). Individuals with erosive hand OA pose a significant clinical challenge because they have greater levels of hand pain, disability, and joint deformity than those with typical hand OA (9). Moreover, as in typical hand OA, there are few effective treatments for erosive hand OA, with currently available therapies only treating symptoms without any known benefits in reducing pathologic progression.

The distinguishing characteristics of erosive hand OA suggest that the pathologic processes differ from those of typical hand OA. Better understanding of the fundamental nature of erosive hand OA could help clarify these processes and identify potential therapeutic targets. In fact, the hypothesis that erosive hand OA represents an inflammatory subtype has already predicated clinical trials of anticytokine therapy; however, these have had mostly negative results (10–12), raising questions about the validity of the thesis that erosive hand OA is an inflammatory arthritis (13). Moreover, scrutiny of erosions in osteoarthritic finger joints reveals heterogeneity in their localization (central versus marginal) (14–18), introducing potential for misclassification among joint diseases (19–21). While marginal erosions are typical in inflammatory joint disease, the prototypical central "erosions" in OA-affected phalangeal joints rather have an appearance of damage of the joint plate and subchondral osteolytic lesions in the context of advanced joint damage (22). Confirming the supposition that the pathologic processes of erosive hand OA differ from those of typical hand OA could lead to an entirely different therapeutic approach focused on bone (23).

These considerations underscore the need to understand the nature of erosive hand OA and its relationship with hand OA, including the fundamental question of whether it represents a separate entity or is simply a more severe manifestation of hand OA (24). Identification of its risk factors and processes involved in its pathogenesis could also form a basis for discovery of potential therapeutic targets. Thus, the aims of the present study were to leverage the large collection of longitudinal data from the Osteoarthritis Initiative (OAI) cohort to evaluate the roles of age, sex, race, OA severity, metabolic factors, and bone health as risk factors for incident erosive hand OA in an enriched population sample (i.e., elevated risk for development of knee OA as required for inclusion in the OAI).

PATIENTS AND METHODS

This was a longitudinal cohort design epidemiologic analysis of the incidence of erosive hand OA among all OAI participants who were eligible for this outcome (i.e., did not currently have erosive hand OA) at the baseline examination. Demographic variables, OA severity measures, and cortical thickness were compared and analyzed over a 48-month observation period.

Study population. The OAI is a multicenter cohort study of 4,796 adults with, or at risk for, knee OA who were recruited between February 2004 and May 2006 from 4 clinical sites (Memorial Hospital of Rhode Island, The Ohio State University, University of Maryland and Johns Hopkins University, and the University of Pittsburgh). The eligibility criteria of the OAI were intended to enrich the cohort with individuals at risk for knee OA and to exclude individuals with end-stage knee OA or inflammatory rheumatic disease. OAI data and protocols are available for free public access at https://nda.nih.gov/oai/ (25).

Ethical considerations. This study received ethics approval from the 4 OAI clinical sites (institutional review boards of Memorial Hospital of Rhode Island, Ohio State University Biomedical Sciences, University of Pittsburgh, and University of Maryland Baltimore) and the OAI coordinating center (Committee on Human Research at University of California, San Francisco; approval no. 10–00532). Each participant provided written informed consent prior to participation. The study was conducted in compliance with the ethical principles of the Declaration of Helsinki, informed consent regulations, and International Conference on Harmonization Good Clinical Practices Guidelines. The source population for the study comprised all participants in the OAI cohort who had complete hand radiographs from both baseline and 48-month visits and who were eligible at baseline for incident erosive hand OA (Figure 1).

Assessment of participant characteristics. A comprehensive inventory of assessments was obtained at baseline and at the 48-month visit. This included posteroanterior radiographs of 1 or both hands, questions about hand pain referencing a homunculus ("During the past 30 days, which of these joints have had pain, aching, or stiffness on most days? By most days, we mean more than half the days of a month") and about diagnosis of hand OA ("Has a doctor ever told you that you have osteoarthritis or degenerative arthritis in your hand or fingers?"), and collection of information on socioeconomic factors, smoking exposure, weight, metabolic risk factors, comorbidities (Charlson Comorbidity Index [26]), and physical activity (Physical Activity Scale for the Elderly [27]).

Classification of exposures. We dichotomized baseline smoking status as never smoker (<100 lifetime cigarettes and no regular pipe, cigar, or cigarillo smoking) or ever smoker (current smoker or >100 cigarettes or regular pipe, cigar, or cigarillo smoking). Weight status was categorized, according to body mass index (BMI), as normal (≤25.0 kg/m^2), overweight (25.1–29.9 kg/m^2), or obese (≥30.0 kg/m^2). Underweight occurred rarely (0.7%) and was included in the normal weight category. We defined central obesity as a waist circumference of ≥102 cm in men and ≥88 cm in women (28,29) and high blood pressure as systolic blood pressure of ≥130 mm Hg and/or diastolic blood pressure of ≥85 mm Hg (29,30) or reported current treatment for diagnosed
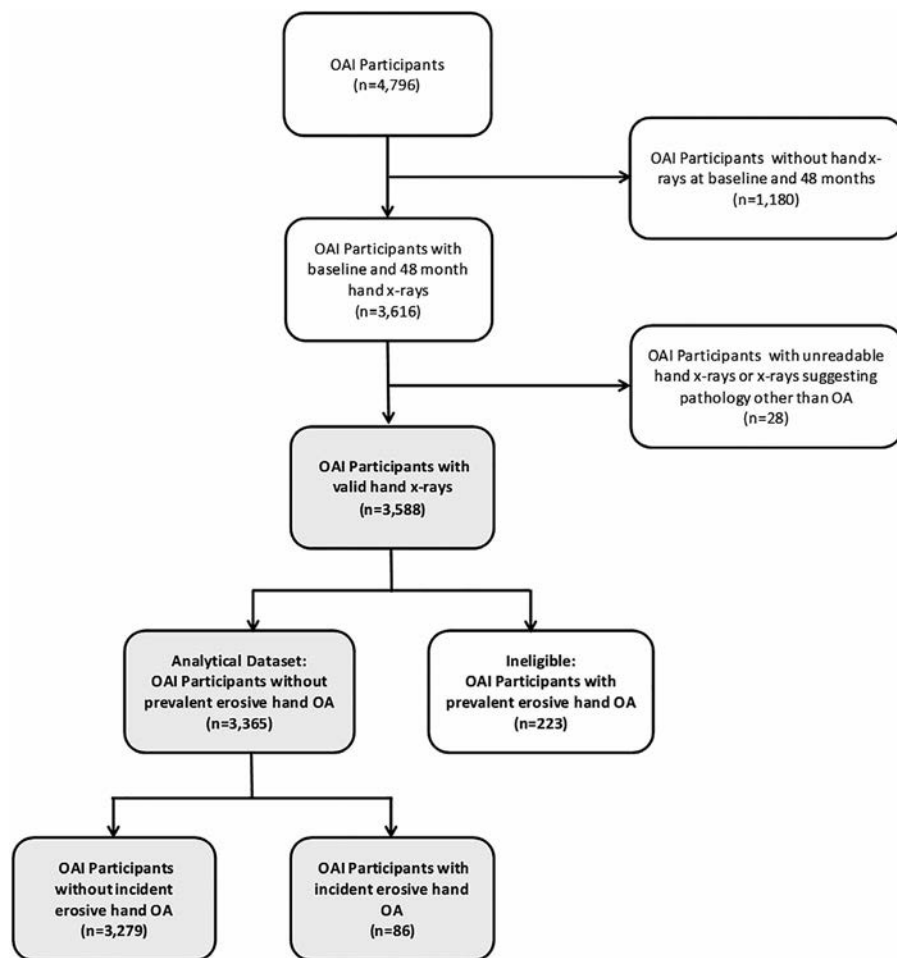
Figure 1. Flow diagram of the subjects who were assessed for the study, those who were found to be ineligible, and those who were found to be eligible and included. OAI = Osteoarthritis Initiative.

hypertension. Self-reported type 2 diabetes mellitus and use of lipid-lowering medications were used as proxies for impaired glucose tolerance and dyslipidemia, respectively.

Radiographic scoring. *Joints evaluated.* We performed each of the OA severity measurements on the second through the fifth distal (DIP) and proximal interphalangeal (PIP) and metacarpophalangeal (MCP) joints, thumb IP joint, and thumb-base joints (i.e., first carpometacarpal [CMC] joint and scaphotrapeziotrapezoidal joint). A musculoskeletal radiologist (LFS) and a rheumatologist (IKH), both experienced with these classification systems, performed the scoring of OA severity, erosions, and joint space narrowing (JSN).

OA severity (Kellgren/Lawrence [K/L] grading). We measured severity of OA according to a modified K/L scale (5) (0 = no OA, 1 = doubtful OA, 2 = mild OA, 3 = moderate OA, 4 = severe OA) (31,32). The modification allows classification of OA based on definite JSN even in the absence of osteophytes (32). The radiologist (LFS) trained in this K/L system and with good intrareader reliability (weighted κ > 0.84) (33) scored paired images, with blinding for chronology and clinical information. The

rheumatologist with expertise in hand OA radiographic scoring (IKH) performed quality control on all of the readings completed by LFS. Grading of joints with disagreements of >1 K/L grade (0.8% of 115,224 readable joints) was resolved in consensus with the musculoskeletal radiologist (SES).

Identification of joint erosions. The presence or absence of central erosions was recorded as a dichotomous variable, with scoring performed on paired radiographs with reference to the Osteoarthritis Research Society International (OARSI) atlas (31) and with the chronological order known. Briefly, in the erosive phase of central erosions, there is damage to the joint plate and presence of subchondral osteolytic lesions. Marginal erosions were classified as absent or present according to previous descriptions (Sharp/van der Heijde method) (34). The reproducibility of the reader's scoring of erosive hand OA erosions, tested in 70 hand radiographs, was excellent (median weighted κ = 0.90).

Measurement of JSN. The rheumatologist (IKH) scored JSN from 0 (no narrowing) to 3 with reference to the OARSI atlas (31). Intrareader reliability, tested in 70 hand radiographs, was excellent (median weighted κ = 0.92).

Measurement of interphalangeal joint space width (JSW). We used a semiautomated software tool to delineate the opposing margins of the MCP, PIP, and DIP joints, define a centrally located region of interest, and generate a measurement of JSW averaged over the second through the fifth fingers (35). For severely eroded joints, the JSW was set equal to 0 (i.e., fully destroyed joint). The reliability of the semiautomated method was determined by 2 readers who measured 30 hands (intraclass correlation coefficient [ICC; 2,1 model] 0.82–0.92). For the PIP and DIP joints, the measurement region covered 50% of the full width of the distal portion of the joint distance between the margins, while for the MCP joint it was 30% (see Supplementary Figure 1, on the *Arthritis & Rheumatology* website at http://onlinelibrary.wiley.com/doi/10.1002/art.41757/abstract).

Classification of hand OA and erosive hand OA. Subjects were classified as having hand OA if radiography revealed definite OA (K/L grade ≥ 2) in at least 1 IP joint on 2 different fingers. Joint analysis was confined to the second through the fifth DIP and PIP joints and all MCP joints, as prevalence of erosions was very low in the thumb-base joints (first CMC joint 0.2%; scaphotrapezial joint 0.3%). Subjects were classified as having erosive hand OA if, in addition, at least 1 DIP or PIP joint was shown to have a central erosion. MCP joints were not used to classify erosive hand OA, to reduce potential for misclassification. Erosive hand OA was then defined as *symptomatic* erosive hand OA when accompanied by a report of hand pain, aching, or stiffness on most days during the previous 30 days. For each outcome, incidence was defined as the presence of erosive hand OA or symptomatic erosive hand OA at 48 months but not at baseline. We did not use marginal erosions to classify erosive hand OA, as they were uncommon (n = 20) and the characteristics of individuals with marginal erosions appear to be fundamentally different from those with central erosions (significantly younger age, predominantly male, and lower frequency of OA). This suggests that marginal erosions may be a manifestation of other processes or possibly other forms of arthritis. For these reasons, we confined our definitions and analyses of erosive hand OA to subjects with central erosions.

Definitions of radiographic hand OA severity and progression. We derived 3 constructs to reflect the overall severity of OA in a hand: 1) the sum of K/L grades across all of the joints evaluated in that hand; 2) mean JSW, calculated as the average of JSW measurements from each joint in the second through the fifth fingers in that hand (irrespective of presence of OA); and 3) maximum JSN, defined as the maximum score from any of the measured joints. These constructs were used in both the cross-sectional analysis (single time point at baseline) and the longitudinal analysis (change from baseline to follow-up). For sensitivity analyses, we also derived measurements of JSW confined to affected joints (K/L grade >1 at baseline) and unaffected joints (K/L grade 0 at both baseline and follow-up).

Metacarpal cortical thickness. We measured metacarpal cortical thickness, a surrogate for bone density of the hands (36), in the second through the fifth metacarpi in the dominant hand. A customized interactive software tool was used to measure cortical thickness as an average width across the central area of each metacarpal (37). Intra- and interreader reliability of this method was determined using 20 samples selected at random. The ICC [3,1 model] for intrareader reliability was >0.98 for cortical thickness and >0.95 for metacarpal length, and the ICC [2,1 model] for interreader reliability was >0.97 for cortical thickness and >0.93 for metacarpal length. At the individual subject level, we defined the metacarpal index as the ratio between the sum of metacarpal length and the sum of cortical thickness in the second through the fifth fingers, such that a higher metacarpal index indicates lower cortical thickness (Supplementary Figure 2, http://onlinelibrary.wiley.com/doi/10.1002/art.41757/abstract).

Statistical analysis. Descriptive statistics were generated to characterize the study sample, including stratifying the sample by men and women. Since there are no clinical cut points for hand OA severity measures, these variables were standardized as Z scores in order to provide easier interpretation. Similarly, all continuous variables were standardized to facilitate comparison in the multivariable models. The statistical approach used to estimate the relative risk (RR) associated with incident erosive hand OA was accomplished through the use of a modified Poisson regression with a robust variance estimator (38,39). Using generalized estimating equations (GEEs) with an underlying Poisson distribution for the dependent variable, a robust variance estimator, an unstructured correlation matrix, and a log link function, the RR for each SD increase in OA severity, with 95% confidence interval (95% CI), was estimated for incident erosive hand OA in both unadjusted and adjusted GEE models. Model covariates included age, sex, race/ethnicity, and BMI. Associations between model covariates and OA severity were examined in order to reduce the influence of potential multicollinearity. All analyses were conducted with SAS, version 9.4.

RESULTS

Characteristics of the study population. The source sample comprised 3,365 eligible participants, of whom 86 participants (2.6%) developed erosive hand OA during the 48-month observation period (Figure 1), representing an occurrence rate of 0.66% per year. Among the 86 participants with incident erosive hand OA, there were 106 incident central erosive joints and 45 incident marginal erosive joints. All of the central erosive joints were localized within an osteoarthritic joint, but only 20 of the marginal erosions (44%) were associated with joint OA. Compared to

Table 1. Characteristics of the hand OA subcohort of the Osteoarthritis Initiative participants*

	No incident erosive hand OA (n = 3,279)	Incident erosive hand OA (n = 86)	P
Age, years	60.4 ± 9.0	64.8 ± 7.7	<0.001
Sex, no. (%)			<0.001
Male	1,472 (44.9)	21 (24.4)	
Female	1,807 (55.1)	65 (75.6)	
Race or ethnicity, no. (%)			0.016
White	2,639 (80.5)	76 (88.4)	
Black	548 (16.7)	6 (7.0)	
Hispanic/other	92 (2.8)	4 (4.7)	
Annual income, no. (%)			0.156
<$25,000	355 (11.6)	8 (10.1)	
$25,000–<$50,000	721 (23.5)	21 (26.6)	
$50,000–<$100,000	1,162 (37.9)	37 (46.8)	
≥$100,000	826 (27.0)	13 (16.5)	
Education level, no. (%)			0.145
High school or lower	447 (13.7)	18 (21.2)	
1–4 years of college	1,469 (45.1)	35 (41.2)	
Graduate school	1,344 (41.2)	32 (37.6)	
Smoking status, no. (%)			0.080
Never	1,799 (54.9)	39 (45.3)	
Ever	1,480 (45.1)	47 (54.7)	
BMI, kg/m^2	28.6 ± 4.8	26.8 ± 4.1	0.001
Abdominal circumference, cm	102.4 ± 12.9	100.9 ± 11.7	0.268
Systolic blood pressure, mm Hg	124 ± 16.1	125 ± 15.3	0.266
Diastolic blood pressure, mm Hg	76 ± 9.7	74 ± 12.7	0.068
BMI category, no. (%)			0.005
Normal	785 (24.0)	26 (30.2)	
Overweight	1,282 (39.1)	43 (50.0)	
Obese	1,210 (36.9)	17 (19.8)	
Waist circumference above cut point, no. (%)†	2,358 (73.8)	71 (83.5)	0.044
PASE score	166 ± 82.5	135 ± 69.9	<0.001
Diabetes, no. (%)	215 (6.7)	8 (9.6)	0.292
Hypertension, no. (%)	1,615 (49.3)	49 (57.0)	0.157
Lipid disorder, no. (%)	894 (27.3)	25 (29.1)	0.711
Charlson Comorbidity Index	0.35 ± 0.81	0.44 ± 0.96	0.334
Knee OA, no. (%)	1,821 (55.5)	45 (52.3)	0.554

* Except where indicated otherwise, values are the mean ± SD. OA = osteoarthritis; BMI = body mass index; PASE = Physical Activity Scale for the Elderly.
† Cut point 88 cm for women and 102 cm for men.

the subjects who did not develop erosive hand OA, the group that developed erosive hand OA was significantly older and less physically active, with a higher proportion of subjects who were female and who were White (Table 1). They also had significantly more frequent and more severe hand OA at baseline (Table 2). Among men, baseline BMI and abdominal circumference did not significantly differ between the group that developed incident erosive hand OA and the group that did not. However, among women, those who developed incident erosive hand OA had lower BMI at baseline (26.2 kg/m^2 versus 28.5 kg/m^2; P = 0.001).

Age and sex distribution. Descriptive analysis of erosive hand OA revealed a striking increase in incidence with age; in women, it occurred both at an earlier age than in men and with greater frequency at all increments of age (Figure 2). Multivariable analysis revealed a highly significant interaction between age and

sex (P < 0.001). In multivariable models stratified by sex, incident erosive hand OA was significantly associated with baseline age in women (RR per SD 1.45 [95% CI 1.16–1.80]) and men (RR 2.39 [95% CI 1.66–3.46]) (Table 3).

Relationship of incident erosive hand OA to hand OA severity. *Hand OA severity at baseline.* Compared to subjects who did not develop erosive hand OA, the erosive hand OA group more frequently reported hand pain and physician-diagnosed OA at baseline (Table 2). They had substantially and significantly more severe hand OA at baseline by all measures, i.e., sum K/L grade (mean 13.9 versus 5.3), maximum JSN grade (mean 2.3 versus 0.8), and IP joint space width (mean 1.14 mm versus 1.36 mm) (Table 2).

At the joint-specific level, each indicator of baseline hand OA severity (i.e., sum K/L grade, average JSW, and maximum

Table 2. Hand OA measurements and cortical thickness*

	No incident erosive hand OA (n = 3,279)	Incident erosive hand OA (n = 86)	P
Baseline measurements			
Physician-diagnosed hand OA, no. (%)	421 (13.3)	29 (34.9)	<0.001
Reported hand pain, no. (%)	635 (19.4)	35 (40.7)	<0.001
Sum hand joint K/L grade (not including thumb base)	5.30 ± 5.71	13.92 ± 5.33	<0.001
No. of hand joints with OA (not including thumb base)	1.81 ± 2.50	5.42 ± 2.58	<0.001
Maximum JSN grade, mm	0.78 ± 0.72	2.28 ± 0.55	<0.001
Average JSW in second through fifth fingers, mm	1.36 ± 0.19	1.36 ± 0.19	<0.001
Average cortical thickness, mm	1.52 ± 0.28	1.38 ± 0.26	<0.001
Longitudinal measurements			
Change in sum hand joint K/L grade (not including thumb base)	0.39 ± 0.94	1.99 ± 2.08	<0.001
Increase in no. of hand joints with OA (not including thumb base)	0.16 ± 0.50	0.51 ± 0.79	<0.001
JSN, mm	0.1032 ± 0.3057	0.6395 ± 0.5404	<0.001
Decrease in average JSW, mm	0.0136 ± 0.0619	0.0522 ± 0.0622	<0.001
Decrease in cortical thickness, mm	0.17 ± 0.10	0.20 ± 0.11	0.007

* Except where indicated otherwise, values are the mean ± SD. OA = osteoarthritis; K/L = Kellgren/Lawrence; JSN = joint space narrowing; JSW = joint space width.

JSN) strongly and independently predicted incident erosive hand OA (Table 4). These associations of baseline hand OA severity with incident erosive hand OA were evident for each severity measure in multivariable models adjusted for age, race/ethnicity, and BMI and were consistent in sex-specific models. For example, for the sum of hand joint K/L grades, the RR for incident erosive hand OA was 3.2 (95% CI 2.5–4.2) in men and 3.5 (95% CI 2.8–4.5) in women. While the sum K/L grade was highly correlated with maximum JSN (r = 0.71, $P < 0.001$), maximum JSN and IP JSW each retained independent associations with incident erosive hand OA when entered simultaneously in

the multivariable models (Supplementary Table 1, on the *Arthritis & Rheumatology* website at http://onlinelibrary.wiley.com/doi/10.1002/art.41757/abstract).

Longitudinal change in hand OA severity. During the observation period, the group that developed incident erosive hand OA also exhibited an increased rate of overall hand OA progression, indicated by aggregated measures of OA severity across all measured hand joints (Table 2). Compared to individuals who did not develop erosive hand OA, and with adjustment for age, sex, race/ethnicity, BMI, and baseline OA severity (sum K/L score), those with incident erosive hand OA had greater loss
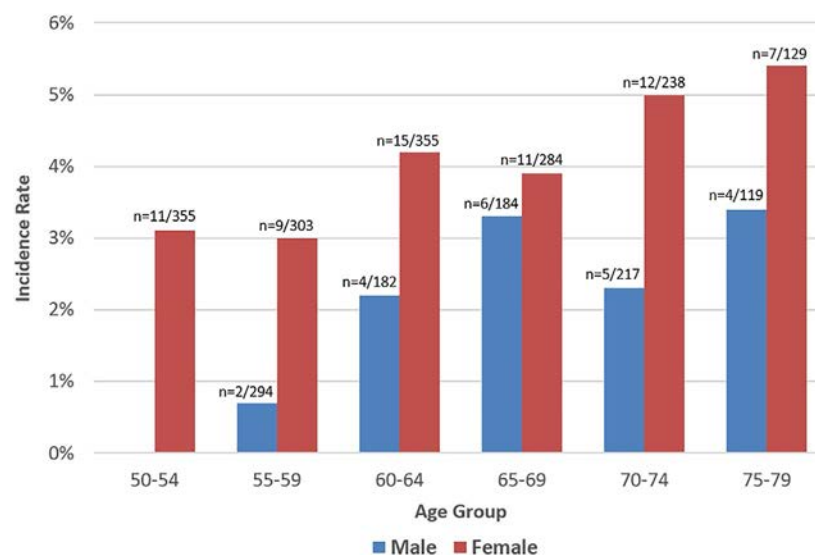
Figure 2. Incidence of erosive hand osteoarthritis by age and sex.

Table 3. Demographic and clinical risk factors for incident erosive hand OA*

	Relative risk (95% CI)		
	All participants (n = 86/3,365)	Men only (n = 21/1,493)	Women only (n = 65/1,872)
Age, per SD	1.63 (1.35–1.97)	2.39 (1.66–3.46)	1.45 (1.16–1.80)
Sex			
Male	Referent	–	–
Female	2.47 (1.52–4.02)	NA	NA
Race or ethnicity			
White	Referent	Referent	Referent
Black/Hispanic	0.56 (0.29–1.08)	0.65 (0.15–2.76)	0.47 (0.23–0.98)
Body mass index, per SD	0.67 (0.54–0.83)	1.00 (0.74–1.34)	0.65 (0.52–0.82)
Sum hand joint K/L grade, per SD	3.01 (2.64–3.44)	3.56 (2.79–4.53)	2.73 (2.33–3.20)

* OA = osteoarthritis; 95% CI = 95% confidence interval; NA = not applicable; K/L = Kellgren/Lawrence.

of mean JSW and greater change in maximum JSN and in sum K/L grade. These associations remained consistent with mutual adjustment and in sex-specific models (Table 4).

Relationship of incident erosive hand OA to JSW in joints without OA. At baseline, average JSW in the normal (K/L grade 0) IP joints in the second through the fifth fingers was similar between the group that developed erosive hand OA and the group that did not (mean ± SD 1.40 ± 0.21 and 1.44 ± 0.21 mm, respectively; P = 0.104). However, in the former group these joints exhibited substantially more loss of JSW over the observation period (0.04 ± 0.08 mm versus 0.02 ± 0.07 mm; P = 0.009).

Relationship of incident erosive hand OA to cortical thickness. Individuals who developed erosive hand OA had substantially lower cortical width at baseline than those who did not (mean ± SD 1.38 mm versus 1.52 mm; $P < 0.001$) and lost more cortical thickness over the observation period (0.20 mm versus 0.17 mm; P = 0.007). With adjustment for age, sex, race/ethnicity, and BMI, the association with baseline cortical thickness

became nonsignificant, although the association with loss of cortical thickness over time persisted (RR per SD 1.23 [95% CI 1.00–1.52]) (Supplementary Table 1, http://onlinelibrary.wiley.com/doi/10.1002/art.41757/abstract).

DISCUSSION

This study revealed several strong characteristics of erosive hand OA that provide a clear picture of a distinct and differentiated clinical endotype. Erosive hand OA occurred exclusively in joints already damaged by osteoarthritis, in most cases with a K/L grade of 2 or 3. This observation is consistent with natural history studies showing that loss of joint space is an early step in erosive evolution (40). However, the association was apparent not only within the joint in which the erosion developed but also across the whole hand, and was consistent for all 3 indicators of hand OA severity (mean K/L grade, mean JSW, and maximum JSN). The association with disease severity was evident not only cross-sectionally but also longitudinally. Thus, erosive hand OA occurs in the setting

Table 4. Relationships of OA severity to incident erosive hand OA*

	Relative risk (95% CI)†		
Model	All participants	Men only	Women only
Baseline severity			
Model 1: sum hand joint K/L grade, per SD	3.37 (2.81–4.05)	3.22 (2.47–4.21)	3.53 (2.78–4.49)
Model 2: average JSW, per SD	0.28 (0.20–0.41)	0.19 (0.12–0.31)	0.33 (0.21–0.51)
Model 3: maximum JSN, per SD	6.35 (5.44–7.40)	5.99 (4.34–8.26)	6.31 (5.33–7.47)
Model 4: all severity measures			
Sum hand joint K/L grade, per SD	1.47 (1.11–1.95)	1.32 (0.70–2.50)	1.47 (1.07–2.02)
Average JSW, per SD	0.67 (0.48–0.96)	0.38 (0.22–0.66)	0.88 (0.56–1.37)
Maximum JSN, per SD	5.18 (3.99–6.73)	4.07 (2.20–7.53)	5.75 (4.24–7.79)
Change in severity			
Model 5: sum hand joint K/L grade, per SD	1.66 (1.54–1.79)	1.71 (1.37–2.12)	1.67 (1.55–1.81)
Model 6: average JSW, per SD	2.03 (1.61–2.57)	1.77 (1.31–2.39)	2.17 (1.61–2.92)
Model 7: maximum JSN, per SD	1.82 (1.66–1.99)	1.82 (1.54–2.15)	1.83 (1.64–2.04)
Model 8: all severity measures			
Sum hand joint K/L grade, per SD	1.35 (1.15–1.58)	1.29 (0.95–1.75)	1.42 (1.19–1.70)
Average JSW, per SD	1.71 (1.37–2.13)	2.04 (1.53–2.73)	1.74 (1.30–2.34)
Maximum JSN, per SD	1.65 (1.40–1.95)	2.11 (1.72–2.58)	1.46 (1.19–1.78)

* OA = osteoarthritis; 95% CI = 95% confidence interval; K/L = Kellgren/Lawrence; JSW = joint space width; JSN = joint space narrowing.
† Adjusted for age, sex, body mass index, and race or ethnicity.

of preexisting hand OA, and in association with progression of OA severity in the hand. The incidence rate in this study was slightly lower than previously reported, likely due to differences in patient selection in the OAI versus other cohort studies (41). Regardless, the incidence rate of erosive hand OA is small enough to suggest that it is not a common end point of hand OA; most patients with hand OA do not develop erosions. Overall, our observations indicate that while the erosions of erosive hand OA develop in joints already damaged by OA, they occur in the context of generalized hand OA that is both more severe and progressing faster than OA in individuals who do not develop erosive hand OA.

We also found that incident erosive hand OA was associated with a greater rate of longitudinal loss of JSW even in joints that had no radiographic manifestations of OA (K/L grade 0) at either baseline or study end. This suggests that those joints, which did not have OA, were losing cartilage at a faster rate than the joints of subjects who did not develop erosive hand OA. The biologic basis for a greater rate of articular cartilage loss in normal joints in hands with erosive hand OA is conjectural but indicates a possible role of systemic processes in pathways to erosive hand OA development. This is especially salient at a time in which the field has moved away from viewing OA as a cartilage disorder (42). All of the associations between indicators of OA severity and erosive hand OA persisted with adjustment for age and potential confounders, and were consistent in sex-specific sensitivity analyses.

One of our prior hypotheses, inferred from the radiographic features characteristic of central erosions, was that erosive hand OA is in part a consequence of subchondral bone fragility. We tested this using measurement of cortical thickness as a proxy for bone health, similar to the method used in a previous study (43). We found that incident erosive hand OA was associated with reduced cortical bone thickness at baseline and with longitudinal loss between baseline and follow-up. The relationship between loss of cortical bone thickness and incident erosive hand OA remained significant after adjustment for age, sex, race/ethnicity, and BMI, but disappeared when measures of hand OA severity were added as covariates in the models. These results indicate that individuals who develop erosive hand OA have thinner bone and lose more bone during erosive hand OA development. While cortical thickness was not independently predictive, it remains biologically plausible that cortical fragility has an intermediary role in subchondral bone attrition and development of erosions. This would be analogous to the role of vertebral osteoporosis (also strongly related to age and sex) as a pathway to osteoporotic fracture (44,45), and would be conceptually consistent with an "osteoporotic" endotype of OA.

Alternatively, it is possible that the observed associations between cortical thickness loss and incident erosions represent co-occurring manifestations of hand OA progression, rather than a causal pathway. In this regard, it is pertinent that prior studies have demonstrated relationships between bone loss and hand OA progression (46,47). A limitation of the present finding with regard to a possible role of cortical thickness is that it was assessed in the metacarpals, therefore not providing a direct measurement at the exact anatomic site of erosion development. These issues predicate the need for further exploration of the interrelationships of bone health with progression of IP joint OA and development of central erosions, especially since they raise the possibility that interventions targeting bone could be a way to mitigate development of erosive hand OA.

We found inverse associations between measures of body weight and incidence of erosive hand OA in women, that were not evident in men. In fact, erosive hand OA in women was associated with lower BMI and smaller waist circumference but not with other factors that characterize metabolic syndrome, such as diabetes, hypertension, or lipid disorder; additionally, systolic and diastolic blood pressure did not differ significantly between the group that developed erosive hand OA and the group that did not. These results are counter to the prevailing perspective of hand OA as a disorder of obesity and metabolic syndrome (48). Instead, the spectrum of characteristics associated with erosive hand OA (more frequent in women, earlier and perimenopausal age at onset in women, lower BMI) suggests an endotype more reminiscent of osteoporosis or musculoskeletal frailty. It should be noted, though, that our findings are limited to subjects who were not morbidly obese since, as a condition of inclusion in the OAI, individuals may not be too obese to fit into a magnetic resonance imaging machine. Hence, incident erosive hand OA may be influenced by very high BMI, but it was not possible to analyze this association in our data set.

Limitations of this study must be considered. We classified central erosions dichotomously based on radiographic findings according to the OARSI atlas. However, there are other scoring and classification systems that may be more sensitive to erosive change (40,49), and classifications may differ between our study and other studies (50–52). The availability of only unilateral hand radiographs is another limitation that might have reduced the rate of detection of incident erosive hand OA in our sample. While this might have reduced case numbers, and possibly the strengths of associations, it should not affect the validity of the associations observed. One caveat regarding our analysis of average JSW is the possibility of bias resulting from nonstandardization of individual joint measurements, which could theoretically be influenced by anatomic variability in joint size. However, the JSW results were consistent with other structural outcomes and also consistent between the cross-sectional and longitudinal analyses. Nevertheless, we recommend development of a standardization approach in order to test this question in future studies. In addition, although the OAI recruited participants from the community, eligibility criteria were applied to assemble a cohort enriched with individuals at elevated risk for development of knee OA, one component of which was the presence of Heberden's nodes. Thus, the frequency of hand OA, and possibly erosive hand OA, may be greater in the OAI than the general population. However, the

incidence of erosive hand OA in our study is rather low compared to other studies (i.e., the Genetics, Arthrosis and Progression study) (41), which may be influenced by eligibility criteria. While these points should not influence the validity of any of the associations detected, they could affect generalizability of the magnitude of the associations to other samples. Our results should therefore be used as a basis for further examination of erosive hand OA in other populations. Finally, baseline dual x-ray absorptiometry scans were not available from the OAI for all subjects, precluding our ability to conduct analyses to complement the cortical thickness measurements. We further recognize the need for circumspection regarding the associations with cortical thickness, as this measure is not a widely used method for assessing bone health.

Taken together, the present findings present a perspective of erosive hand OA as a disorder of aging with a female predominance that occurs in the setting of preexisting osteoarthritis, and is strongly associated with both the severity of articular structural damage and its progression. Individuals who develop erosive hand OA have thinner bones prior to its development and lose more bone and cartilage (even in joints without OA) as the disorder progresses. These observations, together with lower levels of physical activity and lower BMI (in women), suggest that erosive hand OA is a disorder involving musculoskeletal frailty and accelerated aging.

ACKNOWLEDGMENTS

AUTHOR CONTRIBUTIONS

All authors were involved in drafting the article or revising it critically for important intellectual content, and all authors approved the final version to be published. Dr. McAlindon had full access to all of the data in the study and takes responsibility for the integrity of the data and the accuracy of the data analysis.
Study conception and design. McAlindon, Driban, Duryea, Haugen, Eaton.
Acquisition of data. McAlindon, Driban, Duryea, Haugen, Schaefer, Smith, Mathiessen, Eaton.
Analysis and interpretation of data. McAlindon, Driban, Roberts, Eaton.

REFERENCES

1. Dillon CF, Hirsch R, Rasch EK, Gu Q. Symptomatic hand osteoarthritis in the United States: prevalence and functional impairment estimates from the third U.S. National Health and Nutrition Examination Survey, 1991-1994. Am J Phys Med Rehabil 2007;86:12–21.

2. Lawrence RC, Felson DT, Helmick CG, Arnold LM, Choi H, Deyo RA, et al. Estimates of the prevalence of arthritis and other rheumatic conditions in the United States. Part II. Arthritis Rheum 2008;58:26–35.

3. Zhang Y, Niu J, Kelly-Hayes M, Chaisson CE, Aliabadi P, Felson DT. Prevalence of symptomatic hand osteoarthritis and its impact on functional status among the elderly: the Framingham Study. Am J Epidemiol 2002;156:1021–7.

4. Kallman DA, Wigley FM, Scott WW Jr, Hochberg MC, Tobin JD. New radiographic grading scales for osteoarthritis of the hand: reliability for determining prevalence and progression. Arthritis Rheum 1989;32:1584–91.

5. Kellgren JH, Lawrence JS. Radiological assessment of osteoarthrosis. Ann Rheum Dis 1957;16:494–502.

6. Kortekaas MC, Kwok WY, Reijnierse M, Huizinga TW, Kloppenburg M. In erosive hand osteoarthritis more inflammatory signs on ultrasound are found than in the rest of hand osteoarthritis. Ann Rheum Dis 2013;72:930–4.

7. Punzi L, Ramonda R, Oliviero F, Sfriso P, Mussap M, Plebani M, et al. Value of C reactive protein in the assessment of erosive osteoarthritis of the hand. Ann Rheum Dis 2005;64:955–7.

8. Gabriel SE. The epidemiology of rheumatoid arthritis [review]. Rheum Dis Clin North Am 2001;27:269–81.

9. Kwok WY, Kloppenburg M, Rosendaal FR, van Meurs JB, Hofman A, Bierma-Zeinstra SM. Erosive hand osteoarthritis: its prevalence and clinical impact in the general population and symptomatic hand osteoarthritis. Ann Rheum Dis 2011;70:1238–42.

10. Verbruggen G, Wittoek R, Vander Cruyssen B, Elewaut D. Tumour necrosis factor blockade for the treatment of erosive osteoarthritis of the interphalangeal finger joints: a double blind, randomised trial on structure modification. Ann Rheum Dis 2012;71:891–8.

11. Chevalier X, Eymard F, Richette P. Biologic agents in osteoarthritis: hopes and disappointments [review]. Nat Rev Rheumatol 2013;9:400–10.

12. Aitken D, Laslett LL, Pan F, Haugen IK, Otahal P, Bellamy N, et al. A randomised double-blind placebo-controlled crossover trial of HUMira (adalimumab) for erosive hand OsteoaRthritis: the HUMOR trial. Osteoarthritis Cartilage 2018;26:880–7.

13. Banks SE. Erosive osteoarthritis: a current review of a clinical challenge [review]. Clin Rheumatol 2010;29:697–706.

14. Addimanda O, Mancarella L, Dolzani P, Punzi L, Fioravanti A, Pignotti E, et al. Clinical and radiographic distribution of structural damage in erosive and nonerosive hand osteoarthritis. Arthritis Care Res (Hoboken) 2012;64:1046–53.

15. Anandarajah A. Erosive osteoarthritis [review]. Discov Med 2010;9:468–77.

16. Rovetta G, Bianchi G, Monteforte P. Joint failure in erosive osteoarthritis of the hands [review]. Int J Tissue React 1995;17:33–42.

17. Schraml C, Schwenzer NF, Martirosian P, Koetter I, Henes JC, Geiger K, et al. Assessment of synovitis in erosive osteoarthritis of the hand using DCE-MRI and comparison with that in its major mimic, the psoriatic arthritis. Acad Radiol 2011;18:804–9.

18. Tan AL, Grainger AJ, Tanner SF, Shelley DM, Pease C, Emery P, et al. High-resolution magnetic resonance imaging for the assessment of hand osteoarthritis. Arthritis Rheum 2005;52:2355–65.

19. Martel W, Stuck KJ, Dworin AM, Hylland RG. Erosive osteoarthritis and psoriatic arthritis: a radiologic comparison in the hand, wrist, and foot. AJR Am J Roentgenol 1980;134:125–35.

20. Rothschild BM. Distinguishing erosive osteoarthritis and calcium pyrophosphate deposition disease [editorial]. World J Orthop 2013;4:29–31.

21. Tan AL, Grainger AJ, Tanner SF, Emery P, McGonagle D. A high-resolution magnetic resonance imaging study of distal interphalangeal joint arthropathy in psoriatic arthritis and osteoarthritis: are they the same? Arthritis Rheum 2006;54:1328–33.

22. Smythe HA. Osteoarthritis, insulin and bone density. J Rheumatol 1987;14:91–3.

23. Saviola G, Abdi-Ali L, Campostrini L, Sacco S, Baiardi P, Manfredi M, et al. Clodronate and hydroxychloroquine in erosive osteoarthritis: a 24-month open randomized pilot study. Mod Rheumatol 2012;22:256–63.

24. Vlychou M, Koutroumpas A, Alexiou I, Fezoulidis I, Sakkas LI. High-resolution ultrasonography and 3.0 T magnetic resonance imaging

in erosive and nodal hand osteoarthritis: high frequency of erosions in nodal osteoarthritis. Clin Rheumatol 2013;32:755–62.

25. Lionetto L, Negro A, Palmisani S, Gentile G, Del Fiore MR, Mercieri M, et al. Emerging treatment for chronic migraine and refractory chronic migraine [review]. Expert Opin Emerg Drugs 2012;17:393–406.

26. Charlson ME, Pompei P, Ales KL, MacKenzie CR. A new method of classifying prognostic comorbidity in longitudinal studies: development and validation. J Chronic Dis 1987;40:373–83.

27. Washburn RA, Smith KW, Jette AM, Janney CA. The physical activity scale for the elderly (PASE): development and evaluation. J Clin Epidemiol 1993;46:153–62.

28. Alberti KG, Eckel RH, Grundy SM, Zimmet PZ, Cleeman JI, Donato KA, et al. Harmonizing the metabolic syndrome: a joint interim statement of the International Diabetes Federation Task Force on Epidemiology and Prevention; National Heart, Lung, and Blood Institute; American Heart Association; World Heart Federation; International Atherosclerosis Society; and International Association for the Study of Obesity. Circulation 2009;120:1640–5.

29. National Cholesterol Education Program (NCEP) Expert Panel on Detection, Evaluation, and Treatment of High Blood Cholesterol in Adults (Adult Treatment Panel III). Third report of the National Cholesterol Education Program (NCEP) Expert Panel on Detection, Evaluation, and Treatment of High Blood Cholesterol in Adults (Adult Treatment Panel III) final report. Circulation 2002;106:3143–421.

30. Alberti KG, Zimmet P, Shaw J. The metabolic syndrome: a new worldwide definition. Lancet 2005;366:1059–62.

31. Altman RD, Gold GE. Atlas of individual radiographic features in osteoarthritis, revised. Osteoarthritis Cartilage 2007;15:A1–56.

32. Haugen IK, Englund M, Aliabadi P, Niu J, Clancy M, Kvien TK, et al. Prevalence, incidence and progression of hand osteoarthritis in the general population: the Framingham Osteoarthritis Study. Ann Rheum Dis 2011;70:1581–6.

33. Schaefer LF, McAlindon TE, Eaton CB, Roberts MB, Haugen IK, Smith SE, et al. The associations between radiographic hand osteoarthritis definitions and hand pain: data from the Osteoarthritis Initiative. Rheumatol Int 2018;38:403–13.

34. Van der Heijde D. How to read radiographs according to the Sharp/ van der Heijde method. J Rheumatol 2000;27:261–3.

35. Finckh A, de Pablo P, Katz JN, Neumann G, Lu Y, Wolfe F, et al. Performance of an automated computer-based scoring method to assess joint space narrowing in rheumatoid arthritis: a longitudinal study. Arthritis Rheum 2006;54:1444–50.

36. Böttcher J, Malich A, Pfeil A, Petrovitch A, Lehmann G, Heyne J, et al. Potential clinical relevance of digital radiogrammetry for quantification of periarticular bone demineralization in patients suffering from rheumatoid arthritis depending on severity and compared with DXA. Eur Radiol 2004;14:631–7.

37. Duryea J, Driban JB, Roberts M, Eaton C, McAlindon TE. Measurements of metacarpal length and cortical thickness: a longitudinal assessment of hand radiographs from the Osteoarthritis Initiative. Osteoarthritis Cartilage 2018;26:S430–1.

38. McNutt LA, Wu C, Xue X, Hafner JP. Estimating the relative risk in cohort studies and clinical trials of common outcomes. Am J Epidemiol 2003;157:940–3.

39. Zou G. A modified Poisson regression approach to prospective studies with binary data. Am J Epidemiol 2004;159:702–6.

40. Verbruggen G, Veys EM. Numerical scoring systems for the anatomic evolution of osteoarthritis of the finger joints. Arthritis Rheum 1996;39:308–20.

41. Bijsterbosch J, van Bemmel JM, Watt I, Meulenbelt I, Rosendaal FR, Huizinga TW, et al. Systemic and local factors are involved in the evolution of erosions in hand osteoarthritis. Ann Rheum Dis 2011;70:326–30.

42. Brandt KD, Radin EL, Dieppe PA, van de Putte L. Yet more evidence that osteoarthritis is not a cartilage disease. Ann Rheum Dis 2006;65:1261–4.

43. Sharp JT, Tsuji W, Ory P, Harper-Barek C, Wang H, Newmark R. Denosumab prevents metacarpal shaft cortical bone loss in patients with erosive rheumatoid arthritis. Arthritis Care Res (Hoboken) 2010;62:537–44.

44. Buckland-Wright JC, Lynch JA, Rymer J, Fogelman I. Fractal signature analysis of macroradiographs measures trabecular organization in lumbar vertebrae of postmenopausal women. Calcif Tissue Int 1994;54:106–12.

45. Weinstein RS, Majumdar S. Fractal geometry and vertebral compression fractures. J Bone Miner Res 1994;9:1797–802.

46. Güler-Yüksel M, Bijsterbosch J, Allaart CF, Meulenbelt I, Kroon HM, Watt I, et al. Accelerated metacarpal bone mineral density loss is associated with radiographic progressive hand osteoarthritis. Ann Rheum Dis 2011;70:1625–30.

47. Sowers M, Zobel D, Hawthorne VM, Carman W, Weissfeld L. Progression of osteoarthritis of the hand and metacarpal bone loss: a twenty-year followup of incident cases. Arthritis Rheum 1991;34:36–42.

48. Yusuf E, Nelissen RG, Ioan-Facsinay A, Stojanovic-Susulic V, DeGroot J, van Osch G, et al. Association between weight or body mass index and hand osteoarthritis: a systematic review. Ann Rheum Dis 2010;69:761.

49. Verbruggen G, Wittoek R, Cruyssen BV, Elewaut D. Morbid anatomy of 'erosive osteoarthritis' of the interphalangeal finger joints: an optimised scoring system to monitor disease progression in affected joints. Ann Rheum Dis 2010;69:862–7.

50. Pattrick M, Aldridge S, Hamilton E, Manhire A, Doherty M. A controlled study of hand function in nodal and erosive osteoarthritis. Ann Rheum Dis 1989;48:978–82.

51. Olejarova M, Kupka K, Pavelka K, Gatterova J, Stolfa J. Comparison of clinical, laboratory, radiographic, and scintigraphic findings in erosive and nonerosive hand osteoarthritis: results of a two-year study. Joint Bone Spine 2000;67:107–12.

52. Haugen IK, Magnusson K, Turkiewicz A, Englund M. The prevalence, incidence, and progression of hand osteoarthritis in relation to body mass index, smoking, and alcohol consumption. J Rheumatol 2017;44:1402–9.

AMERICAN COLLEGE
of RHEUMATOLOGY
Empowering Rheumatology Professionals

The CRTAC1 Protein in Plasma Is Associated With Osteoarthritis and Predicts Progression to Joint Replacement: A Large-Scale Proteomics Scan in Iceland

Unnur Styrkarsdottir,[1] (ID) Sigrun H. Lund,[1] Saedis Saevarsdottir,[2] Magnus I. Magnusson,[1]
Kristbjorg Gunnarsdottir,[1] Gudmundur L. Norddahl,[1] Michael L. Frigge,[1] Erna V. Ivarsdottir,[1] Gyda Bjornsdottir,[1]
Hilma Holm,[1] Gudmundur Thorgeirsson,[3] Thorunn Rafnar,[1] Ingileif Jonsdottir,[3] Thorvaldur Ingvarsson,[4]
Helgi Jonsson,[5] Patrick Sulem,[1] Unnur Thorsteinsdottir,[6] Daniel Gudbjartsson,[6] and Kari Stefansson[6] (ID)

Objective. Biomarkers for diagnosis and progression of osteoarthritis (OA) are lacking. This study was undertaken to identify circulating biomarkers for OA that could predict disease occurrence and/or progression to joint replacement.

Methods. Using the SomaScan platform, we measured 4,792 proteins in plasma from 37,278 individuals, of whom 12,178 individuals had OA and 2,524 had undergone joint replacement. We performed a case–control study for identification of potential protein biomarkers for hip, knee, and/or hand OA, and a prospective study for identification of biomarkers for joint replacement.

Results. Among the large panel of plasma proteins assessed, cartilage acidic protein 1 (CRTAC1) was the most strongly associated with both OA diagnosis (odds ratio 1.46 [95% confidence interval 1.41–1.52] for knee OA, odds ratio 1.36 [95% confidence interval 1.29–1.43] for hip OA, and odds ratio 1.33 [95% confidence interval 1.26–1.40] for hand OA) and progression to joint replacement (hazard ratio 1.40 [95% confidence interval 1.30–1.51] for knee replacement and hazard ratio 1.31 [95% confidence interval 1.19–1.45] for hip replacement). Patients with OA who were in the highest quintile of risk of joint replacement, based on known risk factors (i.e., age, sex, and body mass index) and plasma CRTAC1 level, were 16 times more likely to undergo knee replacement within 5 years of plasma sample collection than those in the lowest quintile, and 6.5 times more likely to undergo hip replacement. CRTAC1 was not associated with other types of inflammatory arthritis. A specific protein profile was identified in those patients who had undergone joint replacement prior to plasma sample collection.

Conclusion. Through a hypothesis-free approach, we identified CRTAC1 in plasma as a novel promising candidate biomarker for OA that is both associated with occurrence of OA and predictive of progression to joint replacement. This biomarker might also be useful in the selection of suitable patients for clinical trial enrollment.

INTRODUCTION

Osteoarthritis (OA) is a major global health burden affecting >300 million people worldwide (1). Prevalence of OA is increasing since the prevalence of its main risk factors, obesity and older age, continue to rise (2–4). The disease can have a great impact on quality of life due to pain and loss of joint function, mostly affecting the knees, hips, and hands. OA is a heterogeneous disease with variable radiographic and clinical features (5), and there are presently no measures available for early diagnosis before destructive

changes are observable on radiographs. The current therapeutic approach consists of pain medications, lifestyle changes with weight reduction and exercise, and joint arthroplasty for severe disease (3), since no disease-modifying drugs are available. Thus, there is an unmet need for treatment that could effectively slow or halt OA progression.

A biomarker that is associated with OA disease occurrence and/or progression would help to identify cases earlier or monitor the disease course. Lack of such biomarkers has hindered development of effective therapy for this common disease. There are several studies on candidate biomarkers for OA (6–8), with somewhat inconclusive findings, possibly reflecting heterogeneity in the disease definition, study design, or size. However, meta-analyses of the 2 most extensively studied biomarkers for OA, serum cartilage oligomeric matrix protein (COMP) and urinary C-terminal telopeptide of type II collagen (CTX-II), show correlation with both disease occurrence and progression (9–13). These biomarkers are, however, not currently used in clinical settings.

In this study, we conducted a large-scale screen of biomarkers for OA, examining 4,792 human proteins in plasma from 39,155 individuals. We aimed to find a biomarker that is specific for OA development and/or disease progression, preferably a single biomarker since this is most feasible in the clinical setting, but also a more comprehensive tool that could yield better prediction. We included plasma proteins and known risk factors for OA (i.e., age, sex, and body mass index [BMI]) in the association and prediction models. To improve the models, we also included polygenic risk scores for OA, accounting for the role of genetics, as >80 independent sequence variants have been associated with the risk of OA to date (14,15).

SUBJECTS AND METHODS

Study population. We generated proteomics data from plasma collected from 39,155 Icelanders between August 2000 and January 2019, using 4,963 slow off-rate modified aptamers (SOMAmers) (SomaLogic; https://somalogic.com/) that measured 4,792 individual human plasma proteins (Supplementary Figure 1, available on the *Arthritis & Rheumatology* website at http://onlinelibrary.wiley.com/doi/10.1002/art.41793/abstract). We gathered information on OA diagnosis (International Statistical Classification of Diseases and Related Health Problems, Tenth Revision codes M16.0, M16.1, M17.0, M17.1, M15.1, M15.2, M18.0, M18.1, or M18.9, and clinical hand OA) and history of joint replacement (Nordic Medico-Statistical Committee Classification of Surgical Procedures [NCSP] codes NFB or NGB) from hospitals, health care providers, and clinicians (through March 2020). Detailed descriptions of the proteomics data, the OA phenotype definition, and study procedures are provided in Supplementary Methods (http://onlinelibrary.wiley.com/doi/10.1002/art.41793/abstract).

We designed 3 main studies from these 39,155 samples: 1) case–control association studies of OA, including 6,136 subjects with primary OA of the hips, knees, or hands (excluding those with prior joint replacement) and 13,789–16,001 controls without OA, 2) a prospective study of progression to joint replacement, including 10,701 subjects with OA, and 3) a case–control association study of prior joint replacement, including 1,452 cases and 35,826 controls. Subjects with missing information regarding age, sex, or BMI were excluded from all analyses, as were those who had rheumatoid arthritis (RA) or were age <40 years at the time of plasma sampling from analyses 1 and 2 (Figure 1 and Supplementary Methods).

In a secondary analysis of hand OA severity, we used 2 data sets. One included patients with hand OA for whom the severity of disease was evaluated by radiography and clinical findings. The second data set included individuals who participated in the population-based deCODE Health study (16) and had available high-quality hand photographs for analysis of hand OA (17,18). Subjects who participated in the deCODE Health study also answered a simple question regarding pain. Details of these analyses are available in Supplementary Methods.

The study was approved by the National Bioethics Committee of Iceland (VSN_14-015v8, VSN_14-148, and VSN_15-214), and was conducted in accordance with requirements issued by the Data Protection Authority of Iceland. All participants were of Icelandic descent.

Comparison of SOMAmer measurements with Olink assay. To test the specificity of the SomaScan measurements, we measured proteins using a proximity extension assay method (Olink Bioscience) (19). Proteins were measured using a cardiometabolic panel of 92 unique proteins, including cartilage acidic protein 1 (CRTAC1) and COMP. Of 200 samples, all of which had been assayed by SomaScan, 199 passed quality control. The median correlation between proteins was 0.757, ranging from –0.128 to 0.949, with an interquartile range of 0.541 to 0.829.

Polygenic risk scores. A polygenic risk score integrates a large fraction of the genetics contributing to a disease. We generated the polygenic risk scores based on effect estimates from OA genome-wide association study (GWAS) data in the UK Biobank (www.ukbiobank.ac.uk) (14) and calculated the risk scores for genotyped Icelanders, using 600,000 common variants and LDpred software, essentially as previously described (20). Details are provided in the Supplementary Methods (http://online library.wiley.com/doi/10.1002/art.41793/abstract).

Genome-wide association of plasma proteins (protein quantitative trait locus [QTL] study). To identify a set of independent DNA sequence variants that are associated with each protein, we performed a genome-wide association analysis (significance threshold $P < 5 \times 10^{-8}$) with a subsequent recursive
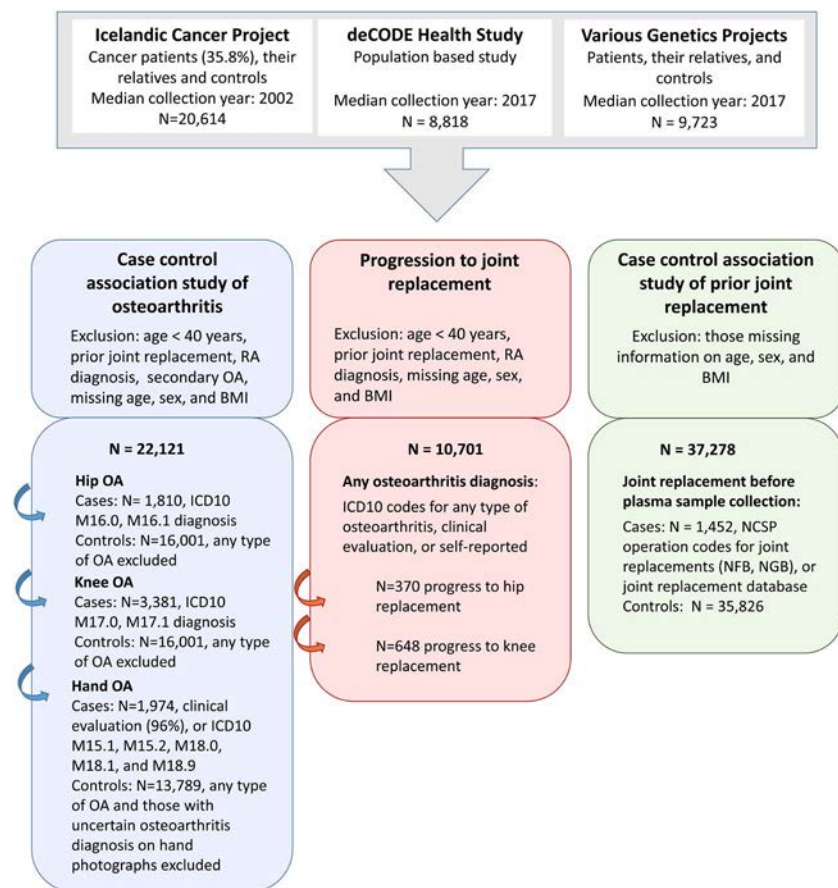
Figure 1. Schematic overview of the osteoarthritis (OA) biomarker study, with exclusion and inclusion criteria for the 3 main studies from which patients were derived. RA = rheumatoid arthritis; BMI = body mass index; ICD-10 = International Statistical Classification of Diseases and Related Health Problems, Tenth Revision; NCSP = Nordic Medico-Statistical Committee Classification of Surgical Procedures. Color figure can be viewed in the online issue, which is available at http://onlinelibrary.wiley.com/doi/10.1002/art.41793/abstract.

conditional analysis, resulting in a list of independent protein QTL sequence variants that were associated with proteins (see Supplementary Methods and Supplementary Note, available on the *Arthritis & Rheumatology* website at http://onlinelibrary.wiley.com/doi/10.1002/art.41793/abstract).

Statistical analysis. Plasma protein levels were adjusted for the age of the individual at the time of plasma collection, sex, collection site, and the storage age of the sample. After adjustment, the plasma protein levels were rank-transformed onto the standard normal distribution with a mean of 0 and SD of 1. All modeling was completed with standardized protein levels, whereas raw unadjusted levels of CRTAC1 were used in visual representations (e.g., correlation with hand OA severity in Figure 2 and Kaplan-Meier curves in Figure 3).

Differences in plasma protein levels after joint replacement as well as their association with hip, knee, and hand OA were estimated with logistic regression, and area under the curve (AUC) was estimated using the bootstrap method. The risk of hip and knee replacement from the time of sample collection was estimated with Cox proportional hazards regression and visualized with Kaplan-Meier curves. Association of plasma protein levels with hand OA severity was estimated by linear regression. We used Bonferroni correction to adjust for multiple testing, yielding the following *P* values for each model: 1) $P \leq 3.3 \times 10^{-6}$ in analyses of association with OA, accounting for 3 phenotypes and 4,983 aptamers (which capture 4,792 proteins); 2) $P \leq 1.0 \times 10^{-5}$ in analyses of association with joint replacement, accounting for 1 phenotype and 4,983 aptamers; and 3) $P \leq 5.0 \times 10^{-6}$ in analyses of risk of progression to joint replacement, accounting for 2 phenotypes and 4,983 aptamers. A detailed description of the statistical methods is provided in the Supplementary Methods (http://onlinelibrary.wiley.com/doi/10.1002/art.41793/abstract).

Data availability. Data supporting the findings of this study are presented herein and in the supplementary data files, and also can be provided upon request from the corresponding author.

RESULTS

Association of plasma proteins with OA diagnosis. We tested whether any of the measured plasma proteins were associated with OA, adjusting the analysis for known disease risk factors (i.e., older age, female sex, and higher BMI). This adjustment is critical
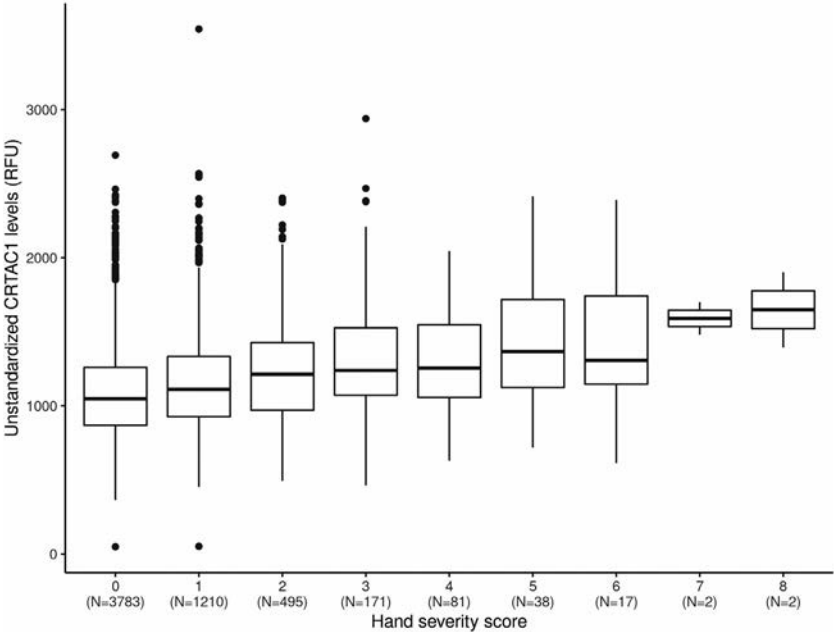
Figure 2. Correlation between cartilage acidic protein 1 (CRTAC1) levels in plasma and hand osteoarthritis severity scores. Correlation between unstandardized levels of CRTAC1 in plasma and hand osteoarthritis severity scores was estimated based on digital photographs (n = 5,445). Photographs were taken at the same time plasma samples were collected from participants in the deCODE Health study (18) and scored for the presence and severity of osteoarthritis, resulting in an aggregate score. Patients with rheumatoid arthritis were excluded. Data are presented as box plots, where the boxes represent the 25th to 75th percentiles, the lines within the boxes represent the median, and the lines outside the boxes represent the 10th to 90th percentiles. Circles represent outliers. All patients were age >40 years. RFU = relative fluorescence units.

to exclude confounders, as a vast number of the 4,792 measured proteins are associated with these traits (e.g., 96% of the proteins tested were significantly associated with BMI in our data set).

We identified 45 proteins associated with knee OA, 7 proteins associated with hip OA, and 44 proteins associated with hand OA,

that met the threshold for significance when accounting for multiple testing ($P \leq 3.3 \times 10^{-6}$; accounting for 3 phenotypes and 4,983 protein aptamers) and after excluding proteins that were also associated with inflammatory arthritis (Supplementary Table 1, available on the *Arthritis & Rheumatology* website at http://onlinelibrary.wiley.
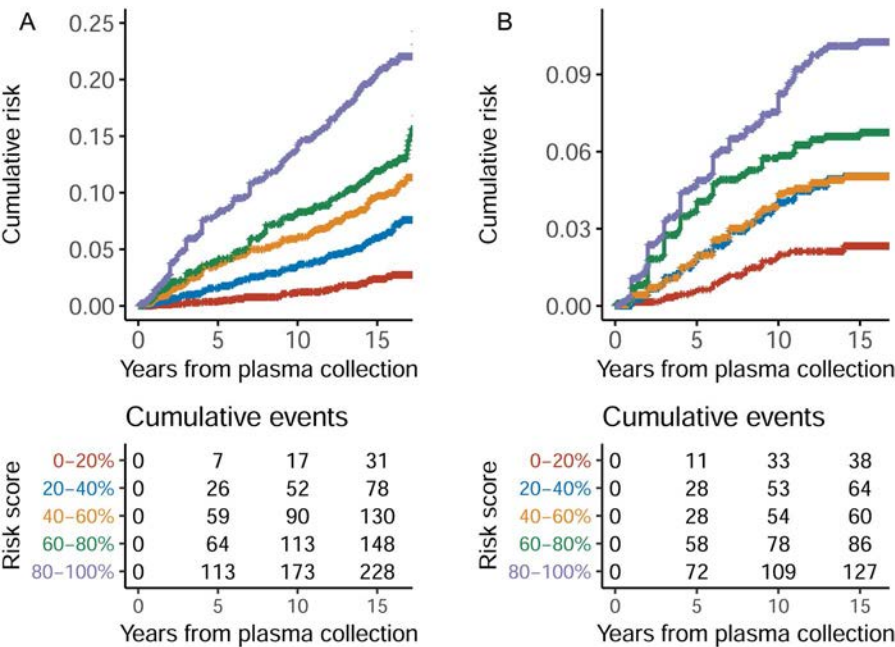
Figure 3. Kaplan-Meier estimates of the cumulative risk of knee replacement (**A**) or hip replacement (**B**) from the time of plasma collection, based on plasma cartilage acidic protein 1 levels and age, sex, and body mass index (top). Cumulative number of joint replacement events over time according to quintiles of risk score among participants (bottom). OA progressed to hip replacement in 376 patients, and to knee replacement in 672 patients.

Table 1. Association of plasma CRTAC1 levels with OA, other joint disorders, joint pain, hand OA severity, and joint replacement*

Phenotype	OR or HR (95% CI)†	P	No. cases/ controls
Hand OA	1.33 (1.26–1.40)	4.6×10^{-27}	1,712/15,242
Hip OA	1.36 (1.29–1.43)	2.1×10^{-35}	1,903/17,644
Knee OA	1.46 (1.41–1.52)	1.2×10^{-86}	3,578/17,644
Joint pain	1.15 (1.04–1.27)	0.0043	724/1,832
RA	0.96 (1.05–0.89)	0.39	525/25,764
Gout	0.94 (1.03–0.87)	0.17	512/24,476
Psoriatic arthritis	0.83 (0.98–0.71)	0.024	158/24,830
Thumb severity score	1.09 (1.01–1.17)	0.022	2,350/0
Finger severity score	1.12 (1.04–1.21)	0.0030	2,350/0
Hand severity score	1.08 (1.05–1.11)	7.6×10^{-10}	5,445/0
Hip replacement	1.31 (1.19–1.45)	8.4×10^{-08}	10,701/0
Knee replacement	1.40 (1.30–1.51)	1.0×10^{-18}	10,701/0

* Subjects were age >40 years at the time of plasma collection. For joint pain and hand severity score, plasma samples were obtained at the time the information on joint pain or hand severity score was collected. For all other phenotypes, the plasma samples were obtained at various time points in relation to osteoarthritis (OA) diagnosis. CRTAC1 = cartilage acidic protein 1; 95% CI = 95% confidence interval; RA = rheumatoid arthritis.
† Hazard ratios (HRs) are shown for risk of hip replacement and knee replacement; for all other variables, odds ratios (ORs) are shown. ORs and HRs are per SD increase in the protein level.

com/doi/10.1002/art.41793/abstract). Of these, CRTAC1, a marker of chondrocyte development, was the protein that showed the most strongly significant association with all 3 OA subtypes (odds ratio [OR] for knee OA 1.46 per SD increase of the standardized protein level [$P = 1.2 \times 10^{-86}$], OR 1.36 for hip OA [$P = 2.1 \times 10^{-35}$], and OR 1.33 for hand OA [$P = 4.6 \times 10^{-27}$]) (Table 1 and Supplementary Tables 1 and 2, available on the *Arthritis & Rheumatology* website at http://onlinelibrary.wiley.com/doi/10.1002/art.41793/abstract). The plasma CRTAC1 level was more strongly associated with OA by several orders of magnitude compared to any of the other proteins measured. COMP, an investigative biomarker for OA, was the second most significantly associated protein (OR 1.31 for knee OA [$P = 8.5 \times 10^{-43}$], 1.26 for hip OA [$P = 4.5 \times 10^{-20}$], and 1.19 for hand OA [$P = 2.3 \times 10^{-10}$]). COMP was somewhat correlated with CRTAC1 in our data ($r^2 = 0.362$ [95% confidence interval 0.355–0.370]). In models conditioning on the CRTAC1 levels, the association of COMP with OA was no longer significant ($P = 0.013$, $P = 0.029$, and $P = 0.97$ for knee, hip, and hand OA, respectively), whereas the association of CRTAC1 with OA remained significant in models conditioning on the COMP levels ($P = 5.3 \times 10^{-47}$, $P = 5.3 \times 10^{-18}$, and $P = 3.0 \times 10^{-18}$ for knee, hip, and hand OA, respectively).

The majority of the associated proteins correlated nominally with all 3 forms of OA. For 5 of these proteins, CRTAC1, COMP, cartilage intermediate-layer protein, retinoblastoma-like 2, and cytokine-like 1, the correlations with all 3 forms of OA were significant (Supplementary Table 1).

Approximately half of our samples were derived from a cancer study (The Icelandic Cancer Project, see Figure 1 and Supplementary Methods), which may have affected the results of our association analysis. However, when we tested the association of the

proteins with any type of cancer, CRTAC1 levels ranked as 1,337. Furthermore, adjusting the association analysis for cancer did not significantly change the results for CRTAC1 (OR 1.46 for knee OA, 1.36 for hip OA, and 1.32 for hand OA) compared to not adjusting for cancer (OR 1.46 for knee OA, 1.33 for hip OA, and 1.26 for hand OA). Likewise, although other comorbidities were more common in OA cases compared to controls (Table 2), these conditions were associated with lower levels of CRTAC1, whereas OA was associated with increased levels of CRTAC1 (Supplementary Table 3, http://onlinelibrary.wiley.com/doi/10.1002/art.41793/abstract). This highlights that CRTAC1 is a biomarker for OA and this association is not influenced by underlying comorbidities.

Correlation of plasma CRTAC1 levels with joint pain and OA disease severity. We further analyzed whether plasma levels of CRTAC1, the most significantly associated protein in OA, correlated with joint pain (a characteristic of OA) or with OA disease severity in the deCODE Health study, where the OA-related information was gathered at the time of plasma collection. Information on joint pain was gathered through a simple yes/no question on pain (answered "yes" by 649 of 2,708 patients), and hand OA severity was scored based on high-quality digital photographs (17,18) (n = 5,445; Supplementary Table 4, http://onlinelibrary.wiley.com/doi/10.1002/art.41793/abstract). We also evaluated whether CRTAC1 levels correlated with the number of each joint type affected.

CRTAC1 levels were associated with both joint pain (OR 1.14, $P = 0.0046$) and the hand OA severity score (OR 1.08, $P = 8.7 \times 10^{-11}$), with a direction of effects consistent with that of the association with OA overall. Figure 2 shows an increase in raw, unstandardized CRTAC1 levels (not adjusted for age or sex) with the hand OA severity score. With each increase in score, CRTAC1 levels were increased by 5.7% ($P = 2.2 \times 10^{-48}$).

We also assessed whether CRTAC1 levels correlated with thumb and finger OA severity scores, defined by radiography and clinical assessment in OA patients (n = 2,347) (Supplementary Table 5, http://onlinelibrary.wiley.com/doi/10.1002/art.41793/abstract). We observed that CRTAC1 levels were associated with severity scores in the finger joints (OR 1.12, $P = 0.0030$), specifically the thumb carpometacarpal joint (OR 1.09, $P = 0.022$) of these patients (Table 1). We noted that CRTAC1 was the only protein associated with both OA joint pain and severity of hand OA (Supplementary Table 1).

We evaluated whether CRTAC1 levels increased with the number of OA-affected joint types. In these analyses, we observed that the CRTAC1 plasma levels increased by 0.22 SD with each incremental increase in the number of OA-affected joint types ($P = 2.2 \times 10^{-82}$) (Supplementary Figure 2, http://onlinelibrary.wiley.com/doi/10.1002/art.41793/abstract).

Plasma CRTAC1 levels as a predictor of joint replacement in patients with OA. Joint replacement is a treatment for severe OA symptoms. We used Cox proportional hazards regression to investigate whether any of the 4,792 proteins measured

Table 2. Characteristics of the study subjects*

Variable	Case–control association study†			Progression to joint replacement study‡	
	Excluded (n = 17,777)	Controls (n = 15,242)	OA (n = 6,136)	No joint replacement (n = 9,654)	Joint replacement (n = 1,047)
Age at time of sample collection, mean ± SD years	48.6 ± 18.9	59.9 ± 13.4	64.0 ± 11.2	63.2 ± 11.5	63.4 ± 10.0
Female sex	10,559 (59.4)	7,847 (51.5)	3,956 (64.5)	6,352 (65.8)	633 (60.5)
Year of sample collection, mean ± SD	2,009.5 ± 7.5	2,007.3 ± 7.0	2,006.8 ± 6.9	2,007.8 ± 7.2	2,003.57 ± 4.3
BMI, mean ± SD kg/m²	27.1 ± 5.2	26.8 ± 4.7	28.4 ± 5.1	28.0 ± 5.0	29.1 ± 4.8
Hip OA	79	0	1,903	1,420	483
Hip replacement	711	0	376	0	376
Age at time of hip replacement, mean ± SD years	65.0 ± 9.3	NA	71.3 ± 9.5	72.7 ± 11.7	70.2 ± 8.9
Knee OA	211	0	3,578	2,801	777
Knee replacement	559	0	672	0	672
Age at time of knee replacement, mean ± SD years	66.3 ± 8.4	NA	69.7 ± 8.5	72.7 ± 11.7	70.3 ± 8.9
Hand OA	97	0	1,721	1,599	122
Hand severity score, mean ± SD	0.52 ± 0.79	0	1.57 ± 1.65	1.07 ± 1.39	1.47 ± 1.56
Follow-up time, median (IQR) years	2.3 (0.9–16.2)	7.6 (1.8–16.0)	10.3 (1.9–16.1)	12.5 (1.8–16.4)	6.0 (2.6–10.6)
Prior joint replacement	1,452	0	0	0	0
RA	691	0	0	0	0
Age <40 years	7,776	0	0	0	0
Any OA diagnosis	6,329	0	6,136	9,654	1,047
Missing BMI	1,877	0	0	0	0
Missing genotype§	2,909	1,418	379	737	23
Comorbidities					
Coronary artery disease	2,415 (15.8)	3,558 (23.3)	1,788 (29.1)	2,622 (27.2)	345 (33.0)
Metabolic syndrome	2,597 (17.0)	2,457 (16.1)	1,429 (23.3)	2,171 (22.5)	270 (25.8)
Type 2 diabetes mellitus	1,491 (9.8)	1,648 (10.8)	867 (14.1)	1,278 (13.2)	176 (16.8)
Hypertension	6,525 (42.8)	6,770 (44.4)	4,029 (65.7)	6,093 (63.1)	726 (69.3)
Depression	1,442 (9.5)	921 (6.0)	442 (7.2)	735 (7.6)	79 (7.5)
Cancer	2,714 (15.3)	4,682 (30.7)	1,835 (29.9)	2,658 (27.5)	386 (36.9)

* Except where indicated otherwise, values are the number (%). All subjects in both studies were age >40 years at the time of plasma collection, had information on body mass index (BMI) within 5 years of plasma collection, had not undergone joint replacement, were not diagnosed as having rheumatoid arthritis (RA), and had protein levels measured using SOMAScan. NA = not applicable; IQR = interquartile range.
† In the case–control association study, patients were required to have a primary diagnosis of hand, knee, or hip osteoarthritis (OA) for inclusion.
‡ In the progression to joint replacement study, a diagnosis of any OA among the individuals undergoing surgery was sufficient for inclusion.
§ Missing genotype is only an exclusion criterion in the full models.

in plasma could predict the time until joint replacement among patients with OA (n = 10,701), limiting the study group to those whose plasma samples were collected before the joint replacement (described below). Since in many cases the specific diagnosis of knee OA or hip OA was not recorded in the electronic health record registries used in this study until the time of joint replacement surgery, we included any patients diagnosed as having OA in this analysis and not only those who were coded as M16.0, M16.1, M17.0, and M17.1 as was the case in the knee and hip association analysis (Figure 1). CRTAC1 was 1 of only 2 proteins that could significantly predict hip replacement, whereas 8 proteins could predict knee replacement (Supplementary Table 6, http://onlinelibrary.wiley.com/doi/10.1002/art.41793/abstract). It was the strongest predictor of both hip replacement (hazard ratio [HR] 1.31, $P = 8.4 \times 10^{-8}$) and knee replacement (HR 1.40, $P = 1.0 \times 10^{-18}$). Therefore, of all the proteins tested, CRTAC1 was most significantly associated with OA diagnosis and was the best predictor of progression to joint replacement.

We assessed the likelihood of joint replacement over time using plasma CRTAC1 levels and classic risk factors for OA (i.e.,

age, sex, and BMI), stratified into quintiles of risk scores, and compared the risk of joint replacement for each quintile of the predicted risk using the Kaplan-Meier estimator. Patients with OA who were in the highest quintile of risk were 16 times more likely to undergo knee replacement within 5 years of plasma sample collection‡ than those in the lowest quintile, and 6.5 times more likely to undergo hip replacement (Figure 3). Using unadjusted CRTAC1 levels in the absence of classic risk factors, those in the highest quintile of risk were 3 times more likely to undergo knee replacement and 2.5 times more likely to undergo hip replacement within 5 years of plasma sample collection than those who were in the lowest quintile, which demonstrated that independent of age, sex, or BMI, the CRTAC1 levels alone substantially increased the likelihood of joint replacement (Supplementary Figure 3, http://onlinelibrary.wiley.com/doi/10.1002/art.41793/abstract).

---

‡Correction added after online publication 18 October 2021: the text was changed from "within 5 years of diagnosis" to "within 5 years of plasma sample collection."
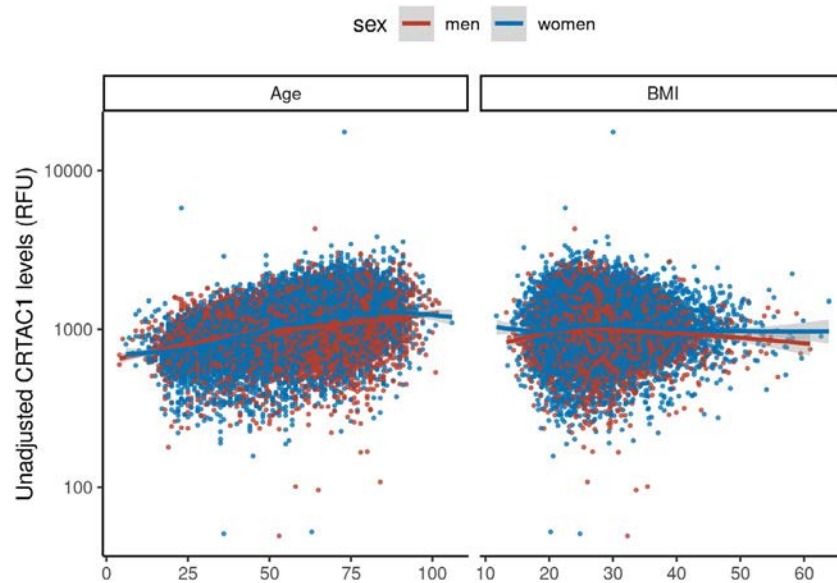
Figure 4. Correlation of unadjusted plasma cartilage acidic protein 1 (CRTAC1) levels with age and body mass index (BMI) in men and women. Results are from the entire data set of 37,278 subjects who had available information on age, sex, and BMI. Each symbol represents an individual subject. RFU = relative fluorescence units. Color figure can be viewed in the online issue, which is available at http://onlinelibrary.wiley.com/doi/10.1002/art.41792/abstract.

Generalizability of CRTAC1 as a biomarker. To address the stability of CRTAC1 levels as a biomarker for OA, we assessed its association with age, sex, and BMI (adjusted for time from sample collection, and source of sample collection). CRTAC1 levels did not correlate with BMI ($P = 0.71$), but they did increase slightly with age (8.24 relative fluorescence units per year, $P < 1 \times 10^{-300}$) (Figure 4). In an association analysis stratified by sex, age, and BMI, we showed that the effect of CRTAC1 on OA risk did not differentiate significantly between any of the groups tested (Supplementary Table 7, http://onlinelibrary.wiley.com/doi/10.1002/art.41793/abstract), demonstrating that CRTAC1 was an independent risk factor for OA.

We also evaluated whether the measurement of CRTAC1 using SOMAmer was consistent with other types of protein measurements using the Olink protein immunoassay (n = 200; https://www.olink.com). The correlation between CRTAC1 SOMAmer measurements and CRTAC1 Olink measurements was 0.86 (95% confidence interval 0.80–0.90), and the association of CRTAC1 level with OA was also significant using the Olink method (Supplementary Figure 4, http://onlinelibrary.wiley.com/doi/10.1002/art.41793/abstract).

Potential role of CRTAC1 in the pathogenesis of OA. To determine whether CRTAC1 levels in plasma contributed to the pathogenesis of OA, we performed a GWAS of DNA sequence variants associated with CRTAC1 levels (protein QTL study) and identified 8 CRTAC1 protein QTL variants, one of which was at the CRTAC1 locus. We then tested those protein QTL variants for association with OA in a combined study population from Iceland

and the UK Biobank (14), with a total of 17,151 patients with hip OA, 23,877 with knee OA, and 9,773 with hand OA, compared to >560,000 controls. None of these sequence variants were associated with OA (Supplementary Table 8, http://onlinelibrary.wiley.com/doi/10.1002/art.41793/abstract). Furthermore, in large meta-analyses of OA, no association with sequence variants at the CRTAC1 locus has been described (14,15). This indicates that the observed increase in CRTAC1 in plasma was unlikely to cause OA. Moreover, adjusting the CRTAC1 association for the OA polygenic risk scores, which integrated a large fraction of the contribution of genetics to the disease, had little impact on CRTAC1 association with OA (Supplementary Figure 5, http://onlinelibrary.wiley.com/doi/10.1002/art.41793/abstract). This suggests that CRTAC1 captured a different component of the disease.

Models for OA association and prediction of progression to joint replacement. Although a single, easily interpreted biomarker is currently most feasible to use in clinical settings, a model incorporating other factors besides CRTAC1 alone may provide more accurate association/prediction of OA development and progression to joint replacement. We therefore aimed to build the best available association model for OA diagnosis and for prediction of progression to joint replacement by including all independently associated proteins and the polygenic risk scores for OA in the model, in addition to age, sex, and BMI. Exclusion/inclusion criteria were the same as before, with the exception that those without genotypes were also excluded. To avoid overfitting of the models, we split the data set in two and used three-fourths of the data to build the model and one-fourth to test it.

We performed backward stepwise selection of associated variables (i.e., proteins, polygenic risk score, age, sex, and BMI) in a single logistic regression model and likewise, to determine a set of proteins that predict OA progression to joint replacement, we used Cox proportional hazards regression. We demonstrated both a good fit between the training and test sets and adequate power of our study to detect association with OA (Supplementary Figure 6, http://onlinelibrary.wiley.com/doi/10.1002/art.41793/abstract).

To evaluate the discriminatory power of our models, we applied a receiver operating characteristic curve and calculated the AUC. In the full model, the AUC was 0.762 for hip OA, 0.770 for knee OA, and 0.800 for hand OA, and the cumulative AUC estimate for joint replacement was 0.661 for hip replacement and 0.734 for knee replacement (Supplementary Table 9, http://online library.wiley.com/doi/10.1002/art.41793/abstract).

Of all the proteins in the models (between 1 and 27), CRTAC1 contributed the most to all 5 models (Supplementary Figures 7 and 8, http://onlinelibrary.wiley.com/doi/10.1002/art.41793/abstract). The polygenic risk score and the classic risk factors, age and sex, contributed to all of the models. BMI, however, did not contribute to the hip replacement model. As expected, given the composition of the sample set, classic risk factors contributed the most in all of the models. However, adding the proteins and polygenic risk scores significantly improved the association of the models with OA ($P = 1.5 \times 10^{-101}$ for hand OA, $P = 3.1 \times 10^{-75}$ for hip OA, and $P = 3.8 \times 10^{-203}$ for knee OA) and prediction of joint replacement ($P = 4.8 \times 10^{-111}$ for knee replacement and $P = 9.3 \times 10^{-71}$ for hip replacement) (Supplementary Table 9).

These OA risk profiles were strongly associated with joint pain, and the hand risk score was strongly associated with hand OA severity (Supplementary Table 10 and Supplementary Figure 9, http://onlinelibrary.wiley.com/doi/10.1002/art.41793/abstract). Patients who were in the highest quintile of joint replacement score were 25 times more likely to undergo knee replacement and 9 times more likely to undergo hip replacement than those in the lowest quintile (Supplementary Figure 10, http://onlinelibrary.wiley.com/doi/10.1002/art.41793/abstract). However, in the full models, additional proteins conferred significant risks of other joint diseases (i.e., RA, gout, and psoriatic arthritis [PsA]) (Supplementary Table 11, http://onlinelibrary.wiley.com/doi/10.1002/art.41793/abstract) and were, therefore, not specific for OA. Furthermore, use of the full models required measuring up to 35 proteins for both OA association and prediction of joint replacement, and genotypes for the polygenic risk score, which would be challenging in clinical settings.

As described above regarding CRTAC1, we also analyzed whether the levels of the plasma proteins selected in the association and prediction models could cause OA by testing protein QTL sequence variants (n = 267) (Supplementary Note, Supplementary Tables 12 and 13, and Supplementary Figure 5, http://onlinelibrary.wiley.com/doi/10.1002/art.41793/abstract). As with CRTAC1, our results indicated that plasma levels of these proteins are unlikely to cause OA, but their altered levels are consequences of the disease.

Induction of a specific protein profile by joint replacement. We observed a striking difference in levels of OA-associated proteins between patients who had undergone a joint replacement before plasma collection (n = 1,452) and those who had not (n = 4,229). In our data, a prior joint replacement was associated with 137 plasma proteins (Supplementary Table 14, http://onlinelibrary.wiley.com/doi/10.1002/art.41793/abstract), a minority of which were associated with OA in patients who had not undergone joint replacement (n = 16 proteins). This indicated that the joint replacement itself was associated with a plasma protein profile that was a consequence of the joint implant rather than the disease. Therefore, we excluded patients who had undergone joint replacement prior to plasma collection from all the OA association studies described above. The protein with the strongest association with prior joint replacement, CUB domain-containing protein 1 (CDCP1) ($P = 1.1 \times 10^{-198}$, OR 2.67), was not associated with OA without joint replacement. Like most proteins associated with joint replacement but not with OA, CDCP1 levels changed very little during the 20 years preceding joint replacement, followed by an increase in levels at the time of arthroplasty ($\beta = 0.866$, $P = 5.7 \times 10^{-16}$) and a continued steady increase thereafter ($\beta = 0.072$ per year, $P = 8.7 \times 10^{-43}$), as demonstrated in data from different individuals at different time points after joint replacement. In contrast, the proteins that were also associated with OA demonstrated an increase in levels prior to joint replacement that either continued (e.g., ASB9) or decreased (e.g., CRTAC1) after surgery (Supplementary Figure 11, http://onlinelibrary.wiley.com/doi/10.1002/art.41793/abstract).

DISCUSSION

In this study of a large panel of plasma proteins (4,792 measured), we determined that plasma CRTAC1 levels were the most strongly associated with OA diagnosis, and CRTAC1 was the best predictor of OA progression to joint replacement. Patients with OA who were in the highest quintile of risk based on known risk factors (i.e., age, sex, and BMI) and plasma CRTAC1 levels were 16 times more likely to undergo knee replacement within 5 years, and 6.5 times more likely to undergo hip replacement than those in the lowest quintile. Furthermore, CRTAC1 levels in plasma were also associated with joint pain and hand OA severity. Importantly, CRTAC1 levels are not associated with other inflammatory joint diseases such as RA, gout, or PsA. We determined that the protein panels of up to 27 proteins, together with the OA polygenic risk scores (in addition to age, sex, and BMI) in the models, performed better than CRTAC1 alone (in combination with age, sex, and BMI). However, these expanded associations and prediction models were not specific to OA. This highlights CRTAC1 as a promising biomarker for OA, since we found that, among all of the disease subphenotypes studied, this protein was not only strongly associated with OA, but also specific for OA with no association with other inflammatory joint diseases. We also

demonstrated that CRTAC1 is a risk factor for OA independent of age, sex, and BMI. Based on CRTAC1 QTL genetic analysis, we demonstrated that CRTAC1 levels in plasma are unlikely to cause OA.

The function of CRTAC1 is not fully understood. It is a glycosylated, calcium-binding extracellular matrix protein that is highly conserved from bacteria to humans (21), that was initially identified as a marker of chondrocyte development from mesenchymal stem cells (22). This protein is found in greater concentrations in knee synovial fluid from OA patients compared to controls (23), and also found at higher levels in OA cartilage (24). Furthermore, CRTAC1 is also involved in apoptosis and pyroptosis of human lens epithelial cells (25,26).

In addition to these findings, we observed that joint replacement was associated with a protein profile in plasma that lacks association with OA and persists long after joint replacement surgery. This profile may therefore reflect the body's reaction to the joint implant. The plasma levels of these proteins could be candidates for prediction of prosthesis survival time or early prosthesis failure.

To our knowledge, this study comprises the largest biomarker study of OA to date. We simultaneously investigated 4,792 plasma proteins in 39,155 individuals of whom 12,178 had OA. This study thus has greatly increased power over previous studies to identify circulating biomarkers for OA. We also demonstrated that plasma levels of COMP, one of the most investigated biomarkers for OA to date (9–12), were associated with hand, hip, and knee OA and predicted knee replacement. Thus, our study supports previous findings indicating that COMP is a likely biomarker for OA. However, we showed that COMP was a substantially weaker predictor than CRTAC1, and because it is also associated with weight, it is a less suitable biomarker. We did not have access to measurements of the other much-studied biomarker for OA, urinary CTX-II, which is a degradation product of type II collagen found in urine. We therefore could not test whether urinary CTX-II correlated with CRTAC1 or whether it was independently associated with OA.

Limitations of this study include the lack of information on age at the onset of OA symptoms or age at first confirmed diagnosis, which reflected the registry nature of the data. Thus, we were unable to determine whether the CRTAC1 levels were already altered at a very early stage of the disease. Furthermore, in the association analysis, we included all patients diagnosed as having OA by March 2020, irrespective of when their plasma sample was collected. This group is therefore heterogeneous, i.e., at the time the plasma sample was collected, some patients had advanced disease whereas others were symptom-free. Moreover, we did not have access to other population studies for replication of our findings. Follow-up studies in other populations of various ancestries, in addition to studies addressing technical issues, are extremely important for validation of CRTAC1 as a general biomarker for OA.

In this large hypothesis-free study on OA and joint replacement, we identified a novel biomarker, CRTAC1, with a strong, and specific, effect on both disease risk and disease severity. It had a stronger effect than biomarkers that were previously established as having the best predictive abilities. If validated in further studies, CRTAC1 will be a promising biomarker both for clinical use and for therapeutic development, where there is currently a large unmet need.

AUTHOR CONTRIBUTIONS

All authors were involved in drafting the article or revising it critically for important intellectual content, and all authors approved the final version to be published. Dr. Styrkarsdottir had full access to all of the data in the study and takes responsibility for the integrity of the data and the accuracy of the data analysis.
Study conception and design. Styrkarsdottir, Lund, Norddahl, Sulem, Thorsteinsdottir, Gudbjartsson, Stefansson.
Acquisition of data. Saevarsdottir, Gunnarsdottir, Norddahl, Bjornsdottir, Holm, Thorgeirsson, Rafnar, Jonsdottir, Ingvarsson, Jonsson, Stefansson.
Analysis and interpretation of data. Styrkarsdottir, Lund, Magnusson, Frigge, Ivarsdottir, Gudbjartsson.

ROLE OF THE STUDY SPONSOR

REFERENCES

1. GBD 2017 Disease and Injury Incidence and Prevalence Collaborators. Global, regional, and national incidence, prevalence, and years lived with disability for 354 diseases and injuries for 195 countries and territories, 1990-2017: a systematic analysis for the Global Burden of Disease Study 2017. Lancet 2018;392:1789–858.

2. Litwic A, Edwards M, Dennison E, Cooper C. Epidemiology and burden of OA [review]. Br Med Bull 2013;105:185–99.

3. Hiligsmann M, Cooper C, Arden N, Boers M, Branco JC, Brandi ML, et al. Health economics in the field of OA: an expert's consensus paper from the European Society for Clinical and Economic Aspects of Osteoporosis and Osteoarthritis (ESCEO). Semin Arthritis Rheum 2013;43:303–13.

4. Hunter DJ, Schofield D, Callander E. The individual and socioeconomic impact of OA [review]. Nat Rev Rheumatol 2014;10:437–41.

5. Felson DT, Lawrence RC, Dieppe PA, Hirsch R, Helmick CG, Jordan JM, et al. Osteoarthritis: new insights. Part 1: the disease and its risk factors. Ann Intern Med 2000;133:635–46.

6. Nguyen LT, Sharma AR, Chakraborty C, Saibaba B, Ahn ME, Lee SS. Review of prospects of biological fluid biomarkers in OA. Int J Mol Sci 2017;18:601.

7. Bay-Jensen AC, Thudium CS, Mobasheri A. Development and use of biochemical markers in OA: current update [review]. Curr Opin Rheumatol 2018;30:121–8.

8. Lennerová T, Pavelka K, Šenolt L. Biomarkers of hand OA [review]. Rheumatol Int 2018;38:725–35.

9. Hoch JM, Mattacola CG, McKeon JM, Howard JS, Lattermann C. Serum cartilage oligomeric matrix protein (sCOMP) is elevated in patients with knee OA: a systematic review and meta-analysis. Osteoarthritis Cartilage 2011;19:1396–404.

10. Bi X. Correlation of serum cartilage oligomeric matrix protein with knee OA diagnosis: a meta-analysis. J Orthop Surg Res 2018;13:262.

11. Van Spil WE, DeGroot J, Lems WF, Oostveen JC, Lafeber FP. Serum and urinary biochemical markers for knee and hip-OA: a systematic review applying the consensus BIPED criteria [review]. Osteoarthritis Cartilage 2010;18:605–12.

12. Valdes AM, Meulenbelt I, Chassaing E, Arden NK, Bierma-Zeinstra S, Hart D, et al. Large scale meta-analysis of urinary C-terminal telopeptide, serum cartilage oligomeric protein and matrix metalloprotease degraded type II collagen and their role in prevalence, incidence and progression of OA. Osteoarthritis Cartilage 2014;22:683–9.

13. Huang M, Zhao J, Huang Y, Dai L, Zhang X. Meta-analysis of urinary C-terminal telopeptide of type II collagen as a biomarker in OA diagnosis. J Orthop Translat 2017;13:50–7.

14. Styrkarsdottir U, Lund SH, Thorleifsson G, Zink F, Stefansson OA, Sigurdsson JK, et al. Meta-analysis of Icelandic and UK data sets identifies missense variants in SMO, IL11, COL11A1 and 13 more new loci associated with OA. Nat Genet 2018;50:1681–7.

15. Tachmazidou I, Hatzikotoulas K, Southam L, Esparza-Gordillo J, Haberland V, Zheng J, et al. Identification of new therapeutic targets for OA through genome-wide analyses of UK Biobank data. Nat Genet 2019;51:230–6.

16. Ivarsdottir EV, Benonisdottir S, Thorleifsson G, Sulem P, Oddsson A, Styrkarsdottir U, et al. Sequence variation at ANAPC1 accounts for 24% of the variability in corneal endothelial cell density. Nat Commun 2019;10:1284.

17. Jonsson H, Helgadottir GP, Aspelund T, Sverrisdottir JE, Eiriksdottir G, Sigurdsson S, et al. The use of digital photographs for the diagnosis of hand OA: the AGES-Reykjavik study. BMC Musculoskelet Disord 2012;13:20.

18. Jonsson H. Age related prevalence of hand OA diagnosed by photography (HOASCORE). BMC Musculoskelet Disord 2017;18:508.

19. Lundberg M, Eriksson A, Tran B, Assarsson E, Fredriksson S. Homogeneous antibody-based proximity extension assays provide sensitive and specific detection of low-abundant proteins in human blood. Nucleic Acids Res 2011;39:e102.

20. Kong A, Frigge ML, Thorleifsson G, Stefansson H, Young AI, Zink F, et al. Selection against variants in the genome associated with educational attainment. Proc Natl Acad Sci U S A 2017;114:E727–32.

21. Anjos L, Morgado I, Guerreiro M, Cardoso JC, Melo EP, Power DM. Cartilage acidic protein 1, a new member of the β-propeller protein family with amyloid propensity. Proteins 2017;85:242–55.

22. Steck E, Benz K, Lorenz H, Loew M, Gress T, Richter W. Chondrocyte expressed protein-68 (CEP-68), a novel human marker gene for cultured chondrocytes. Biochem J 2001;353:169–74.

23. Ritter SY, Subbaiah R, Bebek G, Crish J, Scanzello CR, Krastins B, et al. Proteomic analysis of synovial fluid from the osteoarthritic knee: comparison with transcriptome analyses of joint tissues. Arthritis Rheum 2013;65:981–92.

24. Ge X, Ritter SY, Tsang K, Shi R, Takei K, Aliprantis AO. Sex-specific protection of OA by deleting cartilage acid protein 1. PloS One 2016;11:e0159157.

25. Ji Y, Rong X, Li D, Cai L, Rao J, Lu Y. Inhibition of cartilage acidic protein 1 reduces ultraviolet B irradiation induced-apoptosis through P38 mitogen-activated protein kinase and jun amino-terminal kinase pathways. Cell Physiol Biochem 2016;39:2275–86.

26. Sun Y, Rong X, Li D, Jiang Y, Lu Y, Ji Y. Down-regulation of CRTAC1 attenuates UVB-induced pyroptosis in HLECs through inhibiting ROS production. Biochem Biophys Res Commun 2020;532:159–65.

Effect of Atorvastatin on Knee Cartilage Volume in Patients With Symptomatic Knee Osteoarthritis: Results From a Randomized Placebo-Controlled Trial

Yuanyuan Wang,[1] [iD] Graeme Jones,[2] Catherine Hill,[3] [iD] Anita E. Wluka,[1] [iD] Andrew B. Forbes,[1] Andrew Tonkin,[1] Sultana Monira Hussain,[1] [iD] Changhai Ding,[4] [iD] and Flavia M. Cicuttini[1]

Objective. To determine whether atorvastatin slows tibial cartilage volume loss in patients with symptomatic knee osteoarthritis (OA) in a multicenter, randomized, double-blind, placebo-controlled trial.

Methods. Participants ages 40–70 years were randomized to receive oral atorvastatin (40 mg once daily) (n = 151) or matching placebo (n = 153). The primary end point was annual percentage change in tibial cartilage volume over 2 years, assessed using magnetic resonance imaging (MRI). The prespecified secondary end points were progression of cartilage defects and bone marrow lesions over 2 years, which were assessed using MRI and change in Western Ontario and McMaster Universities Osteoarthritis (WOMAC) Index pain, stiffness, and function scores.

Results. A total of 248 of 304 participants (81.6%) completed the trial (mean age 55.7 years; 55.6% women). The annual change in tibial cartilage volume differed minimally between the atorvastatin and placebo groups (mean change –1.66% versus –2.17%, between-group difference 0.50% [95% confidence interval (95% CI) –0.17%, 1.17%]). There were no significant differences in the progression of cartilage defects (odds ratio [OR] 0.86 [95% CI 0.52, 1.41]) or progression of bone marrow lesions (OR 1.00 [95% CI 0.62, 1.63]). Moreover, there were no significant differences in change in WOMAC pain, stiffness, or function scores over 2 years between the atorvastatin and placebo groups (mean change in pain score –36.0 versus –29.5, adjusted difference –2.7 [95% CI –27.1, 21.7]; mean change in stiffness score –14.2 versus –11.8, adjusted difference –0.2 [95% CI –12.2, 11.8]; mean change in function score –89.4 versus –87.5, adjusted difference 0.3 [95% CI –83.1, 83.6]). The incidence of adverse events (AEs) was similar between the atorvastatin and placebo groups (57 [37.7%] versus 52 [34.0%] experiencing AEs).

Conclusion. Treatment with oral atorvastatin (40 mg once daily), compared to placebo, did not significantly reduce cartilage volume loss over 2 years in patients with symptomatic knee OA. These findings do not support the use of atorvastatin for the treatment of knee OA.

INTRODUCTION

Osteoarthritis (OA) causes pain, disability, and a substantial health care burden and is ranked the thirteenth highest contributor to the incidence and prevalence of disability worldwide (1). Treatment of OA aims to reduce pain and slow structural progression (2).

However, current therapies have only short-term, mild-to-moderate effects on joint pain (3), and there is no approved disease-modifying therapy for slowing structural progression. Knee OA is a multifactorial disease mediated by mechanical, inflammatory, and metabolic mechanisms (4). Increased serum levels of inflammatory biomarkers are associated with the progression of knee OA and

cartilage volume loss (5,6). Increased levels of serum cholesterol are associated with incident bone marrow lesions, which play a role in the pathogenesis of knee OA (7). Statins, the most commonly prescribed and effective treatment for hypercholesterolemia, also target inflammatory and metabolic mechanisms (8), suggesting their potential for slowing the progression of knee OA (9,10).

Findings from large cohort studies have shown that statin use reduced the progression of knee OA (11,12), and statin use over 5 years reduced the risk of developing knee pain (13). In contrast, findings from other studies demonstrated that statin use was associated with the progression of knee OA and worsening physical function (14,15), or findings showed no association between statin use and knee pain or the progression of knee OA (13,15). A recent meta-analysis of observational studies showed no significant association between any statin use and incidence or progression of knee OA, but use of atorvastatin was associated with a reduced risk of OA in a subgroup analysis (16). There was significant heterogeneity among the studies in terms of study populations, definitions of statin use, OA outcomes, and length of follow-up, and observational studies are subject to bias and confounding. Thus, a randomized controlled trial was needed to determine whether statins improve structural and symptomatic outcomes in knee OA.

Radiography does not allow direct visualization of soft tissue joint structures and lacks sensitivity in the assessment of disease progression in OA. Knee cartilage volume, measured using magnetic resonance imaging (MRI), is widely accepted as a valid, reproducible, and sensitive method for assessing structural progression in knee OA (17). The end point of a reduction in the rate of tibial cartilage volume loss is an important marker in patients with OA, as it may be useful in predicting the patient-related outcomes of reduced joint pain or need for knee replacement surgery (18,19). We conducted a randomized controlled trial to determine whether atorvastatin, compared to placebo, reduced knee cartilage volume loss over 2 years in participants with symptomatic knee OA.

PATIENTS AND METHODS

Trial design. The Osteoarthritis of the Knee Statin (OAKS) study was a multicenter, randomized, parallel-group, double-blind, placebo-controlled trial conducted between August 2013 and May 2018 in Australia. This trial was registered with the Australian New Zealand Clinical Trials Registry (ACTRN: 12613000190707) prior to participant recruitment. Ethics approval was obtained from the Alfred Hospital Ethics Committee (approval no. 521/12), Monash University Human Research Ethics Committee (approval no. CF13/595 - 2013000236), Tasmania Health and Medical Human Research Ethics Committee (approval no. H0012971), and Queen Elizabeth Hospital Human Research Ethics Committee (approval no. HREC/13/TQEHLMH/20). All participants provided written informed consent. The study protocol has been published

(20) and is included in the Supplementary Protocol and Statistical Analysis (available on the *Arthritis & Rheumatology* website at http://onlinelibrary.wiley.com/doi/10.1002/art.41760/abstract).

Participants. Participants were recruited using the Osteoarthritis Clinical Trial Network in Melbourne, Hobart, and Adelaide, Australia using a combined strategy including local advertising and advertising through social media and collaboration with general practitioners, rheumatologists, and orthopedic surgeons. Inclusion and exclusion criteria are detailed in the published protocol (20). Participants ages 40–70 years with at least a 6-month history of symptomatic knee OA with a pain score of ≥20 mm on a 100-mm visual analog scale who met the American College of Rheumatology clinical criteria for knee OA (21) were eligible. Exclusion criteria included inability to give informed consent, severe radiographic knee OA (grade 3 joint space narrowing [JSN] according to the Altman atlas [22]), severe knee pain on standing (pain score >80 mm on a 100-mm visual analog scale), inflammatory arthritis, significant knee injury, approved indications for statin therapy (including familial hypercholesterolemia, known atherosclerotic cardiovascular disease [CVD], and diabetes mellitus), current use of lipid-lowering therapy or previous adverse reaction to statins, absolute cardiovascular risk estimated using the Framingham Risk Score of >15% within the next 5 years, fasting total cholesterol level >7.5 mmoles/liter, clinically significant renal disease or abnormal liver function, arthroscopy or open surgery or intraarticular therapy in the index knee in the last 12 months, concomitant use of potent analgesics including opiates, a comorbidity limiting participation, relocation, contraindication to MRI, and, among women, being pregnant, breastfeeding, or trying to become pregnant.

Randomization and blinding. Participants were randomly assigned in a 1:1 ratio to receive either atorvastatin or placebo. Randomization was performed based on computer-generated random numbers prepared by a statistician with no other involvement in the trial. Permuted block randomization was performed using a central automated allocation procedure, stratified according to the study site with random block sizes of 4, 6, and 8. Treatment group allocation was blinded by ensuring that medications were dispensed by pharmacies at participating hospitals, using an identical placebo tablet, and masking the group allocation from participants, research staff collecting participant data, and observers who performed the knee structure measurements.

Intervention. All participants were provided usual care by their treating health practitioners. Participants in the intervention group received 40 mg of atorvastatin once daily (Sandoz), and those in the control group received an inactive matching placebo once daily (Pharmaceutical Packaging Professionals). The duration of the intervention was 2 years.

End points. The primary end point was the annual percentage change in tibial cartilage volume. MRI of the study knee was performed at baseline and at 24-month follow-up using 1.5T or 3T whole-body MRI units with a commercial transmit/receive knee coil. Details on MRI units, sequences, and parameters have been published (20). MR images were read unpaired in blocks of 10 participants within 1 week, by readers who were blinded with regard to group allocation and participant characteristics. Tibial cartilage volume was measured using sagittal T1-weighted images and OsiriX software (University of Geneva). The volumes of medial and lateral tibial cartilage plates were isolated by manually drawing disarticulation contours around the cartilage boundaries on a section-by-section basis, using a previously described method (18,19). Two independent observers performed the measurement, with the mean value used as the final result. The interobserver intraclass correlation coefficient was 0.91. The annual change in tibial cartilage volume was calculated using the following formula: % annual change in tibial cartilage volume = (cartilage volume at follow-up −

cartilage volume at baseline)/(cartilage volume at baseline × years between MRI scans).

Secondary end points were progression of cartilage defects and bone marrow lesions, as well as change in knee pain and function scores over 2 years. Cartilage defects were graded at tibial and femoral sites (score range 0–4) using sagittal images (23), with intraobserver and interobserver intraclass correlation coefficients of 0.85–0.94 (23). Bone marrow lesions were graded at tibial and femoral sites (score range 0–3) using sagittal proton density imaging, with intrareader and interreader intraclass correlation coefficients of 0.88–0.93 (24). Prevalence of cartilage defects was defined as a cartilage defect grade of ≥2 in either the tibial or femoral site, and prevalence of bone marrow lesions was defined as a bone marrow lesion grade of ≥1 in either the tibial or femoral site. Progression of cartilage defects and bone marrow lesions was defined as any increase in grade in either the tibial site or femoral site over 2 years. Knee pain (score range 0–500), stiffness (score range 0–200), and function (score range 0–1,700)
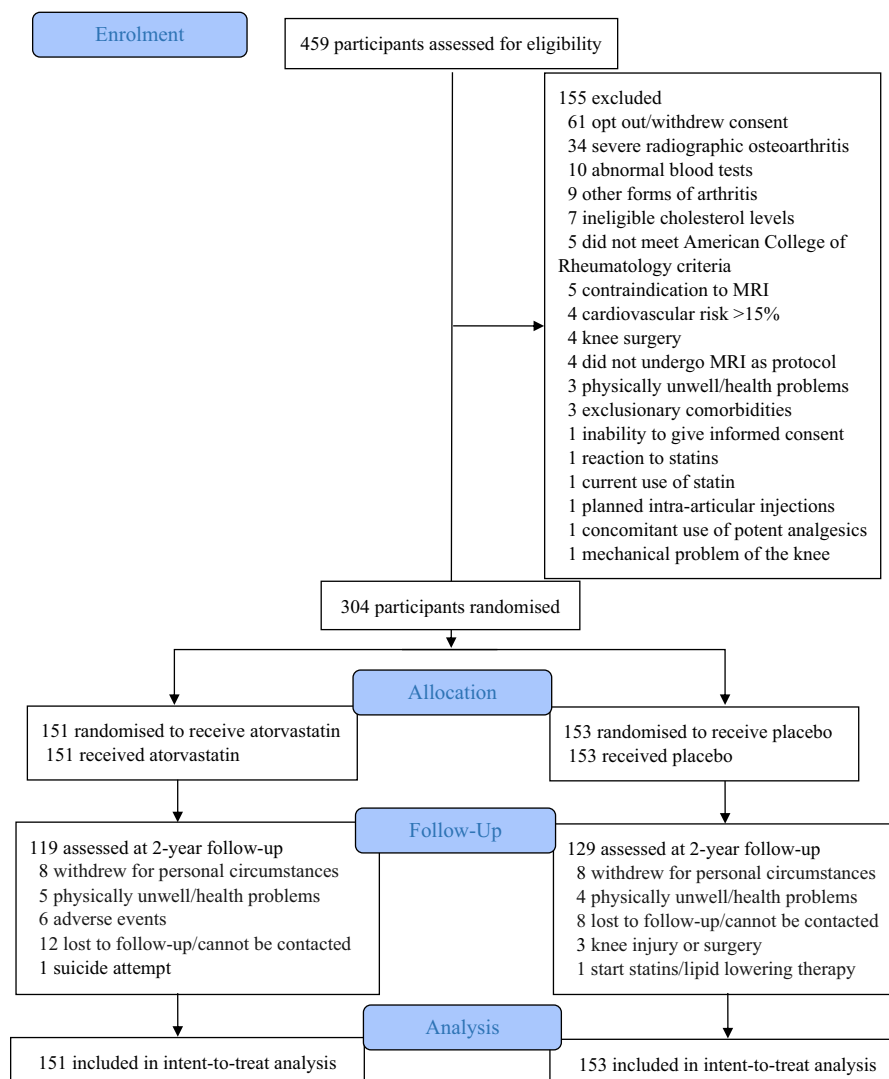

Figure 1. Study flow chart showing the conditions of patient eligibility, the number of patients randomized to receive either atorvastatin or placebo, the number of patients lost to follow-up, and those included in the intent-to-treat analysis. MRI = magnetic resonance imaging.

were assessed using the Western Ontario and McMaster Universities Osteoarthritis Index (WOMAC) scores (25). Changes in knee pain and function scores were calculated using the following formula: WOMAC scores at follow-up – WOMAC scores at baseline.

Adverse events (AEs) were monitored throughout the trial. Participants were requested to report any AEs to the research staff spontaneously at each study visit and by telephone calls between visits after taking study medication. Serious AEs (SAEs) (i.e., death, life-threatening events, disability, nonelective or prolonged hospitalization, or important medical events, such as cancer) were determined by a rheumatologist (including GJ, CH, AEW, and FMC). Details of the AE and its relationship to the intervention were recorded and reported to the ethics committees.

Sample size calculation. Our prior data indicated a rate of tibial cartilage volume loss of 3.0% (SD 3.0%) per year in individuals with knee OA (26). A 1% reduction in this rate was considered clinically significant, decreasing the need for knee replacement surgery by 20% over 4 years (19). The minimum clinically important difference for cartilage volume loss has not been established. We planned on a total of 350 participants (175 in each group) in order for the study to have 80% power to detect a 1% reduction in the rate of cartilage volume loss in the atorvastatin group compared to that in the placebo group (2-sided alpha level of 0.05), allowing for a maximum dropout rate of 20% over 2 years.

Statistical analysis. The complete statistical analysis plan is provided with the study protocol (20). The primary analyses were intent-to-treat analyses of the participants as allocated in their randomized groups. The analyses for primary and secondary end points used all available data, together with imputation of missing data using multiple imputation by chained equations (27), provided that participants had a baseline MRI. Twenty imputation data sets were created and combined using Rubin's rule under a missing at random assumption. For primary and secondary outcomes, age, body mass index (BMI), tibial plateau bone area, grade of JSN, and baseline values of the outcomes were used to impute missing values by treatment group. Differences between treatment groups were assessed using independent-sample t-tests for annual percentage change in tibial cartilage volume, analysis of covariance for the change in WOMAC scores (adjusted for baseline score), and chi-square tests and binary logistic regression analyses for progression of cartilage defects and bone marrow lesions. Multiple linear regression analyses were performed for continuous end points, and logistic regression analyses were performed for binary end points as supplementary analyses to adjust for imbalanced baseline factors, if the imbalances were considered clinically important.

Prespecified subgroup analyses were performed to examine whether the difference in outcomes between randomized groups varied according to the presence versus absence of bone marrow lesions and radiographic grade of JSN at baseline. As secondary analyses, per-protocol analyses were conducted for the primary and secondary end points according to the participants' randomized treatment group, restricted to those with available data on outcome measures at 2 years. Since the medial tibiofemoral compartment is more susceptible to cartilage damage and disease progression compared to the lateral compartment, a sensitivity analysis was performed, in which medial and lateral tibial cartilage volume were examined separately as requested by a reviewer. P values less than 0.05 by 2-sided test were considered significant. Statistical analyses were performed using Stata 15.0 (StataCorp).

RESULTS

From August 2013 to April 2016, 459 participants were screened, and 304 were randomized to receive either atorvastatin (n = 151) or placebo (n = 153), all of whom were included in the intent-to-treat analysis of study end points (Figure 1). The

Table 1. Baseline characteristics of the study participants*

	Atorvastatin (n = 151)	Placebo (n = 153)
Age, mean ± SD years	55.7 ± 7.3	55.8 ± 7.9
Sex, female	92 (60.9)	77 (50.3)
BMI, mean ± SD kg/m²	29.4 ± 5.7	29.5 ± 5.8
JSN†		
Grade 0	64 (43.8)	67 (44.7)
Grade 1	52 (35.6)	50 (33.3)
Grade 2	30 (20.6)	33 (22.0)
Tibial cartilage volume, mean ± SD mm³‡	3,601 ± 1,032	3,748 ± 1,161
Prevalence of tibiofemoral cartilage defects‡	110 (73.3)	111 (72.6)
Prevalence of tibiofemoral bone marrow lesions	103 (68.2)	96 (62.8)
WOMAC pain score (scale 0–500), mean ± SD§	147.4 ± 88.1	141.6 ± 96.6
WOMAC stiffness score (scale 0–200), mean ± SD¶	68.7 ± 46.8	65.3 ± 49.0
WOMAC physical function score (scale 0–1,700), mean ± SD#	483.3 ± 305.7	479.1 ± 347.5
Concomitant medications		
NSAIDs	39 (25.8)	40 (26.1)
Acetaminophen	33 (21.9)	39 (25.5)
Glucosamine/chondroitin	41 (27.2)	49 (32.0)
Other analgesics	8 (5.3)	16 (10.5)

* Except where indicated otherwise, values are the number (%) of patients. BMI = body mass index; JSN = joint space narrowing; WOMAC = Western Ontario and McMaster Universities Osteoarthritis Index; NSAIDs = nonsteroidal antiinflammatory drugs.
† Due to missing radiographs, data were available for a total of 296 participants: n = 146 in the atorvastatin group and n =150 in the placebo group.
‡ Data were available for a total of 303 participants: n = 150 in the atorvastatin group and n = 153 in the placebo group.
§ Data were available for a total of 301 participants: n = 150 in the atorvastatin group and n = 151 in the placebo group.
¶ Data were available for a total of 300 participants: n = 149 in the atorvastatin group and n = 151 in the placebo group.
# Data were available for a total of 302 participants: n = 150 in the atorvastatin group and n = 152 in the placebo group.

planned sample size (n = 350) was not achieved due to budgetary constraints. Participant characteristics are shown in Table 1. The mean age of participants was 55.7 years (SD 7.6), and 169 participants (55.6%) were women. The baseline characteristics were generally well balanced between the atorvastatin and placebo groups, except for a higher proportion of women in the atorvastatin group. Fifty-six participants (18.4%) withdrew from the study (32 participants [21.2%] in the atorvastatin group and 24 participants [15.7%] in the placebo group), and 248 participants (81.6%) completed the study. Based on pill count, 84.6% of participants (85.4% of participants in the atorvastatin group and 83.7% of participants in the placebo group) had >80% compliance with the study medication. Supplementary Table 1 (available on the *Arthritis & Rheumatology* website at http://onlinelibrary.wiley.com/doi/10.1002/art.41760/abstract) shows baseline characteristics of participants who completed the study and those who did not.

Primary end point. Tibial cartilage volume per year over 2 years was reduced by a mean value of 1.66% in the atorvastatin group and 2.17% in the placebo group, with a between-group difference that was not statistically significant (0.50% [95% confidence interval (95% CI) –0.17%, 1.17%]; *P* = 0.14) (Table 2).

Secondary end points. Knee pain, stiffness, and function scores improved in both groups over 2 years, but there were no statistically significant between-group differences in the change in WOMAC scores over 2 years (mean change in pain score –36.0 versus –29.5, adjusted difference –2.7 [95% CI –27.1, 21.7]

Table 2. Effect of atorvastatin on the study end points over 2 years*

	Atorvastatin (n = 151)	Placebo (n = 153)
Primary end point, tibial cartilage volume		
Baseline, mean ± SD mm^3	3,601 ± 1,032	3,748 ± 1,161
Follow-up, mean ± SD mm^3	3,465 ± 1,012	3,581 ± 1,140
Annual change, mean % (95% CI)	–1.66 (–2.13, –1.19)	–2.17 (–2.61, –1.72)
Difference versus placebo, mean (95% CI)	0.50 (–0.17, 1.17)	
P	0.14†	
Secondary end points		
WOMAC pain score		
Baseline, mean ± SD	147.4 ± 88.1	141.6 ± 96.6
Follow-up, mean ± SD	111.4 ± 121.0	112.1 ± 109.2
Change, mean (95% CI)	–36.0 (–58.4, –13.6)	–29.5 (–47.7, –11.3)
Difference versus placebo, mean (95% CI)	–2.7 (–27.1, 21.7)	
P	0.83‡	
WOMAC stiffness score		
Baseline, mean ± SD	68.7 ± 46.8	65.3 ± 49.0
Follow-up, mean ± SD	54.5 ± 59.0	53.5 ± 52.4
Change, mean (95% CI)	–14.2 (–25.3, –3.2)	–11.8 (–20.5, –3.1)
Difference versus placebo, mean (95% CI)	–0.2 (–12.2, 11.8)	
P	0.98‡	
WOMAC physical function score		
Baseline, mean ± SD	483.3 ± 305.7	479.1 ± 347.5
Follow-up, mean ± SD	393.8 ± 429.2	391.7 ± 373.3
Change, mean (95% CI)	–89.4 (–163.3, –15.6)	–87.5 (–146.2, –28.7)
Difference versus placebo, mean (95% CI)	0.3 (–83.1, 83.6)	
P	0.99‡	
Cartilage defects score (scale 0–16)		
Baseline, median (IQR)	5 (2, 7)	5 (2, 7)
Follow-up, median (IQR)	6 (4, 8)	6 (3, 8)
Progression, no. (%)	90 (59.6)	96 (62.7)
Odds ratio for progression (95% CI)	0.86 (0.52, 1.41)	
P	0.54§	
Bone marrow lesion score (scale 0–12)		
Baseline, median (IQR)	2 (0, 5)	2 (0, 4)
Follow-up, median (IQR)	3 (1, 5)	3 (1, 5)
Progression, no. (%)	88 (58.3)	89 (58.2)
Odds ratio for progression (95% CI)	1.00 (0.62, 1.63)	
P	0.99§	

* 95% CI = 95% confidence interval; IQR = interquartile range.
† By independent-sample *t*-test.
‡ By analysis of covariance, adjusted for baseline Western Ontario and McMaster Universities Osteoarthritis Index (WOMAC) subscale score.
§ By chi-square test.

[*P* = 0.83]; mean change in stiffness score –14.2 versus –11.8, adjusted difference –0.2 [95% CI –12.2, 11.8] [*P* = 0.98]; mean change in function score –89.4 versus –87.5, adjusted difference 0.3 [95% CI –83.1, 83.6] [*P* = 0.99]). The progression of cartilage defects (59.6% versus 62.7%; *P* = 0.54) and bone marrow lesions (58.3% versus 58.2%; *P* = 0.99) was similar between groups (Table 2). No statistically significant differences were observed between the groups in level of knee pain, stiffness, or function at any time point (Supplementary Figure 1, available on the *Arthritis & Rheumatology* website at http://onlinelibrary.wiley.com/doi/10.1002/art.41760/abstract). Supplementary Table 2 (http://onlinelibrary.wiley.com/doi/10.1002/art.41760/abstract) shows the power of the study under the sample size achieved.

Prespecified subgroup and sensitivity analyses. Results of the prespecified subgroup analyses based on the presence of bone marrow lesions and radiographic JSN at baseline are available in Supplementary Tables 3 and 4, respectively, on the *Arthritis & Rheumatology* website at http://onlinelibrary.wiley.com/doi/10.1002/art.41760/abstract. There was no differential effect of atorvastatin on study outcomes in participants with and those without bone marrow lesions or those with and those without JSN. However, with regard to the end point of progression of bone marrow lesions over 2 years, we observed a significant (*P* = 0.04) and qualitative interaction between treatment group and baseline presence of bone marrow lesions; in participants without bone marrow lesions at baseline, the 2-year incidence of bone marrow lesions was lower in the atorvastatin group compared to the placebo group, whereas among those with bone marrow lesions at baseline, higher rates of 2-year progression of bone marrow lesions were seen in the atorvastatin group compared to the placebo group. Findings of the per-protocol analyses did not meaningfully change the results from the primary analysis (Supplementary Table 5, available on the *Arthritis & Rheumatology* website at http://onlinelibrary.wiley.com/doi/10.1002/art.41760/abstract).

Since the atorvastatin group had a higher proportion of women compared to the placebo group, additional adjustment for sex was performed for the primary and secondary end points (Supplementary Table 6, available on the *Arthritis & Rheumatology* website at http://onlinelibrary.wiley.com/doi/10.1002/art.41760/abstract). No significant findings were observed. The results did not change when tibial cartilage volume loss in the medial and lateral compartment was examined separately (Supplementary Table 7) (http://onlinelibrary.wiley.com/doi/10.1002/art.41760/abstract).

AEs. AEs are shown in Table 3. There were 89 AEs in the atorvastatin group and 82 in the placebo group. Fifty-seven participants (37.7%) in the atorvastatin group and 52 participants (34.0%) in the placebo group experienced at least one AE. The incidence of AEs was similar in the 2 groups throughout the trial, except that more participants in the atorvastatin group

Table 3. AEs in patients randomized to receive atorvastatin or placebo*

	Atorvastatin (n = 151)	Placebo (n = 153)
No. of AEs	89	82
No. of SAEs	20	26
Participants with AEs		
Any AE	57 (37.7)	52 (34.0)
Any SAE	15 (9.9)	19 (12.4)
Musculoskeletal and connective tissue disorders	15 (9.9)	22 (14.4)
Myalgia	8 (5.3)	2 (1.3)
Injury, falls, fracture, and procedural complications	10 (6.6)	7 (4.6)
Ligament and tendon disorders	3 (2.0)	0 (0.0)
Abnormal blood test result or weight gain	8 (5.3)	5 (3.3)
Skin and subcutaneous tissue disorders	7 (4.6)	3 (2.0)
Infections	4 (2.6)	5 (3.3)
Cardiovascular disorders	3 (2.0)	4 (2.6)
General disorders	3 (2.0)	3 (2.0)
Nervous system disorders	1 (0.7)	5 (3.3)
Cancer	2 (1.3)	3 (2.0)
Metabolism disorders	0 (0.0)	4 (2.6)
Gastrointestinal disorders	3 (2.0)	1 (0.7)
Immune system disorders	1 (0.7)	0 (0.0)
Hepatobiliary disorders	1 (0.7)	0 (0.0)
Other AEs (including elective surgery/ procedures other than knee or hip replacement)	7 (4.6)	13 (8.5)

* Except where indicated otherwise, values are the number (%) of patients. AEs = adverse events; SAEs = serious adverse events.

(n = 8 [5.3%]) had myalgia compared to those in the placebo group (n = 2 [1.3%]). Four participants were withdrawn from the study due to the development of a medical indication for statin therapy during the trial. Twenty SAEs were reported by 15 participants (9.9%) in the atorvastatin group, and 26 were reported by 19 participants (12.4%) in the placebo group. The incidence of SAEs was similar in the 2 groups. None of the SAEs were considered to be treatment related.

DISCUSSION

Oral atorvastatin (40 mg once daily) did not reduce the rate of tibial cartilage volume loss or improve knee pain and function over 2 years compared to placebo in participants with symptomatic knee OA. These findings do not support the use of atorvastatin as a disease-modifying agent in treating established knee OA.

A meta-analysis of observational studies showed that statin use was not associated with the incidence or progression of knee OA, with findings from a subgroup analysis showing a

reduced risk of OA associated with the use of atorvastatin (16). Findings from our randomized controlled trial did not support the notion that atorvastatin has beneficial effect in reducing cartilage volume loss or improving pain in those with symptomatic knee OA. In this clinical trial, we took into account the significant limitations of the methods utilized in previous observational studies and applied methods that were shown to be more reliable. In addition, we reduced the heterogeneity of the study population in our recruitment, and minimized the number of outcomes being assessed. We only examined knee OA, and those with severe JSN were excluded since it is less likely that therapies aimed at preventing cartilage loss will be effective in advanced disease (28). A sensitive assessment of knee structure and disease progression, i.e., cartilage volume measured using MRI, was used as the primary end point. Two-year follow-up is sufficient to detect changes in both structural and clinical outcomes.

Our study participants generally had early-stage radiographic knee OA, with 79% of participants having grade 0 or grade 1 JSN. Early-stage OA is the population that needs to be targeted for treatment in order to reduce the risk of joint replacement surgery. In examining the effect of atorvastatin on cartilage volume, we found that atorvastatin reduced the annual rate of tibial cartilage volume loss by 0.50% (95% CI –0.17%, 1.17%). The upper end point of the confidence limit of 1.17% indicates that a true difference of 1.2% between the atorvastatin and placebo groups is not compatible with our study data. Results of post hoc power analyses showed that this trial had sufficient statistical power to detect the estimated clinically important effect of atorvastatin on cartilage volume loss, pain, and function (Supplementary Table 2, available on the *Arthritis & Rheumatology* website at http://online library.wiley.com/doi/10.1002/art.41760/abstract). Since no clinically important effect was evident on the basis of the 95% CIs for any of these end points, findings from our trial do not support the existence of clinically important effects.

We performed prespecified subgroup analyses to determine whether atorvastatin may have a differential effect in certain patient phenotypes of knee OA. We found some evidence of a potential effect of atorvastatin in reducing the development of bone marrow lesions and the rate of cartilage volume loss in participants without bone marrow lesions at baseline (Supplementary Table 3, available on the *Arthritis & Rheumatology* website at http://onlinelibrary.wiley.com/doi/10.1002/art.41760/abstract). Bone marrow lesions are common in those with knee OA and are associated with cartilage volume loss (24). Increased serum levels of total cholesterol are associated with incident bone marrow lesions (7), and higher high-density lipoprotein cholesterol levels are associated with the resolution of bone marrow lesions (29). We cannot exclude the possibility that there could be an effect of atorvastatin in reducing cartilage volume loss in patients without bone marrow lesions. The widespread use of statins for the prevention of CVD may have a collateral benefit, reducing the structural progression of knee OA.

Although AEs were commonly reported in this study, the incidence was similar between the 2 groups with the exception of myalgia, which was somewhat more common in the atorvastatin group (5.3%) compared to the placebo group (1.3%). None of the SAEs were considered to be treatment related, supporting the previously described ideas regarding the safety and tolerability of statins (30).

This study has several limitations. The prespecified sample size of 350 participants and 280 expected to complete the follow-up period of 2 years was not achieved. Based on the actual sample size, a true between-group difference of 1.2% or greater is not compatible with our study data, as discussed above. Furthermore, post hoc power analyses using the achieved sample size and actual standard deviations of study end points showed that with 304 participants recruited and 248 completing follow-up, our study had 92% power to detect a 1% difference in the rate of cartilage volume loss between the atorvastatin and placebo groups, and the current sample size is sufficiently powered for the secondary end points of knee pain and function (Supplementary Table 2, available on the *Arthritis & Rheumatology* website at http://onlinelibrary.wiley.com/doi/10.1002/art.41760/abstract). The rate of loss to follow-up was 18.4%, which was not significantly different between the atorvastatin and placebo groups (21.2% versus 15.7%; *P* = 0.22). Similar results were observed in the per-protocol analysis, suggesting that loss to follow-up had a minimal influence on the results of the study. In this study, since we could not withhold effective medications for health issues, we excluded those with accepted indications for statin therapy, those who were currently receiving lipid-lowering therapy, or those with an absolute cardiovascular risk (Framingham Risk Score) of >15% within the next 5 years. This group of individuals with metabolic disease and/or low-grade inflammation may be the target population whose knee OA may benefit from statins.

Thus, our results may have underestimated any potential effect of statins on knee OA. The characteristics of statin users with respect to metabolic status (plasma lipids, presence of hypertension, and diabetes) in the previous observational studies, such as the Rotterdam Study (11), were different compared to those of the current study participants. This may explain why the results of this trial differed from the findings indicating reduced progression of knee OA in statin users in previous cohort studies. For example, when we compared the metabolic status of statin users in the Rotterdam Study (11) to that of participants in our study, we found that participants in our study had higher BMIs, probably reflecting the generally higher BMI in the Australian population compared to that of The Netherlands population, but our study participants had a lower plasma total cholesterol level:high-density lipoprotein ratio and a lower prevalence of hypertension and diabetes compared to that of the statin users in the Rotterdam Study. Further investigations are needed to determine the effect of statins on the progression of knee OA in those with metabolic disease. Strengths of our study include the recruitment of participants from the

community, which increases the generalizability of our results to a broad population with symptomatic knee OA, and the validated, quantitative measurement of structural progression (i.e., the rate of cartilage volume loss) using MRI, which has been shown to have high accuracy, reproducibility, and sensitivity to change (17).

In this study we showed that among participants with symptomatic knee OA, oral atorvastatin (40 mg once daily), compared to placebo, did not significantly reduce knee cartilage volume loss over 2 years. These findings do not support the use of atorvastatin in the treatment of knee OA. However, based on the findings from the subgroup analysis, widespread use of statins in the management of CVD may have some benefit in terms of reducing the progression of knee OA, and this is worthy of further targeted study.

ACKNOWLEDGMENTS

AUTHOR CONTRIBUTIONS

All authors were involved in drafting the article or revising it critically for important intellectual content, and all authors approved the final version to be published. Dr. Cicuttini had full access to all of the data in the study and takes responsibility for the integrity of the data and the accuracy of the data analysis.

Study conception and design. Wang, Jones, Hill, Wluka, Forbes, Tonkin, Ding, Cicuttini.

Acquisition of data. Wang, Jones, Hill, Wluka, Forbes, Tonkin, Hussain, Ding, Cicuttini.

Analysis and interpretation of data. Wang, Forbes.

REFERENCES

1. GBD 2015 Disease and Injury Incidence and Prevalence Collaborators. Global, regional, and national incidence, prevalence, and years lived with disability for 310 diseases and injuries, 1990-2015: a systematic analysis for the Global Burden of Disease Study 2015. Lancet 2016;388:1545–602.

2. Bennell KL, Hunter DJ, Hinman RS. Management of osteoarthritis of the knee [review]. BMJ 2012;345:e4934.

3. Zhang W, Nuki G, Moskowitz RW, Abramson S, Altman RD, Arden NK, et al. OARSI recommendations for the management of hip and knee osteoarthritis. Part III: changes in evidence following systematic cumulative update of research published through January 2009. Osteoarthritis Cartilage 2010;18:476–99.

4. Thijssen E, van Caam A, van der Kraan PM. Obesity and osteoarthritis, more than just wear and tear: pivotal roles for inflamed adipose tissue and dyslipidaemia in obesity-induced osteoarthritis. Rheumatology (Oxford) 2015;54:588–600.

5. Pelletier JP, Raynauld JP, Caron J, Mineau F, Abram F, Dorais M, et al. Decrease in serum level of matrix metalloproteinases is predictive of the disease-modifying effect of osteoarthritis drugs assessed by quantitative MRI in patients with knee osteoarthritis. Ann Rheum Dis 2010;69:2095–101.

6. Stannus O, Jones G, Cicuttini F, Parameswaran V, Quinn S, Burgess J, et al. Circulating levels of IL-6 and TNF-α are associated with knee

7. Davies-Tuck ML, Hanna F, Davis SR, Bell RJ, Davison SL, Wluka AE, et al. Total cholesterol and triglycerides are associated with the development of new bone marrow lesions in asymptomatic middle-aged women: a prospective cohort study. Arthritis Res Ther 2009;11:R181.

8. Wierzbicki AS, Poston R, Ferro A. The lipid and non-lipid effects of statins [review]. Pharmacol Ther 2003;99:95–112.

9. Lazzerini PE, Capecchi PL, Selvi E, Lorenzini S, Bisogno S, Baldari CT, et al. Statins and the joint: multiple targets for a global protection? Semin Arthritis Rheum 2011;40:430–46.

10. Baker JF, Walsh P, Mulhall KJ. Statins: a potential role in the management of osteoarthritis? [review]. Joint Bone Spine 2011;78:31–4.

11. Clockaerts S, van Osch GJ, Bastiaansen-Jenniskens YM, Verhaar JA, van Glabbeek F, van Meurs JB, et al. Statin use is associated with reduced incidence and progression of knee osteoarthritis in the Rotterdam study. Ann Rheum Dis 2012;71:642–7.

12. Haj-Mirzaian A, Mohajer B, Guermazi A, Conaghan PG, Lima JA, Blaha MJ, et al. Statin use and knee osteoarthritis outcome measures according to the presence of Heberden nodes: results from the Osteoarthritis Initiative. Radiology 2019;293:396–404.

13. Veronese N, Koyanagi A, Stubbs B, Cooper C, Guglielmi G, Rizzoli R, et al. Statin use and knee osteoarthritis outcomes: a longitudinal cohort study. Arthritis Care Res (Hoboken) 2019;71:1052–8.

14. Eymard F, Parsons C, Edwards MH, Petit-Dop F, Reginster JY, Bruyere O, et al. Statin use and knee osteoarthritis progression: results from a post-hoc analysis of the SEKOIA trial. Joint Bone Spine 2018;85:609–14.

15. Riddle DL, Moxley G, Dumenci L. Associations between statin use and changes in pain, function and structural progression: a longitudinal study of persons with knee osteoarthritis. Ann Rheum Dis 2013;72:196–203.

16. Wang J, Dong J, Yang J, Wang Y, Liu J. Association between statin use and incidence or progression of osteoarthritis: meta-analysis of observational studies. Osteoarthritis Cartilage 2020;28: 1170–9.

17. Hunter DJ, Zhang W, Conaghan PG, Hirko K, Menashe L, Reichmann WM, et al. Responsiveness and reliability of MRI in knee osteoarthritis: a meta-analysis of published evidence. Osteoarthritis Cartilage 2011;19:589–605.

18. Wluka AE, Wolfe R, Stuckey S, Cicuttini FM. How does tibial cartilage volume relate to symptoms in subjects with knee osteoarthritis? Ann Rheum Dis 2004;63:264–8.

19. Cicuttini FM, Jones G, Forbes A, Wluka AE. Rate of cartilage loss at two years predicts subsequent total knee arthroplasty: a prospective study. Ann Rheum Dis 2004;63:1124–7.

20. Wang Y, Tonkin A, Jones G, Hill C, Ding C, Wluka AE, et al. Does statin use have a disease modifying effect in symptomatic knee osteoarthritis? Study protocol for a randomised controlled trial. Trials 2015;16:584.

21. Altman R, Asch E, Bloch D, Bole G, Borenstein D, Brandt K, et al. Development of criteria for the classification and reporting of osteoarthritis: classification of osteoarthritis of the knee. Arthritis Rheum 1986;29:1039–49.

22. Altman RD, Hochberg M, Murphy WA Jr, Wolfe F, Lequesne M. Atlas of individual radiographic features in osteoarthritis. Osteoarthritis Cartilage 1995;3 Suppl A:3–70.

23. Ding C, Garnero P, Cicuttini F, Scott F, Cooley H, Jones G. Knee cartilage defects: association with early radiographic osteoarthritis, decreased cartilage volume, increased joint surface area and type II collagen breakdown. Osteoarthritis Cartilage 2005;13:198–205.

24. Raynauld JP, Martel-Pelletier J, Berthiaume MJ, Abram F, Choquette D, Haraoui B, et al. Correlation between bone lesion changes and

cartilage volume loss in patients with osteoarthritis of the knee as assessed by quantitative magnetic resonance imaging over a 24-month period. Ann Rheum Dis 2008;67:683–8.

25. Bellamy N, Buchanan WW, Goldsmith CH, Campbell J, Stitt LW. Validation study of WOMAC: a health status instrument for measuring clinically important patient relevant outcomes to antirheumatic drug therapy in patients with osteoarthritis of the hip or knee. J Rheumatol 1988;15:1833–40.

26. Bennell KL, Bowles KA, Wang Y, Cicuttini F, Davies-Tuck M, Hinman RS. Higher dynamic medial knee load predicts greater cartilage loss over 12 months in medial knee osteoarthritis. Ann Rheum Dis 2011;70:1770–4.

27. White IR, Royston P, Wood AM. Multiple imputation using chained equations: issues and guidance for practice. Stat Med 2011;30:377–99.

28. Felson DT, Neogi T. Emerging treatment models in rheumatology: challenges for osteoarthritis trials. Arthritis Rheumatol 2018;70:1175–81.

29. Dore D, de Hoog J, Giles G, Ding C, Cicuttini F, Jones G. A longitudinal study of the association between dietary factors, serum lipids and bone marrow lesions of the knee. Arthritis Res Ther 2012;14:R13.

30. Chou R, Dana T, Blazina I, Daeges M, Jeanne TL. Statins for prevention of cardiovascular disease in adults: evidence report and systematic review for the US Preventive Services Task Force. JAMA 2016;316:2008–24.

Erratum

DOI: 10.1002/art.41995

In the article by Merrill et al in the February 2018 issue of *Arthritis & Rheumatology* (Efficacy and Safety of Atacicept in Patients With Systemic Lupus Erythematosus: Results of a Twenty-Four–Week, Multicenter, Randomized, Double-Blind, Placebo-Controlled, Parallel-Arm, Phase IIb Study [pages 266–276]), incorrect versions of Supplementary Table 4 and Supplementary Table 5 were inadvertently published online. The supplementary materials have been updated with the correct tables. There were also minor errors in the safety data reported. The first paragraph of the Safety section on page 273 should have read as follows: "Rates of treatment-emergent AEs (TEAEs) were higher with atacicept 75 mg and 150 mg versus placebo (80.4%, 79.8%, and 70.0%, respectively). The most commonly reported AEs across treatment arms were injection site reactions, headache, injection site pain, urinary tract infections, upper respiratory tract infections, and diarrhea (Supplementary Table 5, available at http://onlinelibrary.wiley.com/doi/10.1002/art.40360/abstract). Incidence rates of TEAEs were similar with atacicept 75 and 150 mg and placebo, except for upper respiratory tract infections (9.8%, 11.5%, and 3.0%, respectively) and diarrhea (6.9%, 11.5%, and 5.0%), which were more common with atacicept, and urinary tract infections (10.8%, 11.5%, and 17.0%), which were more common with placebo. Other commonly reported infections with atacicept 75 and 150 mg included nasopharyngitis (4.9% and 6.7%), bronchitis (1.0% and 3.8%), and influenza (2.9% and 2.9%). Pneumonia occurred in 1 patient (1%) in the atacicept 150 mg group during the treatment period. There were fewer serious TEAEs with atacicept 75 and 150 mg than with placebo (6.9%, 5.8%, and 10.0%, respectively). One patient treated with atacicept 150 mg (1%) reported a serious infection, compared with 5.9% treated with atacicept 75 mg and 5.0% treated with placebo." Finally, in Table 1, the number (percent) of patients in the atacicept 75 mg group who were receiving mycophenolate mofetil at screening should have read "17 (16.7)." None of these corrections affect the overall findings reported or the interpretation of the safety profile of atacicept.

We regret the errors.

DOI: 10.1002/art.41996

In the article by Steen Pettersen et al in the July 2019 issue of *Arthritis & Rheumatology* (Peripheral and Central Sensitization of Pain in Individuals With Hand Osteoarthritis and Associations With Self-Reported Pain Severity [pages 1070–1077]), a minus sign was inadvertently inserted at the proof stage for the upper 95% confidence interval value in two instances where the value was not a negative number. The first full paragraph in the right column of page 1073 should have read as follows: "When repeating the analyses using PPTs at the finger joints as a continuous variable, we found significant inverse associations with NRS pain scores (adjusted β = −0.2 [95% CI −0.3, −0.1] for both the painful and nonpainful finger joints), but not with AUSCAN pain scores (adjusted β = −0.2 [95% CI −0.4, 0.1] for the painful finger joint and −0.1 [95% CI −0.3, 0.1] for the nonpainful finger joint)."

We regret the errors.

The Value of Magnetic Resonance Imaging for Assessing Disease Extent and Prediction of Relapse in Early Peripheral Spondyloarthritis

Thomas Renson,[1] [ID] Philippe Carron,[1] [ID] Ann-Sophie De Craemer,[1] Liselotte Deroo,[1] Manouk de Hooge,[1] Simon Krabbe,[2] [ID] Lennart Jans,[3] Mikkel Østergaard,[2] Dirk Elewaut,[1] [ID] and Filip Van den Bosch[1]

Objective. This study was undertaken to assess the inflammatory burden in peripheral spondyloarthritis (SpA) by magnetic resonance imaging (MRI) of the legs in an early remission–induction strategy study of tumor necrosis factor (TNF) blockade. Furthermore, we sought to determine the value of MRI to predict disease relapse versus sustained remission after treatment discontinuation.

Methods. Thirty-two patients with early peripheral SpA with involvement of the legs determined on clinical examination and confirmed by ultrasonography (US) participated in a remission-induction trial of a TNF inhibitor (TNFi). Patients underwent MRI of the joints and entheses of the legs at baseline and at clinical remission, after which TNFi treatment was withdrawn. Images were evaluated for joint effusion, joint osteitis, entheseal soft tissue inflammation, and entheseal osteitis.

Results. Joint effusion and enthesitis on clinical examination and US correlated well with MRI abnormalities. In addition, a substantial amount of subclinical involvement was seen on MRI, mainly in the ankle joints and heel entheses. Inflammation scores were markedly lower in the subclinically involved joints and entheses versus those that were clinically involved (P values ranged from 0.01 to <0.001). Inflammatory load on MRI decreased significantly upon TNFi treatment ($P < 0.001$). Whereas 80% of the joints that were clinically involved at baseline showed no effusion on remission MRI, 2 of 3 entheses involved at baseline showed residual inflammation. In addition, patients who experienced a relapse after treatment discontinuation displayed more entheseal soft tissue inflammation on remission MRI compared to those who maintained drug-free remission ($P = 0.028$).

Conclusion. Our findings delineate a differential response of synovitis and enthesitis, with enthesitis on MRI being less responsive to TNFi treatment. Furthermore, residual entheseal inflammation might be indicative of the need for continuous therapy.

INTRODUCTION

In clinical practice, spondyloarthritis (SpA) is divided into axial SpA and peripheral SpA based on the predominant clinical presentation. Whereas axial SpA involves inflammation of the sacroiliac joints and/or spine, peripheral SpA affects the joints and entheses of the arms and (predominantly) legs. Monitoring of disease activity and treatment response in peripheral SpA is mainly performed using clinical examination and laboratory tests. The use of imaging techniques is of added value to assess and confirm site-specific inflammation. In this context, magnetic resonance imaging (MRI) is an emerging imaging modality in the field of peripheral

SpA; this technique could provide a more objective measurement of disease activity and treatment response in peripheral SpA (1).

Ultrasonography (US) is more sensitive compared to clinical examination for the detection of peripheral SpA features (2–5). This imaging technique rapidly assesses the presence of joint effusion, and using the power Doppler (PD) technique, active synovitis can be detected. In addition, US evaluates structural abnormalities, such as bone erosions and juxtaarticular new bone formation. However, the presence of periarticular osteitis cannot be assessed, since the US beam cannot penetrate the bony cortex. For the evaluation of osteitis, MRI is a more appropriate imaging modality (5).

The diagnosis of enthesitis, a hallmark of SpA often considered to be the primary disease manifestation, remains challenging (6–10). To date, the clinical diagnosis is based on eliciting pain on pressure, ideally by using a standardized palpation approach (11). Nonetheless, interreader and intrareader variabilities are high. The existing clinical scoring systems lack reliability, validity, sensitivity, and specificity (11,12). Imaging techniques could aid in circumventing these drawbacks. US is increasingly being used for the detection of enthesitis, including in clinical trials. PDUS has shown added value when combined with grayscale US to differentiate between entheseal involvement in SpA and painful pressure points in other non-SpA conditions, such as fibromyalgia (7,13,14). Currently, the use of MRI to assess enthesitis in clinical trials is still limited. Recently, the Outcome Measures in Rheumatology (OMERACT) group has generated consensus-based definitions of enthesitis as assessed by US and MRI for use as outcome measures in trials (15–17).

The aim of the present study was to assess the inflammatory burden in very early peripheral SpA by MRI of the legs at baseline and once patients reached sustained clinical remission upon treatment with a tumor necrosis factor inhibitor (TNFi). An additional aim was to compare MRI findings with joint and entheseal involvement on clinical examination, and to assess the ability of MRI to predict sustained drug-free remission after treatment withdrawal.

PATIENTS AND METHODS

Study subjects. The Clinical Remission in Peripheral Spondyloarthritis (CRESPA) study is a single-center, double-blind, placebo-controlled trial of the TNFi golimumab in 60 patients with very early peripheral SpA (defined as a symptom duration of <12 weeks). The study design has been described previously (18,19). In order to investigate whether early treatment with TNFi would lead to subsequent drug-free remission (the "window of opportunity" hypothesis), medication was withdrawn at the time point of sustained clinical remission, defined as the absence of clinical arthritis, enthesitis, and dactylitis at 2 major consecutive visits planned at weeks 12, 24, 36, and 48. Subsequently, treatment was discontinued and patients were prospectively followed

up to detect a potential peripheral SpA relapse. In this subanalysis, only CRESPA study subjects in whom joint and/or entheseal involvement in the legs was found on clinical examination and confirmed by US were included, since only leg MRI data were available.

Clinical examination. Peripheral synovitis was clinically evaluated by counts of tender and swollen joints (78 and 76 assessed, respectively), and enthesitis was evaluated by assessment of tenderness at the site of an enthesis. Nineteen entheses were evaluated in the CRESPA trial, including the 13 Maastricht Ankylosing Spondylitis Enthesitis Score locations, with the addition of the insertions of the quadriceps tendon, patellar ligament (insertion into the inferior pole of the patella and into the tibial tuberosity), and plantar fascia. Although clinical examination was regarded as the gold standard, only the clinically involved joints and entheses of the legs that also showed abnormalities on US (see below) were analyzed for correlation with MRI findings, in order to increase diagnostic certainty.

Ultrasonography. At baseline, clinical synovitis and enthesitis in the legs was confirmed on US by an experienced ultrasonographer (PC). The subtalar joint and midfoot were evaluated as one anatomic site. Synovitis was scored for each joint on a scale of 0–3 according to the EULAR–OMERACT US task force composite PDUS scale, where 0 = normal, 1 = mild, 2 = moderate, and 3 = severe (20). A EULAR–OMERACT US composite PDUS score of ≥1 was used as a cutoff for the definition of confirmed synovitis. Affected entheses were scored for morphologic severity according to the OMERACT enthesitis composite semiquantitative scale, where 0 = no morphologic abnormalities, 1 = hypoechogenicity, 2 = thickening and hypoechogenicity plus calcifications/enthesophytes, and 3 = thickening and hypoechogenicity plus calcifications/enthesophytes and erosions (15). Intraentheseal PD signal (0–3) was assessed. Clinical enthesitis in the legs was confirmed by US in cases with an OMERACT enthesitis composite score of ≥1.

Magnetic resonance imaging. CRESPA study participants underwent an extensive MRI assessment of the legs, covering several joints and entheses of the legs, at baseline and once sustained clinical remission was reached. Images were obtained on a 1.5T MRI unit (Avanto; Siemens Healthineers). MRI was performed by scanning multiple SpA-specific locations (using different coils) individually over a timeframe of ~2 hours. Dedicated body flexed-array coils, knee coils, and ankle coils were used. Sequences obtained included 3-mm semicoronal, 5-mm coronal, and 6-mm axial STIR images of the pelvis, and 4-mm sagittal fat-saturated T2-weighted images of both knees and both ankles. After an initial calibration exercise, 3 readers (SK, LJ, and MØ) who were blinded with regard to time point and clinical characteristics independently evaluated all images, which were paired per patient.

The following joints were assessed for effusion (synovitis) and bone marrow edema (osteitis) on MRI: hips (osteitis was assessed separately for the femoral head and acetabulum), knees (osteitis was assessed separately for the patella, medial femoral condyle, lateral femoral condyle, medial tibial condyle, and lateral tibial condyle), talocrural joints (osteitis was assessed separately for the talus and crural bones), and subtalar joints and midfoot (talocalcaneonavicular and calcaneocuboid joints). The following entheses were evaluated for soft tissue inflammation and bone marrow edema (osteitis) on MRI: quadriceps femoris tendon insertion into patella, patellar tendon insertion into patella (superior patellar ligament) and tibial tuberosity (inferior patellar ligament), plantar fascia insertion, and Achilles tendon insertion into calcaneus. Involved sites were scored semiquantitatively on a scale of 0–3, where 0 = no abnormalities, 1 = mild, 2 = moderate, and 3 = severe. Synovitis on MRI was defined as a joint effusion score of ≥1, with or without concomitant osteitis. Enthesitis on MRI was defined as a soft tissue inflammation and/or bone marrow edema score of ≥1. For each site the mean of the readers' scores was calculated and used for further analyses.

MRI inflammation indices for joint synovitis, joint osteitis, entheseal soft tissue inflammation, and entheseal osteitis were calculated by adding the respective scores per patient per time point. In addition, a total MRI leg inflammation index was calculated as the sum score of these indices. Changes from baseline scores reflect the difference in inflammatory load at the time point of sustained clinical remission compared to baseline and were calculated as the score at baseline minus the score at remission.

Statistical analysis. Descriptive statistics were used to quantify the baseline demographic and disease characteristics, as well as to calculate the sum scores. Within-group differences between time points in MRI scores were calculated by Wilcoxon's signed rank test. Data for the relapse groups versus the no-relapse groups were compared by the Mann-Whitney U test. P values less than 0.05 were considered significant. All statistical analyses were performed using IBM SPSS Statistics version 25.

RESULTS

Characteristics of the study subjects. Thirty-two CRESPA study subjects with leg involvement were included in this post hoc analysis. All subjects who were included had ≥1 active synovitis or enthesitis in the legs that was confirmed on US. In total, sustained clinical remission was achieved in 27 (84%) of the 32 patients, 10 of whom (37%) experienced a relapse after treatment discontinuation. Only 3 patients reached sustained clinical remission while receiving placebo. Disease characteristics are shown in Table 1.

Baseline MRI findings. Examples of baseline MRI abnormalities in CRESPA study patients and their evolution after patients reached sustained clinical remission are shown in Figure 1. Regarding synovitis, MRI abnormalities were detected in 42 (89%) of the 47 clinically involved joints at baseline (Figure 2): 100% of the hip joints (only 1 patient), 92% of the talocrural joints, 88% of the knee joints, and 86% of the subtalar/midfoot joints showed concordant MRI effusion. A substantial amount of joint effusion on MRI was observed in clinically uninvolved joints: 14 subtalar/midfoot joints, 12 talocrural joints, 6 knee joints, and 5 hip joints (Figure 2). MRI joint synovitis indices and MRI joint osteitis indices were significantly higher in clinically involved joints compared to subclinically involved joints ($P < 0.001$ and $P = 0.01$, respectively). In 11 (26%) of 42 clinically involved joints with effusion on MRI, we also detected concomitant joint osteitis, whereas osteitis was only observed in 2 (5%) of 37 joints with subclinical effusion.

Table 1. Baseline demographic and disease characteristics of all SpA patients in the CRESPA study and patients with clinical involvement of the legs*

	All patients (CRESPA study) (n = 60)	Patients with involvement of the legs (present study) (n = 32)
Age, mean ± SD years	39.7 ± 13.4	37.4 ± 12.7
Sex, no. (%) male	39 (65)	18 (56)
HLA–B27 positive, no. (%)	33 (55)	21 (66)
Duration of joint symptoms, mean ± SD weeks	5.0 ± 2.4	7.6 ± 4.1
Tender joint count, median (IQR) (78 assessed)	4 (3–8)	4 (2–12)
Swollen joint count, median (IQR) (76 assessed)	4 (2–5)	3 (1–6)
Swollen joint count ≥5, no. (%)	14 (23)	10 (31)
Psoriasis (past/present), no. (%)	23 (38)	7 (22)
Anterior uveitis (past/present), no. (%)	1 (2)	0 (0)
Inflammatory bowel disease (past/present), no. (%)	1 (2)	1 (3)
Elevated CRP (≥5 mg/liter) at baseline, no. (%)	39 (65)	21 (66)
CRP, median (IQR) mg/liter	13 (4–36)	19 (4–51)
ESR, median (IQR) mm/hour	23 (10–44)	30 (10–62)

* SpA = spondyloarthritis; CRESPA = Clinical Remission in Peripheral Spondyloarthritis; IQR = interquartile range; CRP = C-reactive protein; ESR = erythrocyte sedimentation rate.
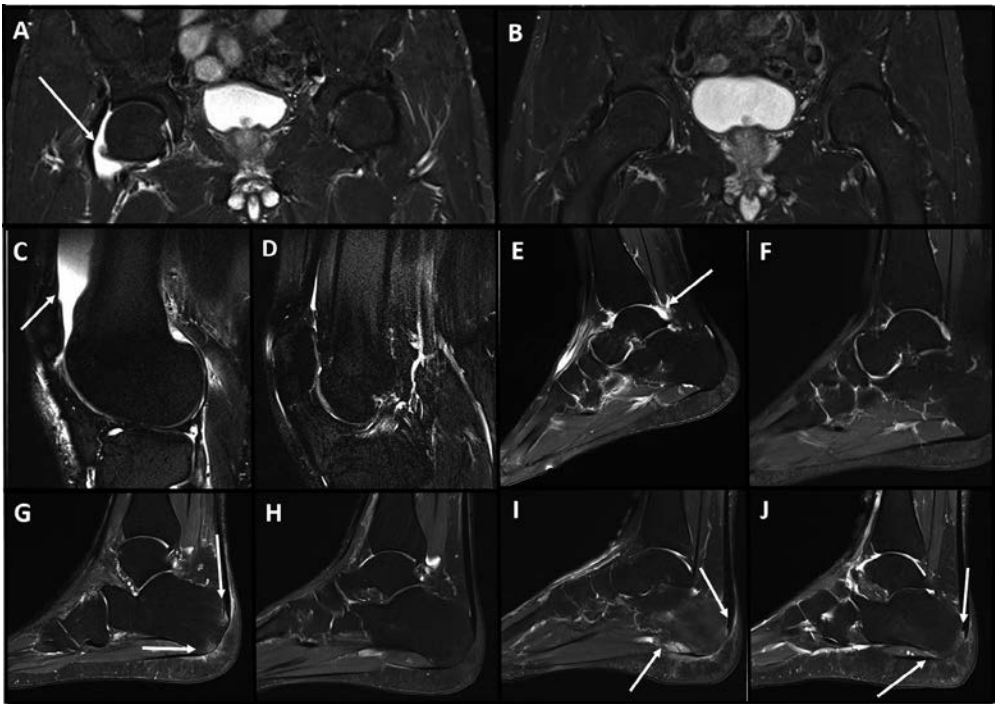
Figure 1. Paired fat-saturated T2 magnetic resonance images (MRIs) showing examples of joint and entheseal involvement in patients with peripheral spondyloarthritis treated with a tumor necrosis factor inhibitor. MRIs were obtained at baseline and the time of sustained clinical remission. The patients with MRIs shown in **A**–**H** remained in drug-free remission during follow-up. The patient with MRIs shown in **I** and **J** experienced a relapse after treatment discontinuation. **A** and **B**, Moderate effusion at the right hip joint (**arrow**) at baseline (**A**) and complete resolution of the hip effusion at remission (**B**). **C** and **D**, Knee effusion (**arrow**) at baseline (**C**) and no residual knee effusion at remission (**D**). **E** and **F**, Severe talocrural (**arrow**) and midfoot effusion and mild subtalar effusion at baseline (**E**) and complete resolution of the joint effusion at remission (**F**). **G** and **H**, Moderate soft tissue inflammation and osteitis at the Achilles tendon enthesis and mild soft tissue inflammation and moderate osteitis at the plantar fascia enthesis (**arrows**) at baseline (**G**) and complete resolution of enthesitis at remission (**H**). **I** and **J**, Moderate soft tissue inflammation and osteitis at the Achilles tendon enthesis and moderate soft tissue inflammation and severe osteitis at the plantar fascia enthesis (**arrows**) at baseline (**I**) and continuing mild soft tissue inflammation and osteitis at both the Achilles tendon enthesis and plantar fascia enthesis (**arrows**) at remission (**J**).

With regard to enthesitis at baseline, we observed MRI abnormalities in 91% of the clinically involved entheses of the heel (Figure 2): 100% of the Achilles tendon entheses and 80% of the plantar fascia entheses showed concordant entheseal soft tissue inflammation and/or osteitis on MRI. Neither clinically involved quadriceps femoris tendon entheses or superior patellar ligament
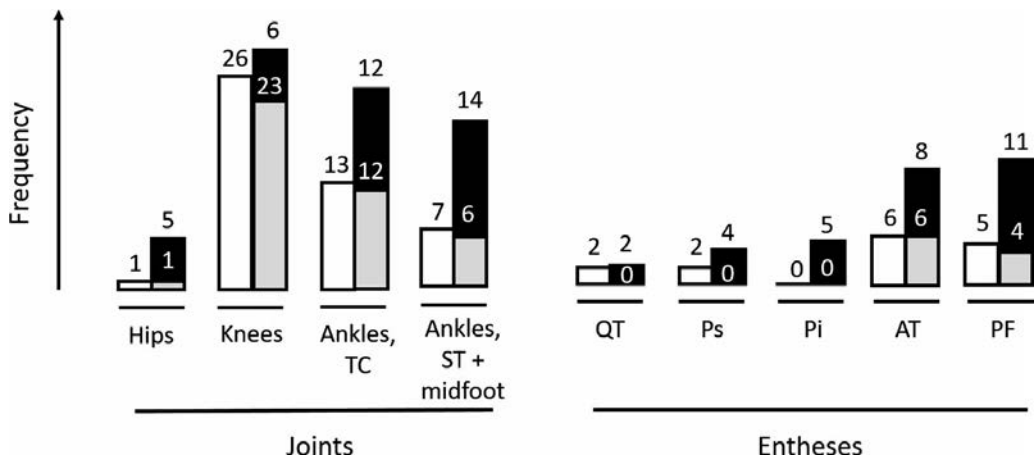
Figure 2. Number of involved joints (synovitis) and entheses (enthesitis) in patients with peripheral spondyloarthritis at baseline, as assessed by clinical examination and magnetic resonance imaging (MRI). Open bars indicate the number of joints or entheses with positive findings on clinical examination and ultrasonography (US); shaded bars indicate the number of joints or entheses with positive findings on clinical examination, US, and MRI; solid bars indicate the number of joints or entheses found to be subclinically involved on MRI. Values refer to the bars directly below them. TC = talocrural joints; ST = subtalar joints; QT = quadriceps femoris tendon: Ps = superior patellar ligament; Pi = inferior patellar ligament; AT = Achilles tendon; PF = plantar fascia.

Table 2. MRI inflammation indices for the joints and entheses at baseline and clinical remission*

MRI index	Baseline	Remission	P†	Change from baseline to remission
Joint synovitis	4.2 ± 3.2	1.4 ± 1.4	<0.001	2.8 ± 3.0
Joint osteitis	0.7 ± 1.1	0.7 ± 1.2	0.87	0.0 ± 1.2
Entheseal soft tissue inflammation	1.7 ± 2.0	0.8 ± 0.8	0.004	1.0 ± 1.7
Entheseal osteitis	0.9 ± 1.8	0.5 ± 0.9	0.12	0.4 ± 1.3
Total inflammation	7.5 ± 5.1	3.4 ± 2.5	<0.001	4.1 ± 4.8

* Values are the mean ± SD. MRI = magnetic resonance imaging.
† By Wilcoxon's signed rank test.

entheses showed MRI abnormalities. However, in 3 of 4 of these entheses an adjacent knee synovitis was present, possibly interfering with the clinical examination of the respective entheses. No inferior patellar ligament entheses were clinically involved at baseline. In addition, in 30 entheses without tenderness at baseline clinical examination, soft tissue inflammation and/or osteitis was detected on MRI: 11 plantar fascia, 8 Achilles tendon, 5 inferior patellar ligament, 4 superior patellar ligament, and 2 quadriceps femoris tendon entheses (Figure 2). MRI entheseal soft tissue inflammation indices and MRI entheseal osteitis indices were significantly higher in clinically affected entheses versus those that were subclinically involved (P = 0.01 and P = 0.002, respectively).

Clinical remission MRI findings. The changes in the MRI inflammation indices from baseline to the time point of sustained clinical remission are shown in Table 2. In general, a significant decrease in the total MRI leg inflammation index was observed upon TNFi treatment. MRI indices for synovitis and entheseal soft tissue inflammation decreased significantly upon treatment, whereas no significant decrease in MRI scores for entheseal osteitis could be detected. Limited joint osteitis was seen at both time points and remained stable over time. Despite sustained clinical remission and the clear improvement in MRI indices upon

treatment, 13 (48%) of 27 patients still showed joint effusion on MRI (in a total of 29 joints) and 11 patients (41%) still showed entheseal soft tissue inflammation and/or osteitis (in a total of 19 entheses); however, inflammation indices in these joints and entheses were low. Nine patients (33%) had neither residual joint nor residual entheseal inflammation on their remission MRI.

In joints and entheses that were clinically affected and displayed MRI abnormalities at baseline, 20% of the joints (6 of 30) were still showing effusion on MRI at remission, whereas in 67% of the entheses (6 of 9) residual abnormalities were observed on MRI at remission. Of note, at the level of the joint, effusion on MRI mainly persisted at the talocrural joints (50% of those involved at baseline), whereas entheseal inflammation persisted at both the plantar fascia and Achilles tendon entheses (75% and 60%, respectively, of those involved at baseline).

Furthermore, we evaluated MRI inflammation indices once sustained clinical remission was achieved in relation to subsequent relapse after treatment discontinuation (Table 3). MRI entheseal soft tissue inflammation indices at remission were significantly higher in patients who experienced a relapse after treatment discontinuation compared to those who maintained drug-free remission (P = 0.028). No significant differences in the other MRI inflammation indices (neither for baseline nor change from baseline) were found between these patient groups.

Table 3. MRI inflammation indices at remission in patients who subsequently experienced a relapse and patients who maintained drug-free remission*

MRI inflammation index	Relapse	Persistent remission
Joint synovitis	1.4	1.5
Joint osteitis	0.6	0.8
Entheseal soft tissue inflammation	1.1	0.6†
Entheseal osteitis	0.9	0.3
Total leg inflammation	4.0	3.1
Change from baseline in joint synovitis score	2.5	2.9
Change from baseline in joint osteitis score	0.3	−0.2
Change from baseline in entheseal soft tissue inflammation score	1.1	0.8
Change from baseline in entheseal osteitis score	0.5	0.3
Change from baseline in total leg inflammation score	4.4	3.9

* Values are the mean. MRI = magnetic resonance imaging.
† P = 0.028 versus relapse, by Mann-Whitney U test.

DISCUSSION

To our knowledge, this is the first study of the value of MRI for the assessment of disease extent and prediction of relapse in early peripheral SpA, revealing several novel and clinically relevant findings with important implications for the management of the disease. First, the baseline MRI findings indicate a much broader pattern of involvement than detected on clinical examination, which may point to a substantially higher inflammatory burden. Second, for patients in whom sustained clinical remission was achieved, the MRI leg inflammation index was greatly reduced after treatment with a TNFi. Nonetheless, despite being in clinical remission, several patients continued to display some low-grade joint and/or entheseal involvement on MRI: two-thirds of the clinical enthesitides showed residual soft tissue inflammation and/or osteitis. In addition, patients who experienced a relapse after treatment discontinuation showed more entheseal soft tissue

inflammation on remission MRI compared to patients in ongoing drug-free remission, suggesting that MRI-determined entheseal inflammation may be indicative of subsequent relapse in early peripheral SpA.

The extent of inflammation on MRI was higher than that determined by clinical (and US) assessment and decreased substantially upon TNFi treatment. Interestingly, at baseline and at clinical remission, MRI frequently visualized ankle effusion that was not detected on clinical examination. A higher threshold (e.g., an MRI joint synovitis index of ≥2) might be needed in the evaluation of clinically affected joints or entheses. The prognostic importance of chronic low-grade subclinical inflammation remains to be determined. Osteitis was almost never observed in joints with subclinical effusion, in contrast to being present in one-fourth of the clinically involved joints with effusion on baseline MRI. This finding indicates that the presence of osteitis may differentiate true synovitis from background noise. Whereas subclinical joint inflammation, particularly osteitis, in rheumatoid arthritis has been documented to have predictive value for subsequent progression of structural joint damage as visualized by both MRI and conventional radiography (21,22), further studies are needed to clarify the predictive value of such findings in the hips, knees, and ankles in peripheral SpA. Osteitis scores did not significantly change after treatment with a TNFi. This finding suggests that osteitis is less responsive than synovitis to TNF blockade within the given timeframe. The reasons for this differential response are elusive. A similar phenomenon is observed in axial SpA, where clinical remission after treatment with TNF blockade is not always accompanied by remission on MRI (23,24).

In the present study, enthesitis on clinical examination and US in general showed a good correlation with abnormalities on MRI. However, MRI identified a substantial amount of subclinical soft tissue inflammation and osteitis at the entheses of the Achilles tendon and plantar fascia. Since enthesitis is an early sign of psoriatic arthritis with a substantially better outcome when treated early, an accurate diagnosis is important (25). Still, both clinical examination and US lack specificity for enthesitis (11,12,25–27). Since entheses are located near joints and fibromyalgia trigger points, the risk of false-positive findings is considerable. Erosions, enthesophytes, and calcifications on entheseal US are also seen in degenerative conditions (27). In addition, US features of active inflammation may also be observed in some healthy subjects (26). This diagnostic challenge is reflected in our study, considering that 3 of 4 patients with a knee enthesitis on clinical examination and US, not detected by MRI, had a synovitis of the respective knee. Considering the differential response of enthesitis and synovitis to treatment with biologic disease-modifying antirheumatic drugs, and the possible role of enthesitis as a prognostic factor, an accurate distinction between joint and entheseal involvement is important.

Thus, MRI could be of added value in identifying true enthesitis. In contrast to US, MRI can visualize the entire entheseal organ, and beyond the bony cortex, by assessing the presence of bone marrow edema. Moreover, MRI can be used to evaluate entheses not readily accessible by US, e.g., the pelvic entheses. Nonetheless, since MRI is very sensitive to signal alterations, entheseal abnormalities are potentially also seen in healthy subjects, warranting the use of higher thresholds (28). In this context, OMERACT recently proposed an MRI enthesitis scoring system, focusing on the heel region in peripheral SpA patients (17). Other limitations of MRI include restricted (and delayed) access, as well as the need for a contrast medium to visualize vascularization. Nonetheless, Poggenborg et al demonstrated a role for MRI in screening for subclinical enthesitis (29). Indeed, our study reveals that this could be of interest, since persisting entheseal soft tissue inflammation over time was more prevalent in patients who experienced a relapse after treatment discontinuation.

While 4 of 5 clinically affected joints showed no residual inflammation on remission MRI, only 1 of 3 clinically affected entheses were completely resolved on remission MRI. These preliminary results may indicate a differential response of enthesitis and synovitis to TNFi treatment. Several hypotheses could explain this striking finding. First, since entheses are poorly vascularized, the entheseal bioavailability of TNFi drugs could be lower than intraarticular levels. Second, the response of enthesitis to TNFi treatment may be slower, warranting longer treatment periods compared to synovitis. Performing the same study using drugs with a different mode of action may show different results (30,31).

This study had several strengths and limitations. Strengths include the very short disease duration and the extensive MRI assessment of specific frequently affected sites in the legs in SpA, both at baseline and at the time point of sustained clinical remission. Another strength is the inclusion of peripheral SpA patients with joint and/or entheseal involvement confirmed by US, reinforcing the clinical assessment in these patients. However, since MRI assessment was only performed for the legs, CRESPA study patients with solely arm and/or forefoot involvement were omitted from this subanalysis, which resulted in a relatively small study population. An additional limitation is the absence of follow-up MRI in patients who did not reach sustained clinical remission. However, this group was relatively small (11 of 60 CRESPA study patients).

In conclusion, this is the first study to conduct MRI of multiple joints and entheses in addition to clinical and US assessment in patients with very early peripheral SpA, at baseline and after treatment with a TNFi. Imaging revealed a more extensive inflammatory burden than clinically suspected. The MRI leg inflammation index was sensitive to change during TNFi treatment. Despite the clear clinical improvement, entheseal inflammation on MRI tended to be less responsive or potentially slower to respond to TNFi treatment compared to synovitis. Patients who experienced a relapse after treatment withdrawal had more entheseal soft tissue inflammation compared to those in ongoing drug-free remission. Imaging could therefore be used

to evaluate disease extent and treatment response in peripheral SpA patients and might play a role in identifying patients with a more severe disease course, in whom prolonged treatment may be warranted. Future studies are needed to clarify this finding, as well the predictive value of MRI findings for long-term clinical and structural outcomes.

AUTHOR CONTRIBUTIONS

All authors were involved in drafting the article or revising it critically for important intellectual content, and all authors approved the final version to be published. Dr. Renson had full access to all of the data in the study and takes responsibility for the integrity of the data and the accuracy of the data analysis.

Study conception and design. Renson, Carron, Elewaut, Van den Bosch.

Acquisition of data. Renson, Carron, Jans.

Analysis and interpretation of data. Renson, De Craemer, Deroo, de Hooge, Krabbe, Jans, Østergaard.

ROLE OF THE STUDY SPONSOR

Janssen Pharmaceutica had no role in the study design or in the collection, analysis, or interpretation of the data, the writing of the manuscript, or the decision to submit the manuscript for publication. Publication of this article was not contingent upon approval by Janssen Pharmaceutica.

REFERENCES

1. Mager AK, Althoff CE, Sieper J, Hamm B, Hermann KG. Role of whole-body magnetic resonance imaging in diagnosing early spondyloarthritis. Eur J Radiol 2009;71:182–8.

2. Balint PV, Kane D, Wilson H, McInnes IB, Sturrock RD. Ultrasonography of entheseal insertions in the lower limb in spondyloarthropathy. Ann Rheum Dis 2002;61:905–10.

3. D'Agostino MA, Said-Nahal R, Hacquard-Bouder C, Brasseur JL, Dougados M, Breban M. Assessment of peripheral enthesitis in the spondylarthropathies by ultrasonography combined with power Doppler: a cross-sectional study. Arthritis Rheum 2003; 48:523–33.

4. Spadaro A, Iagnocco A, Perrotta FM, Modesti M, Scarno A, Valesini G. Clinical and ultrasonography assessment of peripheral enthesitis in ankylosing spondylitis. Rheumatology (Oxford) 2011;50:2080–6.

5. D'Agostino MA. Role of ultrasound in the diagnostic work-up of spondyloarthritis. Curr Opin Rheumatol 2012;24:375–9.

6. Ball J. Enthesopathy of rheumatoid and ankylosing spondylitis. Ann Rheum Dis 1971;30:213–23.

7. D'Agostino MA. Enthesitis detection by ultrasound: where are we now? [review]. Clin Exp Rheumatol 2018;36 Suppl 114:127–30.

8. Mander M, Simpson JM, McLellan A, Walker D, Goodacre JA, Dick WC. Studies with an enthesis index as a method of clinical assessment in ankylosing spondylitis. Ann Rheum Dis 1987; 46:197–202.

9. McGonagle D, Wakefield RJ, Tan AL, D'Agostino MA, Toumi H, Hayashi K, et al. Distinct topography of erosion and new bone formation in Achilles tendon enthesitis: implications for understanding the link between inflammation and bone formation in spondylarthritis. Arthritis Rheum 2008;58:2694–9.

10. McGonagle D, Gibbon W, Emery P. Classification of inflammatory arthritis by enthesitis. Lancet 1998;352:1137–40.

11. Kristensen S, Christensen JH, Schmidt EB, Olesen JL, Johansen MB, Arvesen KB, et al. Assessment of enthesitis in patients with psoriatic arthritis using clinical examination and ultrasound. Muscles Ligaments Tendons J 2016;6:241–7.

12. Hamdi W, Chelli-Bouaziz M, Ahmed MS, Ghannouchi MM, Kaffel D, Ladeb MF, et al. Correlations among clinical, radiographic, and sonographic scores for enthesitis in ankylosing spondylitis. Joint Bone Spine 2011;78:270–4.

13. Marchesoni A, De Lucia O, Rotunno L, De Marco G, Manara M. Entheseal power Doppler ultrasonography: a comparison of psoriatic arthritis and fibromyalgia. J Rheumatol Suppl 2012; 89:29–31.

14. Marchesoni A, De Marco G, Merashli M, McKenna F, Tinazzi I, Marzo-Ortega H, et al. The problem in differentiation between psoriatic-related polyenthesitis and fibromyalgia. Rheumatology (Oxford) 2018;57:32–40.

15. Balint PV, Terslev L, Aegerter P, Bruyn GA, Chary-Valckenaere I, Gandjbakhch F, et al. Reliability of a consensus-based ultrasound definition and scoring for enthesitis in spondyloarthritis and psoriatic arthritis: an OMERACT US initiative. Ann Rheum Dis 2018;77:1730–5.

16. Krabbe S, Eshed I, Gandjbakhch F, Pedersen SJ, Bird P, Mathew AJ, et al. Development and validation of an OMERACT MRI whole-body score for inflammation in peripheral joints and entheses in inflammatory arthritis (MRI-WIPE). J Rheumatol 2019;46:1215–21.

17. Mathew AJ, Krabbe S, Eshed I, Gandjbakhch F, Bird P, Pedersen SJ, et al. The OMERACT MRI in Enthesitis Initiative: definitions of key pathologies, suggested MRI sequences, and a novel heel enthesitis scoring system. J Rheumatol 2019;46:1232–8.

18. Carron P, Varkas G, Cypers H, van Praet L, Elewaut D, Van den Bosch F, on behalf of the CRESPA Investigator Group. Anti-TNF-induced remission in very early peripheral spondyloarthritis: the CRESPA study. Ann Rheum Dis 2017;76:1389–95.

19. Carron P, Varkas G, Renson T, Colman R, Elewaut D, Van den Bosch F. High rate of drug-free remission after induction therapy with golimumab in early peripheral spondyloarthritis. Arthritis Rheumatol 2018;70:1769–77.

20. D'Agostino MA, Terslev L, Aegerter P, Backhaus M, Balint P, Bruyn GA, et al. Scoring ultrasound synovitis in rheumatoid arthritis: a EULAR-OMERACT ultrasound taskforce. Part 1. Definition and development of a standardised, consensus-based scoring system. RMD Open 2017;3:e000428.

21. Hetland ML, Ejbjerg B, Hørslev-Petersen K, Jacobsen S, Vestergaard A, Jurik AG, et al. MRI bone oedema is the strongest predictor of subsequent radiographic progression in early rheumatoid arthritis: results from a 2-year randomised controlled trial (CIMESTRA). Ann Rheum Dis 2009;68:384–90.

22. Baker JF, Ostergaard M, Emery P, Hsia EC, Lu J, Baker DG, et al. Early MRI measures independently predict 1-year and 2-year radiographic progression in rheumatoid arthritis: secondary analysis from a large clinical trial. Ann Rheum Dis 2014;73:1968–74.

23. Van der Heijde D, Sieper J, Maksymowych WP, Lambert RG, Chen S, Hojnik M, et al. Clinical and MRI remission in patients with nonradiographic axial spondyloarthritis who received long-term open-label adalimumab treatment: 3-year results of the ABILITY-1 trial. Arthritis Res Ther 2018;20:61.

24. Renson T, Carron P, De Craemer AS, Deroo L, de Hooge M, Krabbe S, et al. Axial involvement in patients with early peripheral spondyloarthritis: a prospective MRI study of sacroiliac joints and spine. Ann Rheum Dis 2021;80:103–8.

25. D'Angelo S, Palazzi C, Gilio M, Leccese P, Padula A, Olivieri I. Improvements in diagnostic tools for early detection of psoriatic arthritis [review]. Expert Rev Clin Immunol 2016;12:1209–15.

26. Di Matteo A, Filippucci E, Cipolletta E, Martire V, Jesus D, Musca A, et al. How normal is the enthesis by ultrasound in healthy subjects? Clin Exp Rheumatol 2020;38:472–8.

27. Freeston JE, Coates LC, Helliwell PS, Hensor EM, Wakefield RJ, Emery P, et al. Is there subclinical enthesitis in early psoriatic arthritis? A clinical comparison with power doppler ultrasound. Arthritis Care Res (Hoboken) 2012;64:1617–21.

28. Feydy A, Lavie-Brion MC, Gossec L, Lavie F, Guerini H, Nguyen C, et al. Comparative study of MRI and power Doppler ultrasonography of the heel in patients with spondyloarthritis with and without heel pain and in controls. Ann Rheum Dis 2012;71:498–503.

29. Poggenborg RP, Pedersen SJ, Eshed I, Sørensen IJ, Møller JM, Madsen OR, et al. Head-to-toe whole-body MRI in psoriatic arthritis, axial spondyloarthritis and healthy subjects: first steps towards global inflammation and damage scores of peripheral and axial joints. Rheumatology (Oxford) 2015;54:1039–49.

30. Araujo EG, Englbrecht M, Hoepken S, Finzel S, Kampylafka E, Kleyer A, et al. Effects of ustekinumab versus tumor necrosis factor inhibition on enthesitis: results from the enthesial clearance in psoriatic arthritis (ECLIPSA) study. Semin Arthritis Rheum 2019;48:632–7.

31. Gladman DD, Orbai AM, Klitz U, Wei JC, Gallo G, Birt J, et al. Ixekizumab and complete resolution of enthesitis and dactylitis: integrated analysis of two phase 3 randomized trials in psoriatic arthritis. Arthritis Res Ther 2019;21:38.

Clinical Images: Progressive pseudorheumatoid dysplasia—radiographic evolution over twenty years
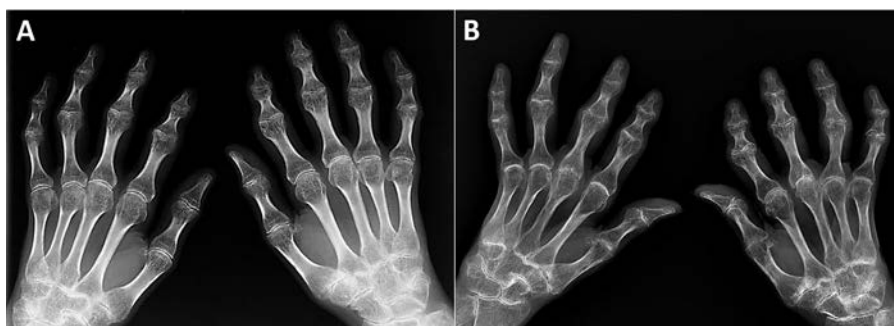
Progressive pseudorheumatoid dysplasia is a rare skeletal dysplasia with autosomal-recessive inheritance, caused by loss-of-function mutations of the Wnt-1–inducible signaling pathway protein 3 (1,2). These radiographic images of the hand present the evolution of progressive pseudorheumatoid dysplasia in a female patient who had been experiencing joint stiffness and pain since early childhood and was originally misdiagnosed as having juvenile idiopathic arthritis. Molecular genetic testing confirmed the diagnosis of progressive pseudorheumatoid dysplasia in 1999 when the patient was age 34 years. A radiographic assessment of the patient's hands, performed in 2000, revealed the typical radiographic characteristics of the disease: wide epiphyses and metaphyses of metacarpal bones and phalanges, juxtaarticular osteoporosis, and the absence of erosions (**A**). No specific treatment is currently available for progressive pseudorheumatoid dysplasia. The patient received disease-modifying antirheumatic drugs, with no improvement, and nonsteroidal antiinflammatory drugs for relief of symptoms. Follow-up radiography of the hands performed 20 years later, when the patient was age 56 years, demonstrated evolution of the disease, characterized by progressive joint space narrowing, epiphyseal enlargement, and secondary osteoarthritis (**B**). Elevation of inflammatory markers or evidence of synovitis were never retrieved. This unique case describes radiographic evolution of progressive pseudorheumatoid dysplasia, and demonstrates the extent to which radiographic features of the disease may change over the course of 20 years. Rheumatologists should recognize this possible differential diagnosis, but awareness about the existence of progressive pseudorheumatoid dysplasia is generally low, and a better knowledge of how the condition evolves over time may help raise the degree of clinical suspicion.

1. Spranger J, Albert C, Schilling F, Bartsocas C, Stöss H. Progressive pseudorheumatoid arthritis of childhood (PPAC): a hereditary disorder simulating rheumatoid arthritis. Eur J Pediatr 1983;140:34–40.

2. Yu Y, Hu M, Xing X, Li F, Song Y, Luo Y, et al. Identification of a mutation in the WISP3 gene in three unrelated families with progressive pseudorheumatoid dysplasia. Mol Med Rep 2015;12:419–25.

Jacopo Ciaffi, MD (iD)
Giancarlo Facchini, MD
Marco Miceli, MD
Istituto Ortopedico Rizzoli, IRCCS
Elena Borlandelli, MD
S. Orsola Malpighi University Hospital
Riccardo Meliconi, MD
Francesco Ursini, MD, PhD
*Istituto Ortopedico Rizzoli, IRCCS
and University of Bologna
Bologna, Italy*

AMERICAN COLLEGE
of RHEUMATOLOGY
Empowering Rheumatology Professionals

BRIEF REPORT

Estrogen-Induced hsa-miR-10b-5p Is Elevated in T Cells From Patients With Systemic Lupus Erythematosus and Down-Regulates Serine/Arginine-Rich Splicing Factor 1

Suruchi A. Ramanujan,[1] Elena N. Cravens,[2] Suzanne M. Krishfield,[2] Vasileios C. Kyttaris,[2] (iD) and Vaishali R. Moulton[2] (iD)

Objective. Autoimmune diseases affect women disproportionately more than men. Estrogen is implicated in immune cell dysfunction, yet its precise molecular roles are not fully known. We recently identified new roles for serine/arginine-rich splicing factor 1 (SRSF1) in T cell function and autoimmunity. SRSF1 levels are decreased in T cells from patients with systemic lupus erythematosus (SLE) and are associated with active disease and comorbidity. However, the molecular mechanisms that control SRSF1 expression are unknown. *Srsf1* messenger RNA (mRNA) has a long 3′-untranslated region (3′-UTR), suggesting posttranscriptional control. This study was undertaken to investigate the role of estrogen and posttranscriptional mechanisms of SRSF1 regulation in T cells and SLE.

Methods. In silico bioinformatics analysis of *Srsf1*–3′-UTR revealed multiple microRNA (miRNA; miR)–binding sites. Additional screening and literature searches narrowed down hsa-miR-10b-5p for further study. Peripheral blood T cells from healthy individuals and SLE patients were evaluated for mRNA and miRNA expression by quantitative reverse transcription–polymerase chain reaction, and SRSF1 protein levels were assessed by immunoblotting. T cells were cultured with β-estradiol, and transient transfections were used to overexpress miRNAs. Luciferase assays were used to measure 3′-UTR activity.

Results. We demonstrated that estrogen increased hsa-miR-10b-5p expression in human T cells, and hsa-miR-10b-5p down-regulated SRSF1 protein expression. Mechanistically, hsa-mir-10b-5p regulated SRSF1 posttranscriptionally via control of its 3′-UTR activity. Importantly, hsa-miR-10b-5p expression levels were elevated in T cells from healthy women compared to healthy men and also elevated in T cells from SLE patients.

Conclusion. We identified a previously unrecognized molecular link between estrogen and gene regulation in immune cells, with potential relevance to systemic autoimmune disease.

INTRODUCTION

Systemic lupus erythematosus (SLE) is a debilitating autoimmune disease that disproportionately affects women (1), and is the fifth leading cause of death in young women (2). Loss of immune tolerance to self antigens leads to a hyperactive immune response and destruction of target organs. SLE typically develops in women during the reproductive years, and flares frequently occur during pregnancy; therefore, sex hormones are implicated

in SLE pathogenesis. Estrogens contribute to the immune dysregulation underlying autoimmunity and disease manifestations (3), yet the precise molecular events controlled by estrogen are unknown.

Besides transcriptional control through classic estrogen receptor–linked pathways and nonclassic pathways, estrogen also controls target genes through posttranscriptional mechanisms (4,5). Posttranscriptional regulation is a powerful mechanism of gene control and involves modulation of messenger

RNA (mRNA) stability and/or translation through regulatory elements frequently found within the 3′-untranslated region (3′-UTR) and conserved through species. Genes with a long 3′-UTR are therefore considered to be significantly regulated at the posttranscriptional level. Besides *cis* elements, *trans*-factors include proteins and noncoding RNA, which bind to and control mRNA expression. MicroRNAs (miRNAs; miRs) are short noncoding RNAs (~23 nucleotides in length) that regulate genes by binding complementary sites within the 3′-UTR of target genes and consequently destabilize mRNA and/or hinder translation. In T cells, miRNAs are crucial for regulating T cell development, differentiation, and function. Therefore, defects in miRNA levels lead to immune dysfunction (6). Aberrant expression of miRNAs is implicated in autoimmune diseases, including SLE. While studies have demonstrated sex-based factors in miRNA expression and have implicated miRNAs in SLE, the role of estrogen in regulating specific miRNA and downstream genes involved in T cell dysfunction is not fully known.

We have recently identified novel roles of the prototypical splicing regulator, serine/arginine-rich splicing factor 1 (SRSF1), in T cells and systemic autoimmunity. Using discovery approaches, we identified SRSF1 in a pull-down assay of proteins binding the mRNA of the T cell receptor–associated CD3 ζ-chain (7). We demonstrated that SRSF1 controls genes involved in T cell signaling and cytokine production (7,8), and mice with T cell–restricted deficiency of SRSF1 display T cell hyperactivity and develop systemic autoimmunity (9). SRSF1 levels are decreased in SLE patients and are associated with active disease and comorbidity (8,10). These studies have demonstrated the relevance of low SRSF1 levels in SLE. Yet, how SRSF1 is regulated in T cells, and whether hormones contribute to its expression, is unknown. Besides transcriptional mechanisms, SRSF1 is controlled via posttranscriptional mechanisms, and this is exemplified by its long 3′-UTR.

In the present study, we used in silico bioinformatics analysis and literature search approaches to screen for miRNAs targeting SRSF1, and we investigated the influence of estrogen on the selected hsa-miR-10b-5p. We demonstrated that hsa-miR-10b-5p overexpression leads to down-regulation of SRSF1 through control of its 3′-UTR activity. Estrogen exposure leads to increased hsa-miR-10b-5p expression in human T cells. Importantly, T cells from healthy women exhibit significantly increased levels of hsa-miR-10b-5p compared to healthy men. Furthermore, hsa-miR-10b-5p levels are elevated in SLE patients regardless of disease activity. Thus, our study provides evidence of hormone- and miRNA-linked posttranscriptional regulation of a key regulator (SRSF1) and insight into its reduced expression in systemic autoimmune disease. These findings reveal molecular links between hormones and gene regulation in the immune system.

MATERIALS AND METHODS

Human subjects. Subjects were recruited from the rheumatology clinic at Beth Israel Deaconess Medical Center. All SLE patients fulfilled 4 of the European Alliance of Associations for Rheumatology/American College of Rheumatology criteria for SLE (11). Written informed consent was obtained from all participants. The study was approved by the local institutional review board.

Cell lines, antibodies, and reagents. HEK 293T cells were cultured in Dulbecco's modified Eagle's medium (DMEM) with 10% fetal bovine serum (FBS) and 1% penicillin/streptomycin (complete DMEM), at 37°C with 5% CO_2. SRSF1 antibody (clone 96) was obtained from Life Technologies, horseradish peroxidase (HRP)–conjugated secondary antibodies from Santa Cruz Biotechnology, anti-CD3 (clone OKT3) from Bio X Cell, anti-CD28 from BioLegend, goat anti-mouse crosslinkers from EMD Millipore, β-estradiol powder from Sigma-Aldrich, and mirVana mimics from ThermoFisher.

Estrogen experiments and T cell activation. Peripheral blood was collected from premenopausal healthy women during the follicular phase of the menstrual cycle. Total T cells were purified by negative selection using a RosetteSep Human T cell kit (StemCell Technologies) and cultured in RPMI 1640 without phenol red, supplemented with charcoal-dextran–stripped FBS (ThermoFisher), and cultured with reconstituted β-estradiol at 37°C. To activate T cells, cells were cultured in complete RPMI and stimulated with soluble anti-CD3 (5 µg/ml), anti-CD28 (2.5 µg/ml), and crosslinker (2.5 µg/ml).

MicroRNA transfections. HEK 293T cells were seeded in complete DMEM overnight. During transfection, complete DMEM was replaced with DMEM without FBS. MicroRNA mimics were transfected using Lipofectamine 2000 (Invitrogen). FBS was added again to cells 2 hours prior to collection.

Luciferase assays. *Srsf1* 3′-UTR was cloned into Topo-TA cloning vector and subcloned into pmirGLO luciferase vector (Promega). HEK 293T cells were cotransfected with 1 µg of pmirGLO-SRSF1-3′-UTR luciferase construct and 10 n*M* of miRNA mimic. As an internal control, pRL-TK *Renilla* luciferase construct (25 ng) was included. Cells were lysed, and luciferase activity was measured by dual-luciferase assay (Promega).

Quantitative reverse transcription–polymerase chain reaction (qRT-PCR). Total RNA was isolated using a miRNeasy kit (Qiagen) and reverse-transcribed with RNA-to-complementary DNA EcoDry premix (Clontech). Real-time qRT-PCR was performed with LightCycler 480 SYBR Green I Master Mix (Roche) under the following conditions: initial denaturation at 95°C for 5 minutes, 40 cycles of amplification; denaturation at 95°C for 15 seconds, annealing at 60°C for 15 seconds, extension

at 72°C for 30 seconds; 1 cycle of melting curves at 95°C for 5 seconds, 65°C for 2 minutes, and 97°C (continuously); and final cooling. Threshold cycle (C_t) values were used to calculate relative expression by the ΔC_t quantification method. The following primer sequences were used: SRSF1 forward 5′-TCTCTGGACTGCCTC-CAAGT-3′, reverse 5′-GGCTTCTGCTACGACTACGG-3′; hsa-miR-10b-5p forward 5′-CGCCTGCTTGGTAACCCTGACC-3′, reverse 5′-GGGTCCCACCCAGAGTGAGGT-3′; U6 forward 5′-CTCGCT-TCGGCAGCACA-3′, reverse 5′-AACGCTTCACGAATTTGCGT-3′.

Western blotting. Cells were lysed in radioimmunoprecipitation assay buffer (Boston BioProducts) with protease inhibitors (Roche). Lysates were resolved in 4–12% Bis-Tris sodium dodecyl sulfate–polyacrylamide gel electrophoresis gels and transferred to

PVDF membranes. Membranes were blocked with 5% nonfat milk in Tris buffered saline–Tween 20 (0.05%) (TBST) for 1 hour, incubated with a primary antibody (1:1,000 or 1:4,000 β-actin) overnight at 4°C or for 1 hour at room temperature (β-actin), washed 3 times with TBST, incubated with an HRP-conjugated secondary antibody (1:2,000) for 1 hour at room temperature, washed 3 times with TBST, developed using enhanced chemiluminescence reagents, and analyzed with a Bio-Rad ChemiDoc-XRS imaging system. Densitometry analysis was performed using Quantity One software (Bio-Rad).

Statistical analysis. Data analysis was performed using GraphPad Prism software. Student's 2-tailed t-test and linear regression were used for statistical analysis. P values less than 0.05 were considered significant.
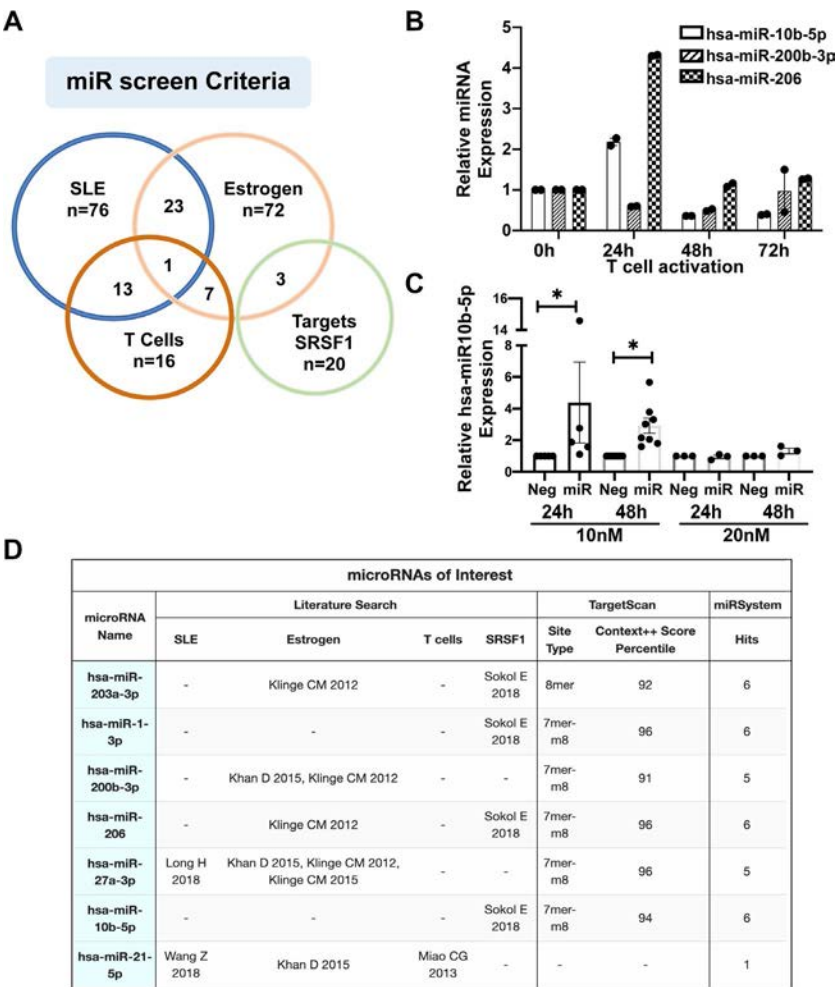
Figure 1. In silico screening and selection of microRNA (miRNA; miR) targeting *Srsf1*. **A**, Web-based bioinformatics prediction tools (TargetScan and miRSystem) were used to screen for microRNAs targeting *Srsf1*, combined with a literature search to curate miRNAs that are up-regulated in systemic lupus erythematosus (SLE), up-regulated by estrogen, up-regulated in T cells, and/or shown to target *Srsf1*. **B**, Quantitative reverse transcription–polymerase chain reaction was performed for 3 selected miRNAs in resting T cells (0 hours) and in activated T cells (24 hours, 48 hours, and 72 hours). Each symbol represents an individual subject; bars show the mean ± SEM relative miRNA expression from duplicates. **C**, Negative control (Neg) or hsa-miR-10b-5p mimics were transiently transfected into HEK 293T cells in 10 n*M* or 20 n*M* concentrations, and cells were collected at 24 hours or 48 hours posttransfection. Expression levels of miRNA were measured by reverse transcription–polymerase chain reaction. Each symbol represents an individual subject; bars show the mean ± SEM relative miRNA expression from at least 3 independent experiments. * = P < 0.05. **D**, The chart shows the miRNAs narrowed for further study based on the above-mentioned criteria. SRSF = serine/arginine-rich splicing factor 1.

RESULTS

In silico analysis and screening for miRNAs targeting *Srsf1*. The *Srsf1* mRNA has a long (~4,000 bp) 3′-UTR suggesting that its expression is controlled at the posttranscriptional level. MicroRNAs silence genes posttranscriptionally either by destabilizing mRNA or by hindering protein translation through binding complementary sites within target mRNA. Therefore, we investigated the role of miRNA on *Srsf1* gene regulation. We performed a bioinformatics analysis of the *Srsf1* 3′-UTR to identify miRNA-binding sites using online prediction tools (TargetScan and the miRSystem), combined with a literature search using NCBI/PubMed (Figures 1A and D). First, we used TargetScan to screen the *Srsf1* 3′-UTR, which yielded a set of putative miRNAs

targeting SRSF1. The Context++ Score percentile provided by TargetScan combines information, including site type, 3′ supplementary pairing, distance from the end of the 3′-UTR, and AU content, to predict the strength of binding between the miRNA and target mRNA. Of the miRNA–mRNA seed sequence match sites, the 8mer is the strongest site type. To supplement this investigation, we performed a literature search using specific search criteria limited to curate miRNAs that have previously been implicated in SLE, that are up-regulated by estrogen or its metabolites, that are up-regulated in T cells, or that are shown to control SRSF1. To further narrow down miRNAs of interest, we used the miRSystem, which evaluates the miRNA–mRNA relationship by integrative analyses of 7 different miRNA prediction databases. The "hits" column in Figure 1D represents the number
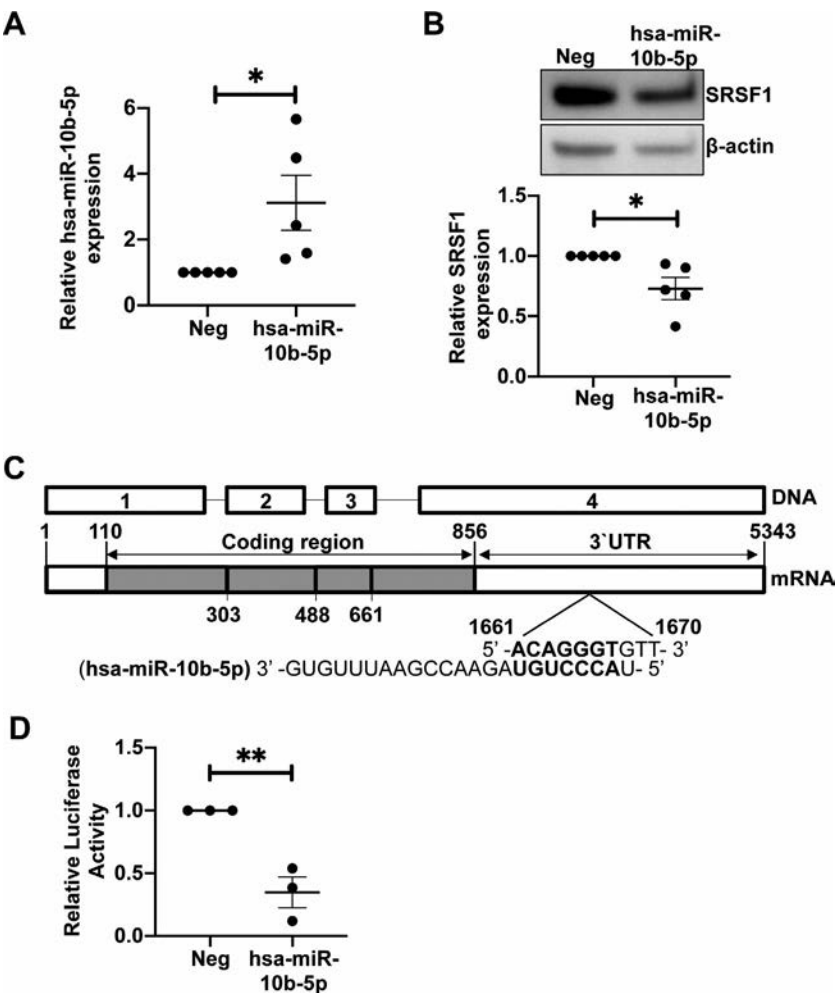
Figure 2. Overexpression of hsa-miR-10b-5p leads to down-regulation of SRSF1 via its 3′-untranslated region (3′-UTR). **A**, Negative control miR mimics or hsa-miR-10b-5p mimics were transiently transfected into HEK 293T cells. Quantitative reverse transcription–polymerase chain reaction was performed to assess the levels of hsa-miR-10b-5p. Each symbol represents an individual subject; bars show the mean ± SEM from 4 experiments. * = $P < 0.05$. **B**, Levels of SRSF1 total protein in transfected cells were assessed by Western immunoblotting. Representative blots are shown (top). Densitometric results from Western blotting were quantified as the expression of SRSF1 protein normalized to β-actin (bottom). Each symbol represents an individual subject; bars show the mean ± SEM from 4 experiments. * = $P < 0.05$. **C**, Schematic shows DNA and mRNA sequence of *Srsf1*. The hsa-miR-10b-5p sequence and its complementary binding site within the 3′-UTR are shown. **D**, HEK 293T cells were cotransfected with the *Srsf1* 3′-UTR–luciferase plasmid and 10 n*M* of hsa-miR-10b-5p mimic or negative control mimic. Cells were collected and 3′-UTR activity was measured by luciferase assay. Each symbol represents an individual subject; bars show the mean ± SEM from 3 experiments. ** = $P < 0.01$. See Figure 1 for other definitions.

of databases, according to the miRSystem, in which a relationship between *Srsf1* and the miRNA is mentioned.

Among the putative miRNAs identified, we selected 7 for further study based on a combination of occurrence in multiple categories of the literature search (4,12–16), Context++ Score >90th percentile, and the number of database hits from the miRSystem (Figure 1D). We tested the expression of these miRNAs by real-time qRT-PCR in T cells. Of these, hsa-miR-10b-5p, hsa-miR-200b-3p, and hsa-miR-206 displayed quantifiable levels (Figure 1B). We further tested these 3 miRNAs for overexpression by transfection of miRNA mimics into HEK 293T cells. Of these, hsa-miR-10b-5p showed reliable and consistently robust overexpression under the conditions tested (Figure 1C). Therefore, we selected hsa-miR-10b-5p for further study.

Overexpression of hsa-miR-10b-5p leads to decreased SRSF1 levels. To investigate the effect of hsa-miR-10b-5p on SRSF1 expression, we used miRVana mimics in transient transfection experiments. We overexpressed hsa-miR-10b-5p by transient transfection of the miRNA mimic into HEK 293T cells. As controls, cells were transfected with a negative control miRNA mimic. Cells were collected 48 hours posttransfection, and hsa-miR-10b-5p mRNA levels were quantified by real-time qRT-PCR, and SRSF1 protein levels were quantified by Western blotting. We confirmed the increased levels of hsa-miR-10b-5p and found that its overexpression led to decreased SRSF1 protein levels compared to controls (Figures 2A and B). These results show that hsa-miR-10b-5p induces the downregulation of SRSF1 expression.

MicroRNA hsa-miR-10b-5p controls the 3'-UTR activity of SRSF1. MicroRNAs mediate their effect at the posttranscriptional level by binding cognate sites within the 3′-UTR and targeting the mRNA for degradation and/or inhibition of translation. Because the overexpression of hsa-miR-10b-5p led to decreased SRSF1 expression (Figure 2B) and *Srsf1* mRNA has an hsa-miR-10b-5p binding site within its 3′-UTR (Figure 2C), we questioned whether hsa-miR-10b-5p regulates the activity of the *Srsf1* 3′-UTR. To evaluate this, we used an *Srsf1* 3′-UTR–luciferase reporter plasmid construct and cotransfected it with either a negative control mimic or an hsa-miR-10b-5p mimic. We collected cells 48 hours posttransfection and measured the 3′-UTR activity by luciferase reporter assays. We found that hsa-miR-10b-5p overexpression led to significantly decreased 3′-UTR luciferase activity compared to the negative control (Figure 2D), suggesting that hsa-miR-10b-5p binds to and controls the activity of the *Srsf1* 3′-UTR, and thus controls SRSF1 expression.

Estrogen up-regulates hsa-miR-10b-5p in human T cells. Given that estrogen is known to control miRNAs in immune cells and our findings showed that hsa-miR-10b-5p controls SRSF1 expression (Figure 2), we wished to examine the relationship between estrogen, miRNA, and SRSF1. To evaluate the influence of estrogen on hsa-miR-10b-5p, we obtained peripheral blood T cells from healthy women during the follicular phase of the menstrual cycle. Circulating estrogen levels are lowest during this phase, and ensuring this criterion enabled comparison between individuals. We treated T cells in vitro with increasing concentrations of β-estradiol and measured the expression of hsa-miR-10b-5p by qRT-PCR. Our results demonstrate that exposure to β-estradiol increases hsa-miR-10b-5p expression levels in a dose-dependent manner (Figure 3A). These results indicate that hsa-miR-10b-5p is responsive to estrogen and may be involved in the downstream gene regulation mediated by estrogen in T cells.

Elevation of hsa-miR-10b-5p in T cells from healthy women and SLE patients. We have previously shown that T cells from SLE patients display lower levels of SRSF1 compared to healthy individuals, which is associated with higher SLE Disease Activity Index (SLEDAI) scores (17) and comorbidity in patients (8,10). To date, hsa-miR-10b-5p has not been implicated in SLE. Thus, we investigated hsa-miR-10b-5p expression in T cells from SLE patients compared to age-, race-, and sex-matched healthy individuals. We found significantly increased levels of hsa-miR-10b-5p in SLE patients compared to healthy controls (Figure 3B). To evaluate sex-based differences, we compared hsa-miR-10b-5p levels between men and women. Levels of hsa-miR-10b-5p were significantly increased in healthy women compared to healthy men (Figure 3C). However, levels were similar in men and women with SLE (Figure 3D). Furthermore, hsa-miR-10b-5p levels did not correlate with SLEDAI scores in patients (Figure 3E). These results indicate that hsa-miR-10b-5p is up-regulated in healthy women and in patients with SLE, and may contribute to the observed decrease in SRSF1 levels in patients with SLE. Overall, our results indicate that estrogen contributes to the induction of hsa-miR-10b-5p, which down-regulates SRSF1. Elevated hsa-miR-10b-5p levels in SLE patients may therefore contribute to decreased SRSF1 expression.

DISCUSSION

In this study, we obtained a number of interesting findings. We demonstrated hsa-mir-10b-5p–mediated posttranscriptional regulation of the prototypical splicing regulator SRSF1 (Figures 1 and 2). Mechanistically, we showed that hsa-miR-10b-5p controls the 3′-UTR activity of SRSF1 (Figure 2C). Furthermore, estrogen increases the expression of hsa-miR-10b-5p in human T cells (Figure 3A). Finally, we showed that hsa-miR-10b-5p levels are elevated in T cells from SLE patients and in T cells from healthy women compared to healthy men (Figures 3B and C).

These findings are significant because SRSF1 controls genes involved in T cell function, and its expression is decreased in SLE patients, which correlates with higher SLEDAI scores (8)
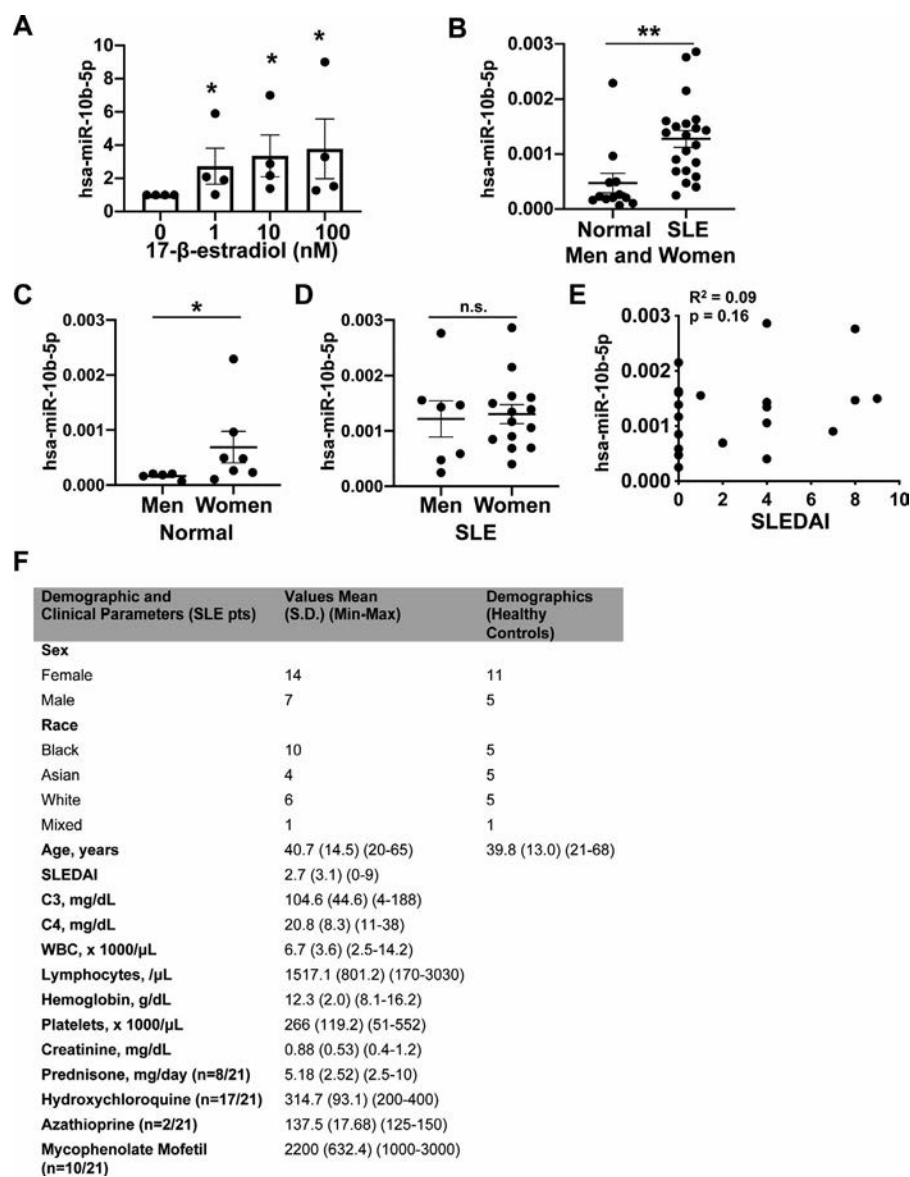
Figure 3. Induction of hsa-miR-10b-5p by estrogen and elevated levels of hsa-miR-10b-5p in T cells from healthy women and systemic lupus erythematosus (SLE) patients. **A**, T cells from healthy women were treated with increasing concentrations of β-estradiol, and hsa-miR-10b-5p levels were assessed by real-time quantitative reverse transcription–polymerase chain reaction. Results are from 4 experiments. * = $P < 0.05$ versus no β-estradiol. **B**, Levels of hsa-miR-10b-5p were measured by quantitative reverse transcription–polymerase chain reaction in T cells from SLE patients (n = 21) and age-, race-, and sex-matched healthy controls (n = 12). ** = $P < 0.01$. **C**, Levels of hsa-miR-10b-5p in healthy men and healthy women are shown. * = $P < 0.05$. **D**, Levels of hsa-miR-10b-5p in men and women with SLE are shown. In **A-D**, each symbol represents an individual subject; bars show the mean ± SEM. **E**, Correlations between Systemic Lupus Erythematosus Disease Activity Index (SLEDAI) scores and hsa-miR-10b-5p levels in patients with SLE are shown. **F**, Demographic and clinical features of the SLE patients and healthy controls are shown. NS = not significant; WBC = white blood cells.

and comorbidity (10). Therefore, understanding how SRSF1 is regulated would guide strategies to correct its expression and potentially improve disease. SRSF1 is a relatively understudied molecule in the immune system. The present study elucidates mechanisms of its regulation in immune cells with implications for autoimmune disease. We showed, for the first time to our knowledge, that T cells from SLE patients display higher expression of hsa-miR-10b-5p. These results imply that hsa-miR-10b-5p may contribute to low SRSF1 levels in SLE.

Furthermore, we showed that hsa-miR-10b-5p is estrogen-responsive in human T cells, thus highlighting its role in the immune system. We also demonstrated that hsa-miR-10b-5p levels are elevated in healthy women compared to healthy men. Elevated hsa-miR-10b-5p levels in SLE implicate its contribution to autoimmune disease. Given its regulation by estrogen, our data showing that hsa-miR-10b-5p is elevated in healthy women compared to healthy men identify a sex-based difference in the physiologic regulation of this miRNA. After disease onset in

SLE patients, multiple factors may be involved, and therefore the sex-based difference may be obviated. Furthermore, hsa-miR-10b-5p expression in SLE does not correlate with disease activity, suggesting that this may be inherent to the disease process rather than due to nonspecific immune activation.

Besides posttranscriptional regulation of miRNA, post-translational mechanisms may be involved in regulating SRSF1 expression. We have previously demonstrated ubiquitin-proteasome–mediated degradation of SRSF1 and ubiquitinated SRSF1 forms in SLE T cells. Lysosome-mediated proteolysis is another mechanism that may be involved in SRSF1 regulation. Recently, the X-linked gene *Cxorf21*, which is involved in lysosomal pH regulation and proteolysis, was found to have single-nucleotide polymorphisms associated with SLE (18). SRSF1 is also known to autoregulate its expression via binding to its 3′-UTR which leads to nonproductive splicing or non–sense-mediated mRNA decay. In addition, SRSF1 controls miRNA expression, and these miRNAs may contribute to a feedback regulatory loop. It would be interesting to investigate whether these proteolytic mechanisms or autoregulatory feedback loops occur in T cells and in systemic autoimmunity.

One limitation of the present study is that we focused on hsa-miR-10b-5p, and other miRNAs may be involved in SRSF1 regulation and controlled by estrogen. Indeed, our miRNA screen revealed potential hits that may be relevant for future studies. Differences in hsa-miR-10b-5p levels in total SLE T cells may result from differences in proportions of CD4/CD8 and other cell lineages, and therefore examination of subset-specific expression is important. Evaluating hsa-miR-10b-5p in other autoimmune diseases would elucidate whether this is specific to SLE or shared by multiple autoimmune diseases.

In conclusion, we have identified sex hormone–linked control of hsa-miR-10b-5p and SRSF1 in immune cells. This finding reveals molecular links between hormones and the immune system with relevance to autoimmunity.

ACKNOWLEDGMENTS

AUTHOR CONTRIBUTIONS

All authors were involved in drafting the article or revising it critically for important intellectual content, and all authors approved the final version to be published. Ms Ramanujan had full access to all of the data in the study and takes responsibility for the integrity of the data and the accuracy of the data analysis.
Study conception and design. Ramanujan, Moulton.
Acquisition of data. Ramanujan, Cravens, Krishfield, Kyttaris, Moulton.
Analysis and interpretation of data. Ramanujan, Cravens, Krishfield, Kyttaris, Moulton.

REFERENCES

1. Moulton VR. Sex hormones in acquired immunity and autoimmune disease. Front Immunol 2018;9:2279.

2. Yen EY, Singh RR. Lupus—an unrecognized leading cause of death in young females: a population-based study using nationwide death certificates, 2000–2015. Arthritis Rheumatol 2018;70:1251–5.

3. Corradetti C, Jog NR, Cesaroni M, Madaio M, Caricchio R. Estrogen receptor α signaling exacerbates immune-mediated nephropathies through alteration of metabolic activity. J Immunol 2018;200:512–22.

4. Klinge CM. miRNAs regulated by estrogens, tamoxifen, and endocrine disruptors and their downstream gene targets [review]. Mol Cell Endocrinol 2015;418:273–97.

5. Rider V, Abdou NI, Kimler BF, Lu N, Brown S, Fridley BL. Gender bias in human systemic lupus erythematosus: a problem of steroid receptor action? Front Immunol 2018;9:611.

6. Jeker LT, Bluestone JA. microRNA regulation of T-cell differentiation and function [review]. Immunol Rev 2013;253:65–81.

7. Moulton VR, Tsokos GC. Alternative splicing factor/splicing factor 2 regulates the expression of the ζ subunit of the human T cell receptor-associated CD3 complex. J Biol Chem 2010;285:12490–6.

8. Moulton VR, Grammatikos AP, Fitzgerald LM, Tsokos GC. Splicing factor SF2/ASF rescues IL-2 production in T cells from systemic lupus erythematosus patients by activating IL-2 transcription. Proc Natl Acad Sci U S A 2013;110:1845–50.

9. Katsuyama T, Li H, Comte D, Tsokos GC, Moulton VR. Splicing factor SRSF1 controls T cell hyperactivity and systemic autoimmunity. J Clin Invest 2019;129:5411–23.

10. Katsuyama T, Martin-Delgado IJ, Krishfield SM, Kyttaris VC, Moulton VR. Splicing factor SRSF1 controls T cell homeostasis and its decreased levels are linked to lymphopenia in systemic lupus erythematosus. Rheumatology (Oxford) 2020;59:2146–55.

11. Aringer M, Costenbader K, Daikh D, Brinks R, Mosca M, Ramsey-Goldman R. 2019 European League Against Rheumatism/American College of Rheumatology classification criteria for systemic lupus erythematosus. Arthritis Rheum 2019;71:1400–12.

12. Long H, Wang X, Chen Y, Wang L, Zhao M, Lu Q. Dysregulation of microRNAs in autoimmune diseases: pathogenesis, biomarkers and potential therapeutic targets [review]. Cancer Lett 2018;428:90–103.

13. Wang Z, Heid B, Dai R, Ahmed SA. Similar dysregulation of lupus-associated miRNAs in peripheral blood mononuclear cells and splenic lymphocytes in MRL/lpr mice. Lupus Sci Med 2018;5:e000290.

14. Khan D, Dai R, Ahmed SA. Sex differences and estrogen regulation of miRNAs in lupus, a prototypical autoimmune disease. Cell Immunol 2015;294:70–9.

15. Miao C, Yang Y, He X, Huang C, Huang Y, Zhang L, et al. The emerging role of microRNAs in the pathogenesis of systemic lupus erythematosus. Cell Signal 2013;25:1828–36.

16. Sokół E, Kędzierska H, Czubaty A, Rybicka B, Rodzik K, Tański Z, et al. microRNA-mediated regulation of splicing factors SRSF1, SRSF2 and hnRNP A1 in context of their alternatively spliced 3′UTRs. Exp Cell Res 2018;363:208–17.

17. Bombardier C, Gladman DD, Urowitz MB, Caron D, Chang CH, and the Committee on Prognosis Studies in SLE. Derivation of the SLEDAI: a disease activity index for lupus patients. Arthritis Rheum 1992;35:630–40.

18. Harris VM, Harley ITW, Kurien BT, Koelsch KA, Scofield RH. Lysosomal pH is regulated in a sex dependent manner in immune cells expressing *CXorf21*. Front Immunol 2019;10:578.

AMERICAN COLLEGE
of RHEUMATOLOGY
Empowering Rheumatology Professionals

What Does It Mean to Be a British Isles Lupus Assessment Group–Based Composite Lupus Assessment Responder? Post Hoc Analysis of Two Phase III Trials

Richard Furie,[1] [ID] Eric F. Morand,[2] [ID] Ian N. Bruce,[3] David Isenberg,[4] [ID] Ronald van Vollenhoven,[5] Gabriel Abreu,[6] Lilia Pineda,[7] and Raj Tummala[7]

Objective. The British Isles Lupus Assessment Group–based Composite Lupus Assessment (BICLA) is a validated global measure of treatment response in systemic lupus erythematosus (SLE) clinical trials. To understand the relevance of BICLA in clinical practice, we investigated relationships between BICLA response and routine SLE assessments, patient-reported outcomes (PROs), and medical resource utilization.

Methods. This was a post hoc analysis of pooled data from the phase III, randomized, placebo-controlled, 52-week TULIP-1 (ClinicalTrials.gov identifier: NCT02446912; n = 457) and TULIP-2 (ClinicalTrials.gov identifier: NCT02446899; n = 362) trials of intravenous anifrolumab (150/300 mg once every 4 weeks) in patients with moderate-to-severe SLE. Changes from baseline to week 52 in clinical assessments, PROs, and medical resource use were compared in BICLA responders versus nonresponders, regardless of treatment assignment.

Results. BICLA responders (n = 318) achieved significantly improved outcomes compared with nonresponders (n = 501), including lower flare rates, higher rates of attainment of sustained oral glucocorticoid taper to ≤7.5 mg/day, greater improvements in PROs (Functional Assessment of Chronic Illness Therapy–Fatigue, Short Form 36 Health Survey), and fewer SLE-related hospitalizations/emergency department visits (all nominal $P < 0.001$). Compared with nonresponders, BICLA responders had greater improvements in global and organ-specific disease activity (Physician's Global Assessment, SLE Disease Activity Index 2000, Cutaneous Lupus Erythematosus Disease Area and Severity Index Activity, and joint counts; all nominal $P < 0.001$). BICLA responders had fewer lupus-related serious adverse events than nonresponders.

Conclusion. BICLA response is associated with clinical benefit in SLE assessments, PROs, and medical resource utilization, confirming its value as a clinical trial end point that is associated with measures important to patient care.

INTRODUCTION

Systemic lupus erythematosus (SLE) is a chronic rheumatic disease with several unmet needs, chief of which is the addition of safer and more efficacious therapies to available treatments. Recognizing the challenges of drug development in SLE that were facing the lupus community, the US Food and Drug Administration (FDA) issued draft guidance in 2005 and a final

guidance document in 2010 that emphasized that improvement in one domain of disease activity could not be accompanied by worsening in another (1). In response to the FDA draft guidance, the first composite index, the SLE Responder Index (SRI), was developed using data from the completed phase II belimumab study (2). The SRI comprises 3 components, with 1 component assessing improvement in disease activity (SLE Disease Activity Index 2000 [SLEDAI-2K] [3]) and the remaining 2 components assessing worsening (British Isles Lupus Assessment Group [BILAG] [4] and physician global assessment of disease activity [PhGA]). Shortly thereafter, the BILAG-based Composite Lupus Assessment (BICLA) was created based on similar principles (5,6).

The BICLA was developed following an expert panel review of disease activity indices used in SLE clinical trials (5,6). A BICLA response requires improvement in all domains affected at baseline, assessed by the BILAG 2004, no worsening of other BILAG 2004 domains, no worsening of SLEDAI-2K or PhGA scores compared with baseline, no initiation of non-protocol treatment or use beyond protocol-allowed thresholds, and no discontinuation of investigational product (5,6). Thus, in contrast to the SRI, the driver of improvement in the BICLA is the BILAG 2004, whereas worsening is assessed using the SLEDAI-2K and PhGA in addition to the BILAG 2004 (7). The BILAG 2004 weighs organ systems equally and distinguishes between inactive disease, partial or complete improvement, and deterioration of disease activity, while the SLEDAI-2K assigns weighted scores to its components and requires complete resolution of disease activity of the specific element to capture improvement (5,7,8).

BICLA response has been used as an end point in more than 20 SLE trials to date (5,9–14), including the phase II MUSE trial and the phase III TULIP-1 and TULIP-2 trials of anifrolumab, a human monoclonal antibody to type I interferon (IFN) receptor subunit 1 (12–14). BICLA response was a secondary end point in the MUSE and TULIP-1 studies and was the primary end point in the TULIP-2 study (12–14). BICLA response rate treatment differences of >16% between anifrolumab and placebo were observed at week 52 in all 3 studies.

Composite SLE assessment results incorporated as end points in clinical trials are not used in clinical practice, and thus the relevance of treatment response assessed in this way may not be appreciated by clinicians. We therefore investigated the relationship between BICLA response and other SLE disease measures that are meaningful in clinical practice, including flares, oral glucocorticoid daily dose and sustained oral glucocorticoid taper, patient-reported outcomes (PROs), medical resource utilization, and clinical and laboratory measures of global and organ-specific disease. These relationships were assessed between BICLA responders and nonresponders using pooled data from the phase III TULIP-1 and TULIP-2 trials of anifrolumab, regardless of treatment group assignment.

PATIENTS AND METHODS

Patients and study design. This was a post hoc analysis of pooled data from the phase III, randomized, placebo-controlled, double-blind, 52-week TULIP-1 and TULIP-2 trials, for which patient disposition and study details have been previously published (13,14). In brief, eligible patients were ages 18–70 years, fulfilled the American College of Rheumatology revised classification criteria for SLE (15), and had seropositive moderate-to-severe SLE despite standard treatment. Patients with active severe lupus nephritis or neuropsychiatric SLE were excluded. Patients were randomized to receive intravenous infusions of placebo or anifrolumab every 4 weeks for 48 weeks in addition to standard treatment (TULIP-1: placebo, anifrolumab 150 mg, or anifrolumab 300 mg [2:1:2]; TULIP-2: placebo or anifrolumab 300 mg [1:1]). Primary end points were assessed at week 52. Other treatments were stable throughout the trial except for those resulting from protocol-determined intent-to-taper oral glucocorticoids. For patients receiving oral glucocorticoids ≥10 mg/day (prednisone or equivalent) at baseline, an attempt to taper oral glucocorticoids to ≤7.5 mg/day was required between weeks 8 and 40; tapering was also permitted for patients receiving oral glucocorticoids <10 mg/day at baseline. Stable oral glucocorticoid dosage was required between weeks 40 and 52.

Study end points and assessments. BICLA response was defined as all of the following: reduction of all baseline BILAG 2004 A and B domain scores to B/C/D and C/D domains, respectively, and no worsening in other BILAG 2004 organ systems, as defined by ≥1 new BILAG 2004 A domain scores or ≥2 new BILAG 2004 B domain scores; no increase in SLEDAI-2K score (from baseline); no increase in PhGA score (≥0.3 points from baseline); no discontinuation of investigational product; and no use of restricted medications beyond protocol-allowed thresholds (5). Pooled data were analyzed according to the TULIP-2 restricted medication analytical rules to classify responders/nonresponders (14).

Clinical outcome measures were compared between BICLA responders and nonresponders at week 52, regardless of treatment group assignment, and results are presented in a hierarchy of clinical relevance, agreed upon by consensus between the authors. Outcome measures include the percentage of patients with flares (defined as ≥1 new BILAG 2004 A domain score or ≥2 new BILAG 2004 B domain scores compared with the prior visit) through week 52, as well as an analysis by flare severity (percentage of patients with ≥1 new BILAG 2004 A domain score or ≥2 new BILAG 2004 B domain scores versus prior visit through week 52), annualized flare rates, percentage of patients achieving sustained oral glucocorticoid taper (defined as oral glucocorticoid dosage reduction to ≤7.5 mg/day prednisone or equivalent, achieved by week 40 and sustained through week 52, in patients receiving ≥10 mg/

day at baseline), and change in daily oral glucocorticoid dosage from baseline to week 52.

Changes in PROs were assessed from baseline to week 52, including responses in Functional Assessment of Chronic Illness Therapy–Fatigue (FACIT–F) (defined as an improvement of >3 points) (16), responses in Short Form 36 health survey (SF-36) version 2 (acute) physical component summary (PCS) and mental component summary (MCS) (defined as an improvement of >3.4 in the PCS and >4.6 in the MCS) (17), and changes from baseline in patient global assessment of disease activity (PtGA).

Attainment of Lupus Low Disease Activity State (LLDAS) (18) was assessed as previously described (19). Medical resource utilization (health care visits, emergency department [ED] use, and hospital visits) was also assessed. Other indices compared between BICLA responders and nonresponders included changes from baseline to week 52 in SLEDAI-2K score, PhGA score, joint counts (active, swollen, tender), and the Cutaneous Lupus Erythematosus Disease Area and Severity Index Activity (CLASI) (20) responses (defined as a ≥50% reduction in CLASI activity score among patients with a CLASI activity score ≥10 at baseline).

Table 1. Patient demographic data and baseline clinical characteristics*

Baseline characteristic	BICLA responders at week 52 (n = 318)	BICLA nonresponders at week 52 (n = 501)
Age, mean ± SD years	41.5 ± 11.67	41.7 ± 12.13
Sex, female	294 (92.5)	466 (93.0)
Time from SLE diagnosis to randomization, median (range) months	85.5 (0–555)	84.0 (4–503)
IFN gene signature test-high at screening	261 (82.1)	415 (82.8)
BILAG 2004 score, mean ± SD	18.9 ± 5.20	19.2 ± 5.59
≥1 A item	171 (53.8)	222 (44.3)
No A and ≥2 B items	126 (39.6)	254 (50.7)
No A and <2 B items	21 (6.6)	25 (5.0)
SLEDAI-2K score, mean ± SD	10.8 ± 3.19	11.7 ± 4.01
<10	104 (32.7)	127 (25.3)
≥10	214 (67.3)	374 (74.7)
PhGA score, mean ± SD	1.76 ± 0.425	1.81 ± 0.396
Oral GC use†	263 (82.7)	410 (81.8)
<10 mg/day	98 (30.8)	152 (30.3)
≥10 mg/day	165 (51.9)	258 (51.5)
Antimalarial use	225 (70.8)	361 (72.1)
Immunosuppressant use	158 (49.7)	230 (45.9)
CLASI activity score, mean ± SD	8.5 ± 7.56	7.8 ± 7.18
<10	215 (67.6)	373 (74.5)
≥10	103 (32.4)	128 (25.5)
0	13 (4.1)	20 (4.0)
>0	305 (95.9)	481 (96.0)
SDI global score, mean ± SD	0.6 ± 1.08	0.5 ± 0.89
SJC, mean ± SD	6.5 ± 5.27	7.4 ± 6.08
TJC, mean ± SD	9.8 ± 6.94	11.1 ± 7.85
AJC, mean ± SD‡	6.1 ± 5.22	6.9 ± 5.97
Anti-dsDNA positive§	142 (44.7)	224 (44.7)
Anti-dsDNA level, median (range) IU/ml¶	48.2 (15–3,790)	57.0 (15–4,404)
Anti-dsDNA level, mean ± SD, IU/ml§	142.5 ± 401.84	220.4 ± 526.38
Abnormal C3 level#	123 (38.7)	178 (35.5)
C3 level, median (range) gm/liter§	0.729 (0.36–0.90)	0.715 (0.18–0.90)
C3 level, mean ± SD, gm/liter§	0.711 ± 0.1279	0.685 ± 0.1603
Abnormal C4 level**	72 (22.6)	118 (23.6)
C4 level, median (range) gm/liter§	0.080 (0.05–0.10)	0.072 (0.05–0.10)
C4 level, mean ± SD, gm/liter§	0.075 ± 0.0168	0.071 ± 0.0145

* Except where indicated otherwise, values are the number (%) of patients. BICLA = British Isles Lupus Assessment Group (BILAG)–based Composite Lupus Assessment; SLE = systemic lupus erythematosus; IFN = interferon; BILAG 2004 = 2004 Update of the BILAG; SLEDAI-2K = SLE Disease Activity Index 2000; PhGA = physician global assessment of disease activity; CLASI = Cutaneous Lupus Erythematosus Disease Area and Severity Index; SDI = Systemic Lupus International Collaborating Clinics/American College of Rheumatology Damage Index; SJC = swollen joint count; TJC = tender joint count; AJC = active joint count.
† Oral glucocorticoids (GCs) include prednisone or equivalent.
‡ Defined as a joint with swelling and tenderness.
§ Positivity defined as >15 IU/ml.
¶ Only patients with anti–double-stranded DNA (anti-dsDNA) antibodies and abnormal complement levels at baseline are included in the summary statistics for the respective variables.
# Abnormal levels defined as <0.9 gm/liter.
** Abnormal levels defined as <0.1 gm/liter.

Serologies (anti–double-stranded DNA [anti-dsDNA] antibodies and complement C3 and C4) were evaluated; anti-dsDNA antibody levels were classified as "positive" (>15 IU/ml) or "negative" (≤15 IU/ml), and complement levels were classified as "abnormal" (C3, <0.9 gm/liter; C4, <0.1 gm/liter) or "normal" (C3, ≥0.9 gm/liter; C4, ≥0.1 gm/liter). Adverse events (AEs) were also assessed.

Statistical analysis. The similar designs of the TULIP-1 and TULIP-2 studies allowed for the results to be pooled. Sample sizes were selected for TULIP-1 and TULIP-2 based on powering of the primary and key secondary end points and to ensure an adequate safety database. In TULIP-1 and TULIP-2, 180 subjects per arm yielded >99% and 88% power, respectively, to reject the hypothesis (no difference in the primary end point) using a 2-sided alpha value of 0.05. Responder versus nonresponder rates were calculated using a stratified Cochran-Mantel-Haenszel approach (21), which included stratification factors of SLEDAI-2K score at screening (<10 or ≥10), baseline oral glucocorticoid dosage (<10 mg/day or ≥10 mg/day), type I IFN gene signature test status at screening (test-low or test-high); the study in which the patients participated (TULIP-1 or TULIP-2) was also included in the model. For all responder analyses, patients were considered nonresponders if they received restricted medications beyond the protocol-allowed thresholds or discontinued the investigational drug before the week 52 assessment. Comparison of estimated change from baseline to week 52 between BICLA responders and nonresponders was assessed using a mixed repeated-measures model with fixed effects for baseline value, group, visit, study, and the stratification factors used at screening; a group-by-visit interaction term was used, and visit was a repeated variable in the model. Missing data were imputed using the last observation carried forward for the first visit with missing data; subsequent visits with missing data were not imputed. For responder analyses, if any component of the variable could not be derived owing to missing data, the patient was classified as a nonresponder for that visit.

Study approval. The TULIP-1 and TULIP-2 trials were conducted in accordance with the principles of the Declaration of Helsinki and followed the International Conference on Harmonisation Guidelines for Good Clinical Practice, and all patients provided written informed consent in accordance with local requirements (13,14). As this was a post hoc analysis of anonymized data, no ethics committee or institutional review board approvals were required—all such approvals were obtained in the original trials (13,14).

RESULTS

Trial populations. Data were pooled for 457 patients in TULIP-1 and 362 patients in TULIP-2 (n = 819). Across both trials, 360 patients received anifrolumab 300 mg, 93 patients received anifrolumab 150 mg (in TULIP-1 only), and 366 patients

received placebo. Regardless of treatment group assignment, at week 52 there were 318 BICLA responders (anifrolumab 300 mg, n = 171; anifrolumab 150 mg, n = 35; placebo, n = 112) and 501 BICLA nonresponders (anifrolumab 300 mg, n = 189; anifrolumab 150 mg, n = 58; placebo, n = 254).

Patient demographics and baseline clinical characteristics were generally balanced across BICLA responders and nonresponders (Table 1 and Supplementary Table 1, available on the *Arthritis & Rheumatology* website at http://onlinelibrary.wiley.com/doi/10.1002/art.41778/abstract). The majority of patients were female (92.5% of responders, 93.0% of nonresponders), and the mean ± SD age was 41.5 ± 11.67 years for responders and 41.7 ± 12.13 years for nonresponders. Similar proportions of BICLA responders and nonresponders were white (67.0% versus 65.9%), Black/African American (14.2% versus 12.6%), or Asian (9.1% versus 11.0%).

Flares. More BICLA responders than nonresponders were flare-free over the 52-week treatment period (76.1% versus 52.2%), meaning that fewer BICLA responders than nonresponders experienced ≥1 flare (23.9% versus 47.8%; difference −23.9% [95% confidence interval (95% CI) −30.4, −17.5]; nominal $P < 0.001$) (Figure 1A and Supplementary Table 2, http://onlinelibrary.wiley.com/doi/10.1002/art.41778/abstract). Compared with their prior visits, fewer BICLA responders than nonresponders experienced ≥1 new BILAG 2004 A domain score or ≥2 new BILAG 2004 B domain scores. Fewer patients experienced 1, 2, or ≥3 flares, and the annualized flare rate was lower for BICLA responders than nonresponders (rate ratio [RR] 0.36 [95% CI 0.29, 0.47]; nominal $P < 0.001$) (Supplementary Table 2).

Oral glucocorticoid use and steroid sparing. At baseline, similar percentages of BICLA responders and nonresponders were receiving oral glucocorticoids at any dosage and at ≥10 mg/day (Table 1). Compared with BICLA nonresponders, BICLA responders had greater reductions in daily oral glucocorticoid dosage from baseline to week 52 (least squares mean [LSM] difference −4.29 mg/day [95% CI −5.37, −3.20]; nominal $P < 0.001$) (Figure 1B). The key secondary end point of sustained oral glucocorticoid dosage reduction to ≤7.5 mg/day among patients who were receiving oral glucocorticoids ≥10 mg/day at baseline was achieved by more BICLA responders than nonresponders (79.2% versus 19.1%; difference 60.1% [95% CI 52.1%, 68.1%]; nominal $P < 0.001$) (Figure 1C). The mean ± SD cumulative oral glucocorticoid dose through week 52 was 31.3% lower in BICLA responders compared with nonresponders (mean ± SD 2,159.20 ± 1,661.39 mg versus 3,140.81 ± 3,081.19 mg) (Figure 1D).

PROs. FACIT–F, SF-36 MCS, and SF-36 PCS scores were similar among BICLA responders and nonresponders at baseline (Supplementary Table 3, http://onlinelibrary.wiley.com/doi/10.1002/art.41778/abstract). Improvement in FACIT–F scores
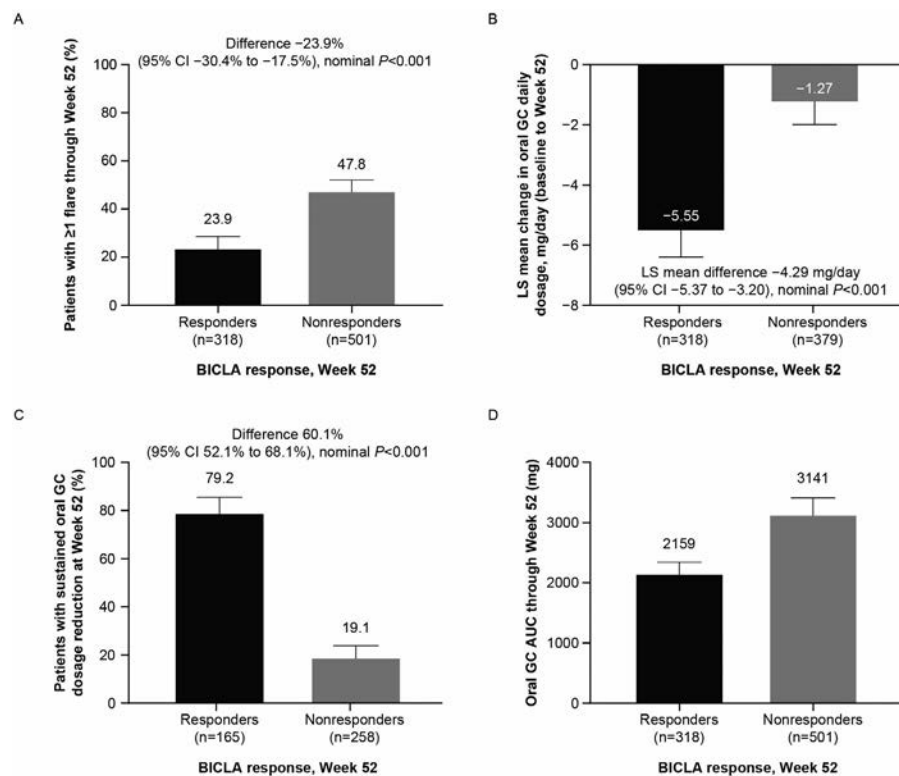
Figure 1. Flares and oral glucocorticoid (GC) use in British Isles Lupus Assessment Group (BILAG)–based Composite Lupus Assessment (BICLA) responders compared with nonresponders. **A**, Patients with ≥1 BILAG 2004 flare through week 52. Bars show the mean and 95% confidence interval (95% CI). **B**, Least squares mean (LSM) change in oral glucocorticoid daily dosage from baseline to week 52 in all patients regardless of baseline oral glucocorticoid dosage. Bars show the LSM change and 95% CI. **C**, Patients achieving sustained oral glucocorticoid dosage reduction to ≤7.5 mg/day among patients receiving oral glucocorticoids ≥10 mg/day at baseline. Sustained oral glucocorticoid dosage reduction is defined as oral glucocorticoid dosage of ≤7.5 mg/day sustained from weeks 40 to 52. Bars show the mean and 95% CI. **D**, Oral glucocorticoids area under the curve (AUC) through week 52 for all patients regardless of baseline oral glucocorticoid dosage. Bars show the mean ± SD. Rate difference, 95% CIs, and nominal *P* values were calculated using a stratified Cochran-Mantel-Haenszel approach.

was reported in more BICLA responders than nonresponders (55.6% versus 15.7%; difference 40.0% [95% CI 33.6%, 46.3%]; nominal *P* < 0.001) (Figure 2A). Similarly, more BICLA responders than nonresponders had improvement above the predefined threshold in SF-36 PCS scores (57.9% versus 12.8%; difference 45.1% [95% CI 38.9%, 51.3%]; nominal *P* < 0.001) and SF-36 MCS scores (42.6% versus 12.3%; difference 30.3% [95% CI 24.1%, 36.5%]; nominal *P* < 0.001) (Figures 2B–C). PtGA scores were similar for BICLA responders and nonresponders at baseline (Supplementary Table 2). Greater improvements in PtGA scores from baseline to week 52 were reported for BICLA responders compared with nonresponders (LSM difference –11.1 [95% CI –14.9, –7.3]; nominal *P* < 0.001) (Figure 2D).

Medical resource utilization. During the 52-week trials, fewer BICLA responders than nonresponders had health care visits (62.5% versus 70.7%; difference –8.3 [95% CI –14.9%, –1.6%]; nominal *P* = 0.015) (Table 2). Fewer BICLA responders required ED visits compared with nonresponders (11.9% versus

21.8%; difference –9.9% [95% CI –15.2%, –4.5%]; nominal *P* < 0.001), and fewer ED visits were related to increased SLE activity (2.6% versus 24.0%; difference –21.4% [95% CI –35.3%, –7.5%]; nominal *P* = 0.003). Similarly, fewer BICLA responders than nonresponders had hospital visits (4.5% versus 14.4%; difference –10.0% [95% CI –14.3%, –5.7%]; nominal *P* < 0.001), and no hospital visits were related to increased SLE activity among BICLA responders, compared with 38.5% among BICLA nonresponders (difference –38.5% [95% CI –58.8%, –18.2%]; nominal *P* < 0.001).

SLEDAI-2K, PhGA, and LLDAS. The mean ± SD of SLE-DAI-2K and PhGA scores were similar among responders and nonresponders at baseline (Table 1). From baseline to week 52, greater improvements were observed for BICLA responders compared with nonresponders in total SLEDAI-2K scores (LSM difference –3.5 [95% CI –4.1, –3.0]; nominal *P* < 0.001) (Figure 3A) and PhGA scores (LSM difference –0.59 [95% CI –0.67, –0.51]; nominal *P* < 0.001) (Figure 3B).
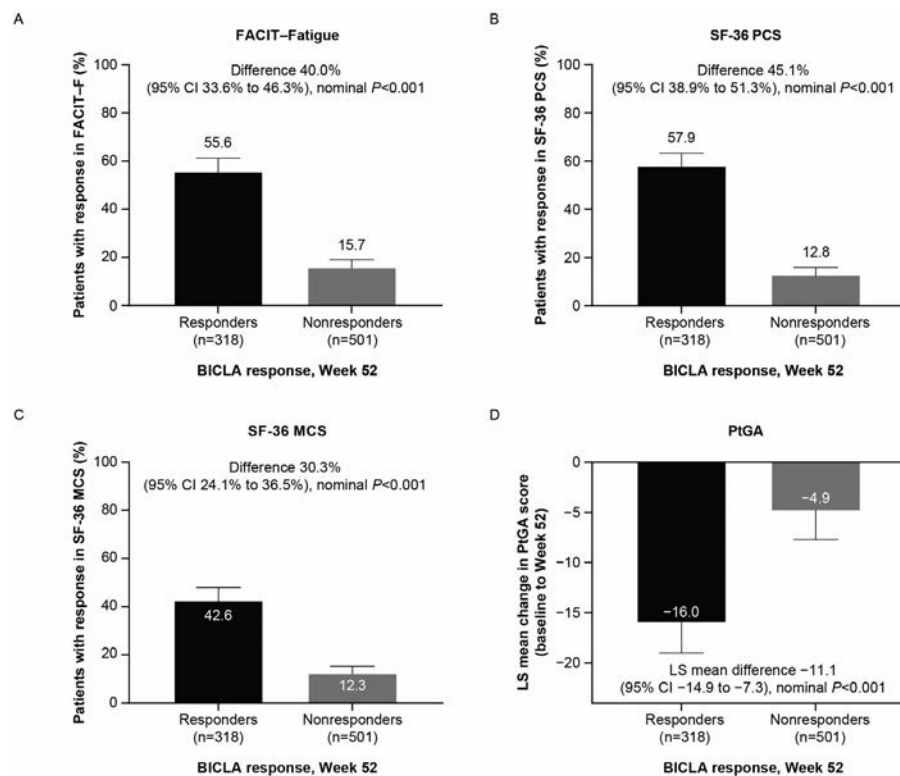
Figure 2. Patient-reported outcomes at week 52 in BICLA responders compared with nonresponders. **A–C**, Patients with a response according to following assessments: the Functional Assessment of Chronic Illness Therapy–Fatigue (FACIT–F), defined as an improvement of >3 points from baseline to week 52 (**A**), Short Form 36 health survey (SF-36) physical component summary (PCS), defined as an increase of >3.4 in the PCS domain from baseline to week 52 (**B**), and SF-36 mental component summary (MCS), defined as an increase of >4.6 in the MCS domain from baseline to week 52 (**C**). Bars show the mean and 95% CI. Response rates, 95% CIs, and nominal *P* values were calculated using a stratified Cochran-Mantel-Haenszel approach. **D**, LSM change in patient global assessment (PtGA) score from baseline to week 52. Bars show the LSM change and 95% CI. LSM difference, 95% CIs, and nominal *P* values were calculated using mixed-model repeated measures. See Figure 1 for other definitions.

At week 52, 32.0% of BICLA responders versus 2.3% of BICLA nonresponders had attained LLDAS (difference 29.7% [95% CI 24.3%, 35.1%]; nominal *P* < 0.001) (Supplementary Table 4, http://onlinelibrary.wiley.com/doi/10.1002/art.41778/abstract). Accordingly, 89.5% of patients who attained LLDAS were BICLA responders.

Table 2. Medical resource utilization for BICLA responders and nonresponders*

Medical resource utilization	BICLA responders at week 52 (n = 318)	BICLA nonresponders at week 52 (n = 501)	Difference between groups (95% CI)	Nominal *P*
Health care visits (specialist and primary care)				
Patients with ≥1 health care visit†	198 (62.5)	348 (70.7)	−8.3 (−14.9, −1.6)	0.015
ED visits				
Patients with ≥1 ED visit†	38 (11.9)	107 (21.8)	−9.9 (−15.2, −4.5)	<0.001
Visit related to increase in SLE activity†	1 (2.6)	25 (24.0)	−21.4 (−35.3, −7.5)	0.003
No. of ED visits per patient, mean ± SD‡	1.4 ± 0.86	1.7 ± 1.48	–	–
Hospitalizations				
Patients with ≥1 hospital visit†	14 (4.5)	71 (14.4)	−10.0 (−14.3, −5.7)	<0.001
Visits related to increase in SLE activity†	0	25 (38.5)	−38.5 (−58.8, −18.2)	<0.001
No. of hospital visits per patient, mean ± SD‡	1.6 ± 2.13	1.4 ± 0.72	–	–
Length of hospital stay, mean ± SD days‡	5.7 (2.64)	7.4 (8.02)	–	–
Total days in ICU‡	0	5	–	–
No. of days in ICU, mean ± SD	–	1.8 (0.45)	–	–

* Except where indicated otherwise, values are the number (%) of patients. ICU = intensive care unit (see Table 1 for other definitions).
† Percentages, differences, 95% confidence intervals (95% CIs), and nominal *P* values were calculated using a stratified Cochran-Mantel-Haenszel approach.
‡ Data on hospital visits and emergency department (ED) visits were missing for 8 patients in the BICLA nonresponders group.
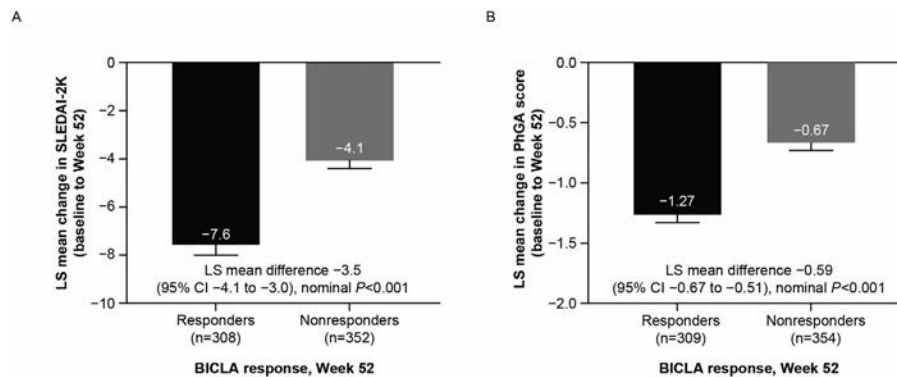
Figure 3. Change in Systemic Lupus Erythematosus Disease Activity Index 2000 (SLEDAI-2K) (**A**) and physician global assessment (PhGA) scores (**B**) from baseline to week 52 in BICLA responders compared with nonresponders. Bars show the mean and 95% CI. LSM difference, 95% CIs, and nominal *P* values were calculated using mixed-model repeated measures. See Figure 1 for other definitions.

Skin disease. Overall, 32.4% of BICLA responders and 25.5% of nonresponders had a baseline CLASI activity score ≥10 (Table 1). Among these patients, more BICLA responders achieved a ≥50% reduction in CLASI activity score at week 52 compared with nonresponders (92.0% versus 23.2%; difference 68.8% [95% CI 59.2%, 78.3%]; nominal *P* < 0.001) (Figure 4A).

Arthritis. The mean ± SD active joint counts (defined as joints with both swelling and tenderness) were 6.1 ± 5.22 (BICLA responders) and 6.9 ± 5.97 (nonresponders), the mean ± SD swollen joint counts were 6.5 ± 5.27 (BICLA responders) and 7.4 ± 6.08 (nonresponders), and the mean ± SD tender joint counts were 9.8 ± 6.94 (BICLA responders) and 11.1 ± 7.85 (nonresponders) (Table 1). From baseline to week 52, joint counts improved more for
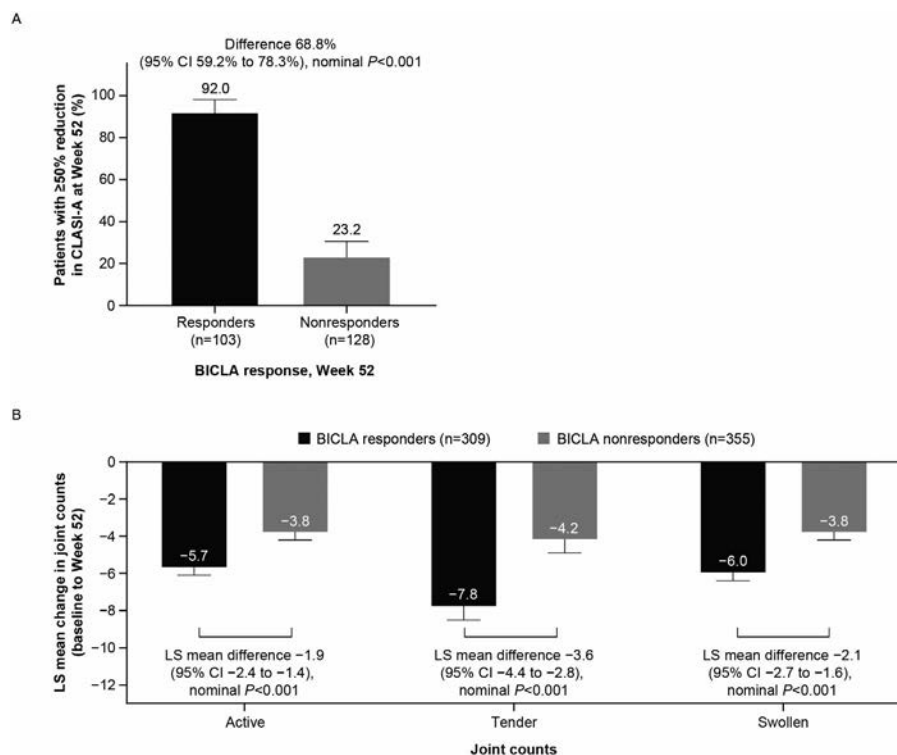
Figure 4. Cutaneous Lupus Erythematosus Disease Area and Severity Index (CLASI) response and joint counts in BICLA responders compared with nonresponders. **A**, Patients with a CLASI response at week 52 (defined as ≥50% reduction from baseline to week 52) among patients with a CLASI activity score of ≥10 at baseline. Bars show the mean and 95% CI. Response rates, 95% CIs, and nominal *P* values were calculated using a stratified Cochran-Mantel-Haenszel approach. **B**, Change in LSM joint counts from baseline to week 52 for active joints (defined as a joint with swelling and tenderness), tender joints, and swollen joints. Bars show the mean and 95% CI. LSM difference, 95% CIs, and nominal *P* values were calculated using mixed-model repeated measures. See Figure 1 for other definitions.

BICLA responders compared with nonresponders, for the active joint count (LSM difference −1.9 [95% CI −2.4, −1.4]; nominal $P < 0.001$), tender joint count (LS mean difference −3.6 [95% CI −4.4, −2.8]; nominal $P < 0.001$), and swollen joint count (LS mean difference −2.1 [95% CI −2.7, −1.6]; nominal $P < 0.001$) (Figure 4B).

Serology. Equal percentages of BICLA responders and nonresponders were positive for anti-dsDNA antibodies at baseline (Table 1). Improvement from positive to negative anti-dsDNA antibody status was observed in similar percentages of BICLA responders and nonresponders (5.0% versus 4.4%) (Supplementary Table 5, http://onlinelibrary.wiley.com/doi/10.1002/art.41778/abstract).

Similar proportions of BICLA responders and nonresponders had abnormal C3 and C4 levels at baseline (Table 1). Percentage changes from baseline to week 52 in complement levels did not differ between BICLA responders and nonresponders for C3 (LSM difference 2.82 [95% CI −4.185, 9.819]; nominal $P = 0.429$) or C4 (LSM difference −9.63 [95% CI −25.174, 5.910]; nominal $P = 0.223$) (Supplementary Table 5, http://onlinelibrary.wiley.com/doi/10.1002/art.41778/abstract). More BICLA responders than nonresponders showed improvement from abnormal to normal C3 levels (10.4% versus 7.0%) and C4 levels (7.5% versus 4.8%).

Safety. AE frequencies were similar between BICLA responders and nonresponders (83.6% versus 85.2%) (Supplementary Table 6, http://onlinelibrary.wiley.com/doi/10.1002/art.41778/abstract). Mild and moderate AEs were reported in similar percentages of BICLA responders and nonresponders, whereas fewer BICLA responders than nonresponders experienced severe AEs (3.8% versus 9.4%). There were no AEs leading to discontinuation in BICLA responders compared with 8.2% in nonresponders. Fewer BICLA responders than nonresponders experienced serious AEs (SAEs) (5.0% versus 19.0%), including SAEs due to lupus nephritis or SLE (0.3% versus 3.0%). Fewer BICLA responders than nonresponders had non-opportunistic serious infections (2.2% versus 6.8%). The percentage of patients with herpes zoster was similar in BICLA responders and nonresponders (4.7% versus 3.6%), as was the percentage of patients with influenza (1.9% versus 2.0%) or malignancy (0.6% versus 1.0%).

DISCUSSION

BICLA response is a dichotomous SLE trial end point that classifies a patient as a responder or nonresponder based on changes in organ domain activity (5,6). As BICLA response is primarily used in the clinical trial setting, the aim of this study was to assess the meaningfulness of BICLA response in terms of outcomes that are relevant to patients and physicians. In this post hoc analysis of pooled data acquired from 819 patients enrolled in the TULIP-1 and TULIP-2 trials, BICLA response was significantly associated with improved clinical outcomes across a range of SLE assessments, key PROs, and medical resource utilization measures.

Flares, with or without an increase in glucocorticoid dosage, pose significant risks to patients with SLE. In the long term, both disease flares and oral glucocorticoid use have been linked to organ damage, which itself increases mortality (22–26). Flares are also associated with reduced health-related quality of life, and flare severity together with oral glucocorticoid use correlate with health care costs (27–31). A key SLE treatment goal therefore is to prevent flares while minimizing oral glucocorticoid exposure, which in turn is expected to reduce medical resource utilization (27–30,32,33). BICLA responders had fewer disease flares, and there were more BICLA responders who were flare-free, consistent with the BICLA response definition, which requires improvement in all BILAG 2004 organs affected at baseline and no new activity in the remaining organ systems. BICLA responders also had a lower daily oral glucocorticoid dosage, indicating that the observed responses were not due to greater oral glucocorticoid use. A greater percentage of BICLA responders achieved sustained oral glucocorticoid reduction to target dosage, and they also had fewer hospitalizations and ED visits than did nonresponders, including those related to increased SLE activity.

In addition, greater improvements in global and organ-specific disease activity were observed in BICLA responders compared with nonresponders, as measured by PhGA, SLEDAI-2K, LLDAS attainment, skin disease as measured by CLASI activity score, and joint counts. Since improved disease activity, reduced oral glucocorticoid exposure, and LLDAS attainment have been shown to be associated with reduced health care costs (29,30), BICLA responders may incur lower health care costs than nonresponders.

We also assessed AEs in BICLA responders and nonresponders occurring during the TULIP trials. There were fewer SAEs in BICLA responders compared with nonresponders, potentially because of greater disease control and/or reduced oral glucocorticoid dosage in the BICLA responder group. There were also fewer SAEs related to lupus nephritis or SLE disease worsening in BICLA responders, consistent with the efficacy findings of lower flare rates and fewer SLE-related ED visits and hospitalizations associated with BICLA response. BICLA nonresponders had a greater propensity to discontinue treatment due to an AE than BICLA responders, consistent with the BICLA response definition, where patients who discontinued investigational product were classified as nonresponders.

PROs have been incorporated into nearly all SLE clinical trials. However, analyses have often yielded discordance between clinical outcomes and PROs, as patient perceptions of disease activity and illness are heavily impacted by fatigue and quality of life, which are not captured by measures of disease activity (34–38). Furthermore, fatigue and other PROs do not always associate with disease activity measures in clinical practice (39–41). In the TULIP trials, BICLA responders had improvements in

validated PROs, including the physical and mental components of the SF-36 health survey and the FACIT assessment of fatigue. Fatigue, a common symptom in patients with SLE, interferes with daily life (42), and more than half of the patients in the TULIP trials with BICLA responses experienced improvement in fatigue. PtGA and PhGA scores both showed greater degrees of improvement among BICLA responders compared with nonresponders. Our results suggest that BICLA response translates to general improvements in the physical and mental well-being of patients with SLE.

Investigation of the correlations of SRI-4 response to clinical outcomes in pooled data from 2 phase IIb trials (sifalimumab and anifrolumab), as well as 2 phase III trials of belimumab, demonstrated improved general clinical outcomes in SRI-4 responders compared with nonresponders, including improved fatigue (36,43). While changes in serologic outcomes were not significantly different between BICLA responders and nonresponders in the TULIP trials, SRI-4 response was associated with significant improvements in anti-dsDNA antibody and complement C3 levels (but not C4 levels) in the belimumab phase III trials (43). This discordance may reflect the different mechanisms of action of the 2 evaluated drugs, and/or because the BILAG 2004, on which the BICLA is anchored, does not include serology in its scoring system (4,44).

The limitations of this study include the post hoc nature of the analyses, as groups were compared based on postrandomization characteristics, which may have resulted in imbalances of baseline characteristics and stratification factors. Furthermore, these results were assessed with a single intervention and used predetermined inclusion and exclusion criteria. As such, results may not translate to other interventions or patient populations. For example, the TULIP trials excluded patients with severe active renal disease and central nervous system lupus. Therefore, future work is needed to assess the relationship between BICLA response and clinical outcomes across the full spectrum of SLE disease. In addition, because we assessed SF-36 score improvement using meaningful change thresholds established in the general population (17), future work will be needed to measure improvements in PROs in BICLA responders using SLE-specific meaningful change thresholds.

Our data confirm the value of BICLA as a clinical trial end point and that a BICLA response is associated with improvements in a range of important outcomes that resonate with the priorities of both clinicians and patients in everyday practice.

ACKNOWLEDGMENTS

AUTHOR CONTRIBUTIONS

All authors were involved in drafting the article or revising it critically for important intellectual content, and all authors approved the final version to be published. Dr. Tummala had full access to all of the data in the study and takes responsibility for the integrity of the data and the accuracy of the data analysis.

Study conception and design. Furie, Morand, Bruce, Isenberg, Abreu, Pineda, Tummala.
Acquisition of data. Furie, Bruce, Pineda, Tummala.
Analysis and interpretation of data. Furie, Morand, Bruce, Isenberg, van Vollenhoven, Abreu, Tummala.

ROLE OF THE STUDY SPONSOR

REFERENCES

1. US Food and Drug Administration. Systemic lupus erythematosus–developing medical products for treatment. June 2010. URL: https://www.fda.gov/regulatory-information/search-fda-guidance-documents/systemic-lupus-erythematosus-developing-medical-products-treatment.

2. Furie RA, Petri MA, Wallace DJ, Ginzler EM, Merrill JT, Stohl W, et al. Novel evidence-based systemic lupus erythematosus responder index. Arthritis Rheum 2009;61:1143–51.

3. Gladman DD, Ibanez D, Urowitz MB. Systemic Lupus Erythematosus Disease Activity Index 2000. J Rheumatol 2002;29:288–91.

4. Isenberg DA, Rahman A, Allen E, Farewell V, Akil M, Bruce IN, et al. BILAG 2004. Development and initial validation of an updated version of the British Isles Lupus Assessment Group's disease activity index for patients with systemic lupus erythematosus. Rheumatology (Oxford) 2005;44:902–6.

5. Wallace DJ, Kalunian K, Petri MA, Strand V, Houssiau FA, Pike M, et al. Efficacy and safety of epratuzumab in patients with moderate/severe active systemic lupus erythematosus: results from EMBLEM, a phase IIb, randomised, double-blind, placebo-controlled, multicentre study. Ann Rheum Dis 2014;73:183–90.

6. Wallace D, Strand V, Furie R, Petri M, Kalunian K, Pike M, et al. Evaluation of treatment success in systemic lupus erythematosus clinical trials: development of the British Isles Lupus Assessment Group-based Composite Lupus Assessment Endpoint [poster]. Presented at the Annual Meeting of the American College of Rheumatology; 2011 November 5–9; Chicago, Illinois.

7. Mikdashi J, Nived O. Measuring disease activity in adults with systemic lupus erythematosus: the challenges of administrative burden and responsiveness to patient concerns in clinical research. Arthritis Res Ther 2015;17:183.

8. Yee CS, Farewell V, Isenberg DA, Griffiths B, Teh LS, Bruce IN, et al. The BILAG-2004 index is sensitive to change for assessment of SLE disease activity. Rheumatology (Oxford) 2009;48:691–5.

9. Wallace D, Popa S, Spindler A, Eimon A, González-Rivera T, Utset T, et al. Improvement of disease activity and reduction of severe flares following subcutaneous administration of an IL-6 monoclonal antibody (mAb) in subjects with active generalized systemic lupus erythematosus (SLE) [abstract]. Arthritis Rheumatol 2014;66:3531.

10. ClinicalTrials.gov. National Library of Medicine: NIH clinical trials database. URL: https://clinicaltrials.gov/.

11. Clowse ME, Wallace DJ, Furie RA, Petri MA, Pike MC, Leszczyński P, et al. Efficacy and safety of epratuzumab in moderately to severely active systemic lupus erythematosus: results from two phase III randomized, double-blind, placebo-controlled trials. Arthritis Rheumatol 2017;69:362–75.

12. Furie R, Khamashta M, Merrill JT, Werth VP, Kalunian K, Brohawn P, et al. Anifrolumab, an anti–interferon-α receptor monoclonal antibody, in moderate-to-severe systemic lupus erythematosus. Arthritis Rheumatol 2017;69:376–86.

13. Furie R, Morand E, Bruce I, Manzi S, Kalunian K, Vital E, et al. Type I interferon inhibitor anifrolumab in active systemic lupus erythematosus (TULIP-1): a randomised, controlled, phase 3 trial. Lancet Rheumatol 2019;1:E208–19.

14. Morand EF, Furie R, Tanaka Y, Bruce IN, Askanase AD, Richez C, et al. Trial of anifrolumab in active systemic lupus erythematosus. N Engl J Med 2020;382:211–21.

15. Hochberg MC for the Diagnostic and Therapeutic Criteria Committee of the American College of Rheumatology. Updating the American College of Rheumatology revised criteria for the classification of systemic lupus erythematosus [letter]. Arthritis Rheum 1997;40:1725.

16. Lai JS, Beaumont JL, Ogale S, Brunetta P, Cella D. Validation of the functional assessment of chronic illness therapy–fatigue scale in patients with moderately to severely active systemic lupus erythematosus, participating in a clinical trial. J Rheumatol 2011;38:672–9.

17. Maruish ME. User's manual for the SF-36v2 Health Survey. 3rd ed. Lincoln, (Rhode Island): QualityMetric Incorporated; 2011.

18. Franklyn K, Lau CS, Navarra SV, Louthrenoo W, Lateef A, Hamijoyo L, et al. Definition and initial validation of a Lupus Low Disease Activity State (LLDAS). Ann Rheum Dis 2016;75:1615–21.

19. Morand EF, Trasieva T, Berglind A, Illei GG, Tummala R. Lupus Low Disease Activity State (LLDAS) attainment discriminates responders in a systemic lupus erythematosus trial: post-hoc analysis of the Phase IIb MUSE trial of anifrolumab. Ann Rheum Dis 2018;77:706–13.

20. Albrecht J, Taylor L, Berlin JA, Dulay S, Ang G, Fakharzadeh S, et al. The CLASI (Cutaneous Lupus Erythematosus Disease Area and Severity Index): an outcome instrument for cutaneous lupus erythematosus. J Invest Dermatol 2005;125:889–94.

21. Stokes ME, Davis CS, Koch GG. Categorical data analysis using SAS. 3rd ed. Carey (North Carolina): SAS Institute; 2012.

22. Bruce IN, O'Keeffe AG, Farewell V, Hanly JG, Manzi S, Su L, et al. Factors associated with damage accrual in patients with systemic lupus erythematosus: results from the Systemic Lupus International Collaborating Clinics (SLICC) inception cohort. Ann Rheum Dis 2015;74:1706–13.

23. Apostolopoulos D, Kandane-Rathnayake R, Louthrenoo W, Luo SF, Wu Y, Lateef A, et al. Factors associated with damage accrual in patients with systemic lupus erythematosus with no clinical or serological disease activity: a multicentre cohort study. Lancet Rheumatol 2020;2:e24–30.

24. Bonakdar ZS, Mohtasham N, Karimifar M. Evaluation of damage index and its association with risk factors in patients with systemic lupus erythematosus. J Res Med Sci 2011;16 Suppl 1:S427–32.

25. Tsang AS, Bultink IE, Heslinga M, Voskuyl AE. Both prolonged remission and Lupus Low Disease Activity State are associated with reduced damage accrual in systemic lupus erythematosus. Rheumatology (Oxford) 2017;56:121–8.

26. Murimi-Worstell IB, Lin DH, Nab H, Kan HJ, Onasanya O, Tierce JC, et al. Association between organ damage and mortality in systemic lupus erythematosus: a systematic review and meta-analysis. BMJ Open 2020;10:e031850.

27. Katz P, Wan GJ, Daly P, Topf L, Connolly-Strong E, Bostic R, et al. Patient-reported flare frequency is associated with diminished quality of life and family role functioning in systemic lupus erythematosus. Qual Life Res 2020;29:3251–61.

28. Katz P, Nelson WW, Daly RP, Topf L, Connolly-Strong E, Reed ML. Patient-reported lupus flare symptoms are associated with worsened patient outcomes and increased economic burden. J Manag Care Spec Pharm 2020;26:275–83.

29. Yeo AL, Koelmeyer R, Kandane-Rathnayake R, Golder V, Hoi A, Huq M, et al. Lupus low disease activity state and reduced direct health care costs in patients with systemic lupus erythematosus. Arthritis Care Res (Hoboken) 2020;72:1289–95.

30. Kan HJ, Song X, Johnson BH, Bechtel B, O'Sullivan D, Molta CT. Healthcare utilization and costs of systemic lupus erythematosus in Medicaid. Biomed Res Int 2013;2013:808391.

31. Zhu TY, Tam LS, Lee VW, Lee KK, Li EK. The impact of flare on disease costs of patients with systemic lupus erythematosus. Arthritis Rheum 2009;61:1159–67.

32. Fanouriakis A, Kostopoulou M, Alunno A, Aringer M, Bajema I, Boletis JN, et al. 2019 update of the EULAR recommendations for the management of systemic lupus erythematosus. Ann Rheum Dis 2019;78:736–45.

33. Van Vollenhoven RF, Mosca M, Bertsias G, Isenberg D, Kuhn A, Lerstrøm K, et al. Treat-to-target in systemic lupus erythematosus: recommendations from an international task force. Ann Rheum Dis 2014;73:958–67.

34. Alarcón GS, McGwin G Jr, Brooks K, Roseman JM, Fessler BJ, Sanchez ML, et al. Systemic lupus erythematosus in three ethnic groups. XI. Sources of discrepancy in perception of disease activity: a comparison of physician and patient visual analog scale scores. Arthritis Rheum 2002;47:408–13.

35. Elera-Fitzcarrald C, Vega K, Gamboa-Cárdenas RV, Zúñiga K, Medina M, Pimentel-Quiroz V, et al. Discrepant perception of lupus disease activity: a comparison between patients' and physicians' disease activity scores. J Clin Rheumatol 2020;26: S165–9.

36. Furie R, Wang L, Illei G, Drappa J. Systemic Lupus Erythematosus (SLE) Responder Index response is associated with global benefit for patients with SLE. Lupus 2018;27:955–62.

37. Mahieu M, Yount S, Ramsey-Goldman R. Patient-reported outcomes in systemic lupus erythematosus. Rheum Dis Clin North Am 2016;42:253–63.

38. Strand V, Berry P, Lin X, Asukai Y, Punwaney R, Ramachandran S. Long-term impact of belimumab on health-related quality of life and fatigue in patients with systemic lupus erythematosus: six years of treatment. Arthritis Care Res (Hoboken) 2019;71:829–38.

39. Wang B, Gladman DD, Urowitz MB. Fatigue in lupus is not correlated with disease activity. J Rheumatol 1998;25:892–5.

40. Bruce IN, Mak VC, Hallett DC, Gladman DD, Urowitz MB. Factors associated with fatigue in patients with systemic lupus erythematosus. Ann Rheum Dis 1999;58:379–81.

41. Nantes SG, Strand V, Su J, Touma Z. Comparison of the sensitivity to change of the 36-item Short Form Health Survey and the lupus quality of life measure using various definitions of minimum clinically important differences in patients with active systemic lupus erythematosus. Arthritis Care Res (Hoboken) 2018;70:125–33.

42. Morgan C, Bland AR, Maker C, Dunnage J, Bruce IN. Individuals living with lupus: findings from the LUPUS UK Members Survey 2014. Lupus 2018;27:681–7.

43. Van Vollenhoven RF, Stohl W, Furie RA, Fox NL, Groark JG, Bass D, et al. Clinical response beyond the Systemic Lupus Erythematosus Responder Index: post-hoc analysis of the BLISS-SC study. Lupus Sci Med 2018;5:e000288.

44. Ceccarelli F, Perricone C, Massaro L, Cipriano E, Alessandri C, Spinelli FR, et al. Assessment of disease activity in systemic lupus erythematosus: lights and shadows [review]. Autoimmun Rev 2015; 14:601–8.

AMERICAN COLLEGE
of RHEUMATOLOGY
Empowering Rheumatology Professionals

Protein Mannosylation as a Diagnostic and Prognostic Biomarker of Lupus Nephritis: An Unusual Glycan Neoepitope in Systemic Lupus Erythematosus

Inês Alves,[1] ID Beatriz Santos-Pereira,[1] ID Hans Dalebout,[2] Sofia Santos,[3] Manuel M. Vicente,[4] ID Ana Campar,[5] Michel Thepaut,[6] Franck Fieschi,[6] Sabine Strahl,[7] Fanny Boyaval,[2] Ramon Vizcaíno,[8] Roberto Silva,[9] Stephanie Holst-Bernal,[2] Carlos Vasconcelos,[10] Lélita Santos,[11] Manfred Wuhrer,[2] António Marinho,[10] Bram Heijs,[2] and Salomé S. Pinho[12] ID

Objective. Changes in protein glycosylation are a hallmark of immune-mediated diseases. Glycans are master regulators of the inflammatory response and are important molecules in self–nonself discrimination. This study was undertaken to investigate whether lupus nephritis (LN) exhibits altered cellular glycosylation to identify a unique glycosignature that characterizes LN pathogenesis.

Methods. A comprehensive tissue glycomics characterization was performed in kidney specimens from patients with systemic lupus erythematosus and biopsy-proven LN. A combination of advanced tissue mass spectrometry, in situ glyco-characterization, and ex vivo glycophenotyping was performed to structurally map the repertoire of *N*-glycans in LN tissue samples.

Results. LN exhibited a unique glycan signature characterized by increased abundance and spatial distribution of unusual mannose-enriched glycans that are typically found in lower microorganisms. This glycosignature was specific for LN, as it was not observed in other kidney diseases. Exposure of mannosylated glycans in LN was shown to occur at the cell surface of kidney cells, promoting increased recognition by specific glycan-recognizing receptors expressed by immune cells. This abnormal glycosignature of LN was shown to be due to a deficient complex *N*-glycosylation pathway and a proficient *O*-mannosylation pathway. Moreover, mannosylation levels detected in kidney biopsy samples from patients with LN at the time of diagnosis were demonstrated to predict the development of chronic kidney disease (CKD) with 93% specificity.

Conclusion. Cellular mannosylation is a marker of LN, predicting the development of CKD, and thus representing a potential glycobiomarker to be included in the diagnostic and prognostic algorithm of LN.

INTRODUCTION

Systemic lupus erythematosus (SLE) is an autoimmune disease characterized by a loss of immune tolerance and sustained autoantibody production that may potentially lead to multiorgan inflammation and injury (1). Lupus nephritis (LN) is one of the most common and severe clinical manifestations of SLE, affecting up to 60% of patients. However, this percentage may depend on the population studied, ancestry, as well as sex and age (2). LN remains a major risk factor for overall morbidity and mortality in SLE and may evolve to chronic kidney disease (CKD) or end-stage renal disease in ~25% of patients (3).

Accumulating evidence suggests that genetic and environmental factors contribute to the pathogenesis of SLE (4,5);

however, the exact mechanism underlying the immune dysfunction is far from being elucidated. Therefore, SLE remains a chronic, lifelong, relapsing, and disabling disorder that mainly affects young women, imposing a negative impact on quality of life.

Glycosylation is a major posttranslational mechanism characterized by the addition of glycans to proteins through the synchronized action of a portfolio of specific glycosyltransferase enzymes in the endoplasmic reticulum/Golgi compartments of essentially all cells (6). Changes in glycan presentation on the cell surface can occur in response to environmental and genetic stimuli, often associated with the acquisition of altered cellular phenotypes, and is an essential characteristic in distinguishing self glycans from nonself glycans (7). Accumulating evidence has demonstrated that glycans act as master regulators of the inflammatory response, either directly by regulating immune cell activity and function or through cellular recognition by specific glycan-recognizing receptors expressed by immune cells during inflammation and infection (8–11).

Changes in protein glycosylation have been shown to play an instrumental role in the immunopathogenesis of many immune-mediated diseases such as inflammatory bowel disease (12), rheumatoid arthritis (13), and multiple sclerosis (14). However, changes in protein glycosylation in SLE development and progression are still unknown. In this study, we demonstrated for the first time that LN is characterized by an abnormal pattern of cellular glycosylation in the kidney that is not observed in other kidney conditions, revealing an unusual exposure of altered self glycan antigens. This unique and specific glycosignature, which is potentially associated with the loss of self tolerance, was demonstrated to have prognostic applications in SLE.

PATIENTS AND METHODS

Patients and controls. Formalin-fixed paraffin-embedded (FFPE) stored kidney biopsy samples collected from 41 patients with LN between 1992 and 2015 were obtained from the Nephrology Department at Porto University Centre Hospital (CHUP) and the Nephrology Department at Coimbra University Centre Hospital. As healthy kidney control samples, 20 FFPE kidney sections from healthy subjects (specifically excluding autoimmune diseases, cancer, and inflammatory-mediated diseases) were

obtained from the Department of Pathology, São João University Hospital. In addition, 27 FFPE kidney biopsy samples were obtained from patients with other diseases affecting the kidney (including amyloidosis, type 2 diabetes mellitus, IgA nephropathy, antineutrophil cytoplasmic antibody–associated vasculitis, and chronic and acute kidney rejection) in the Nephrology Department at CHUP (additional details on the study subjects are provided in Supplementary Tables 1 and 2, available on the *Arthritis & Rheumatology* website at http://onlinelibrary.wiley.com/doi/10.1002/art.41768/abstract). Clinicopathologic and treatment data on each patient with LN were collected at the time of LN diagnosis and 1 year post-biopsy. The data include Systemic Lupus Erythematosus Disease Activity Index (SLEDAI) score (15) and proteinuria at the time of diagnosis and 1 year post-biopsy, and response to treatment, need for biologic treatment and/or glucocorticoids >10 mg/day, and number of renal flares at least 1 year post-biopsy (Supplementary Table 2).

Response to treatment was defined in accordance with the updated European Alliance of Associations for Rheumatology (EULAR)/European Renal Association–European Dialysis and Transplant Association recommendations for the management of LN (5). Patients were classified as either responders or nonresponders to standard therapy (i.e., glucocorticoids and immunosuppressants), with nonresponders defined as those who experienced <50% reduction in proteinuria or persistent nephrotic proteinuria (5). Flares were defined using the Safety of Estrogens in Lupus Erythematosus National Assessment version of the SLEDAI (the SELENA–SLEDAI flare index), in accordance with the EULAR recommendations for clinical studies (16,17). Good versus poor prognosis was defined in accordance with the 2012 Kidney Disease: Improving Global Outcomes classification recommendations, with a poor prognosis defined as the development of CKD (estimated glomerular filtration rate <60 ml/minute/1.73 m^2 and albuminuria ≥30 mg/24 hours) and a good prognosis defined as no development of CKD at 1 year post-biopsy (18).

Ethics approval and consent to participate. This study was approved by the ethics committee of the CHUP and Coimbra University Centre Hospital (no. 123-DEFI/127-CE). Patients and healthy controls were recruited based on their scheduled

Medical Center, Leiden, The Netherlands; [3]Sofia Santos, MD: Department of Nephrology, Porto University Hospital Center, Porto, Portugal; [4]Manuel M. Vicente, MSc: Institute for Research and Innovation in Health (i3S), University of Porto, Porto, Portugal, and Institute of Biomedical Sciences Abel Salazar (ICBAS), University of Porto, Porto, Portugal; [5]Ana Campar, MD: Clinical Immunology Unit, Porto University Hospital Center, Porto, Portugal, Institute for Research and Innovation in Health (i3S), University of Porto, Porto, Portugal, and Institute of Biomedical Sciences Abel Salazar (ICBAS), University of Porto, Porto, Portugal; [6]Michel Thepaut, MSc, Franck Fieschi, PhD: University Grenoble Alpes, CNRS, CEA, Institut de Biologie Structurale, Grenoble, France; [7]Sabine Strahl, PhD: Center for Organismal Studies (COS), Glycobiology, Heidelberg University, Heidelberg, Germany; [8]Ramon Vizcaíno, MD: Pathology Department, Porto University Hospital Center, Porto, Portugal; [9]Roberto Silva, MD: Pathology Department, Centro

Hospitalar São João, Porto, Portugal; [10]Carlos Vasconcelos, MD, PhD, António Marinho, MD, PhD: Clinical Immunology Unit, Porto University Hospital Center, Porto, Portugal, and Institute of Biomedical Sciences Abel Salazar (ICBAS), University of Porto, Porto, Portugal; [11]Lélita Santos, MD: Department of Internal Medicine, Coimbra University Centre Hospital, Coimbra, Portugal; [12]Salomé S. Pinho, DVM, PhD: Institute for Research and Innovation in Health (i3S), University of Porto, Porto, Portugal, Faculty of Medicine, University of Porto, Porto, Portugal, and Institute of Biomedical Sciences Abel Salazar (ICBAS), University of Porto, Porto, Portugal.

appointments at the 2 Portuguese referral hospital centers and were informed of the main content and goal of the study. All subjects provided written informed consent.

Matrix-assisted laser desorption ionization–imaging mass spectrometry. Sections of the FFPE tissue samples were obtained from 6 female patients with LN and 6 healthy kidney controls (3 men and 3 women). The mean age of the patients with LN was 53 years (range 41–66 years), and the mean age of the healthy kidney controls was 59 years (range 51–74 years). The collected samples were cut and mounted on indium tin oxide–coated glass slides (Bruker Daltonics), previously coated with poly-L-lysine. Slides were processed as previously described (19). *N*-glycan matrix-assisted laser desorption ionization–imaging mass spectrometry (MALDI-IMS) analyses were performed using a rapifleX MALDI–time-of-flight/time-of-flight instrument (Bruker Daltonics). Data were recorded in reflectron positive-ion mode covering a mass range of m/z 900–3200, using 500 laser shots per spot and a $50 \times 50 \ \mu m^2$ pixel size. A detailed protocol is described in the Supplementary Methods (http://onlinelibrary.wiley.com/doi/10.1002/art.41768/abstract).

Following MALDI-IMS analysis, excess of the MALDI matrix was removed, and slides were stained with hematoxylin and eosin and scanned using an IntelliSite Pathology Solution ultra-fast scanner (Philips). Histologic images were coregistered with the MALDI-IMS data in FlexImaging 5.0 (Bruker Daltonics). Annotations of regions of interest (glomeruli, stroma, and tubular zones) were recorded by an expert pathologist.

A representative average spectrum for each tissue structure (glomeruli, stroma, and tubular zone) was created using SCiLS Lab software; mMass (20) and GlycoWorkbench, version 1.2.4105 (21) were used to construct a theoretical composition list (containing 90 *N*-glycan compositions) and a calibration list from the representative average spectra. Spectral processing was performed using mMass. Data recalibration extraction was performed using MassyTools, version 0.1.8.1.

Lectin histochemistry and immunohistochemistry. The glycan profiles of FFPE tissue obtained from 20 healthy kidney controls, 27 patients with other kidney diseases, and 41 patients with LN were analyzed by lectin histochemistry. The expression of β1,6 *N*-acetylglucosamine β1–6-branched *N*-glycans was assessed by tissue immunoreactivity using phytohemagglutinin leukoagglutinin (PHA-L), and the expression of mannosylated *N*-glycans was assessed using Galanthus nivalis agglutinin (GNA). Tissue sections were incubated with biotinylated lectins, and the avidin-biotin-peroxidase complex was detected using a Vectastain ABC kit (both from Vector). For the detection of *O*-mannosylated proteins, tissue sections were incubated with α-*O*-Man–directed monoclonal antibody (clone RKU-1-3-5) (22) and

processed with EnVision+ Dual Link System-HRP (Dako). DC-SIGN–binding motifs were measured using biotinylated DC-SIGN-ECD (lot 54416) (23) and detected using a Vectastain ABC kit. GNA reactivity was evaluated by 3 independent observers (IA, BS-P, and SSP) and scored as 0–25%, 25–50%, 50%–75%, or >75% positive GNA reactivity; the observers were blinded with regard to the source of the kidney sample (patient with LN, patient with other kidney conditions, or healthy). Quantitative characterization of GNA reactivity was performed using the optical density of deconvoluted images with ImageJ software (National Institutes of Health). Clinical evaluation was performed 1 year after diagnosis, with the assessor blinded with regard to the glycobiomarker signature.

Ex vivo glycoprofile of kidney biopsy tissue. To characterize the glycoprofile of ex vivo tissue, fresh kidney biopsy samples were obtained from 3 patients with LN and 4 patients with other kidney diseases (2 patients with amyloidosis and 2 patients with IgA nephropathy) in the Nephropathy Department at CHUP at the time of diagnosis. Single-cell suspensions were obtained as previously described (24). Cells were incubated with fixable viability dye-allophycocyanin-Cy7, for dead cell exclusion, followed by lectin staining with biotinylated PHA-L and fluorescein isothiocyanate–conjugated GNA (both from Vector). Then, cells were incubated with Streptavidin-PeCy7 and CD45-BV510 (both from BioLegend). Using the same samples, but in an independent mix, cells were incubated with biotinylated DC-SIGN-ECD (lot 54416) (23) followed by Streptavidin-PE and CD45-BV510. Data acquisition was performed using a FACSCanto II flow cytometer (Becton Dickinson) and analyzed using FlowJo version 10 software (Tree Star). Live nonimmune cells were first gated based on their lack of CD45 expression, and the median fluorescence intensity of PHA-L and GNA was recorded.

Real-time quantitative polymerase chain reaction. Total RNA from FFPE tissue from 18 healthy kidney controls, 17 patients with LN, and 4 patients with other kidney conditions (1 patient with chronic kidney rejection, 1 patient with acute kidney rejection, and 2 patients with type 2 diabetes) was obtained using a RecoverAll Total Nucleic Acid Isolation Kit, according to the instructions of the manufacturer (Invitrogen). Of the total RNA, 100 μg was reverse transcribed to single-stranded complementary DNA using Superscript II Reverse Transcriptase and random hexamer primers (Invitrogen). Quantitative reverse transcriptase–polymerase chain reaction was carried out in duplicate for the target genes (*MAN2A1*-FAM, Hs.01123591 and *POMT1*-FAM, Hs.01123591) and the housekeeping gene (*HPRT*-VIC, Hs.02800695) (all TaqMan probes from Applied Biosystems). Quantitative polymerase chain reaction was performed with ABI Prism 7000 Sequence Detection System. Data were analyzed by the $2(-\Delta\Delta C_t)$ method. The Mann-Whitney test was used for all data comparisons.

Statistical analysis. A receiver operating characteristic analysis (for the average score of tubules and glomeruli, the nonimmune compartment) was performed, and the cutoff of 50% GNA reactivity was determined. Kidney sections exhibiting ≥50% GNA lectin reactivity were classified as high expression, and sections with <50% GNA lectin reactivity were classified as low expression. Univariable binary logistic regression analysis was performed to test the ability of high GNA reactivity and clinical variables in predicting poor prognosis. Moreover, multivariable logistic regression analysis was performed to determine the variables that could independently predict progression to CKD. In logistic regressions, the best fitting model was assessed using the Hosmer-Lemeshow goodness-of-fit test. Pearson's chi-square test was used to determine the associations between GNA levels and clinical features. All statistical analyses were performed using SPSS, version 25.0.
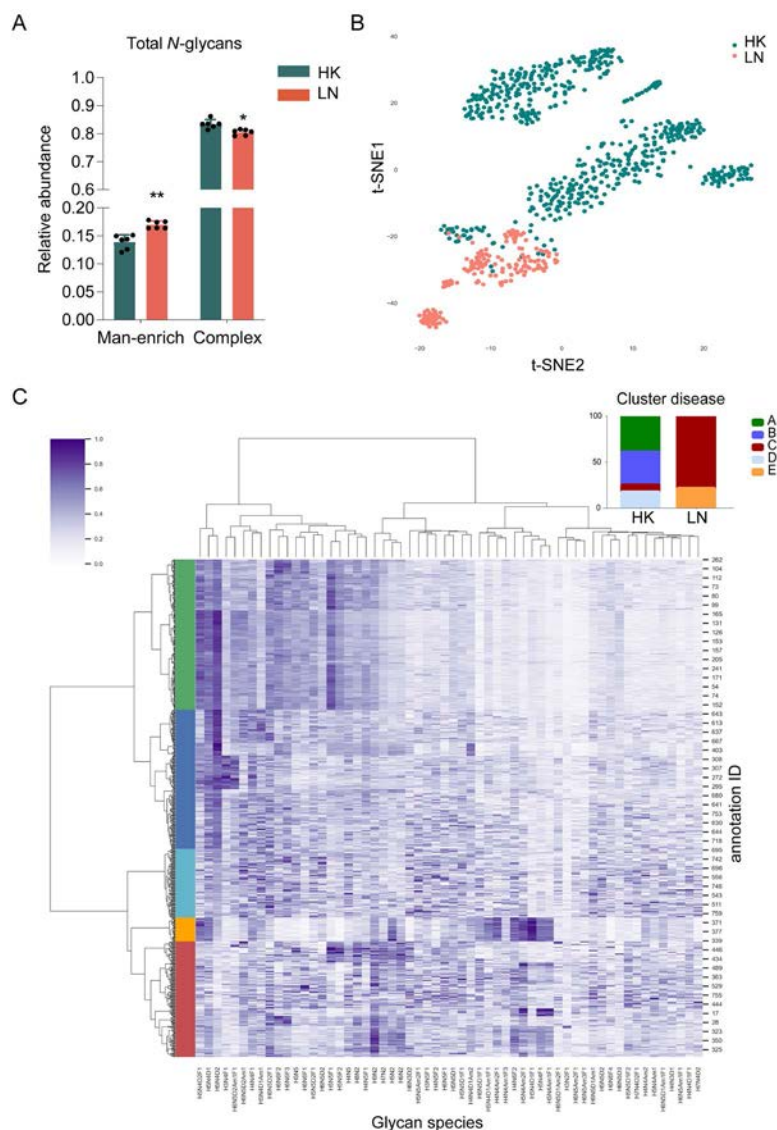
Figure 1. **A**, Matrix-assisted laser desorption ionization–imaging mass spectrometry (MALDI-IMS) analysis of derivatized *N*-glycans from 12 kidney biopsy samples (6 from patients with lupus nephritis [LN] and 6 from healthy kidneys [HKs]). An increase in the overall relative abundance of mannose-enriched (Man-enrich) *N*-glycans (high-mannose and hybrid) was accompanied by a relative decrease in complex *N*-glycans in the LN samples. The data presented were obtained from 6 biologic replicates from each group, and represent the average of glycan abundance considering all regions of interest. Circles represent individual subjects; bars show the mean ± SD. * = $P < 0.05$; ** = $P < 0.01$ versus healthy kidneys, by Mann-Whitney test. **B**, Two-dimensional representation of MALDI-IMS acquisitions from LN or healthy kidney samples (represented by the same colors as in **A**), obtained via t-distributed stochastic neighbor embedding (t-SNE) and including all kidney regions. Each symbol represents an IMS acquisition/annotation; t-SNE was performed with the full set of glycans measured. **C**, Unsupervised hierarchical clustering and heatmap of MALDI-IMS acquisitions showing glycan abundance levels, scaled according to the maximum value of each glycan. Clusters were identified using a 50-linkage distance threshold and are represented by the 5 colors on the left. Healthy kidney– and LN-derived annotations in the 5 identified clusters are shown. Color figure can be viewed in the online issue, which is available at http://onlinelibrary.wiley.com/doi/10.1002/art.41768/abstract.

RESULTS

Two-dimensional mapping of the *N*-glycosylation signature of LN tissues. As a first approach, the glycome in LN tissue was characterized using MALDI-IMS, a cutting-edge mass spectrometry–based glycomics technique that allows comprehensive analysis of the spatial distribution of *N*-glycans directly from FFPE kidney tissue samples. Evaluation of the MALDI-IMS data revealed a differential overall distribution of *N*-glycans in the tissue of 6 patients with LN compared to 6 healthy kidney controls (Figure 1A). The results demonstrated that mannose-enriched *N*-glycans were significantly more abundant in the stroma, tubules, and glomeruli regions of kidney tissue from patients with LN (Supplementary Figure 1A, available on the *Arthritis & Rheumatology* website at http://onlinelibrary.wiley.com/doi/10.1002/art.41768/abstract) compared to healthy kidney controls. The increased overall abundance of mannose-enriched glycans (high-mannose and hybrid-type *N*-glycans) in all regions was accompanied by a consequent decrease in complex branched *N*-glycans (Figure 1A).

Additionally, using a t-distributed stochastic neighbor embedding approach, we demonstrated a clear dissimilarity in *N*-glycan signature between patients with LN and healthy kidney controls (Figure 1B). This glycan-based segregation between patients with LN and healthy kidney controls was shown to be disease-specific,

which highlights the potential of this glycomic signature to be useful in discriminating LN tissue from healthy kidney tissue.

Furthermore, in order to specifically identify the *N*-glycan moieties that were enriched in LN tissue versus healthy kidney tissue, annotated regions were hierarchically clustered using the relative abundance of the glycans. The clustering analysis provided information on specific glycosignatures of the different samples, resulting in 5 segmented groups (Figure 1C). These clusters were found to be strongly associated with LN disease, as shown by the unique prevalence of cluster E and the predominant existence of cluster C in patients with LN. Cluster E showed the highest levels of mannose-enriched *N*-glycans: high-mannose glycans (H5N2, where H = hexose and N = *N*-acetylhexosamine) and biantennary complex-type glycans (H5N4D2F1, H5N4D1, H4N4Am2F1, H5N4F1, and H5N4Am2F1, where F = fucose, D = α2,6-linked sialic acid, and Am = α2,3-linked sialic acid). Accordingly, cluster C also showed increased abundance of high-mannose *N*-glycans (H5N2, H6N2, H7N2, H8N2, and H9N2), biantennary galactosylated (H5N4F1), and sialylated complex-type glycans (H5N4Am2F1), as well as lower abundances of biantennary sialylated (H5N4D2), triantennary sialylated (H6N5D3 and H6N5D2Am1), and tetraantennary galactosylated (H6N6F4) *N*-glycan species.

We next analyzed *N*-glycan expression in the nonimmune/epithelial compartment (tubules and glomeruli) of the kidney samples (Figure 2A). This analysis demonstrated a significant accumulation
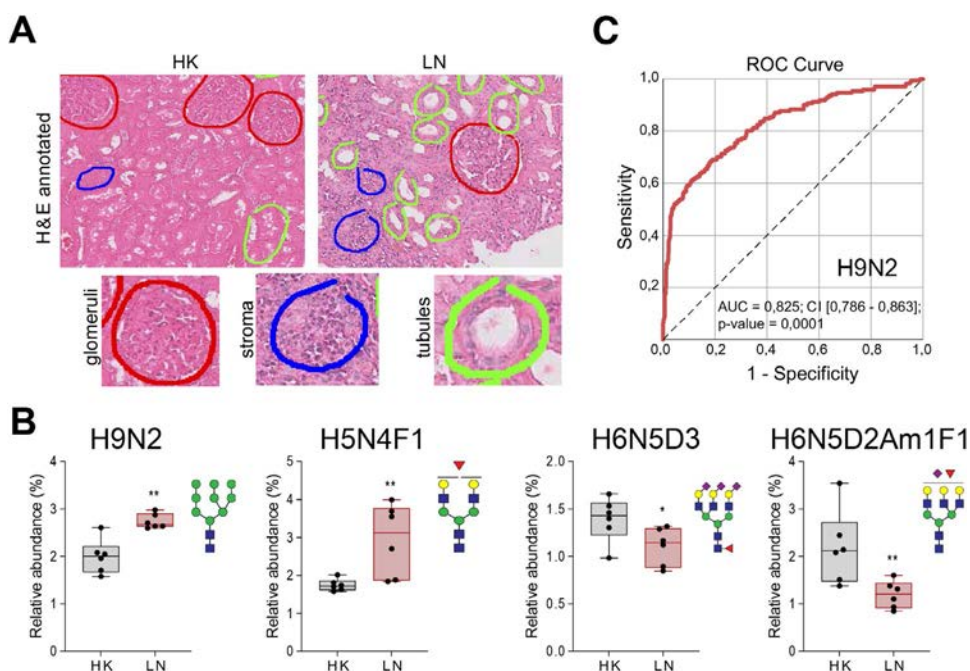
Figure 2. **A**, Representative images of hematoxylin and eosin (H&E)–stained healthy kidney and LN kidney samples. Regions of interest used in the MALDI-IMS analysis are circled in red (glomeruli), blue (stroma), or green (renal tubules). **B**, Relative abundance of the most significantly altered *N*-glycan structures in the epithelial/nonimmune compartment (tubules and glomeruli) of patients with LN compared to healthy kidney controls. Data are presented as box plots, where the boxes represent the 25th to 75th percentiles, the lines within the boxes represent the median, and the lines outside the boxes represent the 10th and 90th percentiles. Each symbol represents an individual subject. * = P < 0.05; ** = P < 0.01, by Mann-Whitney test. **C**, Receiver operating characteristic (ROC) curve analysis of H9N2 *N*-glycan species for each MALDI-IMS acquisition in the epithelial/nonimmune compartment tubules and glomeruli. AUC = area under the curve; CI = 95% confidence interval (see Figure 1 for other definitions). Color figure can be viewed in the online issue, which is available at http://onlinelibrary.wiley.com/doi/10.1002/art.41768/abstract.
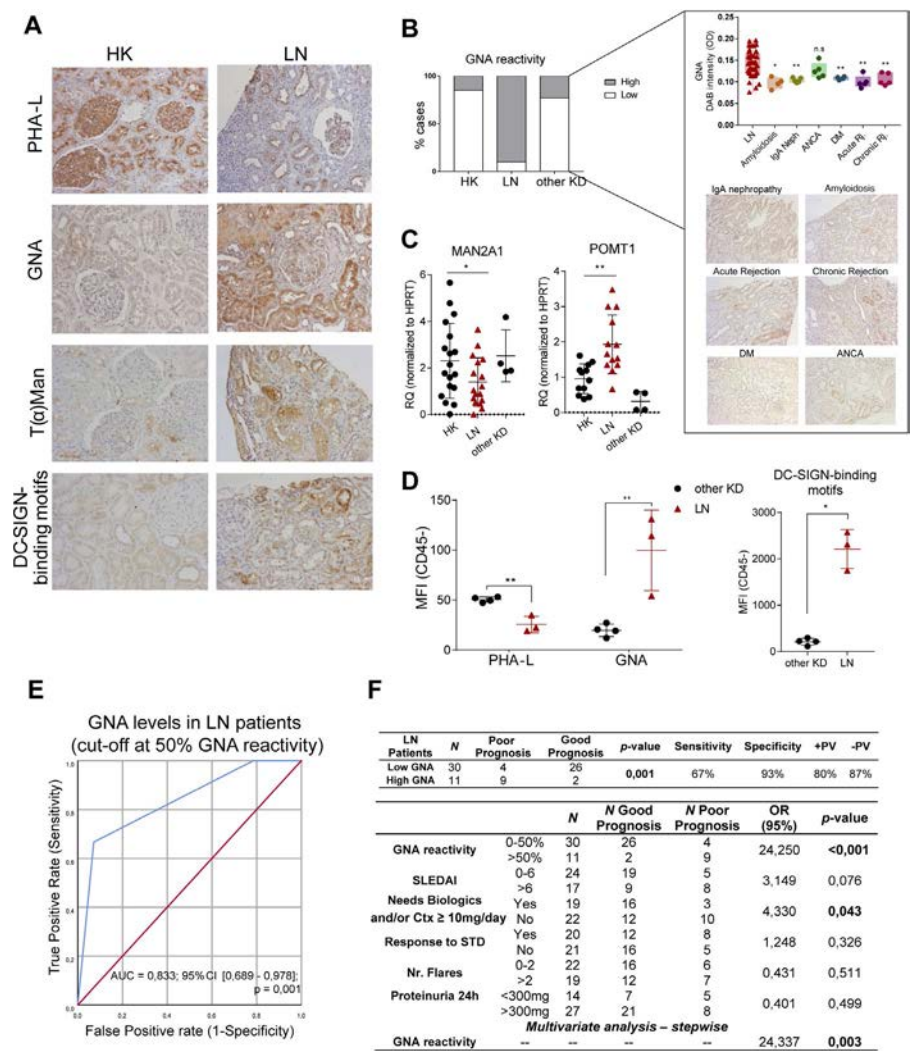
Figure 3. **A**, Representative images of kidney cortex from healthy controls and patients with LN, showing low phytohemagglutinin leukoagglutinin (PHA-L), and high Galanthus nivalis agglutinin (GNA) reactivity in LN biopsy samples. *O*-mannosylation and DC-SIGN–binding motifs are increased in LN biopsy samples. **B**, Left, Distribution of high GNA reactivity (≥50%) and low GNA reactivity (<50%) among healthy kidney controls, patients with LN, and patients with other kidney conditions (KDs). Right, Quantitative analysis of diaminobenzidine (DAB) staining intensity and representative histologic images showing GNA reactivity in LN and other kidney conditions (negative control shown in Supplementary Figure 1C, http://onlinelibrary. wiley.com/doi/10.1002/art.41768/abstract). The analysis was performed on kidney specimens collected from 41 LN patients, 27 patients with other kidney conditions, and 20 healthy kidney controls. Data are shown as box plots, where the boxes represent the 25th and 75th percentiles, the lines within the boxes represent the median, and the lines outside the boxes represent the 10th and 90th percentiles. Each symbol represents an individual subject. * = $P < 0.05$; ** = $P < 0.01$ versus patients with LN, by Mann-Whitney test. **C**, Relative quantification (RQ) of *MAN2A1* and *POMT1* mRNA expression levels in formalin-fixed paraffin-embedded kidney biopsy samples from healthy kidney controls, patients with LN, and patients with other kidney conditions (2 with chronic rejection [Rj], 1 with acute rejection, and 1 with type 2 diabetes mellitus [DM]). * = $P < 0.05$; ** = $P < 0.01$, by Mann-Whitney test. **D**, Flow cytometry analysis of levels of PHA-L, GNA, and DC-SIGN–binding motifs on CD45-negative cells (representing the nonimmune/epithelial cell compartment) in fresh kidney biopsy samples from patients with LN or with other kidney conditions (2 with amyloidosis and 2 with IgA nephropathy [Neph]), obtained at the time of diagnosis. In **C** and **D**, symbols represent individual subjects; bars show the mean ± SD. * = $P < 0.05$; ** = $P < 0.01$, by Mann-Whitney test. **E**, Receiver operating characteristic curve for GNA reactivity in samples from patients with LN that progressed to chronic kidney disease. **F**, Predictive capacity of high GNA reactivity and other clinicopathologic parameters in distinguishing patients with LN that will progress to chronic kidney disease (poor prognosis). T(α)Man = T(alpha) mannose; ANCA = antineutrophil cytoplasmic antibody; NS = not significant; MFI = mean fluorescence intensity; AUC = area under the curve; 95% CI = 95% confidence interval; +PV = positive predictive value; –PV = negative predictive value; OR = odds ratio; SLEDAI = Systemic Lupus Erythematosus Disease Activity Index; Ctx = glucocorticoids; STD = standard therapy; Nr = number (see Figure 1 for other definitions).

of less complex/mannose-enriched *N*-glycans (H9N2 and H5N4F1) together with decreased expression of complex *N*-glycans (sialylated *N*-glycans, H6N5D3, and H6N5D2Am1F1) in LN tissue compared to healthy kidney tissue (Figure 2B and Supplementary Figure 1A, available on the *Arthritis & Rheumatology* website at http://onlinelibrary.wiley.com/doi/10.1002/art.41768/abstract). This

abundance of high-mannose *N*-glycans significantly correlated with LN disease status (specificity ≥0.8 and *P* = 0.0001) (Figure 2C).

Taken together, these results provide evidence for the existence of a unique glycosignature that characterizes LN. This suggests that *N*-glycomes in tissue define the phenotype of LN, thus representing a potential glycobiomarker for diagnosis of LN.

Glycosylation profile of renal parenchyma in LN patients reveals unusual exposure of mannose-enriched neoglycoantigens not observed in other kidney conditions. The in situ glycoprofile at the time of diagnosis was characterized in 41 LN tissue samples obtained from patients with LN, 27 kidney biopsy samples from patients with other kidney conditions, and 20 healthy kidney controls.

When compared to healthy kidney controls and patients with other kidney conditions, the tissue samples obtained from the patients with LN showed a significant increase in mannose-enriched *N*-glycan expression (detected with GNA lectin). This increase in mannose-enriched *N*-glycan expression was accompanied by decreased expression of complex branched *N*-glycans (PHA-L positive), predominantly in tubules and glomeruli (Figures 3A and B, and Supplementary Figures 1B and C, http://online library.wiley.com/doi/10.1002/art.41768/abstract), thus confirming the IMS findings.

This in situ glycosignature was further confirmed at a transcriptional level by determining the expression of specific glycogenes involved in the generation of mannose-enriched glycan, such as *MAN2A1* and *POMT1*, in LN tissue samples (Supplementary Figure 1D). Accordingly, a significant reduction in the expression of glycogene *MAN2A1,* encoding for α-mannosidase II enzyme, was observed in patients with LN when compared to healthy kidney controls (Figure 3C). Moreover, LN tissue exhibited up-regulation of the mannosyltransferase gene *POMT1* (Figure 3C), which is in accordance with increased expression of *O*-mannosylated glycans observed by T(α)mannose immunochemistry. Other glycogenes, such as *MGAT1*, *MGAT3*, and *MGAT5*, were also analyzed, and no differences were observed (Supplementary Figure 1E).

To gain further insight into the glycosylation profile at a cellular level, we analyzed the cell surface glycosignature of CD45-negative nonimmune cells from fresh kidney biopsy samples obtained from 3 patients with LN and 4 patients with other kidney conditions using flow cytometry. Kidney nonimmune cells from patients with LN, compared to patients with other kidney conditions, showed significantly lower levels of branched *N*-glycans and a significant increase in high-mannose *N*-glycans (Figure 3D). This overexposure of mannose epitopes at the surface of kidney nonimmune cells was further confirmed by the recognition of a specific glycan-recognizing receptor, DC-SIGN. Consistent with this, nonimmune/epithelial cells from LN tissue samples showed increased levels of DC-SIGN–binding motifs, compared to

healthy kidney controls and patients with other kidney conditions (Figures 3A and D).

In a longitudinal analysis, we observed that high GNA reactivity (detection of high mannosylated glycan expression) at the time of diagnosis could be used to stratify patients according to the risk of developing CKD, with a specificity of 93% and a sensitivity of 67% (Figure 3F). Univariable analysis further demonstrated that high GNA reactivity detected at the time of LN diagnosis increased the odds of developing CKD by 24-fold (*P* < 0.001) when compared to LN patients with low GNA reactivity. Moreover, multivariable analysis revealed that among other clinical parameters, high GNA reactivity at the time of LN diagnosis was the only variable that independently predicted the development of CKD (Figure 3F).

Taken together, these results represent the first identification of a potential glycobiomarker based on abnormal expression of mannose-enriched glycan epitopes at the surface of kidney epithelial cells, with diagnostic and prognostic applications in SLE. This accumulation of mannosylated glycan structures appears to be the result of a deficient *N*-glycosylation pathway that converges with an increased *O*-mannosylation pathway to generate mannose-enriched neoglycoantigens.

DISCUSSION

To our knowledge, this is the first study to show that LN is characterized by an unusual and specific glycosignature not observed in healthy kidney controls or in patients with other kidney conditions. This has prognostic value as demonstrated by the correlation with development of CKD.

The increased accumulation of mannosylated glycans in the kidney of LN patients was found to be due to an incomplete *N*-glycosylation pathway, demonstrated by the down-regulation of glycogene *MAN2A1* and the up-regulation of the *O*-mannosylation pathway through increased *POMT1* transcription. The coordinated action of both the deficient *N*-glycosylation pathway and the proficient *O*-mannosylation appears to converge to promote this unusual overexpression of mannose-enriched glycans. This is in accordance with findings in the *Man2a1*−/− mice, which develop a systemic autoimmune-like disease similar to SLE in humans (25). Interestingly, and consistent with our observations, a previous case report described 2 sisters with α-mannosidosis, an autosomal-recessive disorder characterized by intralysosomal accumulation of less complex glycans, who developed SLE (26).

The abnormal accumulation of high-mannose *N*-glycans as well as *O*-mannose was shown to be a unique signature that distinguishes the kidneys of patients with LN from healthy kidneys and other kidney conditions. In fact, mannosylated glycans are considered a marker of immunogenicity, acting as a glycan-epitope that is able to trigger the recognition and activation of

antigen-presenting cells through specific recognition by glycan-recognizing receptors such as DC-SIGN (27). In accordance with this, oligomanose epitopes are typically found on the surface of several pathogens (i.e., virus, fungi, and parasites), representing an important trigger for immune activation.

Abnormal exposure of altered self glycoantigens in LN may promote the creation of a damage-associated molecular pattern, sensed as a sterile sign of infection by immune cells. This is demonstrated by the increased expression of DC-SIGN–binding motifs, which appears to contribute to alteration of the balance between homeostasis and loss of self tolerance associated with SLE pathogenesis.

Further studies are needed to confirm the accuracy of the glycobiomarker as a novel diagnostic and prognostic tool in LN by testing in larger and well-characterized multicentric cohorts, as well as in longitudinal cohorts. Moreover, and since our cohort comprises mainly White female patients, it would also be important to confirm these findings in male patients and in patients of different ethnicities. Envisioning a clinical applicability of this glycobiomarker, it would also be beneficial to validate the predictive performance of the glycobiomarker combined with other clinico-pathologic parameters currently used in the management of SLE and CKD.

In conclusion, we identified a glycobiomarker with prognostic value in LN and SLE. This may provide a new avenue in the clinical and therapeutic algorithm of these diseases, potentially leading to the development of novel biomarkers and targeted therapies.

ACKNOWLEDGMENTS

AUTHOR CONTRIBUTIONS

All authors were involved in drafting the article or revising it critically for important intellectual content, and all authors approved the final version to be published. Dr. Alves had full access to all of the data in the study and takes responsibility for the integrity of the data and the accuracy of the data analysis.

Study conception and design. Alves, Wuhrer, Heijs, Pinho.
Acquisition of data. Alves, Santos-Pereira, Dalebout, Thepaut, Fieschi, Strahl, Boyaval, Holst-Bernal, Heijs.
Analysis and interpretation of data. Alves, S. Santos, Vicente, Campar, Vizcaíno, Silva, Vasconcelos, L. Santos, Marinho, Pinho.

REFERENCES

1. Tsokos GC, Lo MS, Costa Reis P, Sullivan KE. New insights into the immunopathogenesis of systemic lupus erythematosus [review]. Nat Rev Rheumatol 2016;12:716–30.

2. Davidson A. What is damaging the kidney in lupus nephritis? [review]. Nat Rev Rheumatol 2016;12:143–53.

3. Almaani S, Meara A, Rovin BH. Update on lupus nephritis [review]. Clin J Am Soc Nephrol 2017;12:825–35.

4. Choi J, Kim ST, Craft J. The pathogenesis of systemic lupus erythematosus: an update [review]. Curr Opin Immunol 2012;24:651–7.

5. Fanouriakis A, Kostopoulou M, Cheema K, Anders HJ, Aringer M, Bajema I, et al. 2019 update of the joint European League Against Rheumatism and European Renal Association-European Dialysis and Transplant Association (EULAR/ERA–EDTA) recommendations for the management of lupus nephritis. Ann Rheum Dis 2020;79:713–23.

6. Ohtsubo K, Marth JD. Glycosylation in cellular mechanisms of health and disease. Cell 2006;126:855–67.

7. Pinho SS, Reis CA. Glycosylation in cancer: mechanisms and clinical implications [review]. Nat Rev Cancer 2015;15:540–55.

8. Rabinovich GA, van Kooyk Y, Cobb BA. Glycobiology of immune responses [review]. Ann N Y Acad Sci 2012;1253:1–15.

9. Marth JD, Grewal PK. Mammalian glycosylation in immunity [review]. Nat Rev Immunol 2008;8:874–87.

10. Pereira MS, Alves I, Vicente M, Campar A, Silva MC, Padrão NA, et al. Glycans as key checkpoints of T cell activity and function [review]. Front Immunol 2018;9:2754.

11. Verhelst X, Dias AM, Colombel JF, Vermeire S, van Vlierberghe H, Callewaert N, et al. Protein glycosylation as a diagnostic and prognostic marker of chronic inflammatory gastrointestinal and liver diseases [review]. Gastroenterology 2020;158:95–110.

12. Dias AM, Correia A, Pereira MS, Almeida CR, Alves I, Pinto V, et al. Metabolic control of T cell immune response through glycans in inflammatory bowel disease. Proc Natl Acad Sci U S A 2018;115:E4651–60.

13. Axford J, Lydyard P, Isenberg D, Mackenzie L, Hay F, Roitt I. Reduced B-cell galactosyltransferase activity in rheumatoid arthritis. Lancet 1987;330:1486–8.

14. Li CF, Zhou RW, Mkhikian H, Newton BL, Yu Z, Demetriou M. Hypomorphic MGAT5 polymorphisms promote multiple sclerosis cooperatively with MGAT1 and interleukin-2 and 7 receptor variants. J Neuroimmunol 2013;256:71–6.

15. Bombardier C, Gladman DD, Urowitz MB, Caron D, Chang CH, and the Committee on Prognosis Studies in SLE. Derivation of the SLEDAI: a disease activity index for lupus patients. Arthritis Rheum 1992;35:630–40.

16. Isenberg D, Sturgess J, Allen E, Aranow C, Askanase A, Sang-Cheol B, et al. Study of flare assessment in systemic lupus erythematosus based on paper patients. Arthritis Care Res (Hoboken) 2018;70:98–103.

17. Petri M, Kim MY, Kalunian KC, Grossman J, Hahn BH, Sammaritano LR, et al, for the OC-SELENA Trial. Combined oral contraceptives in women with systemic lupus erythematosus. N Engl J Med 2005;353:2550–8.

18. Levin A, Stevens PE, Bilous RW, Coresh J, de Francisco AL, de Jong PE, et al. Kidney disease: improving global outcomes (KDIGO) CKD work group. KDIGO 2012 clinical practice guideline for the evaluation and management of chronic kidney disease. Kidney Int Suppl 2013;3:1–150.

19. Holst S, Heijs B, de Haan N, van Zeijl RJ, Briaire-de Bruijn IH, van Pelt GW, et al. Linkage-specific in situ sialic acid derivatization for N-glycan mass spectrometry imaging of formalin-fixed paraffin-embedded tissues. Anal Chem 2016;88:5904–13.

20. Strohalm M, Hassman M, Košata B, Kodíček M. mMass data miner: an open source alternative for mass spectrometric data analysis. Rapid Commun Mass Spectrom 2008;22:905–8.

21. Ceroni A, Maass K, Geyer H, Geyer R, Dell A, Haslam SM. GlycoWorkbench: a tool for the computer-assisted annotation of mass spectra of glycans. J Proteome Res 2008;7:1650–9.

22. Bartels MF, Winterhalter PR, Yu J, Liu Y, Lommel M, Möhrlen F, et al. Protein O-mannosylation in the murine brain: occurrence of mono-O-mannosyl glycans and identification of new substrates. PLoS One 2016;11:e0166119.

23. Tabarani G, Thépaut M, Stroebel D, Ebel C, Vivès C, Vachette P, et al. DC-SIGN neck domain is a pH-sensor controlling oligomerization:

SAXS and hydrodynamic studies of extracellular domain. J Biol Chem 2009;284:21229–40.

24. Arazi A, Rao DA, Berthier CC, Davidson A, Liu Y, Hoover PJ, et al. The immune cell landscape in kidneys of patients with lupus nephritis. Nat Immunol 2019;20:902.

25. Chui D, Sellakumar G, Green R, Sutton-Smith M, McQuistan T, Marek K, et al. Genetic remodeling of protein glycosylation in vivo induces autoimmune disease. Proc Natl Acad Sci U S A 2001;98:1142–7.

26. Urushihara M, Kagami S, Yasutomo K, Ito M, Kondo S, Kitamura A, et al. Sisters with α-mannosidosis and systemic lupus erythematosus. Eur J Pediatr 2004;163:192–5.

27. Van Kooyk Y, Rabinovich GA. Protein-glycan interactions in the control of innate and adaptive immune responses. Nat Immunol 2008;9:593–601.

Clinical Images: Rice bodies in cinematic rendering
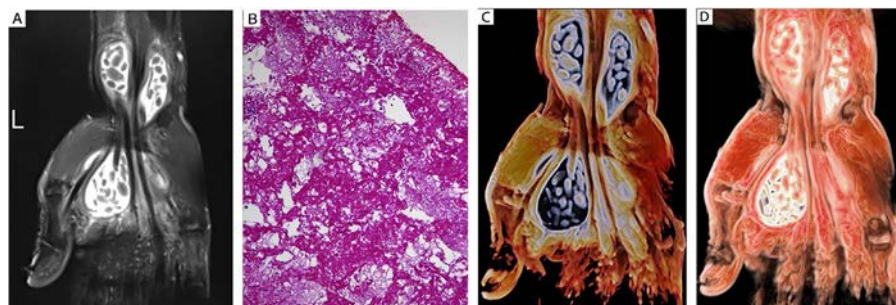
The patient, a 56-year-old man who had undergone resection of a cyst in his left wrist 2 years ago, presented to the orthopedics outpatient clinic with gradually increasing swelling over his left wrist and pain and numbness in the fingers of his left hand. The patient did not have a history of rheumatoid arthritis. Coronal magnetic resonance imaging (MRI) of the left wrist demonstrated the presence of fluid in the wrist and palmar tendon and multiple hypointense nodules within the effusion on T2-weighted imaging, indicating synovitis with "rice bodies" (**A**). The patient underwent surgery and numerous pea-sized loose bodies were extruded. Rice bodies are formed through hypertrophy and infarction, they primarily consist of collagen, fibrinogen, and inflammatory cells, and they are associated with rheumatoid arthritis and chronic infections (1). Findings of laboratory tests for rheumatoid factor, antinuclear antibodies, and anti–cyclic citrullinated peptide antibodies were normal; however, the patient's history, which included chronic pain and a previous cyst resection, suggested that the rice bodies resulted from chronic inflammation. Histopathologic analysis of the rice bodies showed prominent acidophilic, amorphous necrotic areas (**B**) (hematoxylin and eosin stained, original magnification × 200). Synovial hypertrophy in the patient's left wrist was further assessed using cinematic rendering on coronal MRI (**C** and **D**), which showed in greater detail the small white rice bodies (**C**) and the synovial hypertrophy and effusion (**D**). Cinematic rendering is a new 3-dimensional reconstruction technique that is a physically based volume rendering method (2). The technique models the real-life physical propagation of light by creating complex lighting effects such as ambient occlusion, shadows, multi-scattering, and color transmittance, which can provide more photorealistic images and describe complex anatomic structures more accurately (3). Cinematic rendering can more realistically show synovial hypertrophy and rice bodies, thereby allowing orthopedic surgeons and patients to more easily assess the severity of this disease.

1. Okura Y, Tsumagari S, Nawate M, Yoshioka M, Shikano T, Takahashi Y. Juvenile idiopathic arthritis with rice bodies in a 2-year-old girl. J Pediatr 2016;172:220.

2. Elshafei M, Binder J, Baecker J, Brunner M, Uder M, Weber GF, et al. Comparison of cinematic rendering and computed tomography for speed and comprehension of surgical anatomy. JAMA Surg 2019;154:738–44.

3. Dappa E, Higashigaito K, Fornaro J, Leschka S, Wildermuth S, Alkadhi H. Cinematic rendering: an alternative to volume rendering for 3D computed tomography imaging. Insights Imaging 2016;7:849–56.

Jian Liu, MS [ID]
Xinge Cheng, MS
Zunyi Medical University
Zunyi, China
and Guizhou Provincial People's Hospital
Guiyang, China
Rongpin Wang, PhD
Xianchun Zeng, MD [ID]
Guizhou Provincial People's Hospital
Guiyang, China

American College
of Rheumatology
Empowering Rheumatology Professionals

Prevalence of Antineutrophil Cytoplasmic Antibody–Associated Vasculitis and Spatial Association With Quarries in a Region of Northeastern France: A Capture–Recapture and Geospatial Analysis

Stéphane Giorgiutti,[1] (iD) Yannick Dieudonne,[1] Olivier Hinschberger,[2] Benoît Nespola,[3] Julien Campagne,[4] Hanta Nirina Rakotoarivelo,[5] Thierry Hannedouche,[3] Bruno Moulin,[3] Gilles Blaison,[5] Jean-Christophe Weber,[3] Marie-Caroline Dalmas,[3] Frédéric De Blay,[3] Dan Lipsker,[3] François Chantrel,[2] Jacques-Eric Gottenberg,[6] Yves Dimitrov,[7] Olivier Imhoff,[8] Pierre-Edouard Gavand,[9] Emmanuel Andres,[3] Christian Debry,[3] Yves Hansmann,[3] Alexandre Klein,[5] Caroline Lohmann,[2] François Mathiaux,[5] Aurélien Guffroy,[1] (iD) Vincent Poindron,[1] Thierry Martin,[1] Anne-Sophie Korganow,[1] and Laurent Arnaud[6] (iD)

Objective. Silica is an environmental substance strongly linked with autoimmunity. The aim of this study was to assess the prevalence of antineutrophil cytoplasmic antibody (ANCA)–associated vasculitis (AAV), including granulomatosis with polyangiitis (GPA), microscopic polyangiitis (MPA), and renal limited vasculitis, in a northeastern region of France and to evaluate whether there was a geospatial association between the localization of quarries in the region and the prevalence of these AAVs.

Methods. Potential AAV patients were identified using 3 sources: hospital records, immunology laboratories, and the French National Health Insurance System. Patients who resided in the Alsace region of France as of January 1, 2016 and who fulfilled the American College of Rheumatology criteria for GPA or the 2012 Chapel Hill Consensus Conference definitions for GPA or MPA were included. Incomplete case ascertainment was corrected using a capture–recapture analysis. The spatial association between the number of cases and the presence of quarries in each administrative entity was assessed using regression analyses weighted for geographic region.

Results. Among 910 potential AAV patients, we identified 185 patients fulfilling inclusion criteria: 120 patients with GPA, 35 patients with MPA, and 30 patients with renal limited vasculitis. The number of cases missed by any source as estimated by capture–recapture analysis was 6.4 (95% confidence interval [95% CI] 3.6–11.5). Accordingly, the estimated prevalence in Alsace in 2016 was 65.5 GPA cases per million inhabitants (95% CI 47.3–93.0), 19.1 MPA cases per million inhabitants (95% CI 11.3–34.3), and 16.8 renal limited vasculitis cases per million inhabitants (95% CI 8.7–35.2). The risk of AAV was significantly increased in communities with quarries (odds ratio 2.51 [95% CI 1.66–3.80]), and geographic-weighted regression analyses revealed a significant spatial association between the proximity to quarries and the number of GPA cases ($P = 0.039$). In analyses stratifying the AAV patients by ANCA serotype, a significant association between the presence of quarries and positivity for both proteinase 3 ANCAs ($P = 0.04$) and myeloperoxidase ANCAs ($P = 0.03$) was observed.

Conclusion. In a region with a high density of quarries, the spatial association between the presence of and proximity to quarries and the prevalence of AAVs supports the idea that silica may have a role as a specific environmental factor in this disease.

[1]Stéphane Giorgiutti, MD, Yannick Dieudonne, MD, Aurélien Guffroy, MD, PhD, Vincent Poindron, MD, PhD, Thierry Martin, MD, PhD, Anne-Sophie Korganow, MD, PhD: Le Centre National de Reference pour les Maladies Autoimmunes Systemiques Rares (CNR RESO), Hôpitaux Universitaires de Strasbourg, and Université de Strasbourg, INSERM UMR S1109, Strasbourg, France; [2]Olivier Hinschberger, MD, François Chantrel, MD, Caroline Lohmann, PharmaD: Hôpital Emile Muller, Groupe Hospitalier de la Région de Mulhouse et Sud Alsace, Mulhouse, France; [3]Benoît Nespola, PharmaD, Thierry Hannedouche, MD, PhD, Bruno Moulin, MD, PhD, Jean-Christophe Weber, MD, PhD, Marie-Caroline Dalmas, MD, Frédéric De Blay, MD, PhD, Dan Lipsker, MD, PhD, Emmanuel Andres, MD, PhD, Christian Debry, MD, PhD, Yves Hansmann, MD, PhD: Hôpitaux Universitaires de Strasbourg, Strasbourg, France; [4]Julien Campagne, MD: Hôpitaux Privés de Metz, Metz, France; [5]Hanta Nirina Rakotoarivelo, MD, Gilles Blaison, MD, Alexandre Klein, MD, François Mathiaux, MD: Hôpitaux Civils de Colmar, Colmar, France; [6]Jacques-Eric Gottenberg, MD, PhD, Laurent Arnaud, MD, PhD: Le Centre National de Reference pour les Maladies Autoimmunes Systemiques Rares (CNR RESO), Hôpitaux Universitaires de Strasbourg, Strasbourg,

INTRODUCTION

Granulomatosis with polyangiitis (GPA) and microscopic polyangiitis (MPA) are 2 types of primary systemic antineutrophil cytoplasmic antibody–associated vasculitis (AAV) that mainly affect small vessels (1). AAV commonly causes life-threatening multisystem manifestations with substantial long-term morbidity (2). GPA and MPA share many clinical and histopathologic systemic features, whereas renal limited AAV is characterized by pauci-immune glomerulonephritis without evidence of extrarenal disease. Studies addressing the epidemiology of AAV in different countries have shown various prevalence rates, ranging from 23.7 to 218 GPA cases per million inhabitants and 9 to 184 MPA cases per million inhabitants (3). Available data also suggest that AAV prevalence increases over time in different regions of the world (3–6). In 2000, in a northeastern suburb of Paris, France, the prevalence of AAV was estimated to be 23.7 GPA cases per million adults and 25.1 MPA cases per million adults (7).

The etiology of AAV remains largely unknown, but it is usually considered to be multifactorial. A specific genetic background, involving both the major histocompatibility complex (MHC) and non–MHC-linked loci, has been identified in genome-wide association studies (8). Environmental factors may also play an important role in the development of AAV. Since AAV frequently involves the respiratory tract, inhaled noninfectious agents are the leading candidates among putative triggers. Exposure to silica (SiO_2), an environmental substance strongly associated with causing overall autoimmunity, has particularly been associated with a higher risk of developing AAV (9). Quarries are important sources of crystalline silica exposure. However, to date, no study has demonstrated a geographic association between proximity to quarries and AAV.

Studying the epidemiology of rare diseases remains challenging, especially with regard to ensuring complete case detection. Alsace is a small region in northeastern France located next to Germany and Switzerland. Access to health care is high in Alsace, and there is a high density of physicians (10). Notably, due to the proximity of the Vosges mountains to the west, the density of quarries in Alsace is high compared to that of other French regions (11).

In the present study, we assessed the prevalence of GPA, MPA, and renal limited vasculitis in the Alsace region in 2016 using triple-source ascertainment and a capture–recapture analysis. Furthermore, considering the high density of quarries in Alsace, we assessed the spatial association between these diseases and the presence of quarries using geospatial analyses.

PATIENTS AND METHODS

Study area and population. The study was carried out in Alsace, an 8,280 km² region in northeastern France (see Supplementary Methods, available on the *Arthritis & Rheumatology* website at http://onlinelibrary.wiley.com/doi/10.1002/art.41767/abstract). This area has previously been used for epidemiologic studies of autoimmune and inflammatory diseases by our group (12,13). According to the French national Census, the population of Alsace in 2016 was 1,884,150 residents with an age distribution close to that of the global metropolitan French population. According to the French National Institute of Statistics and Economic Studies (Institut National des Statistiques et des Etudes Economiques [INSEE]), the population size has remained quite stable (within 1.7% of the current estimate) since the last census was conducted in 2011. Alsace comprised a total of 866 administrative entities in 2016 (French "communes," the smallest administrative geographic unit in France), with 93.3% of the subjects living in the same municipality as was reported by the subjects in 2015.

Study period and case ascertainment. The study encompassed the entire calendar year of 2016. Patients were identified using the following 3 separate sources: hospital records, ANCA serology, and the French National Health Insurance System.

All departments of medical specialties that were likely to diagnose AAV (internal medicine, rheumatology, nephrology, dermatology, pneumology, and otorhinolaryngology) in public hospitals or private clinics in the study area were approached. We contacted department heads and, when appropriate, additional medical staff members via email or telephone and asked them to participate in the study. Each department was contacted at least twice. Then, if the physician agreed, hospital personnel were asked to report the diagnosis applied to patients who received care in each department, using International Classification of Diseases, Tenth Revision (ICD-10) codes M31.3 (for diagnosis of GPA), M31.7 (for diagnosis of MPA), or M31.8 (for diagnosis of other conditions related to necrotizing vasculitis, including renal-limiting vasculitis) between January 1, 2007 and December 31, 2016.

Staff at 3 main publicly funded reference immunology laboratories in Alsace (Strasbourg, Mulhouse, and Colmar) were contacted and asked to report all patients with proteinase 3 (PR3)– and myeloperoxidase (MPO)–ANCA positivity from January 1, 2007 to December 31, 2016. Most hospitals and private practitioners from the study area work with these 3 accredited reference laboratories to screen or confirm ANCA positivity. ANCAs were assessed using indirect immunofluorescence staining in

France; [7]Yves Dimitrov, MD: Centre Hospitalier de Haguenau, Haguenau, France; [8]Olivier Imhoff, MD: Clinique Saint-Anne, Strasbourg, France; [9]Pierre-Edouard Gavand, MD: Clinique Rhéna, Strasbourg, France.

Drs. Giorgiutti and Dieudonne contributed equally to this work. Drs. Korganow and Arnaud contributed equally to this work.

No potential conflicts of interest relevant to this article were reported.

Address correspondence to Stéphane Giorgiutti, MD, Hôpitaux Universitaires de Strasbourg, Département d'Immunologie Clinique et de Médecine Interne, 1 Place de l'Hopital, Strasbourg 67091, France. Email: stephane.giorgiutti@chru-strasbourg.fr.

ethanol-fixed neutrophils, and PR3- or MPO-ANCA detection was performed using enzyme-linked immunosorbent assay.

The French National Health Insurance System (Caisse Primaire d'Assurance-Maladie) is compulsory for French residents and covers health care–related expenses for chronic and costly diseases, which allows for a reduction or elimination of health care costs for all patients, including those with chronic AAVs. In this system, detailed demographic and clinical information is provided by physicians. For the present study, members of the French National Health Insurance agency screened the database to identify all patients with ICD-10 diagnostic classifications of M31.3, M31.7, or M31.8 who were inhabitants of the study area and insured under the French National Health Insurance System. Patients provided their consent with regard to collection of these data.

For all 3 sources, the patient data, including the patient's initials, date of birth, sex, and postal code of residency, as well as the identity of the treating physician, were anonymized. The study was approved by the Commission Nationale de l'Informatique et des Libertés (National Commission of Informatics and Freedom approval no. 2001404) and by the Ethics Committee of the University of Strasbourg (approval no. 2017-46).

Case reviews and inclusion criteria. Duplicate cases were identified by matching the patient's initials, sex, and date of birth. A standardized questionnaire was used to collect demographic data, including the postal code of residence at the time of diagnosis and information to verify inclusion and classification criteria (including clinical, radiologic, histologic, and serologic features). All the medical charts were reviewed by 2 independent physicians (SG and YD) and were discussed with other investigators (A-SK and LA) in cases of discrepancy, until consensus was reached. A case was included if the patient was alive and resided in Alsace on January 1, 2016 and fulfilled either the American College of Rheumatology classification criteria for GPA (14) or the Chapel Hill Consensus Conference 2012 revised definition of systemic vasculitides for both GPA and MPA (1). Patients satisfying criteria for eosinophilic GPA (15) were excluded. Then, the European Medicines Agency (EMA) algorithm for the classification of AAV was used to distinguish between GPA and MPA (16). According to this algorithm, histologic evidence of vasculitis was not systematically required. Renal limited vasculitis was defined as pauci-immune glomerulonephritis without any extrarenal disease on the day of medical records review (1).

Statistical analysis and capture–recapture estimates. For descriptive statistics, continuous variables are presented as the median and range. Categorical variables are presented as numbers and percentages.

Capture–recapture analysis was used to estimate the degree of overlap in patient data collected from the 3 separate sources. Findings were used to identify the number of cases missed

by any of the sources and therefore the total number of cases. Some assumptions are required for an appropriate application of capture–recapture methods. 1) The individuals who appear in different sources can be matched. 2) Each individual has the same probability of ascertainment for each single source. 3) The sources of case ascertainment are independent. 4) The study population is closed (17). JMP 13 (SAS Institute) was used to build log-linear Poisson regression models in order to estimate the number of missed cases (with 95% confidence interval [95% CI]), after accounting for possible overlap between sources. Eight models were built, including one without any interaction term and others with all first-order interactions between the 3 sources (see Supplementary Methods, available on the *Arthritis & Rheumatology* website at http://onlinelibrary.wiley.com/doi/10.1002/art.41767/abstract). Model fit with and without interaction terms was assessed using Akaike's Information Criterion (AIC). The model without interaction between sources had the lowest AIC value and was selected as the best fitting model. The prevalence of GPA, MPA, and renal limited vasculitis in the region in 2016 was calculated using the prevalent number of cases of each disease as the numerator and the population in the Alsace region according to the 2016 French national Census as the denominator. The same method was applied in assessing the prevalence of AAV according to ANCA serotype (PR3 or MPO ANCAs).
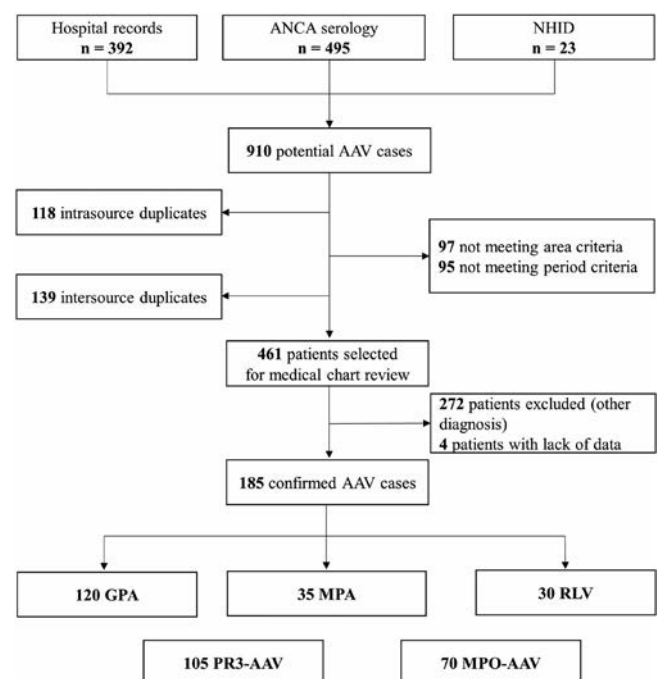

Figure 1. Flow chart depicting the identification of antineutrophil cytoplasmic antibody (ANCA)–associated vasculitis (AAV) cases. NHID = French National Health Insurance database; GPA = granulomatosis with polyangiitis; MPA = microscopic polyangiitis; RLV = renal limited vasculitis; PR3 = proteinase 3; MPO = myeloperoxidase.

Geostatistical analysis. Detailed information regarding the administrative divisions of Alsace and reference populations of those entities (communes) for the year 2016 was extracted from the French National Geographic Database Institut National de l'information Géographique et Forestière, Paris, France). Information on the localization of quarries in the Alsace region (as listed in on the Observatoire des matériaux website at http://infoterre.brgm.fr/page/geoservices-ogc) was obtained through the French National Bureau for Geological and Mining Research. Both active and closed quarries were included in the analysis. The odds ratios (ORs) for the risk of AAV in communes with quarries in comparison to the risk in communes without quarries were determined.

The spatial association between AAV cases and quarries in each administrative entity was then assessed using geographic-weighted regression models built using the R package geographic-weighted model. For these analyses, geographic Poisson regression models were built using the number of AAV cases in Alsace at the time of diagnosis as the dependent variable and the number of extraction sites within each administrative entity as the independent variable, with the 2016 French national Census reference population of the entity as an offset. The significance of the spatial variability of the geographic-weighted regression model coefficients was assessed using Monte Carlo simulation with 999 permutations (geographic-weighted model R package). Additionally, we simulated a random distribution of "virtual quarries" in Alsace and tested the spatial association between these random points and the number of AAV cases using the same approach.

The density of quarries in Alsace and Seine-Saint-Denis was calculated using the number of quarries divided by the surface of these areas (in km²) and compared using a multivariate Poisson regression model adjusted for the surface of these entities. Statistical analyses were performed using R version 3.6.1 software, JMP 13 (SAS institute), and GIS version 3.12 software QGIS. The same methodology was used to assess potential associations between each organ involved in AAV and proximity to quarries.

RESULTS

Sources and identification of AAV cases. A total of 910 potential eligible cases were identified. All hospitals that were contacted participated in the study except one primary-level hospital. A total of 392 potential cases were accessed from the hospital records. These cases were reported by the internal medicine departments (n = 238 cases), nephrology departments (n = 71), rheumatology departments (n = 35), dermatology departments (n = 19), pneumology departments (n = 24), and otorhinolaryngology departments (n = 5). The 3 laboratories and the French National Health Insurance System identified 495 and 23 potential cases, respectively. A total of 118 intra-source and 139 inter-source duplicates were excluded, and 192 additional cases were immediately eliminated based on demographic data indicating that they did not meet inclusion criteria for the study area or period. The remaining 461 cases were selected for medical chart review (Figure 1). None of the potentially eligible AAV patients declined to be included in the study.

Table 1. Characteristics of the study patients at the time of clinical assessment*

	Total (n = 185)	GPA (n = 120)	MPA (n = 35)	Renal limited vasculitis (n = 30)
Age at diagnosis, median (range) years	61 (12–91)	58 (13–91)	67 (12–89)	61 (30–82)
Sex, male	105 (57)	71 (59)	15 (43)	19 (63)
Disease duration, median (range) years	5 (0–26)	5 (0–22)	4 (0–19)	5 (0–26)
Organ involvement				
Renal	152 (82)	88 (73)	34 (97)	30 (100)
ENT	80 (43)	77 (64)	3 (9)	–
Pulmonary	103 (56)	83 (69)	20 (57)	–
Nervous system	41 (22)	35 (29)	6 (17)	–
Cutaneous	35 (19)	30 (25)	5 (14)	–
Eyes	22 (12)	21 (18)	1 (3)	–
Cardiovascular	15 (8)	9 (8)	6 (17)	–
Gastrointestinal	11 (6)	9 (8)	2 (6)	–
ANCA positivity	175 (95)	111 (93)	35 (100)	29 (97)
PR3	105 (57)	96 (80)	1 (3)	9 (30)
MPO	70 (38)	17 (14)	34 (97)	20 (67)
Histologic evidence of AAV	139 (75)	89 (74)	20 (57)	30 (100)
FFS at diagnosis, median (range)	1 (0–3)	1 (0–3)	1 (0–3)	–
BVAS at diagnosis, median (range)	14 (1–39)	15 (1–39)	15.5 (5–21)	–

* Except where indicated otherwise, values are the number (%) of patients. GPA = granulomatosis with polyangiitis; MPA = microscopic polyangiitis; ENT = ear, nose, and throat; ANCA = antineutrophil cytoplasmic antibody; PR3 = proteinase 3; MPO = myeloperoxidase; AAV = ANCA-associated vasculitis; FFS = Five-Factor Score (see ref. 30); BVAS = Birmingham Vasculitis Activity Score (see ref. 31).

Characteristics of the AAV patients. The thorough review of all medical charts resulted in exclusion of 272 patients (Figure 1). In most cases, exclusion was due to alternative diagnoses, especially in patients with positivity for ANCAs associated with other disorders, mainly inflammatory bowel diseases (n = 23), malignant diseases (n = 16), infectious diseases (n = 15), systemic lupus erythematosus (n = 12), autoimmune hepatitis (n = 5), drug-induced ANCA positivity (n = 6), large vessel vasculitis (n = 3), or other immune-related conditions (n = 42). Retrospective diagnosis data were not provided for 4 patients. The remaining 185 patients were thus included. The main clinical and demographic characteristics of these patients are summarized in Table 1. Most of the patients were male (57%), with a median age of 61 years at diagnosis (range 12–91). The median disease duration was 5 years (range 0–26). Based on an EMA algorithm, 120 patients were classified as having GPA, 35 were classified as having MPA, and 30 were classified as having renal limited vasculitis. Histopathologic evidence of vessel inflammation and/or granuloma was observed in 139 patients (75%). All the remaining patients with no histopathologic documentation tested positive for ANCAs. Anti-PR3 antibodies were the most frequently identified antibodies (n = 105 patients [57%]).

Capture–recapture analysis and prevalence estimates. Figure 2 shows the number of cases ascertained from each of the 3 sources and the source overlap. Fifty-four cases were derived from a single source, 123 were derived from 2 sources, and 8 were derived from all 3 sources. Hospital records were the source of the most cases, identifying 160 of the 185 patients (86%). Accordingly, the number of cases missed by any source as estimated by capture–recapture analysis was 6.4 (95% CI 3.6–11.5), yielding an estimated total number of 191 AAV cases and a 96.6% completeness of case finding. Based on this model, the estimated prevalence of AAV (excluding eosinophilic GPA) in Alsace in 2016 was 101.5 cases per million inhabitants (95% CI 76.3–137.7), with 65.5 GPA cases per million inhabitants (95% CI 47.3–93.0), 19.1 MPA cases per million inhabitants (95% CI 11.3–34.3), and 16.8 renal limited vasculitis cases per million inhabitants (95% CI 8.7–35.2). Regarding ANCA serotype, the prevalence was 56.9 PR3-AAV cases per million inhabitants (95% CI 29.7–90.2) and 38.1 MPO-AAV cases per million inhabitants (95% CI 18.6–64.8).

Findings from geostatistical analyses. Among the 185 patients, 6 who did not reside in Alsace at the time of diagnosis were excluded from the geospatial analysis. The risk of AAV was significantly increased in communes with quarries versus those without quarries (OR 2.51 [95% CI 1.66–3.80]); specifically, there was an increased risk for GPA (OR 3.21 [95% CI 1.96–5.25]) and for renal limited vasculitis (OR 3.1 [95% CI 1.12–8.51]), but not for MPA (OR 1.10 [95% CI 0.50–2.41]).

We confirmed these findings using geographic-weighted regression analyses taking into account the spatial interactions between communes. The results of this analysis demonstrated a
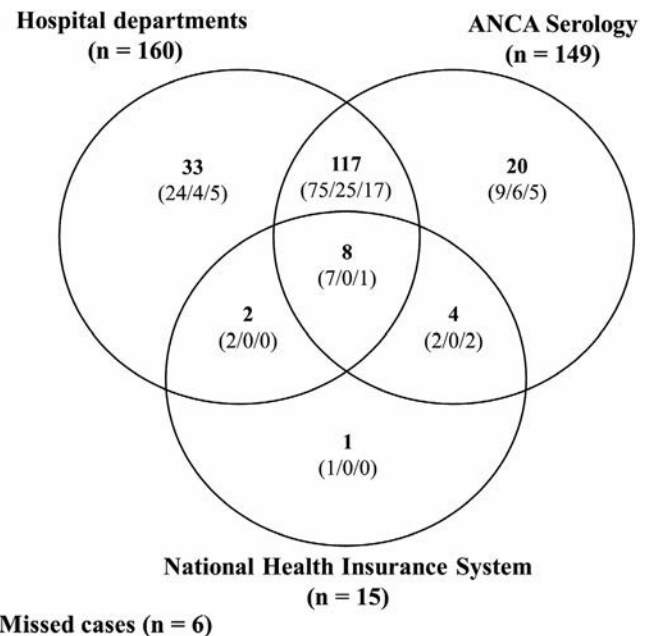
Figure 2. Venn diagram showing the distribution of cases ascertained using each of the 3 sources (hospital departments, ANCA serology, and the French National Health Insurance System). The values in parentheses within the diagram are the number of cases of GPA/MPA/renal limited AAV. See Figure 1 for definitions.

significant spatial association between the number of GPA cases and proximity to quarries (P = 0.039) (Figure 3). Conversely, we detected no spatial association between the number of GPA cases and the number of randomly distributed points as there are quarries in Alsace (P = 0.58) (for details, see Supplementary Methods, available on the *Arthritis & Rheumatology* website at http://online library.wiley.com/doi/10.1002/art.41767/abstract). This further suggests that the significant spatial association between GPA cases and proximity to quarries was not random. Although findings were close to the significance threshold, we found no significant association between the number of MPA cases (P = 0.067) or the number of renal limited vasculitis cases (P = 0.066) and proximity to extraction sites. Moreover, results of the geospatial analysis were not statistically significant when we considered AAV as a whole group (P = 0.18).

When we applied the same method based on ANCA serotype, the risk of PR3-AAV and MPO-AAV was found to be significantly increased in communes with quarries versus those without quarries (OR 2.95 [95% CI 1.76–4.94] and OR 2.32 [95% CI 1.22–4.39], respectively). Using geographic-weighted regression models, we found a significant association between the presence of quarries and PR3-AAV (P = 0.04) as well as MPO-AAV (P = 0.03) (Supplementary Figure 1, available on the *Arthritis & Rheumatology* website at http://onlinelibrary.wiley.com/doi/10.1002/art.41767/abstract). Furthermore, the risk of respiratory involvement, renal involvement, and ear, nose, and throat (ENT) involvement was significantly increased in communes with quarries versus those without quarries (OR 1.96 [95% CI 1.20–3.20], OR 2.41 [95% CI
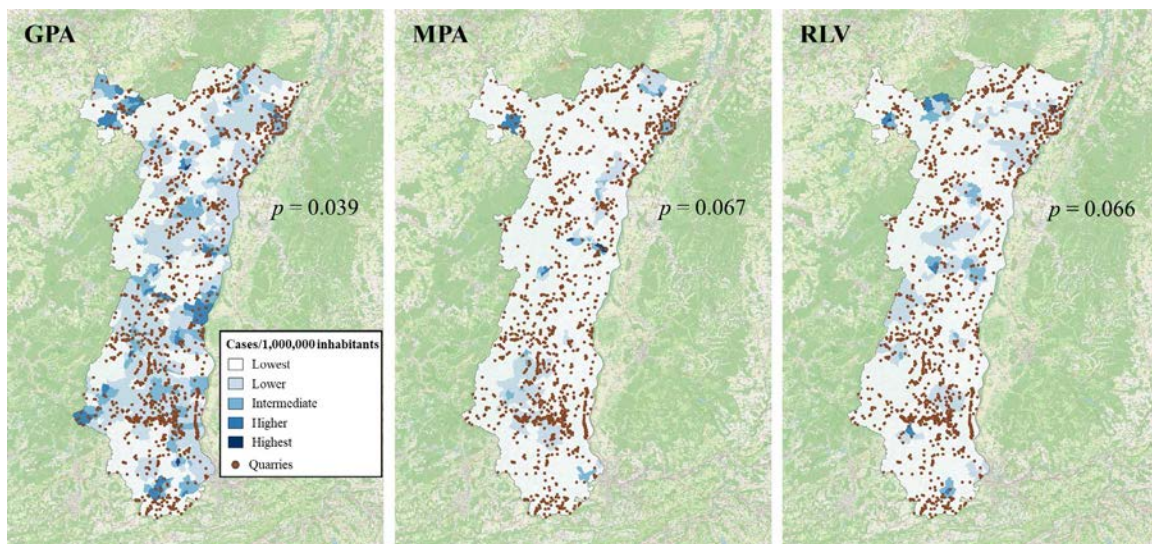
Figure 3. Spatial association between the number of AAV cases per million inhabitants and proximity to quarries. Each panel shows the significance of the spatial association between quarries in the Alsace region of France and the normalized prevalence of GPA, MPA, and RLV. Data were subjected to spatial Bayesian smoothing using Jenks natural breaks. See Figure 1 for definitions.

1.55–3.76], and OR 3.33 [95% CI 1.80–6.16], respectively), but using geographic-weighted regression, a significant spatial association with quarries was only identified for renal involvement and ENT involvement (Supplementary Table 1).

DISCUSSION

Using a capture–recapture technique, our population-based study provides a detailed analysis of the epidemiology and characteristics of AAV in the Alsace region of France, an area of western Europe. The estimated prevalence of GPA, MPA, and renal limited vasculitis in this region of France in 2016 was 65.5, 19.1, and 16.8 cases per million inhabitants, respectively. Findings of the geospatial analysis demonstrated a significant spatial association in Alsace between proximity to quarries and GPA but not between proximity to quarries and MPA or renal limited vasculitis.

The prevalence estimates for GPA and MPA in Alsace are similar to those observed in other European countries over the last 20 years. Studies addressing the epidemiology of AAV in the UK, Germany, or Sweden showed a prevalence of GPA ranging from 58 to 160 cases per million inhabitants and a prevalence of MPA ranging from 9 to 94 cases per million inhabitants (5,18,19). In France, only one study has used the same methodology as our study. In that prior study, the prevalence of AAV was reported to be 25.1 cases per million adults, and the prevalence of GPA was reported to be 23.7 cases per million adults in the year 2000 in Seine-Saint-Denis, a northeastern suburb of Paris (7). Notably, the prevalence of GPA in our study was almost 3 times higher than that observed in the study from Seine-Saint-Denis, while the prevalence of MPA was comparable.

In our study, the higher prevalence of GPA may reflect either an increase in the incidence of AAV, improvement in disease diagnosis

or patient survival, or differences in study population or inclusion criteria. However, we used the same criteria as those applied by Mahr et al (7), although histologic evidence of diagnostic classification was not required for inclusion in our study, in accordance with the EMA algorithm (16). In their study, Mahr and colleagues did not distinguish renal limited vasculitis from MPA, which may have increased the MPA prevalence estimation, since renal limited vasculitides are more likely associated with anti-MPO antibodies than with anti-PR3 antibodies (20). Also, while no information about the ethnic background of participants was formally collected due to French laws, it is likely that the mix of ethnicities in the two areas differs between our study and the study by Mahr et al (21), suggesting a possible different genetic background. Indeed, the proportion of immigrants in Alsace was 11.2% in 2016 according to the INSEE census, suggesting that most of our patients are of White descent, whereas immigrants with differing ethnic backgrounds represent ~30% of the population in Seine-Saint-Denis.

Another possible explanation for the higher prevalence of AAV in Alsace could be environmental factors, which is supported by studies showing temporal and/or seasonal fluctuations of disease occurrence (22) and a north–south gradient, with GPA occurring more frequently in northern countries and MPA occurring more frequently in southern countries (23). In a multivariate analysis, Weiner et al showed an association between ANCA serotype and latitude and ultraviolet radiation levels (24). Among other environmental triggers, infections (including infection attributable to *Staphylococcus*), solvents, or pesticides are worthwhile candidates for future study (22,25).

Despite the controversial aspects of these findings and the heterogeneity of the studies, exposure to crystalline silica has also been associated with a higher risk of developing AAV (9), especially in workers with specific jobs such as farming, mill and textile work,

sandblasting, and drilling (26). However, to the best of our knowledge, our study is the first to demonstrate a geospatial association between AAV and proximity to quarries. Quarries are an important source of dust emissions, including crystalline silica. Few data are available regarding nonoccupational exposure to silica dust in the vicinity of quarries, but Peng et al reported that quarry mining dust contributed to 6% of the fine particle exposure in a city adjacent to a limestone quarry in China (27). In Alsace, most of the quarries are related to the alluvial plains of the Rhine river, where sand and gravel are used for the creation of concrete (11). Interestingly, the density of quarries was significantly higher in Alsace than in Seine-Saint-Denis (0.19/km² compared to 0.14/km²; $P = 0.002$) according to the French National Geographic database. The geospatial association between MPA or renal limited vasculitis and quarries was not statistically significant. However, the study may have been underpowered to demonstrate such an association, due to the limited number of cases of those two diseases. Nevertheless, the association between quarries and both PR3- and MPO-AAV further supports idea that silica exposure has a role in AAV, regardless of clinical subgroup such as GPA, MPA, or renal limited vasculitis.

The pathogenic link between silica exposure and the development of AAV is not well understood, but in several studies, researchers have found MPO positivity after silica exposure (28), which is presumed to increase apoptosis of neutrophils and exposure of corresponding antigens to the adaptative immune system (26). Silica may also induce the inflammatory response and apoptosis of pulmonary macrophages. As a consequence, the increased exposure to self antigens in a proinflammatory environment may lead to loss of tolerance and systemic manifestations (29). Of interest, a spatial association was found between proximity to quarries and renal involvement using geographic-weighted regression models. This finding supports the findings of the meta-analysis by Gómez-Puerta et al, which included 6 studies predominantly examining renal involvement (9).

The main strengths of our study include extensive case identification using a capture–recapture analysis of 3 independent sources, and the low estimated number of missing cases, although the limited number of cases identified using the French National Health Insurance System may raise concerns regarding incomplete ascertainment. We hypothesize that some patients may have refused to be included in the French National Health Insurance System database or that some cases of AAV may have been under-declared or incorrectly declared due to the frequency of comorbidities, such as chronic kidney disease. Furthermore, Alsace is a small region with a high density of medical centers and is the location of a national reference center for rare autoimmune diseases. Therefore, patients are unlikely to seek care outside of the region, supporting the idea that the number of AAV cases identified in the region was fairly complete (12,13). Independent review of each case file by different investigators has likely also helped confirm the accuracy of the diagnoses in the region.

The main limitation of our study is that the geospatial association between proximity to quarries and AAV cases is merely an indirect representation of crystalline silica exposure. First, the address recorded for each patient at the time of diagnosis does not necessarily correspond to the location where the patient resided for most of the prediagnosis period, thus confounding the relationship between environmental exposures and AAV risk. The latency period between the beginning of the exposure to silica and the diagnosis of AAV is frequently >20 years (9). Second, we were not able to quantify the degree of exposure or establish a "dose effect" relationship. Quarry dust contains other crystalline materials, such as aluminum or iron oxides, and the involvement of other inhaled particles in the development of AAV cannot be excluded.

In conclusion, the present study reveals a higher prevalence of GPA in a northeastern French region with a high density of quarries, compared to results from a previous study in France. Findings demonstrate a geospatial association between AAV and proximity to quarries and support the idea that silica may have a role as a specific environmental factor. Further studies should investigate the relationship of the duration and intensity of exposure to inhaled particles, including crystalline silica, development of AAV.

AUTHOR CONTRIBUTIONS

All authors were involved in drafting the article or revising it critically for important intellectual content, and all authors approved the final version to be published. Dr. Giorgiutti had full access to all of the data in the study and takes responsibility for the integrity of the data and the accuracy of the data analysis.

Study conception and design. Giorgiutti, Dieudonne, Poindron, Martin, Korganow, Arnaud.

Acquisition of data. Giorgiutti, Dieudonne, Hinschberger, Nespola, Campagne, Rakotoarivelo, Hannedouche, Moulin, Blaison, Weber, Dalmas, De Blay, Lipsker, Chantrel, Gottenberg, Dimitrov, Imhoff, Gavand, Andres, Debry, Hansmann, Klein, Lohmann, Mathiaux, Guffroy, Poindron, Martin, Korganow, Arnaud.

Analysis and interpretation of data. Giorgiutti, Dieudonne, Gavand, Guffroy, Korganow, Arnaud.

REFERENCES

1. Jennette JC, Falk RJ, Bacon PA, Basu N, Cid MC, Ferrario F, et al. 2012 revised International Chapel Hill Consensus Conference Nomenclature of Vasculitides. Arthritis Rheum 2013;65:1–11.

2. Flossmann O, Berden A, de Groot K, Hagen C, Harper L, Heijl C, et al. Long-term patient survival in ANCA-associated vasculitis. Ann Rheum Dis 2011;70:488–94.

3. Mohammad AJ. An update on the epidemiology of ANCA-associated vasculitis [review]. Rheumatology (Oxford) 2020;59 Suppl 3:iii42–50.

4. Berti A, Cornec D, Crowson CS, Specks U, Matteson EL. The epidemiology of antineutrophil cytoplasmic autoantibody–associated vasculitis in Olmsted County, Minnesota: a twenty-year US population–based study. Arthritis Rheumatol 2017;69:2338–50.

5. Herlyn K, Buckert F, Gross WL, Reinhold-Keller E. Doubled prevalence rates of ANCA-associated vasculitides and giant cell arteritis between 1994 and 2006 in northern Germany. Rheumatology (Oxford) 2014;53:882–9.

6. Nilsen AT, Karlsen C, Bakland G, Watts R, Luqmani R, Koldingsnes W. Increasing incidence and prevalence of ANCA-associated vasculitis in Northern Norway. Rheumatology (Oxford) 2020;59:2316–24.

7. Mahr A, Guillevin L, Poissonnet M, Aymé S. Prevalences of polyarteritis nodosa, microscopic polyangiitis, Wegener's granulomatosis, and Churg-Strauss syndrome in a French urban multiethnic population in 2000: a capture–recapture estimate. Arthritis Rheum 2004;51:92–9.

8. Lyons PA, Rayner TF, Trivedi S, Holle JU, Watts RA, Jayne DR, et al. Genetically distinct subsets within ANCA-associated vasculitis. N Engl J Med 2012;367:214–23.

9. Gómez-Puerta JA, Gedmintas L, Costenbader KH. The association between silica exposure and development of ANCA-associated vasculitis: systematic review and meta-analysis. Autoimmun Rev 2013;12:1129–35.

10. Institut national de la statistique et des études économiques. Professionnels de santé au 1 janvier 2018. April 2020. URL: https://www.insee.fr/fr/statistiques/2012677#tableau-TCRD_068_tab1_departements.

11. Les Schémas Départementaux des carrières: DREAL Grand Est. April 2021. URL: http://www.grand-est.developpement-durable.gouv.fr/les-schemas-departementaux-des-carrieres-r143.html.

12. Spielmann L, Arnaud L, Severac F, Messer L, Mahé A, Meyer A, et al. Population-based prevalence of eosinophilic fasciitis (Shulman syndrome): a capture-recapture study. Br J Dermatol 2018;179:516–7.

13. Meyer A, Chifflot H, Chatelus E, Kleinmann JF, Ronde-Ousteau C, Klein D, et al. Spatial heterogeneity of systemic sclerosis in France: high prevalence in the northeast region. Arthritis Rheumatol 2016;68:1731–7.

14. Leavitt RY, Fauci AS, Bloch DA, Michel BA, Hunder GG, Arend WP, et al. The American College of Rheumatology 1990 criteria for the classification of Wegener's granulomatosis. Arthritis Rheum 1990;33:1101–7.

15. Masi AT, Hunder GG, Lie JT, Michel BA, Bloch DA, Arend WP, et al. The American College of Rheumatology 1990 criteria for the classification of Churg-Strauss syndrome (allergic granulomatosis and angiitis). Arthritis Rheum 1990;33:1094–100.

16. Watts R, Lane S, Hanslik T, Hauser T, Hellmich B, Koldingsnes W, et al. Development and validation of a consensus methodology for the classification of the ANCA-associated vasculitides and polyarteritis nodosa for epidemiological studies. Ann Rheum Dis 2007;66:222–7.

17. Hook EB, Regal RR. Capture-recapture methods in epidemiology: methods and limitations [review]. Epidemiol Rev 1995;17:243–64.

18. Mohammad AJ, Jacobsson LT, Mahr AD, Sturfelt G, Segelmark M. Prevalence of Wegener's granulomatosis, microscopic polyangiitis, polyarteritis nodosa and Churg-Strauss syndrome within a defined population in southern Sweden. Rheumatology (Oxford) 2007;46:1329–37.

19. Watts RA, Lane SE, Bentham G, Scott DG. Epidemiology of systemic vasculitis: a ten-year study in the United Kingdom. Arthritis Rheum 2000;43:414–19.

20. Jennette JC, Nachman PH. ANCA glomerulonephritis and vasculitis [review]. Clin J Am Soc Nephrol 2017;12:1680–91.

21. Institut national de la statistique et des études économiques. IMG1B–population immigrée par sexe, âge et pays de naissance en 2009: département de la Seine-Saint-Denis (93). June 2012. URL: https://www.insee.fr/fr/statistiques/2044111?sommaire=2131811&geo=DEP-93.

22. Watts RA, Mahr A, Mohammad AJ, Gatenby P, Basu N, Flores-Suárez LF. Classification, epidemiology and clinical subgrouping of antineutrophil cytoplasmic antibody (ANCA)-associated vasculitis [review]. Nephrol Dial Transplant 2015;30 Suppl 1:i14–22.

23. Watts RA, Gonzalez-Gay MA, Lane SE, Garcia-Porrua C, Bentham G, Scott DG. Geoepidemiology of systemic vasculitis: comparison of the incidence in two regions of Europe. Ann Rheum Dis 2001;60:170–2.

24. Weiner M, Bjørneklett R, Hrušková Z, Mackinnon B, Poulton CJ, Sindelar L, et al. Proteinase-3 and myeloperoxidase serotype in relation to demographic factors and geographic distribution in antineutrophil cytoplasmic antibody-associated glomerulonephritis. Nephrol Dial Transplant 2019 01;34:301–8.

25. Knight A, Sandin S, Askling J. Occupational risk factors for Wegener's granulomatosis: a case-control study. Ann Rheum Dis 2010;69:737–40.

26. Chen M, Kallenberg CG. The environment, geoepidemiology and ANCA-associated vasculitides [review]. Autoimmun Rev 2010;9:A293–8.

27. Peng X, Shi GL, Zheng J, Liu JY, Shi XR, Xu J, et al. Influence of quarry mining dust on PM2.5 in a city adjacent to a limestone quarry: seasonal characteristics and source contributions. Sci Total Environ 2016;550:940–9.

28. De Lind van Wijngaarden RA, van Rijn L, Hagen EC, Watts RA, Gregorini G, Tervaert JW, et al. Hypotheses on the etiology of antineutrophil cytoplasmic autoantibody associated vasculitis: the cause is hidden, but the result is known. Clin J Am Soc Nephrol 2008;3:237–52.

29. Pollard KM. Silica, silicosis, and autoimmunity [review]. Front Immunol 2016;7:97.

30. Guillevin L, Pagnoux C, Seror R, Mahr A, Mouthon L, Le Toumelin P, French Vasculitis Study Group. The Five-Factor Score revisited: assessment of prognoses of systemic necrotizing vasculitides based on the French Vasculitis Study Group (FVSG) cohort. Medicine (Baltimore) 2011;90:19–27.

31. Mukhtyar C, Lee R, Brown D, Carruthers D, Dasgupta B, Dubey S, et al. Modification and validation of the Birmingham Vasculitis Activity Score (version 3). Ann Rheum Dis 2009;68:1827–32.

AMERICAN COLLEGE
of RHEUMATOLOGY
Empowering Rheumatology Professionals

B Cell Depletion Inhibits Fibrosis via Suppression of Profibrotic Macrophage Differentiation in a Mouse Model of Systemic Sclerosis

Hiroko Numajiri,[1] Ai Kuzumi,[1] Takemichi Fukasawa,[1] Satoshi Ebata,[1] (iD) Asako Yoshizaki-Ogawa,[1] Yoshihide Asano,[1] Yutaka Kazoe,[2] Kazuma Mawatari,[3] Takehiko Kitamori,[3] Ayumi Yoshizaki,[1] (iD) and Shinichi Sato[1]

Objective. We undertook this study to investigate the effect of B cell depletion on fibrosis in systemic sclerosis (SSc) and its mechanism of action.

Methods. Mice with bleomycin-induced SSc (BLM-SSc) were treated with anti-CD20 antibody, and skin and lung fibrosis were histopathologically evaluated. T cells and macrophages were cocultured with B cells, and the effect of B cells on their differentiation was assessed by flow cytometry. We also cocultured B cells and monocytes from SSc patients and analyzed the correlation between fibrosis and profibrotic macrophage induction by B cells.

Results. B cell depletion inhibited fibrosis in mice with BLM-SSc. B cells from mice with BLM-SSc increased proinflammatory cytokine–producing T cells in coculture. In mice with BLM-SSc, B cell depletion before BLM treatment (pre-depletion) inhibited fibrosis more strongly than B cell depletion after BLM treatment (post-depletion) ($P < 0.01$). However, the frequencies of proinflammatory T cells were lower in the post-depletion group than in the pre-depletion group. This discrepancy suggests that the effect of B cell depletion on fibrosis cannot be explained by its effect on T cell differentiation. On the other hand, profibrotic macrophages were markedly decreased in the pre-depletion group compared to the post-depletion group ($P < 0.05$). Furthermore, B cells from mice with BLM-SSc increased profibrotic macrophage differentiation in coculture ($P < 0.05$). In SSc patients, the extent of profibrotic macrophage induction by B cells correlated with the severity of fibrosis ($P < 0.0005$).

Conclusion. These findings suggest that B cell depletion inhibits tissue fibrosis via suppression of profibrotic macrophage differentiation in mice with BLM-SSc, providing a new rationale for B cell depletion therapy in SSc.

INTRODUCTION

Systemic sclerosis (SSc) is an autoimmune disease primarily consisting of 3 pathologic manifestations: fibrosis, vasculopathy, and autoimmune abnormalities. Fibrosis of internal organs, interstitial lung disease (ILD) in particular, is often life-threatening (1). Although the pathogenesis of SSc is still unknown, a previous study has shown that B cells from SSc patients are activated via downstream signaling of CD19, a positive regulator molecule specifically expressed on the surface of B cells, suggesting that B cells play an important role in the development of SSc (2).

Recent advances in immunology have shown that B cells not only produce antibodies but also have a variety of functions and play a central role in the immune system (3–6). One of the important functions of B cells is to produce a variety of cytokines. For example, interleukin-6 (IL-6) produced by B cells binds to the IL-6 receptor and induces phosphorylation of STAT3 (7). Phosphorylated STAT3 acts as a transcription factor, leading to the production of inflammatory cytokines and increased expression of cell adhesion molecules, resulting in a further inflammatory response. It has been also suggested that B cells activate and differentiate immune cells, such as T cells and macrophages, through cytokines.

[1]Hiroko Numajiri, MD, PhD, Ai Kuzumi, MD, PhD, Takemichi Fukasawa, MD, PhD, Satoshi Ebata, MD, PhD, Asako Yoshizaki-Ogawa, MD, PhD, Yoshihide Asano, MD, PhD, Ayumi Yoshizaki, MD, PhD, Shinichi Sato, MD, PhD: University of Tokyo Graduate School of Medicine, Tokyo, Japan; [2]Yutaka Kazoe, PhD: Keio University School of Integrated Design Engineering, Tokyo, Japan; [3]Kazuma Mawatari, PhD, Takehiko Kitamori, PhD: University of Tokyo Graduate School of Engineering, Tokyo, Japan.

Drs. Numajiri and Kuzumi contributed equally to this work.

B cells are thought to play a central role in autoimmune diseases. It has been suggested that T cells differentiated into Th2 cells produce Th2 cytokines such as IL-4 and IL-13 and exacerbate fibrotic lesions in SSc (8). Macrophages can be classified into antifibrotic macrophages and profibrotic macrophages according to their functions (9). Antifibrotic macrophages have an inflammatory function, leading to tissue destruction by producing free radicals. In contrast, profibrotic macrophages produce profibrotic mediators, such as CCL18, and the resulting tissue remodeling exacerbates fibrosis (10,11). Taken together, these findings suggest that profibrotic macrophages are more closely involved in SSc development than antifibrotic macrophages. Thus, the immune cells differentiated by B cells are thought to be involved in the pathogenesis of SSc.

Many studies have suggested that B cell depletion therapy using antibodies against CD20, which is specifically expressed on B cells, is an outstanding treatment for many autoimmune diseases (12). Recently, it has been shown that B cell depletion therapy is also effective for SSc (13–17). However, it is still poorly understood how B cell depletion inhibits SSc pathogenesis. In this study, we examined the impact of B cell depletion on SSc development using a mouse model of bleomycin-induced SSc (BLM-SSc), a widely used model of SSc, and using specimens from human SSc patients. Moreover, we investigated the mechanism by which B cell activity may lead to the development of SSc.

PATIENTS AND METHODS

BLM-SSc mouse model. BLM (200 μg; Nippon Kayaku) dissolved in phosphate buffered saline (PBS) or control PBS was injected subcutaneously into a single location on the backs of 8-week-old female wild-type (WT) mice (C57BL/6) or CD22$^{-/-}$

mice, every other day (referred to as the non-depletion group). CD22$^{-/-}$ mice were backcrossed for more than 10 generations onto the C57BL/6 background. Anti-mouse CD20 monoclonal antibodies (BioLegend), which deplete mouse B cells, were injected every 2 weeks from either 1 week before BLM treatment (the pre-depletion group) or 2 weeks after BLM treatment (the post-depletion group). After 4 weeks of BLM treatment, samples were collected (Figures 1A and B). Mice were obtained from The Jackson Laboratory. In this study, every experiment was performed ≥3 times with a minimum of 5 mice. All studies and procedures were approved by the Institutional Animal Care and Use Committee of the University of Tokyo.

Histologic assessment and immunohistochemistry. All skin sections were obtained from the paramidline, lower back region in mice. Sections were stained with hematoxylin and eosin. Immunohistochemistry was performed using antibodies against CD206 (Abcam) and secondary Alexa Fluor 488–conjugated antibodies (Abcam).

Flow cytometry. Single-cell suspensions from the spleen and lungs of mice were prepared as previously described (18). For surface staining, cells were stained with antibodies against CD19 (eBioscience), CD4 (BioLegend), F4/80 (BioLegend), CD11b (BioLegend), CD11c (BioLegend), CD206 (BioLegend), I-A/I-E (eBioscience), CD80 (eBioscience), and CD86 (eBioscience). For intracellular cytokine staining, cells were stimulated with 10 ng/ml phorbol myristate acetate and 1 μg/ml ionomycin (Sigma-Aldrich) in the presence of 1 mg/ml brefeldin A (BioLegend) for 5 hours. Cells were washed, stained for CD19 or CD4, treated with fixation/permeabilization buffer, and stained with antibodies against
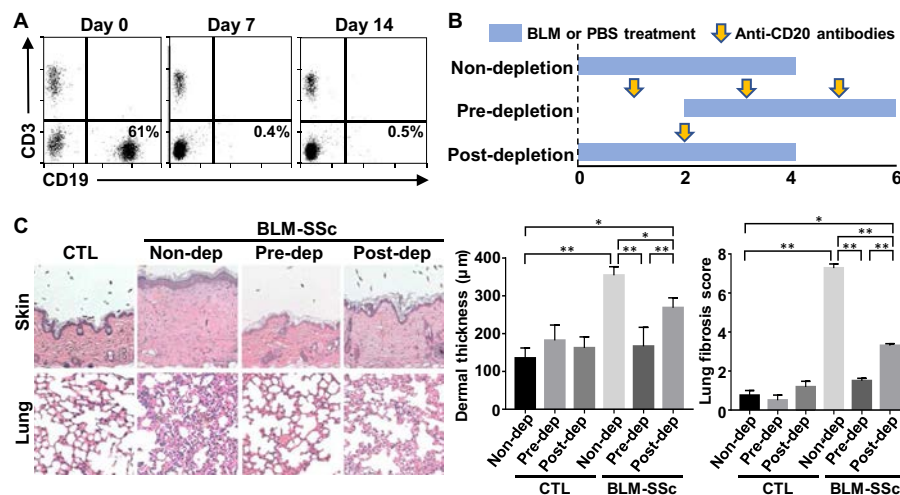
Figure 1. Antifibrotic effects of B cell depletion on mice with bleomycin-induced systemic sclerosis (BLM-SSc). **A**, In mice treated with anti-CD20 antibody, splenic B cells were almost completely eliminated after 7 days, and the elimination effect was maintained 14 days later. **B**, The effect of B cell depletion on mice with BLM-SSc was studied in the B cell non-depletion (Non-dep) group, the pre-depletion (Pre-dep) group, and the post-depletion (Post-dep) group. **C**, B cell depletion inhibited skin sclerosis and pulmonary fibrosis in mice with BLM-SSc, and the inhibitory effect of anti-CD20 antibody treatment was higher in the pre-depletion group than in the post-depletion group. Original magnification × 100. Bars show the mean ± SD. * = $P < 0.05$; ** = $P < 0.01$. PBS = phosphate buffered saline; CTL = control.

interferon-γ (IFNγ), IL-4, IL-6, IL-10, and IL-17A (all from eBioscience). For staining of transcriptional factors and intracellular proteins, antibodies against STAT3 (BioLegend), arginase 1 (eBioscience), Ym1 (R&D Systems), and FIZZ-1 (eBioscience) were used. Antifibrotic macrophages were defined as CD11b+F4/80+CD206– CD11c+ cells, and profibrotic macrophages were defined as CD11b+F4/80+CD206+CD11c– cells, as previously described (19,20). Cells were analyzed using a FACSVerse flow cytometer (BD Biosciences) and Kaluza (Beckman Coulter).

Coculture assay. Murine splenic macrophages, B cells, and T cells from control mice and mice with BLM-SSc were prepared. Cells were isolated with CD45R/B220 magnetic particles, CD4 T Lymphocyte Enrichment Set-DM, and CD11b magnetic particles (all from BD Bioscience). The purity of these cells was measured by flow cytometry. T cells (1×10^6 cells) and B cells (1×10^6 cells), or macrophages (1×10^6 cells) and B cells (1×10^6 cells), were cocultured in 60-mm plates or Transwells (Falcon) for 72 hours. Next, cells were analyzed on a flow cytometer. In some experiments, cocultured cells were treated with anti-mouse IL-4 (eBioscience), IL-6 (eBioscience), CD11a (Abcam), or CD22 (R&D Systems) antibodies. In some experiments, B cells were cultured 24 hours with monensin (eBioscience) before the coculture and were confirmed to be viable and to show no IL-6 release. Cytokine expression in culture supernatant was analyzed by specific enzyme-linked immunosorbent assay (ELISA) kits for CCL18 (LSBio), tumor necrosis factor (TNF) (R&D Systems), IL-10 (R&D Systems), and transforming growth factor β1 (TGFβ1) (R&D Systems). To analyze the secretion of TNF, IL-10, and TGFβ1 from macrophages cocultured with B cells, macrophages were isolated using CD11b magnetic particles (BD Bioscience) and stimulated for 5 hours with 100 ng/ml lipopolysaccharide (Sigma).

Human peripheral blood B cells and monocytes were also obtained from 5 healthy controls and 15 SSc patients who fulfilled the American College of Rheumatology and European Alliance of Associations for Rheumatology criteria (21). Human B cells and monocytes were isolated using magnetic bead isolation kits according to the manufacturer's instructions (Stem Cell Technologies). Each of these cells was cocultured in a 96-well plate with 5×10^4 cells per well for 72 hours. These cells were homogenized with lysis buffer containing complete protease inhibitor mixture (Roche Diagnostics), as previously described (22). The homogenates were centrifuged at 12,000 revolutions per minute for 15 minutes, and the supernatants were analyzed using a microfluidic ELISA system (23–25). This system can measure very low concentrations (10–1,000 fg/ml) of several proteins using a bead-bed immunoassay located in a microchip composed of 5–100-μm depth of flow channels. In this study, CD206 expression levels were measured by a microfluidic ELISA system using capture and detection antibodies obtained commercially (eBioscience). This study was approved by the Ethics Committee of the University of Tokyo Graduate School of Medicine and was performed according to the Declaration of Helsinki.

RNA isolation and real-time polymerase chain reaction (PCR). Total RNA was isolated from the skin and lung tissue of mice by RNeasy Spin Columns according to the manufacturer's instructions (Qiagen). Total RNA was reverse-transcribed into complementary DNA (cDNA). Gene expression was quantified using SYBR Green Real-Time PCR Master Mix (Toyobo) and analyzed with an ABI Prism 7000 Sequence Detector (Applied Biosystems). To normalize the amounts of loaded cDNA, GAPDH was used as an internal control. Relative fold differences were calculated by the comparative C_t method as previously described (22). The sequences of primers for TGFβ1 are as follows: forward 5′-GCAACATGTGGAACTCTACCAGAA-3′, reverse 5′-GACGTCAAAAGACAGCCACTCA-3′.

Statistical analysis. Distributions of 2 unmatched groups were statistically compared using the Mann-Whitney U test. One-way analysis of variance followed by Tukey's post hoc comparison test was used for multiple-group comparisons. P values less than 0.05 were considered significant.

RESULTS

Effect of B cell depletion with anti-CD20 antibody on fibrosis in mice with BLM-SSc. First, we confirmed that mouse anti-CD20 antibodies eliminated mouse B cells (Figure 1A). B cells, which accounted for about 60% of the mononuclear cells in the spleen prior to administration of anti-CD20 antibody, were almost completely eliminated, decreasing to 0.4% 7 days after it was administered. After 14 days of treatment, this elimination effect was maintained.

B cell depletion markedly inhibited skin and lung fibrosis of mice with BLM-SSc in both the pre-depletion and post-depletion groups ($P < 0.05$) (Figure 1C). In addition, the pre-depletion group showed significant inhibition of skin and lung fibrosis compared to the post-depletion group ($P < 0.01$) (Figure 1C).

Capacity of B cells to produce cytokines and affect T cell differentiation in mice with BLM-SSc. To investigate how the properties of B cells are altered in mice with BLM-SSc, we examined the ability of B cells to produce cytokines, using B cells obtained from PBS-treated control mice and mice with BLM-SSc. Mice with BLM-SSc had fewer regulatory B cells producing IL-10 compared to controls ($P < 0.05$) (Figure 2A). In contrast, IL-6–producing B cells were increased in mice with BLM-SSc ($P < 0.05$). The frequencies of IFNγ-producing B cells were comparable between controls and mice with BLM-SSc. We also evaluated the effect of B cells on T cells in coculture. B cells from mice with BLM-SSc enhanced the IL-4, IL-6, IL-17A, and IFNγ production by CD4+ T cells from control mice but did not affect IL-10 production (Figure 2B). We obtained similar results in B cells and T cells from the lungs of controls and mice with BLM-SSc (Supplementary Figures
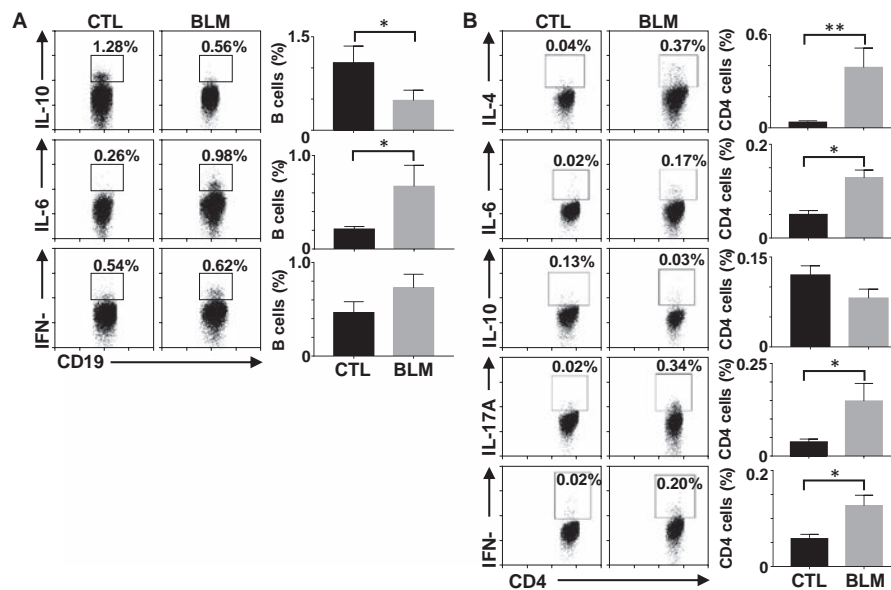
Figure 2. Cytokine production ability of B cells in mice with bleomycin-induced systemic sclerosis (BLM-SSc) and its effect on T cell differentiation. **A**, The frequencies of interleukin-10 (IL-10), IL-6, and interferon-γ (IFNγ) production induced by B cells in the spleen were compared between phosphate buffered saline–treated control (CTL) mice and mice with BLM-SSc. **B**, B cells were cocultured with CD4+ T cells extracted from the spleens of control mice, and frequencies of cytokine-producing T cells were examined. Bars show the mean ± SD. * = $P < 0.05$; ** = $P < 0.01$.

1A and B, available on the *Arthritis & Rheumatology* website at http://onlinelibrary.wiley.com/doi/10.1002/art.41798/abstract). These results suggest that the increased proportions of inflammation-inducible B cells in mice with BLM-SSc may affect T cell differentiation and consequently differentiate CD4+ T cells into Th1, Th2, and Th17 cells.

Alteration of T cell fractions by B cell depletion in mice with BLM-SSc. To investigate whether the difference in T cell fractions is responsible for the difference in the extent of fibrosis inhibition in mice with BLM-SSc according to the timing of B cell depletion, we examined CD4+ T cell fractions in each group. Mice with BLM-SSc showed an increase in IFNγ-, IL-4–, IL-17A–, and
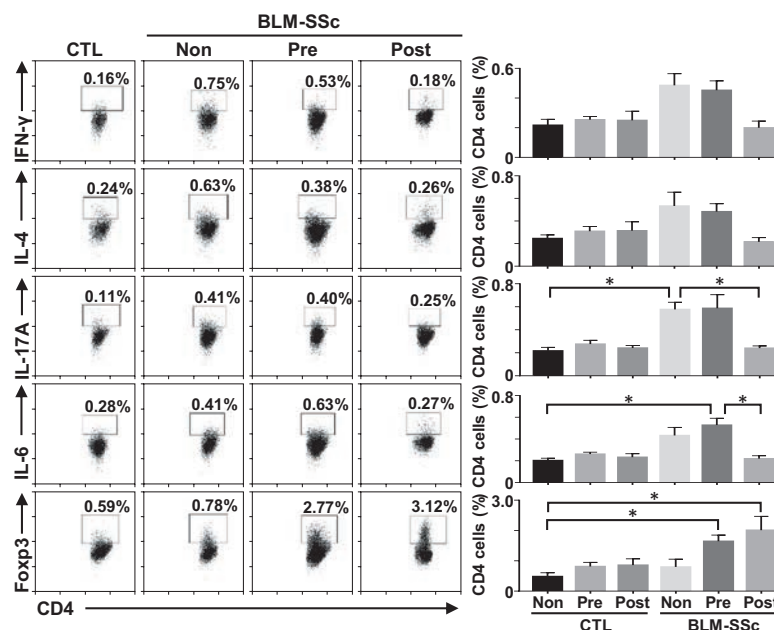
Figure 3. Effects of B cell depletion on T cell differentiation in mice with BLM-SSc. Flow cytometry was used to examine cytokine production by T cells in B cell non-depletion (Non), pre-depletion (Pre), and post-depletion (Post) groups of mice with BLM-SSc. Frequencies of IFNγ-, IL-4–, IL-17A–, and IL-6–producing CD4+ T cells, in addition to FoxP3+CD4+ T cells, were measured. Bars show the mean ± SD. * = $P < 0.05$. See Figure 2 for other definitions.

IL-6–producing CD4+ T cells compared to controls, and the difference was significant for IL-17A–producing CD4+ T cells ($P < 0.05$) (Figure 3). Comparing the non-depletion and pre-depletion groups in mice with BLM-SSc, the frequencies of IFNγ-, IL-4–, IL-17A–, and IL-6–producing CD4+ T cells were similar, and the frequencies of FoxP3+CD4+ T cells tended to increase in the pre-depletion group. The comparison of the pre-depletion and post-depletion groups in mice with BLM-SSc showed a decrease in IFNγ-, IL-4–, IL-17A–, and IL-6–producing CD4+ T cells in the post-depletion group, with a significant difference in IL-6–producing CD4+ T cells ($P < 0.05$). However, we observed an increase in FoxP3+CD4+ T cells in the post-depletion group compared to the pre-depletion group in mice with BLM-SSc, even though it was not significant.

Although previous studies have suggested that TGFβ induces regulatory T cells (26), B cell depletion decreased TGFβ1 expression levels in the skin and lungs of mice with BLM-SSc in both the pre-depletion and post-depletion groups in the present study (Supplementary Figure 2, http://onlinelibrary.wiley.com/doi/10.1002/art.41798/abstract). Therefore, the increase in FoxP3+CD4+ T cells by B cell depletion might not be attributable to the altered expression of TGFβ1, but these findings indicate that post-depletion of B cells is more potent than pre-depletion in inhibiting inflammatory CD4+ T cells and increasing regulatory T cells. However, this is inconsistent with the fact that, in mice with BLM-SSc, B cell pre-depletion more strongly inhibits fibrosis than post-depletion. Therefore, the differential inhibitory effect of SSc on fibrosis caused by the timing of B cell depletion cannot be explained by the ability of B cells to regulate T cell differentiation.

Effects of B cell depletion on macrophage differentiation in mice with BLM-SSc. It has been suggested that macrophages play an important role in fibrosis in SSc
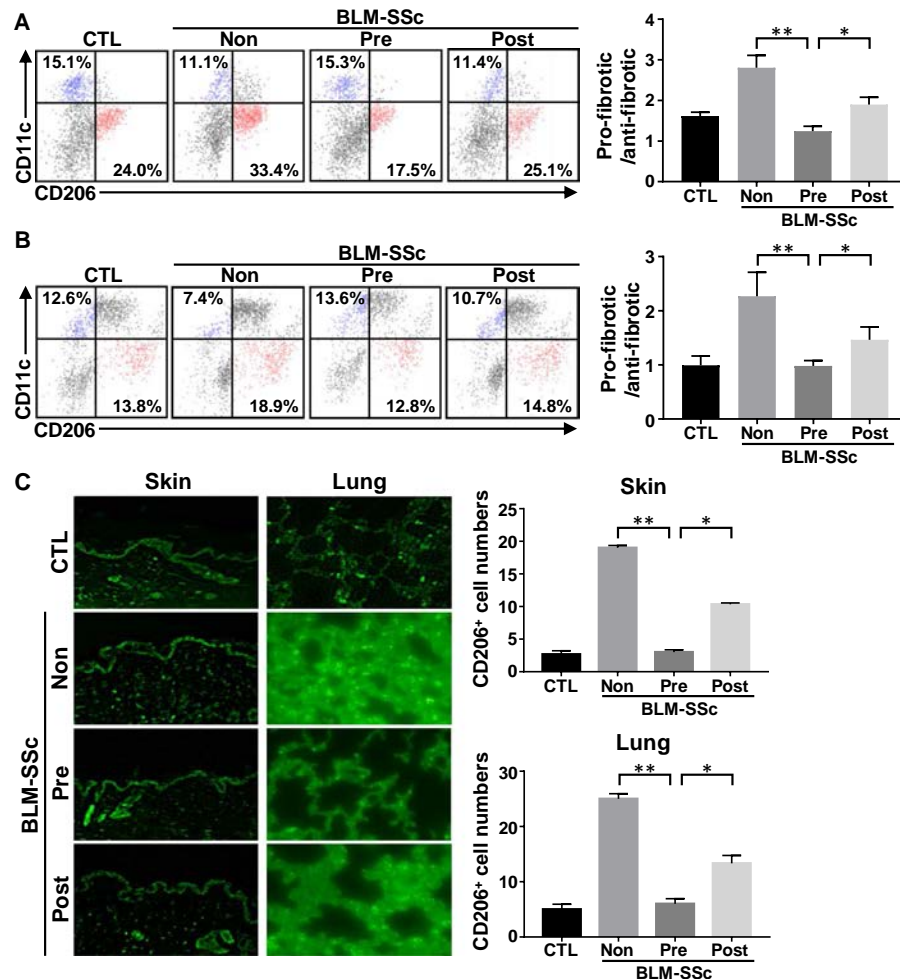
Figure 4. Effects of B cell depletion on macrophage differentiation in mice with BLM-SSc. **A** and **B**, Macrophages from the spleen (**A**) and lungs (**B**) of control mice and mice with BLM-SSc in the B cell non-depletion (Non), pre-depletion (Pre), and post-depletion (Post) groups were examined by flow cytometry. Results were quantified as the ratio of profibrotic to antifibrotic macrophages. Antifibrotic macrophages were defined as CD11b+F4/80+CD206–CD11c+ cells (blue) and profibrotic macrophages were defined as CD11b+F4/80+CD206+CD11c– cells (red). **C**, CD206-expressing cells in the skin (original magnification × 40) and lungs (original magnification × 100) were examined using fluorescence immunohistochemistry. Bars show the mean ± SD. * = $P < 0.05$; ** = $P < 0.01$. See Figure 2 for other definitions. Color figure can be viewed in the online issue, which is available at http://onlinelibrary.wiley.com/doi/10.1002/art.41798/abstract.

(27,28). Therefore, we next examined the effects of B cell depletion on macrophages in mice with BLM-SSc. The ratio of profibrotic macrophages to antifibrotic macrophages in the spleen was reduced in mice with BLM-SSc that had been depleted of B cells (Figure 4A). The decrease in the ratio of profibrotic macrophages to antifibrotic macrophages was more pronounced in the pre-depletion group than in the post-depletion group (P < 0.05). Consistent with this, expression levels of profibrotic macrophage markers, such as arginase 1, Ym1, FIZZ-1, IL-10, and TGFβ1, were more suppressed in the pre-depletion group than in the post-depletion group (Supplementary Figures 3A and B, http://onlinelibrary.wiley.com/doi/10.1002/art.41798/abstract). Expression levels of antifibrotic macrophage markers, such as I-A/I-E, CD80, CD86, and TNF, were higher in the pre-depletion group than in the post-depletion group. Similar results were obtained in the lungs of mice with BLM-SSc, where the ratio of profibrotic macrophages to antifibrotic macrophages was decreased more markedly in the pre-depletion group than in the post-depletion group (P < 0.05) (Figure 4B). In accordance with these results, when analyzed with immunofluorescence staining, the pre-depletion group showed significantly fewer cells expressing profibrotic marker CD206 in the skin and lungs, compared to the post-depletion group (P < 0.05) (Figure 4C). These results suggest that both fibrosis and profibrotic macrophage differentiation were inhibited more strongly in the pre-depletion group than in the post-depletion group. Thus, the antifibrotic effect of B cell depletion in SSc was associated with suppressed profibrotic macrophage differentiation.
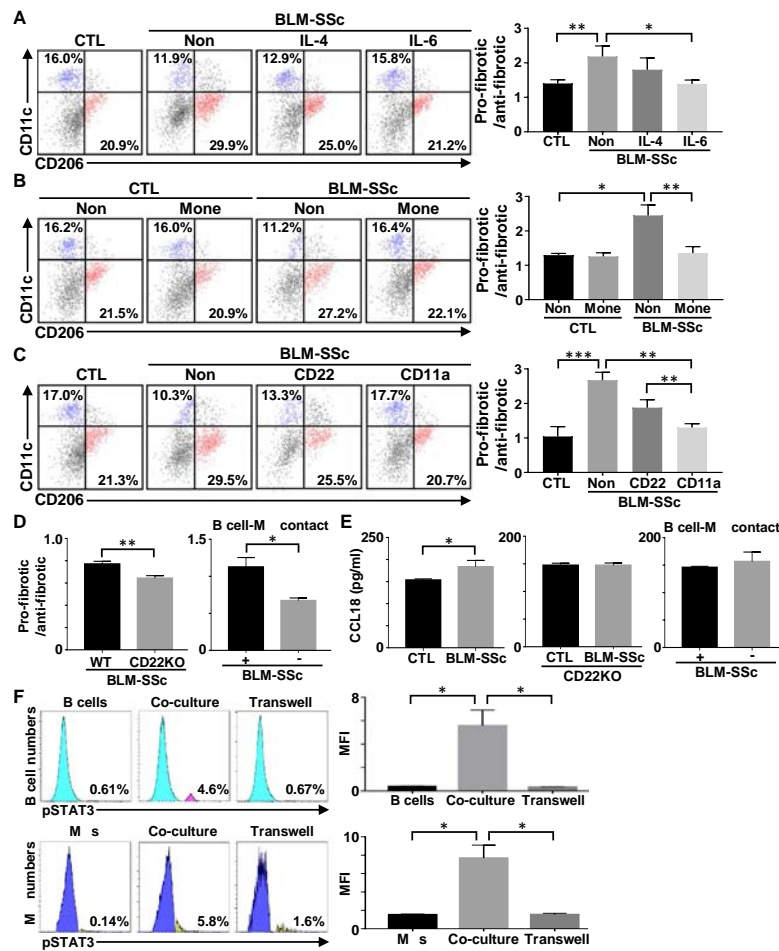
Figure 5. Factors mediating the induction of profibrotic macrophages (Mφ) by B cells in mice with BLM-SSc. **A**, B cells from mice with BLM-SSc and macrophages from control mice were cocultured in the presence of anti–IL-4 or anti–IL-6 antibodies. **B**, B cells pretreated with monensin (Mone) were cocultured with control macrophages. **C**, B cells and macrophages were cocultured in the presence of anti-CD22 or anti-CD11a antibodies. **D**, B cells from mice with BLM-SSc generated from wild-type (WT) and CD22$^{-/-}$ (knockout [KO]) mice were cocultured with WT macrophages (left). Also, B cells from mice with BLM-SSc were cocultured with or without WT macrophages (right). Transwells were used to prevent cell-to-cell contact between B cells and macrophages. In **A–D**, the ability of B cells to induce profibrotic macrophages was examined as the ratio of profibrotic to antifibrotic macrophages. **E**, WT macrophages were cocultured with B cells from controls or mice with BLM-SSc, and CCL18 production was examined. **F**, BLM-SSc B cells and WT macrophages were cultured alone or in coculture, and STAT3 phosphorylation was examined. Transwells were used to prevent contact between B cells and macrophages during coculture. Bars show the mean ± SD. * = P < 0.05; ** = P < 0.01; *** = P < 0.001. See Figure 2 for other definitions. Color figure can be viewed in the online issue, which is available at http://onlinelibrary.wiley.com/doi/10.1002/art.41798/abstract.

Influence of BLM-SSc B cells on macrophage differentiation and its mechanism. Next, the effect of B cells from mice with BLM-SSc on macrophage differentiation was directly investigated by extracting B cells and macrophages and coculturing them. Compared to cocultures with B cells from control mice, in cocultures with B cells from mice with BLM-SSc, control macrophages were markedly skewed toward an increase in profibrotic macrophages relative to antifibrotic macrophages (Figure 5A). In the coculture of B cells and macrophages, anti–IL-6 antibodies inhibited profibrotic macrophage differentiation ($P < 0.05$), but anti–IL-4 antibodies did not significantly affect profibrotic macrophage differentiation. Pretreatment of B cells with monensin to block cytokine production inhibited profibrotic macrophage differentiation induced by B cells from mice with BLM-SSc (Figure 5B). Furthermore, the addition of anti-CD22 or anti-CD11a antibodies during coculture inhibited the ability of BLM-SSc B cells to induce profibrotic macrophage differentiation, and in particular, anti-CD11a antibodies significantly inhibited profibrotic macrophage induction ($P < 0.01$) (Figure 5C). Similar results were obtained by evaluating antifibrotic and profibrotic macrophage markers (Supplementary Figures 4–6, http://onlinelibrary.wiley.com/doi/10.1002/art.41798/abstract).

B cells from mice with BLM-SSc generated using CD22$^{-/-}$ mice had a weaker ability to induce profibrotic macrophage differentiation than B cells from mice with BLM-SSc generated using WT mice ($P < 0.01$) (Figure 5D). Moreover, inhibition of B

cell–macrophage binding using Transwells significantly inhibited profibrotic macrophage differentiation ($P < 0.05$). Several studies have shown that profibrotic macrophages induce CCL18-mediated fibrosis (27,28). Indeed, previous studies have shown that CCL18 promotes collagen production in skin and lung fibroblasts (29). In particular, serum CCL18 has emerged as one of the most reliable markers for monitoring SSc-associated ILD, a major cause of death among SSc patients (30,31). B cells from mice with BLM-SSc promoted an increase in CCL18 production from macrophages compared to B cells from controls (mean ± SD 183.4 ± 41.2 pg/ml versus 153.4 ± 7.0 pg/ml; $P < 0.05$) (Figure 5E). In contrast, B cells from mice with BLM-SSc generated using CD22$^{-/-}$ mice did not enhance CCL18 production from macrophages compared to PBS-treated CD22$^{-/-}$ mice (mean ± SD 147.3 ± 12.1 pg/ml versus 147.5 ± 10.6 pg/ml; $P = 0.98$), and similarly, inhibition of B cell–macrophage adhesion using Transwells inhibited enhanced CCL18 production induced by B cells from mice with BLM-SSc (mean ± SD 156.5 ± 45.9 pg/ml versus 145.9 ± 5.6 pg/ml; $P = 0.29$).

When B cells obtained from mice with BLM-SSc were cocultured with control macrophages, the phosphorylation of STAT3 in macrophages was enhanced ($P < 0.05$) (Figure 5F). Inhibition of B cell–macrophage adhesion using Transwells inhibited the induction of STAT3 phosphorylation in macrophages by B cells. Similarly, enhancement of STAT3 phosphorylation in B cells was also observed when they were cocultured with macrophages, and this
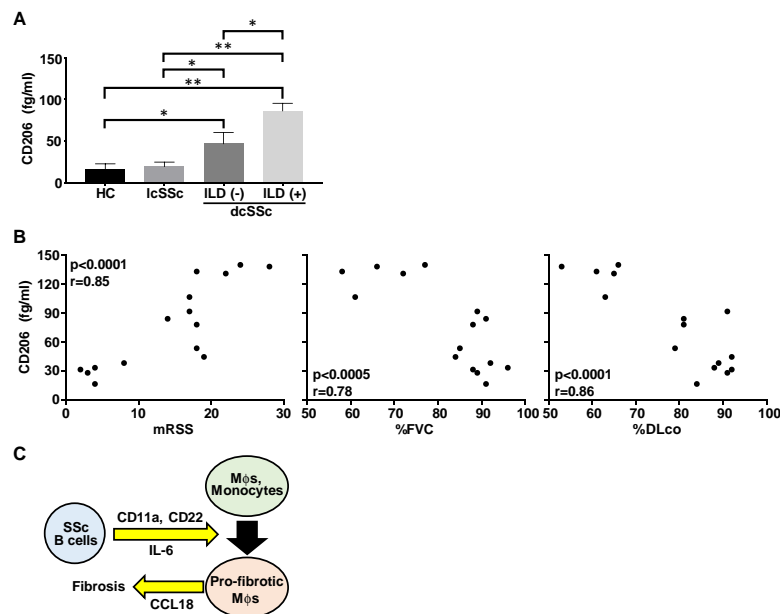
Figure 6. Ability of B cells from human systemic sclerosis (SSc) patients to induce profibrotic macrophage (Mφ) differentiation. **A**, B cells and monocytes were extracted from the peripheral blood of patients with diffuse cutaneous SSc (dcSSc) with or without interstitial lung disease (ILD), patients with limited cutaneous SSc (lcSSc), and healthy controls (HC). Expression levels of CD206 on macrophages were examined using microfluidic enzyme-linked immunosorbent assay after coculture. Samples from 5 subjects in each group were obtained. Bars show the mean ± SD. * = $P < 0.05$; ** = $P < 0.01$. **B**, Correlations between CD206 expression and modified Rodnan skin thickness score (mRSS), forced vital capacity percent predicted (%FVC), and diffusing capacity for carbon monoxide percent predicted (%DLco) were examined. **C**, Relationship between B cells and macrophages in the development of SSc fibrosis is shown. IL-6 = interleukin-6. Color figure can be viewed in the online issue, which is available at http://onlinelibrary.wiley.com/doi/10.1002/art.41798/abstract.

enhancement was not observed when Transwells were used to inhibit their adhesion. These results suggest that B cells and macrophages are activated by the stimulation of adhesion to each other.

Induction of profibrotic macrophages by B cells from SSc patients. B cells from SSc patients were extracted to evaluate their ability to differentiate monocytes into profibrotic macrophages. Compared to B cells from healthy controls, macrophages induced by B cells from patients with diffuse cutaneous SSc (dcSSc) showed significantly enhanced CD206 expression ($P < 0.05$) (Figure 6A). Furthermore, B cells from dcSSc patients with ILD induced CD206 expression in macrophages more strongly than B cells from those without ILD ($P < 0.05$). Considering that the baseline expression levels of CD206 on isolated monocytes were comparable between healthy controls and dcSSc patients with ILD (Supplementary Figure 7, http://onlinelibrary.wiley.com/doi/10.1002/art.41798/abstract), these results suggest that B cells from dcSSc patients with ILD induce CD206 expression on monocytes more prominently than B cells from healthy controls. We further examined the correlation between the expression levels of CD206 and clinical symptoms in SSc patients (Figure 6B). B cell–induced CD206 expression levels positively correlated with modified Rodnan skin thickness scores and negatively correlated with the forced vital capacity percent predicted and diffusing capacity for carbon monoxide percent predicted. Therefore, we concluded that B cell–induced CD206 expression on monocytes correlated with the severity of fibrosis in SSc patients.

DISCUSSION

In the present study, B cell depletion markedly inhibited skin and lung fibrosis in mice with BLM-SSc (Figure 1). Mice with BLM-SSc showed a decrease in IL-10–producing regulatory B cells and an increase in IL-6–producing B cells compared to controls (Figure 2). Coculture experiments with B cells from mice with BLM-SSc and T cells from controls showed that these B cells were capable of differentiating CD4+ T cells into IL-4–, IL-6–, IL-17A–, and IFNγ-producing T cells. In contrast, mice with BLM-SSc receiving B cell depletion showed a decrease in IL-17A– and IL-6–producing T cells and an increase in Treg cells in the post-depletion group compared to the non-depletion group; the pre-depletion group showed little change in the T cell fractions other than Treg cell differentiation (Figure 3).

Because these findings did not explain why B cell pre-depletion inhibited fibrosis in mice with BLM-SSc more strongly than post-depletion, we continued our investigation by focusing on macrophages, which are one of the key players in fibrosis. Mice with BLM-SSc subjected to B cell pre-depletion showed a marked decrease in profibrotic macrophages compared to the post-depletion group (Figure 4). Coculture experiments of B cells and macrophages revealed that B cells from mice with BLM-SSc induced profibrotic macrophage differentiation (Figure 5).

In addition, IL-6 produced by B cells and CD22- and CD11a-mediated engagement of B cells and macrophages are important for the induction of profibrotic macrophages by B cells.

B cells from patients with severely fibrotic dcSSc with ILD enhanced the expression of CD206, an indicator of profibrotic macrophages, on monocytes (Figures 6A and B). Furthermore, the strength of CD206 induction in B cells from SSc patients correlated with the severity of skin and lung fibrosis. These results suggest that profibrotic macrophages induced by B cells contribute to fibrosis in SSc (Figure 6C). Taken together with the finding of reductions in fibrosis and profibrotic macrophage differentiation by B cell depletion in mice with BLM-SSc, our study provides a new rationale for B cell depletion therapy in SSc.

Mice with BLM-SSc are widely used as a model of SSc because they exhibit autoimmune abnormalities and skin and lung fibrosis (32–34). BLM-mediated tissue damage via reactive oxygen species production induces intracellular antigen exposure and generation of hyaluronic acid, an endogenous ligand for Toll-like receptors. They activate immune cells, including B cells, leading to fibrosis as a result of autoimmune abnormalities and increased cytokine production. Furthermore, mice with BLM-SSc that lack CD19, which promotes B cell activation, show markedly reduced skin and lung fibrosis and inflammation, suggesting that aberrant B cell activation in mice with BLM-SSc plays an important role in the development of SSc, as is the case with human SSc (35). Although there have been few studies of B cell depletion in mice with BLM-SSc, this study has shown that B cell depletion markedly suppresses fibrosis in mice with BLM-SSc. Therefore, the results obtained here could be applied to human SSc.

In the present study, B cell depletion inhibited profibrotic macrophage differentiation as well as fibrosis. Studies in tumor areas such as squamous cell carcinoma have suggested that B cell depletion inhibits profibrotic macrophage differentiation (36,37). However, the interaction between B cells and macrophages in SSc and its effect on fibrosis are largely unknown. Because previous studies have suggested an important role of B cell–derived IL-6 in SSc (38–40), we explored the effect of B cell–derived IL-6 on macrophage activation and demonstrated that IL-6 was essential for profibrotic macrophage differentiation induced by B cells in mice with BLM-SSc (Figure 5A). Although further studies using conditional IL-6$^{-/-}$ mice are needed to assess the contribution of IL-6 from other cell types in an in vivo context, our findings suggest that B cell–derived IL-6 promotes profibrotic macrophage differentiation in mice with BLM-SSc. Indeed, previous studies have shown that IL-6 induces profibrotic macrophage differentiation (41,42). In addition, IL-6 increases phosphorylated STAT3 in macrophages and induces increased expression of IL-4 receptor. This indicates that IL-6 is a potent profibrotic macrophage inducer.

Our results suggest that CD11a- and CD22-mediated binding of B cells to macrophages is required for induction of profibrotic macrophage differentiation by B cells. CD11a is one of the cell adhesion molecules that binds to the intercellular adhesion molecule

1 expressed in macrophages and vascular endothelial cells. The binding of cell adhesion molecules not only serves to infiltrate cells into tissues but also transmits activation stimuli into cells (43–45). However, CD22 is one of the membrane surface molecules that is specifically expressed on B cells (46,47). Although a specific ligand for CD22 has not been identified in vivo, it has been shown that CD22 recognizes glycoproteins as ligands. Recent studies have demonstrated that many of the cell adhesion molecules are glycoproteins (48). Thus, CD22 might be involved in the adhesion of B cells and macrophages as well as CD11a. Interestingly, in the present study, not only macrophages but also B cells showed increased STAT3 phosphorylation when they attached to macrophages. These results support the notion that B cells from mice with BLM-SSc are activated by adhesion to macrophages and enhance profibrotic macrophage differentiation capacity.

In SSc, profibrotic macrophages have been shown to directly induce fibrosis via IL-4, IL-6, IL-13, TGFβ, and CCL18 (9–11,49). In this study, profibrotic macrophages differentiated by coculture with B cells from mice with BLM-SSc also produced CCL18. Furthermore, B cells from SSc patients promoted profibrotic macrophage differentiation, the extent of which correlated with the severity of fibrosis. In conclusion, our findings suggest that profibrotic macrophages induced by B cells play an important role in SSc fibrosis. Inhibiting profibrotic macrophage induction using B cells could be a novel therapeutic strategy for the treatment of SSc.

AUTHOR CONTRIBUTIONS

All authors were involved in drafting the article or revising it critically for important intellectual content, and all authors approved the final version to be published. Dr. Yoshizaki had full access to all of the data in the study and takes responsibility for the integrity of the data and the accuracy of the data analysis.

Study conception and design. Yoshizaki, Sato.

Acquisition of data. Numajiri, Kuzumi, Fukasawa, Ebata, Yoshizaki-Ogawa, Asano, Kazoe, Mawatari, Kitamori, Yoshizaki.

Analysis and interpretation of data. Numajiri, Kuzumi, Yoshizaki-Ogawa, Kazoe, Mawatari, Kitamori, Yoshizaki.

REFERENCES

1. Steen VD, Medsger TA. Changes in causes of death in systemic sclerosis, 1972–2002. Ann Rheum Dis 2007;66:940–4.

2. Yoshizaki A, Sato S. Abnormal B lymphocyte activation and function in systemic sclerosis [review]. Ann Dermatol 2015;27:1–9.

3. Sakkas LI, Bogdanos DP. Systemic sclerosis: new evidence re-enforces the role of B cells [review]. Autoimmun Rev 2016;15:155–61.

4. Yoshizaki A. Pathogenic roles of B lymphocytes in systemic sclerosis [letter]. Immunol Lett 2018;195:76–82.

5. Yoshizaki A. B lymphocytes in systemic sclerosis: abnormalities and therapeutic targets. J Dermatol 2016;43:39–45.

6. Yoshizaki A, Miyagaki T, DiLillo DJ, Matsushita T, Horikawa M, Kountikov EI, et al. Regulatory B cells control T-cell autoimmunity through IL-21-dependent cognate interactions [letter]. Nature 2012;491:264–8.

7. Barnes TC, Anderson ME, Moots RJ. The many faces of interleukin-6: the role of IL-6 in inflammation, vasculopathy, and fibrosis in systemic sclerosis. Int J Rheumatol 2011;2011:721608.

8. Gasparini G, Cozzani E, Parodi A. Interleukin-4 and interleukin-13 as possible therapeutic targets in systemic sclerosis. Cytokine 2020;125:154799.

9. Torroella-Kouri M, Rodriguez D, Caso R. Alterations in macrophages and monocytes from tumor-bearing mice: evidence of local and systemic immune impairment. Immunol Res 2013;57:86–98.

10. Prasse A, Probst C, Bargagli E, Zissel G, Toews GB, Flaherty KR, et al. Serum CC-chemokine ligand 18 concentration predicts outcome in idiopathic pulmonary fibrosis. Am J Respir Crit Care Med 2009;179:717–23.

11. Gkika E, Vach W, Adebahr S, Schimek-Jasch T, Brenner A, Brunner TB, et al. Is serum level of CC chemokine ligand 18 a biomarker for the prediction of radiation induced lung toxicity (RILT)? PLoS One 2017;12:e0185350.

12. Hale M, Rawlings DJ, Jackson SW. The long and the short of it: insights into the cellular source of autoantibodies as revealed by B cell depletion therapy. Curr Opin Immunol 2018;55:81–8.

13. Panopoulos S, Chatzidionysiou K, Tektonidou MG, Bournia VK, Drosos AA, Liossis SC, et al. Treatment modalities and drug survival in a systemic sclerosis real-life patient cohort. Arthritis Res Ther 2020;22:56.

14. Tang R, Yu J, Shi Y, Zou P, Zeng Z, Tang B, et al. Safety and efficacy of Rituximab in systemic sclerosis: a systematic review and meta-analysis. Int Immunopharmacol 2020;83:106389.

15. Ebata S, Yoshizaki A, Fukasawa T, Miura S, Takahashi T, Sumida H, et al. Rituximab therapy is more effective than cyclophosphamide therapy for Japanese patients with anti-topoisomerase I-positive systemic sclerosis-associated interstitial lung disease. J Dermatol 2019;46:1006–13.

16. Ebata S, Yoshizaki A, Fukasawa T, Nakamura K, Yamashita T, Miura S, et al. Unprecedented success of rituximab therapy for prednisolone- and immunosuppressant-resistant systemic sclerosis-associated interstitial lung disease. Scand J Rheumatol 2017;46:247–52.

17. Goswami RP, Ray A, Chatterjee M, Mukherjee A, Sircar G, Ghosh P. Rituximab in the treatment of systemic sclerosis-related interstitial lung disease: a systematic review and meta-analysis. Rheumatology (Oxford) 2021;60:557–67.

18. Moro K, Ealey KN, Kabata H, Koyasu S. Isolation and analysis of group 2 innate lymphoid cells in mice. Nat Protoc 2015;10:792–806.

19. Kloepper J, Riedemann L, Amoozgar Z, Seano G, Susek K, Yu V, et al. Ang-2/VEGF bispecific antibody reprograms macrophages and resident microglia to anti-tumor phenotype and prolongs glioblastoma survival. Proc Natl Acad Sci U S A 2016;113:4476–81.

20. Lumeng CN, Bodzin JL, Saltiel AR. Obesity induces a phenotypic switch in adipose tissue macrophage polarization. J Clin Invest 2007;117:175–84.

21. Van den Hoogen F, Khanna D, Fransen J, Johnson SR, Baron M, Tyndall A, et al. 2013 classification criteria for systemic sclerosis: an American College of Rheumatology/European League Against Rheumatism collaborative initiative. Arthritis Rheum 2013;65:2737–47.

22. Yoshizaki A, Yanaba K, Ogawa A, Asano Y, Kadono T, Sato S. Immunization with DNA topoisomerase I and Freund's complete adjuvant induces skin and lung fibrosis and autoimmunity via interleukin-6 signaling. Arthritis Rheum 2011;63:3575–85.

23. Sato K, Yamanaka M, Takahashi H, Tokeshi M, Kimura H, Kitamori T. Microchip-based immunoassay system with branching multichannels for simultaneous determination of interferon-γ. Electrophoresis 2002;23:734–9.

24. Fukasawa T, Yoshizaki A, Ebata S, Nakamura K, Saigusa R, Miura S, et al. Contribution of soluble forms of programmed death 1 and programmed death ligand 2 to disease severity and progression in systemic sclerosis. Arthritis Rheumatol 2017;69:1879–90.

25. Numajiri H, Yoshizaki A, Fukasawa T, Ebata S, Nakamura K, Yamashita T, et al. Rapid alteration of serum interleukin-6 levels may predict the reactivity of i.v. cyclophosphamide pulse therapy

in systemic sclerosis-associated interstitial lung disease. J Dermatol 2018;45:1221–4.

26. Sharabi A, Tsokos MG, Ding Y, Malek TR, Klatzmann D, Tsokos GC. Regulatory T cells in the treatment of disease [review]. Nat Rev Drug Discov 2018;17:823–44.

27. Schupp JC, Binder H, Jager B, Cillis G, Zissel G, Muller-Quernheim J, et al. Macrophage activation in acute exacerbation of idiopathic pulmonary fibrosis. PLoS One 2015;10:e0116775.

28. Stahl M, Schupp J, Jager B, Schmid M, Zissel G, Muller-Quernheim J, et al. Lung collagens perpetuate pulmonary fibrosis via CD204 and M2 macrophage activation. PLoS One 2013;8:e81382.

29. Atamas SP, Luzina IG, Choi J, Tsymbalyuk N, Carbonetti NH, Singh IS, et al. Pulmonary and activation-regulated chemokine stimulates collagen production in lung fibroblasts. Am J Respir Cell Mol Biol 2003;29:743–9.

30. Kodera M, Hasegawa M, Komura K, Yanaba K, Takehara K, Sato S. Serum pulmonary and activation-regulated chemokine/CCL18 levels in patients with systemic sclerosis: a sensitive indicator of active pulmonary fibrosis. Arthritis Rheum 2005;52:2889–96.

31. Elhai M, Hoffmann-Vold AM, Avouac J, Pezet S, Cauvet A, Leblond A, et al. Performance of candidate serum biomarkers for systemic sclerosis–associated interstitial lung disease. Arthritis Rheumatol 2019;71:972–82.

32. Yamamoto T, Takagawa S, Katayama I, Yamazaki K, Hamazaki Y, Shinkai H, et al. Animal model of sclerotic skin. I: Local injections of bleomycin induce sclerotic skin mimicking scleroderma. J Invest Dermatol 1999;112:456–62.

33. Yamamoto T. The bleomycin-induced scleroderma model: what have we learned for scleroderma pathogenesis? [review]. Arch Dermatol Res 2006;297:333–44.

34. Yoshizaki A, Yanaba K, Ogawa A, Iwata Y, Ogawa F, Takenaka M, et al. The specific free radical scavenger edaravone suppresses fibrosis in the bleomycin-induced and tight skin mouse models of systemic sclerosis. Arthritis Rheum 2011;63:3086–97.

35. Yoshizaki A, Iwata Y, Komura K, Ogawa F, Hara T, Muroi E, et al. CD19 regulates skin and lung fibrosis via Toll-like receptor signaling in a model of bleomycin-induced scleroderma. Am J Pathol 2008;172:1650–63.

36. Affara NI, Ruffell B, Medler TR, Gunderson AJ, Johansson M, Bornstein S, et al. B cells regulate macrophage phenotype and response to chemotherapy in squamous carcinomas. Cancer Cell 2014;25:809–21.

37. Yamamoto T. Animal model of systemic sclerosis [review]. J Dermatol 2010;37:26–41.

38. Dumoitier N, Chaigne B, Régent A, Lofek S, Mhibik M, Dorfmüller P, et al. Scleroderma peripheral B lymphocytes secrete interleukin-6 and transforming growth factor β and activate fibroblasts. Arthritis Rheumatol 2017;69:1078–89.

39. Hasegawa M, Hamaguchi Y, Yanaba K, Bouaziz JD, Uchida J, Fujimoto M, et al. B-lymphocyte depletion reduces skin fibrosis and autoimmunity in the tight-skin mouse model for systemic sclerosis. Am J Pathol 2006;169:954–66.

40. Matsushita T, Kobayashi T, Mizumaki K, Kano M, Sawada T, Tennichi M, et al. BAFF inhibition attenuates fibrosis in scleroderma by modulating the regulatory and effector B cell balance. Sci Adv 2018;4:eaas9944.

41. Mantovani A, Sica A, Sozzani S, Allavena P, Vecchi A, Locati M. The chemokine system in diverse forms of macrophage activation and polarization. Trends Immunol 2004;25:677–86.

42. Fu XL, Duan W, Su CY, Mao FY, Lv YP, Teng YS, et al. Interleukin 6 induces M2 macrophage differentiation by STAT3 activation that correlates with gastric cancer progression. Cancer Immunol Immunother 2017;66:1597–608.

43. Xu J, Grewal IS, Geba GP, Flavell RA. Impaired primary T cell responses in L-selectin-deficient mice. J Exp Med 1996;183:589–98.

44. Catalina MD, Carroll MC, Arizpe H, Takashima A, Estess P, Siegelman MH. The route of antigen entry determines the requirement for L-selectin during immune responses. J Exp Med 1996;184:2341–51.

45. Van Seventer GA, Shimizu Y, Horgan KJ, Shaw S. The LFA-1 ligand ICAM-1 provides an important costimulatory signal for T cell receptor-mediated activation of resting T cells. J Immunol 1990;144:4579–86.

46. Sato S, Tuscano JM, Inaoki M, Tedder TF. CD22 negatively and positively regulates signal transduction through the B lymphocyte antigen receptor [review]. Semin Immunol 1998;10:287–97.

47. Crocker PR, Paulson JC, Varki A. Siglecs and their roles in the immune system [review]. Nat Rev Immunol 2007;7:255–66.

48. Varki A. Selectin ligands [review]. Proc Natl Acad Sci U S A 1994;91:7390–7.

49. Manetti M. Deciphering the alternatively activated (M2) phenotype of macrophages in scleroderma [editorial]. Exp Dermatol 2015;24:576–8.

AMERICAN COLLEGE
of RHEUMATOLOGY
Empowering Rheumatology Professionals

Assessing the Causal Relationships Between Insulin Resistance and Hyperuricemia and Gout Using Bidirectional Mendelian Randomization

Natalie McCormick,[1] (ID) Mark J. O'Connor,[2] (ID) Chio Yokose,[3] (ID) Tony R. Merriman,[4] (ID) David B. Mount,[5] Aaron Leong,[6] (ID) and Hyon K. Choi[1] (ID)

Objective. Hyperuricemia is closely associated with insulin resistance syndrome (and its many cardiometabolic sequelae); however, whether they are causally related has long been debated. We undertook this study to investigate the potential causal nature and direction between insulin resistance and hyperuricemia, along with gout, by using bidirectional Mendelian randomization (MR) analyses.

Methods. We used genome-wide association data (n = 288,649 for serum urate [SU] concentration; n = 763,813 for gout risk; n = 153,525 for fasting insulin) to select genetic instruments for 2-sample MR analyses, using multiple MR methods to address potential pleiotropic associations. We then used individual-level, electronic medical record–linked data from the UK Biobank (n = 360,453 persons of European ancestry) to replicate our analyses via single-sample MR analysis.

Results. Genetically determined SU levels, whether inferred from a polygenic score or strong individual loci, were not associated with fasting insulin concentrations. In contrast, genetically determined fasting insulin concentrations were positively associated with SU levels (0.37 mg/dl per log-unit increase in fasting insulin [95% confidence interval (95% CI) 0.15, 0.58]; $P = 0.001$). This persisted in outlier-corrected ($\beta = 0.56$ mg/dl [95% CI 0.45, 0.67]) and multivariable MR analyses adjusted for BMI ($\beta = 0.69$ mg/dl [95% CI 0.53, 0.85]) ($P < 0.001$ for both). Polygenic scores for fasting insulin were also positively associated with SU level among individuals in the UK Biobank ($P < 0.001$). Findings for gout risk were bidirectionally consistent with those for SU level.

Conclusion. These findings provide evidence to clarify core questions about the close association between hyperuricemia and insulin resistance syndrome: hyperinsulinemia leads to hyperuricemia but not the other way around. Reducing insulin resistance could lower the SU level and gout risk, whereas lowering the SU level (e.g., allopurinol treatment) is unlikely to mitigate insulin resistance and its cardiometabolic sequelae.

INTRODUCTION

The incidence, prevalence, and disability burden of gout have risen substantially over the past decades, especially in the US (1).

Gout and hyperuricemia, its causal precursor, frequently coexist with metabolic syndrome (2) and are associated with an elevated burden of cardiovascular disease and type 2 diabetes mellitus (3). However, despite the close association between hyperuricemia and

the insulin resistance syndrome (4,5), the nature and direction of any causal relations are unclear. Observational studies have identified hyperuricemia as an independent risk factor for insulin resistance and prediabetes (6), but these findings may represent a case of reverse causality or residual confounding. Conversely, findings from some human physiologic experiments suggest that induced hyperinsulinemia can raise serum urate (SU) concentrations (4,7), but its casual impact at the population level remains unknown.

Clarifying the reason and direction behind the close association between insulin resistance and hyperuricemia could inform the treatment and prevention of these frequently overlapping problems. This endeavor can be accomplished using Mendelian randomization (MR) analysis, which employs genetic variants as instrumental variables for exposures, allowing one to obtain unconfounded estimates of potential causal effects. Leveraging newly released genome-wide association studies (GWAS), which identified substantially more variants associated with SU level and fasting insulin compared to their predecessors, we performed a bidirectional MR analysis to investigate potential causal relationships between insulin resistance and hyperuricemia, with gout itself as a secondary outcome measure.

PATIENTS AND METHODS

Study design. We performed both 1- and 2-sample MR analyses. First, we conducted a series of univariable 2-sample analyses to examine the relationship between SU concentration and fasting insulin concentration, a surrogate measure of insulin resistance (8). We looked for causal relationships in both directions. We also examined gout in place of SU to ensure consistency of our findings. Given the known correlations between fasting insulin, SU, and body mass index (BMI), we then performed multivariable analyses (9) using BMI-associated genetic variants to partition the total effects of fasting insulin on SU from its direct effects, independent of BMI. Finally, we replicated our findings in a single-sample context, using individual-level data from the UK Biobank to assess the relationship between a polygenic score for fasting insulin concentrations and our 2 outcome measures: SU level and gout. The UK Biobank obtained ethical approval from the North West - Haydock Research Ethics Committee (no. 16/NW/0274); all participants provided written informed consent.

Data source and study population. *Two-sample MR analyses.* For our 2-sample analyses, we used summary-level data from the largest available GWAS. For urate level and gout, we used summary statistics from the Chronic Kidney Disease Genetics (CKDGen) consortium, consisting of many European-ancestry cohorts (10). The summary statistics were derived from 288,649 participants for SU level and from 13,179 cases and 750,634 controls for gout. For fasting insulin, we used the Meta-Analysis of Glucose- and Insulin-related traits Consortium (MAGIC) (11), which provided summary statistics for fasting insulin concentrations, adjusted for measured BMI, based on 153,525 European-ancestry participants without diabetes, as insulin concentrations are affected by diabetes or medication to treat diabetes. Finally, for our multivariable 2-sample MR analysis with adjustment for BMI, we used BMI association statistics from a recent meta-analysis of the Genetic Investigation of Anthropometric Traits consortium and the UK Biobank, which featured 681,275 total participants of European ancestry (12).

One-sample MR analysis. For our 1-sample analysis, we used individual-level data from the UK Biobank (application no. 27892), a prospective cohort of ~500,000 individuals ages 40–69 years recruited across the UK. Genotypic and phenotypic data were available, as well as biomarker measurements such as SU level. Genotyping in this cohort was performed using either the Affymetrix UK Bileve Axiom array or the Affymetrix UK Biobank Axiom array. Quality control and imputation were performed centrally by researchers affiliated with the UK Biobank itself. We limited our analyses to people of European ancestry due to the fact that our polygenic score for fasting insulin was based on data from European populations. To do so, we first used principal component analysis to identify genetically European individuals, and then, from this population, removed individuals who did not self-report as White or "do not know/prefer not to answer," following prior UK Biobank analyses (13). We also excluded related individuals. Relatedness was determined according to Bycroft et al (14), in which individuals were considered related if they were third-degree relatives or closer (kinship coefficient $\geq 1/2^{9/2}$), using kinship coefficients provided by the UK Biobank. In total, our final 1-sample analysis involved 378,065 individuals.

Outcome measures. *Two-sample MR analyses.* The primary outcomes for the bidirectional 2-sample analyses were age- and sex-adjusted concentrations of SU (mg/dl), as defined by the CKDGen consortium (10), and fasting insulin (log pmoles/liter), as defined by the MAGIC study (11,15). The mean ± SD SU concentration was 5.1 ± 1.5 mg/dl among European-ancestry members of the Atherosclerosis Risk in Communities (ARIC) cohort, one of the largest European-ancestry population-based cohorts in the CKDGen consortium. The mean ± SD fasting insulin concentrations were 1.90 ± 1.7 and 1.82 ± 1.7 log pmoles/liter, in men and women, respectively, in one of the largest European-ancestry cohorts in the MAGIC study.

One-sample MR analysis. Since fasting insulin was not measured in the UK Biobank cohort, the 1-sample individual-level MR analysis was unidirectional, with SU concentration serving as the primary outcome measure. Gout was examined as a secondary outcome measure in both the 1- and 2-sample analyses. For the 1-sample analysis using data from the UK Biobank, gout was defined based on either patient report (20% of cases), diagnoses recorded during primary care encounters (39%), inpatient hospitalizations (12%), or a combination thereof (30%). This case definition

builds upon one concluded to have high precision for detecting association in genetic epidemiologic studies of gout (16) and used in other published studies of gout using the UK Biobank (17,18).

Genetic instruments (2-sample and 1-sample MR analyses). We identified 123 single-nucleotide polymorphisms (SNPs) for SU (total R^2 7.2%) and 55 SNPs for gout (total R^2 1.4%) (10), combining these to produce polygenic instruments for each exposure. We also separately examined the effects of SNPs from 2 highly influential SU genes, *SLC2A9* (R^2 = 2.4% alone) and *ABCG2* (R^2 = 0.7% alone), which are strongly associated with SU concentration (0.33 mg/dl and 0.25 mg/dl, respectively) and gout risk (odds ratio [OR] 1.51 [95% confidence interval (95% CI) 1.47, 1.56] and OR 2.04 [95% CI 1.96, 2.12], respectively), with little to no evidence of pleiotropy (e.g., associations with related cardiometabolic traits) (19). For fasting insulin concentration, we identified 95 SNPs (total R^2 1%) (11), and for BMI, we identified 941 SNPs (total R^2 6%) (12). We subsequently pruned these SNPs for linkage disequilibrium at a threshold of R^2 < 0.001, leaving 121 independent SNPs for SU (F statistic 182), 54 for gout (F statistic 198), 83 for fasting insulin (F statistic 25), and 925 for BMI (F statistic 47) (Supplementary Table 1, available on the *Arthritis & Rheumatology* website at http://onlinelibrary.wiley.com/doi/10.1002/art.41779/abstract). The F statistic is a measure of the strength of association between these genetic instruments and the exposure (20); values >10 indicate that the instrument is sufficiently strong with a low potential for weak instrument bias (21), which would otherwise drive a 2-sample MR estimate toward the null.

Statistical analysis. *Primary 2-sample MR analyses.* We first assessed the associations between genetically determined SU concentration/gout risk and fasting insulin concentration using multiplicative random-effects inverse variance–weighted (IVW) meta-analysis methods; Wald ratios were generated for the single-SNP estimates (22). In the opposite direction, we assessed the association between genetically determined fasting insulin concentrations on changes in SU levels and the odds of gout. Our primary analysis used BMI-adjusted beta coefficients as exclusively reported in the latest MAGIC GWAS (n = 95 SNPs) (11), whereas our secondary analysis used unadjusted betas from an earlier MAGIC GWAS (n = 12 SNPs) (15), in which both BMI-unadjusted and BMI-adjusted summary statistics were available (Supplementary Table 2, http://onlinelibrary.wiley.com/doi/10.1002/art.41779/abstract).

Multivariable 2-sample MR analyses. We performed multivariable MR analyses to isolate the direct effects of fasting insulin, independent of (or conditional on) BMI, which is known to impact concentrations of both fasting insulin (15) and SU (23,24). Based on procedures for 2-sample multivariable MR published by Sanderson et al (9), these models included variants significantly associated with either fasting insulin or BMI.

Sensitivity MR analysis for pleiotropy. We assessed the presence of horizontal pleiotropy using the MR-Egger intercept test (25), wherein the intercept represents the average pleiotropic effect. An intercept term that is significantly different from 0 indicates the presence of unbalanced (directional) pleiotropy, which can bias the IVW estimate (25). Along with our main (IVW) effect estimates, we generated additional estimates shown to be robust to the presence of horizontal pleiotropy. These included univariable (25) and multivariable (26) MR-Egger estimates and univariable weighted median- and mode-based estimates (27,28). We conducted leave-one-out analyses (Supplementary Figures 1 and 2, http://onlinelibrary.wiley.com/doi/10.1002/art.41779/abstract), systematically recalculating the main IVW estimate after removing 1 variant at a time to visually inspect for influential variants (Supplementary Figures 3 and 4, http://onlinelibrary.wiley.com/doi/10.1002/art.41779/abstract), and regenerated all estimates after removing outliers identified by the MR-PRESSO (Pleiotropy RESidual Sum and Outlier) test (29).

Power calculations. Post hoc power calculations for the 2-sample analysis were performed using the mRnd power calculator (30) and were based on the proportion of variance explained by the instruments, the numbers of participants in the CKDGen and MAGIC studies, and the observed epidemiologic associations and their 95% confidence intervals (31) (Supplementary Table 3, http://onlinelibrary.wiley.com/doi/10.1002/art.41779/abstract).

Polygenic scores. Polygenic scores were constructed for the UK Biobank participants using the same fasting insulin SNPs used in the 2-sample analysis. To calculate the scores, we used PLINK version 1.9 (www.cog-genomics.org/plink/1.9). Each SNP was weighted according to its effect size for fasting insulin in the latest MAGIC GWAS, as fasting insulin values were not measured in the UK Biobank cohort. The polygenic scores were normalized, setting the mean to 0 and the SD to 1. Participants with urate concentrations ≥4 SDs from the mean were excluded. For the analysis of urate concentration as a function of the fasting insulin score, linear regression models were used. For gout, a binary outcome measure, we used logistic regression. Models were adjusted for age, sex, 10 principal components to control for population stratification, and the genotyping platform used. We also controlled for BMI in some models.

Software. The 1- and 2-sample analyses were conducted using R software (http://www.R-project.org); the R packages TwoSampleMR, MendelianRandomization, and MVMR; and the MR-Base portal (32).

RESULTS

Effects of genetically determined SU concentration and gout risk on fasting insulin concentration, according to 2-sample MR analysis. In the main IVW analysis, neither genetically determined concentrations of SU (β = 0.0038 log pmoles/liter fasting insulin per 1 mg/dl increase in SU level

[95% CI –0.0390, 0.0466]; *P* = 0.86), nor genetically determined gout risk (β = –0.0026 log pmoles/liter [95% CI –0.0235, 0.0183]; *P* = 0.81) had significant effects on fasting insulin (Figure 1). These findings were consistent across all MR estimates (Figure 1) and did not materially change after removal of the outliers identified by the MR-PRESSO test (Supplementary Table 4, http://onlinelibrary. wiley.com/doi/10.1002/art.41779/abstract). Furthermore, while the SNPs mapping to *SLC2A9* and *ABCG2* were strongly associated with SU level and odds of gout, neither was associated with changes in fasting insulin concentration (Figure 1). Estimates were similar when using the BMI-unadjusted summary statistics for fasting insulin (Supplementary Table 5, http://onlinelibrary. wiley.com/doi/10.1002/art.41779/abstract). Furthermore, genetically determined SU level was not associated with BMI, and thus, no multivariable MR analysis was performed.

Effects of genetically determined fasting insulin concentration on SU concentration, according to 2-sample MR analysis. In the opposite direction, genetically determined concentrations of fasting insulin (adjusted for BMI) were positively associated with SU level (Figure 2A). In the main IVW analysis, a 1-unit (1 log pmole/liter) increase in fasting insulin was associated with an increase in SU concentration of 0.37 mg/dl (95% CI 0.15, 0.58) (*P* = 0.001). This translates to a 0.63 mg/dl increase in SU per 1 SD (1.7 log pmoles/liter) increase in fasting insulin. No pleiotropy was detected (MR-Egger intercept = 0.008; *P* = 0.09). All other MR estimates were significant and were numerically larger than the main IVW estimate except for the MR-Egger regression estimate (Figure 2A).

Nine outlier SNPs were identified by the MR-PRESSO test (Supplementary Table 4). As shown in the leave-one-out plots in Supplementary Figure 2 and scatter plots in Supplementary Figure 4 (http://onlinelibrary.wiley.com/doi/10.1002/art.41779/ abstract), the most influential SNP was rs1260326, mapped to the *GCKR* gene. Upon the removal of all 9 outliers, the IVW estimate strengthened (β = 0.56 mg/dl [95% CI 0.45, 0.67]; *P* < 0.001), as did the MR-Egger regression estimate (β = 0.54 mg/dl [95% CI 0.22, 0.87]; *P* = 0.002) (Figure 2A), and there remained little evidence of pleiotropy (MR-Egger intercept < 0.001; *P* = 0.90).
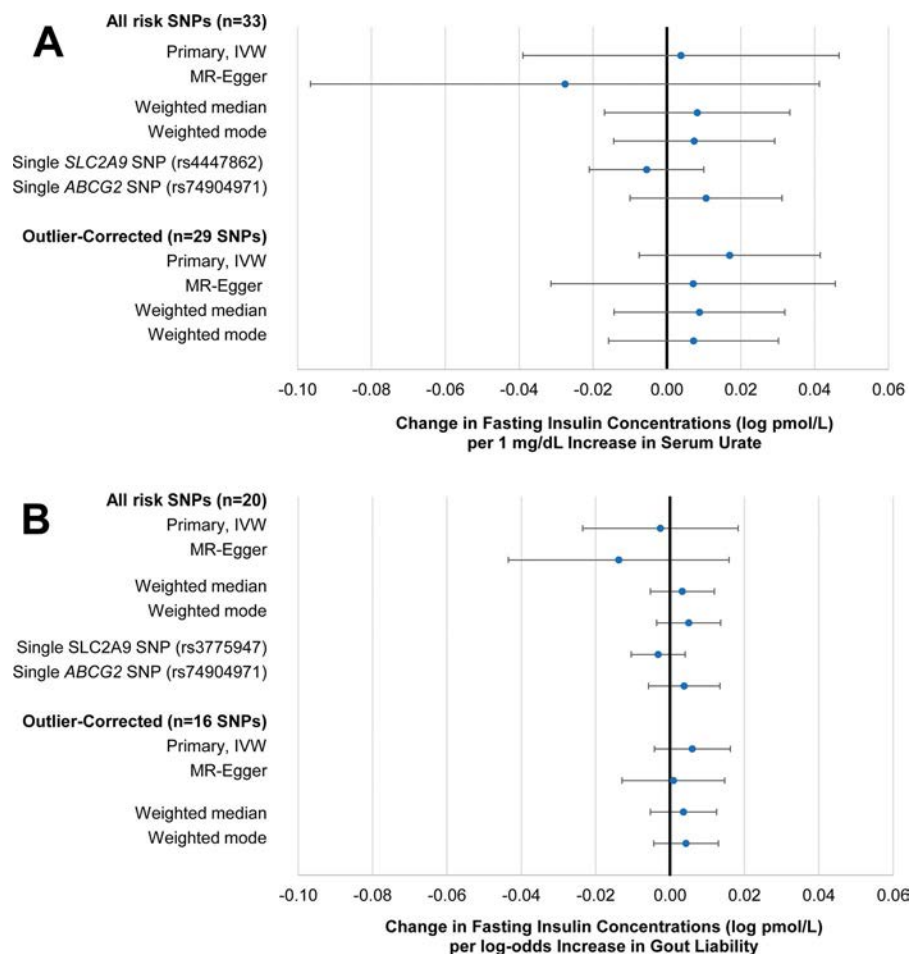
Figure 1. Causal effect estimates (with 95% confidence intervals) for genetically determined concentration of serum urate (per 1 mg/dl) (**A**) and odds of gout (**B**) on body mass index–adjusted concentrations of fasting insulin (log pmoles/liter), obtained from subjects without diabetes mellitus, using a 2-sample analysis. SNPs = single-nucleotide polymorphisms; IVW = inverse probability–weighted; MR-Egger = Mendelian randomization analysis method. Color figure can be viewed in the online issue, which is available at http://onlinelibrary.wiley.com/doi/10.1002/ art.41779/abstract.
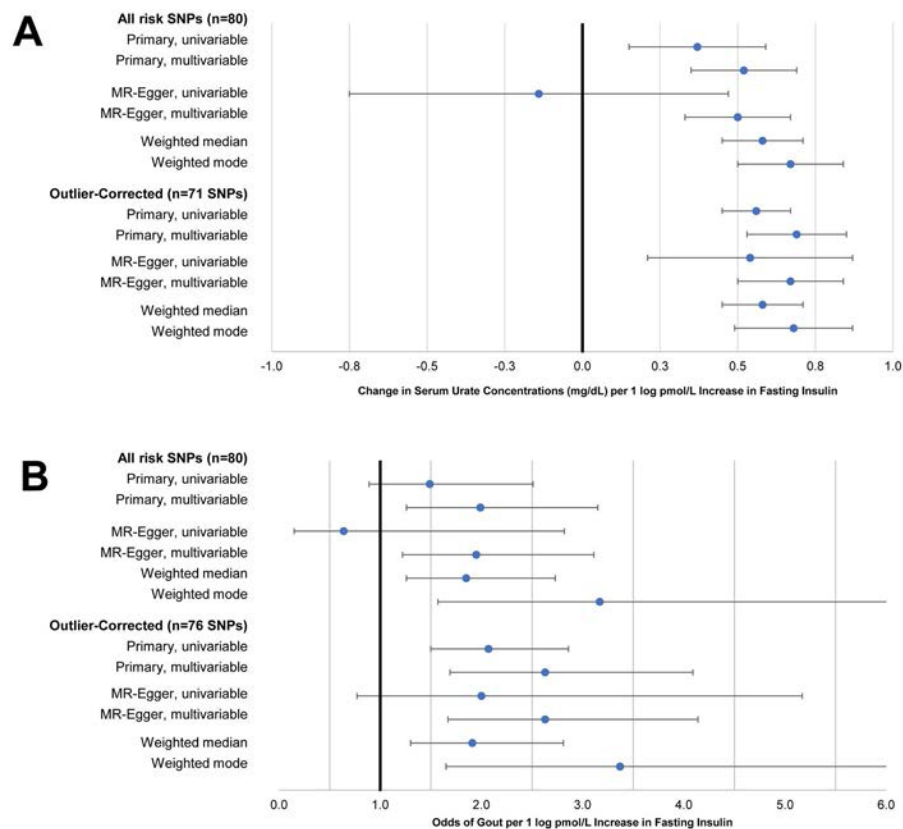
Figure 2. Causal effect estimates (with 95% confidence intervals) for genetically determined concentration of fasting insulin (per log pmole/liter) on concentrations of serum urate (mg/dl) (**A**) and odds of gout (**B**), obtained from subjects without diabetes mellitus, using a 2-sample analysis. One of the candidate risk SNPs for fasting insulin was removed during harmonization due to ambiguity in the strand direction, leaving 80 SNPs in the final analysis. See Figure 1 for definitions.

As displayed in Figure 2A, the multivariable IVW estimates for fasting insulin, representing its direct effect on SU level conditioned on genetically determined BMI, were larger than their univariable counterparts, reaching 0.52 mg/dl (95% CI 0.35, 0.69) per 1 log pmole/liter of fasting insulin, which translates to 0.88 mg/dl per SD increase in fasting insulin, including outliers, and 0.69 mg/dl (95% CI 0.53, 0.85), or 1.18 mg/dl per SD increase of fasting insulin, excluding outliers ($P < 0.001$ for both). The same pattern was observed for the univariable and multivariable MR-Egger estimates. The univariable and multivariable estimates of the effect of genetically determined BMI on SU level were virtually identical, with SU increases of 0.32 and 0.31 mg/dl per 1-SD increase in BMI, respectively ($P < 0.001$ for both).

Effects of genetically determined fasting insulin concentration on SU level, according to 1-sample MR analysis. These findings were replicated at the individual level with UK Biobank data, using polygenic risk scores for fasting insulin concentration (Figure 3). Among all eligible UK Biobank participants (n = 360,453), there was a mean ± SD SU concentration of 5.19 ± 1.34 mg/dl; 26% of participants had hyperuricemia (SU ≥ 6 mg/dl) (Supplementary Table 6, http://onlinelibrary.wiley.com/doi/10.1002/art.41779/abstract). Consistent with findings

from the 2-sample MR analysis, we found that a 1-SD increase in the polygenic risk score corresponded to a significant increase in SU level ($P = 6.3 \times 10^{-33}$) (Table 1). This effect strengthened after removing the outliers identified in the 2-sample MR analysis and was further amplified with additional adjustment for measured BMI. When we excluded individuals receiving urate-lowering therapy, our effect estimates remained the same to 2 decimal places.

Effects of genetically determined fasting insulin concentration on risk of gout, according to 1- and 2-sample MR analyses. The estimated effects of genetically determined fasting insulin concentration on gout risk followed a pattern similar to SU level. In the 2-sample MR analysis, the OR for gout (per 1 log pmole/liter insulin) increased from 1.49 (95% CI 0.89, 2.51) ($P = 0.13$) in the initial analysis to 2.07 (95% CI 1.50, 2.86) ($P < 0.001$) when 4 outliers were excluded (Figure 2B). As with SU, the multivariable OR was larger than the univariable, reaching 2.63 (95% CI 1.69, 4.10) ($P < 0.001$). In the 1-sample analysis (n = 12,920), we observed a similar result, namely that there was a statistically significant positive association between the polygenic score for fasting insulin and OR for gout ($P = 9.5 \times 10^{-4}$) (Table 1), which increased when we adjusted for BMI and excluded outlier SNPs. Our definition of gout captured 93% of participants
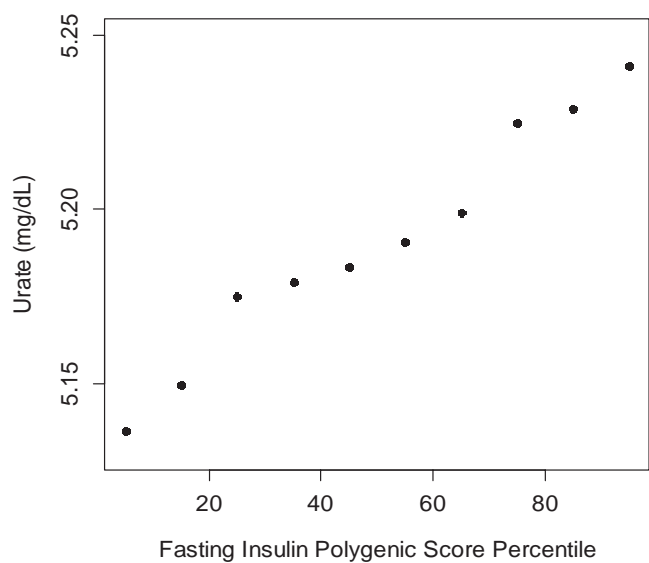
Figure 3. Mean serum urate concentration by decile of the polygenic score for fasting insulin in the UK Biobank. The 71–single-nucleotide polymorphism polygenic score, which excluded outliers, was used to generate this figure.

receiving urate-lowering therapy. Limiting our definition of gout to only self-reported cases did not change the significance of our results or the direction of effect.

DISCUSSION

This first bidirectional MR analysis of SU and fasting insulin concentrations provides evidence that genetically elevated fasting insulin concentration, a measure of insulin resistance and precursor to cardiometabolic diseases, is causally associated with hyperuricemia, as well as the clinical end point of gout. Effects were consistent across summary-level and individual-level analyses and strengthened upon the removal of outliers and controlling for BMI. Conversely, our data do not support a causal effect of SU on fasting insulin concentrations.

Our null findings on the effects of SU concentration are consistent with an earlier, individual-level MR analysis of multiple population-based cohorts (e.g., ARIC, Framingham) within the CHARGE consortium (33), in which an 8-SNP genetic risk score for SU was not associated with fasting insulin concentrations. These findings are also consistent with prior MR analyses which similarly identified no causal effects between SU level and clinical cardiometabolic end points (19), including coronary heart disease (34,35) and type 2 diabetes (19). Furthermore, the 2 pivotal individual genes (*SLC2A9* and *ABCG2*) accounting for 34% and 10%, respectively, of the total proportion of variance in SU concentration explained by the polygenic instrument for SU (10), were not associated with fasting insulin concentrations in this MR analysis nor in the prior CHARGE consortium analysis (33). Therefore, a causal role of SU on insulin resistance seems highly unlikely.

Conversely, fasting insulin concentrations were positively associated with SU concentration, and this relationship grew larger when outliers were removed. The most prominent outlier was rs1260326, mapped to the *GCKR* gene, which affects multiple cardiometabolic pathways (19,33). This SNP was significantly associated with fasting insulin concentrations but is also likely a causal variant of SU (10), which makes a strong case for its removal on the basis of horizontal pleiotropy. The unidirectional causal effects observed for fasting insulin in our study are consistent with another causal indicator reported by the CKDGen consortium (i.e., genetic causality proportion –0.49; $P = 2.80 \times 10^{-2}$) (10), which suggests that fasting insulin is partially genetically causal to urate concentrations.

Our findings also corroborate those from previous physiologic experiments demonstrating insulin's anti-uricosuric property, with exogenous insulin reducing the renal excretion of urate in both healthy individuals and patients with hypertension (7,36). Insulin may increase renal urate reabsorption via stimulation of facilitated glucose transporter 9 (encoded by *SLC2A9*) and other renal urate transporters involved in urate reabsorption (37). Insulin resistance manifests early in the progression to type 2 diabetes (38), and the early pathophysiologic changes could increase SU concentrations before dysglycemia becomes clinically evident, a theory supported by the Whitehall II cohort study (39), in which participants who eventually developed type 2 diabetes already had

Table 1. Association of polygenic scores for fasting insulin with SU level and gout risk based on UK Biobank data (1-sample analysis)*

	Change in SU level (mg/dl) per SD increase in fasting insulin score (95% CI)	P	OR for gout per SD increase in fasting insulin score (95% CI)	P
Unadjusted for BMI				
All SNPs	0.023 (0.019, 0.026)	6.3×10^{-33}	1.03 (1.01, 1.05)	9.5×10^{-4}
Excluding outliers	0.031 (0.027, 0.035)	8.2×10^{-61}	1.05 (1.03, 1.07)	1.0×10^{-7}
Adjusted for BMI				
All SNPs	0.031 (0.028, 0.034)	1.8×10^{-69}	1.05 (1.03, 1.07)	8.8×10^{-7}
Excluding outliers	0.040 (0.036, 0.043)	8.6×10^{-114}	1.07 (1.05, 1.09)	9.8×10^{-13}

* All models were adjusted for age and sex as well as 10 principal components and the genotyping platform used. SU = serum urate; 95% CI = 95% confidence interval; OR = odds ratio; BMI = body mass index; SNPs = single-nucleotide polymorphisms.

lower levels of insulin sensitivity at baseline (up to 13 years prior to diagnosis) compared to those who did not develop diabetes.

While obesity and insulin resistance are positively correlated, we provide evidence that a portion of the effects of fasting insulin on SU are independent of genetically determined BMI, with multivariable effect estimates that were larger compared to the univariable effect estimates. At the same time, our results suggest that there is at least some portion of the SU-increasing effect of obesity independent of the insulin pathway. Negative confounding by BMI is consistent with prior reports from MAGIC investigators (15,40), and the phenomenon of lipodystrophic insulin resistance (41), wherein a lack (or dysfunction) of white adipose tissue, especially subcutaneous gluteofemoral fat, leads to insulin resistance and metabolic syndrome in nonobese or lean individuals (42). Subtle lipodystrophy is believed to be a major contributor to metabolic syndrome at the population level (42).

Related to this, a potential caveat of our analysis is that the SNP–insulin association estimates from the MAGIC summary statistics were adjusted for age, sex, and BMI (as measured in study participants who underwent genotyping), while the corresponding estimates for SU were not adjusted for BMI. MAGIC investigators opted to adjust for BMI as this had increased the number of insulin-associated variants detected in their previous GWAS (15), including some insulin-increasing alleles associated with lower BMI. While this adjustment can help isolate SNPs impacting insulin resistance independently of BMI, it can also raise concerns about collider bias (43) (e.g., inducing a spurious association between the SNP and fasting insulin). However, MAGIC investigators evaluated this possibility and found no evidence of collider bias in the vast majority of SNPs tested (11,41). Moreover, there were no meaningful differences in the effect estimates we generated using the BMI-unadjusted and BMI-adjusted fasting insulin summary statistics from the earlier MAGIC GWAS (Supplementary Table 2, http://onlinelibrary.wiley.com/doi/10.1002/art.41779/abstract). Our examination of the impact of fasting insulin on SU with a multivariable MR model that included BMI-associated SNPs (the potential collider) (9) should further alleviate these concerns.

Our novel findings explain the core reason and direction underpinning the close association between hyperuricemia and insulin resistance syndrome, with implications for the prevention and management of both conditions and their cardiometabolic sequelae. Large-scale pharmaceutical trials of drugs that substantially lowered SU have not, to date, demonstrated cardiometabolic benefits, such as weight change, lipid profile, blood pressure, or renal function (44,45). Building upon this, our data suggest that interventions targeting SU alone (e.g., urate-lowering drugs) are unlikely to lower insulin concentrations and, in turn, the risk of insulin resistance or metabolic syndrome and its cardiometabolic consequences. Instead, our data suggest that lifestyle modifications specifically shown to improve insulin concentrations and insulin resistance (e.g., a "green" Mediterranean diet emphasizing consumption of plant proteins instead of red/processed meats

and other animal proteins [46]) would lower SU concentrations, in addition to providing other cardiometabolic risk benefits. Indeed, a higher-protein, low-carbohydrate diet was associated with reductions in BMI (median 2.7 kg/m^2) and SU level (median 1.6 mg/dl), and improvements in dyslipidemia, according to a pilot open-label trial of gout patients (47), while in a recent analysis of the Dietary Intervention Randomized Controlled Trial, 3 healthy weight-loss diets significantly reduced SU levels, particularly among those with baseline hyperuricemia (by 1.9–2.4 mg/dl over 6 months, the maximum weight-loss phase, and by 1.1–1.4 mg/dl over 24 months) (48). This reduction was independently driven by reductions in plasma insulin concentrations in addition to weight reduction.

Our analysis has some limitations. While the genetic association data were sourced from large, multinational disease consortia, they pertained mainly to European-ancestry/White British populations. This served to minimize confounding by differences in population structure (21), but our findings should be confirmed in other ancestral populations. Since insulin concentrations were not measured in the UK Biobank cohort, we could not replicate our analysis of the effect of genetically determined SU on fasting insulin in the single-sample setting. However, none of the estimates from the 2-sample analysis suggested a causal role for these exposures. With an R^2 of 1.3%, the 80-SNP instrument for fasting insulin explained a comparatively low proportion of the phenotypic variance (e.g., overall variance in measured fasting insulin concentrations) than did the instruments for SU (R^2 = 7.1%) and BMI (R^2 = 6%). This was evident in the 1-sample MR analysis, wherein the polygenic risk score for fasting insulin was positively correlated with measured SU concentrations (Figure 3), although the absolute difference between the extreme deciles of the risk score was small (~0.10 mg/dl).

Of note, since fasting insulin concentrations were not measured in the UK Biobank cohort, different methods were required for the 1- and 2-sample analyses, and the resultant effect estimates cannot be directly compared. The estimates generated by the 2-sample MR analysis represent the change in concentrations of SU (and odds of gout) associated with a 1-unit change in genetically determined concentrations of fasting insulin itself, while the estimates generated by the 1-sample MR analysis represent the changes associated with a 1-SD change in the polygenic score for fasting insulin, which is less sensitive. As such, the findings of our 1-sample analysis served to reinforce the presence of causal effects of fasting insulin observed in our 2-sample analysis, rather than to quantify the magnitude of these effects (49). Importantly, the variants are a proxy for the genetic predisposition toward increased fasting insulin concentrations, while environmental factors appear to make a larger contribution to the total phenotypic variance in fasting insulin (50). BMI, for example, accounted for one-third of the variance in fasting insulin concentrations in one MAGIC cohort (15).

While weak instrument bias would drive the 2-sample MR estimates toward the null (in the absence of substantial overlap

between samples), we observed significant causal effects for fasting insulin, but not SU concentration, whose instrument was stronger. Indeed, we had >99% power to detect a causal effect of SU concentrations on fasting insulin concentrations matching that observed in a representative sample of US adults (31) (Supplementary Table 4, http://onlinelibrary.wiley.com/doi/10.1002/art.41779/abstract). We sourced data from recently published, mainly population-based GWAS, and the findings of the 2-sample univariable and multivariable analyses were generally consistent with these for SU and gout, and robust to sensitivity analyses, especially after outliers were removed. Moreover, the positive associations between genetically instrumented fasting insulin concentrations and SU concentrations were replicated at the individual level, before and after adjustment for measured BMI.

In conclusion, this study provides robust evidence that insulin resistance has a positive causal effect on SU concentrations, with this relationship operating only in one direction. Interventions to reduce insulin resistance may lower SU concentrations and gout risk, conferring additional metabolic health benefits.

AUTHOR CONTRIBUTIONS

All authors were involved in drafting the article or revising it critically for important intellectual content, and all authors approved the final version to be published. Dr. McCormick had full access to all of the data in the study and takes responsibility for the integrity of the data and the accuracy of the data analysis.
Study conception and design. McCormick, O'Connor, Leong.
Acquisition of data. Leong.
Analysis and interpretation of data. McCormick, O'Connor, Yokose, Merriman, Mount, Leong, Choi.

REFERENCES

1. Safiri S, Kolahi AA, Cross M, Carson-Chahhoud K, Hoy D, Almasi-Hashiani A, et al. Prevalence, incidence, and years lived with disability due to gout and its attributable risk factors for 195 Countries and territories 1990–2017: a systematic analysis of the Global Burden of Disease study 2017. Arthritis Rheumatol 2020;72:1916–27.

2. Choi HK, Ford ES. Prevalence of the metabolic syndrome in individuals with hyperuricemia. Am J Med 2007;120:442–7.

3. Zhu Y, Pandya BJ, Choi HK. Comorbidities of gout and hyperuricemia in the US general population: NHANES 2007–2008. Am J Med 2012;125:679–87.

4. Facchini F, Chen YD, Hollenbeck CB, Reaven GM. Relationship between resistance to insulin-mediated glucose uptake, urinary uric acid clearance, and plasma uric acid concentration. JAMA 1991;266:3008–11.

5. Rathmann W, Funkhouser E, Dyer AR, Roseman JM. Relations of hyperuricemia with the various components of the insulin resistance syndrome in young Black and White adults: the CARDIA study. Ann Epidemiol 1998;8:250–61.

6. Krishnan E, Pandya BJ, Chung L, Hariri A, Dabbous O. Hyperuricemia in young adults and risk of insulin resistance, prediabetes, and diabetes: a 15-year follow-up study. Am J Epidemiol 2012;176:108–16.

7. Ter Maaten JC, Voorburg A, Heine RJ, Ter Wee PM, Donker AJ, Gans RO. Renal handling of urate and sodium during acute physiological hyperinsulinaemia in healthy subjects. Clin Sci (Lond) 1997;92:51–8.

8. Laakso M. How good a marker is insulin level for insulin resistance? Am J Epidemiol 1993;137:959–65.

9. Sanderson E, Smith GD, Windmeijer F, Bowden J. An examination of multivariable Mendelian randomization in the single-sample and two-sample summary data settings. Int J Epidemiol 2019;48:713–27.

10. Tin A, Marten J, Kuhns VL, Li Y, Wuttke M, Kirsten H, et al. Target genes, variants, tissues and transcriptional pathways influencing human serum urate levels. Nat Genet 2019;51:1459–74.

11. Chen J, Spracklen CN, Marenne G, Varshney A, Corbin LJ, Luan J, et al. The trans-ancestral genomic architecture of glycaemic traits. URL: http://biorxiv.org/lookup/doi/10.1101/2020.07.23.217646. bioRxiv. July 2020.

12. Yengo L, Sidorenko J, Kemper KE, Zheng Z, Wood AR, Weedon MN, et al. Meta-analysis of genome-wide association studies for height and body mass index in ~700,000 individuals of European ancestry. Hum Mol Genet 2018;27:3641–9.

13. Cole JB, Florez JC, Hirschhorn JN. Comprehensive genomic analysis of dietary habits in UK Biobank identifies hundreds of genetic associations. Nat Commun 2020;11:1467.

14. Bycroft C, Freeman C, Petkova D, Band G, Elliott LT, Sharp K, et al. The UK Biobank resource with deep phenotyping and genomic data. Nature 2018;562:203–9.

15. Scott RA, Lagou V, Welch RP, Wheeler E, Montasser ME, Luan J, et al. Large-scale association analyses identify new loci influencing glycemic traits and provide insight into the underlying biological pathways. Nat Genet 2012;44:991–1005.

16. Cadzow M, Merriman TR, Dalbeth N. Performance of gout definitions for genetic epidemiological studies: analysis of UK Biobank. Arthritis Res Ther 2017;19:181.

17. Tai V, Narang RK, Gamble G, Cadzow M, Stamp LK, Merriman TR, et al. Do serum urate–associated genetic variants differentially contribute to gout risk according to body mass index? Analysis of the UK Biobank. Arthritis Rheumatol 2020;72:1184–91.

18. Sandoval-Plata G, Nakafero G, Chakravorty M, Morgan K, Abhishek A. Association between serum urate, gout and comorbidities: a case-control study using data from the UK Biobank. Rheumatology (Oxford) 2020. doi: 10.1093/rheumatology/keaa773. E-pub ahead of print.

19. Keenan T, Zhao W, Rasheed A, Ho WK, Malik R, Felix JF, et al. Causal assessment of serum urate levels in cardiometabolic diseases through a mendelian randomization study. J Am Coll Cardiol 2016;67:407–16.

20. Burgess S, Butterworth A, Thompson SG. Mendelian randomization analysis with multiple genetic variants using summarized data. Genet Epidemiol 2013;37:658–65.

21. Davies NM, Holmes MV, Smith GD. Reading Mendelian randomisation studies: a guide, glossary, and checklist for clinicians. BMJ 2018;362:k601.

22. Wald A. The fitting of straight lines if both variables are subject to error. Ann Math Stat 1940;11:284–300.

23. Larsson SC, Burgess S, Michaëlsson K. Genetic association between adiposity and gout: a Mendelian randomization study. Rheumatology (Oxford) 2018;57:2145–8.

24. Lyngdoh T, Vuistiner P, Marques-Vidal P, Rousson V, Waeber G, Vollenweider P, et al. Serum uric acid and adiposity: deciphering causality using a bidirectional Mendelian randomization approach. PLoS One 2012;7:e39321.

25. Burgess S, Thompson SG. Interpreting findings from Mendelian randomization using the MR-Egger method. Eur J Epidemiol 2017;32:377–89.

26. Rees JM, Wood AM, Burgess S. Extending the MR-Egger method for multivariable Mendelian randomization to correct for both measured and unmeasured pleiotropy. Stat Med 2017;36:4705–18.

27. Bowden J, Smith GD, Haycock PC, Burgess S. Consistent estimation in Mendelian randomization with some invalid instruments using a weighted median estimator. Genet Epidemiol 2016;40:304–14.

28. Hartwig FP, Smith GD, Bowden J. Robust inference in summary data Mendelian randomization via the zero modal pleiotropy assumption. Int J Epidemiol 2017;46:1985–98.

29. Verbanck M, Chen CY, Neale B, Do R. Detection of widespread horizontal pleiotropy in causal relationships inferred from Mendelian randomization between complex traits and diseases. Nat Genet 2018;50:693–8.

30. Brion MJ, Shakhbazov K, Visscher PM. Calculating statistical power in Mendelian randomization studies. Int J Epidemiol 2013;42:1497–501.

31. Choi HK, Ford ES. Haemoglobin A1c, fasting glucose, serum C-peptide and insulin resistance in relation to serum uric acid levels: the Third National Health and Nutrition Examination Survey. Rheumatology (Oxford) 2008;47:713–7.

32. Hemani G, Zheng J, Elsworth B, Wade KH, Haberland V, Baird D, et al. The MR-Base platform supports systematic causal inference across the human phenome. Elife 2018;7:e34408.

33. Yang Q, Kottgen A, Dehghan A, Smith AV, Glazer NL, Chen MH, et al. Multiple genetic loci influence serum urate levels and their relationship with gout and cardiovascular disease risk factors. Circ Cardiovasc Genet 2010;3:523–30.

34. White J, Sofat R, Hemani G, Shah T, Engmann J, Dale C, et al. Plasma urate concentration and risk of coronary heart disease: a Mendelian randomisation analysis. Lancet Diabetes Endocrinol 2016;4:327–36.

35. Efstathiadou A, Gill D, McGrane F, Quinn T, Dawson J. Genetically determined uric acid and the risk of cardiovascular and neurovascular diseases: a Mendelian randomization study of outcomes investigated in randomized trials. J Am Heart Assoc 2019;8:e012738.

36. Muscelli E, Natali A, Bianchi S, Bigazzi R, Galvan AQ, Sironi AM, et al. Effect of insulin on renal sodium and uric acid handling in essential hypertension. Am J Hypertens 1996;9:746–52.

37. Mount D, Mandal A. Insulin: genetic and physiological influences on human uric acid homeostasis [abstract]. Arthritis Rheumatol 2018;70 Suppl 10. URL: https://acrabstracts.org/abstract/insulin-genetic-and-physiological-influences-on-human-uric-acid-homeostasis.

38. Weir GC, Bonner-Weir S. Five stages of evolving β-cell dysfunction during progression to diabetes. Diabetes 2004;53:S16–21.

39. Tabák AG, Jokela M, Akbaraly TN, Brunner EJ, Kivimäki M, Witte DR. Trajectories of glycaemia, insulin sensitivity, and insulin secretion before diagnosis of type 2 diabetes: an analysis from the Whitehall II study. Lancet 2009;373:2215–21.

40. Scott RA, Fall T, Pasko D, Barker A, Sharp SJ, Arriola L, et al. Common genetic variants highlight the role of insulin resistance and body fat distribution in type 2 diabetes, independent of obesity. Diabetes 2014;63:4378–87.

41. Lotta LA, Gulati P, Day FR, Payne F, Ongen H, van de Bunt M, et al. Integrative genomic analysis implicates limited peripheral adipose storage capacity in the pathogenesis of human insulin resistance. Nat Genet 2017;49:17–26.

42. Mann JP, Savage DB. What lipodystrophies teach us about the metabolic syndrome [review]. J Clin Invest 2019;129:4009–21.

43. Aschard H, Vilhjálmsson BJ, Joshi AD, Price AL, Kraft P. Adjusting for heritable covariates can bias effect estimates in genome-wide association studies. Am J Hum Genet 2015;96:329–39.

44. White WB, Saag KG, Becker MA, Borer JS, Gorelick PB, Whelton A, et al. Cardiovascular safety of febuxostat or allopurinol in patients with gout. N Engl J Med 2018;378:1200–10.

45. Doria A, Galecki AT, Spino C, Pop-Busui R, Cherney DZ, Lingvay I, et al. Serum urate lowering with allopurinol and kidney function in type 1 diabetes. N Engl J Med 2020;382:2493–503.

46. Tsaban G, Meir AY, Rinott E, Zelicha H, Kaplan A, Shalev A, et al. The effect of green Mediterranean diet on cardiometabolic risk; a randomised controlled trial. Heart 2020. doi: 10.1136/heartjnl-2020-317802. E-pub ahead of print.

47. Dessein PH, Shipton EA, Stanwix AE, Joffe BI, Ramokgadi J. Beneficial effects of weight loss associated with moderate calorie/carbohydrate restriction, and increased proportional intake of protein and unsaturated fat on serum urate and lipoprotein levels in gout: a pilot study. Ann Rheum Dis 2000;59:539–43.

48. Yokose C, McCormick N, Rai SK, Lu N, Curhan G, Schwarzfuchs D, et al. Effects of low-fat, Mediterranean, or low-carbohydrate weight loss diets on serum urate and cardiometabolic risk factors: a secondary analysis of the Dietary Intervention Randomized Controlled Trial (DIRECT). Diabetes Care 2020;43:2812–20.

49. VanderWeele TJ, Tchetgen Tchetgen EJ, Cornelis M, Kraft P. Methodological challenges in Mendelian randomization. Epidemiology 2014;25:427–35.

50. Snieder H, Boomsma DI, van Doornen LJ, Neale MC. Bivariate genetic analysis of fasting insulin and glucose levels. Genet Epidemiol 1999;16:426–46.

AMERICAN COLLEGE
of RHEUMATOLOGY
Empowering Rheumatology Professionals

Augmentation of Stimulator of Interferon Genes–Induced Type I Interferon Production in COPA Syndrome

Takashi Kato,[1] [ID] Masaki Yamamoto,[2] Yoshitaka Honda,[3] [ID] Takashi Orimo,[4] Izumi Sasaki,[1] [ID]
Kohei Murakami,[5] [ID] Hiroaki Hemmi,[6] Yuri Fukuda-Ohta,[1] Kyoichi Isono,[1] Saki Takayama,[2]
Hidenori Nakamura,[2] Yoshiro Otsuki,[2] Toshiaki Miyamoto,[2] Junko Takita,[7] Takahiro Yasumi,[7]
Ryuta Nishikomori,[8] [ID] Tadashi Matsubayashi,[2] Kazushi Izawa,[7] and Tsuneyasu Kaisho[1] [ID]

Objective. Coatomer subunit alpha (COPA) syndrome, also known as autoinflammatory interstitial lung, joint, and kidney disease, is caused by heterozygous mutations in *COPA*. We identified a novel *COPA* variant in 4 patients in one family. We undertook this study to elucidate whether and how the variant causes manifestations of COPA syndrome by studying these 4 patients and by analyzing results from a gene-targeted mouse model.

Methods. We performed whole-exome sequencing in 7 family members and measured the type I interferon (IFN) signature of the peripheral blood cells. We analyzed the effects of *COPA* variants in in vitro experiments and in *Copa* mutant mice that were generated.

Results. We identified a heterozygous variant of *COPA* (c.725T>G, p.Val242Gly) in the 4 affected members of the family. The IFN score was high in the members carrying the variant. In vitro analysis revealed that *COPA* V242G, as well as the previously reported disease-causing variants, augmented stimulator of interferon genes (STING)–induced type I IFN promoter activities. *Copa*^V242G/+ mice manifested interstitial lung disease and STING-dependent elevation of IFN-stimulated gene expression. In *Copa*^V242G/+ dendritic cells, the STING pathway was not constitutively activated but was hyperactivated upon stimulation, leading to increased type I IFN production.

Conclusion. V242G, a novel *COPA* variant, was found in 4 patients from one family. In gene-targeted mice with the V242G variant, interstitial lung disease was recapitulated and augmented responses of the STING pathway, leading to an increase in type I IFN production, were demonstrated.

INTRODUCTION

Coatomer subunit alpha (COPA) syndrome (OMIM no. 616414), also known as autoinflammatory interstitial lung, joint, and kidney disease, is caused by heterozygous mutations in *COPA* located on chromosome 1q23.2 (1). It is inherited in an autosomal-dominant manner with incomplete penetrance and variable expressivity. Inflammatory markers are typically elevated, including C-reactive protein level and erythrocyte sedimentation rate. Additional indicators of immune dysregulation seen in COPA syndrome patients include positivity for antinuclear antibody as well as rheumatoid factor and myeloperoxidase/proteinase 3–antineutrophil cytoplasmic antibody, indicating that COPA syndrome is not only an autoinflammatory disease but also an autoimmune disease. *COPA* encodes the alpha subunit of the coatomer protein complex I, a carrier complex required for retrograde protein trafficking from the Golgi to the endoplasmic reticulum (ER). Impaired retrograde vesicle transport results in ER stress, followed by unfolded protein and systemic inflammatory responses, causing a variety of phenotypes (1–5). COPA syndrome has recently been reported to be a type I interferonopathy (6,7). Furthermore, findings in human cell lines and murine embryonic fibroblasts from *Copa*[E241K/+] mice suggest that this type I interferonopathy is caused by constitutive activation of the stimulator of interferon (IFN) genes (STING) pathway, which induces type I IFN production in response to cytosolic DNAs (8–10).

In the present study, we showed that 4 patients with COPA syndrome from one family had a novel variant, p.Val242Gly. In vitro analysis revealed that this novel variant, as well as the previously reported variants, showed enhanced activity to transactivate the type I IFN promoters in synergy with STING. We also generated mice that had the newly identified *COPA* variant. *Copa*[V242G/+] mice showed interstitial lung disease (ILD) similar to the patients with COPA syndrome and *Copa*[E241K/+] mice (8,11). *Copa*[V242G/+] mice also exhibited STING-dependent elevation of IFN-stimulated gene (ISG) expression. Furthermore, in dendritic cells (DCs) from *Copa*[V242G/+] mice, the STING pathway was not constitutively activated but was hyperactivated by ligand stimulation, thereby leading to an increase in type I IFN production.

PATIENTS AND METHODS

Mutation analysis. Genomic DNA was extracted from whole blood (patients I-2, II-1, II-2, III-2, III-3, and IV-1) or paraffin-embedded lung tissues (patient III-1). Whole-exome sequencing was performed in the family members to identify the causative variants (patients II-1, II-2, III-2, III-3, and IV-1). Genomic DNA was enriched for protein-coding sequences using SureSelect XT Auto Human All Exon V5 (Agilent Technologies), followed by massively parallel sequencing (HiSeq 1000; Illumina). Sequence data were mapped against the human reference genome (Genome Reference Consortium Human Build 37) using Burrows-Wheeler

Aligner software. Variants were called using the Genome Analysis Toolkit. Annotation of each variant was performed using an in-house program, and then nonsynonymous and splice-site variants with minor allele frequencies of >0.01 were removed as previously described (12). Finally, rare variants shared only by the affected family members (II-1, III-2, and IV-1) were listed as candidates. Sanger sequencing of the family members was performed to confirm the complete segregation of the candidate variants.

The study protocol was approved by the Kyoto University Ethical Committee, and written informed consent was obtained from all participants or their legal guardians in accordance with the Declaration of Helsinki.

IFN signature. Total RNA was extracted from human blood samples collected in PAXgene Blood RNA tubes (no.762165; Becton Dickinson). Blood was drawn once from patients I-2 and III-2 and twice from patient II-1 (before and after JAK inhibitor treatment). Quantitative polymerase chain reaction (PCR) was performed using TaqMan Gene Expression Master Mix (no.4369016; Applied Biosystems) and probes (IFI27, Hs01086370_m1; IFIT1, Hs00356631_g1; RSAD2, Hs01057264_m1; SIGLEC1, Hs00988063_m1; ISG15, Hs00192713_m1; IFI44L, Hs00199115_m1; BACT, Hs01060665_g1; all from Applied Biosystems) on a StepOnePlus Real-Time PCR system (ThermoFisher Scientific), as previously described (12,13). The expression levels of each transcript were determined in triplicate and normalized to the level of β-actin. Results were shown relative to a single calibrator. The median of the relative quantification of the 6 ISGs was used to calculate the IFN score for each patient. IFN scores that exceeded the mean IFN score in 11 healthy controls +2 SD (i.e., >5.04) were considered positive.

In vitro analysis of the *COPA* variants. Detailed methods of luciferase reporter gene assay and Western blot analysis on *COPA* variants are described in Supplementary Methods (available on the *Arthritis & Rheumatology* website at http://onlinelibrary.wiley.com/doi/10.1002/art.41790/abstract).

Generation and analysis of *Copa*[V242G/+] mice. Detailed methods on the generation and analysis of *Copa*[V242G/+] mice are described in Supplementary Methods.

Statistical analysis. Statistical significance was calculated by Student's 2-tailed *t*-test using Prism 7 (GraphPad Software). Calculated data are presented as the mean ± SEM. *P* values less than 0.05 were considered significant.

RESULTS

Patient profiles. The index patient (III-2) and patients III-1 and IV-1 had similar manifestations of the following characteristics: onset during infancy, development of ILD before arthritis, no renal involvement, ground-glass opacities with cysts on radiologic

examinations, nonspecific interstitial pneumonia pattern with lymphoid follicle formation and proliferation of alveolar macrophages on lung biopsy, and autoantibody positivity on serologic tests (Figures 1A–C and Supplementary Table 1, http://online library.wiley.com/doi/10.1002/art.41790/abstract). Patient III-1 developed huge pulmonary bullae, in which *Mycobacterium intracellulare* was detected, and his lung function rapidly declined. He underwent bilateral living-related lung transplantation from his parents (II-1 and II-2) but died of sepsis caused by multidrug-resistant *Pseudomonas aeruginosa* 5 months after the transplantation.

In patient IV-1, the plasma level of β-D-glucan was markedly elevated (464 pg/ml) at initial presentation. *Pneumocystis jirovecii* and cytomegalovirus (CMV) DNA was detected in the bronchoalveolar
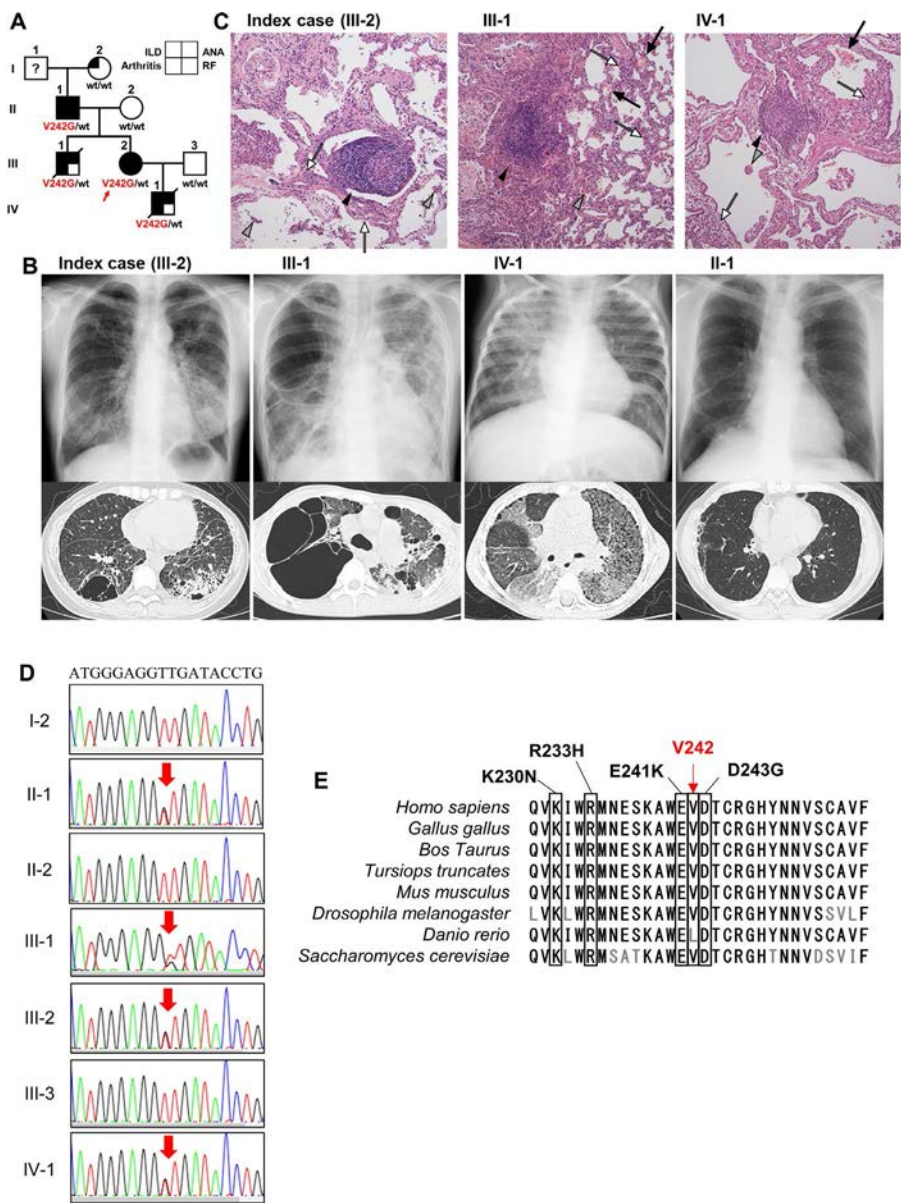
Figure 1. Pedigree of and findings on the family with a novel *COPA* variant. **A**, Pedigree of the family. Genotypes of *COPA* (wild-type [WT] allele and V242G mutant allele) are shown. Closed symbols denote positive findings of interstitial lung disease (ILD), arthritis, antinuclear antibody (ANA), and rheumatoid factor (RF), open symbols denote negative findings, and slashed lines denote deceased patients. **Arrow** indicates the proband. **B**, Radiologic findings. Chest radiography and high-resolution computed tomography scans show diffuse or localized reticular and ground-glass opacities with cyst formation. **C**, Histopathology of the biopsied samples from the lungs. Diffuse fibrosis of the alveolar septum and lymphocyte infiltration with lymphoid follicle formation are indicated by **solid arrowheads**. Inflammatory cell infiltration detected in the alveolar walls is indicated by **open arrowheads**. Alveolar macrophages and alveolar hemorrhage are indicated by **gray-shaded arrowheads** and **solid arrows**, respectively. **D**, Results of Sanger sequencing analysis of genomic DNA from whole blood (patients I-2, II-1, II-2, III-2, III-3, and IV-1) or paraffin-embedded lung (patient III-1). **Arrows** indicate the presence of the V242 variant. **E**, Comparison of variants. V242 is as highly conserved among species as the other previously reported disease-causing variants.
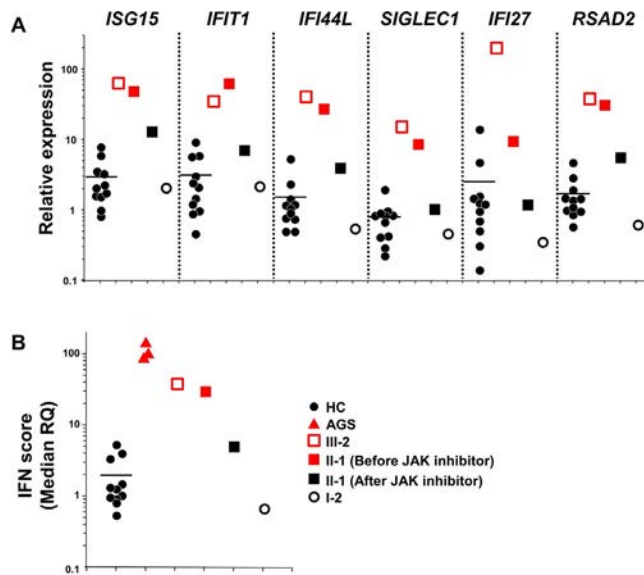
Figure 2. Increased interferon (IFN) signature in the patients with coatomer subunit alpha (COPA) syndrome. **A**, Relative expression levels of each IFN-stimulated gene (ISG) in patients (II-1 and III-2), a family member without COPA syndrome (I-2), and healthy controls (HC). Bars show the mean. **B**, IFN score in patients II-1 and III-2, healthy family member I-2, patients with Aicardi-Goutières syndrome (AGS) as a positive control, and healthy controls. IFN scores were calculated as the median relative quantification of 6 ISGs (same as those shown in **A**) and designated as positive if they exceeded the mean IFN score in 11 healthy controls +2 SD (i.e., >5.04). For patient II-1, relative expression levels of each ISG and IFN score were examined before and after baricitinib treatment.

lavage fluid. No other microorganisms were detected. Although β-ᴅ-glucan and CMV DNA levels drastically decreased to normal levels with the disappearance of *P jirovecii* and CMV (after commencement treatment with of trimethoprim/sulfamethoxazole and ganciclovir), this patient's respiratory symptoms did not significantly improve. His immunologic screening tests showed normal results, including complete blood cell count, complement levels, immunoglobulin, lymphocyte subset analysis, and mitogen-induced lymphocyte proliferation by phytohemagglutinin and pokeweed mitogen testing. Thereafter, the patient's lung function deteriorated steadily, and he received bilateral lung transplantation from a donor with no brain activity. However, he developed progressive respiratory failure, and diffuse ground-glass opacities reappeared on chest radiography (Supplementary Figure 1, http://onlinelibrary.wiley.com/doi/10.1002/art.41790/abstract). He had no signs of infection, and aggressive immunosuppressive therapies targeting the possible graft rejection were ineffective. He died 8 months after the transplantation. Histopathologic examination of the autopsied lungs in patient IV-1 showed diffuse alveolar damage with alveolar hemorrhage and bronchiolitis obliterans.

The clinical picture of patient II-1 was slightly different from those of other family members: the initial presentation of COPA syndrome occurred in middle age (53 years old), ILD was mild based on radiologic examination, and joint disease preceded

development of the lung disease. Patient II-1 had been experiencing arthritis with poor response to disease-modifying antirheumatic drugs and biologics, including an anti–interleukin-6 (anti–IL-6) receptor antibody, tocilizumab, and anti–tumor necrosis factor antibodies. In the index patient (III-2), a painless induration of the neck appeared at 35 years of age, and a biopsy of this revealed papillary thyroid cancer. Thyroidectomy is currently under consideration.

Patient I-2 recently developed subclinical ILD, in her 80s, which was identified by a computed tomography scan. A higher age at onset and quite different clinical course from those observed in other family members suggest that the subclinical ILD observed in patient I-2 was caused by aging.

Novel missense heterozygous variant of *COPA* identified by whole-exome sequencing. There was no consanguinity in the family. Similar clinical manifestations led us to consider genetic abnormalities. To determine the cause of the disease, we performed whole-exome sequencing on the family. Among the rare variants shared only by the affected patients (Supplementary Table 2, http://onlinelibrary.wiley.com/doi/10.1002/art.41790/abstract), we focused on a novel heterozygous missense variant of the *COPA* gene (c.725T>G, V242G) (Figures 1A and D), because the clinical features of our patients were compatible with those previously described in COPA syndrome patients. Sanger sequencing confirmed the complete segregation of this variant; that is, all affected family members (II-1, III-1, III-2, and IV-1) harbored the same variant, whereas unaffected family members (I-2, II-2, and III-3) did not (Figures 1A and D). Several prediction programs (SIFT, PROVEAN, MutationTaster, and PolyPhen-2 scores) predicted this variant to be damaging and disease-causing, and V242 is highly
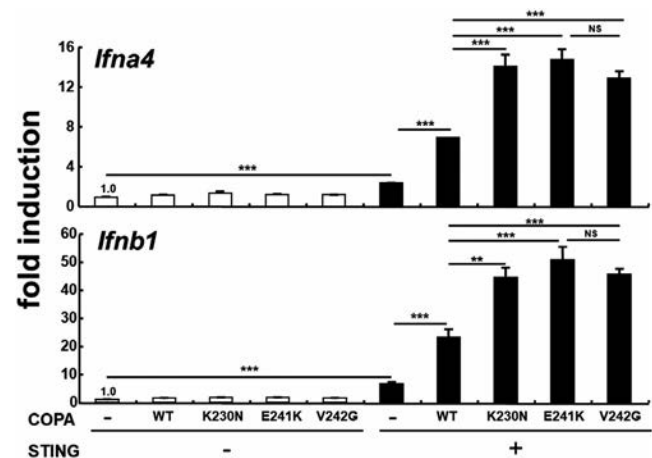
Figure 3. Enhanced ability of mutant *COPA* to activate type I interferon (IFN) promoters in synergy with stimulator of IFN genes (STING). HEK 293T cells were transiently transfected with *Ifna4* or *Ifnb1* promoter–driven luciferase reporter plasmid alone or together with a combination of STING and/or *COPA* expression plasmids (100 ng/well). After 18 hours, cell lysates were prepared and subjected to luciferase assay. Bars show the mean ± SEM. ** = $P < 0.01$; *** = $P < 0.001$, by Student's 2-tailed *t*-test. WT = wild-type; NS = not significant.

conserved among species (Figure 1E). According to the American College of Medical Genetics and Genomics standards and guidelines (14), this variant has been determined to be "pathogenic" (evidence of pathogenicity fulfills PM1, PM2, PM5, PP3, and PP4). In addition, the novel variant resides in the hotspot of the mutants causing COPA syndrome, the WD-40 repeat domain. These data suggest that the family members had COPA syndrome due to the novel heterozygous missense variant, V242G.

Increased IFN signature in patients with COPA syndrome. COPA syndrome often presents as a type I interferonopathy, so we measured the type I IFN signature using whole blood cells from 2 patients as well as another family member (I-2) to confirm the clinical phenotype of the consequences caused by the genetic alteration. IFN score was increased in the members carrying the variant (II-1 and III-2) (Figure 2) but not in family member I-2, who did not have the variant. Recently, JAK inhibitors have been shown to be effective in COPA syndrome (15,16), so we prescribed baricitinib treatment in patient II-1. The IFN score in this patient normalized from 30.5 to 5.04 at 16 weeks (Figure 2B), and articular symptoms were also improved after initiation of baricitinib treatment. The symptoms improved further after treatment was switched from baricitinib to upadacitinib, a potent, orally active, and selective JAK1 inhibitor. ILD symptoms and related laboratory markers, such as KL-6/SP-D, were also stable during the observation period (14 months with baricitinib, 1 month with upadacitinib).

Enhanced ability of mutant *COPA* to activate type I IFN promoters in synergy with STING. STING, which is an adaptor molecule critical for cytosolic DNA–induced type I IFN production, is known to reside in the ER in resting states and move to the Golgi after its activation (17,18). Gain-of-function mutations in *TMEM173*, which encodes STING, cause an autoinflammatory disease, known as STING-associated vasculopathy with onset

in infancy (SAVI), which manifests as type I interferonopathy and ILD and is similar to COPA syndrome (19,20), although there are some clinical differences (21). These mutant STINGs tend to localize in the Golgi in resting states and hyperactivate the signaling pathways leading to type I IFN production (19,20,22–24). Several studies have shown that the STING pathway is hyperactivated by *COPA* variants (8–10).

We analyzed the effects of the *COPA* variants, including K230N, E241K (1), and V242G, on type I IFN promoter activity by using the luciferase assay in an overexpression system in HEK 293T cells (Figure 3). Wild-type (WT) *COPA* and all tested *COPA* variants failed to activate the *Ifna4* and *Ifnb1* promoters. STING overexpression in HEK 293T cells led to the activation of both *Ifna4* and *Ifnb1* promoters, and this activation was synergistically augmented with disease-causing *COPA* variants as well as WT *COPA*. Notably, all COPA syndrome–associated variants showed more potent abilities to activate both promoters than WT *COPA*. Thus, *COPA* V242G as well as the previously reported disease-causing *COPA* variants showed enhanced ability to activate type I IFN promoters in synergy with STING.

COPA syndrome–like pulmonary lesions and T cell abnormalities in *Copa*[V242G/+] mice. In order to delineate the in vivo effects of the *COPA* V242G variant, we generated *Copa*[V242G/+] mice by clustered regularly interspaced short palindromic repeat (CRISPR)/CRISPR-associated protein 9 (Cas9) gene editing (Supplementary Figure 2, http://onlinelibrary.wiley.com/doi/10.1002/art.41790/abstract). *Copa*[V242G/+] mice appeared healthy at a glance, and their survival rates beyond 40 weeks of age were similar to those of WT mice. However, histologic analysis revealed several abnormalities in the lungs of these mice (Figures 4A–F). Alveolar walls were thickened with infiltration of inflammatory cells and congestion. Lymphocytic infiltration was also detected, with lymphoid follicle–like formation in the alveolar walls. Notably, infiltrating cells included alveolar macrophages and a small number
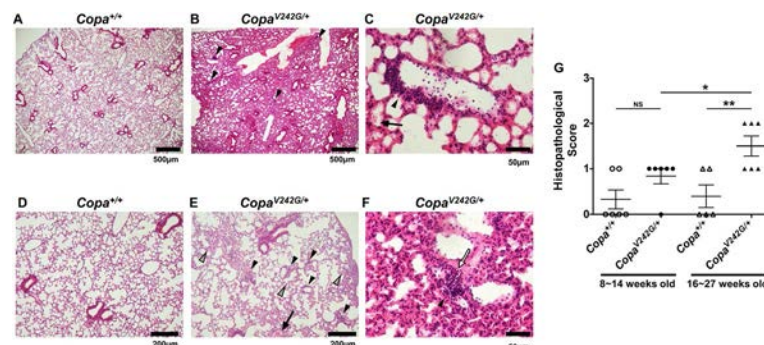
Figure 4. Lung pathology in *Copa* [V242G/+] mice. **A–F**, Representative lung sections from 1 *Copa*^{+/+} mouse (**A** and **D**) and 2 *Copa*[V242G/+] mice (**B**, **C**, and **F** from 1 mouse and **E** from another mouse), stained with hematoxylin and eosin. Inflammatory cell infiltration was detected in the alveolar wall as indicated by **solid arrowheads**. Alveolar macrophages, eosinophils, and alveolar hemorrhage are indicated with by **gray-shaded arrowheads** (**E**), an **open arrow** (**F**), and **solid arrows** (**C** and **E**). **G**, Histopathologic scoring of the lungs. *Copa*^{+/+} mice were littermates of *Copa*[V242G/+] mice. Each symbol represents an individual mouse. Bars show the mean ± SEM. * = P < 0.05; ** = P < 0.01, by Student's 2-tailed *t*-test. NS = not significant. Color figure can be viewed in the online issue, which is available at http://onlinelibrary.wiley.com/doi/10.1002/art.41790/abstract.

Figure 5. T cell abnormalities in *Copa*[V242G/+] mice. **A**, Flow cytometry analysis of splenocytes. Percentages and absolute numbers of B220+ cells, CD3+ cells , CD4+ T cells, and CD8+ T cells among total splenocytes are shown. **B**, Dot plots of CD4+ and CD8+ T cell subsets. Naive, central memory (CM), and effector memory (EM) T cells are CD62L+44−, CD62L+44+, and CD62L−44+ T cell subsets, respectively. **C**, Percentages of naive, CM, and EM T cells. **D**, Intracellular cytokine staining of CD4+ and CD8+ T cells. **E**, Percentages of interferon-γ (IFNγ)–positive and interleukin-17A (IL-17A)–positive T cells. **F**, Dot plots of Treg cells among CD4+ T cells. Treg cells are FoxP3+ T cells. **G**, Percentages and absolute numbers of FoxP3+ T cells. *Copa*^{+/+} mice were littermates of *Copa*[V242G/+] mice. Mice used in **A–E** were 8–16 weeks old, and those used in **F** and **G** were 23–27 weeks old. Numbers in the dot plots indicate the percentages of the corresponding quadrants. In **A** (right and bottom), **C**, **E**, and **G**, each symbol represents an individual mouse. Bars show the mean ± SEM. * = $P < 0.05$; ** = $P < 0.01$; *** = $P < 0.001$, by Student's 2-tailed *t*-test. NS = not significant. Color figure can be viewed in the online issue, which is available at http://onlinelibrary. wiley.com/doi/10.1002/art.41790/abstract.

of eosinophils. These pathologic findings in *Copa*[V242G/+] mice were quite similar to those found in human patients with COPA syndrome (Figure 1C). Lesions were more prominent in *Copa*[V242G/+] mice older

than 16 weeks of age (Figure 4G). In joints, *Copa*[V242G/+] mice did not show any signs of swelling, bone erosion, or histologic abnormalities such as immune cell infiltration or cartilage damage (Supplementary
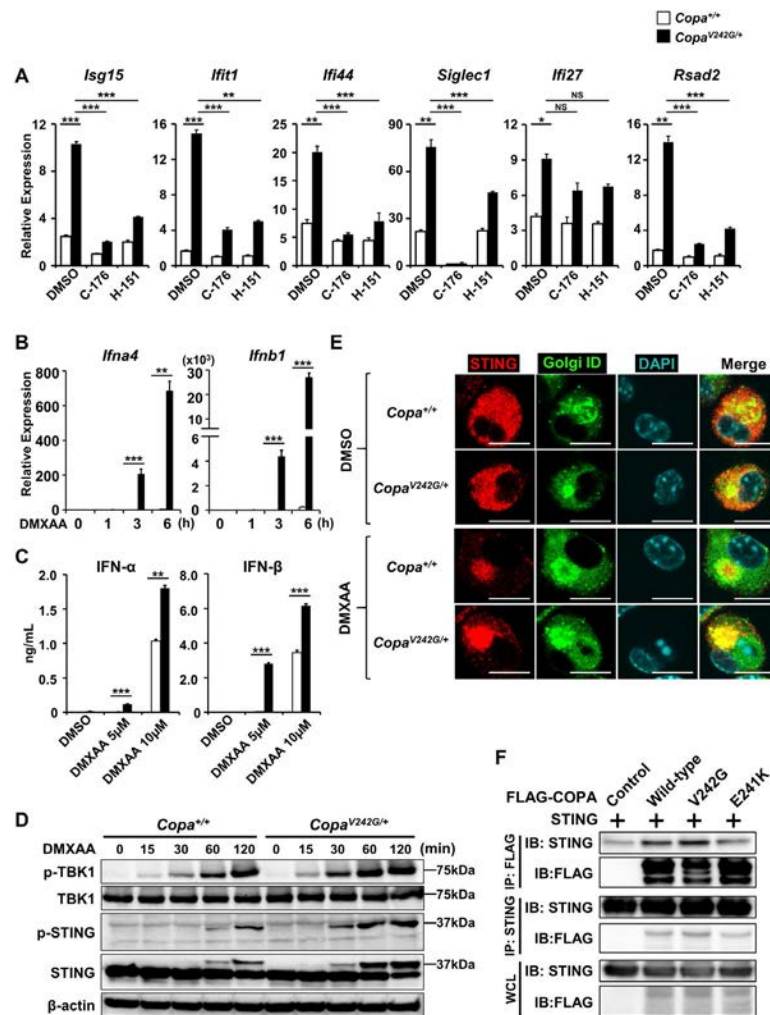
Figure 6. Enhancement of STING-induced type I IFN production in *Copa*[V242G/+] mice. **A**, IFN-stimulated gene (ISG) expression of splenocytes in the absence (DMSO only) or presence of STING inhibitors C-176 or H-151. **B**, *Ifna4* and *Ifnb1* expression in granulocyte–macrophage colony-stimulating factor (GM-CSF)–induced bone marrow dendritic cells (GM-DCs) stimulated with 5 μ*M* 5,6-dimethyl-9-oxo-9H-xanthene-4-acetic acid (DMXAA) for the indicated periods. **C**, IFNα/β production from GM-DCs stimulated with DMXAA for 24 hours. **D**, Western blot analysis of GM-DCs stimulated with 20 μ*M* DMXAA for the indicated periods. **E**, Subcellular localization of STING in GM-DCs. The cells were unstimulated (DMSO only) or stimulated with 20 μ*M* DMXAA for 60 minutes and stained with anti-STING monoclonal antibody (mAb), Golgi ID, or DAPI. Bars = 10 μm. **F**, Interaction of STING and WT or mutant *COPA*. After transfection, HEK 293T cell lysates were immunoprecipitated (IP) and immunoblotted (IB) with anti-STING mAb or anti-FLAG mAb. In **A–E**, *Copa*^{+/+} mice (n = 3) were littermates of *Copa*[V242G/+] mice (n = 3), and they were 12–22 weeks old. In **A–C**, bars show the mean ± SEM of >3 independent experiments. * = $P < 0.05$; ** = $P < 0.01$; *** = $P < 0.001$, by Student's 2-tailed *t*-test. In **D–F**, data represent 3 independent experiments. WCL = whole-cell lysate (see Figure 3 for other definitions). Color figure can be viewed in the online issue, which is available at http://onlinelibrary.wiley.com/doi/10.1002/art.41790/abstract.

Figure 3, http://onlinelibrary.wiley.com/doi/10.1002/art.41790/abstract). *Copa*[V242G/+] mice therefore showed COPA syndrome–like pulmonary lesions without any signs of arthritis.

We then analyzed immunologic phenotypes. Numbers and percentages of CD4+CD8+ (double-positive) cells were decreased, and percentages of CD4+ (single-positive) and CD8+ (single-positive) cells were increased, in the thymus of *Copa*[V242G/+] mice (Supplementary Figure 4, http://onlinelibrary.wiley.com/doi/10.1002/art.41790/abstract). Splenic T and B cell populations were comparable between WT and *Copa*[V242G/+] mice (Figure 5A). However, *Copa*[V242G/+] mice showed a decrease in percentages of naive CD8+ T

cells and an increase in percentages of central and effector memory CD8+ T cells (Figures 5B and C). Similar patterns were also observed in CD4+ T cells of *Copa*[V242G/+] mice, although without statistical significance. Furthermore, in *Copa*[V242G/+] mice, splenic IFNγ-producing CD4+ and CD8+ T cells were significantly increased, while IL-17A–producing CD4+ T cells were not (Figures 5D and E). Percentages of CD4+FoxP3+ T cells, i.e., Treg cells, were decreased (Figures 5F and G). T cells in *Copa*[V242G/+] mice therefore showed hyperactivation and skewed toward Th1 cells. These T cell phenotypes were similar to those of *Copa*[E241K/+] mice, although skewing toward Th17 cells was more apparent in *Copa*[E241K/+] mice (11).

Enhanced production of type I IFN in response to STING signaling in DCs from _Copa_^{V242G/+} mice. We next analyzed the expression of ISG, which was significantly elevated in splenocytes from _Copa_^{V242G/+} mice (Figure 6A). In thymocytes from _Copa_^{V242G/+} mice, surface expression of a type I IFN–inducible marker, Qa2, was enhanced in CD4+ cells (single-positive) and CD8+ cells (single-positive) (Supplementary Figures 5A and B, http://onlinelibrary.wiley.com/doi/10.1002/art.41790/abstract). Type I IFNs drive thymocyte maturation from semi-mature cells to mature cells (25). In both CD4+ (single-positive) and CD8+ (single-positive) cells from _Copa_^{V242G/+} mice, percentages of semi-mature and mature cells were decreased and increased, respectively (Supplementary Figures 5C and D). Thus, ISG expression was elevated, and thymic phenotype was altered, in _Copa_^{V242G/+} mice, as described in _Copa_^{E241K/+} mice (8).

To elucidate whether STING signaling is augmented by the _COPA_ V242G variant, we further analyzed responses of bone marrow–derived DCs from WT mice and _Copa_^{V242G/+} mice to STING signaling. In response to a synthetic STING agonist, 5,6-dimethyl-9-oxo-9H-xanthene-4-acetic acid (DMXAA), _Copa_^{V242G/+} DCs showed prominently higher levels of messenger RNA for _Ifna4_ and _Ifnb1_ compared to WT DCs (Figure 6B). DMXAA-induced IFNα/β production was also higher in _Copa_^{V242G/+} DCs compared to WT DCs (Figure 6C).

Next, we investigated the downstream molecules in STING signaling. In resting states, phosphorylation of TANK-binding kinase 1 (TBK1) and STING was not observed in WT or _Copa_^{V242G/+} DCs (Figure 6D). After stimulation, however, their phosphorylation was detected more rapidly and prominently in _Copa_^{V242G/+} DCs (Figure 6D). STING localizes in the ER in resting states and moves to the Golgi upon stimulation, thereby activating TBK1. Expression of the _COPA_ E241K variant leads to constitutive activation and localization in the Golgi of STING (8–10). In resting _Copa_^{V242G/+} DCs, STING localized broadly in the cytoplasm as in WT DCs. After stimulation, however, STING colocalized in the Golgi more prominently in _Copa_^{V242G/+} DCs (Figure 6E). We also tested the binding of COPA variants to STING, because _COPA_ E241K caused constitutive activation of STING due to decreased binding to STING (8–10). However, with _COPA_ V242G, binding to STING was retained (Figure 6F). _COPA_ V242G therefore led to enhancement of ligand-induced STING signaling, leading to type I IFN production in a manner distinct from _COPA_ E241K.

Furthermore, enhanced expression of ISGs in _Copa_^{V242G/+} splenocytes was attenuated not only by a STING antagonist, H-151, but by a palmitoylation inhibitor, C-176, which also functions as a STING inhibitor (Figure 6A). This indicates that the V242G mutation of COPA leads to enhancement of ISG expression through STING.

Double-stranded RNAs, such as polyinosinic:polycytidylic acids [poly(I-C)], can also induce type I IFNs through cytosolic sensors, retinoic acid–inducible gene 1–like receptors (RLRs) (26). In response to poly(I-C), _Copa_^{V242G/+} DCs produced fewer

type I IFNs than WT DCs (Supplementary Figure 6A, http://onlinelibrary.wiley.com/doi/10.1002/art.41790/abstract). Signaling through nucleic acid–sensing Toll-like receptors (TLRs) such as TLR-7 or TLR-9 has also been shown to induce type I IFN production (26). In addition, the induction was attenuated in _Copa_^{V242G/+} DCs (Supplementary Figures 6B and C). These data suggest that STING signaling is selectively enhanced in _Copa_^{V242G/+} mice.

DISCUSSION

We detected a novel heterozygous missense variant, V242G in _COPA_, in 4 patients from one family. Several pieces of evidence suggest that the _COPA_ V242G variant is responsible for the patients' disease manifestations. First, V242 is well conserved among species and is located in the WD-40 repeat domain, which is the site of localization for all disease-causing variants reported to date in patients with COPA syndrome. Second, _Copa_^{V242G/+} mice showed pulmonary lesions with interstitial infiltration of inflammatory cells and alveolar hemorrhage, similar to the observations in the 4 patients carrying the _COPA_ V242G variant. The lesions were also similar to those in _Copa_^{E241K/+} mice (11). Third, a representative feature of COPA syndrome, elevation of ISG expression, was observed in both the patients and the _Copa_^{V242G/+} mice. In the patients, the IFN scores were prominently higher than those observed in healthy controls. In the mutant mice, DCs showed enhanced production of type I IFN in response to STING signaling and splenocytes showed STING-dependent elevation of ISG expression. Furthermore, _Copa_^{V242G/+} mice showed T cell abnormalities reflecting activation of the type I IFN pathway, as observed in _Copa_^{E241K/+} mice. These results indicate that _COPA_ V242G is a novel disease-causing variant of COPA syndrome.

How do mutant _COPA_ including _COPA_ V242G cause enhanced STING signaling? Both WT and mutant _COPA_, including _COPA_ V242G, _COPA_ K230N, and _COPA_ E241K, failed to activate type I IFN promoters, excluding the possibility that mutant _COPA_ directly activate type I IFN promoters. In the presence of STING, however, _COPA_ V242G, _COPA_ K230N, and _COPA_ E241K showed augmented ability to activate type I IFN promoters, compared to WT COPA. Consistent with these in vitro findings, DCs from _Copa_^{V242G/+} mice showed higher expression of type I IFN genes and proteins in response to STING signaling, and enhanced expression of ISGs in the mutant splenocytes was attenuated by STING inhibitors. Furthermore, type I IFN induction by RLRs or TLRs was impaired in _Copa_^{V242G/+} DCs, although it remains unclear how the induction was defective. These results suggest that mutant _COPA_ enhance STING-induced type I IFN production.

Upon stimulation, STING moves from the ER to the Golgi. Mutant STINGs derived from SAVI patients localize in the Golgi rather than the ER and cause constitutive activation of TBK1, which can lead to type I IFN gene up-regulation (20,23,24). In

Copa[E241K/+] mice and *COPA* E241K–expressing cell lines, STING localization is also skewed toward the Golgi and is constitutively activated without ligand stimulation (8,10). *Copa*[V242G/+] DCs, in resting states, did not show any signs of STING pathway activation. Upon stimulation, however, such signs were more prominent in *Copa*[V242G/+] DCs than WT DCs, which is consistent with enhanced induction of type I IFN production by STING signaling. Retained binding to STING of *COPA* V242G compared to *COPA* E241K might contribute to this phenotype of *Copa*[V242G/+] DCs. However, at present, it is unclear what causes the distinct effects of *COPA* V242G and E241K on the STING pathway.

The lungs of *Copa*[V242G/+] mice showed pulmonary diseases, similar to the manifestations in COPA syndrome patients and *Copa*[E241K/+] mice (11). In *Copa*[E241K/+] mice, adoptive T cell transfer causes the pulmonary lesions, but it is unknown whether type I interferonopathy contributes to the lesions. ILD has also been observed in mice carrying gain-of-function mutations, N153S or V154M of STING (27–29). The lung disease in these mutant STING mice was absent on T cell–deficient backgrounds but still observed on IFNα/β receptor–deficient backgrounds, indicating that ILD depends on T cells, which are affected by the mutant STING-induced type I IFN–independent pathways (28–30). Although amino acids E241 and V242 are next to each other, mutation-specific mechanisms cannot be excluded, given that STING N153M and V154M mice show distinct phenotypes and underlying mechanisms (30). Further studies are needed to elucidate the pathogenesis of lung disease in *Copa*[V242G/+] and *Copa*[E241K/+] mice.

The family members carrying the *COPA* V242G variant experienced the following different complications: pulmonary *Mycobacterium intracellulare* complex infection (patient III-1), thyroid cancer (patient III-2), and CMV/*P jirovecii* pneumonia (patient IV-1). Taveira-DaSilva et al described a 56-year-old patient who developed a carcinoid tumor of the lung and clear cell carcinoma of the kidney (31). Although COPA syndrome mainly involves the lungs, joints, and kidneys, *COPA* is expressed ubiquitously. COPA syndrome patients might require careful long-term follow-up for cancer complications. In addition, the coincidence of *Mycobacterium* (as in patient III-1), CMV and *P jirovecii* pneumonia (as in patient IV-1), and ILD is intriguing, as these infections are rare even in early infancy. Patient IV-1 showed normal results of immunologic screening tests, and members of this family had no clinical manifestations indicating vulnerability to pathogens. As exome sequencing did not reveal any additional pathogenic variants in known primary immunodeficiency genes, the comorbidity of primary immunodeficiency seemed unlikely. One SAVI patient developed *P jirovecii* pneumonia at 2 months of age, followed by ILD (32). In addition, a gain-of-function mutation of *STAT1* has been reported to be associated with enhanced type I IFN signature and predisposition to *Mycobacterium* infection (33). COPA syndrome, SAVI, and gain-of-function *STAT1* (34) are all associated with enhanced type I IFN signature, so there may be a common mechanism that makes these patients susceptible to *Mycobacterium* or *P jirovecii* infections.

There is no established standard treatment for COPA syndrome. A variety of treatments have been reported, mainly as part of single-case reports or within small case series. We treated our patients with various drugs including immunosuppressive and antifibrotic agents, all of which failed to improve disease severity. Several recent case reports have described improvement of clinical manifestations as well as IFN scores with JAK inhibitor treatment in patients with COPA syndrome (15,16). Consistent with this, JAK inhibitors ameliorated not only the IFN score but also articular symptoms of one of our patients (II-1). JAK inhibitors have demonstrated efficacy for type I interferonopathies, such as Aicardi-Goutières syndrome, proteasome-associated autoinflammatory syndrome, and SAVI (35), and could be promising therapies for COPA syndrome, although more evidence is needed to confirm their efficacy and ensure that there are no adverse effects.

Lung transplantation may be an option for COPA syndrome patients with progressively impaired respiratory function despite receiving maximum and optimal medical interventions. Graft survival after lung transplantation for COPA syndrome requires investigation, as it is very important to establish an effective treatment strategy for COPA syndrome with intractable ILD. There have been previous reports of only 4 patients with genetically confirmed COPA syndrome who received lung transplantation, however (36), and their outcomes have not yet been reported. In our study, 2 patients received lung transplantation: patient III-1 from his parents (II-1 and II-2) and patient IV-1 from a donor with no brain activity. Patient III-1 died due to sepsis, 5 months after lung transplantation, and patient IV-1 died of respiratory failure. The autopsied lungs of patient IV-1 revealed diffuse alveolar damage as well as alveolar hemorrhage and bronchiolitis obliterans, all of which are relatively common postmortem histologic findings in patients with adult respiratory distress syndrome, which can result from acute lung allograft rejection, idiopathic pulmonary fibrosis, infection, or drug/radiation-induced lung damage (37,38). However, aggressive immunosuppressive treatment targeting acute rejection was ineffective, and there was no evidence of infection in patient IV-1. We therefore speculate that the posttransplantation respiratory failure in this patient may have been associated with a recurrence of COPA-related ILD in the donor lungs.

Copa[E241K/+] mice showed ILD similar to that in COPA syndrome, and it was demonstrated that T cell dysfunction based on thymic nonhematopoietic cell disorders led to ILD (11). This T cell dysfunction could contribute to the recurrence of ILD in donor lungs transplanted into recipients with COPA syndrome, as in the patient described above. If the recurrence rate is high, therapeutic intervention intended to control the immune dysfunction of COPA syndrome needs to be addressed when considering lung transplantation.

In this study, we have identified a novel *COPA* variant, V242G, in 4 patients from one family. The lung diseases were

recapitulated in the *Copa*^{V242G/+} mice. Notably, in vitro and in vivo analyses demonstrated that the mutant *COPA*, as well as *COPA* E241K, enhanced STING-induced type I IFN production, strengthening the hypothesis that COPA syndrome and SAVI partly share the same pathologic mechanisms leading to the enhanced type I IFN signaling pathway. However, there are some clinical differences, i.e., age at onset and other organ involvement, such as the skin and kidneys (21). It should be noted that the *COPA* V242G variant exhibited similar but distinct effects from the *COPA* E241K variant, as shown by the findings in DCs. Taken together with findings on the *COPA* E241K variant (9–11), this study provides insight into a link between COPA syndrome and SAVI and introduces a new therapeutic strategy for COPA syndrome by focusing on STING pathway activation. Furthermore, our present findings are important in identifying *COPA* as a novel regulator of STING signaling, which is critical for anticancer and antiviral immune responses.

ACKNOWLEDGMENTS

AUTHOR CONTRIBUTIONS

All authors were involved in drafting the article or revising it critically for important intellectual content, and all authors approved the final version to be published. Drs. Izawa and Kaisho had full access to all of the data in the study and take responsibility for the integrity of the data and the accuracy of the data analysis.
Study conception and design. Kato, Yamamoto, Honda, Orimo, Sasaki, Hemmi, Nakamura, Miyamoto, Nishikomori, Izawa, Kaisho.
Acquisition of data. Kato, Yamamoto, Honda, Orimo, Murakami, Fukuda-Ohta, Isono, Takayama, Miyamoto, Matsubayashi.
Analysis and interpretation of data. Nakamura, Otsuki, Takita, Yasumi, Nishikomori, Izawa, Kaisho.

REFERENCES

1. Watkin LB, Jessen B, Wiszniewski W, Vece TJ, Jan M, Sha Y, et al. COPA mutations impair ER-Golgi transport and cause hereditary autoimmune-mediated lung disease and arthritis [letter]. Nat Genet 2015;47:654–60.
2. Vece TJ, Watkin LB, Nicholas S, Canter D, Braun MC, Guillerman RP, et al. Copa syndrome: a novel autosomal dominant immune dysregulatory disease [review]. J Clin Immunol 2016;36:377–87.
3. Jensson BO, Hansdottir S, Arnadottir GA, Sulem G, Kristjansson RP, Oddsson A, et al. COPA syndrome in an Icelandic family caused by a recurrent missense mutation in COPA. BMC Med Genet 2017;18:129.
4. Noorelahi R, Perez G, Otero HJ. Imaging findings of Copa syndrome in a 12-year-old boy. Pediatr Radiol 2018;48:279–82.
5. Patwardhan A, Spencer CH. An unprecedented COPA gene mutation in two patients in the same family: comparative clinical analysis of newly reported patients with other known COPA gene mutations [review]. Pediatr Rheumatol Online J 2019;17:59.
6. Volpi S, Tsui J, Mariani M, Pastorino C, Caorsi R, Sacco O, et al. Type I interferon pathway activation in COPA syndrome. Clin Immunol 2018;187:33–6.
7. Khalifi SB, Viel S, Lahoche A, Frémond ML, Lopez J, Lombard C, et al. COPA syndrome as a cause of lupus nephritis. Kidney Int Rep 2019;4:1187–9.
8. Deng Z, Chong Z, Law CS, Mukai K, Ho FO, Martinu T, et al. A defect in COPI-mediated transport of STING causes immune dysregulation in COPA syndrome. J Exp Med 2020;217:e20201045.
9. Lepelley A, Martin-Niclós MJ, Le Bihan M, Marsh JA, Uggenti C, Rice GI, et al. Mutations in COPA lead to abnormal trafficking of STING to the Golgi and interferon signaling. J Exp Med 2020;217:e20200600.
10. Mukai K, Ogawa E, Uematsu R, Kuchitsu Y, Kiku F, Uemura T, et al. Homeostatic regulation of STING by retrograde membrane traffic to the ER. Nat Commun 2021;12:61.
11. Deng Z, Law CS, Ho FO, Wang KM, Jones KD, Shin JS, et al. A defect in thymic tolerance causes T cell-mediated autoimmunity in a murine model of COPA syndrome. J Immunol 2020;204:2360–73.
12. Oda H, Nakagawa K, Abe J, Awaya T, Funabiki M, Hijikata A, et al. Aicardi-Goutières syndrome is caused by IFIH1 mutations. Am J Hum Genet 2014;95:121–5.
13. Rice GI, Forte GM, Szynkiewicz M, Chase DS, Aeby A, Abdel-Hamid MS, et al. Assessment of interferon-related biomarkers in Aicardi-Goutières syndrome associated with mutations in TREX1, RNASEH2A, RNASEH2B, RNASEH2C, SAMHD1, and ADAR: a case-control study. Lancet Neurol 2013;12:1159–69.
14. Monaghan KG, Lyon E, Spector EB. ACMG standards and guidelines for fragile X testing: a revision to the disease-specific supplements to the standards and guidelines for clinical genetics laboratories of the American College of Medical Genetics and Genomics. Genet Med 2013;15:575–86.
15. Krutzke S, Rietschel C, Horneff G. Baricitinib in therapy of COPA syndrome in a 15-year-old girl [review]. Eur J Rheumatol 2019;7 Suppl 1:1–4.
16. Frémond ML, Legendre M, Fayon M, Clement A, Filhol-Blin E, Richard N, et al. Use of ruxolitinib in COPA syndrome manifesting as life-threatening alveolar haemorrhage. Thorax 2020;75:92–5.
17. Ishikawa H, Ma Z, Barber GN. STING regulates intracellular DNA-mediated, type I interferon-dependent innate immunity. Nature 2009;461:788–92.
18. Motwani M, Pesiridis S, Fitzgerald KA. DNA sensing by the cGAS-STING pathway in health and disease. Nat Rev Genet 2019;20:657–74.
19. Liu Y, Jesus AA, Marrero B, Yang D, Ramsey SE, Sanchez GA, et al. Activated STING in a vascular and pulmonary syndrome. N Engl J Med 2014;371:507–18.
20. Jeremiah N, Neven B, Gentili M, Callebaut I, Maschalidi S, Stolzenberg MC, et al. Inherited STING-activating mutation underlies a familial inflammatory syndrome with lupus-like manifestations. J Clin Invest 2014;124:5516–20.
21. Frémond ML, Crow YJ. STING-mediated lung inflammation and beyond [review]. J Clin Immunol 2021;41:501–14.
22. Dobbs N, Burnaevskiy N, Chen D, Gonugunta VK, Alto NM, Yan N. STING activation by translocation from the ER is associated with infection and autoinflammatory disease. Cell Host Microbe 2015;18:157–68.
23. Mukai K, Konno H, Akiba T, Uemura T, Waguri S, Kobayashi T, et al. Activation of STING requires palmitoylation at the Golgi. Nat Commun 2016;7:11932.
24. Ogawa E, Mukai K, Saito K, Arai H, Taguchi T. The binding of TBK1 to STING requires exocytic membrane traffic from the ER. Biochem Biophys Res Commun 2018;503:138–45.

25. Xing Y, Wang X, Jameson SC, Hogquist KA. Late stages of T cell maturation in the thymus involve NF-κB and tonic type I interferon signaling. Nat Immunol 2016;17:565–73.

26. Akira S, Uematsu S, Takeuchi O. Pathogen recognition and innate immunity. Cell 2006;124:783–801.

27. Warner JD, Irizarry-Caro RA, Bennion BG, Ai TL, Smith AM, Miner CA, et al. STING-associated vasculopathy develops independently of IRF3 in mice. J Exp Med 2017;214:3279–92.

28. Bouis D, Kirstetter P, Arbogast F, Lamon D, Delgado V, Jung S, et al. Severe combined immunodeficiency in stimulator of interferon genes (STING) V154M/wild-type mice. J Allergy Clin Immunol 2019;143:712–25.

29. Luksch H, Stinson WA, Platt DJ, Qian W, Kalugotla G, Miner CA, et al. STING-associated lung disease in mice relies on T cells but not type I interferon. J Allergy Clin Immunol 2019;144:254–66.

30. Motwani M, Pawaria S, Bernier J, Moses S, Henry K, Fang T, et al. Hierarchy of clinical manifestations in SAVI N153S and V154M mouse models. Proc Natl Acad Sci U S A 2019;116:7941–50.

31. Taveira-DaSilva AM, Markello TC, Kleiner DE, Jones AM, Groden C, Macnamara E, et al. Expanding the phenotype of COPA syndrome: a kindred with typical and atypical features. J Med Genet 2019;56:778–82.

32. Saldanha RG, Balka KR, Davidson S, Wainstein BK, Wong M, Macintosh R, et al. A mutation outside the dimerization domain causing atypical STING-associated vasculopathy with onset in Infancy. Front Immunol 2018;9:1535.

33. Pedraza-Sánchez S, Lezana-Fernández JL, Gonzalez Y, Martínez-Robles L, Ventura-Ayala ML, Sadowinski-Pine S, et al. Disseminated tuberculosis and chronic mucocutaneous candidiasis in a patient with a gain-of-function mutation in signal transduction and activator of transcription 1. Front Immunol 2017;8:1651.

34. Al Shehri T, Gilmour K, Gothe F, Loughlin S, Bibi S, Rowan AD, et al. Novel gain-of-function mutation in STAT1 sumoylation site leads to CMC/CID phenotype responsive to ruxolitinib. J Clin Immunol 2019;39:776–85.

35. Sanchez GA, Reinhardt A, Ramsey S, Wittkowski H, Hashkes PJ, Berkun Y, et al. JAK1/2 inhibition with baricitinib in the treatment of autoinflammatory interferonopathies. J Clin Invest 2018;128:3041–52.

36. Tsui JL, Estrada OA, Deng Z, Wang KM, Law CS, Elicker BM, et al. Analysis of pulmonary features and treatment approaches in the COPA syndrome. ERJ Open Res 2018;4:00017-2018.

37. Leuschner G, Behr J. Acute exacerbation in interstitial lung disease [review]. Front Med (Lausanne) 2017;4:176.

38. Parambil JG, Myers JL, Aubry MC, Ryu JH. Causes and prognosis of diffuse alveolar damage diagnosed on surgical lung biopsy. Chest 2007;132:50–7.

American College
of Rheumatology
Empowering Rheumatology Professionals

Pyrin Inflammasome Activation Abrogates Interleukin-1 Receptor Antagonist, Suggesting a New Mechanism Underlying Familial Mediterranean Fever Pathogenesis

Sussi B. Mortensen,[1] Ann-Brit E. Hansen,[2] Trine H. Mogensen,[3] Marianne A. Jakobsen,[1] Hans C. Beck,[4] Eva B. Harvald,[1] Kate L. Lambertsen,[1] Isik S. Johansen,[1] and Ditte C. Andersen[1]

Objective. Aberrant pyrin inflammasome activity triggers familial Mediterranean fever (FMF) pathogenesis, but the exact mechanism remains elusive and an obstacle to efficient treatment. We undertook this study to identify pyrin inflammasome–specific mechanisms to improve FMF treatment and diagnostics in the future.

Methods. Pyrin-specific protein secretion was assessed by proteome analysis in U937-derived macrophages, and specific findings were confirmed in pyrin inflammasome–activated monocytes from healthy blood donors and patients with FMF, stratified according to *MEFV* genotype categories corresponding to a suspected increase in FMF disease severity.

Results. Proteome data revealed a differential secretion pattern of interleukin-1 receptor antagonist (IL-1Ra) from pyrin- and NLRP3-activated U937-derived macrophages, which was verified by enzyme-linked immunosorbent assay and quantitative polymerase chain reaction. Moreover, pyrin activation significantly reduced *IL1RN* messenger RNA expression ($P < 0.001$) and IL-1Ra secretion ($P < 0.01$) in healthy donor and FMF monocytes, respectively. Independent of *MEFV* genotype, unstimulated FMF monocytes from colchicine-treated patients secreted lower amounts of IL-1Ra compared to healthy donors ($P < 0.05$) and displayed decreased ratios of IL-1Ra:IL-1β ($P < 0.05$), suggesting a reduced antiinflammatory capacity.

Conclusion. Our data show an inherent lack of IL-1Ra expression specific to pyrin inflammasome activation, suggesting a new mechanism underlying FMF pathogenesis. The reduced IL-1Ra levels in FMF monocytes suggest a diminished antiinflammatory capacity that potentially leaves FMF patients sensitive to proinflammatory stimuli, regardless of receiving colchicine therapy. Thus, considering the potential clinical consequence of reduced monocyte IL-1Ra secretion in FMF patients, we suggest further investigation into IL-1Ra dynamics and its potential implications for FMF treatment in the future.

INTRODUCTION

The pyrin inflammasome was recently discovered as an intracellular indirect pattern-recognition receptor of the innate immune system. It is a new member of the inflammasome macromolecular complex family that initiates proinflammatory responses by activating caspase 1–dependent interleukin-1β (IL-1β) processing (1,2). Pyrin inflammasome assembly is facilitated by pyrin that has been activated by bacterial modifications of RhoA activity (2) through downstream effector kinase release of inhibitory pyrin

phosphorylation (1). Pyrin is encoded by the *MEFV* (Mediterranean fever) gene and located on chromosome 16 in humans. In 1997, mutations in the *MEFV* gene were identified and found to be associated with the autoinflammatory disease, familial Mediterranean fever (FMF) (3,4). As a monogenic hereditary disease, FMF is characterized by periodic flares of fever accompanied by varying degrees of serositis, myalgia, skin involvement, and elevated levels of acute-phase reactants (5,6). It mainly affects people of Mediterranean origin with a reported prevalence in the range of 1:400–1:1,000 (7,8). However, with increasing rates of immigrants

and refugees coming from high-prevalence areas (9), FMF prevalence is expected to increase in previously low-prevalence areas.

Even though a diagnosis of FMF is mainly established based on clinical symptoms, diagnostic tests, and disease monitoring, it is highly dependent on genetic screening for *MEFV* variants and assessment of unspecific acute-phase reactants such as C-reactive protein, erythrocyte sedimentation rate, and serum amyloid A in patient blood. In addition, clinical symptoms are heterogeneous and many FMF patients, including apparently healthy carriers of low-penetrant *MEFV* variants, exhibit varying degrees of subclinical inflammation (10,11). Colchicine, the standard treatment for FMF patients (12), reduces the number and severity of flares and reduces the prevalence of chronic subclinical inflammation, amyloidosis, and associated kidney failure among others (10,12), but the underlying mechanism of action is unknown. However, treatment is still not curative, as patients with severe disease often experience treatment resistance (13,14), and the maximum-tolerated colchicine dose is not always adequate to control FMF activity (15). As in a few other autoinflammatory disorders (16), patients with FMF that does respond to colchicine may alternatively be treated with IL-1 receptor antagonists (IL-1Ra) or IL-1 antibodies to relieve symptoms (17–20). Thus, the limited knowledge of how *MEFV* variant properties affect FMF pathogenesis and shape disease phenotype hinders effective treatment of this increasing population of patients. We therefore investigated macrophage pyrin inflammasome activation to gain more mechanistic insight into FMF pathogenesis, which may improve the treatment of FMF patients.

PATIENTS AND METHODS

U937-derived macrophage cultures. The U937 line (ATCC CRL-1593.2) was maintained in medium consisting of RPMI 1640 (ATCC-modified formulation; A1049101; ThermoFisher Scientific) supplemented with 10% fetal bovine serum (16140071; ThermoFisher Scientific) and 1% penicillin/streptomycin (15140122; ThermoFisher Scientific) at 37°C. For differentiation, cells were plated at 50,000 cells/cm^2 and treated with 100 ng/ml phorbol 12-myristate 13-acetate (PMA) (P1585; Sigma-Aldrich) for 72 hours in extracellular matrix–coated (E1270; Sigma-Aldrich) culture plates, followed by a resting period of 72 hours in PMA-free complete culture medium. Optimal conditions for differentiation were established prior to study execution (data not shown). Differentiation was verified by morphologic changes and increased messenger RNA (mRNA) expression of macrophage markers CD11b, CD14, CD86, and HLA–DRB1 (see Supplementary Figure 1, avaiable on the *Arthritis & Rheumatology* website at http://onlinelibrary.wiley.com/doi/10.1002/art.41770/abstract).

Inflammasome activation in U937-derived macrophages. Inflammasome activation in macrophages was obtained by priming them for 4 hours with 1 μg/ml ultrapure *Escherichia coli* lipopolysaccharide (LPS) (tlrl-3pelps; InvivoGen)

followed by an activation step that included the following: 1 μg/ml C3 toxin (CT04-B; Cytoskeleton) (referred to as LPS/C3) for pyrin activation, 2.5 m*M* ATP (A6419; Sigma-Aldrich) (referred to as LPS/ATP) for NLRP3 activation, and no stimuli for LPS-induced effects. All activation steps were conducted in serum-free medium for 16 hours. Unprimed cells in serum-free medium were included as unstimulated controls. Inflammasome activation was performed in 4 biologic replicates according to previously described protocols (1,21) and in preliminary model setup experiments with varying concentrations of activators and time periods (Supplementary Figures 2B–E, http://onlinelibrary.wiley.com/doi/10.1002/art.41770/abstract). Cell supernatants were collected, cleared by centrifugation, and stored at –30°C until protein quantification. Cells were detached by incubation in phosphate buffered saline at 37°C, counted, lysed in RNeasy Mini kit lysis buffer (RLT), and stored at –80°C until RNA extraction.

Human plasma samples and isolation of primary monocytes. Blood samples were collected from healthy blood donors and patients with FMF upon signing written consent. Patients were stratified into 3 *MEFV* genotype groups: FMF patients with *MEFV* variants classified as variants of unknown significance or no detected variants (n = 10), FMF patients with variants classified as pathogenic or likely pathogenic in monoallelic form (n = 7), and FMF patients with variants classified as pathogenic or likely pathogenic in biallelic form (n = 6) (Supplementary Table 1, http://online library.wiley.com/doi/10.1002/art.41770/abstract).

The study protocol was approved by The Regional Committees on Health Research Ethics for Southern Denmark (S-20170020). Blood was collected in plasma separation tubes (no. 368270; Becton Dickinson) and citrate–phosphate–dextrose (CPD) tubes (no. 455056; Greiner Bio-One) for peripheral blood mononuclear cell (PBMC) isolation. Plasma samples were centrifuged at 1,500*g* for 10 minutes and stored at –80°C, and PBMCs were isolated from CPD samples by density gradient centrifugation of whole blood using Ficoll-Paque Plus (no. 17144002; GE Healthcare) in SepMate separation tubes (no. 85450; Stem-Cell Technologies). Cells were processed within 24 hours after blood sampling, and PBMCs were stored in liquid nitrogen until use. Monocytes were enriched from thawed PBMCs by negative selection using an EasySep enrichment kit without CD16 depletion (no. 19058) according to recommendations of the manufacturer (StemCell Technologies).

Inflammasome activation in primary isolated human monocytes. Pyrin inflammasome activation was obtained by adding 10 ng/ml ultrapure *E coli* LPS and 1 μg/ml C3 toxin to reduced serum medium Opti-MEM (no. 31985062; ThermoFisher Scientific) for 16 hours. Monocytes that had been incubated in Opti-MEM for 16 hours with or without the addition of 10 ng/ml LPS were included as LPS-stimulated and unstimulated controls, respectively. For peroxisome proliferator–activated

receptor α (PPARα) activation, PPARα agonist WY14643 (C7081; Merck) or vehicle (DMSO) was added at 50 ng/ml for 16 hours, together with LPS (10 ng/ml) and C3 (1 μg/ml). Cell supernatant was removed, cleared by centrifugation, and stored at –30°C until protein quantifications. Cells were lysed by adding TRI Reagent (AM9738; ThermoFisher Scientific), and cell lysate was stored at –80°C until RNA extraction.

RNA extraction and relative quantitative polymerase chain reaction (qPCR). Total RNA was extracted from U937-derived macrophages using an RNeasy Mini kit (no. 74104; Qiagen) or from primary isolated monocytes using TRI Reagent according to the manufacturer's instructions. RNA concentrations were assessed by NanoDrop. For complementary DNA (cDNA) synthesis, 0.2–0.4 μg total RNA was reverse-transcribed using a High Capacity cDNA RT kit (no. 4368813; ThermoFisher Scientific), and real-time qPCR was performed in technical triplicates with 2 ng cDNA and 3 pM of forward and reverse primer in a 10-μl reaction mixture using Power SYBR Green Master Mix (no. 4367659; ThermoFisher Scientific). Primers were designed to preferably span exon–exon junctions using the NCBI Primer-Blast software (22). Primer sequences are listed in Supplementary Table 2 (http://onlinelibrary.wiley.com/doi/10.1002/art.41770/abstract). PCR was run on a QuantStudio 7 Flex (no. 4485698; ThermoFisher Scientific) or LightCycler 480 II (no. 05015278001; Roche), under PCR conditions of 95°C for 10 minutes prior to 45 PCR cycles of the following: denaturation at 94°C for 15 seconds, annealing at 60°C for 30 seconds, and elongation at 72°C for 30 seconds. Robust and valid real-time qPCR data were obtained by normalizing raw data against multiple stably expressed endogenous control genes, as determined by the geNorm algorithm in qBasePlus version 3.2 (Biogazelle) (23).

Measurements of cytokines in cell supernatant and plasma samples. Quantifications of cytokines in cell media supernatants and human plasma were performed using a custom-designed Luminex Magnetic assay (LXSAHM-04; R&D Systems), by Uplex Assay (K15067L-1, Meso Scale Diagnostics), or by individual enzyme-linked immunosorbent assay kits (human IL-1β/IL-1F2 [DLB50]) according to the manufacturer's instructions.

Proteome analysis. Proteins were isolated from cell media supernatant of inflammasome-activated U937-derived macrophages (n = 4) as described above, by acetone precipitation. The protein pellet was redissolved in 0.2M tetraethylammonium bicarbonate followed by dithiothreitol reduction (5 mM at 50°C for 30 minutes), iodoacetamide alkylation (15 mM at room temperature for 30 minutes), and proteolysis using 1 μg trypsin. The resulting tryptic digests were labeled with isobaric tags using tandem mass tag (TMT) 10-plex reagent (no. 90110) according to recommendations of the manufacturer (ThermoFisher Scientific). Each sample set was split into 24 fractions using hydrophilic

interaction liquid chromatography fractionation and analyzed by nano–liquid chromatography tandem mass spectrometry (nano-LC-MS/MS) as previously described (24), with the following modifications: peptide mixtures were separated using a 30-minute linear gradient from 95% A (0.1% formic acid) to 30% B (100% acetonitrile), and maximum ion injection time for MS/MS analysis was set to 500 msec.

Raw data were processed using the Proteome Discoverer 2.1.0.81 software integrated with Mascot (version 2.4) and the Sequest database search program (25). Search parameters were set to the following: MS accuracy 8 parts per million, MS/MS accuracy 0.05 daltons with 2 missed cleavages allowed, fixed modifications of N-terminal, lysine (both 10-plex TMT) and cysteine blocked with carbamidomethyl, and variable modification (methionine oxidation and deamidated asparagine and glutamine). Tandem mass spectra were searched against the Swiss-Prot protein databank and restricted to humans. Proteins were inferred on the basis of ≥1 unique peptide identified with high confidence (false discovery rate [FDR] <1%). FDRs were obtained using the Percolator selecting identification with a q value of ≤0.01. TMT quantification was performed using Proteome Discoverer with reporter ion area integration within a 20-ppm window, and protein abundances were relative to a pool of all samples.

Proteome data analysis. Log$_2$ fold ratios for each treatment versus controls (LPS-treated versus control, LPS/C3-treated versus control, and LPS/ATP-treated versus control) were calculated from the mean relative abundance of each identified protein. Keratins are well-known contaminants in MS and were excluded from the analysis. Based on the DAVID Functional Annotation Table for gene ontology (GO) term cellular component analysis (Bioinformatic Database, version 6.8) (26,27), and to avoid identification of contaminating unspecific intracellularly associated proteins, we selected only terms that referred to the extracellular space and cell surface: GO:1903561 (extracellular vesicle), GO:0070062 (extracellular exosome), GO:0043230 (extracellular organelle), GO:0044421 (extracellular region part), GO:0005615 (extracellular space), GO:0019898 (extrinsic component of membrane), GO:0009986 (cell surface), GO:0044420 (extracellular matrix [ECM] component), GO:0005578 (proteinaceous ECM), GO:0097610 (cell surface furrow).

Up-regulated and down-regulated proteins were defined as having a log$_2$ fold change of >0.1 or <0.1, respectively. Lists of regulated proteins (treatment versus control) were uploaded to the functional annotation tool DAVID (26,27) for GO enrichment analysis. Significance was tested using a modified Fisher's exact test with FDR correction, and an FDR less than 0.05 was considered significant. Pyrin inflammasome (C3/LPS)–specific proteins were presented according to their level of up- or down-regulation compared to LPS treatment, after subtracting proteins similarly regulated by NLRP3 inflammasome (LPS/ATP) activation.

Statistical analysis. Statistical significance of the difference between means was determined by 2-tailed *t*-tests, or by one-way or two-way analysis of variance (ANOVA) followed by post hoc tests. Repeated-measures tests were used for analysis of monocyte gene and protein expression upon inflammasome activation, as observed in healthy donors and patients with FMF. A mixed-effect model was used instead of repeated measures when baseline values were below detection levels. Values of relative normalized gene expression and protein concentrations in cell supernatants are presented as the mean ± SD, including individual values. Monocytes displaying a "preactivated" profile were excluded from experiments and are not included in the presented data (monocytes from healthy donors, n = 1; monocytes from patients with FMF, n = 2). Preactivation was defined as an *IL1B* mRNA normalized relative quantity of >1,000 (scaled to the sample with lowest expression using qBasePlus software) at baseline or an IL-1β protein concentration in cell supernatant >1,000 pg/ml at baseline.

Effects of PPARα agonist WY14643 treatment are presented as the mean ± SD of individual expression ratios to DMSO (vehicle), including individual subject values. Three observations were missing from the PPARα agonist experiment due to failed measures of relative normalized gene expression or protein concentration in cell supernatant. For cell line experiments, the value denotes the number of performed experiments with cell cultures separated by ≥3 passages, and for experiments involving plasma or monocytes from healthy donors and patients with FMF, the value denotes the number of subjects. Continuous variables (cytokine mRNA and protein expression) from patient and healthy donor data were log-transformed to obtain Gaussian distribution and fulfill the requirements for two-way ANOVA statistics prior to statistical analysis, as required.

GraphPad Prism (version 7.04) was used for statistical analysis, and significance of enrichment analysis was tested using modified Fisher's exact test with FDR correction by built-in tests in the DAVID tool.

RESULTS

Impeded IL-1Ra expression in the presence of pyrin inflammasome activation in U937-derived macrophages. With the intent of mimicking FMF pathogenesis, we differentiated the human promonocytic cell line U937 from macrophages and primed them with LPS to induce proinflammatory gene expression (28) prior to specific inflammasome activation (Supplementary Figures 1 and 2B, http://onlinelibrary.wiley.com/doi/10.1002/art.41770/abstract). We designed the model with the intent of discriminating between the effects derived from LPS-induced Toll-like receptor 4 (TLR-4)–mediated cell activation (LPS-treated cells) (29), from its potential LPS-induced cross-activation of NLRP3 inflammasome (LPS/ATP-treated cells) (30), and from pyrin inflammasome activation (LPS/C3-treated cells) (1) (Figure 1A). As expected, LPS priming alone elicited a strong proinflammatory transcriptional response, including increased expression of IL-1β (Supplementary Figure 1F) as well as cell swelling and loss of membrane integrity (Supplementary Figures 2B–E). This inflammatory phenotype of the U937-derived macrophages was exacerbated by the addition of ATP and C3 in a dose- and time-dependent manner in our initial model setup experiments (Supplementary Figures 2C–E), and, taken together, these findings confirmed our in vitro design.

We next used MS of media supernatants from stimulated U937-derived macrophages (n = 4) to specifically identify molecular networks that distinguish between LPS-induced cell activation, NLRP3 inflammasome (LPS/ATP) signaling, and pyrin inflammasome (LPS/C3) signaling. Initially, the proinflammatory response of U937-derived macrophages was confirmed by measurements of IL-1β and tumor necrosis factor (TNF) in cell supernatants (Figure 1B). Using MS data, we identified a total of 1,556 robustly present proteins in the media, and GO enrichment analysis of the up-regulated proteins for the 3 subsets (n = 101, 434, and 344 for LPS-treated, NLRP3 inflammasome–activated, and pyrin inflammasome–activated, respectively), when compared to controls (nonstimulated), revealed enrichment (FDR < 0.05) of biologic processes related to neutrophil chemotaxis, inflammatory response, and positive regulation of inflammatory response for LPS-stimulated U937-derived macrophages (Supplementary Figure 3A, http://onlinelibrary.wiley.com/doi/10.1002/art.41770/abstract). Further stimulation of the pyrin or NLRP3 inflammasome with C3 or ATP revealed 18 and 12 annotated biologic processes, respectively (Supplementary Figures 3B and C), 3 of which were shared, and some that remained specific to each treatment. This confirmed the onset of LPS-induced inflammatory effects (31,32) and that the underlying mode of action for NLRP3 inflammasome activation and pyrin inflammasome activation clearly differs, which supports our study design.

We next identified mechanisms involving secretion of proteins specific to pyrin inflammasome activation and FMF disease by conducting cell compartment analysis, classifying 924 proteins as secreted or associated with the cell surface. As such, we identified 86 up-regulated and 179 down-regulated proteins unique to pyrin inflammasome activation (Figure 1C). Interestingly, when listing and evaluating the top 10 up- and down-regulated pyrin-specific proteins (Figure 1C), we recognized IL-1Ra, a key regulator of IL-1 signaling used for treating other immune-affected patients and FMF colchicine nonresponders (17–19,33). We therefore decided to analyze in detail whether IL-1Ra–dependent mechanisms are specifically associated with the FMF phenotype.

Abrogation of IL-1Ra expression by pyrin inflammasome activation in U937-derived macrophages and compromised IL-1Ra secretion in unstimulated FMF monocytes. Initially, we verified the MS data on differential IL-1Ra abundance in pyrin and NLRP3 inflammasome–activated U937-derived macrophage medium supernatants, and found that
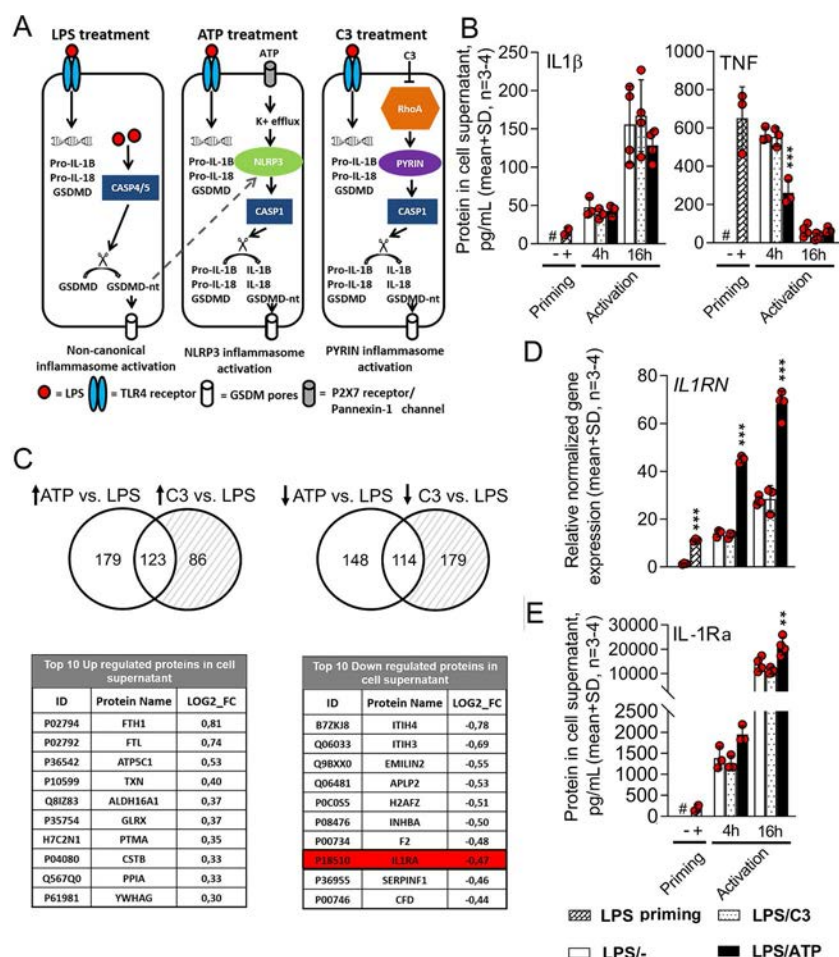
Figure 1. Pyrin and NLRP3 inflammasome activation in U937-derived macrophages exerts differential effects on interleukin-1 receptor antagonist (IL-1Ra) expression. **A**, Overview of the inflammasome activation model design, with differentiation between lipopolysaccharide (LPS)–derived effects, NLRP3 (LPS/ATP) inflammasome activation, and pyrin (LPS/C3) inflammasome activation. Dashed lines indicate the potential cross-activating effects of LPS on NLRP3 inflammasome activity. **B**, IL-1β and tumor necrosis factor (TNF) in cell supernatant of U937-derived macrophages (n = 4) upon LPS priming and inflammasome activation. **C**, Venn diagrams of up-regulated (log$_2$ fold change >0.1) and down-regulated (log$_2$ fold change <0.1) proteins in cell supernatant of pyrin inflammasome– and NLRP3 inflammasome–activated cells as compared to LPS-treated cells, and the top 10 pyrin up- and down-regulated proteins ranked according to log$_2$ fold change. **D** and **E**, *IL1RN* mRNA expression (**D**) and protein release (**E**) in cultures of U937-derived macrophages upon LPS priming and inflammasome activation with ATP or C3. Significance of the effect of LPS priming was tested using a 2-sample *t*-test, and significance of the effect of pyrin (LPS/C3) and NLRP3 (LPS/ATP) inflammasome activation in comparison to LPS-treated cells at each time point was tested using one-way analysis of variance. Correction for multiple comparisons was conducted using the Holm-Sidak method. ** = $P < 0.01$; *** = $P < 0.001$ versus LPS/C3 treatment and unstimulated controls (LPS/–); # = below assay detection limit. TLR-4 = Toll-like receptor 4; GSDMD-NT = gasdermin D N-terminal cleavage product; CASP1 = caspase 1; TH-1 = ferritin heavy chain 1; FTL = ferritin light chain; ATPSC-1 = ATP synthase F1 subunit gamma; TXN = thioredoxin; ALDH16A1 = aldehyde dehydrogenase 16 family member A1; GLRX = glutaredoxin; PTMA = prothymosin α; CSTB = cystatin B; PPIA = peptidylprolyl isomerase A; YWHAG = tyrosine 3-monooxygenase/tryptophan 5-monooxygenase activation protein γ; ITIH-4 = inter-α-trypsin inhibitor heavy chain 4; EMLIN2 = elastin microfibril interfacer 2; APLP-2 = amyloid β precursor-like protein 2; INHBA = inhibin subunit βA; CFD = human complement factor D.

an increase in *IL1RN* mRNA expression was associated with NLRP3-mediated inflammasome activation, but this association was not present for pyrin inflammasome activation (Figure 1D). Consistent with this finding, LPS-induced IL-1Ra protein expression was amplified from a mean ± SD of 13,866 ± 2,913 pg/ml to 21,265 ± 3,650 pg/ml by NLRP3 activation (*P* < 0.001), whereas IL-1Ra remained unaltered at a mean ± SD of 11,042 ± 1,171 pg/ml in pyrin-stimulated U937-derived macrophages (n = 4) (Figure 1E). This may indicate an inherent absence of IL-1Ra dampening

IL-1 signaling in the monocyte cell lineage of patients with FMF, which potentially exacerbates the FMF disease. Monocytes were therefore isolated from FMF patients presenting biallelic, pathogenic exon-10 *MEFV* variants and healthy blood donors (Figure 2A and Supplementary Table 2, http://onlinelibrary.wiley.com/doi/10.1002/art.41770/abstract).

Both LPS activation and pyrin inflammasome activation induced a substantial proinflammatory response, as seen in levels of IL-1β and TNF protein secretion (Figures 2B and C), but only

Figure 2. Pyrin inflammasome activation abrogates IL-1 receptor antagonist (IL-1Ra) expression in healthy donor (HD) and familial Mediterranean fever (FMF) primary monocytes. **A**, Experimental setup. Healthy donor and FMF monocytes were en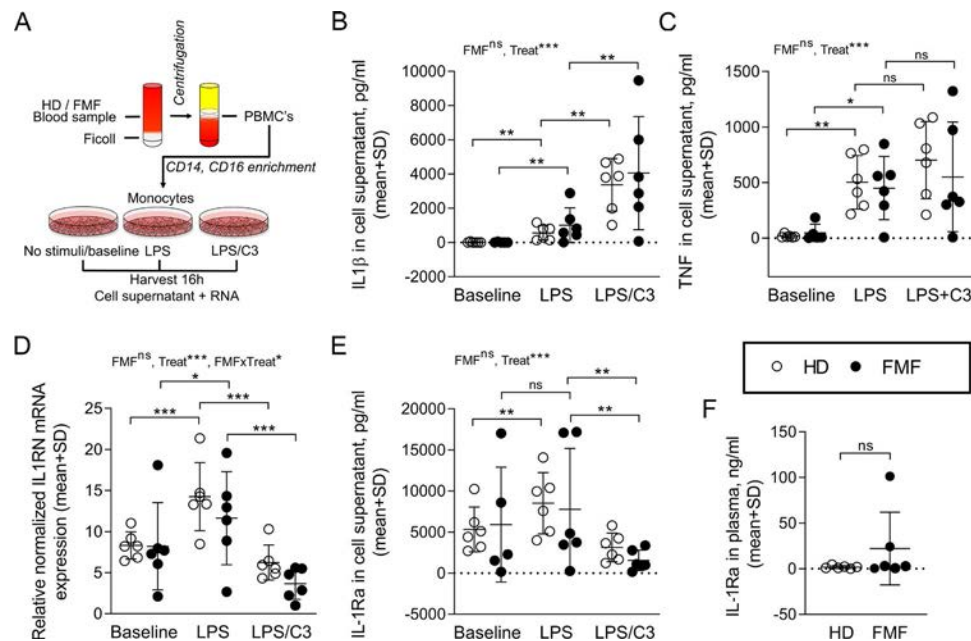riched from peripheral blood mononuclear cells (PBMCs) and left unstimulated or stimulated with LPS or LPS/C3 (pyrin) for 16 hours before obtaining cell supernatant and RNA. FMF patients were *MEFV*-genotyped with biallelic pathogenic exon-10 variants (see Supplementary Table 2, http://onlinelibrary.wiley. com/doi/10.1002/art.41770/). **B** and **C**, IL-1β (**B**) and TNF (**C**) levels in cell supernatant, to confirm proinflammatory cytokine stimulation. **D–F**, *IL1RN* mRNA expression (**D**) and IL-1Ra secretion (**E**) upon monocyte activation (as depicted in **A**), and plasma IL-1Ra levels (**F**) in samples from healthy donors and FMF patients. The significance of LPS-derived effects and pyrin inflammasome activation (LPS/C3) was tested using repeated-measures or mixed-effect two-way analysis of variance, followed by Holm-Sidak correction for multiple comparisons, in comparing LPS stimulation versus no stimulation and LPS/C3 stimulation versus LPS stimulation in healthy donor and FMF monocytes. Significance of difference in plasma IL-1Ra levels was tested using Mann-Whitney test. In **B–F**, each symbol represents an individual subject; bars show the mean ± SD. * = $P < 0.05$; ** = $P < 0.01$; *** = $P < 0.001$. NS = not significant (see Figure 1 for other definitions).

IL-1β levels were significantly affected by additional pyrin inflammasome activation. This indicates that TNF expression is mainly controlled by LPS activation of the TLR-4 receptor, while IL-1β expression is further triggered by pyrin inflammasome activation (34,35). The magnitude of the proinflammatory response was not affected by FMF disease under the present experimental conditions (Figures 2B and C). Confirming our U937 cell model derived data (Figure 1), we found a substantial increase in IL-1Ra for both FMF and healthy donor monocytes with LPS treatment (Figures 2D and E). However, pyrin inflammasome activation abrogated IL-1Ra expression, with *IL1RN* mRNA levels declining below baseline, from a mean ± SD of 14.3 ± 4.1 to 6.2 ± 2.1 in healthy donors (n = 6; $P < 0.001$) and from a mean ± SD of 11.6 ± 5.7 to 1.9 in FMF patients (n = 6; $P < 0.001$), compared to LPS-treated monocytes (Figure 2D). This was supported by a reduction in cell supernatant IL-1Ra from a mean ± SD of 8,521 ± 3,733 pg/ml to 3,143 ± 1,742 pg/ml in healthy donors (n = 6; $P < 0.01$) and from a mean ± SD of 7,761 ± 7,423 pg/ml to 1,549 ± 1,248 pg/ml in FMF patients (n = 6; $P < 0.01$) compared to LPS-treated monocytes (Figure 2E). Plasma IL-1Ra levels did not show any robust changes between FMF patients and healthy donors. Instead, elevated plasma IL-1Ra levels seemed to coincide, to some degree, with the presence of

an ongoing FMF flare (Figure 2F), which is consistent with IL-1Ra also being a liver-secreted acute-phase reactant (36).

To delineate the mechanism underlying macrophages' and monocytes' inability to mount an appropriate IL-1Ra response upon pyrin inflammasome activation, we investigated the nuclear receptor PPARα–retinoid X receptor α (RXRα) complex. It is known that the RXRα facilitates PPARα-mediated *IL1RN* transcription from the *IL1RN* promoter (37–39); thus, we sought to investigate whether *IL1RN* transcription and expression could be rescued by addition of the PPARα agonist WY14643 to pyrin-activated monocytes (Figure 3A). Contrary to our expectations, we found that while PPARα agonist treatment failed to induce or rescue the abrogated *IL1RN* transcription in pyrin-activated monocytes ($P < 0.001$), it did confer an inhibitory effect on the proinflammatory *IL1B* mRNA transcription in both healthy donor and FMF monocytes ($P < 0.001$) (Figure 3B). This was confirmed at the protein level, where secreted concentrations of IL-1Ra and IL-1β were reduced by PPARα agonist treatment ($P < 0.01$) (Figures 3B and C), suggesting that WY14643 successfully agonized the RXRα-independent transrepressing PPARα effect, while failing to agonize the RXRα-dependent transactivating effect on pyrin inflammasome activation ($P < 0.05$) (Figure 3E). Additionally, *RXRA* mRNA expression declined but was
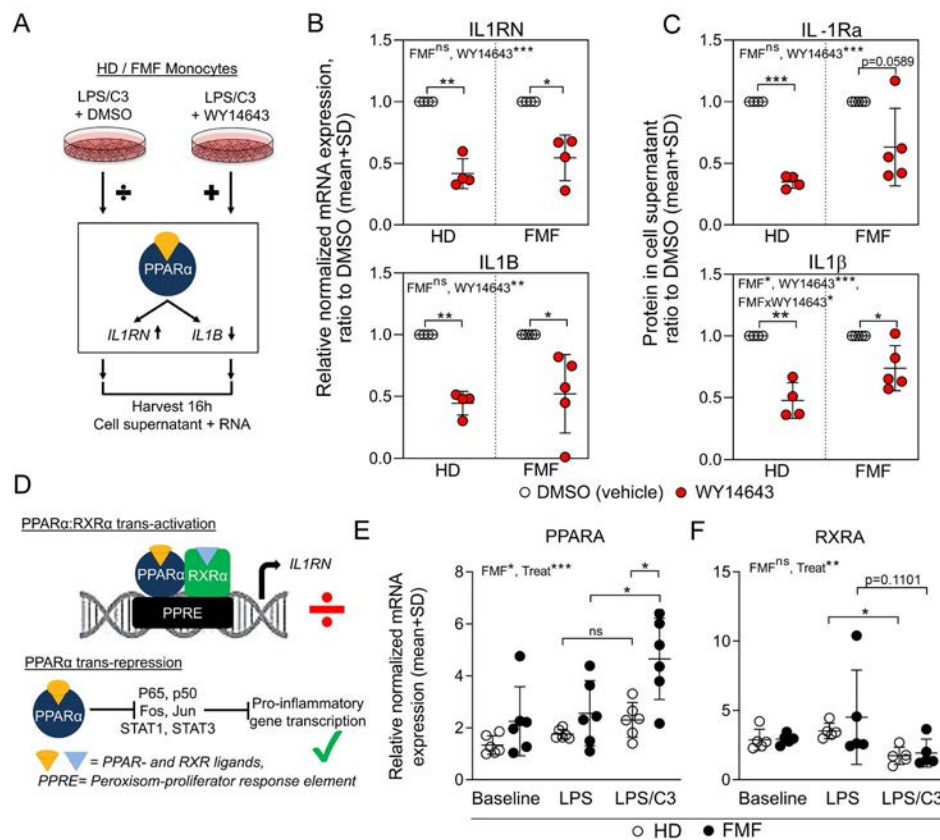
Figure 3. Peroxisome proliferator–activated receptor α (PPARα) agonist WY14643 failed to rescue the abrogated IL-1Ra expression in pyrin inflammasome–activated monocytes. **A**, Experimental setup. Pyrin inflammasome–activated (LPS/C3) healthy donor (HD) and familial Mediterranean fever (FMF) monocytes were treated with PPARα agonist WY14643 or vehicle (DMSO) for 16 hours. FMF patients were *MEFV*-genotyped with biallelic pathogenic exon-10 variants (see Supplementary Table 2, http://onlinelibrary.wiley.com/doi/10.1002/art.41770/). **B** and **C**, *IL1RN* and *IL1B* mRNA expression (**B**) and IL-1Ra and IL-1β protein secretion (**C**) upon PPARα agonist treatment. Data are presented as a ratio relative to the mean values with DMSO treatment (set at 1.0). **D**, Theoretical drawing of PPARα involvement in the regulation of antiinflammatory and proinflammatory gene transcription. **E** and **F**, *PPARA* (**E**) and *RXRA* (**F**) mRNA expression upon pyrin inflammasome activation, as described in Figure 2A. Significance of WY14643 treatment compared to DMSO treatment was tested by one-sample *t*-test. The significance of the effect of pyrin inflammasome activation (LPS/C3) on *PPARA* and *RXRA* levels in healthy donor and FMF monocytes was tested using repeated-measures two-way analysis of variance, followed by paired *t*-test comparison of LPS stimulation versus LPS/C3 stimulation. In **B**, **C**, **E**, and **F**, each symbol represents an individual subject; bars show the mean ± SD. * = $P < 0.05$; ** = $P < 0.01$; *** = $P < 0.001$. NS = not significant; RXRα = retinoid X receptor α (see Figure 1 for other definitions).

only significant ($P < 0.05$) in healthy donor monocytes, compared to LPS treatment (Figure 3F).

Therefore, our data indicate a specific failure in monocytes to mount an appropriate IL-1Ra response upon pyrin inflammasome activation, which could at least partly be mediated by an RXRα-dependent antiinflammatory mechanism of PPARα. However, the exact mechanism and its implications for IL-1Ra dynamics in FMF patients require further investigation. We then finally tested IL-1Ra release from untreated monocytes, LPS-treated monocytes, and pyrin inflammasome–activated monocytes from a larger group of FMF patients who did not experience flares while receiving colchicine, representing a more diverse variety of *MEFV* variants, grouped according to the expected clinical significance (Supplementary Table 2, http://onlinelibrary.wiley.com/doi/10.1002/art.41770/abstract).

Monocytes were isolated and stimulated as described above (Figure 2A), and cell supernatant IL-1Ra and IL-1β concentrations were assessed at baseline and upon LPS and pyrin inflammasome activation, respectively. Consistent with our above findings, pyrin inflammasome activation reduced IL-1Ra secretion to below baseline levels, but now with a significant difference between healthy donor and FMF monocytes ($P < 0.05$) (Figure 4A). In addition, we found that unstimulated FMF monocytes released significantly lower amounts of IL-1Ra (mean ± SD 1,347 ± 1,159 pg/ml; n = 23) extracellularly than healthy donors (mean ± SD 3,049 ± 1,728 pg/ml; n = 6) ($P < 0.05$) (Figure 4A). However, there was no difference in secretion levels of IL-1Ra ($P > 0.7556$) or in the IL-1Ra:IL-1β ratio ($P > 0.3746$) between the 3 different FMF groups (Supplementary Table 2), either at baseline or after treatment with LPS or LPS/C3 (Figures 4A and B).
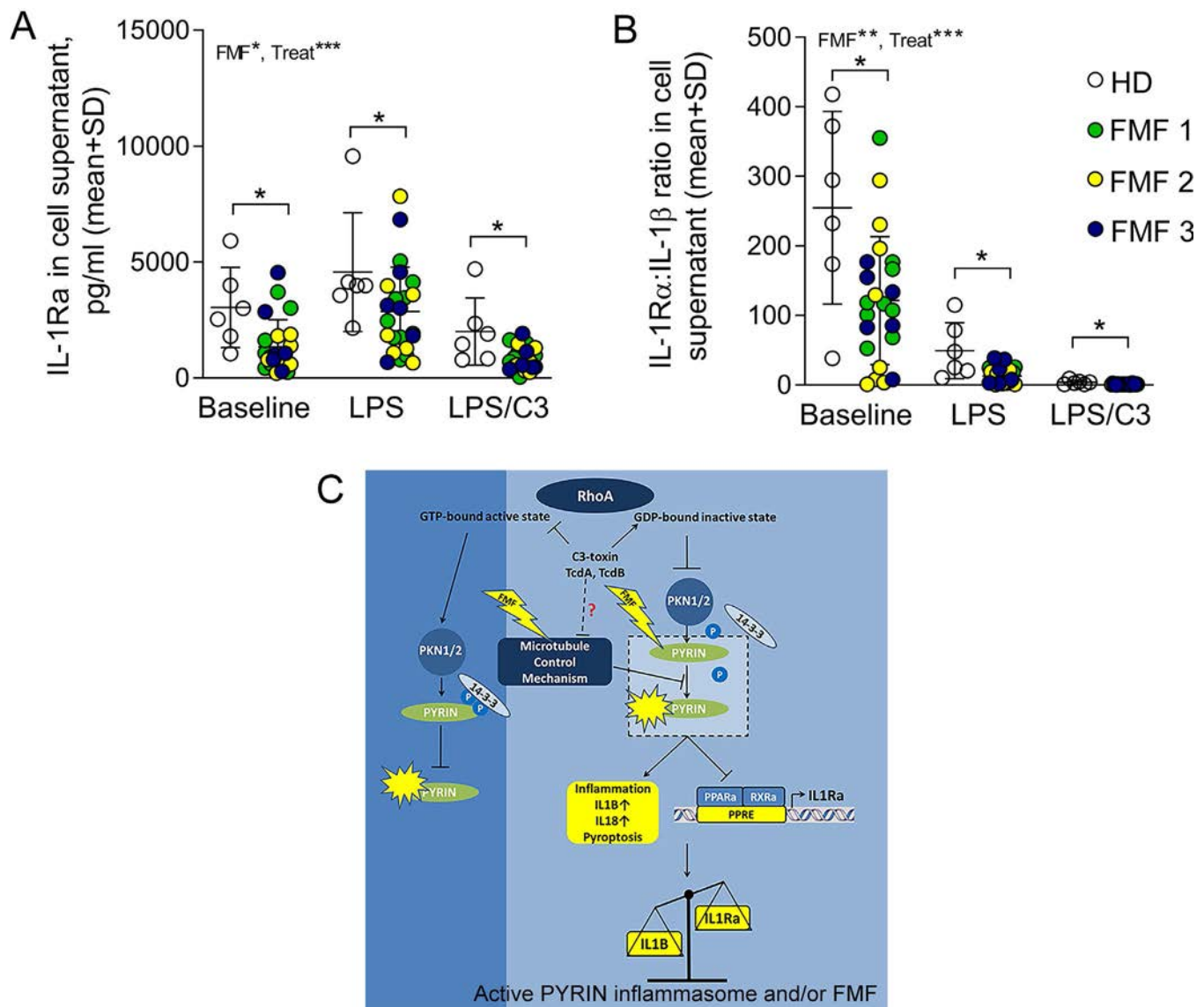
Figure 4. Cell supernatant IL-1Ra levels and the IL-1Ra:IL-1β ratio decreased in colchicine-treated FMF patient monocytes compared to healthy donor monocytes. **A** and **B**, Healthy donor (HD) and familial Mediterranean fever (FMF) monocytes were enriched from peripheral blood mononuclear cells (PBMCs) and stimulated as described in Figure 2A. FMF patients were grouped based on *MEFV* genotypes, as follows: no variants or variants with uncertain significance (FMF 1, n = 10), monoallelic pathogenic or likely pathogenic exon-10 variants (FMF 2, n = 7), and biallelic pathogenic or likely pathogenic exon-10 variants (FMF 3, n = 6). IL-1Ra levels (**A**) and the IL-1Ra:IL-1β ratio (**B**) were evaluated in the cell supernatant after 16 hours of stimulation. Each symbol represents an individual subject; bars show the mean ± SD. * = $P < 0.05$; ** = $P < 0.01$; *** = $P < 0.001$. **C**, Theoretical view of a proposed pyrin inflammasome–dependent IL-1Ra–altering mechanism underlying FMF pathogenesis. Significance of the effects of LPS and LPS/C3 activation was tested using repeated-measures two-way analysis of variance, followed by Holm-Sidak correction for multiple comparisons, in comparing the main LPS- and LPS/C3-derived effects (not shown), and comparing FMF monoctyes to healthy donor monocytes in each treatment group. NS = not significant; PKN1/2 = protein kinase N 1/2; PPARα = peroxisome proliferator–activated receptor α; RXRα = retinoid X receptor α; PPRE = peroxisome proliferator response element (see Figure 1 for other definitions).

An IL-1Ra:IL-1β ratio above 100 is considered to reflect an antiinflammatory functional phenotype (40,41). In the FMF monocytes, IL-1Ra:IL-1β ratios were just balancing around this threshold (mean ± SD 121.5 ± 92.0; n = 23), whereas healthy donor monocytes exhibited a clear antiinflammatory phenotype (mean ± SD 255.0 ± 138.5; n = 6) (Figure 4B). As expected, LPS and pyrin inflammasome activation caused an overall reduction of the IL-1Ra:IL-1β ratio, while maintaining the significant difference between healthy donor and FMF monocytes ($P < 0.05$) (Figure 4B). These low IL-1Ra concentrations and IL-1Ra:IL-1β ratios at baseline in FMF monocytes likely imply a more sensitive monocyte phenotype with reduced capacity to control and shut down potential proinflammatory responses, thereby triggering the FMF disease flares.

DISCUSSION

Deficiency of pyrin inflammasome assembly and regulation due to *MEFV* mutations is the most recently suggested molecular explanation of FMF pathogenesis, but many questions regarding the specific mechanism by which mutationally altered pyrin proteins confer the proinflammatory phenotype in FMF patients remain. Here, we have demonstrated how activation of the pyrin inflammasome, contrary to LPS and NLRP3 inflammasome activation, abrogates IL-1Ra expression, suggesting a pyrin inflammasome–specific deregulation of IL-1 signaling (Figure 4C). Taken together with the reduced IL-1Ra levels and IL-1Ra:IL-1β ratios in unstimulated FMF monocytes, these findings call for further investigation into how this may have translational potential for treating FMF patients. While colchicine is effective in reducing symptoms in most patients, IL-1Ra therapy in addition to colchicine may augment the abnormally reduced IL-1Ra–mediated antiinflammatory capacity of FMF monocytes, thereby potentially providing substantial relief of symptoms, especially for certain groups of FMF patients in whom standard colchicine treatment is insufficient to control symptoms.

While previous findings have shown a delayed IL-1Ra response in TLR-stimulated monocytes from patients with the autoinflammatory disease known as cryopyrin-associated periodic syndrome (42), our finding of decreased steady-state antiinflammatory capacity in FMF monocytes with an absence of an IL-1Ra response upon pyrin inflammasome activation is, to the best of our knowledge, novel. IL-1 signaling has recently been linked to the induction of trained immunity in myeloid cells by introducing epigenetic changes that increase monocyte and macrophage responsiveness to proinflammatory stimuli (43,44). Interestingly, IL-1Ra treatment has proven important for reversing this process in primary human monocytes (45) and in hematopoietic mouse stem cells (43). When lacking the IL-1 dampening capacity of IL-1Ra in FMF monocytes as described here, it is likely that even minute amounts of microbial constituents (pathogen-associated molecular patterns) or other fluctuations in cell homeostasis (homeostasis-associated molecular patterns) may shift the antiinflammatory:inflammatory balance (Figure 4C). As such, FMF monocytes may be shifted to the modified "trained" state upon every disease flare (44), exhibiting an exacerbated proinflammatory phenotype. However, whether the decreased IL-1Ra secretion in monocytes, as observed in this study, leads to consecutive aggravated immune deregulation in FMF patients remains to be seen. The efficacy of IL-1Ra for certain subgroups of FMF patients has been confirmed, where IL-1 antagonists in FMF patients who are unresponsive to colchicine reduces the number of flares and levels of acute-phase reactants (18,46,47).

Moreover, IL-1Ra have been shown to lower proteinuria in patients with complicating AA amyloidosis (48–50). Therefore, our data suggest further investigation of the clinical relevance of monocyte IL-1Ra secretion in FMF pathology, considering the potential beneficial effects of extending IL-1Ra therapy to a broader spectrum of FMF patients. Since our data show that FMF patients, independent of *MEFV* genotypes and despite receiving colchicine treatment, have compromised IL-1Ra monocyte capacity, all FMF patients may likely benefit from IL-1 antagonist treatment in combination with colchicine. This is consistent with a very recent hypothesis proposed during the finalization of our study, that IL-1 blockade should be considered as first-line treatment to prevent irreversible loss of beneficial effects in treatment-naive patients with AA amyloidosis, proteinuria, or renal impairment (51).

Our data also suggest that measuring baseline IL-1Ra secretion or IL-1Ra:IL-1β balance in patient monocytes may serve as an obvious new clinical tool for monitoring disease activity and treatment progress. However, since we focused on circulatory monocytes in patients, we cannot exclude the possibility that IL-1Ra dynamics in resident macrophages or neutrophils infiltrating serosal fluids may behave differently. In addition, whether other treatment schedules can be developed from our new knowledge must be further investigated. For instance, it is known that PPARα exerts its antiinflammatory effect by 2 different routes: by heterodimerizing with RXRα in the PPARα–RXRα complex to induce *IL1RN* transcription through binding to PPAR response element in the promoter of *IL1RN* (37), and by transrepressing proinflammatory gene transcription through inhibitory binding of transcription factors activating protein 1 and NF-κB (39). In the present study, agonizing PPARα–RXRα activity did not induce *IL1RN* transcription, while RXRα-independent transrepression of *IL1B* was successfully achieved. Recent findings suggest that PPARα and RXRα also play key roles in bridging metabolism and inflammation through lipid activation, which may potentially explain part of the observed FMF phenotype heterogeneity (52,53). Taken together, these findings suggest that dietary restrictions may benefit FMF patients.

A limitation of this study includes the absence of *MEFV* variant–matched FMF patients who were not treated with colchicine in order to investigate whether the low IL-1Ra levels are caused by colchicine treatment. However, whether or not this is colchicine-induced, it is likely disadvantageous for the antiinflammatory capacity of FMF monocytes.

In conclusion, our data collectively point to aberrant IL-1Ra dynamics underlying FMF pathogenesis, and we therefore propose further investigation into IL-1Ra dynamics in FMF patients and its implications for developing new treatment schedules for patients with poor responsiveness or tolerance to colchicine.

AUTHOR CONTRIBUTIONS

All authors were involved in drafting the article or revising it critically for important intellectual content, and all authors approved the final version to be published. Dr. Andersen had full access to all of the data in the study and takes responsibility for the integrity of the data and the accuracy of the data analysis.

Study conception and design. Mortensen, Hansen, Jakobsen, Johansen, Andersen.

Acquisition of data. Mortensen, Hansen, Mogensen, Beck, Lambertsen, Johansen, Andersen.

Analysis and interpretation of data. Mortensen, Beck, Harvald, Lambertsen, Johansen, Andersen.

REFERENCES

1. Park YH, Wood G, Kastner DL, Chae JJ. Pyrin inflammasome activation and RhoA signaling in the autoinflammatory diseases FMF and HIDS. Nat Immunol 2016;17:914–21.

2. Xu H, Yang J, Gao W, Li L, Li P, Zhang L, et al. Innate immune sensing of bacterial modifications of Rho GTPases by the Pyrin inflammasome [letter]. Nature 2014;513:237–41.

3. French FMF Consortium, Bernot A, Clepet C, Dasilva C, Devaud C, Petit JL, et al. A candidate gene for familial Mediterranean fever. Nat Genet 1997;17:25–31.

4. The International FMF Consortium. Ancient missense mutations in a new member of the RoRet gene family are likely to cause familial Mediterranean fever. Cell 1997;90:797–807.

5. Ben-Chetrit E, Levy M. Familial Mediterranean fever. Lancet 1998;351:659.

6. Kastner DL. Hereditary periodic fever syndromes. Hematology AM Soc Hematol Educ Program 2005;2005:74–81.

7. Ben-Chetrit E, Touitou I. Familial Mediterranean fever in the world [review]. Arthritis Rheum 2009;61:1447–53.

8. Sohar E, Gafni J, Pras M, Heller H. Familial Mediterranean fever: a survey of 470 cases and review of the literature [review]. Am J Med 1967;43:227–53.

9. Farkas M, Dovenyi Z. Migration to Europe and its demographic background. Regional Statistics 2018;8:29–48.

10. Ben-Zvi I, Livneh A. Chronic inflammation in FMF: markers, risk factors, outcomes and therapy [review]. Nat Rev Rheumatol 2011;7:105–12.

11. Lachmann HJ, Sengul B, Yavuzsen TU, Booth DR, Booth SE, Bybee A, et al. Clinical and subclinical inflammation in patients with familial Mediterranean fever and in heterozygous carriers of MEFV mutations. Rheumatology (Oxford) 2006;45:746–50.

12. Dinarello CA, Wolfe SM, Goldfinger SE, Dale DC, Alling DW. Colchicine therapy for familial Mediterranean fever: a double-blind trial. N Engl J Med 1974;291:934–7.

13. Ozen S, Demirkaya E, Erer B, Livneh A, Ben-Chetrit E, Giancane G, et al. EULAR recommendations for the management of familial Mediterranean fever. Ann Rheum Dis 2016;75:644.

14. Ter Haar N, Lachmann H, Ozen S, Woo P, Uziel Y, Modesto C, et al. Treatment of autoinflammatory diseases: results from the Eurofever Registry and a literature review. Ann Rheum Dis 2013;72:678–85.

15. Alghamdi M. Familial Mediterranean fever, review of the literature. Clin Rheumatol 2017;36:1707–13.

16. Masters SL, Simon A, Aksentijevich I, Kastner DL. Horror autoinflammaticus: the molecular pathophysiology of autoinflammatory disease [review]. Annu Rev Immunol 2009;27:621–68.

17. Dinarello CA, Simon A, van der Meer JW. Treating inflammation by blocking interleukin-1 in a broad spectrum of diseases [review]. Nat Rev Drug Discov 2012;11:633–52.

18. Meinzer U, Quartier P, Alexandra JF, Hentgen V, Retornaz F, Koné-Paut I. Interleukin-1 targeting drugs in familial Mediterranean fever: a case series and a review of the literature. Semin Arthritis Rheum 2011;41:265–71.

19. Roldan R, Ruiz AM, Miranda MD, Collantes E. Anakinra: new therapeutic approach in children with familial Mediterranean fever resistant to colchicine. Joint Bone Spine 2008;75:504–5.

20. De Benedetti F, Gattorno M, Anton J, Ben-Chetrit E, Frenkel J, Hoffman HM, et al. Canakinumab for the treatment of autoinflammatory recurrent fever syndromes. N Engl J Med 2018;378:1908–19.

21. Jamilloux Y, Lefeuvre L, Magnotti F, Martin A, Benezech S, Allatif O, et al. Familial Mediterranean fever mutations are hypermorphic mutations that specifically decrease the activation threshold of the pyrin inflammasome. Rheumatology (Oxford) 2018;57:100–11.

22. Ye J, Coulouris G, Zaretskaya I, Cutcutache I, Rozen S, Madden TL. Primer-BLAST: a tool to design target-specific primers for polymerase chain reaction. BMC Bioinformatics 2012;13:134.

23. Vandesompele J, De Preter K, Pattyn F, Poppe B, van Roy N, De Paepe A, et al. Accurate normalization of real-time quantitative RT-PCR data by geometric averaging of multiple internal control genes. Genome Biol 2002;3:research0034.

24. Beck HC, Jensen LO, Gils C, Ilondo AM, Frydland M, Hassager C, et al. Proteomic discovery and validation of the confounding effect of heparin administration on the analysis of candidate cardiovascular biomarkers. Clin Chem 2018;64:1474–84.

25. Kall L, Canterbury JD, Weston J, Noble WS, MacCoss MJ. Semi-supervised learning for peptide identification from shotgun proteomics datasets. Nat Methods 2007;4:923–5.

26. Huang DW, Sherman BT, Lempicki RA. Systematic and integrative analysis of large gene lists using DAVID bioinformatics resources. Nat Protoc 2009;4:44–57.

27. Huang DW, Sherman BT, Lempicki RA. Bioinformatics enrichment tools: paths toward the comprehensive functional analysis of large gene lists. Nucleic Acids Res 2009;37:1–13.

28. Li X, Qin J. Modulation of Toll-interleukin 1 receptor mediated signaling. J Mol Med (Berl) 2005;83:258–66.

29. Shi J, Zhao Y, Wang Y, Gao W, Ding J, Li P, et al. Inflammatory caspases are innate immune receptors for intracellular LPS. Nature 2014;514:187–92.

30. Liston A, Masters SL. Homeostasis-altering molecular processes as mechanisms of inflammasome activation [review]. Nat Rev Immunol 2017;17:208.

31. Viganò E, Diamond CE, Spreafico R, Balachander A, Sobota RM, Mortellaro A. Human caspase-4 and caspase-5 regulate the one-step non-canonical inflammasome activation in monocytes. Nat Commun 2015;6:8761.

32. Awad F, Assrawi E, Louvrier C, Jumeau C, Georgin-Lavialle S, Grateau G, et al. Inflammasome biology, molecular pathology and therapeutic implications [review]. Pharmacol Ther 2018; 187:133–49.

33. Ozdogan H, Ugurlu S. Canakinumab for the treatment of familial Mediterranean fever [review]. Expert Rev Clin Immunol 2017;13:393–404.

34. Lee MS, Kim YJ. Signaling pathways downstream of pattern-recognition receptors and their cross talk [review]. Annu Rev Biochem 2007;76:447–80.

35. Martinon F, Burns K, Tschopp J. The inflammasome: a molecular platform triggering activation of inflammatory caspases and processing of proIL-β. Molecular Cell 2002;10:417–26.

36. Gabay C, Smith MF, Eidlen D, Arend WP. Interleukin 1 receptor antagonist (IL-1Ra) is an acute-phase protein. J Clin Invest 1997;99:2930–40.

37. Stienstra R, Mandard S, Tan NS, Wahli W, Trautwein C, Richardson TA, et al. The interleukin-1 receptor antagonist is a direct target gene of PPARα in liver. J Hepatol 2007;46:869–77.

38. Desvergne B, Wahli W. Peroxisome proliferator-activated receptors: nuclear control of metabolism [review]. Endocr Rev 1999;20: 649–88.

39. Delerive P, De Bosscher K, Besnard S, Vanden Berghe W, Peters JM, Gonzalez FJ, et al. Peroxisome proliferator-activated receptor α negatively regulates the vascular inflammatory gene response by negative cross-talk with transcription factors NF-κB and AP-1. J Biol Chem 1999;274:32048–54.

40. Arend WP, Malyak M, Guthridge CJ, Gabay C. Interleukin-1 receptor antagonist: role in biology [review]. Annu Rev Immunol 1998;16:27–55.

41. Firestein GS, Boyle DL, Yu C, Paine MM, Whisenand TD, Zvaifler NJ, et al. Synovial interleukin-1 receptor antagonist and interleukin-1 balance in rheumatoid arthritis. Arthritis Rheum 1994;37:644–52.

42. Carta S, Tassi S, Delfino L, Omenetti A, Raffa S, Torrisi MR, et al. Deficient production of IL-1 receptor antagonist and IL-6 coupled to oxidative stress in cryopyrin-associated periodic syndrome monocytes. Ann Rheum Dis 2012;71:1577–81.

43. Mitroulis I, Ruppova K, Wang B, Chen LS, Grzybek M, Grinenko T, et al. Modulation of myelopoiesis progenitors is an integral component of trained immunity. Cell 2018;172:147–61.

44. Moorlag SJ, Röring RJ, Joosten LA, Netea MG. The role of the interleukin-1 family in trained immunity [review]. Immunol Rev 2018;281:28–39.

45. Dos Santos JC, de Figueiredo AM, Silva MV, Cirovic B, de Bree LC, Damen MS, et al. β-glucan-induced trained immunity protects against Leishmania braziliensis infection: a crucial role for IL-32. Cell Rep 2019;28:2659–72.

46. Ben-Zvi I, Kukuy O, Giat E, Pras E, Feld O, Kivity S, et al. Anakinra for colchicine-resistant familial Mediterranean fever: a randomized, double-blind, placebo-controlled trial. Arthritis Rheumatol 2017;69:854–62.

47. Soriano A, Verecchia E, Afeltra A, Landolfi R, Manna R. IL-1β biological treatment of familial Mediterranean fever [review]. Clin Rev Allergy Immunol 2013;45:117–30.

48. Leslie KS, Lachmann HJ, Bruning E, McGrath JA, Bybee A, Gallimore JR, et al. Phenotype, genotype, and sustained response to anakinra in 22 patients with autoinflammatory disease associated with CIAS-1/NALP3 mutations. Arch Dermatol 2006;142:1591–7.

49. Thornton BD, Hoffman HM, Bhat A, Don BR. Successful treatment of renal amyloidosis due to familial cold autoinflammatory syndrome using an interleukin 1 receptor antagonist. Am J Kidney Dis 2007;49:477–81.

50. Nalcacioglu H, Ozkaya O, Genc G, Ayyildiz S, Kefeli M, Elli M, et al. Efficacy of anakinra in a patient with systemic amyloidosis presenting as amyloidoma. Int J Rheum Dis 2018;21:552–9.

51. Tezcan ME. IL-1 blockers together with colchicine may be administered as first line therapy in familial Mediterranean fever with amyloidosis. Med Hypotheses 2019;130:109269.

52. De Cosmo S, Mazzoccoli G. Retinoid X receptors intersect the molecular clockwork in the regulation of liver metabolism [review]. Front Endocrinol (Lausanne) 2017;8:24.

53. Pontis S, Ribeiro A, Sasso O, Piomelli D. Macrophage-derived lipid agonists of PPAR-α as intrinsic controllers of inflammation. Crit Rev Biochem Mol Biol 2016;51:7–14.

AMERICAN COLLEGE
of RHEUMATOLOGY
Empowering Rheumatology Professionals

Prediction of Differential Pharmacologic Response in Chronic Pain Using Functional Neuroimaging Biomarkers and a Support Vector Machine Algorithm: An Exploratory Study

Eric Ichesco,[1] (iD) Scott J. Peltier,[1] Ishtiaq Mawla,[1] (iD) Daniel E. Harper,[1] Lynne Pauer,[2] Steven E. Harte,[1] Daniel J. Clauw,[1] and Richard E. Harris[1]

Objective. There is increasing demand for prediction of chronic pain treatment outcomes using machine-learning models, in order to improve suboptimal pain management. In this exploratory study, we used baseline brain functional connectivity patterns from chronic pain patients with fibromyalgia (FM) to predict whether a patient would respond differentially to either milnacipran or pregabalin, 2 drugs approved by the US Food and Drug Administration for the treatment of FM.

Methods. FM patients participated in 2 separate double-blind, placebo-controlled crossover studies, one evaluating milnacipran (n = 15) and one evaluating pregabalin (n = 13). Functional magnetic resonance imaging during rest was performed before treatment to measure intrinsic functional brain connectivity in several brain regions involved in pain processing. A support vector machine algorithm was used to classify FM patients as responders, defined as those with a ≥20% improvement in clinical pain, to either milnacipran or pregabalin.

Results. Connectivity patterns involving the posterior cingulate cortex (PCC) and dorsolateral prefrontal cortex (DLPFC) individually classified pregabalin responders versus milnacipran responders with 77% accuracy. Performance of this classification improved when both PCC and DLPFC connectivity patterns were combined, resulting in a 92% classification accuracy. These results were not related to confounding factors, including head motion, scanner sequence, or hardware status. Connectivity patterns failed to differentiate drug nonresponders across the 2 studies.

Conclusion. Our findings indicate that brain functional connectivity patterns used in a machine-learning framework differentially predict clinical response to pregabalin and milnacipran in patients with chronic pain. These findings highlight the promise of machine learning in pain prognosis and treatment prediction.

INTRODUCTION

Suboptimal management of chronic pain has contributed to a pain-related health crisis, including the ongoing opioid epidemic in the US. As a result, discovery of biologic markers of pain to supplement self-report measures of clinical pain has been garnering attention, and become a priority for organizations like the National Institutes of Health (e.g., The Helping to

End Addiction Long-term [HEAL] initiative [heal.nih.gov]). Ultimately, such biomarkers will aid diagnosis, forecast longitudinal outcomes, and predict treatment efficacy.

One clinical pain disorder where biomarker development has become imperative is fibromyalgia (FM), a chronic condition characterized by widespread pain, fatigue, hypersensitivity to sensory stimuli (1), and increased prevalence of multiple negative health outcomes. Research in the past 2 decades has shown that augmented pain and sensory processing in the central nervous system is a primary mechanism underlying pain in FM patients (2,3). Multiple brain loci have been identified as being related to FM pain, including subregions of the salience, default mode, and somatosensory networks (3,4). Some regions of the default mode network have been shown to have increased connectivity to the salience and somatosensory networks in FM. This type of connectivity might be a marker for chronic pain intensity in this population (3,4).

Functional magnetic resonance imaging (fMRI) studies have demonstrated that aberrant pain processing in FM can be modulated with US Food and Drug Administration–approved pharmacologic compounds, such as pregabalin, milnacipran, and duloxetine. However, only 30% of FM patients report clinically significant pain improvements with any of these drugs (5–7). Patients who fail to receive immediate analgesic effects may receive other treatments in a "trial and error" approach that is both inefficient and costly. The identification of tools that can predict the effectiveness of specific pharmacologic agents used to treat pain at the individual patient level would be of significant clinical benefit and an important step toward personalized analgesia.

With the advent of sophisticated multivariate data analytic techniques such as machine learning, prediction of analgesic response from neuroimaging data has become a promising avenue for biomarker development (8). Briefly, machine-learning techniques "learn" the underlying data patterns (e.g., neuroimaging voxels) to form a model using labels (e.g., pregabalin responder versus milnacipran responder), which can then be applied to unseen or new data to make predictions. Such models have rarely been used in clinical pain populations to predict treatment efficacy. To the best of our knowledge, this study is the first to assess fMRI-derived biomarkers as predictors of differential analgesic response in chronic pain.

We built machine-learning models, using a support vector machine (SVM), from fMRI data obtained from 2 separate, double-blind, placebo-controlled crossover trials in FM patients, one with pregabalin (9) and another with milnacipran (10). These 2 medications are thought to work differently on pain processing, with pregabalin reducing pain-promoting neural activity (9) and milnacipran increasing pain inhibitory pathways (10). We reasoned that given the central mechanisms of action of the 2 drugs, pretreatment brain connectivity (i.e., communication between brain structures) might be able to differentially predict drug responsiveness.

PATIENTS AND METHODS

Subjects. Fifty women with FM who were previously enrolled in 2 independent double-blind, placebo-controlled crossover studies investigating the effects of pregabalin versus placebo and milnacipran versus placebo (9,10) were eligible for this secondary analysis (Consolidated Standards of Reporting Trials [CONSORT] diagrams are included in Supplementary Figures 1 and 2, available on the *Arthritis & Rheumatology* website at http://onlinelibrary.wiley.com/doi/10.1002/art.41781/abstract). Twenty-seven FM patients were enrolled in the original pregabalin study. A total of 14 patients were excluded (9 were excluded in the original study) (9). Five additional patients were excluded from the present study: 4 for head motion using more stringent translational or rotational thresholds after assessment of brain images (see below for additional details), and 1 for incomplete clinical data. This resulted in 13 patients taking pregabalin being included in the present analysis. Twenty-three female patients with FM were enrolled in the original milnacipran study (8 were excluded as previously reported) (10). Brain images for the remaining 15 patients passed quality inspection and were included in the present analysis.

All study participants gave written informed consent. Study protocols and informed consent documents were approved by the University of Michigan Institutional Review Board and the sponsor of the respective studies: Pfizer for pregabalin and Forest Laboratories for milnacipran. All clinical symptom data from both trials were previously verified for accuracy and the database was locked before analysis. Neuroimaging data were stored, validated, analyzed, and assessed for quality at the University of Michigan independent of Pfizer and Forest Laboratories personnel. Patient demographic characteristics, medications, inclusion/exclusion criteria, and treatment effects have been reported previously (9,10). Patient demographic characteristics and medications are listed in Table 1, while brief descriptions of the inclusion and exclusion criteria are included in the Supplementary Methods, available on the *Arthritis & Rheumatology* website at http://onlinelibrary.wiley.com/doi/10.1002/art.41781/abstract.

Clinical pain and mood measures. For participants enrolled in the pregabalin study, clinical pain was assessed using a 10-cm visual analog scale (VAS) bounded by the anchors "no pain" and "worst pain imaginable." Subjects from the milnacipran study reported their clinical pain with an itemized question from the Brief Pain Inventory (BPI) that ranged from 0–10, where 0 was anchored with the words "no pain" and 10 was anchored with the words "pain as bad as you can imagine" (11). Depression and anxiety were assessed using the Hospital Anxiety and Depression Scale (HADS), a 14-item measure with each item rated on a 4-point severity scale (12). The HADS produces 2 scales, one for anxiety and one for depression. The BPI, VAS, and HADS were administered prior to the baseline neuroimaging session. Differences in clinical pain and mood were measured using

Table 1. Characteristics of the patients with FM, and medications taken, in the pregabalin and milnacipran studies*

Patient	Age, years	Race	BMI	Medications and supplements
Pregabalin study				
1	44	White	25	Augmentin, Motrin
2	29	White	21	Albuterol, erythromycin eye lotion, Extra Strength Tylenol, ibuprofen, Ortho Tri-Cyclen, Zantac, Zyrtec
3	25	White	23	Children's Tylenol Plus Cough and Runny Nose, Motrin
4	43	White	25	Triamcinolone acetonide 0.5%
5	36	White	21	Amoxicillin, Augmentin, Motrin, Synthroid, Tylenol
6	42	White	27	Sudafed, Tylenol, Zyrtec
7	42	White	26	Advil, CVS Sinus Allergy, Effexor, Nyquil, Tylenol
8	39	White	25	Claritin, melatonin, NuvaRing, propionate fluticasone, Tylenol
9	44	White	30	Amoxicillin, Nyquil, prednisone, Proventil, Rocephin, Tylenol
10	59	White	29	Colchicine, Flexeril, hydrochlorothiazide, melatonin, nabumetone, Omacor, Prilosec trazodone
11	19	White	23	Bupropion, Concerta, Loestrin
12	19	White	26	Claritin, Concerta, Loestrin
13	39	White	25	Effexor, Excedrin ES, fluticasone propionate nasal spray, ibuprofen, Maxalt, Proventil HFA, pseudoephedrine, Seasonale, Topamax, zonisamide
Milnacipran study				
1	54	White	33	Tramadol
2	26	White	36	Pregabalin, metformin
3	30	White	31	Metronidazole, Benadryl, Motrin
4	42	White	27	Ibuprofen, Sudafed
5	53	White	33	Dinox, Anacin, Aleve, ibuprofen, prednisone, Mobic, Mucinex, Ventolin, Airborne
6	36	African American	37	Amlodipine besylate, lisinopril/hydrochlorothiazide, Aleve
7	40	White	24	NuvaRing, ibuprofen, Skelaxin, Vicodin, Tylenol, Quasense
8	36	White	21	Synthroid, Tylenol, acetaminophen, Motrin, ibuprofen
9	39	White	21	Nasonex
10	50	White	29	Lisinopril/hydrochlorothiazide, amoxicillin
11	30	White	28	Xanax, Cataphlam, Aleve
12	40	White	23	Motrin
13	53	African American	26	Motrin, Excedrin
14	27	White	32	Levothyroxine, Singulair, albuterol sulfate, Vicodin, cyclobenzaprine, Maxalt, Tylenol, Cortizone shots, cephalexin
15	55	White	35	Avapro, Norvasc, Aldactazide, Detrol LA, pregabalin, Synthroid, Taclonex, Diprolene Gel, aspirin, Tylenol, Motrin, minocycline, methotrexate

* FM = fibromyalgia; BMI = body mass index.

paired-sample *t*-tests (predrug versus postdrug). In both studies, drug responders were defined as those who had a reduction in clinical pain of ≥20% from predrug to postdrug, since this criterion provided a sufficient number of subjects who did respond to either drug for meaningful SVM classification (see below). In both studies, anxiety/depression responders were defined as those who had a decrease in anxiety or depression, and nonresponders were defined as having no change or an increase in anxiety or depression.

Resting-state functional connectivity MRI as predictive of drug response. *Data acquisition.* Functional connectivity MRIs, including a 6-minute resting-state scan and a high-resolution T1 structural scan, were acquired for all participants at baseline. All scans were performed on a 3.0T GE Signa Scanner (LX VH3 release, quadrature birdcage transmit–receive radiofrequency coil, neuro-optimized gradients). Resting-state fMRI data for both studies were acquired using a custom T2*-weighted spiral-in sequence (repetition time [TR] 2,000 msec, echo time [TE] 30 msec, flip angle 90°, matrix size 64 × 64 pixels with 43 slices, and 3.13 × 3.13 × 3 mm voxels; 5 discarded dummy acquisitions). During each resting-state scan (180 volumes), participants were asked to remain awake with eyes open. To reduce head motion, participants' heads were secured in the head coil using foam padding around the sides of the head and a strap across the forehead. A fixation cross was displayed on a presentation screen. Participants were asked to lie still and fixate on the cross throughout the scan. It has been shown that cognitive tasks such as staring at a cross do not typically disrupt resting-state networks (13).

Physiologic data were collected simultaneously with fMRI data because cardiorespiratory fluctuations are known to influence fMRI intrinsic connectivity within several brain networks. Cardiac data were collected for each participant using an infrared pulse oximeter (GE) attached to the right middle finger. Respiratory volume data were acquired using a GE magnetic resonance–compatible chest plethysmograph that was secured around the abdomen. Further, previously mentioned T1 high-resolution images were acquired using a spoiled gradient-echo inversion recovery sequence (for the pregabalin study: TR 10.5 msec, TE 3.4 msec, flip angle 25°, matrix size 256 × 256 pixels with 106 slices, and 0.94 × 0.94 × 1.5 mm voxels; for the milnacipran study: TR 1,400 msec, TE 1.8 msec, flip angle 15°, matrix size 256 × 256 pixels with 124 slices, and 1.02 × 1.02 × 1.2 mm voxels). Inspection of individual T1 MRIs revealed no gross morphologic abnormalities for any participant.

Preprocessing. Data were preprocessed and analyzed using FSL (www.fmrib.ox.ac.uk/fsl) and statistical parametric mapping (SPM) (version 8; Functional Imaging Laboratories) as well as the functional connectivity toolbox Conn (Cognitive and Affective Neuroscience Library, Massachusetts Institute of Technology) (14) and the GIFT toolbar (15). Following collection of functional data, cardiorespiratory artifacts were corrected for using RETROICOR (16). Subsequent preprocessing steps were conducted within SPM and included motion correction (realignment to the first image of the time series), registration of all images to the mean motion-corrected functional image, normalization to the standard SPM Montreal Neurological Institute template (generating 2 × 2 × 2 mm resolution images), and spatial smoothing (convolution with an 8-mm full-width half-maximum Gaussian kernel). Head motion from each participant was assessed by evaluating 3 translations and 3 rotations. Translational thresholds were set to ±2 mm. Rotation thresholds were limited to ±1°. Subjects were excluded from the analysis if head motion exceeded either of the thresholds in 1 of the 6 dimensions.

Seed-to–whole brain functional connectivity maps were generated using the Conn toolbox (14). Within the Conn toolbox, seed regions' time series were extracted; white matter, cerebrospinal fluid, and realignment parameters were entered into the analysis as covariates of no interest. A band-pass filter (frequency window 0.01–0.1 Hz) was applied, thus removing linear drift artifacts and high-frequency noise. First-level analyses were performed correlating seed region time series signal with averaged time series voxel signal throughout the whole brain, thereby creating bivariate Fisher Z-transformation correlation seed region–to-voxel connectivity maps (one map per seed per individual). Machine-learning analyses were implemented using a linear SVM, performed using the libsvm toolbox version 3.18 (17) in MATLAB 7.5b.

Our prior studies (9,10) identified regions with functional connectivity patterns that were related to drug response to pregabalin and milnacipran. We therefore chose these as seed regions to test responders to the 2 drugs in a machine-learning framework for prediction. These seed regions encompass various known ascending and descending pain circuits in the brain. Seed-to–whole brain functional connectivity maps were generated for the following regions (Supplementary Table 1, available on the *Arthritis & Rheumatology* website at http://onlinelibrary.wiley.com/doi/10.1002/art.41781/abstract): the left posterior cingulate cortex (PCC) and left inferior parietal lobule (based on pregabalin study results) (9) and the bilateral periaqueductal gray, subgenual anterior cingulate cortex (ACC), perigenual ACC, dorsal ACC, and bilateral dorsolateral prefrontal cortex (DLPFC) (based on milnacipran study results) (10).

Support vector machine classification. Machine-learning analyses were implemented using a linear SVM, performed using the libsvm toolbox version 3.18 (https://www.csie.ntu.edu.tw/~cjlin/libsvm/) in MATLAB 7.5b. Briefly, linear SVM tries to separate 2 distinct classes (i.e., pregabalin responder versus milnacipran responder) of features (i.e., data from brain voxels) by creating a hyperplane that separates the 2 classes in the most optimal manner. SVM was implemented on brain connectivity maps of pregabalin responders versus milnacipran responders. SVM classification was performed using a linear kernel with parameter C = 1 (no improvement was found using a C parameter line search), and while it is true that a nonlinear kernel may capture higher-order features, we found no advantage to using a radial basis function with this data set.

Leave-one-out cross-validation was used to calculate classification accuracies and predicted values. Accuracies >75% for identifying a drug responder were deemed clinically significant. SVM model weights were averaged across all leave-one-out iterations to investigate the spatial distribution of the classification weights. Significance levels for the model weights were generated by permuting the treatment labels 100 times for each leave-one-out instance, resulting in 1,300 model weight instances for each voxel location for the pregabalin responder versus milnacipran responder analysis, allowing significance to be calculated by the number of times a model weight occurred in the histogram. Significant values ($P < 0.05$) were overlaid on reference anatomy, and the connectivity maps of the most significant areas were plotted to examine their relationship to the multivariate pattern. A chance-level classification outcome was taken to reaffirm that the given predictive model was specific and minimally affected by confounders.

To determine if predrug VAS ratings can predict responders to pregabalin versus responders to milnacipran with high accuracy, we performed a logistic regression analysis. Then, to investigate if there was an additive effect on classification accuracy, we included predrug clinical pain ratings as a vector to the connectivity maps of each patient and performed SVM classification.

Assessment of confounders and investigation of separation accuracy in SVM classification. Subsequent steps were taken to confirm that a classifier did not possess any confounders. First, to confirm the specificity of the pregabalin versus milnacipran

classifier to responders, the model was also tested in the non-responders. Second, since milnacipran is an antidepressant, we also investigated whether the classifier was specific to predicting changes in pain as opposed to changes in anxiety or depression using the HADS questionnaire (12). The model was first tested in pregabalin responders versus milnacipran responders for depression, and was then tested in responders versus nonresponders with regard to anxiety and depression (where a responder was defined as having a decrease in anxiety or depression and a nonresponder was defined as having no change or an increase in anxiety or depression). Third, to investigate whether subject motion influenced the classification, the model was tested in high-motion versus low-motion groups. Finally, to confirm that the classifier was not predicting differences in sequence and hardware status between the pregabalin

and milnacipran studies, an SVM analysis was performed comparing baseline placebo scans for all seeds between the 2 studies. This SVM analysis was performed exactly as was described above for the responder versus responder analysis, except that the input was placebo data for all subjects from both studies (n = 13 for pregabalin and n = 15 for milnacipran).

RESULTS

Subject demographic characteristics, clinical pain, and psychological measures. There was no significant difference in age between patients in the 2 studies (mean ± SD 35.7 ± 11.4 years in the pregabalin study and 40.7 ± 10.2 in the milnacipran study; P = 0.228). Pregabalin responders (n = 6) and milnacipran responders (n = 7) reported less pain after

Table 2. Clinical pain, anxiety, and depression in all FM patients and responders/nonresponders to pregabalin or milnacipran based on pain improvement*

	Pretreatment	Posttreatment	P
Clinical pain, 0–10-cm VAS			
Pregabalin study			
Responders	5.4 ± 2.5	1.6 ± 2.3	0.0003
Nonresponders	1.3 ± 1.0	1.7 ± 2.3	0.60
All patients	3.2 ± 2.7	1.7 ± 1.9	0.06
Milnacipran study			
Responders	5.6 ± 1.5	2.1 ± 2.0	0.00009
Nonresponders	4.8 ± 2.4	6.0 ± 2.6	0.13
All patients	5.1 ± 2.0	4.2 ± 3.0	0.23
Pretreatment clinical pain, 0–10-cm VAS			0.85
Pregabalin responders	5.4 ± 2.5	–	
Milnacipran responders	5.6 ± 1.5	–	
Anxiety and depression data			
Pregabalin study			
HADS anxiety score			
Responders	9.5 ± 2.3	7.8 ± 4.9	0.31
Nonresponders	2.9 ± 2.9	2.6 ± 3.2	0.17
All patients	5.9 ± 4.3	5.0 ± 4.7	0.40
HADS depression score			
Responders	6.5 ± 3.3	4.0 ± 3.8	0.22
Nonresponders	1.7 ± 2.2	2.3 ± 2.4	0.46
All patients	3.9 ± 3.6	3.1 ± 3.1	0.40
Milnacipran study			
HADS anxiety score			
Responders	7.0 ± 3.5	3.9 ± 3.1	0.01
Nonresponders	6.1 ± 2.5	5.6 ± 3.3	0.53
All patients	6.5 ± 2.9	4.8 ± 3.3	0.02
HADS depression score			
Responders	4.9 ± 3.0	3.1 ± 2.9	0.03
Nonresponders	4.1 ± 2.5	4.5 ± 2.1	0.53
All patients	4.5 ± 2.7	3.9 ± 2.5	0.24
Pretreatment HADS anxiety score			0.16
Pregabalin responders	9.5 ± 2.3	–	
Milnacipran responders	7.0 ± 3.5	–	
Pretreatment HADS depression score			0.37
Pregabalin responders	6.5 ± 3.3	–	
Milnacipran responders	4.9 ± 3.0	–	

* Responders were defined as having a ≥20% reduction in clinical pain (on a visual analog scale [VAS]) following treatment. The pregabalin sample included 13 patients (46% were responders [n = 6]; 54% were nonresponders [n = 7]). The milnacipran sample included 15 patients (47% were responders [n = 7]; 53% were nonresponders [n = 8]). Values are the mean ± SD. FM = fibromyalgia; HADS = Hospital Anxiety and Depression Scale.

receiving the drug compared to nonresponders. Full results for clinical pain effects in responders, nonresponders, and all patients are shown in Table 2. Results for anxiety and depression in these groups (responders and nonresponders determined by clinical pain improvement) are included in Table 2. We focused our analyses on the ability of pretreatment functional connectivity MRI to predict differential analgesic responsiveness.

Differential classification of response to pregabalin versus milnacipran. We were unable to predict differential response to pregabalin versus milnacipran using predrug clinical pain ratings (62% accuracy; $\beta = -0.065$, $P = 0.782$). Whole-brain connectivity patterns to the left PCC seed differentiated pregabalin responders from milnacipran responders with 77% accuracy (Figure 1A). Significant average model weights
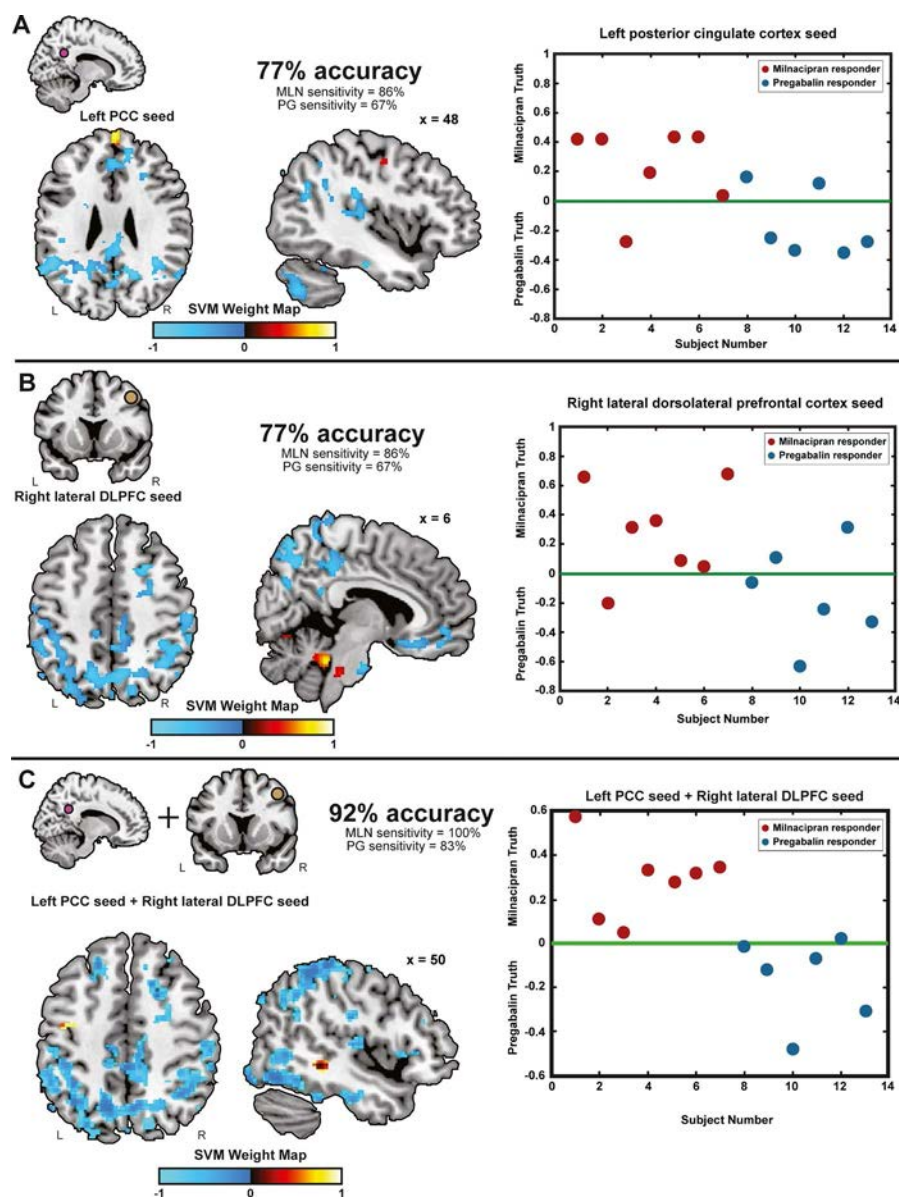
Figure 1. Baseline resting-state functional connectivity between the seed region (posterior cingulate cortex [PCC] or right lateral dorsolateral prefrontal cortex [DLPFC]) and whole brain differentiates patients with fibromyalgia (FM) who respond to pregabalin (PG) from patients with FM who respond to milnacipran (MLN) with high accuracy. **A**, Resting-state functional connectivity between the left PCC seed and regions including the precuneus, inferior parietal lobule, PCC, and left insular cortex classifies pregabalin responders versus milnacipran responders with 77% accuracy. **B**, Resting-state functional connectivity between the right lateral DLPFC seed and regions including the superior parietal lobule, precuneus, primary somatosensory cortex, and left insular cortex classifies pregabalin responders versus milnacipran responders with 77% accuracy. **C**, Baseline resting-state functional connectivity between the left PCC and the right lateral DLPFC seeds combined and the superior parietal lobule, precuneus, perigenual anterior cingulate cortex, mid cingulate cortex, and PCC classifies pregabalin responders versus milnacipran responders with 92% accuracy. Warm colors (red to yellow) designate positive support vector machine (SVM) weights where milnacipran responders have greater connectivity compared to pregabalin responders; cool colors (dark blue to light blue) designate negative SVM weights where pregabalin responders have more connectivity compared to milnacipran responders. Graphs show prediction values for each subject.

contributing to successful classification included greater connectivity for pregabalin responders versus milnacipran responders to regions such as the left inferior parietal lobule, left precuneus, left and right PCC, right perigenual ACC, and right primary motor/somatosensory cortex. In addition, significant average model weights where connectivity to the left PCC was found to be greater for milnacipran responders as compared to pregabalin responders included the left primary visual cortex, bilateral superior medial frontal gyrus, bilateral superior parietal lobule, and the right superior temporal gyrus (Figure 1A and Table 3).

Whole-brain connectivity patterns of the right lateral DLPFC differentiated pregabalin responders from milnacipran responders with 77% accuracy (Figure 1B). Significant average model weights contributing to successful classification included greater connectivity for pregabalin responders versus milnacipran responders to regions including the left precuneus, bilateral superior and inferior parietal lobules, left middle frontal gyrus, right superior frontal gyrus, and the left posterior insular cortex (Table 3). Additionally, significant average model weights where connectivity of the DLPFC was found to be greater in the milnacipran responders as compared to the pregabalin responders included the right anterior cerebellum, right superior frontal gyrus, right middle temporal gyrus, and the right superior temporal gyrus. Many of these connected regions are found to be involved in the frontoparietal, dorsal attention, and sensorimotor networks. The remaining seed regions included in this study did not yield high predictive accuracy. When pretreatment clinical pain ratings were included as an additional feature, the combination model did not improve the predictive power beyond using the whole-brain connectivity maps alone (for left PCC, 77% accuracy; for right lateral DLPFC, 77% accuracy).

In order to enhance classification performance of the aforementioned models, a combinatorial SVM model was produced using connectivity maps from both the left PCC and the right lateral DLPFC. This combinatorial classification model was able to synergistically differentiate responders to pregabalin from responders to milnacipran with 92% accuracy (Figure 1C). Significant average model weights contributing to this result included the combination of those brain regions previously described individually—regions within the default mode network such as the precuneus, PCC, and inferior parietal lobule, the mid cingulate cortex, the posterior insular cortex, the perigenual ACC, and multiple regions within the cerebellum (Figure 1). Complete results are found in Table 3. As with our PCC and DLPFC models alone, the addition of the pretreatment clinical pain ratings did not improve the predictive power of the combined SVM model including the left PCC and right lateral DLPFC, yielding 92% accuracy.

Assessment of confounders and investigation of separation accuracy in SVM classification. To confirm that these significant average model weights of connectivity were specific to responders and not nonresponders for these compounds,

the average model weights from these analyses were then applied to the nonresponders from both the pregabalin study (n = 7) and the milnacipran study (n = 8). There were below-chance classification accuracies of 47% for the PCC connectivity maps and 40% for the DLPFC, with the remaining seeds resulting in classification accuracies found to be less than the relevant clinical threshold set for this study (range 13–73%).

We also confirmed that classification weights were specific to pain and not related to changes in anxiety and depression following treatment. In this pregabalin responder versus milnacipran responder analysis, the PCC and DLPFC maps did not yield significant classification for anxiety (left PCC, 15%; right lateral DLPFC, 54%) or depression (left PCC, 54%; right lateral DLPFC, 54%). In an exploratory analysis, responder and nonresponder labels were created for anxiety and depression scores for both the pregabalin and milnacipran groups. The only significant classification in the milnacipran group was for perigenual ACC connectivity, which classified responders versus nonresponders in terms of depression scores, with 73% accuracy (Supplementary Figure 3 and Supplementary Table 2, available on the *Arthritis & Rheumatology* website at http://onlinelibrary.wiley.com/doi/10.1002/art.41781/abstract).

Furthermore, we confirmed that head motion during acquisition of fMRI images did not confound classification performance. For each subject, a composite motion value was created from the average of all time points along the 6 dimensions (3 rotation and 3 translation). This was used to split subjects into high-motion or low-motion groups. The goal was to see if the prediction model obtained from pregabalin responders versus milnacipran responders was able to predict high-motion and low-motion labels. All comparisons yielded below-chance classification, with accuracy ranging from 8% to 31%, demonstrating that the drug classification models obtained from brain images were not confounded by head motion.

We wanted to be sure our classifier was not predicting differences in sequences or MRI hardware between the pregabalin and milnacipran studies despite both studies using the same scan sequences and MRI scanner. When adding baseline placebo scans from both studies, we were unable to differentiate between functional connectivity MRI data from the milnacipran study (n = 15) and the pregabalin study (n = 13) with high accuracy for any seed included in this study (accuracy values ranged from 25% to 64%).

DISCUSSION

FM is a complex condition that is difficult to treat, with pharmacologic interventions providing significant pain relief in only a minority of cases. There has been a recent surge of interest in utilizing candidate pain biomarkers in a predictive, machine-learning framework to improve the management of FM and related chronic pain conditions (18). Here, we utilized machine learning on

Table 3. Significant multivariate SVM prediction of response to pregabalin versus response to milnacipran according to baseline resting-state connectivity between brain regions in patients with FM*

Seed region, regions with significant connectivity weights	Accuracy, %	Size, mm³	Coordinates		
			x	y	z
Left PCC seed region	77				
Left inferior parietal lobule: BA 40 (−)	−	19,488	−52	−50	44
Left precuneus (−)	−	−	−6	−68	38
Left ventral PCC (−)	−	−	−6	−46	14
Right medial frontal gyrus (−)	−	18,984	6	60	0
Right perigenual ACC (−)	−	−	8	44	−2
Right inferior parietal lobule (−)	−	4,800	46	−50	44
Right medial frontal gyrus/superior frontal gyrus (−)	−	3,296	16	32	42
Right primary motor/primary somatosensory cortex (−)	−	2,744	38	−30	62
Left posterior cerebellum: Crus 1, Crus 2 (−)	−	2,728	−40	−66	−42
Left posterior insular cortex/superior temporal gyrus (−)	−	1,512	−40	−26	14
Right posterior insular cortex (−)	−	744	50	−10	8
Left superior frontal gyrus (−)	−	736	−20	32	46
Right/left superior medial frontal gyrus (+)	−	680	2	60	30
Right superior parietal lobule (+)	−	640	26	−60	60
Right superior temporal gyrus (+)	−	448	56	8	−8
Left superior parietal lobule (+)	−	360	−32	−66	60
Right putamen (−)	−	328	26	16	−2
Right midbrain/pons (−)	−	328	4	−24	−20
Right lateral DLPFC seed region	77				
Right superior parietal lobule (−)	−	36,656	14	−80	54
Right inferior parietal lobule (−)	−	−	46	−46	54
Left precuneus (−)	−	−	−4	−66	44
Left superior parietal lobule (−)	−	−	−16	−70	56
Left inferior parietal lobule (−)	−	−	−40	−62	54
Left primary somatosensory cortex (−)	−	−	−50	−18	58
Left middle frontal gyrus (−)	−	8,184	−24	34	−18
Left inferior frontal gyrus (−)	−	−	−32	30	−12
Right superior frontal gyrus (−)	−	−	34	44	−16
Right pons (−)	−	1,800	20	−14	34
Right parahippocampal gyrus (−)	−	−	22	−4	−28
Left pons (+)	−	1,592	0	−34	−32
Right anterior cerebellum (+)	−	−	10	−48	−28
Left precentral gyrus (−)	−	1,000	−50	−2	26
Right superior frontal gyrus (+)	−	720	16	24	64
Left inferior occipital gyrus (+)	−	544	−44	−78	−6
Right middle temporal gyrus (+)	−	464	52	−6	−22
Right superior temporal gyrus (+)	−	456	42	−50	16
Right posterior cerebellum (+)	−	440	−46	−50	−46
Left posterior insular cortex (−)	−	360	−34	−28	14
Left PCC and right lateral DLPFC seed regions combined	92				
Right superior parietal lobule (−)	−	36,928	34	−50	62
Right primary somatosensory cortex (−)	−	−	58	−18	48
Right inferior parietal lobule: BA 40 (−)	−	−	44	−40	46
Left precuneus (−)	−	−	−8	−64	44
Right precuneus (−)	−	−	6	−62	42
Left inferior parietal lobule: BA 40 (−)	−	−	−40	−50	46
Right perigenual ACC (−)	−	19,408	4	36	−4
Right medial frontal gyrus (−)	−	−	4	58	−6
Left inferior parietal lobule: BA 40 (−)	−	18,800	−48	−50	44
Left precuneus (−)	−	−	−10	−62	42
Left ventral PCC (-)	−	−	−2	−46	20
Left mid cingulate cortex (−)	−	−	−2	−34	46
Left inferior orbital frontal gyrus (−)	−	9,672	−26	30	−10
Right mid orbital frontal gyrus (−)	−	−	18	48	−22
Left precuneus (−)	−	5,072	−6	−42	70
Right mid cingulate (−)	−	−	6	−28	44
Right primary somatosensory cortex (−)	−	2,160	50	−28	62

(Continued)

Table 3. (*Cont'd*)

Seed region, regions with significant connectivity weights	Accuracy, %	Size, mm³	Coordinates		
			x	y	z
Right anterior cerebellum (+)	–	1,376	10	−48	−24
Right pons (+)	–	–	8	−30	−36
Right supplementary motor area (−)	–	1,176	36	0	58
Left cuneus (+)	–	1,136	−14	−78	8
Left superior frontal gyrus (−)	–	880	−16	28	52
Right supplementary motor area (+)	–	880	14	24	64
Left posterior cerebellum (+)	–	760	−6	−78	−34
Left inferior occipital gyrus (+)	–	696	−48	−82	−4
Left posterior cerebellum (+)	–	496	−42	−52	−50
Right mid temporal gyrus (+)	–	488	50	−4	−20
Left superior parietal lobule (+)	–	472	22	−56	62
Left mid cingulate cortex (−)	–	464	−10	−24	54
Left premotor cortex (+)	–	448	−34	−8	54
Right posterior insular cortex (−)	–	416	44	−10	10
Right posterior cerebellum (+)	–	360	6	−68	−46
Right superior temporal gyrus (+)	–	352	60	10	−8
Right superior frontal gyrus (+)	–	336	14	24	62

* Support vector machine (SVM) accuracy values indicate the frequency with which the model correctly identifies pregabalin responders and milnacipran responders. Group labels were chosen based on median splits (for both drugs, responders had a ≥20 point reduction in pain following treatment), and patients deemed to be responders to each respective drug were entered into this analysis. Results are significant at $P < 0.05$, derived from permutation testing (1,300 iterations), and are reported for clusters >320 mm³. (+) denotes greater functional connectivity for milnacipran responders compared to pregabalin responders. (−) denotes greater functional connectivity for pregabalin responders compared to milnacipran responders. FM = fibromyalgia; PCC = posterior cingulate cortex; BA 40 = Brodmann area 40; ACC = anterior cingulate cortex; DLPFC = dorsolateral prefrontal cortex.

resting-state fMRI data collected from 2 cohorts of FM patients who underwent longitudinal therapy with pregabalin or milnacipran. The 2 drugs have differential neurochemical properties and mechanisms of action in the central nervous system. Pregabalin is thought to act through inhibition of calcium-dependent release of excitatory neurotransmitters, whereas milnacipran likely works through increasing norepinephrine and serotonin signaling in descending inhibitory pathways (9,10). Therefore, we sought to understand if functional connectivity between brain regions implicated in pain processing and modulation may be a candidate biomarker that predicts differential response to pregabalin and milnacipran in patients with FM.

Machine-learning models showed that baseline patterns of brain connectivity distinguished responders to pregabalin from responders to milnacipran, significantly above the level of chance. To further distinguish that these markers were specific to pain only, we confirmed that improvements in anxiety (left PCC, 15%; right lateral DLPFC, 54%) and depression (left PCC, 54%; right lateral DLPFC, 54%) were not identified by our classifiers. Moreover, motion, scanner, and sequence parameters did not seem to contribute to our results. Finally, our approach did not classify nonresponsiveness to the 2 drugs, suggesting that our markers predict differential analgesic response.

Our results highlight classification differences between milnacipran and pregabalin. We assessed brain connectivity patterns of the PCC, a key node of the default mode network,

and found that within–default mode network connectivity patterns were higher in pregabalin responders than in milnacipran responders. Interestingly, our PCC seed region was placed in a dorsal subregion of the PCC which has been found to be associated with pain widespreadness in FM (19), while the resultant connected ventral subregion of the PCC has been shown to be associated with pain catastrophizing in patients with FM (20). This suggests that our classifier identified multiple default mode network regions that influence chronic pain. Further, we explored connectivity of the DLPFC, an antinociceptive node that has shown modifications in connectivity with treatment in previous studies of chronic pain (21). Here we observed that greater connectivity of the DLPFC with subregions of networks including frontoparietal, dorsal attention, and sensorimotor networks differentially predict pregabalin versus milnacipran responders.

Recent machine-learning neuroimaging studies in chronic pain have shown that combining data across different tasks (22) or modalities (23) can bolster classification and prediction accuracy. We combined whole-brain–seed connectivity maps of the PCC and the DLPFC and found increased classification performance (92%) in distinguishing pregabalin versus milnacipran outcomes, which was substantially higher than the individual performance of either seed in isolation (77%). These results underscore the fact that these 2 drugs may act on different brain regions and combining results from different networks can capture unique aspects of pain pathology and bolster classification performance.

In recent years there has been a push toward personalized or precision medicine for numerous medical conditions ranging from cancer to depression (24). Given that most of these conditions are etiologically complex, there are likely multiple pathologies across individuals who share a common diagnosis. The situation is similar for chronic pain. There may be multiple pain-processing pathways wherein plasticity may promote chronic pain that outlasts peripheral nociceptive drive. Therefore, the effectiveness of an analgesic, with a specific set of molecular targets, may be more or less suited to any individual person based on their specific pathology. While the concept of personalized or precision analgesia has been discussed for over 2 decades (25), it still remains largely unrealized for chronic pain.

There are several limitations to this study. The sample size used in this study is small due to the design of our 2 previous studies, and we were unable to include an independent replication cohort. Machine-learning studies typically need larger sample sizes to be robust. Therefore, in future studies, training the model on larger sample sizes with out-of-sample validation is needed to determine if these results are reproducible. Furthermore, to optimize our SVM analyses, we used an unorthodox cutoff to identify our pregabalin and milnacipran responder groups (20% reduction in clinical pain). Studies with larger samples may be able to use a more traditional cutoff point of 30% improvement in pain to identify drug responders. Other machine-learning techniques could have been chosen, but one of our main motivations to use SVM for this study was that it is designed to deal with small sample sizes and high-dimensional data (26). While we were able to achieve high accuracy with leave-one-out cross-validation, we also attempted a k-fold cross-validation analysis where we used a 5-fold cross-validation. This approach yielded the same accuracy values (77% each for the DLPFC and PCC independently, and 92% for the combination of the DLPFC and PCC maps), suggesting that our findings are consistent across multiple methods. Finally, only women were enrolled in this study, and other factors such as age, race, and concurrent medications were not included as part of the SVM.

While our study has limitations, we see this work as a first step toward building robust, generalizable, and predictive markers of pharmacologic response in chronic pain. Machine learning combined with functional connectivity MRI is not yet ready for clinical application. There have been studies that have taken steps to close this gap (27), but it is yet to be confirmed as a viable tool in a clinical setting. To this end, ongoing work will investigate using whole-brain correlation matrices, feature selection techniques, and nonlinear kernels as additional approaches to analgesic prediction.

In summary, our results demonstrate that brain connectivity at baseline, prior to commencing therapy, may be leveraged to differentially predict responders *between* analgesics. The predictive ability may be due to the mechanism of action of these pharmacologic agents on the endogenous pain circuits in the central nervous system. Larger, multisite, and systematic trials with multimodal biomarkers are needed in the future to validate these findings and utilize them in a precision medicine framework.

REFERENCES

1. Clauw DJ. Fibromyalgia: a clinical review. JAMA 2014;311:1547–55.
2. Gracely RH, Petzke F, Wolf JM, Clauw DJ. Functional magnetic resonance imaging evidence of augmented pain processing in fibromyalgia. Arthritis Rheum 2002;46:1333–43.
3. Napadow V, LaCount L, Park K, As-Sanie S, Clauw DJ, Harris RE. Intrinsic brain connectivity in fibromyalgia is associated with chronic pain intensity. Arthritis Rheum 2010;62:2545–55.
4. Kutch JJ, Ichesco E, Hampson JP, Labus JS, Farmer MA, Martucci KT, et al. Brain signature and functional impact of centralized pain: a multidisciplinary approach to the study of chronic pelvic pain (MAPP) network study. Pain 2017;158:1979–91.
5. Derry S, Cording M, Wiffen PJ, Law S, Phillips T, Moore RA. Pregabalin for pain in fibromyalgia in adults. Cochrane Database Syst Rev 2016;9:CD011790.
6. Derry S, Gill D, Phillips T, Moore RA. Milnacipran for neuropathic pain and fibromyalgia in adults. Cochrane Database Syst Rev 2012:CD008244.
7. Arnold LM, Clauw DJ, Wohlreich MM, Wang F, Ahl J, Gaynor PJ, et al. Efficacy of duloxetine in patients with fibromyalgia: pooled analysis of 4 placebo-controlled clinical trials. Prim Care Companion J Clin Psychiatry 2009;11:237–44.
8. Tracey I, Woolf CJ, Andrews NA. Composite pain biomarker signatures for objective assessment and effective treatment. Neuron 2019;101:783–800.
9. Harris RE, Napadow V, Huggins JP, Pauer L, Kim J, Hampson J, et al. Pregabalin rectifies aberrant brain chemistry, connectivity, and functional response in chronic pain patients. Anesthesiology 2013;119:1453–64.
10. Schmidt-Wilcke T, Ichesco E, Hampson JP, Kairys A, Peltier S, Harte S, et al. Resting state connectivity correlates with drug and placebo response in fibromyalgia patients. Neuroimage Clin 2014;6:252–61.
11. Cleeland CS, Ryan KM. Pain assessment: global use of the Brief Pain Inventory [review]. Ann Acad Med Singap 1994;23:129–38.
12. Bjelland I, Dahl AA, Haug TT, Neckelmann D. The validity of the Hospital Anxiety and Depression Scale: an updated literature review. J Psychosom Res 2002;52:69–77.
13. Greicius MD, Krasnow B, Reiss AL, Menon V. Functional connectivity in the resting brain: a network analysis of the default mode hypothesis. Proc Natl Acad Sci U S A 2003;100:253–8.
14. Whitfield-Gabrieli S, Nieto-Castanon A. Conn: a functional connectivity toolbox for correlated and anticorrelated brain networks. Brain Connect 2012;2:125–41.

15. Calhoun VD, Adali T, Pekar JJ. A method for comparing group fMRI data using independent component analysis: application to visual, motor and visuomotor tasks. Magn Reson Imaging 2004;22:1181–91.

16. Hu X, Le TH, Parrish T, Erhard P. Retrospective estimation and correction of physiological fluctuation in functional MRI. Magn Reson Med 1995;34:201–12.

17. Chang CC, Lin CJ. LIVSVM: a library for support vector machines. ACM Trans Intell Syst Technol 2011;2:27.

18. Van der Miesen MM, Lindquist MA, Wager TD. Neuroimaging-based biomarkers for pain: state of the field and current directions [review]. Pain Rep 2019;4:e751.

19. Ellingsen DM, Beissner F, Alsady TM, Lazaridou A, Paschali M, Berry M, et al. A picture is worth a thousand words: linking fibromyalgia pain widespreadness from digital pain drawings with pain catastrophizing and brain cross-network connectivity. Pain 2020;162:1352–63.

20. Lee J, Protsenko E, Lazaridou A, Franceschelli O, Ellingsen DM, Mawla I, et al. Encoding of self-referential pain catastrophizing in the posterior cingulate cortex in fibromyalgia. Arthritis Rheumatol 2018;70:1308–18.

21. Čeko M, Shir Y, Ouellet JA, Ware MA, Stone LS, Seminowicz DA. Partial recovery of abnormal insula and dorsolateral prefrontal connectivity to cognitive networks in chronic low back pain after treatment. Hum Brain Mapp 2015;36:2075–92.

22. López-Solà M, Pujol J, Wager TD, Garcia-Fontanals A, Blanco-Hinojo L, Garcia-Blanco S, et al. Altered functional magnetic resonance imaging responses to nonpainful sensory stimulation in fibromyalgia patients. Arthritis Rheumatol 2014;66:3200–9.

23. Lee J, Mawla I, Kim J, Loggia ML, Ortiz A, Jung C, et al. Machine learning-based prediction of clinical pain using multimodal neuroimaging and autonomic metrics. Pain 2019;160:550–60.

24. National Research Council. Toward precision medicine: building a knowledge network for biomedical research and a new taxonomy of disease. Washington, DC: The National Academic Press; 2011.

25. Woolf CJ, Max MB. Mechanism-based pain diagnosis: issues for analgesic drug development. Anesthesiology 2001;95:241–9.

26. LaConte S, Strother S, Cherkassky V, Anderson J, Hu X. Support vector machines for temporal classification of block design fMRI data. Neuroimage 2005;26:317–29.

27. Wager TD, Atlas LY, Lindquist MA, Roy M, Woo CW, Kross E. An fMRI-based neurologic signature of physical pain. N Engl J Med 2013;368:1388–97.

AMERICAN COLLEGE
of RHEUMATOLOGY
Empowering Rheumatology Professionals

Industry Payments to Practicing US Rheumatologists, 2014–2019

Michael S. Putman,[1] (iD) Jay E. Goldsher,[1] Cynthia S. Crowson,[2] (iD) and Alí Duarte-García[2] (iD)

Objective. Payments from the pharmaceutical industry to practicing physicians may influence prescribing behavior. This study was undertaken to investigate the nature, quantity, and geographic distribution of payments to US rheumatologists.

Methods. General payments from industry sponsors to US rheumatologists from 2014 to 2019 were extracted from the Centers for Medicare and Medicaid Services Open Payments database. Gender was identified by linking physicians to the National Plan and Provider Enumeration System registry. Data were reported in aggregate, trends over time were assessed using linear regression models, and differences by gender were analyzed using the Wilcoxon rank sum test.

Results. Over the 6-year time period from 2014 to 2019, a total of 1,610,668 payments totaling $221,254,966 were made to 5,723 rheumatologists. The median payment was $15 (interquartile range [IQR] $10 to $22), and the median total amount received by individual rheumatologists over the 6-year period was $2,818 (IQR $464 to $11,560). The majority of rheumatologists (3,416 of 5,723 [60%]) received less than $5,000, but 368 of 5,723 (6%) received more than $100,000 each and accounted for 78% of the total. The yearly value of payments increased over time ($3,703,264 per year; $P < 0.001$), and the median payment to male rheumatologists was significantly higher than the median payment to female rheumatologists ($3,723 [IQR $542 to $15,841] versus $2,084 [IQR $394 to $8,186]; $P < 0.001$).

Conclusion. The value of industry payments has increased over time, and a large amount is concentrated among a small number of rheumatologists. Future studies should investigate the degree to which industry payments have influenced prescribing in the field of rheumatology.

INTRODUCTION

Conflicts of interest have been identified by rheumatologists as an important ethical concern (1–3), but the nature, geographic distribution, and quantity of industry payments to rheumatologists have yet to be investigated. Such payments have been characterized in multiple other medical subspecialties using the Centers for Medicare and Medicaid Services (CMS) Open Payments Database (4–8). This database was established as part of the 2010 Sunshine Act, which mandated reporting of pharmaceutical industry payments to physicians. Subsequent investigations revealed that roughly half of US physicians have received some form of payment from industry sponsors (9,10), which ranges from small

disbursements for food and travel to large payments for educational activities and consulting. The degree to which industry payments influence practice is difficult to quantify, but they have been associated with higher utilization of medical devices (11) and with prescribing patterns (12–19).

Industry payments to rheumatologists may be of particular interest. Rheumatologists frequently prescribe expensive biologic and targeted disease-modifying antirheumatic drugs (DMARDs), the majority of which remain under patent. Over the past 20 years, the frequency of trials investigating such agents has increased from 1 in 9 rheumatology randomized controlled trials (RCTs) to 4 in 5 rheumatology RCTs (20). Prior studies using CMS Open Payments data have identified associations between

industry payments to rheumatologists and positive trial outcomes in rheumatoid arthritis (21) and the use of hyaluronic acid in osteoarthritis (22). Such associations do not imply causality, however, and should be interpreted with caution. A recent investigation of industry payments to authors of rheumatology clinical practice guidelines (23) revealed that the majority had accepted payments, though most had accepted less than $10,000 in total payments and only 1 in 5 had accepted payments relevant to the clinical practice guidelines. No studies to date have characterized the volume or geographic distribution of payments to rheumatologists. The objective of this study was to describe the nature, quantity, geographic distribution, and secular trends in pharmaceutical industry payments to practicing US rheumatologists from 2014 to 2019.

METHODS

The CMS Open Payments database is a publicly available database of payments from applicable manufacturers and group purchasing organizations to physicians, including fellows and part-time physicians. Internal reviews have found <1% of records to be missing, inaccurate, or inconsistent (24). For this study, data from the CMS Sunshine Act Open Payments database were downloaded from https://openpaymentsdata.cms.gov/ on October 1, 2020. General payments from the years 2014–2019 were included. Payments from 2013 were excluded because of partial reporting; physician ownership and investments as well as research payments were excluded because of a different reporting format. Rheumatologists were identified by specialty ("Allopathic & Osteopathic Physicians/Internal Medicine/Rheumatology") using the Physician Supplement File for All Program Years and matched to payments using physician identification numbers.

The variables assessed included recipient identification number, recipient state, applicable manufacturer, total payment in US dollars, date of payment, nature of payment, and name of associated covered drug or biologic agent. The payment type "compensation for services other than consulting, including serving as faculty or as a speaker at a venue other than a continuing education program" was analyzed as "speakers fees" for clarity in reporting. Payment types that accounted for >4% of the total were analyzed without change (food and beverage, travel and lodging, consulting fee, and honoraria). Payment types that accounted for <4% of the total were aggregated in the category "other" for readability and included the following payment types: grants, education, current or prospective ownership or investment interest, compensation for serving as faculty or as a speaker for an accredited or certified continuing education program, gift, entertainment, royalty or license, and charitable contributions.

Parent companies of pharmaceutical industry sponsors as of November 1, 2020 who made over $100 in payments were identified by hand search of online databases and company websites by one of the authors (JEG). Duplicate and alternative names for the first listed covered drug or biologic agent were identified by one of the authors (MSP) and used for analysis of each product. The top 10 medications were then identified by calculating the sum of all payments for all agents over the entire period of analysis and selecting the top 10 highest grossing products. To identify physician gender, the National Plan and Provider Enumeration System (NPPES) National Provider Identifier registry was downloaded (https://download.cms.gov/nppes/NPI_Files.html) and all providers who listed the healthcare provider taxonomy code for "Rheumatology Physician" (207RR0500X) were extracted. Gender from the NPPES database was matched to physician profile IDs from the CMS Open Payments database using all unique combinations of first name, last name, and state. The number of rheumatologists per state was identified using the 2015 American College of Rheumatology workforce report and analyzed with respect to state and US Census Division (25).

The total amount of spending, number of payments, and rheumatologist payees are reported in aggregate. Payments were described by calculating the median and interquartile range (IQR) for both payments overall and for payments to each physician ID over the 6-year period of analysis. The value and number of payments over time were analyzed using separate linear regression models and reported with respect to yearly payments. The nature of payments and the total payments per company were expressed as totals and percent. Payments by gender were analyzed using the Wilcoxon rank sum test over the entire 6-year period of analysis. The likelihood of receiving more than $100,000 for female versus male rheumatologists was analyzed using odds ratios. Chi-square tests were used to assess the total value and number of each type of payment with respect to high or low earners and female or male rheumatologists. All analyses were performed using R software version 4.04.

RESULTS

A total of $221,254,966 from 1,610,668 payments was received by 5,723 rheumatologists from 2014 to 2019. The median payment was $15 (IQR $10 to $22), with a minimum payment of $0.01 and maximum payment of $1,989,343. The median total amount received by individual rheumatologists from 2014 to 2019 was $2,818 (IQR $464 to $11,560), with a minimum amount of $8 and a maximum amount of $5,612,254. Overall, 1,306,528 payments (81%) were less than $25, and 60,813 payments (4%) were more than $1,000. The majority of rheumatologists (3,416 of 5,723 [60%]) received less than $5,000 during the 6-year period, but 368 of 5,723 (6%) received more than $100,000 each and accrued 78% of the total value of payments (Table 1). These physicians were more likely to receive payments for speaking fees (10% versus 1% for physicians earning less than $100,000), consulting fees (3% versus 1% for physicians earning less than $100,000) or travel and lodging (16% versus 1% for physicians earning less than $100,000), and less likely to receive payments for food

Table 1. Value of industry payments to US rheumatologists from 2014 to 2019, per payment and per rheumatologist

Payment value, dollars	Per payment (n = 1,610,668)		Per rheumatologist (n = 5,723)	
	No. (%) of payments	Cumulative %	No. (%) of rheumatologists	Cumulative %
<25	1,306,528 (81.1)	81.1	190 (3.3)	3.3
25–50	81,221 (5.0)	86.2	167 (2.9)	6.2
50–100	52,379 (3.3)	89.4	229 (4.0)	10.2
100–500	89,158 (5.5)	94.9	904 (15.8)	26.0
500–1,000	20,569 (1.3)	96.2	500 (8.7)	34.8
1,000–5,000	57,501 (3.6)	99.8	1,426 (24.9)	59.7
5,000–10,000	2,772 (0.2)	100.0	724 (12.7)	72.3
10,000–50,000	479 (0.0)	100.0	992 (17.3)	89.7
50,000–100,000	31 (0.0)	100.0	223 (3.9)	93.6
100,000–500,000	28 (0.0)	100.0	265 (4.6)	98.2
500,000–1,000,000	0 (0.0)	100.0	59 (1.0)	99.2
1,000,000–2,000,000	2 (0.0)	100.0	33 (0.6)	99.8
>2,000,000	0 (0.0)	100.0	11 (0.2)	100.0

and beverage (62% versus 96% for physicians earning less than $100,000) ($P < 0.001$) (Supplementary Tables 1 and 2 and Supplementary Figure 1, available on the *Arthritis & Rheumatology* website at http://onlinelibrary.wiley.com/doi/10.1002/art.41896/abstract). The top 1% of rheumatologists received 39% of the total value of payments, and 44 rheumatologists received more than $1,000,000 each over the 6-year period of analysis.

The value of payments per year increased by 56% over the 6-year period, from a value of $29,755,133 in 2014 to $46,308,926 in 2019, which was a significant increase of $3,703,264 per year ($r^2 = 0.96$, $P < 0.001$). The number of payments per year increased by 14%, from 243,918 payments in 2014 to 277,305 payments in 2019, which was a significant increase of 7,632 payments per year ($r^2 = 0.79$, $P = 0.02$). The largest single total expenditure was for speaking fees (47%), followed by consulting fees (23%), food and beverage (13%), travel and lodging (12%), honoraria (5%), and other (1%) (Table 2 and Figure 1A). Speaking fees underwent the greatest absolute growth per year (105%), followed by honoraria (101%) and travel and lodging (35%). As a proportion of the total, speaking fees grew by 32% per year and honoraria grew by 29% per year, while all other payment types decreased in relative terms (Table 2).

The top 3 companies by total spending from 2014 to 2019 accounted for 49% of the total and included Bristol Myers Squibb (20%), AbbVie (17%), and Pfizer (12%) (Figure 1B and Supplementary Table 3, available on the *Arthritis & Rheumatology*

website at http://onlinelibrary.wiley.com/doi/10.1002/art.41896/abstract). The top 10 medications accounted for 51% of the total spending from 2014 to 2019 and included apremilast (Otezla; $20,724,517), adalimumab (Humira; $17,581,683), and tofacitinib (Xeljanz; $13,700,701) (Figure 2A).

Gender matching was successful for 5,407 of the physicians (94%). Female rheumatologists comprised 43% of the total sample and received 34% of the total value of payments. With respect to total payments, male physicians received significantly higher average payments ($52,974 versus $21,349 for female rheumatologists; $P < 0.001$), a significantly higher median payment ($3,723 [IQR $542 to $15,841] versus $2,084 for female rheumatologists [IQR $394 to $8,186]; $P < 0.001$), and were significantly more likely to receive more than $100,000 in total value of payments (odds ratio 3.24 [95% confidence interval 2.47–4.29]). Female rheumatologists were less likely to receive payments for speaking fees (2% versus 4% for male rheumatologists) or travel and lodging (3% versus 6% for male rheumatologists) and more likely to receive food and beverage (92% versus 86% for male rheumatologists) (overall $P < 0.001$) (Supplementary Tables 4 and 5, available on the *Arthritis & Rheumatology* website at http://onlinelibrary.wiley.com/doi/10.1002/art.41896/abstract).

The highest total spending by state occurred in California ($27,769,124) followed by New York ($26,832,342) and Texas ($17,071,556). Per rheumatologist, the highest spending by state occurred in Arizona ($143,559) followed by Alabama ($98,734)

Table 2. Industry payments to US rheumatologist from 2014 to 2019, by type of payment

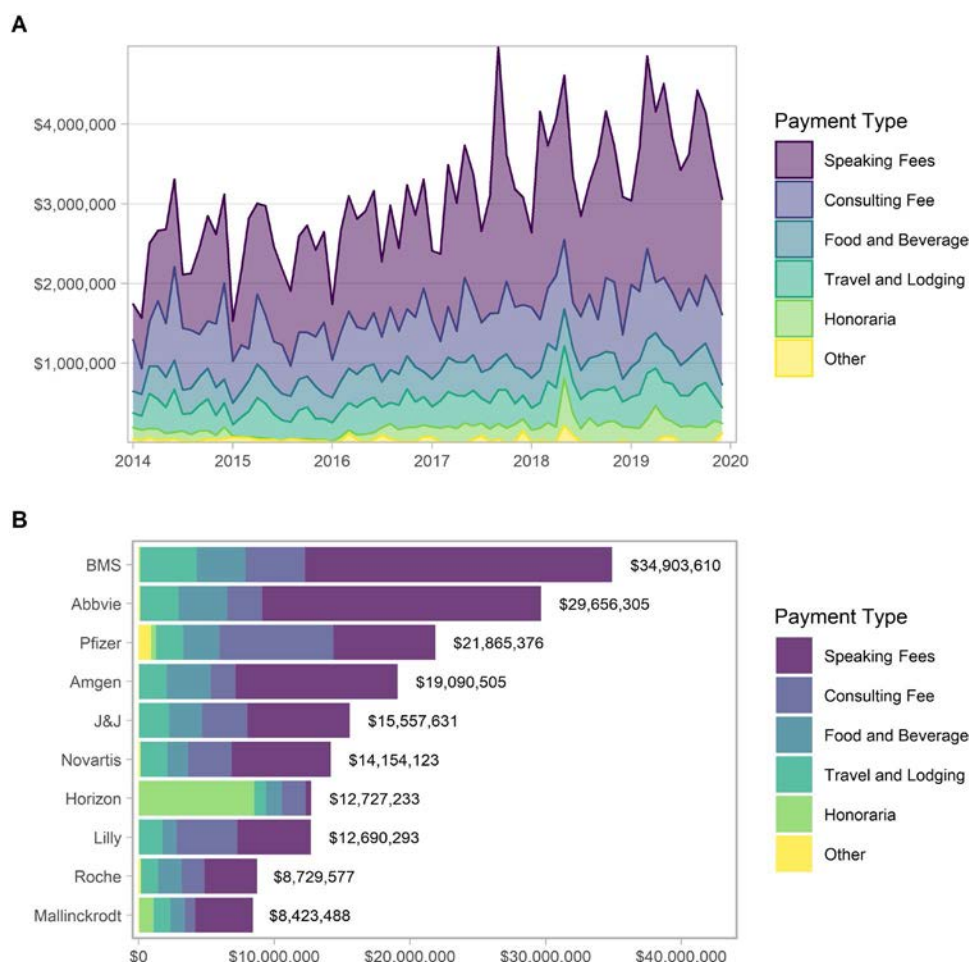| Type of payment	Total value, dollars	Percent of total	Absolute growth, 2014–2019, %	Relative growth, 2014–2019, %
Speaking fees	103,273,996.55	46.7	105.0	31.6
Consulting fees	51,008,312.10	23.1	13.3	−27.2
Food and beverage	27,858,696.48	12.6	24.0	−20.3
Travel and lodging	25,738,528.22	11.6	35.4	−13.0
Honoraria	10,581,087.44	4.8	101.3	29.4
Other	2,794,345.68	1.3	−21.9	−49.8

Figure 1. Total value of monthly industry payments (**A**) and total value of payments per company (**B**) to US rheumatologists from 2014 to 2019, stratified by payment type.

and the District of Columbia ($72,294) (Supplementary Table 6, available on the *Arthritis & Rheumatology* website at http://online library.wiley.com/doi/10.1002/art.41896/abstract). The highest spending by US Census Division occurred in the Middle Atlantic Division ($46,327,351) followed by the South Atlantic Division ($44,047,624), and the Pacific Division ($35,573,508). Per rheumatologist, the highest spending by US Census Division occurred in the East South Central Division ($49,605) followed by the Middle Atlantic Division ($45,197) and the West South Central Division ($40,064) (Figure 2B and Supplementary Table 7, available on the *Arthritis & Rheumatology* website at http://onlinelibrary.wiley.com/doi/10.1002/art.41896/abstract).

DISCUSSION

Six years of data from the CMS Open Payments database revealed more than $220 million of payments from the pharmaceutical industry to practicing rheumatologists. The majority of payments were less than $25, and the majority of rheumatologists received less than $5,000 over the 6-year period of analysis. A small number of physicians received larger payments, resulting in three-quarters of the total value accruing to the top 5% of rheumatologists. Male rheumatologists received more than twice as much on average as female rheumatologists. Almost half of all payments were made by 3 pharmaceutical companies, and almost all payments were associated with biologic DMARDs or targeted synthetic DMARDs. The total value of payments increased over time, which was primarily secondary to increases in speaking fees and honoraria.

These data suggest that industry payments in rheumatology have followed two distinct patterns, which have been observed in other medical subspecialties (8). First, many small payments are made to a large number of rheumatologists. The impact of such payments cannot be discounted, as even small gifts may affect behavior (26) and are associated with prescribing patterns (27). Second, large payments are made to a small number of physicians, including 44 who accrued more than $1,000,000 each from 2014 to 2019. The degree to which such payments influence behavior and their impact on practice should be investigated in future studies, but it is notable that a recent evaluation of rheumatology clinical practice guidelines identified substantial involvement from rheumatologists who had accepted large values of industry payments (23).
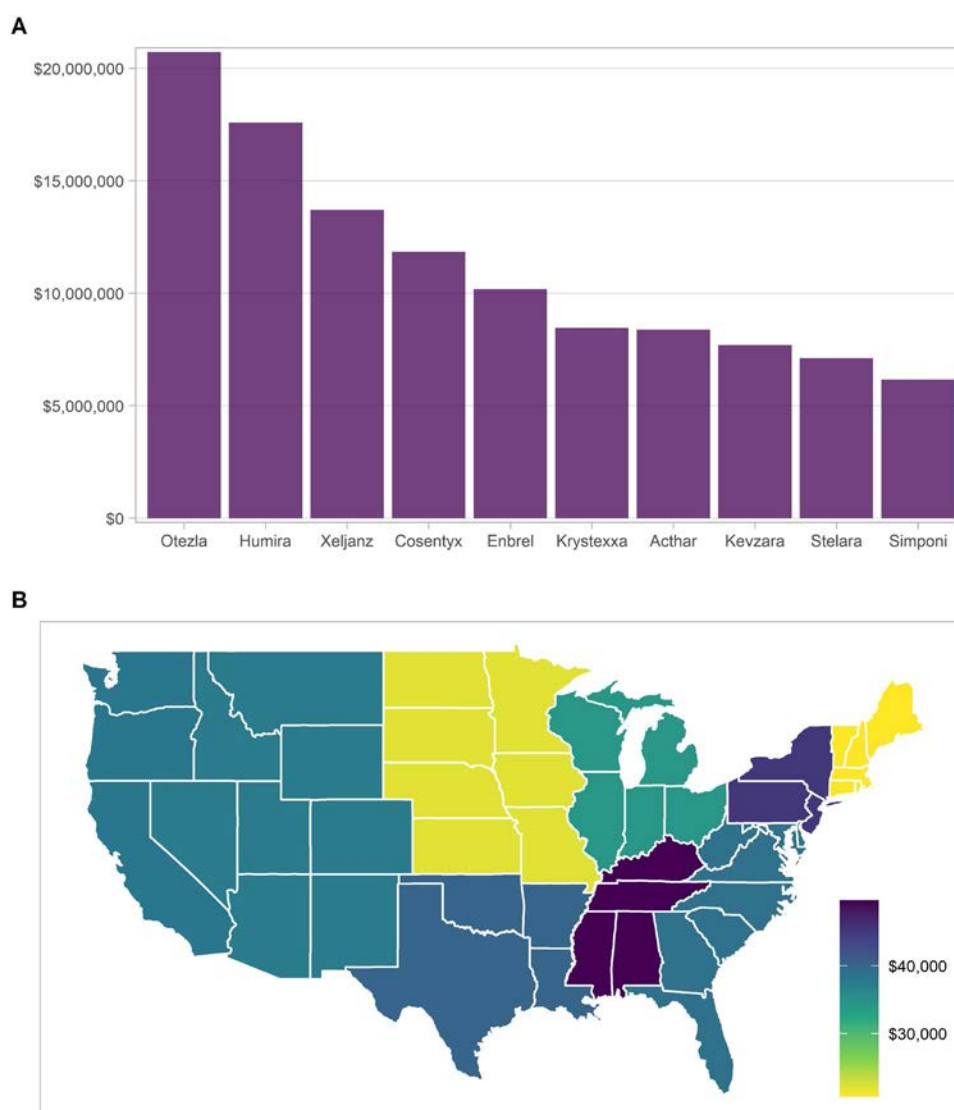
Figure 2. **A**, Total value of industry payments per product to US rheumatologists from 2014 to 2019. Data are shown for the top 10 products: apremilast (Otezla), adalimumab (Humira), tofacitinib (Xeljanz), secukinumab (Cosentyx), etanercept (Enbrel), pegloticase (Krystexxa), repository corticotropin (Acthar), sarilumab (Kevzara), ustekinumab (Stelara), and golimumab (Simponi). **B**, Average value of industry payments per US rheumatologist from 2014 to 2019, stratified by US Census Division. Color figure can be viewed in the online issue, which is available at http://onlinelibrary.wiley.com/doi/10.1002/art.41896/abstract.

Differences were observed in payments with respect to gender and to geographic distribution. The average total payment to male rheumatologists was more than twice the average total payment to female rheumatologists, and male rheumatologists were 3 times more likely to earn more than $100,000. Similar disparities have been observed in other specialties and have previously been attributed to less willingness to accept industry payments, different preferences for or types of involvement with the pharmaceutical industry, or gender bias resulting in fewer speaking engagements or consulting opportunities (9,28–30). Any of these explanations may be supported by this study, as female rheumatologists received fewer payments per rheumatologist as well as a different distribution of payment types. Substantial

heterogeneity in spending per rheumatologist by state and by US Census Division was also observed. Because payments were linked to the practice address of the accepting physician, as opposed to where payments occurred, these differences may reflect the presence of "key opinion leaders" in a particular geographic location. Other possibilities, such as regional differences in practice patterns (31), population density, or the prevalence of academic medical centers may also be considered.

Three companies and 10 products accounted for nearly half of the total value of payments. Eight of the top 10 products were novel biologic or targeted synthetic DMARDs, all of which were still under patent as of this writing. While not unexpected, the degree of concentration in spending is notable. Curiously, repository

corticotropin (H.P. Acthar gel) was one of the top 10 agents with respect to total payments. H.P. Acthar gel was initially approved in 1952 and has no high-quality evidence supporting its use (32). Despite these limitations and the availability of affordable alternatives in adult medicine, such as prednisone, the manufacturer of H.P. Acthar gel provided a large portion of the overall payments to rheumatologists. Notably, >90% of rheumatologists who frequently prescribe H.P. Acthar gel have also received H.P. Acthar–related payments, (16) raising the possibility that such payments have influenced prescribing behavior.

This project has a number of limitations. Only general payments to rheumatologists were included; payments related to research, payments related to ownership, and payments to other clinicians involved in the care of rheumatic disease patients, such as nurse practitioners or physician assistants, were not assessed. The CMS Open Payments database depends upon accurate reporting by manufacturers; external sources were not used to verify payments. Relevant physician characteristics, such as practice type or clinical volume, were not available. The degree to which payments were accepted by clinicians who train future rheumatologists was not assessed; future studies should investigate this influential subset of rheumatologists. Most importantly, this was a descriptive study, and the degree to which payments have influenced physician behavior lies outside the scope of this work.

Limitations notwithstanding, these data suggest that the bulk of payments from the pharmaceutical industry to rheumatologists are concentrated among a small number of rheumatologists and a short list of novel therapeutic agents. Payments have increased over time, primarily due to increases in speaking fees, and have not been evenly distributed with respect to gender or geographic region. Future studies should investigate the degree to which industry payments have influenced prescribing in the field of rheumatology.

AUTHOR CONTRIBUTIONS

All authors were involved in drafting the article or revising it critically for important intellectual content, and all authors approved the final version to be published. Dr. Putman had full access to all of the data in the study and takes responsibility for the integrity of the data and the accuracy of the data analysis.
Study conception and design. Putman, Crowson, Duarte-García.
Acquisition of data. Putman, Goldsher, Crowson, Duarte-García.
Analysis and interpretation of data. Putman, Duarte-García.

REFERENCES

1. MacKenzie CR, Meltzer M, Kitsis EA, Mancuso CA. Ethical challenges in rheumatology: a survey of the American College of Rheumatology membership. Arthritis Rheum 2013;65:2524–32.

2. Sen R, Caplan L. The never-ending conflict (of interest) [editorial]. Arthritis Rheumatol 2020;72:1412–4.

3. Scher JU, Schett G. Key opinion leaders: a critical perspective [review]. Nat Rev Rheumatol 2021;17:119–24.

4. Feng H, Wu P, Leger M. Exploring the industry-dermatologist financial relationship: insight from the Open Payment Data. JAMA Dermatol 2016;152:1307.

5. Tseng AS, Hu TY, Lee JZ, Amin M, Vaidya V, Deshmukh AJ, et al. Trends in reported industry payments to physicians practicing cardiac electrophysiology from 2013 to 2018 in the United States. J Cardiovasc Electrophysiol 2020;31:3106–14.

6. Ahlawat A, Narayanaswami P. Financial relationships between neurologists and industry: the 2015 Open Payments database. Neurology 2019;92:1006–13.

7. Harada Y, Sheng S, Thombre VA, Ounpraseuth S, Tommee CG, Annapureddy AR, et al. A neuromuscular-based analysis of the open payments program. Muscle Nerve 2021;63:96–9.

8. Tarras ES, Marshall DC, Rosenzweig K, Korenstein D, Chimonas S. Trends in industry payments to medical oncologists in the United States since the inception of the Open Payments Program, 2014 to 2019. JAMA Oncol 2021;7:440–4.

9. Tringale KR, Marshall D, Mackey TK, Connor M, Murphy JD, Hattangadi-Gluth JA. Types and distribution of payments from industry to physicians in 2015. JAMA 2017;317:1774–84.

10. Marshall DC, Tarras ES, Rosenzweig K, Korenstein D, Chimonas S. Trends in industry payments to physicians in the United States from 2014 to 2018 [letter]. JAMA 2020;324:1785–8.

11. Annapureddy AR, Henien S, Wang Y, Minges KE, Ross JS, Spatz ES, et al. Association between industry payments to physicians and device selection in ICD implantation. JAMA 2020;324:1755–64.

12. Mitchell AP, Trivedi NU, Gennarelli RL, Chimonas S, Tabatabai SM, Goldberg J, et al. Are financial payments from the pharmaceutical industry associated with physician prescribing? A systematic review. Ann Intern Med 2021;174:353–61.

13. Fleischman W, Agrawal S, King M, Venkatesh AK, Krumholz HM, McKee D, et al. Association between payments from manufacturers of pharmaceuticals to physicians and regional prescribing: cross sectional ecological study. BMJ 2016;354:i4189.

14. Fleischman W, Agrawal S, Gross CP, Ross JS. Association of pharmaceutical manufacturer payments to physicians and prescribing dosage of opioids. J Gen Intern Med 2019;34:1074–6.

15. Brunt CS. Physician characteristics, industry transfers, and pharmaceutical prescribing: empirical evidence from Medicare and the Physician Payment Sunshine Act. Health Serv Res 2019;54:636–49.

16. Hartung DM, Johnston K, Cohen DM, Nguyen T, Deodhar A, Bourdette DN. Industry payments to physician specialists who prescribe repository corticotropin. JAMA Netw Open 2018;1:e180482.

17. Mitchell AP, Winn AN, Lund JL, Dusetzina SB. Evaluating the strength of the association between industry payments and prescribing practices in oncology. Oncologist 2019;24:632–9.

18. Inoue K, Figueroa JF, Orav EJ, Tsugawa Y. Association between industry payments for opioid products and physicians' prescription of opioids: observational study with propensity-score matching. J Epidemiol Community Health 2020;74:647–54.

19. Singh P, Forman H, Adamson AS, Mostaghimi A, Ogdie AR, Oganisian A, et al. Impact of industry payments on prescribing patterns for tumor necrosis factor inhibitors among Medicare beneficiaries. J Gen Intern Med 2019;34:176–8.

20. Putman MS, Ragle AH, Ruderman EM. The quality of randomized controlled trials in high impact rheumatology journals, 1998–2018. J Rheumatol 2020;47:1446–9.

21. Khan NA, Nguyen CL, Khawar T, Spencer H, Torralba KD. Association of author's financial conflict of interest with characteristics and outcome of rheumatoid arthritis randomized controlled trials. Rheumatology (Oxford) 2019;58:776–85.

22. Printz JO, Lee JJ, Knesek M, Urquhart AG. Conflict of interest in the assessment of hyaluronic acid injections for osteoarthritis of the knee: an updated systematic review. J Arthroplasty 2013;28 Suppl:30–3.

23. Wayant C, Walters C, Zaaza Z, Gilstrap C, Combs T, Crow H, et al. Evaluation of financial conflicts of interest among physician-authors of American College of Rheumatology clinical practice guidelines. Arthritis Rheumatol 2020;72:1427–34.

24. US Department of Health and Human Services. Open Payments Data: review of accuracy, precision, and consistency in reporting. August 2018. URL: https://oig.hhs.gov/oei/reports/oei-03-15-00220.asp.

25. Battafarano DF, Ditmyer M, Bolster MB, Fitzgerald JD, Deal C, Bass AR, et al. 2015 American College of Rheumatology workforce study: supply and demand projections of adult rheumatology workforce, 2015–2030. Arthritis Care Res (Hoboken) 2018;70:617–26.

26. Dana J, Loewenstein G. A social science perspective on gifts to physicians from industry [letter]. JAMA 2003;290:252–5.

27. DeJong C, Aguilar T, Tseng CW, Lin GA, Boscardin WJ, Dudley RA. Pharmaceutical industry-sponsored meals and physician prescribing patterns for Medicare beneficiaries. JAMA Intern Med 2016;176:1114–22.

28. Teplitsky S, Perez T, Leong JY, Xie K, Murphy A, Shenot PJ. Industry payments to female pelvic medicine and reconstructive surgeons: an analysis of Sunshine Act open payments from 2014–2017. Int Urogynecol J 2020;31:799–807.

29. Raber I, McCarthy CP, Al Rifai M, Vaduganathan M, Michos ED, Wood MJ, et al. Gender differences in industry payments among cardiologists. Am Heart J 2020;223:123–31.

30. Rose SL, Sanghani RM, Schmidt C, Karafa MT, Kodish E, Chisolm GM. Gender differences in physicians' financial ties to industry: a study of national disclosure data. PLoS One 2015;10:e0129197.

31. Chen C, Petterson S, Phillips R, Bazemore A, Mullan F. Spending patterns in region of residency training and subsequent expenditures for care provided by practicing physicians for Medicare beneficiaries. JAMA 2014;312:2385–93.

32. Duarte-García A, Matteson EL, Shah ND. Older drugs with limited trial evidence: are they worth the expense? The case of repository corticotropin marketed as H.P. Acthar gel. Ann Intern Med 2019;170:791–2.

AMERICAN COLLEGE
of RHEUMATOLOGY
Empowering Rheumatology Professionals

LETTERS

DOI 10.1002/art.41804

Cardiovascular and renal morbidity in Takayasu arteritis: comment on the article by Goel et al

To the Editor:

We read with great interest the article by Dr. Goel and colleagues about cardiovascular disease in Takayasu arteritis (TAK) (1). Goel et al conducted an open retrospective matched cohort study to estimate the risk of comorbidities among patients with TAK. Their study demonstrated that cardiovascular morbidity was increased among TAK patients. The investigators posed excellent study questions and suggested very innovative ideas. However, a few matters need to be addressed.

First, models in this study were adjusted only for sex, age, body mass index, and Townsend Deprivation Score. Though this would be limited by the small sample size, we still suggest adding confounders like hyperlipidemia and steroid use, which could further increase the accuracy of the results of this study.

Second, we noticed that the hazard of developing hypertension and heart failure was not significantly different between patients with TAK and controls. However, hypertension and heart failure are widely known as comorbidities of TAK. We suggest that the authors further explore this finding.

Third, the median age at diagnosis of TAK was 50.19 years. However, there are some studies in Europe in which the median age at diagnosis was <40 years (2–5). This may indicate that the onset of TAK among different European populations does not vary widely. Diagnostic delay would be a more suitable explanation for this difference in age at disease onset.

We appreciate the work done by the authors and are looking forward to their response.

Mr. Liu and Dr. Tsai contributed equally to this work.

Hsuan-Hsien Liu (iD)
School of Medicine, Chung Shan Medical University
Hao-Hung Tsai, MD, MS
*Department of Medical Imaging, Chung Shan
   Medical University Hospital and Institute of
   Medicine, College of Medicine, Chung Shan
   Medical University*
James Cheng-Chung Wei, MD, PhD
*Department of Allergy, Immunology and
   Rheumatology, Chung Shan Medical University
   Hospital*
*Institute of Medicine, College of Medicine, Chung
   Shan Medical University and Graduate Institute
   of Integrated Medicine, China Medical University*
Taichung, Taiwan

1. Goel R, Chandan JS, Thayakaran R, Adderley NJ, Nirantharakumar K, Harper L. Cardiovascular and renal morbidity in Takayasu arteritis: a population-based retrospective cohort study from UK. Arthritis Rheumatol 2021;73:504–11.
2. Arnaud L, Haroche J, Limal N, Toledano D, Gambotti L, Chalumeau NC, et al. Takayasu arteritis in France: a single-center retrospective study of 82 cases comparing white, North African, and black patients. Medicine (Baltimore) 2010;89:1–17.
3. Dreyer L, Faurschou M, Baslund B. A population-based study of Takayasu's arteritis in eastern Denmark. Clin Exp Rheumatol 2011;29 Suppl 64:S40–2.
4. Gudbrandsson B, Molberg Ø, Garen T, Palm Ø. Prevalence, incidence, and disease characteristics of Takayasu arteritis by ethnic background: data from a large, population-based cohort resident in southern Norway. Arthritis Care Res (Hoboken) 2017;69:278–85.
5. Mohammad A, Mandl T. Takayasu's arteritis in southern Sweden. J Rheumatol 2015;42:853–8.

DOI 10.1002/art.41809

Reply

To the Editor:

We thank Dr. Liu and colleagues for their interest in our article. Our responses to their queries are as follows.

Due to the relatively small number of outcomes in our study, we decided that it was best to be conservative in the number of covariates we included in the Cox proportional hazards regression models. We therefore restricted the covariates to age, sex, body mass index (BMI), Townsend Deprivation Score quintile, and smoking status. We provided information on statin use, steroid use, and comorbidities in the exposed and unexposed groups in Table 1.

However, following Liu and colleagues' recommendation, we have now performed an additional analysis for cardiovascular disease outcome (ischemic heart disease, stroke/transient ischemic attack, or heart failure) in which baseline statin use (as a marker of hyperlipidemia) and steroid use were included as covariates in the regression model. We found that the hazard ratio (HR) was very similar to that previously reported; in the original model, the adjusted HR for cardiovascular outcomes in patients with TAK (adjusted for age, sex, BMI, Townsend Deprivation Score, and smoking) was 3.04 (95% confidence interval [95% CI] 1.64–5.63), and in the model adding statin use and steroid use at baseline as covariates, the adjusted HR was 3.18 (95% CI 1.65–6.12).

The effect estimates for the association between TAK and hypertension or heart failure were suggestive of an increased risk of both conditions in patients with TAK; however, these results did not reach statistical significance, perhaps due to the relatively small sample size and small number of outcomes.

We agree that the higher age at diagnosis in TAK patients in the UK compared to other countries may be related to either diagnostic delays or differences in recording of TAK in primary care data. However, our study was not designed to determine this.

Drs. Nirantharakumar and Harper contributed equally to this work.

Ruchika Goel, DM iD
University of Birmingham
 and Queen Elizabeth Hospital Birmingham
Birmingham, UK
 and Christian Medical College
 Vellore, India
Joht Singh Chandan, PhD iD
Rasiah Thayakaran, PhD
Nicola J. Adderley, PhD
Krishnarajah Nirantharakumar, MD
University of Birmingham
Lorraine Harper, PhD iD
University of Birmingham
 and Queen Elizabeth Hospital Birmingham
Birmingham, UK

Noncoding RNAs, osteoarthritis, and the microbiome: new therapeutic targets? Comment on the article by Wei et al

To the Editor:

We read with great interest the article by Dr. Wei and colleagues which sheds light on the association between the gut microbiome and the presence of symptomatic hand osteoarthritis (OA) (1). Their findings will help investigators understand the role of the gut microbiome in the development of symptomatic hand OA (1) and could lead to the gut microbiome becoming the target for emerging therapies (2). There is a need for individualized interventions targeting the pathogenesis of OA (3).

In the setting of OA, microRNAs (miRNAs), circular RNAs, and microbiome dysbiosis seem to be potential target therapies. Genetic, hormonal, and lifestyle factors drive the pathogenesis of OA (4). Epigenetics, which includes recognition of the role of deregulated noncoding RNAs, represents the study of potential links between disease susceptibility and the influence of environmental factors. In OA, miRNAs have a pivotal role in cartilage development and homeostasis, and the host miRNA profile can be modulated by the activity of bacterial organisms through various distinct mechanisms (5). The modulation of specific miRNA may change some cell processes such as proliferation, metabolism, apoptosis, and differentiation and could help manage the disease.

Understanding the mechanisms that regulate the relationships between miRNA and the microbiome may present new perspectives on the treatment and prevention of OA. A new frontier in the treatment of osteoporosis and other bone resorption–related skeletal diseases such as OA (6) could emerge from the development of interventions targeting the microbiota as a strategy to modify expression of noncoding genetic material (7,8). Several disease-related challenges hinder the development of new treatments for OA. To move to individualized interventions aimed at the pathogenesis of OA, it is necessary to broaden the horizons and to implement all possible strategies utilizing novel therapeutic targets in the management of this disease (2).

Maddalena Sirufo, MD
Lia Ginaldi, MD
Massimo De Martinis, MD iD
Department of Life, Health and
Environmental Sciences
University of L'Aquila
L'Aquila, Italy
 and Allergy and Clinical Immunology Unit
 Center for the Diagnosis and Treatment of Osteoporosis
 AUSL04 Teramo
 Teramo, Italy

1. Wei J, Zhang C, Zhang Y, Zhang W, Doherty M, Yang T, et al. Association between gut microbiota and symptomatic hand osteoarthritis: data from the Xiangya Osteoarthritis Study. Arthritis Rheumatol 2021;73:1656–62.
2. Boer CG, Radjabzadeh D, Medina-Gomez C, Garmaeva S, Schiphof D, Arp P, et al. Intestinal microbiome composition and its relation to joint pain and inflammation. Nat Commun 2019;10:4881.
3. Latourte A, Kloppenburg M, Richette P. Emerging pharmaceutical therapies for osteoarthritis [review]. Nat Rev Rheumatol 2020;16:673–88.
4. Biver E, Berenbaum F, Valdes AM, de Carvalho IA, Bindels LB, Brandi ML, et al. Gut microbiota and osteoarthritis management: an expert consensus of the European society for clinical and economic aspects of osteoporosis, osteoarthritis and musculoskeletal diseases (ESCEO) [review]. Ageing Res Rev 2019;55:100946.
5. Layton E, Fairhurst AM, Griffiths-Jones S, Grencis RK, Roberts IS. Regulatory RNAs: a universal language for inter-domain communication [review]. Int J Mol Sci 2020;21:8919.
6. Duan L, Liang Y, Xu X, Wang J, Li X, Sun D, et al. Noncoding RNAs in subchondral bone osteoclast function and their therapeutic potential for osteoarthritis [review]. Arthritis Res Ther 2020;22:279.
7. Sirufo MM, Ginaldi L, De Martinis M. MicroRNAs, bone and microbiota [letter]. Bone 2021;144:115824.
8. De Martinis M, Ginaldi L, Allegra A, Sirufo MM, Pioggia G, Tonacci A, et al. The osteoporosis/microbiota linkage: the role of miRNA [review]. Int J Mol Sci 2020;21:8887.

Reply

To the Editor:

We thank Dr. Sirufo and colleagues for their interest in our article describing the association between gut microbiota and symptomatic hand OA. Hand OA is a common joint disorder. Individuals with hand OA often report pain and functional limitations, including difficulty in undertaking daily activities. To date, few risk factors have been identified for the development of hand OA, and there is no effective treatment that can halt disease progression.

In managing hand OA, the primary goals are to control pain and improve joint function. However, the treatment of pain with pharmacologic agents may result in various side effects. Thus, the development of novel preventive and therapeutic strategies for the treatment of this disease is urgently needed.

We agree with Sirufo and colleagues that our findings will help investigators understand the role of the microbiome in the development of symptomatic hand OA and could reveal new perspectives on the development of novel therapeutic strategies for OA. We believe that future studies assessing the causal associations of key microbial species and related metabolites with OA should further address the underlying mechanisms (i.e., interactions between microRNAs and the microbiome [1,2]) and explore potential targets for intervention, which could provide novel alternatives to current treatment regimens for this common and disabling disease.

Jie Wei, PhD
Xiangya Hospital
Central South University
Changsha, China
Yuqing Zhang, DSc iD
Massachusetts General Hospital
  and Harvard Medical School
Boston, MA
Chao Zeng, MD, PhD
Guanghua Lei, MD, PhD iD
Xiangya Hospital
  Central South University
  and Hunan Key Laboratory of
  Joint Degeneration and Injury
Changsha, China

1. Thomas H. Gut microbiota: host faecal miRNA regulates gut microbiota [review]. Nat Rev Gastroenterol Hepatol 2016;13:122–3.
2. Dong J, Tai JW, Lu LF. miRNA-microbiota interaction in gut homeostasis and colorectal cancer. Trends Cancer 2019;5:666–9.

Outcomes and Western Ontario and McMaster Universities Osteoarthritis Index score reporting in a trial of the efficacy and safety of diclofenac–hyaluronate conjugate: comment on the article by Nishida et al

To the Editor:

Nishida and colleagues conducted a phase III, placebo-controlled repeated knee injection study in patients with symptomatic knee osteoarthritis confirmed on radiography (1). This design allowed for the determination of the true effects of the active ingredient (diclofenac etalhyaluronate) over effects attributable to placebo (contextual features indicating characteristics of the patients, treatment providers, and settings) injection and nonspecific effects (2). My comments on the trial relate to 3 issues.

First, many secondary outcomes were used, including the Western Ontario and McMaster Universities Osteoarthritis Index version 3.1 (WOMAC) (3) stiffness subscale score, WOMAC physical function subscale score, WOMAC total score, pain score after a 50-foot walking test, daily pain score, rates of responders, patient global assessment, physician global assessment, Medical Outcomes Study Short Form 36 health survey, EuroQol 5-domain, and acetaminophen consumption. In the clinical trial registry (JapicCTI no. 173537), the only secondary outcomes listed are the WOMAC total score, 50-foot walking test (not pain after the test), and adverse events. Inconsistencies between the article and the registry in terms of clarity (e.g., pain after walking or distance walked during a 50-foot walking test), type of outcome, and timing of outcome assessment raise concerns regarding preferential outcome reporting. The 2010 Consolidated Standards of Reporting Trials statement (4) warns about the potentially serious risk of selective outcome reporting bias.

Second, Nishida et al used the WOMAC pain subscale score for their primary outcome measure. My concern relates to the way in which WOMAC pain subscale scores were reported. The authors state that "the primary outcome measure was the WOMAC pain subscale score, measured on a 100-mm visual analog scale (VAS)." Woolacott et al conducted a systematic review to determine if randomized trials adhere to appropriate use of the WOMAC scoring system (5). They found that in 32 of 60 trials using WOMAC scores, researchers incorrectly reported the scale version or type of scale used. There are two visual analog scales that can be applied in calculating the WOMAC pain subscale score, one with a 0–10-mm VAS per item (total score range 0–50) and one with a 0–100-mm VAS per item (total score range 0–500). A third option is a numeric rating scale in which the scale used is 0–10 per item, with a total score range of 0–50. Nishida and colleagues appeared to apply the incorrect scale when calculating WOMAC pain subscale scores.

My last point relates to the heavy reliance on statistical significance with little attention paid to clinical importance. Reliance on secondary outcomes not specified in the registry (i.e., Outcome Measures in Rheumatology–Osteoarthritis Research Society International responder criteria) is inadequate for reasons discussed earlier in this letter. Rather, I would have expected a discussion of the clinical importance of group differences for the primary outcome and prespecified secondary outcomes.

Daniel L. Riddle, PT, PhD, FAPTA iD
Virginia Commonwealth University
Richmond, VA

1. Nishida Y, Kano K, Nobuoka Y, Seo T. Efficacy and safety of diclofenac–hyaluronate conjugate (diclofenac etalhyaluronate) for knee osteoarthritis: a randomized phase III trial in Japan. Arthritis Rheumatol 2021;73:1646–55.
2. Cashin AG, McAuley JH, Lamb SE, Lee H. Disentangling contextual effects from musculoskeletal treatments [editorial]. Osteoarthritis Cartilage 2021;29:297–9.
3. Bellamy N, Buchanan WW, Goldsmith CH, Campbell J, Stitt LW. Validation study of WOMAC: a health status instrument for measuring clinically important patient relevant outcomes to antirheumatic drug therapy in patients with osteoarthritis of the hip or knee. J Rheumatol 1988;15:1833–40.

4. Moher D, Hopewell S, Schulz KF, Montori V, Gøtzsche PC, Devereaux PJ, et al. CONSORT 2010 explanation and elaboration: updated guidelines for reporting parallel group randomised trials. BMJ 2010;340:c869.

5. Woolacott NF, Corbett MS, Rice SJ. The use and reporting of WOMAC in the assessment of the benefit of physical therapies for the pain of osteoarthritis of the knee: findings from a systematic review of clinical trials. Rheumatology (Oxford) 2012;51:1440–6.

Reply

To the Editor:

We thank Dr. Riddle for stating his concerns regarding potential methodologic issues in our study. We would like to address these concerns.

First, our article was prepared in compliance with the Consolidated Standards of Reporting Trials statement (1), including all prespecified methods and results; therefore, there is no concern of selective outcome reporting. Diclofenac etalhyaluronate (DF-HA) is a developmental product and has never been on the market in any country. To protect our intellectual property, only the minimum information was provided to the registry. Therefore, some of the secondary outcomes reported in this article differ from those registered. However, the registered contents in the JapicCTI registry follow the International Federation of Pharmaceutical Manufacturers and Associations guidelines (2). We plan to add this article to the JapicCTI registry after DF-HA becomes available in the first country to implement it.

As for the second concern, we used the WOMAC scoring system (3) correctly because we followed the instructions in the WOMAC user guide to normalize dimensions on a subscale-by-scale basis and express the scores on 0–10 or 0–100 scales (4). Dr. Riddle also raised the issue of incorrect reporting of scale version and type of scale, as described by Woolacott et al (5). In the outcomes section of our article, however, we clearly state that we used a 100-mm VAS to evaluate the WOMAC pain subscale scores. Therefore, we do not inadequately report or misreport any application or explanations of the WOMAC pain subscale scoring system.

Third, it is necessary to examine multiple factors in order to evaluate the clinical importance of group differences (6). We discussed results of the responder analysis, improvement of multiple symptoms, early response to treatment with DF-HA, and maintenance of the treatment effect. In addition, to examine the magnitude of group differences for the primary and secondary outcomes, the mean effect size over 12 weeks was calculated using the least squares mean change and the pooled SD at each time point for the post hoc analyses (7). The results indicated that

Table 1. Difference and effect size in primary and secondary outcomes of DF-HA over 12 weeks*

	Difference (95% CI)	Effect size, SD units
Primary outcome		
WOMAC pain score, mm†	−6.1 (−9.4, −2.8)	0.30
Secondary outcomes		
WOMAC stiffness score, mm†	−4.6 (−8.0, −1.2)	0.20
WOMAC physical function score, mm†	−5.7 (−8.9, −2.5)	0.29
Total score	−5.6 (−8.7, −2.4)	0.29
50-foot walking test pain score, mm†	−6.8 (−10.5, −3.2)	0.30
Mean daily pain score‡	−0.56 (−0.82, −0.31)	0.35
Patient global assessment score, mm†	−6.5 (−9.7, −3.3)	0.31
Physician global assessment score, mm†	−4.5 (−7.2, −1.9)	0.24

* Differences are the between-group difference (95% confidence interval [95% CI]) in least squares mean change from baseline. DF-HA = diclofenac etalhyaluronate; WOMAC = Western Ontario and McMaster Universities Osteoarthritis Index.
† On a 100-mm visual analog scale (0–100).
‡ On an 11-point numeric rating scale (0–10).

the mean effect size of DF-HA treatment on WOMAC pain subscale scores over 12 weeks was 0.30. Similar effect sizes were observed when secondary outcomes were evaluated in the DF-HA group over 12 weeks (Table 1). Although this study was not an active treatment–controlled clinical trial, and it is difficult to evaluate the clinical importance of group differences only by effect size, the effect size of DF-HA was in the low-to-moderate range for improvement in primary and secondary outcomes (8). Thus, some benefits of DF-HA were confirmed, but further studies are needed to evaluate the clinical usefulness of DF-HA.

Yoshihiro Nishida, MD [ID]
Nagoya University Hospital
Nagoya, Japan
Kazuyuki Kano, BSc
Yuji Nobuoka, MSc
Takayuki Seo, PhD
Seikagaku Corporation
Tokyo, Japan

1. Moher D, Hopewell S, Schulz KF, Montori V, Gøtzsche PC, Devereaux PJ, et al. CONSORT 2010 explanation and elaboration: updated guidelines for reporting parallel group randomised trials. BMJ 2010; 340:c869.

2. International Federation of Pharmaceutical Manufacturers and Associations, European Federation of Pharmaceutical Industries and

Associations, Juvenile Products Manufacturers Association, Pharmaceutical Research and Manufacturers of America. Joint position on the disclosure of clinical trial information via clinical trial registries and databases. URL: https://www.ifpma.org/wp-content/uploads/2010/11/Joint-Position-on-Disclosure-of-CT-Info-via-CT-Registries-Revised-Jan2018-vFINAL.pdf.

3. Bellamy N, Buchanan WW, Goldsmith CH, Campbell J, Stitt LW. Validation study of WOMAC: a health status instrument for measuring clinically important patient relevant outcomes to antirheumatic drug therapy in patients with osteoarthritis of the hip or knee. J Rheumatol 1988;15:1833–40.

4. Bellamy N. WOMAC osteoarthritis index user guide XI. Brisbane (Australia); 2015.

5. Woolacott NF, Corbett MS, Rice SJ. The use and reporting of WOMAC in the assessment of the benefit of physical therapies for the pain of osteoarthritis of the knee: findings from a systematic review of clinical trials. Rheumatology (Oxford) 2012;51:1440–6.

6. Dworkin RH, Turk DC, McDermott MP, Peirce-Sandner S, Burke LB, Cowan P, et al. Interpreting the clinical importance of group differences in chronic pain clinical trials: IMMPACT recommendations [review]. Pain 2009;146:238–44.

7. Dworkin RH, Peirce-Sandner S, Turk DC, McDermott MP, Gibofsky A, Simon LS, et al. Outcome measures in placebo-controlled trials of osteoarthritis: responsiveness to treatment effects in the REPORT database [review]. Osteoarthritis Cartilage 2011;19:483–92.

8. Zhang W, Nuki G, Moskowitz RW, Abramson S, Altman RD, Arden NK, et al. OARSI recommendations for the management of hip and knee osteoarthritis. Part III: changes in evidence following systematic cumulative update of research published through January 2009 [review]. Osteoarthritis Cartilage 2010;18:476–99.

More steps forward to optimize the dosing of hydroxychloroquine: comment on the article by Petri et al

To the Editor:

We read with great interest the article by Dr. Petri and colleagues describing their study in which it was demonstrated that higher hydroxychloroquine (HCQ) blood levels were associated with lower risk of thrombotic events in patients with systemic lupus erythematosus (SLE) (1). A threshold of ≥1,068 ng/ml for whole blood HCQ levels (based on tertiles of mean levels observed in SLE patients) and a most recent HCQ level of ≥1,192 ng/ml had a protective effect. The dose response observed in that study implies that HCQ has a therapeutic threshold with which to determine protective versus deleterious effects. However, a previous study indicated that an HCQ blood level ranging from 1,177 ng/ml to 3,513 ng/ml was predictive of HCQ retinopathy (2). Obviously, there is a great overlap between HCQ blood levels that are protective against thrombosis and toxic levels associated with retinopathy. The optimal therapeutic range is so narrow (1,068–1,177 ng/ml) that dose titration to target this level would be difficult in clinical practice. It seems that the dilemma of avoiding retinopathy while maintaining the benefit of HCQ still exists.

To further clarify this problem, we believe more comprehensive risk stratification is helpful. As "triple positivity" for antiphospholipid antibodies carries higher risk of thrombotic events (3), the presence of anti–β_2-glycoprotein I and anticardiolipin antibodies would have been important to identify, but was not reported in the analysis by Petri and colleagues. The concomitant use of aspirin may modify the risk of thrombosis, which was also not specified in the report. In addition, Petri and colleagues demonstrated that the risk of thrombosis was reduced by 13% with every 200-ng/ml increase in HCQ blood level. We are curious if this observation still holds true for higher HCQ blood levels (e.g., >1,500 or >2,000 ng/ml). Similarly, the risk of retinopathy should be assessed in stratified groups of patients displaying higher ranges of HCQ blood levels, in order to clarify the extent of hazard conferred by each HCQ blood level range among patients who require this therapy. This would help physicians and patients manage the disease in a way that balances the risks and benefits of treatment with HCQ.

Finally, the strategy of adapting HCQ dose based on blood level with an aim at reducing thrombotic risk should be investigated in the future. A similar approach was shown to be ineffective in decreasing disease flares of SLE in the PLUS study (4). Although personalized drug dosing and risk management will likely be the future paradigm in the treatment of SLE, we still need more details on the relationship between the dose of HCQ and the benefit or toxicity associated with this treatment.

Jui-Hung Kao, MD [iD]
Ting-Yuan Lan, MD [iD]
Ko-Jen Li, MD, PhD
National Taiwan University Hospital
Taipei, Taiwan

1. Petri M, Konig MF, Li J, Goldman DW. Higher hydroxychloroquine blood levels are associated with reduced thrombosis risk in systemic lupus erythematosus. Arthritis Rheumatol 2021;73:997–1004.

2. Petri M, Elkhalifa M, Li J, Magder LS, Goldman DW. Hydroxychloroquine blood levels predict hydroxychloroquine retinopathy. Arthritis Rheumatol 2020;72:448–53.

3. Pengo V, Ruffatti A, Legnani C, Testa S, Fierro T, Marongiu F, et al. Incidence of a first thromboembolic event in asymptomatic carriers of high-risk antiphospholipid antibody profile: a multicenter prospective study. Blood 2011;118:4714–8.

4. Costedoat-Chalumeau N, Galicier L, Aumaître O, Francès C, Le Guern V, Lioté F, et al. Hydroxychloroquine in systemic lupus erythematosus: results of a French multicentre controlled trial (PLUS Study). Ann Rheum Dis 2013;72:1786–92.

Reply

To the Editor:

We would like to thank Dr. Kao and colleagues for their comments regarding our article, and we have some thoughts in response.

First, regarding the importance of identifying "triple positivity" (i.e., positive for lupus anticoagulant, anticardiolipin, and anti–β_2-glycoprotein), we did not find "triple positivity" to be useful in predicting thrombotic events in our cohort. For one thing, we have observed that the blood levels of lupus anticoagulant fluctuate over time in patients with SLE, but even when found to be only intermittently positive over the course of the disease, this antibody is still a risk factor for thrombosis (1). Furthermore, we have shown that anticardiolipin does not add to thrombotic risk in SLE (2) over and above lupus anticoagulant. Finally, "triple positivity" also was not valid in the PROMISSE study of pregnancy outcomes in antiphospholipid-positive women (a study not limited to SLE), in that only lupus anticoagulant was associated with adverse pregnancy outcomes (3).

Second, we agree that there is an overlap between the range of HCQ blood levels we found to be protective against thrombosis and the range that increased the risk of retinopathy. However, we note that the cutoffs we used in our analysis were simply chosen to divide the concentrations equally into tertiles to gain insight into the relationship between blood concentration and protection or risk. We agree that it would be important to identify a range of HCQ blood concentration that conferred protection without increasing risk. Unfortunately, given the small number of cases of thrombosis and retinopathy in our database at the time of our analysis, we were not able to determine if such a range exists. Hopefully we can address that issue in the future.

Third, observations from our prospective studies have shown that the risk of retinopathy is greater in patients with SLE (4) than has been thought historically, but is much lower than the reported risk in patients receiving HCQ therapy in a retrospective Kaiser Permanente study (5).

Michelle Petri, MD, MPH [iD]
Johns Hopkins University School of Medicine
Laurence S. Magder, PhD, MPH
University of Maryland School of Medicine
Baltimore, MD

1. Petri MA, Avci M, Magder LS. Evaluation of different ways to identify persistent positivity of lupus anticoagulant in systemic lupus erythematosus. Lupus Sci Med 2020;7:e000406.
2. Domingues V, Magder LS, Petri M. Assessment of the independent associations of IgG, IgM and IgA isotypes of anticardiolipin with thrombosis in SLE. Lupus Sci Med 2016;3:e000107.
3. Lockshin MD, Kim M, Laskin CA, Guerra M, Branch DW, Merrill J, et al. Prediction of adverse pregnancy outcome by the presence of lupus anticoagulant, but not anticardiolipin antibody, in patients with antiphospholipid antibodies. Arthritis Rheum 2012;64:2311–8.
4. Petri M, Elkhalifa M, Li J, Magder LS, Goldman DW. Hydroxychloroquine blood levels predict hydroxychloroquine retinopathy. Arthritis Rheumatol 2020;72:448–53.
5. Melles RB, Marmor MF. The risk of toxic retinopathy in patients on long-term hydroxychloroquine therapy. JAMA Ophthalmol 2014;132:1453–60.